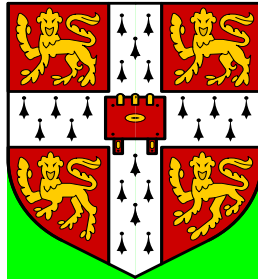


**UNIVERSITY OF CAMBRIDGE**

DEPARTMENT OF ENGINEERING



Soil conditioning for pipe-jacking and tunnelling

François Xavier BORGHI

*A dissertation submitted for the degree of Doctor of Philosophy  
at the University of Cambridge*

---

**Declaration**

I hereby declare that, except where specific reference is made to the work of others, the contents of this dissertation are original and have not been submitted in whole or in part for consideration for any other degree or qualification in this, or any other university. This dissertation is entirely the result of my own work, and includes nothing, except where explicitly mentioned, which is the outcome of work done in collaboration. This dissertation contains less than the revised limit of 80,000 words and less than 150 figures.

F.X. Borghi  
January 2006

---

## Abstract

In pipe jacking, reduction of jacking forces may be achieved by injecting bentonite, polymer solutions, or other additives into a thin overcut annulus excavated around the pipes. Physicochemical interactions, including clay swelling inhibition and filter-cake formation at or near the cavity boundary, are believed to alter the process of cavity contraction. This may help reduce radial effective stresses on the pipe and, in turn, the jacking forces. However, the interplay between the contracting cavity, the overcut size, the lubricant chemistry and its injection pressure are not understood with sufficient confidence to allow informed decisions to be made when selecting lubrication schemes. A physical model replicating the pipe jacking process at laboratory-scale has been devised to identify the key interactions and measure the effects of the lubricant chemistry on the radial effective stresses between the pipe and the clay. A cylindrical cavity was excavated in an overconsolidated kaolin clay model using a low-disturbance drilling system. During excavation, lubricant fluids were injected at controlled pressures in an annulus around the pipe. Tests performed using different chemical compositions but under otherwise identical conditions have demonstrated that the lubricant composition significantly affects the rate of build-up of effective stresses on the model pipe, as well as their final magnitude. In comparison to water, polymer achieved a 65% reduction of radial effective stress on the pipe.

In earth pressure balance (*EPB*) tunnelling machines, the provision of a supporting pressure to the tunnel face often demands that the properties of the excavated ground be altered by means of soil conditioning. Foam and polymer are almost invariably injected into the excavation chamber to help remould the excavated ground into a mixture that may be discharged by the screw conveyor in a controllable manner. Again, little guidance is available to recommend appropriate types and quantities of soil conditioners in different ground conditions, and serious difficulties have sometimes arisen from the common sense and experience approach usually adopted in industry. The effects of soil conditioning on the operational parameters of the *EPB* machines used on the Channel Tunnel Rail Link project have been back-analysed. It has been shown that the 8.15 m diameter machines could be driven efficiently in a wide variety of ground conditions and that appropriate soil conditioning allowed the machines to be operated in closed-mode in the very stiff clays of the Lambeth Group as well as in the London Clay. Remarkably well-controlled face pressures have been achieved in London Clay. Polymer injection ratios of about 15% reduced the undrained shear strengths of the London Clay to about 25 kPa. Little or no foam was injected when the *EPB* machines were in the London Clay, suggesting that foam only has limited benefits in stiff clays. Volume losses of below 1% were achieved throughout the tunnel drives, with only a few instances of larger volume loss.

---

## Acknowledgements

I would like to thank my supervisor Professor Robert Mair for his practical insight and immense enthusiasm which have encouraged and enlightened me throughout my research.

I have learnt much from discussions with Professor Malcolm Bolton, who acted as my advisor and I am indebted for the constant help and support that he generously provided. I owe an incalculable debt to Professor Sarah Springman, who will no doubt be aware of her countless contributions. Sarah and Malcolm fomented my aspirations towards research, and I would never have embarked into this work, had I not be inspired and motivated by them.

The financial support of the Engineering and Physical Science Research Council is gratefully acknowledged. I would like to extend my gratitude to the British Pipe Jacking Association, the British Tunnelling Society as well as Clare College Cambridge, who all made important contributions towards my maintenance as well as my College and University fees. I would like to thank all members of the Pipe Jacking Research Group, in particular Arthur Moss and George Milligan for their enthusiasm and technical advice.

This research has benefited from the collaboration of Nishimatsu Construction Company Ltd, contractor of Contract 220 of the Channel Tunnel Rail Link in London. The collaboration of Messrs Sugiyama, Hagiwara, Minami and Yamasaki is gratefully acknowledged. The author is particularly indebted to Doug Allenby and Ivor Thomas of Edmund Nuttall Ltd (Contract 250), for the exceptional interest he took in helping me while on site.

During the slow and often interrupted evolution of the experimental apparatus, I have accumulated many debts towards Chris Collison and Chrissie McGinnie, who provided vital technical assistance in the laboratory; their continuous support will be remembered with recognition. I would also like to thank Keith Wilkinson who helped design parts of the experimental apparatus. My sincerest thanks go to Clive Dalton and co-workers at Cambridge Insitu Ltd and, for their exceptional generosity and enthusiasm throughout my research.

Among my colleagues of the Geotechnical Group, I will especially remember the friendship of Helena Coumoulos, Lis Bowman, Barnali Ghosh, Sang & Rina Ratnam, Francisco Hernandez-Martinez, George Marketos, and Gabrielle Pepe and James Rombi, and Dominic Joray, Yukihiro Ishiara, Angelique Quentin, Ana Carla and Paul Dimmock as well as the various contributions of Johnny Cheuk, Andy Take, Stuart Haigh, Andrew Brennan, SW Jacobsz and Alec Marshall. I am grateful to Dave

---

White, who has always shown interest in my research and has been available to share ideas or provide useful criticism. I would also like to thank Michele Buono Mascagni, Marco Barla, Markus Sidler, Andrew Merritt and Jarungwit Wongsaroj for their collaborations and valuable contributions.

I cannot imagine having completed this work without the support of my dear friends Paulo Coelho, Aleksandar Spasojevic and Marcelo Silva. In addition, I am particularly grateful for the friendship and assistance of my colleagues Kensuke Date and Masoud Hajjalilue Bonab and for the exceptional support of Anama Lowday. You all contributed to make my stay in Cambridge worthwhile and enjoyable. I would also like to thank Dodly Alexandre, José Manuel Diego and Guido Ribí who continuously provided friendship and encouragements from abroad.

*Finally, Mei Tzeang, you made it all possible, I will never forget – merci!*

---

## Table of Content

Declaration .....	i
Abstract .....	ii
Acknowledgments .....	iii
Table of content .....	v
List of Tables .....	xi
List of Figures .....	xiii
Notation .....	xx
<b>CHAPTER 1: BACKGROUND AND OBJECTIVES .....</b>	<b>- 0 -</b>
1.1 INTRODUCTION .....	- 0 -
1.2 BACKGROUND: LUBRICATION IN PIPE JACKING .....	- 1 -
1.2.1 <i>The method</i> .....	2
1.2.2 <i>Jacking forces</i> .....	- 1 -
1.2.3 <i>Lubrication</i> .....	- 2 -
1.2.4 <i>Need for research</i> .....	- 3 -
1.3 BACKGROUND: SOIL CONDITIONING IN EPB MACHINES .....	- 4 -
1.3.1 <i>The technology</i> .....	- 4 -
1.3.2 <i>Spoil properties</i> .....	- 5 -
1.3.3 <i>Soil conditioning</i> .....	- 5 -
1.3.4 <i>Need for research</i> .....	- 6 -
1.4 OBJECTIVES .....	- 7 -
1.5 LAYOUT OF THE DISSERTATION .....	- 8 -
<b>CHAPTER 2: LITERATURE REVIEW: EFFECTS OF LUBRICATION IN PIPE JACKING.....</b>	<b>12</b>
2.1 SCOPE AND OBJECTIVES .....	12
2.2 FIELD OBSERVATIONS AND MEASUREMENTS OF LUBRICATION EFFECTS .....	13
2.2.1 <i>Introduction</i> .....	13
2.2.2 <i>Effects of lubricant on jacking forces</i> .....	14
2.2.2.1 Honor Oak, London, UK.....	14
2.2.2.2 Leytonstone, London, UK.....	14
2.2.2.3 Seaham, UK.....	15
2.2.2.4 Thurrock, UK.....	15
2.2.2.5 Nimitmai Road, Bangkok, Thailand .....	16
2.2.2.6 Vibhavadi, Bangkok, Thailand .....	17
2.2.3 <i>Effects of lubricants on pipe-soil contact stresses</i> .....	18
2.2.3.1 Thurrock, UK.....	18
2.2.3.2 Seaham, UK.....	19
2.2.4 <i>Summary</i> .....	20
2.3 GROUND RESPONSE TO CYLINDRICAL CAVITY CONTRACTION .....	21
2.3.1 <i>Introduction</i> .....	21
2.3.2 <i>Stability of unloaded cylindrical cavities</i> .....	22
2.3.3 <i>Short-term stress changes around an unloaded cylindrical cavity</i> .....	24
2.3.3.1 Applicability and assumptions .....	24
2.3.3.2 Total stress models.....	25
2.3.3.3 Effective stress models .....	27

---

---

2.3.4	<i>Consolidation around a contracting cavity</i> .....	29
2.3.4.1	Terminology .....	29
2.3.4.2	Semi-analytical consolidation solution for contracting cavities .....	31
2.3.4.3	Numerical analyses .....	34
2.3.5	<i>Ground loading on the lining</i> .....	36
2.3.5.1	Introduction.....	36
2.3.5.2	Method of characteristic curves .....	36
2.3.5.3	Numerical analysis.....	38
2.3.6	<i>Summary</i> .....	39
2.4	PHYSICOCHEMICAL INTERACTION NEAR THE EXCAVATION BOUNDARY .....	40
2.4.1	<i>Introduction</i> .....	40
2.4.2	<i>Relevance of wellbore drilling fluids for pipe jacking lubrication</i> .....	41
2.4.3	<i>Composition and properties of drilling fluids and lubricants</i> .....	42
2.4.3.1	Generalities .....	42
2.4.3.2	Bentonite.....	43
2.4.3.3	Polymers .....	44
2.4.3.4	Inorganic chemical solutions .....	45
2.4.4	<i>Interaction mechanisms</i> .....	45
2.4.4.1	Permeability reduction near the cavity boundary .....	46
2.4.4.2	Osmotic potential .....	51
2.4.4.3	Cation exchange processes and interparticle forces .....	54
2.4.5	<i>Summary</i> .....	56
2.5	CONCLUSIONS.....	58
<b>CHAPTER 3: EXPERIMENTAL APPARATUS.....</b>		<b>124</b>
3.1	OBJECTIVES .....	125
3.2	MODELLING TECHNIQUE .....	126
3.2.1	<i>Idealisation of the construction process</i> .....	126
3.2.1.1	Excavation of a cavity.....	126
3.2.1.2	Lubrication.....	127
3.2.1.3	Model pipe .....	129
3.2.2	<i>Modelling of ground conditions</i> .....	130
3.2.3	<i>Numerical or physical?</i> .....	130
3.2.4	<i>Centrifuge or 1-g?</i> .....	131
3.2.5	<i>Stress and strain boundary conditions imposed to the soil model</i> .....	132
3.2.6	<i>Selection and implications of model dimensions</i> .....	134
3.2.6.1	Side-boundary effects .....	134
3.2.6.2	Selection of the model dimensions.....	135
3.2.6.3	Scaling laws .....	136
3.2.7	<i>Summary</i> .....	137
3.3	APPARATUS DESIGN .....	138
3.3.1	<i>Strongbox design</i> .....	138
3.3.2	<i>Provision of consolidation and surcharge pressure</i> .....	139
3.3.3	<i>Model Pipe</i> .....	141
3.3.4	<i>Self-boring mechanism</i> .....	141
3.3.4.1	Principles of low disturbance drilling .....	141
3.3.4.2	Design of a new cutting tool .....	142
3.3.4.3	Drilling fluid .....	144

---

---

3.3.5	<i>Lubricant injection</i> .....	145
3.3.5.1	Injection method .....	145
3.3.5.2	Lubricant fluids.....	146
3.3.6	<i>Model pipe assembly and driving equipment</i> .....	146
3.3.6.1	Guiding cylinder .....	146
3.3.6.2	Pipe carrier unit.....	147
3.3.6.3	Jacking actuation.....	148
3.3.6.4	Pipe-strongbox interface .....	149
3.4	SOIL MODEL PREPARATION .....	150
3.4.1	<i>Material selection</i> .....	150
3.4.2	<i>Soil Model Preparation</i> .....	151
3.4.2.1	Slurry preparation .....	151
3.4.2.2	Top and bottom boundary drainage .....	151
3.4.2.3	Consolidation procedure .....	151
3.5	APPARATUS INSTRUMENTATION .....	153
3.5.1	<i>Summary</i> .....	153
3.5.2	<i>Model pipe instrumentation</i> .....	153
3.5.2.1	Earth pressure cells .....	153
3.5.2.2	Pore pressure cells.....	154
3.5.2.3	Displacement transducers .....	156
3.5.3	<i>Pore pressure measurements in the soil</i> .....	157
3.5.3.1	Generalities .....	157
3.5.3.2	Transducer technology.....	158
3.5.3.3	<i>PPT</i> saturation.....	160
3.5.3.4	<i>PPT</i> calibration .....	162
3.5.3.5	Quality control of <i>PPT</i> measurements .....	163
3.5.3.6	<i>PPT</i> insertion into the soil model.....	164
3.5.4	<i>Monitoring of boundary conditions</i> .....	165
3.5.4.1	Total stress boundary condition ( <i>LI</i> ) .....	165
3.5.4.2	Hydraulic boundary condition ( <i>PTI</i> ) .....	165
3.5.4.3	Height of the soil model ( <i>DW1</i> ).....	165
3.5.5	<i>Monitoring of lubricant injection</i> .....	166
3.5.5.1	Lubricant pressure ( <i>PT2</i> and <i>PT3</i> ).....	166
3.5.5.2	Lubricant volume ( <i>L2</i> ) .....	166
3.5.6	<i>Monitoring of pipe insertion</i> .....	167
3.5.6.1	Model pipe position ( <i>DW2</i> ).....	167
3.5.6.2	Jacking force ( <i>L3</i> ) .....	167
3.5.7	<i>Signal conditioning, data acquisition and raw data processing</i> .....	167
3.5.7.1	Model Pipe instrumentation .....	168
3.5.7.2	<i>PPT</i> and ancillary instrumentation.....	168
3.6	TESTING PROCEDURE .....	168
3.6.1	<i>Soil model preparation</i> .....	168
3.6.2	<i>Preparation of the model pipe assembly</i> .....	170
3.6.3	<i>Insertion of model pipe</i> .....	171
3.6.4	<i>Post-mortem proceedings</i> .....	172
3.7	TEST PROGRAMME.....	172
3.8	FINAL REMARKS .....	173

---

---

<b>CHAPTER 4: EXPERIMENTAL RESULTS .....</b>	<b>186</b>
4.1 INTRODUCTION .....	186
4.1.1 <i>Scope and objectives</i> .....	186
4.1.2 <i>Chapter layout</i> .....	187
4.2 PRESENTATION AND PROCESSING OF TEST DATA .....	187
4.2.1 <i>Definitions, conventions, and references</i> .....	187
4.2.2 <i>Scaling of test results</i> .....	187
4.2.3 <i>Raw data processing</i> .....	189
4.3 SOIL MODEL CHARACTERISATION .....	190
4.3.1 <i>Stress history of the soil model</i> .....	191
4.3.2 <i>Compression and consolidation parameters</i> .....	192
4.3.3 <i>Horizontal-to-vertical stress ratio</i> .....	193
4.3.4 <i>Moisture content and voids ratio</i> .....	194
4.3.5 <i>Undrained shear strength</i> .....	195
4.3.5.1 <i>Shear-vane measurements</i> .....	195
4.3.5.2 <i>Undrained shear strength prediction</i> .....	196
4.4 BOUNDARY CONDITIONS .....	196
4.4.1 <i>Applied stresses at the soil model boundaries</i> .....	196
4.4.1.1 <i>Total stress</i> .....	196
4.4.1.2 <i>Back-pressure</i> .....	197
4.4.1.3 <i>Effective stresses</i> .....	198
4.4.2 <i>Model pipe installation</i> .....	198
4.4.3 <i>Lubricant injection</i> .....	198
4.4.3.1 <i>Method and monitoring</i> .....	198
4.4.3.2 <i>Test T5</i> .....	199
4.4.3.3 <i>Test T6</i> .....	200
4.4.3.4 <i>Test T8</i> .....	201
4.5 PORE WATER PRESSURE MEASUREMENTS .....	201
4.5.1 <i>Preliminary remarks</i> .....	201
4.5.1.1 <i>Labelling of instruments</i> .....	201
4.5.1.2 <i>Normalisation of pore water pressure data</i> .....	202
4.5.1.3 <i>Hydrostatic conditions before excavation</i> .....	202
4.5.2 <i>Generated excess pore water pressure</i> .....	203
4.5.2.1 <i>Symmetry of pore water pressure measurements</i> .....	204
4.5.2.2 <i>Effect of container shape on excess pore water pressure</i> .....	205
4.5.2.3 <i>Initial distribution of excess pore water pressure</i> .....	206
4.5.3 <i>Dissipation of excess pore water pressure</i> .....	207
4.5.3.1 <i>Presentation of excess pore water pressure dissipation</i> .....	207
4.5.3.2 <i>Evolution of fluid pressure at cavity boundary</i> .....	208
4.5.3.3 <i>Dissipation of <math>\Delta u/\sigma_{vo}'</math> before sealing of the gap (<math>0 &lt; T &lt; 0.4</math>)</i> .....	209
4.5.3.4 <i>Dissipation <math>\Delta u/\sigma_{vo}'</math> after sealing of the gap (<math>T &gt; 0.4</math>)</i> .....	210
4.5.3.5 <i>Pore water pressures at steady state (<math>T &gt; 30</math>)</i> .....	211
4.6 GROUND LOADING ON PIPE .....	212
4.6.1 <i>Preliminary remarks</i> .....	212
4.6.2 <i>Fluid pressure on the pipe</i> .....	213
4.6.3 <i>Total stress on the pipe</i> .....	214
4.6.4 <i>Effective stresses at the pipe-clay interface</i> .....	216

---

---

4.7	MODEL LIMITATIONS AND SOURCES OF ERRORS .....	217
4.7.1	<i>Errors related to modelling</i> .....	217
4.7.2	<i>Errors related to test execution</i> .....	219
4.8	SUMMARY OF OBSERVATIONS.....	220
<b>CHAPTER 5: DISCUSSION OF EXPERIMENTAL RESULTS.....</b>		<b>223</b>
5.1	INTRODUCTION .....	223
5.1.1	<i>Scope and objectives</i> .....	223
5.1.2	<i>Chapter layout</i> .....	223
5.2	ELEMENTS OF SOIL BEHAVIOUR AND OF CLAY-POLYMER INTERACTION .....	224
5.2.1	<i>Model for the behaviour of overconsolidated clay</i> .....	224
5.2.2	<i>PHPA Polymer and kaolin</i> .....	226
5.3	INTERPRETATION OF THE MODEL BEHAVIOUR.....	227
5.3.1	<i>Preliminary remarks</i> .....	227
5.3.2	<i>Undrained cavity unloading (stage I)</i> .....	228
5.3.3	<i>Consolidation under constant cavity pressure (stage II)</i> .....	229
5.3.4	<i>Change of cavity pressure after sealing of the gap (stage III)</i> .....	230
5.3.5	<i>Build up of pipe-soil stresses (stage IV)</i> .....	233
5.4	REPERCUSSIONS FOR FIELD APPLICATION OF LUBRICATION .....	233
5.4.1	<i>Effect of lubricant composition</i> .....	233
5.4.2	<i>Effect of injection procedure</i> .....	235
5.5	FINAL REMARKS .....	237
<b>CHAPTER 6: LITERATURE REVIEW: SOIL CONDITIONING IN EARCH PRESSURE BALANCE MACHINES .....</b>		<b>226</b>
6.1	SCOPE AND OBJECTIVES.....	226
6.2	EARTH PRESSURE BALANCE MACHINE TECHNOLOGY .....	227
6.2.1	<i>Provision of face pressure</i> .....	227
6.2.2	<i>Control of pressure in the excavation chamber</i> .....	228
6.2.3	<i>Mechanics of screw conveyors</i> .....	229
6.2.4	<i>Monitoring and operation of EPB machine</i> .....	230
6.3	SOIL CONDITIONING IN EPB MACHINES .....	230
6.3.1	<i>Aim and methods</i> .....	230
6.3.2	<i>Parameters involved in soil conditioning</i> .....	231
6.3.3	<i>Effects of conditioning agents on engineering properties of the soil</i> .....	232
6.3.4	<i>Recommendations for selection of soil conditioning parameters</i> .....	236
6.3.5	<i>Field observation of soil conditioning effects</i> .....	237
6.4	IMPACT OF EPB MACHINES.....	238
6.4.1	<i>Face stability</i> .....	238
6.4.2	<i>Ground movements</i> .....	239
6.5	CONCLUSIONS.....	240
<b>CHAPTER 7: FIELD DATA OF EPB MACHINES.....</b>		<b>244</b>
7.1	INTRODUCTION .....	244
7.1.1	<i>Background and objectives</i> .....	244
7.1.2	<i>Chapter layout</i> .....	245

---

---

7.2	CHANNEL TUNNEL RAIL LINK PROJECT; <i>CONTRACT 220</i> .....	245
7.2.1	<i>Project overview</i> .....	245
7.2.2	<i>Ground conditions</i> .....	246
7.2.3	<i>Design and instrumentation of the EPB machines</i> .....	248
7.3	APPLICATION AND EFFECTS OF SOIL CONDITIONING .....	249
7.3.1	<i>Definition and presentation of data</i> .....	249
7.3.2	<i>Tunnelling in Thanet Sand</i> .....	253
7.3.2.1	Soil conditioning.....	253
7.3.2.2	Effect of the liquid injection ratio ( <i>LIR</i> ).....	253
7.3.2.3	Effect of the foam injection ratio ( <i>FIR</i> ) .....	254
7.3.3	<i>Tunnelling in the Lambeth Group</i> .....	254
7.3.3.1	Soil conditioning.....	254
7.3.3.2	Effect of the liquid injection ratio ( <i>LIR</i> ).....	254
7.3.3.3	Effect of the foam injection ratio ( <i>FIR</i> ) .....	254
7.3.4	<i>Tunnelling in London Clay and Harwich Formation</i> .....	254
7.3.4.1	Soil conditioning.....	254
7.3.4.2	Effect of the liquid injection ratio ( <i>LIR</i> ).....	254
7.3.4.3	Effect of the foam injection ratio ( <i>FIR</i> ) .....	254
7.4	EFFECT OF MACHINE PARAMETERS ON GROUND VOLUME LOSS .....	254
7.4.1	<i>Overview</i> .....	254
7.4.2	<i>Ground volume loss in Thanet Sand</i> .....	254
7.4.3	<i>Ground volume loss in the Lambeth Group</i> .....	254
7.4.4	<i>Ground volume loss in London Clay and Harwich Formation</i> .....	254
7.5	DISCUSSION .....	254
7.5.1	<i>Soil conditioning compared recommendation</i> .....	255
7.5.2	<i>Provision and control of face pressure</i> .....	255
7.5.3	<i>Effect of machine parameters on ground volume loss</i> .....	255
7.6	SUMMARY .....	255
	<b>CHAPTER 8: CONCLUSIONS.....</b>	<b>256</b>
8.1	OUTLINE.....	256
8.2	LUBRICATION IN PIPE JACKING.....	257
8.2.1	<i>Conclusions</i> .....	257
8.2.2	<i>Recommendation for further work</i> .....	258
8.3	SOIL CONDITIONING IN EPB MACHINES.....	258
8.3.1	<i>Conclusions</i> .....	258
8.3.2	<i>Recommendation for further work</i> .....	258
8.4	FINAL REMARKS .....	258

---

---

## List of Tables

### Chapter 2

Table 2.1. Summary of the reported pipe jacking projects

Table 2.2. Direct and coupled flow phenomena in soil (after Mitchell, 1993 and Keijzer, 2000)

Table 2.3. Test combinations and achieved permeability reductions (Ballard *et al.*, 1994)

### Chapter 3

Table 3.1. Mechanical components of the experimental apparatus and manufacturer details

Table 3.3. Calibration factors of PPTs and ancillary instrumentation

Table 3.4. Test parameters

Table 3.5. Summary of technical difficulties and remediation measures

### Chapter 4

Table 4.1. Summary of properties and engineering parameters of E-Grade kaolin (after Barker, 1998; Merritt, 2004)

### Chapter 6

Table 6.1. Guideline for the application of soil conditioning (EFNARC, 2005)

Table 6.2. Soil conditioning application in *EPB* machine (Milligan, 2001)

Table 6.3. Case-studies of soil conditioning (Boone *et al.*, 2005)

Table 6.4. Other case-studies of soil conditioning

### Chapter 7

Table 7.1. Stratigraphic formation and unit names (Union Railways, 1997)

Table 7.2. Ground conditions at tunnel level along the route (based on 32 boreholes)

Table 7.3. Screw conveyor characteristics – Kawasaki machines  
Contract 220 CTRL

Table 7.4. Selection of monitored machine parameters

Table 7.5. Summary of soil conditioning parameters in different ground conditions

Table 7.6. Summary of average machine parameters in different ground conditions

- 
- Table 7.7. Summary of average face components in different ground conditions (see Fig. 7.12)
- Table 7.8. Summary of correlation coefficient between soil conditioning parameters and machine parameters (the data corresponding to the shaded parts are plotted in Fig. 7.13)
- Table 7.9. Summary of average soil conditioning and machine parameters for the rings plotted in Fig. 7.14 to 7.16
- Table 7.10. Summary of average soil conditioning and machine parameters for the rings plotted in Fig. 7.17 to 7.19
- Table 7.11. Mean and range of total and face volume loss in different ground conditions (Upline tunnel)

---

## List of Figures

### Chapter 1

- Fig. 1.1. Overview of the pipe jacking method (courtesy Herrenknecht AG)  
Fig. 1.2. Diagrammatic section of an EPB machine (Maidl *et al.*, 1996)

### Chapter 2

- Fig. 2.1. Jacking record Honor Oak, London, UK (Norris, 1992)  
Fig. 2.2. Jacking record, Leytonstone, London, UK (Marshall, 1998)  
Fig. 2.3. Jacking record Seaham, UK (Marshall, 1998)  
Fig. 2.4. Jacking record, Thurrock, UK (Marshall, 1998)  
Fig. 2.5. Jacking record, Nimitmai, Thailand (Broomfield, 2004)  
Fig. 2.6. Interface stresses at Thurrock, UK (Marshall, 1998) (a) Invert rear; (b) Crown Centre; (c) Spring line right front  
Fig. 2.7. Pore pressure variation at pipe front during lubricant pumping, Seaham, UK (Marshall, 98)  
Fig. 2.8. Variation in average shear and effective stresses at the pipe centre, Seaham, UK (Marshall, 1998)  
Fig. 2.9. Summary of unit jacking forces in different schemes  
Fig. 2.10. Variable definition for cavity contraction  
Fig. 2.11. Upper and lower bound stability ratios for plane strain circular tunnels (Davis *et al.*, 1980)  
Fig. 2.12. Comparison of stability ratios for circular tunnels in soils whose undrained shear strength increases linearly with depth (Sloan & Assadi, 1993)  
Fig. 2.13. Measured and predicted changes in pore water pressure around a deep tunnel in Boom Clay (Mair & Taylor, 1993)  
Fig. 2.14. Large-strain cylindrical cavity contraction solution for soil behaviour around tunnel in original Cam clay with OCR = 1.0 (a), 2.0 (b) and 5.0 (c), respectively (Yu & Rowe, 1999)  
Fig. 2.15. Isochrones of excess pore water pressure for different sets of boundary conditions (Carter, 1988)  
Fig. 2.16. Method of the characteristic curves (Panet & Guenot, 1982)  
Fig. 2.17. Excess pore water pressure distribution and characteristic curves during transient ground loading (Gärber, 2002)  
Fig. 2.18. Flow rate reduction  $Q/Q_d$  as a function of the permeability reduction  $k/k_d$  of an annulus of radius  $r_d$  around the cavity (after Muskat, 1949)

- 
- Fig. 2.19. A polymer coil entering a pre-adsorbed cylindrical pore (Denys, 2003)
- Fig. 2.20. The mechanism of polymer bridging adsorption (Denys & Zaitoun)
- Fig. 2.21. Permeability reduction due to potassium silicate fluid (Bailey *et al.*, 1998)

### **Chapter 3**

- Fig. 3.1. Overview of experimental apparatus
- Fig. 3.2. Line diagram of test set-up
- Fig. 3.3. Boundary conditions at the cavity wall
- Fig. 3.4. Soil model dimensions and initial stress conditions
- Fig. 3.5. Strongbox piston; cross-section, top, bottom and side view
- Fig. 3.6. Strongbox cross-section and side view
- Fig. 3.7. Guiding cylinder-strongbox assembly
- Fig. 3.8. Photograph of the pipe-strongbox interface (without spacer)
- Fig. 3.9. Overview of the load cell pressuremeter (courtesy Cambridge Insitu Ltd)
- Fig. 3.10. Overall dimensions of the load cell pressuremeter
- Fig. 3.11. Design details of the low-disturbance drilling system
- Fig. 3.12. Components of the excavation tools
- Fig. 3.13. Clay cutter with injection nozzle for drilling fluid
- Fig. 3.14. Pipe-carrier unit; longitudinal section
- Fig. 3.15. Pipe carrier unit
- Fig. 3.16. Model pipe assembly
- Fig. 3.17. Paraffin wax seal (top left: clay surface before pouring wax; top right: after setting of wax; bottom middle: cutting edge break through after end of test)
- Fig. 3.18. Consolidation history of the soil model
- Fig. 3.19. Synoptic diagram of LCPM instrumentation
- Fig. 3.20. Instrument compartments on the LCPM
- Fig. 3.21. Pore pressure cell (PPC) on the LCPM
- Fig. 3.22. Set-up for the saturation of the pore pressure cells (PPCs)
- Fig. 3.23. Overview of the pore pressure cells (PPCs) saturation set-up
- Fig. 3.24. Displacement transducer design
- Fig. 3.25. Displacement transducer components
- Fig. 3.26. Miniature Druck and Entran PPTs
- Fig. 3.27. Saturation set-up for miniature PPTs
- Fig. 3.28. Calibration set-up for miniature PPTs

---

Fig. 3.29. Typical response of a poorly-saturated (Entran) PPT

Fig. 3.30. Typical response of a well-saturated (Entran) PPT

Fig. 3.31. Post-mortem view of the exposed *PPTs*

## Chapter 4

Fig. 4.1. Spatial reference frame

Fig. 4.2. Raw and filtered data ( $N = 61, n = 10$ )

Fig. 4.3. Raw and filtered data ( $N = 31, n = 5$ )

Fig. 4.4. Undrained shear strength measurements

Fig. 4.5. (a) Total stress; (b) back-pressure; and (c) effective stress at boundary

Fig. 4.6. (a) Trajectory and (b) advance rate of model pipe

Fig. 4.7. (a) Lubricant pressure; (b) lubricant volume

Fig. 4.8. Position and designation of *PPTs*

Fig. 4.9. Excess pore water pressure due to changes in deviator stress

Fig. 4.10. Measured pore water pressure at equilibrium

Fig. 4.11. Overview of excess pore water pressure measurements during excavation

Fig. 4.12. Overview of excess pore water pressure measurements during equilibration period

Fig. 4.13. Symmetry of pore water pressure T5 PPT\_A

Fig. 4.14. Symmetry of pore water pressure T5 PPT\_B

Fig. 4.15. Symmetry of pore water pressure T6 PPT\_A

Fig. 4.16. Symmetry of pore water pressure T6 PPT\_B

Fig. 4.17. Symmetry of pore water pressure T8 PPT\_A

Fig. 4.18. Generated pore water pressure and isochrones  $x/D = -4$

Fig. 4.19. Generated pore water pressure and isochrones  $x/D = -2$

Fig. 4.20. Generated pore water pressure and isochrones  $x/D = -1$

Fig. 4.21. Generated pore water pressure and isochrones  $x/D = 0$

Fig. 4.22. Generated pore water pressure and isochrones  $x/D = 1$

Fig. 4.23. Generated pore water pressure and isochrones  $x/D = 2$

Fig. 4.24. Predicted and measured excess pore water pressure

Fig. 4.25. Dissipation of excess pore pressure  $T = 0.05$

Fig. 4.26. Dissipation of excess pore pressure  $T = 0.3$

Fig. 4.27. Dissipation of excess pore pressure  $T = 0.8$

Fig. 4.28. Dissipation of excess pore pressure  $T = 2$

- 
- Fig. 4.29. Dissipation of excess pore pressure  $T = 5$
- Fig. 4.30. Dissipation of excess pore pressure  $T = 10$
- Fig. 4.31. Dissipation of excess pore pressure  $T = 30$
- Fig. 4.32. Two-dimensional pore water pressure isochrone ( $T = 0.03$ )
- Fig. 4.33. Pore water pressure contour around the advancing excavation face
- Fig. 4.34. Total stress on pipe during installation test T8
- Fig. 4.35. Fluid pressure on pipe during installation test T8
- Fig. 4.36. Comparison of total stresses during pipe installation (T5, T6 and T8)
- Fig. 4.37. Comparison of total stresses during consolidation (T5, T6 and T8)
- Fig. 4.38. Comparison of fluid pressure during pipe installation (T5, T6 and T8)
- Fig. 4.39. Comparison of fluid pressure during consolidation (T5, T6 and T8)
- Fig. 4.40. Comparison of effective stresses during pipe installation (T5, T6 and T8)
- Fig. 4.41. Comparison of effective stresses during consolidation (T5, T6 and T8)

## Chapter 5

- Fig. 5.1. Cam-Clay yield model: (a) stress plane, (b) compression plane
- Fig. 5.2. Stress components on an element of soil at the springline of the excavation
- Fig. 5.3. Idealised cavity pressure evolution in test T6 and T8
- Fig. 5.4. Stress paths for undrained unloading (stage I and II)
- Fig. 5.5. Stress paths after change of boundary conditions (stage III)
- Fig. 5.6. Stress paths during consolidation and stress build-up (stage IV)
- Fig. 5.7. Zones of softened soil around excavation

## Chapter 6

- Fig. 6.1. Horizontal forces acting on an idealised *EPB* machine
- Fig. 6.2. Example design of cutting wheel of *EPB* machine: (a) Herrenknecht machine (Metrosur, Madrid, Spain), 9.4 m diameter, 31% face opening (Maynar *et al.*, 2000); (b) Kawasaki (CTRL, London, UK), 8.5 m diameter, 57% face opening (courtesy Rail Link Engineering).
- Fig. 6.3. Foam injection ratio (*FIR*) versus slump test results (Leinala *et al.*, 2000)
- Fig. 6.4. Soil conditioning needs in different types of ground (Jancsecz *et al.*, 1999)

---

## Chapter 7

- Fig. 7.1. Machine parameters in relation to soil conditioning parameters: effect of total liquid injection ratio (*LIR*) in Thanet Sand
- Fig. 7.2. Machine parameters in relation to soil conditioning parameters: effect of foam injection ratio (*FIR*) in Thanet Sand
- Fig. 7.3. Machine parameters in relation to soil conditioning parameters: effect of foam injection rate (*FIR*) in the Lambeth Group
- Fig. 7.4. Machine parameters in relation to soil conditioning parameters: effect of Total liquid injection ratio (*LIR*) in the Lambeth Group
- Fig. 7.5. Machine parameters in relation to soil conditioning parameters: effect of liquid injection ratio (*LIR*) in London Clay
- Fig. 7.6. Machine parameters in relation to soil conditioning parameters: effect of foam injection ratio (*FIR*) in London Clay
- Fig. 7.7. Relationships between face pressure and volume loss components in Lambeth Group and Lambeth Group/Harwich Formation
- Fig. 7.8. Relationships between face pressure and volume loss components London Clay and London Clay/Harwich/Lambeth Group
- Fig. 7.9. Chamber pressure (a) and total thrust (b) during for excavation face progresses through the 7.5 m preceding monitoring section
- Fig. 7.10. Chamber pressure (a) and total thrust (b) during for excavation face progresses through the 7.5 m preceding monitoring section
- Fig. 7.11. Chamber pressure (a) and total thrust (b) during for excavation face progresses through the 7.5 m preceding monitoring section
- Fig. 7.12. Chamber pressure (a) and total thrust (b) during for excavation face progresses through the 7.5 m preceding monitoring section
- Fig. 7.13. Chamber pressure (a) and total thrust (b) during for excavation face progresses through the 7.5 m preceding monitoring section
- Fig. 7.14. Chamber pressure (a) and total thrust (b) during for excavation face progresses through the 7.5 m preceding monitoring section
- Fig. 7.15. Chamber pressure (a) and total thrust (b) during for excavation face progresses through the 7.5 m preceding monitoring section
- Fig. 7.16. Chamber pressure (a) and total thrust (b) during for excavation face progresses through the 7.5 m preceding monitoring section
- Fig. 7.17. Chamber pressure (a) and total thrust (b) during for excavation face progresses through the 7.5 m preceding monitoring section
- Fig. 7.18. Chamber pressure (a) and total thrust (b) during for excavation face progresses through the 7.5 m preceding monitoring section
- Fig. 7.19. Machine parameters in relation to soil conditioning parameters: effect of foam injection ratio (*FIR*) in London Clay

- 
- Fig. 7.20. Conditioned London Clay sample strength and liquid injection ratio (Merritt *et al.*, 2002)
- Fig. 7.21. Definition of volume loss components and related machine parameters (after Wongsaroj *et al.*, 2006)
- Fig. 7.22. Volume loss along Contract 220 derived from transverse ground surface settlement monitoring profiles (Bowers & Moss, 2006)
- Fig. 7.23. Relationship between face volume loss and sum of shield and tail volume loss components
- Fig. 7.24. Relationships between face pressure and volume loss components Thanet Sand and Upnor/Thanet Sand
- Fig. 7.25. Relationships between face pressure and volume loss components in Lambeth Group and Lambeth Group/Harwich Formation
- Fig. 7.26. Relationships between face pressure and volume loss components London Clay and London Clay/Harwich/Lambeth Group
- Fig. 7.27. Chamber pressure (a) and total thrust (b) during excavation face progress through the 7.5 m preceding monitoring section
- Fig. 7.28. Chamber pressure (a) and total thrust (b) during excavation face progress through the 7.5 m preceding monitoring section
- Fig. 7.29. Chamber pressure (a) and total thrust (b) during excavation face progress through the 7.5 m preceding monitoring section
- Fig. 7.30. Chamber pressure (a) and total thrust (b) during excavation face progress through the 7.5 m pre
- Fig. 7.31. Chamber pressure (a) and total thrust (b) during excavation face progress through the 7.5 m preceding monitoring section
- Fig. 7.32. Chamber pressure (a) and total thrust (b) during excavation face progress through the 7.5 m preceding monitoring section
- Fig. 7.33. Chamber pressure (a) and total thrust (b) during excavation face progress through the 7.5 m preceding monitoring section
- Fig. 7.34. Chamber pressure (a) and total thrust (b) during excavation face progress through the 7.5 m preceding monitoring section
- Fig. 7.35. Chamber pressure (a) and total thrust (b) during excavation face progress through the 7.5 m preceding monitoring section
- Fig. 7.36. Case history data of volume loss presented against load factor (Macklin, 1999)

---

## Appendix A

- Fig. A.1 Total stress on pipe during installation T5
- Fig. A.2 Total stress on pipe during consolidation T5
- Fig. A.3 Total stress on pipe during installation T6
- Fig. A.4 Total stress on pipe during consolidation T6
- Fig. A.5 Total stress on pipe during consolidation T8
- Fig. A.6 Fluid pressure on pipe during installation T5
- Fig. A.7 Fluid pressure on pipe during consolidation T5
- Fig. A.8 Fluid pressure on pipe during installation T6
- Fig. A.9 Fluid pressure on pipe during consolidation T6
- Fig. A.10 Fluid pressure on pipe during consolidation T8
- Fig. A.11 Effective stresses on pipe during installation T5
- Fig. A.12 Effective stresses on pipe during consolidation T5
- Fig. A.13 Effective stresses on pipe during installation T6
- Fig. A.14 Effective stresses on pipe during consolidation T6
- Fig. A.15 Effective stresses on pipe during installation T8
- Fig. A.16 Effective stresses on pipe during consolidation T8

---

## Notation

### Acronymes

$\text{\AA}$	Angström
<i>ASCE</i>	American Society of Civil Engineers
<i>BIR</i>	Bentonite injection ratio
<i>CMC</i>	Carboxymethylcellulose
<i>CPT</i>	Cone penetration test
<i>CTRL</i>	Channel Tunnel Rail Link
<i>EPB</i>	Earth pressure balance
<i>FE</i>	Finite Element
<i>FER</i>	Foam expansion ratio
<i>FIR</i>	Foam injection ratio
<i>ICE</i>	Institution of Civil Engineers
<i>ID</i>	Internal diameter
<i>LCPM</i>	Load cell pressuremeter
<i>LIR</i>	Liquid injection ratio
<i>MCC</i>	Modified Cam-Clay
<i>NC</i>	Normally consolidated
<i>OBM</i>	Oil-based mud
<i>OCR</i>	Overconsolidation ratio
<i>OC</i>	Overconsolidated
<i>OCC</i>	Original Cam-Clay
<i>OD</i>	Outer diameter
<i>PAC</i>	Polyanionic cellulose
<i>PHPA</i>	Partially hydrolysed polyacrylamide
<i>PIR</i>	Polymer injection ratio
<i>PJA</i>	Pipe Jacking Association, UK.
<i>PPC</i>	Pore pressure cell (on the <i>LCPM</i> )
<i>PPT</i>	Pore (water) pressure transducer
<i>rpm</i>	Revolutions per minute
<i>SPE</i>	Society of Petroleum Engineers
<i>TBM</i>	Tunnel boring machine
<i>WBM</i>	Water-based mud

### Symbols

#### *Roman*

<i>a</i>	At-rest rebound parameter
<i>C</i>	Depth of tunnel crown
<i>c<sub>p</sub></i>	Polymer concentration
<i>c<sub>s</sub></i>	Surfactant concentration
<i>c<sub>v</sub></i>	Coefficient of consolidation
<i>D</i>	Excavation/cavity diameter, $D = 2 \cdot r_o$
<i>e<sub>o</sub></i>	Initial voids ratio
<i>G</i>	Shear modulus
<i>G<sub>s</sub></i>	Specific mass of the soil grains

---

$I_l$	Liquidity index, $(w_l - w)/I_p$
$I_c$	Consistency index, $(w - w_p)/I_p$
$i_r, i_x$	Radial and longitudinal components of the hydraulic gradient
$I_p$	Plasticity index of the clay
$k$	Coefficient of permeability
$K_{no}$	Coefficient of earth pressure at rest, normally consolidated state
$K_{oc}$	Coefficient of earth pressure at rest, overconsolidated state
$LF$	Load factor, $= N/N_c$
$n$	Reduction factor for raw data matrices
$N$	Stability ratio, Savitzky-Golay parameter (frame length)
$N_c$	Critical stability ratio
$p$	Mean normal effective stress
$p$	Savitzky-Golay parameter (in § 4.2.3)
$p_o$	Fluid pressure at the cavity boundary or pipe-soil interface
$p_c'$	Preconsolidation pressure
$p_1$	Shear stress between ground and <i>EPB</i> machine shield
$p_2$	Total pressure in excavation chamber of <i>EPB</i> machine
$p_{2,drop}$	Reduction of $p_2$ during erection of one ring (build time)
$p_{2,excav}$	Average value of $p_2$ during excavation of one ring
$p_{2,IQR}$	Interquartile range of $p_2$
$p_{2,mean}$	Average value of $p_2$
$p_{2,min}$	Minimum value of $p_2$
$p_{2,10\%}$	10%-percentile of $p_2$
$p_3$	Pressure between cutting head of <i>EPB</i> machine and excavation face
$q$	Deviator stress
$r$	Radial coordinate of cylindrical reference frame
$r_o$	Initial cavity radius
$R_h$	Characteristic pore radius of the soil
$R_p$	Hydrodynamic radius of polymer coil (in § 2.4)
$R_p$	Radius of the plastic zone (in § 2.3)
$S_r$	Saturation ratio
$S_u$	Undrained shear strength
$t$	Time
$T$	Dimensionless time factor, $T = c_v \cdot t / r_o^2$
$u$	Pore water pressure
$u_o$	Initial pore water pressure at pipe axis depth
$u_p$	Water back pressure under consolidation piston
$v$	Specific volume of the soil, $v = 1 + e$
$V_L$	Ground volume loss
$V_{L,face}$	Face component of ground volume loss
$V_{fl}$	Volume of foaming liquid solution
$V_p$	Volume of polymer solution
$V_s$	Volume of excavated soil
$w$	Water content of the clay, $w = S_r \cdot e / G_s$
$w_l, w_p$	Water content at the limits of liquidity and plasticity
$x$	Abscissa of cylindrical reference frame

---

---

## Greek

$\gamma$	Specific weight of submerged soil
$\gamma_w$	Specific weight of water
$\delta$	Radial soil displacement
$\Delta u$	Excess pore water pressure
$\Gamma_{CSL}$	Ordinate of critical state line in $v: \ln p'$ plane
$\lambda$	Gradient of compression line in $v: \ln p'$ plane
$\Lambda$	Parameter relating swelling with compression, $\Lambda = (\lambda - \kappa) / \kappa$
$\kappa$	Gradient of swelling line in $v: \ln p'$ plane
$M$	Critical state frictional constant
$\eta$	Ratio of deviator to mean effective stress, $\eta = q/p'$
$\eta$	Opening ratio of cutting head (Chapter 6 and 7)
$\nu, \nu'$	Drained and undrained Poisson's ratio
$\sigma_T$	Total cavity support pressure
$\sigma_{vo}, \sigma_{vo}'$	Total and effective initial vertical stress at model pipe axis
$\sigma_{vp}, \sigma_{vp}'$	Total and effective initial vertical stress under consolidation piston
$\sigma_{ro}, \sigma_{ro}'$	Total and effective radial stresses acting on the model pipe
$\tau$	Shear stress between the <i>EPB</i> machine shield and the excavation wall
$\phi_{crit}'$	Angle of friction at critical state
$\psi$	Dilatancy angle
$\theta$	Azimuthal angle of cylindrical reference frame

## **CHAPTER 1: BACKGROUND AND OBJECTIVES**

### **1.1 Introduction**

This thesis is concerned with two applications of soil conditioning to soft ground tunnelling: lubrication in pipe jacking (§ 1.2) and soil conditioning in earth pressure balance (*EPB*) tunnelling machines (§ 1.3). Recent advances and innovations in these methods now allow tunnels with diameters ranging from 0.5 to over 14 meters to be constructed even in the most adverse conditions, such as those prevailing in urban areas, where the congestion levels demand that the tunnelling work be carried out in ever more sensitive and complex settings. In such environments, it is of utmost importance that the safety and the efficiency of underground construction be continuously improved, so that the costs, the time and the considerable risks associated with the tunnels' construction may be reduced. Ideally, the tunnelling engineer and contractor must carry out the excavation and provide a temporary as well as a permanent support to the tunnel in such a way that the entire construction process causes minimum disturbance to the surrounding ground and structures. While the available technology makes this possible under certain circumstances, severe damages and collapses of tunnels under construction still occur, causing unacceptable casualties and exorbitant material damages.

It is the need for further improvement of these technologies that motivated the present research. Both *EPB* machines and the pipe jacking method critically depend on the use of soil conditioning. *EPB* machines may otherwise fail to operate, or only do so under unsafe and much impaired conditions, while pipe jacking may become unviable as jacking forces rise beyond acceptable levels. In spite of its importance, soil conditioning, or research thereon, is sometimes regarded with distrust and the ‘common sense and experience’ approach has tended to be preferred in the field. This attitude is perfectly reasonable for less demanding projects or in cases where only a low standard of performance is required. However, as the efficiency and control of the machine operation becomes critical or when the project conditions grow in complexity, a deeper understanding of the fundamental mechanics becomes crucial to complement the experience-driven approach to soil conditioning. Only then can the best possible benefits of the methods be obtained, and dangerous mistakes leading to loss of lives, exorbitant construction damage and costs overruns be avoided.

## **1.2 Background: lubrication in pipe jacking**

### 1.2.1 The method

The ‘trenchless’ technique of pipe jacking allows installing underground ducts and pipelines with diameters ranging from 0.5 to approximately 3 meters without causing excessive surface disruption. As illustrated in Fig. 1.1, the technique involves pushing a string of pipes through the ground from a launch shaft towards a reception shaft, while excavating the soil at the front end using either a mechanised or manually-operated excavation system. As the excavation progresses, pipes are placed one by one into the launch shaft, added at the rear end of the pipe string and pushed forward a distance allowing insertion of the next pipe. This cycle is repeated until the pipe string breaks through at the reception shaft, which may lie a distance of 50 to 500 m from the launch shaft. Detailed descriptions of this technology may be found in Stein *et al.* (1989) or Thomsen (1993).

### 1.2.2 Jacking forces

The technical viability and the cost-effectiveness of pipe jacking predominantly depend on the magnitude of the jacking forces. They determine the required capacity of the jacking rig, the design of the thrust wall reacting the jacking forces and the stresses in the concrete segments. When jacking forces cause the capacity of one of these elements to be exceeded, the distance between the launch and the reception shafts has to be reduced, or intermediate jacking stations have to be

inserted at regular intervals in the pipe string to overcome excessive jacking forces. Excavating additional shafts may not only be too expensive but also causes surface disruption, which may not be acceptable or possible in certain environments. Intermediate jacking stations carry operational complications which also result in a significant increase of the overall project cost as well as a significant increase in construction time.

Various authors (*e.g.*: Auld, 1982; Craig, 1983; Norris, 1992; Pellet, 1997; Bennett, 1998; Marshall, 1998; Chapman & Ichioka, 1999 or Phelipot, 2000) have discussed the factors affecting the magnitude of jacking forces. These factors may be classified as being either site-related or construction-related. Amongst the construction-related factors, the pressure applied to the excavation face, the size of the overcut excavated around the pipes, the frequency and duration of jacking stoppages, the dewatering of the launching and the reception shafts as well as the misalignment of the pipe string are those considered to be most relevant. All the parameters upon which total jacking forces depend may vary with time and location along the pipe string, as a result of variation in geological and hydro-geological conditions, or following alterations of the lubrication method or changes of support pressure at the tunnel face.

The friction developing along the pipe shafts accounts for the most part of the jacking force. Friction per unit length of pipe predominantly depends on whether the excavation is stable or if the excavated ground converges onto the pipe. In the case of a stable cavity, friction per unit length primarily relates to the weight (or to the buoyant weight) of the pipe. In the case of unstable cavities, the ground may lie in full contact with the pipe, thus increasing both the contact area between the soil and the pipe and their contact stresses. Frictional forces are naturally much larger in this latter case. As a guide, it has been suggested that the average shear stress per unit surface area of pipe installed in firm clay ranges from 5 to 20 kPa (Craig, 1983), yielding jacking forces of up to 18'000 kN for a 3-m diameter pipe installed on a length of 100 m.

### 1.2.3 Lubrication

Although small diameter (< 3 m) excavations in clay may often be stable, stress relief and subsequent swelling occurring around the cavity can cause large radial pressures on the pipes. This results in high jacking forces, and severely limits the distance that may be jacked and hence, the distance between the launch and the reception shafts. In an attempt to decrease the frictional forces between the pipes and the soil, the ground is always excavated to a diameter 20 to 80 mm larger than that of

the pipes. Thus, an annular void (also referred to as ‘gap’ or ‘overcut’) is left around the pipe and a water-based lubricant is usually injected into this overcut. It is intended that this measure helps mitigate large jacking forces by (1) delaying the radial stresses build-up on the pipes, (2) reducing the interface friction angle between the ground and the pipes and (3) achieving partial buoyancy of the pipes and hence reduce the frictional resistance to their installation. However, such fluid provides a source of free water that can be absorbed by the surrounding clay and, which can increase the rate and magnitude of ground loading on the pipes. Hence, under certain circumstances, lubrication might prove counterproductive. Recent approaches to counteracting this process have suggested the use of polymers and inorganic salts, either as water-solutions or in combination with bentonite slurries. Such chemical agents are thought to act as ‘swelling inhibitors’ in that they reduce the rate of water intake into the ground and thereby delay the swelling process and the build-up of jacking forces on the pipes (Milligan, 2001).

#### 1.2.4 Need for research

Despite the routine application of lubrication, insufficient evidence exists to predict its net effect on pipe jacking forces. In particular, little is known about the way in which the chemical properties of the lubricant and its injection procedures affect the build-up of pipe-soil stresses. Products such as polymers or so-called clay swelling inhibitors are increasingly being used as additives to enhance the lubricant fluid properties. However, the conditions under which they might be beneficial as well as the mechanisms and magnitudes by which they help reduce swelling pressures remain unclear. The legacy of this lack of fundamental understanding is the absence of practical guidance for the selection and mode of injection of lubricants, which in turn prevents the full benefits of lubrication to be achieved. Understanding the effect of the chemical composition of the lubricant and of their injection pressure is required. This will help select effective lubricant fluids, and will provide the basis to decide when and at what pressure the lubricants should be injected. Effective lubrication could greatly reduce jacking forces, allowing significantly longer drives to be achieved. In additions, overcut ratios around the pipes could be decreased, thus reducing the impact of pipe jacking in terms of ground and structure settlements around the pipes.

### 1.3 Background: soil conditioning in *EPB* machines

#### 1.3.1 The technology

The control of ground volume loss and the stability requirements during tunnelling operations in soft ground often demands that continuous support of the excavation face be provided during the excavation. The magnitude of the required face support mainly depends on the depth and diameter of the excavation, as well as on the ground conditions and the tolerated volume loss agreed with the client and the owners of nearby infrastructures. In most instances, face pressures ranging from 50 to 300 kPa are required. The principle of closed-face tunnelling machines - *i.e.* those allowing continuous support of the face during excavation - consists in confining a support medium into a sealed excavation chamber at the front of the tunnelling machine. Different types of tunnelling machine evolved from the use of different support media, each technology bearing its own advantages and drawbacks. Slurry shields rely on pumping large quantities of bentonite slurry into the excavation chamber of the tunnelling machine, where it is mixed with the excavated soil and discharged at a controlled rate to maintain the slurry pressure at the desired level. The bentonite creates a filtercake on the excavation surface to prevent the loss of slurry into the ground, hence allowing a support pressure to be applied to the excavation face (*e.g.*: Steiner, 1996b; Anagnostou & Kovári, 1996).

*EPB* machines, in contrast, achieve face support by confining the excavated soil in the head chamber, thus obviating the costly injection and recycling of bentonite slurry. While slurry shield machines rely on the formation of an impermeable filtercake on or ahead of the excavation surface to ensure that the slurry pressure imparts effective stress to the tunnel face, it is intended that *EPB* machines transmit effective stresses to the face via the remoulded soil in their head chamber. The shear strength of this remoulded spoil prevents local collapse of the face. As shown in Fig. 1.2, continuous discharge of the spoil from the head chamber is achieved by means of an Archimedean screw conveyor. The control of face pressure in *EPB* machines occurs by altering the rate of spoil discharge by the conveyor, matching it to the rate of excavated soil, which can itself be influenced by the thrust applied on the tunnelling machine. The rate of discharge depends on the angular velocity of the screw conveyor, but also on the soil-screw interaction during the extrusion process. Changes in soil properties alter the soil-screw interaction and, in turn, the rate of spoil discharge as well as the face pressure. In order to keep a constant magnitude of face pressure, the operation of the machine must be altered by the driver: he may chose to reduce the thrust on the shield, adjust the angular velocity of the screw conveyor,

inject soil conditioning products at various locations in the machine or even to restrict the outlet size of the screw conveyor by deploying guillotine valves. In most instances, several parameters will be varied simultaneously, hence causing complex interactions between the different machine components and the conditioned spoil.

### 1.3.2 Spoil properties

The success of the *EPB* technology critically depends on the physical properties of the excavated soil mass. If the shear resistance between the spoil and the conveyor drops below a *critical value*, the pressure does not dissipate sufficiently along the screw conveyor and the soil may gush or extrude in an uncontrollable manner through the screw conveyor. In such cases, the face pressure would reduce instantly, potentially causing instability of the face or excessive ground movements around the tunnel. If, on the contrary, the shear resistance between the soil and the screw conveyor becomes *excessive*, problems will be encountered in extruding the soil from the chamber and the machine may clog or fail to operate efficiently. Because the properties of the natural ground seldom suit the machine requirements, they usually have to be modified by soil conditioning agents. This involves the injection of various conditioning products at different points in the machine and aims to modify the soil in a way that allows efficient and controllable excavation. However, accurate statements on what these *critical* and *excessive values* of shear resistance may be are at present not available.

### 1.3.3 Soil conditioning

A wide range of conditioning agents is available for application in *EPB* machines. Foam and polymers, either used separately or in combination, are the most commonly employed products. Foam has proven an effective additive for granular soil (sand and gravels), where its bubbles integrate the sand matrix and reduce the friction as well as the permeability of the natural soil. Foam also provides some compressibility to the sand (Maidl, 1995; Quebaud, 1996; Houlsby & Psomas, 2001). However, less is known on the interactions between foam and clay, and the mechanisms that make foam a successful additive for clay are not properly understood. Foam is also thought to prevent clay from recompacting and sticking to the machine by lubricating the steel surface and reducing the friction between the cuttings, but others suggested it is ineffective in clay (Merritt, 2005). Polymers influence the adsorption of water of the clay and are believed to be efficient in reducing its stickiness and adhesion onto metal surfaces. They are believed to have a binding effect on the soil and to reduce friction between the clay and the machine

---

parts, and are often recommended by their supplier for improving the stability and performance of foam.

#### 1.3.4 Need for research

Despite common use in practice, the effects of different combination of foam and polymer conditioning agents on *EPB* machine operations in clay are not clear. As a result, the selection of conditioning agents and appropriate injection volumes is often done on a trial and error basis or following the recommendations of the product supplier. Although some recommendations exist to determine suitable injection volumes of conditioning agents for *EPB* operations in sands and gravels (*e.g.*: Maidl, 1995 or Kusakabe *et al.*, 1999), little guidance exists for soil conditioning in clays. Guidelines for the use of specialist products in tunnelling have recently been published by the EFNARC (2005). They contain some recommendations regarding the selection of soil conditioning product and parameters in different ground conditions. However, these recommendations are based on the particle size distribution of the ground only and ignore its fundamental engineering properties such as plasticity, moisture content and shear strength. The fact that some of the recommended injection quantities for foam and polymer cover a range of 1:50 illustrates the uncertainties and the difficulties associated with the application of soil conditioning in practice.

To date, there has been little formal research into the key parameters involved in soil conditioning, and the governing mechanisms that make conditioning treatment successful are not yet properly understood. Uncertainties remain as to where to inject the conditioning agents, what agent to use in a particular type of ground and at what concentrations and injection rates. The complexity of the interactions associated with conditioning has also been illustrated by Langmaack (2001), who pointed out that when used to condition clays, certain foams that are not recommended by the manufacturer for use in clayey grounds perform better than those actually recommended for these conditions. This suggests that some of the key interactions and mechanisms remain poorly understood. This relative lack of guidance and understanding is in contrast with the stake and risk associated with the application of soil conditioning. The most favourable outcome of a erroneous decision as to the selection of soil conditioning is a temporary drop in production rate, then more or less quickly followed by a readjustment of the additive type and quantities injected into the excavation chamber. However, when tunnelling in high-risk environment, such as in the vicinity of sensitive structures, or when water pressures in the ground have to

be withstood, poor control of the *EPB* machine may initiate a sequence of events leading to the serious consequences discussed above.

## **1.4 Objectives**

The research reported in this thesis aims to advance the understanding of the technology of lubrication and soil conditioning in pipe jacking and *EPB* machines. The purpose is to advance the fundamental understanding of the underlying mechanisms so that, ultimately, recommendations for optimal conditioning of clay soils in pipe jacking and *EPB* machines may be provided. The specific objectives pursued in this research comprise of two separate aspects that may be summarised as follows:

### ***I. Lubrication in pipe jacking:***

- To measure the effect of lubricants composition and injection pressure on the radial pipes-clay stresses.
- To identify the fundamental parameters governing the mechanical as well as the physicochemical interactions between the pipe, the clay and the lubricant injected into the overcut.
- To suggest directions for further research to contribute to the elaboration of guidelines to help select lubricant type and injection methods in any specific situation.

### ***II. Soil conditioning in EPB machines:***

- To analyse the operational parameters of full-size *EPB* machines and identify the way in which their behaviour is affected by various conditioning agents.
- To improve the understanding of how (and which/what) the properties of the spoil affect the machine operation and, in turn, the performance, the safety and the impact of the tunnelling process.
- To investigate how these properties can be affected by means of soil conditioning and to reassess existing recommendations for conditioning clay soils in *EPB* machines.

## 1.5 Layout of the dissertation

This thesis is presented in eight chapters, broadly divided in two main sections: the dissertation begins with four chapters (2 to 5) on pipe jacking lubrication, then proceeds with two chapters (6 and 7) dealing with soil conditioning in *EPB* machines. The contents of each chapter may be outlined as follows:

### *I. Lubrication in pipe jacking:*

- **Chapter 2** reviews literature relevant to the problem of lubrication in pipe jacking. Lessons learned from case-studies are first summarised; an overview of cylindrical cavity contraction mechanics is then provided, and, finally, the physicochemical interactions between clay and drilling fluids near the boundary of contracting cavities are revised.
- **Chapter 3** details the scientific objectives, which motivated the experimental work on lubrication in pipe jacking. The selection of the modelling technique is discussed, before describing the design evolution of the experimental apparatus, the instrumentation, as well as the model preparation technique and the experimental procedure.
- **Chapter 4** presents the data gained from the experiment described in chapter 3. The properties of the soil model and the boundary conditions imposed to the soil model are first examined, before presenting the effects of the different lubricant types on the clay behaviour as well as on the ground loading onto the pipe.
- **Chapter 5** proposes an explanation for the observations made in chapter 4; namely the contrasting pipe-soil interactions resulting from the use of different lubricants. The proposed explanation for the effect of lubricants is used to suggest implications of the experimental results for practical application of lubrication.

### *II. Soil conditioning in EPB machines:*

- **Chapter 6** reviews the literature dealing with soil conditioning of clayey soils in *EPB* machines. The fundamental interactions involved in the machine operation are first discussed, before reviewing the effects of soil conditioning on the engineering properties of soil. The current guidelines for soil conditioning are then reviewed, and the conclusions drawn from published case-studies are summarised. Finally, the impact of *EPB* machines on tunnel stability and ground volume loss is addressed.

- **Chapter 7** presents monitoring data of the *EPB* machines used on the Channel Tunnel Rail Link project in London. The soil conditioning applied in each different type of ground is summarised and its effects are discussed in relation to the machine behaviour. In addition, the effects of the magnitude and control of the chamber pressure in the *EPB* machine is related to measurements of ground volume loss due to the tunnel construction.
- **Chapter 8** brings together the conclusions from the experimental and the field work, highlighting the practical applications of these contributions and suggesting areas where further work might be appropriate.

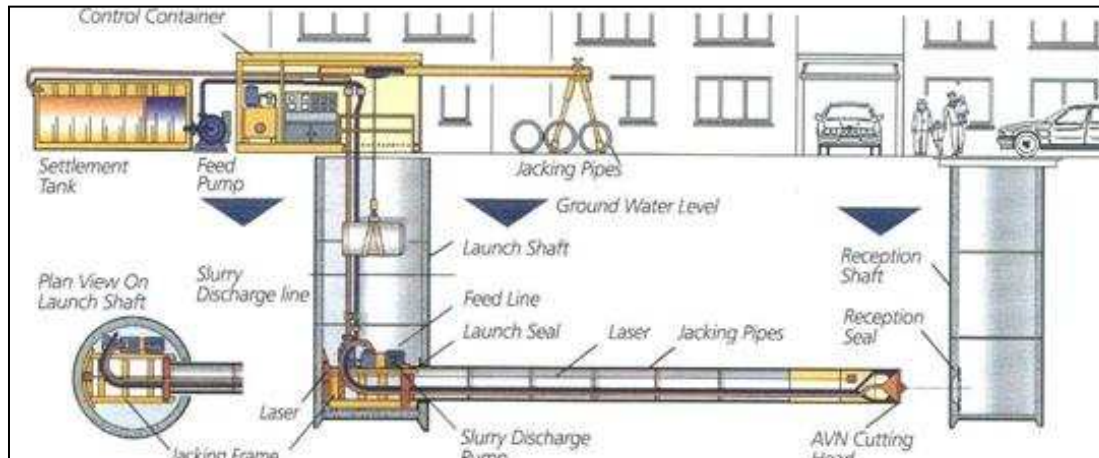


Fig. 1.1. Overview of the pipe jacking method (by courtesy of Herrenknecht AG)

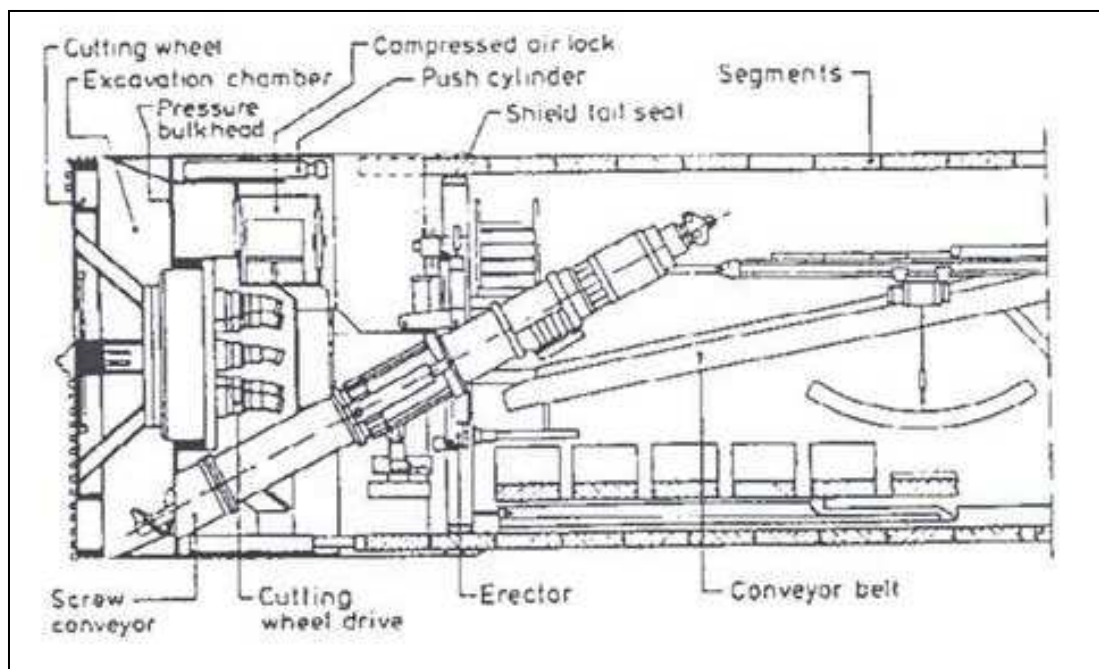


Fig. 1.2. Diagrammatic section through an EPB machine (Maidl *et al.*, 1996)

## **CHAPTER 2: LITERATURE REVIEW: EFFECTS OF LUBRICATION IN PIPE JACKING**

### **2.1 Scope and objectives**

This chapter reviews the physical understanding of lubrication in pipe jacking. The objective is to provide a detailed description of the mechanisms governing the pipe-soil interactions. The processes undergone by the ground surrounding the excavation are discussed, and the way in which the interaction between the ground and the pipes may be affected by lubricant is considered. Except for section 2.2, the focus of this work is directed towards the normal stresses exerted on the pipes and only limited insight is given into the interface shear stresses acting on the pipes during jacking.

The review is subdivided in three sections: it begins by synthesising published field-experience (§ 2.2), then proceeds by reviewing the current understanding of stress changes around contracting cylindrical cavities in clay (§ 2.3), and finally discusses the physicochemical interactions between the ground and the lubricant near the cavity wall (§ 2.4). Summaries of observations are provided at the end of each section and the chapter is concluded with a critical commentary and suggesting areas where improved understanding could benefit the industry.

---

## 2.2 Field observations and measurements of lubrication effects

### 2.2.1 Introduction

This section summarises case-studies of pipe jacking in clay. Lessons learned from the field are summarised and an attempt is made to quantify the net effect of lubrication by comparing pipe jacking forces in lubricated and un-lubricated drives, or in drives where lubrication was only partially used. Other factors affecting the jacking forces are briefly discussed in order to establish the extent to which the lubrication contributes to the reduction of jacking forces. Relatively few well-documented projects may be found in the technical literature. In addition, the large majority of the published site records only report jacking loads versus the installed length of pipes, and details of the lubrication procedure are often lacking.

Assessing the effects of lubrication by directly comparing jacking loads in different projects is not appropriate. This is because jacking loads are, in addition to geological and hydro-geological conditions, influenced by several factors such as the pipe diameter, the installation depth, the over-cutting ratio, the installation rate and the pipe line misalignment, as well as, to some extent, the surface coating of the pipes. Normalising jacking load with a combination of these variables might be misleading. Indeed, the mechanism of friction build-up between the ground and the pipes may involve further operating variables than just these and overlooking them may lead to misrepresentation of the physical behaviour. In particular, the way in which lubrication should be accounted for remains uncertain. Also, expressing average shear stresses by dividing the jacking loads by the total surface area of the pipes (as is sometimes done) is inappropriate when the effective contact area between the pipe and the ground is not known with confidence.

Such manipulation of the data is therefore avoided. Instead, the jacking forces are compared in terms of force per unit length of pipe (kN/m), after deduction of the jacking load component caused by the resistance of the tunnel face (cutting edge or face pressure). The overall effects of lubrication on jacking forces are first discussed by comparing jacking records on representative projects completed with and without lubrication, or where lubrication was introduced partway through the drives (§ 2.2.2). Local measurements of pipe-soil stresses are then analysed in order to highlight the interactions that give rise to the jacking forces (§ 2.2.3). Details of the projects presented in this section are recapitulated in Table 2.1 and a summary of the observations is provided in § 2.2.4.

## 2.2.2 Effects of lubricant on jacking forces

### 2.2.2.1 Honor Oak, London, UK

Norris (1992) reports measurements of jacking loads during the installation of a pipe jack in stiff overconsolidated London Clay at Honor Oak in London, UK. The outer diameter of the pipes was 2.27 m and the average depth to axis varied between 11 and 21 m as the pipe jack was installed under a reservoir embankment. The excavation was performed by hand, therefore resulting in a variable magnitude of the overcut ratio around the pipe (the shield diameter was not reported). No lubrication was used for this 70-m long drive.

Jacking forces per unit length as high as 54 kN/m were required to install the pipes, as shown by the jacking record in Fig. 2.1. Maximum forces of nearly 5200 kN were necessary to resume jacking after a short stoppage near the end of the drive. Although stability analyses (§ 2.3.2) suggest that, owing to the large undrained shear strength (measured between 101 and 603 kPa) of the clay, the excavation should have remained open, it appears to have closed onto the pipe. This caused large normal stresses on the pipe and, in turn, high jacking forces. With reference to this project, Milligan & Marshall (1998) noted the tendency of highly plastic and heavily overconsolidated clays to swell upon stress relief. They warn that the use of aqueous lubricants may accelerate the swelling process and therefore prove counter-productive, and suggest that swelling inhibiting chemicals be added to the lubricant to prevent that problem.

### 2.2.2.2 Leytonstone, London, UK

Jacking forces in similar ground conditions were measured by Milligan & Marshall (1998) during the installation of a 1.8 m OD sewer at Leytonstone, UK. The 75-m long drive lay wholly in London Clay, at a depth of 8.5 m to axis.

As may be seen in Fig. 2.2, jacking load increased linearly throughout the drive, at an average rate of 12.7 kN/m. Peaks exceeding the average force by 50% were observed after production stoppages. These forces are approximately four times smaller than those measured by Norris (1992) at Honor Oak. This may be partially attributed to the shallower installation depth, to the slightly smaller diameter, and possibly to the smaller undrained shear strength of the London Clay at Leytonstone, which was reported to be in the region of  $S_u = 100$  kPa at pipe axis depth. Also, lubrication was partially used by injecting bentonite slurry from the excavation shield at three

occasions during the drive. The authors reported the absence of noticeable changes of jacking load patterns following these injection episodes. A possible explanation for not having observed a reduction of jacking load is the irregularity and possibly large overcut around the pipes. Hand excavation was performed approximately 0.5 m ahead of the open-face shield; it is therefore likely that over-excavation occurred as a result of the highly fissured London Clay, hence leaving a leakage path around the shield and causing loss of bentonite slurry. Details on the lubricant injection procedure and the magnitude of the overcut were not reported, which makes it difficult to fully explain the contrasting magnitude of jacking forces observed at Honor Oak and Leytonstone.

### 2.2.2.3 Seaham, UK

High jacking forces such as those measured by Norris (1992) at Honor Oak were also recorded by Milligan & Marshall (1998) on a 310-m long drive at Seaham, UK. The 1.8 m ID pipes were installed above the groundwater table in stiff glacial till (boulder clay) at a depth to axis of about 7 m.

Unit jacking forces of 48 kN/m were measured on the first 20 m of the drive; a similar magnitude to those measured at Honor Oak. However, lubrication was then used for the remainder of the drive, causing the jacking force to reduce steadily on the 15 m following the onset of bentonite injection. The unit jacking forces plotted in Fig. 2.3 then increased at a steady rate of about 15 kN/m until the end of the drive, although large restart peaks were consistently observed after production breaks over week-ends. The restart forces typically exceeded those before stoppage by approximately 80%. The gradual reduction of total jacking load (and not only its rate of increase with jacked length) upon injection of bentonite suggests that the lubrication is effective over the entire length of the pipe jack. Measurements of pipe-soil contact stresses at a distance of 182 m behind the tunnel heading seemed to indicate intermittent pipe-soil contact as well as pipe buoyancy within the overcut. Evidence is lacking to explain the delayed reduction of jacking load upon introduction of lubrication, but this observation is likely to be associated with a partial closure of the overcut around the pipe. The original misalignment and subsequent straightening effects of the bore as jacking proceeds are likely to allow the bentonite slurry to gradually penetrate around the pipe in the originally non-lubricated section, hence giving rise to a gradual reduction of jacking force.

#### 2.2.2.4 Thurrock, UK

The same authors (Milligan & Marshall, 1998) identified a similar pattern of jacking force reduction for another drive in clay material, albeit much softer than the glacial till at Seaham. This drive at Thurrock consisted in just over 200 m of 1.5-m outer diameter pipes installed in very soft alluvial peaty clay at a depth between 5.5 and 6.0 m, approximately 4.0 m below the groundwater table. A distance of 130 m was driven prior to the commencement of lubrication. Since large forces were required to resume jacking after a week-end production break, lubrication was introduced.

As shown in Fig. 2.4, the jacking force, which increased at a rate of 25 kN/m in the un-lubricated section, then began to reduce sharply to approximately 60% of the value that was measured before the stoppage. The jacking loads then increased at a rate of 14 kN/m for the remainder of the drive, hence showing a 50% reduction of jacking force per unit length compared to the un-lubricated section of the drive. It is worth noting that lubricants were only pumped during the day shift, whilst jacking continued overnight. No corresponding patterns can be detected when scrutinising the jacking load record. Measurements of pipe-soil stresses (§ 2.2.3.1) in a pipe situated 48 m behind the excavation suggested that the soft clay had converged onto the pipe to fully close the overcut. Under such conditions, the effectiveness of the lubricant over the entire length of the pipe line would a priori not be expected. Again, the reduction of jacking load upon injection of bentonite disproves this logical supposition, for if the lubricant only reduced friction over the pipe ahead of the point at which injection began, only a drop in the rate of increase would be observed. However, an effect on the entire length of the pipe jack cannot be ruled out when analysing the pipe jacking record of Fig. 2.4.

#### 2.2.2.5 Nimitmai Road, Bangkok, Thailand

In the three projects described above, lubrication was introduced partially through the drives to mitigate large jacking forces and prevent them from exceeding the limiting design load. Despite successful completion of the drives, jacking loads in excess of 5,200 kN were necessary to complete the 70-m long un-lubricated drive at Honor Oak and the 220-m long lubricated pipe jack at Thurrock. In contrast to these high jacking forces, Broomfield (2004) describes a project in Bangkok where three pipe jacks with individual lengths of over 500 m were installed using an ‘automatic’ lubrication system from the commencement of the drive. Steel pipes with an outer diameter of 1.63 m were jacked at approximately 4 m depth to axis (as inferred from

a photograph) in soft Bangkok clay. The magnitude of the overcut was not reported. Bentonite slurry was injected through triplets of ports arranged at 60° angle around the pipe circumference and every 18 m along the pipeline.

Jacking records for the three drives completed with this system are provided in Fig. 2.5. After subtraction of a jacking force component of approximately 500 kN required to propel the full-face earth pressure balance (EPB) machine, jacking forces per unit length of between 2.0 and 3.7 kN/m were calculated. This yields total installation forces of the order 1,250 kN at 500 m drive, and allowed the drive to be completed without using intermediate jacking stations. The unit jacking forces reported by Broomfield are up to an order of magnitude lower than those measured by Norris (1992) and Milligan & Marshall (1998). Other effects are likely to have influenced the magnitude of these jacking forces: the straightness of the pipeline which consisted in welded pipes ensured that no additional jacking resistance was caused by misalignments, such as might be the case when using shorter, spigot-jointed pipes; the shallow installation depth and the low undrained shear strength of the marine clay and the double-shift working, which resulted in production rates sometimes exceeding 35 m per 24 hours. Therefore, the reduction of jacking forces on this project is perhaps not wholly, but at least partly due to the high-standard lubrication procedure that was utilised. It is worth noting that the precise meaning of ‘automatic’ in the context of the lubrication procedure is not explained.

#### 2.2.2.6 Vibhavadi, Bangkok, Thailand

Alexanderson (2001) summarises the observation made on the construction of the 7.8-km long Vibhavadi cable tunnel in Bangkok, Thailand. Spun concrete pipes with outer diameter of 3.04 m were installed well below the groundwater table, in medium stiff marine Bangkok Clay, at a depth of between 13 and 15 m. A radial overcut of 40 mm was excavated around the pipe extradoses, and bentonite slurry was injected throughout the initial drives using an ‘automatic’ lubrication system from the same manufacturer as in the project described by Broomfield. Three injection ports were arranged in the pipe line every 15 m. Several lubrication sections were separated by electronic valves and a computerised system controlled the injection station by station according to a pre-programmed sequence (Alexanderson, 2005). However, no detail of the injection pressure was provided.

The author reports that values of average skin friction ranging from 2 to 3 kPa had been experienced when jacking pipes in the marine clay when using only water as a lubricant. Assuming full contact between the ground and the pipe these values

integrate to jacking loads per unit length of the 3.04 m diameter pipe of 19 and 28 kN/m, respectively. Jacking loads of this magnitude did, on occasion, cause the concrete pipes to crack (Alexanderson, 2005). The lubricant type was subsequently changed to a water-solution of anionic acrylamide copolymer (Alexanderson, 2005), and a considerable reduction of jacking forces was observed as a result. Jacking force per unit length of pipe reduced to as low as 4.7 kN/m, achieving a fivefold reduction compared to the unit forces measured when bentonite lubrication was used. This corresponds to a mere 0.5 kPa average skin friction assuming total contact between the pipe and the clay. It is not clear however if these values account for face resistance or not.

Alexanderson (2001) attributed the relatively large skin friction measured when using bentonite as a lubricant to the swelling of poorly-hydrated bentonite, causing in turn pressure between the pipe and the clay. There is, however, no direct evidence to corroborate this explanation but the effect proposed by Alexanderson (2001) cannot be ruled out and is one that requires further investigation. The benefits of polymer over the bentonite lubricant seem undeniable when considering the large reduction of jacking load measured after the introduction of polymer lubricant. In contrast to the jacking load patterns in the section lubricated with bentonite, no jacking load increase arose from production stops when using the polymeric lubricant.

### 2.2.3 Effects of lubricants on pipe-soil contact stresses

#### 2.2.3.1 Thurrock, UK

Pipe-soil contact stresses were measured in one instrumented pipe of the Thurrock pipe jack already described in section 2.2.2.4 and summarised in Table 2.1 (Milligan & Marshall, 1998). Total normal stresses, fluid pressures and interface shear stresses were measured at 12 locations on a pipe located 50 m behind the excavation face. Three instrument clusters were arranged on the pipe crown, three on the invert and another three on each of the spring lines. As may be seen in Fig. 2.4, lubrication was introduced at chainage 130 m, when the instrumented pipe was already 80 m into the drive.

The total stresses acting on the instrumented pipes increased linearly from zero upon its insertion into the ground, and rapidly reached values of the order of the overburden pressure at pipe axis level. As shown in Fig. 2.6, total stresses were between 100 and 150 kPa at the pipe bottom, between 90 and 120 kPa at the crown and in excess of 100 kPa at the spring lines. The total normal stresses acting on the

pipe prior to lubrication appeared to be relatively uniform around the pipe and approximately constant during this first portion of the drive. As may be seen in Fig. 2.6, fluid pressures on the pipe increased from zero until reaching a threshold of approximately 100 kPa, *i.e.* about twice the hydrostatic pressure at pipe axis depth. Of the twelve fluid pressure transducers, nine returned consistent measurements indicating these large pore water pressures. The large fluid pressure acting on the pipe is perhaps surprising, at least on the first portion of the drive where no lubricant was injected around the pipes. A 2.6-m long slurry shield TBM was used on this drive and Marshall noted that sever roll of the machine occurred during the excavation. This suggests ‘weak’ contact between the ground and the shield, and the high pore water pressure measured 50 m behind the excavation face might be due to a leakage of pressurised slurry into the overcut annulus.

The effective stresses acting on the pipes were calculated as the difference between total stress and fluid pressure measurements. They were found to be roughly uniform around the pipe and constant on the pre-lubricated section of the pipe. Values around 20 kPa were calculated, clearly indicating closure of the ground onto the pipes. Shear stresses acting on the instrumented pipe were also constant, in the region of 10 kPa, which corresponds to the value of undrained shear strength measured at pipe axis depth. Contact stresses measured after lubrication are also shown in Fig. 2.6. A slight decrease of effective stress acting on the invert may be discerned, while the reverse trend is apparent at the pipe crown, suggesting onset of buoyancy. Shear stresses do not display the anticipated reduction upon lubrication, not even after the instrumented pipe was driven an extra 50 m into the ‘fully’ lubricated section. Instead, after a temporary reduction (at the invert) or increase (at the crown) of between 2 and 7 kPa, the trend reverted and shear stresses returned to the pre-lubrication value. Toward the end of the drive, when the instrumented section was pushed through the section of the bore that was always in contact with lubricant, shear stresses actually increased, quite the opposite of what might be desired and expected. Fig. 2.8 shows the average shear stresses versus average effective stresses for three distinct phases of the interface stress records shown in Fig. 2.6. Phase (a) corresponds to the portion of the drive before the introduction of lubrication (chainage 0 to 130 m), phase (b) to the section soon after lubrication was introduced (chainage 130 to 170 m), and phase (c) to the remainder of the drive.

### 2.2.3.2 Seaham, UK

Similar measurements were performed by Marshall (1998) at Seaham. There, the instrumented pipe was inserted after lubrication had begun, so that a

contrast between pre and post lubrication was not possible. The salient conclusion derived from contact stress measurements was that large differences of fluid pressure were recorded between adjacent transducers, as may be seen in Fig. 2.7. In this figure, the pore water pressure measured at the pipe crown, invert and spring lines are plotted versus time during an injection episode and the subsequent jacking event. Injection of lubricant occurred from sockets that were situated a few meters on either sides of the instrumented pipe. The initial fluid pressures are considerably different around the circumference of the pipe. Pumping lubricant in the overcut a few meters away did not have an immediate effect on the fluid pressure around the instrumented pipe, which again suggests that the overcut around the pipe had been closed by the converging ground. However, the pressures immediately departed from their steady values once jacking of the pipes was resumed, though not all in the same direction. In particular, the measured fluid pressure at the pipe crown covered a range of over 200 kPa, initially rising to approximately 150 kPa (the drive was above the groundwater table), before dropping rapidly to a measure suction of -50 kPa. These confusing observations are likely to be associated with a combination of shear-induced excess negative pore water pressure and equalisation of transient pore water pressures generated by the different injection episodes of lubricant.

Marshall suggested that the local variations of fluid occurred because “bentonite only charged section of the new bore”. This, however, is not in full agreement with his interpretation of the jacking record (§ 2.2.2.3, Fig. 2.3), namely that lubrication was “effective on the entire length of the drive”.

#### 2.2.4 Summary

The jacking force per unit length of pipe are summarised in Fig. 2.9 for each of the project discussed in the section. For reasons already explained, attempts to rationalise the friction data or the jacking forces per unit length using dimensionless expressions failed to produce consistent trends and are therefore not presented. The injection procedure (port location, injection sequence and pressure) and lubricant composition are often not reported in sufficient detail, and the interpretation of the observed jacking load patterns in relation to lubrication is therefore difficult. Some qualitative comments may nevertheless be extracted from the case-studies discussed in this section:

- The unit jacking forces vary from 2 to 54 kN/m. Little correlation with the pipe diameter or undrained shear strength of the clay is apparent. While shaft spacing

---

of 500 m were sometimes possible as a result of low jacking forces, jacking forces exceeded their limiting value after only 70 m in other cases.

- The introduction of lubrication at some distance into the drive generally halved the jacking force per unit length, however not in all cases. In addition to reducing the rate of jacking force increase, lubrication seems to reduce the total jacking force, suggesting that lubrication is effective over the entire length of the drive.
- While effectiveness of the lubricant over the entire length of the drive is expected when the ground does not fully close onto the pipes, it is perhaps surprising to measure a reduction of the total jacking force in cases where full ground closure was clearly indicated by interface stress measurements, such as was the case in Thurrock and Seaham.
- Integrating local values of shear stresses over the pipe area yields jacking forces per unit length that exceed the measured value by a factor of 2, hence indicating shear stress non-uniformity along the pipe length.
- The use of ‘automatic’ lubrication systems from the beginning of the drives has been reported and resulted in remarkably small jacking forces. However, it is not clear if the low jacking forces result from (a) the early introduction of lubrication, (b) the ‘automatic’ lubrication system or (c) from a lubricant composition of superior quality.
- Remarkably low unit jacking forces were measured in the medium stiff Bangkok clay when lubricating the pipeline with polymer. This product resulted in lower jacking forces than bentonite slurry. While bentonite lubrication resulted in higher restart forces after stoppages, the use of polymer was reported to obviate this problem.

## **2.3 Ground response to cylindrical cavity contraction**

### **2.3.1 Introduction**

The jacking forces reviewed in section 2.2 have been shown to vary over an order of magnitude depending on the ground conditions, the overcut ratio and the lubricant procedure, amongst other factors. The complex interactions between the ground and the lubricant largely determine the build-up of ground loading on the pipes and the associated jacking load. An understanding of these interactions is required to select the overcut size and to decide upon the necessity and method of

lubrication. These parameters will, together with the ground conditions, determine if the excavation remains open or if full contact between the ground and the pipe occurs and, in such instances, the magnitude of the ground loading. The loading area and the stresses exerted onto the pipe are then rather difficult to predict. This section summarises the methods available to analyse this problem.

At a distance of approximately three diameters behind the tunnel face, the excavation of the pipe jack may be idealised as the unloading of a cylindrical cavity in plane-strain conditions (*e.g.*: Mair & Taylor, 1993). When the supporting total stresses acting on the boundary of a cylindrical cavity prior to its excavation are reduced, the soil responds elastically until the onset of plastic yielding at the cavity wall. If the support pressure is further reduced, a plastic zone forms around the cavity and excess pore water pressures are generated in this zone (Yu, 2000). Under certain conditions, instabilities may occur around the excavation, either in the form of a local collapse mechanism or one that reaches to the ground surface (§ 2.3.2). Stable cavities nevertheless deform and the unloading causes both immediate (undrained) and time-dependant (drained) inward displacement of the cavity wall. Elasto-plastic solutions describing the immediate, undrained response, as well as the subsequent radial consolidation around the cavity are presented in § 2.3.3 and 2.3.4, respectively. When, as a result of excess pore water pressure dissipation, the magnitude of this convergence reaches that of the over-excavated annulus around the pipe, contact occurs and radial effective stresses will build up on the pipes; the existing method for estimating the magnitude of these interactions is provided in § 2.3.6. Finally, a summary of the observation made in this section is provided in § 2.3.7.

Lubricants may significantly influence the ground response by altering the flow regime and the fluid pressure near the excavation boundary. However, only the particular idealised situation in which no lubricant fluids interact with the cavity wall is considered in this section. The mechanisms by which the lubricant and their chemical composition affect the boundary condition at the cavity wall are addressed in § 2.4.

The variables involved in the idealised problem are represented in Fig. 2.10; wherever necessary, the notation adopted by other authors was altered to be consistent with the terminology defined in this thesis.

### 2.3.2 Stability of unloaded cylindrical cavities

In cases where no lubricants are injected around the pipes, or when the pressure of the lubricant is near atmospheric pressure, the cylindrical cavity behind the excavation shield undergoes a complete removal of the supporting total stress  $\sigma_{ro}$ . Depending on the diameter, the cover depth, and the strength of the ground, collapse mechanisms may be triggered by the excavation, leading to overall instabilities of the ground. Such instabilities may result in the full closure of the overcut and potentially large pressures on the pipe. Whether such a mechanism develops and causes instability of the cavity can be predicted using the limit theorems of classical plasticity. Rigorous upper and lower bound solutions for the limiting tunnel pressure,  $\sigma_T$ , have been derived for soils assumed to behave as a linear elastic perfectly plastic material with undrained shear strength  $S_u$ .

Davis *et al.* (1980) summarise upper and lower bounds for the undrained collapse load of a plane-strain tunnel in clay. Upper bounds were computed using several kinematically admissible block mechanisms with geometry suggested by the observation of failures induced in model tunnel tests conducted by Cairncross (1973), Seneviratne (1979) and Mair (1979). The calculations assume the undrained shear strength to be constant with depth and are derived for soil with both zero and finite unit weight,  $\gamma$ . Upper and lower bounds are summarised in Fig. 2.11 using the dimensionless depth of cover to diameter ratio,  $C/D$ , and the stability number,  $N$ , defined by Broms & Bennermark (1967):

$$N = \left[ \sigma_s - \sigma_T + \gamma \left( C + \frac{D}{2} \right) \right] / S_u \quad (2.1)$$

and where the other variables are as defined in Fig. 2.10.

While the experimental results are remarkably bracketed by the plasticity solutions, this data suggests that the failure mechanism predicted by classical plasticity is inappropriate once the cover to depth ratio  $C/D$  exceeds 3 (Sloan & Assadi, 1973). Collapse of deeper tunnels may be caused by local mechanisms not immediately propagating to the ground surface. Using an upper bound mechanism for local collapse, Davis *et al.* (1980) were able to show that no local instabilities could occur as long as the condition  $\gamma D/S_u < 4$  was satisfied, and this, irrespective of the ratio  $C/D$ .

Upper and lower bound solutions were proposed by Sloan & Assadi (1993) for soils whose undrained shear strength is given by the following relationship:

$$S_u(z) = S_{uo} + \rho \cdot z \quad (2.2)$$

where  $z$  is the depth below ground surface and  $\rho$  a factor representing the rate of undrained shear strain increase with depth. The dimensionless stability charts obtained by Sloan & Assadi show that the assumption of constant  $S_u$  with depth ( $\rho = 0$ ) is conservative. Their stability ratios for different cover to depth ratios and different gradients of undrained shear strength are reproduced in Fig. 2.12.

It is important to note that for overconsolidated clays, the bounds for undrained stability are only valid in the short period of time immediately following the excavation. As soon as the negative excess pore water pressures generated during the cavity unloading begin to dissipate, the effective stresses and the strength of the clay will gradually reduce, potentially leading to collapse. Hence, although the stability of openings in clays dry of critical state may be satisfied immediately upon unloading, failure may occur during consolidation as the strength deteriorates.

Time-dependent stability ratios applicable to the partially drained stage following undrained conditions were computed by Eisenstein & Samarasekera (1992). Their analysis incorporated the effect of a geostatic stress field by varying the earth pressure coefficients at rest,  $K_o$ , and assumed an initial parabolic undrained shear strength distribution with depth. Charts were produced for the long-term stand-up time of the cavities by computing pore water pressure dissipation in an uncoupled FE model.

### 2.3.3 Short-term stress changes around an unloaded cylindrical cavity

#### 2.3.3.1 Applicability and assumptions

Total stresses and pore water pressures in the ground are significantly altered by the excavation of the cavity. Excess pore water pressures are generated as a result of the radial unloading, and their subsequent dissipation are associated with transient changes of effective stress as water migrates under the effect of the hydraulic gradient caused by the excavation. Because the build-up of effective stresses on the pipe and the interactions between the ground and the lubricant considerably depend on the stress distribution in the ground, an understanding of the stress changes is essential.

This section discusses the stress changes immediately following the excavation. In most instances when tunnelling in low permeability clay, the cavity unloading resulting from the excavation is sufficiently rapid so that significant changes in stress due to migration of pore water during the construction may be neglected. *Undrained* conditions and zero volume change may therefore be assumed to evaluate the excess pore water pressure and the cavity deformation just after the excavation. The cavity deformation and the excess pore water pressures in the undrained stage will later serve as initial conditions for the consolidation problem arising as the excess pore water pressure dissipates (§ 2.3.4). Unless otherwise indicated, the solutions discussed in the following paragraphs are derived for conditions of plane-strain and axial symmetry, which implies that the effect of the free ground surface is ignored. The consequences of these assumptions and the conditions under which the proposed solutions may be applied to the problem in general will be briefly discussed.

### 2.3.3.2 Total stress models

Mair & Taylor (1993) report plasticity solutions that give a simple and robust insight into the response of the ground to tunnel excavation. Ground response to excavation is idealised as the complete or partial unloading of a cylindrical cavity in a linear-elastic perfectly plastic (Tresca material) and isotropic soil model. Closed-form solutions for the radius of the plastic zone,  $R_p$ , the cavity wall displacement,  $\delta$ , and the excess pore water pressure,  $\Delta u$ , may be derived by combining the radial equilibrium of the cavity, the kinematical compatibility of strains under the constant-volume condition, the yield criteria of the material as well as continuity of radial stress at the elastic-plastic interface. Rigorous derivation of these relations are given elsewhere (*e.g.*: Mair *et al.*, 1992 or Yu, 2000). Using the stability ratio  $N$  for weightless soil:

$$N = \frac{\sigma_o - \sigma_T}{S_u} \quad (2.3)$$

where  $\sigma_T$  is the radial support pressure in terms of total stress, the radius of the plastic zone,  $R_p$ , may be expressed by:

$$\frac{R_p}{r_o} = \exp\left(\frac{N-1}{2}\right) \quad (2.4)$$

where  $r_o$  is the excavation radius; while the inward radial displacement  $\delta$  at radius  $r$  is given by:

$$\frac{\delta(r)}{S_u} = \frac{1}{2G} \left( \frac{r_o^2}{r} \right) \cdot \exp(N-1) \quad (2.5)$$

in which  $G$  is the shear modulus; and the excess pore water pressure distribution in the plastic zone by:

$$\frac{\Delta u(r)}{S_u} = 1 - N + 2 \ln \left( \frac{r}{r_o} \right) \quad (2.6)$$

In pipe jacking, as a result of the excavated overcut, the support pressure is either zero, in cases where no lubricants are injected into the overcut, or the magnitude of the lubricant pressure in the overcut. Matters are complicated when the overcut closes as a result of undrained cavity wall displacement, as discussed in § 3.2.1.1. Because of the extremely high radial stiffness of the pipes, the radial convergence at the cavity boundary,  $\delta$ , is limited to the radial magnitude of the overcut, so that equation 2.3 and 2.5 may be combined to give a direct expression of the total stress building up on the pipe when full contact occurs in undrained conditions. It is worth noting that no excess pore water pressures are predicted in the zone where the soil remains elastic, since radial equilibrium demands that the total mean stresses remain constant in the elastic zone (and without yield the mean effective stress is unchanged in undrained conditions).

Results predicted with equations 2.3 and 2.4 are compared to field measurements in Fig. 2.13. Mair & Taylor (1993) concluded that sub-surface ground movements measured at a number of tunnelling sites in London Clay and during the construction of a 223-m deep tunnel in Boom Clay agreed reasonably well with the simple plasticity predictions, although the consequences of the non-axisymmetric geometry were apparent even for a tunnel constructed at a depth to cover ratio  $C/D = 7$ . Centrifuge tests on model tunnels in soft reconstituted kaolin clay at a cover depth to diameter ratio  $C/D = 3.1$  showed that significant excess pore water pressure developed beyond the predicted plastic zone. A similar conclusion was drawn from the construction of the repository tunnel in Boom Clay, where excess pore water pressures of the order of 800 kPa were measured at radii up to twice the predicted

plastic radius assuming a linear elastic perfectly plastic soil model (Mair & Taylor, 1993).

Therefore, although the solutions based on linear-elastic perfectly plastic soil models have the advantage of producing convenient closed-form solutions, the predicted excess pore water pressures around the cavity depart substantially from field measurements, especially beyond the expected plastic radius  $R_p$ . In addition to the approximations introduced with the assumptions of axisymmetry and isotropy, this is likely to be due to the assumption that the clay behaves as a Tresca material (Mair & Taylor 1993). As pointed out by Randolph *et al.* (1979), these models only account for excess pore water pressures resulting from changes in mean effective stress and any pore water pressure generated as a result of pure shear are ignored.

It is important to realise that modelling the excavation as a cylindrical cavity contraction is a simplification of the problem. In reality, the alteration of the stress regime produced by the excavation can be seen as the combined effect of (1) a spherical cavity contraction at the tunnel face (or expansion if an unusually high face pressure is applied), (2) shearing along the shield of the tunnelling machine, and (3), a cylindrical cavity contraction due to the radial unloading behind the oversized shield. While item (1) can be assumed to be negligible in cases where the support to the tunnel face is approximately equal to the horizontal *in situ* stress, item (2) can result in considerable changes of pore water pressure. Excess pore water pressure generated as a result of shearing between the clay and the shield are likely to affect the measurements discussed in § 2.2.3.

#### 2.3.3.3 Effective stress models

Total stress models have the merit of simplicity, but also suffer some limitations. Yu & Rowe (1999) point out that the main drawbacks of total stress models are (1) that they ignore the effect of stress history (*OCR*), (2) that the variation of stiffness with stress level and void ratio is generally not taken into account and (3) that strain-hardening/softening is not considered. While total volumetric strains are zero in undrained unloading, plastic volumetric strains are generally non-zero unless the soil yields at critical state. It follows that elastic volumetric strains of the same magnitude but opposite sign must accompany plastic straining. Therefore, changes of mean effective stress occur when the loading of a soil element proceeds beyond plastic yielding. When strength and deformation parameters are pressure dependent, a constitutive model in terms of effective stress is required to refine the models discussed in § 2.3.3.2. Several cavity expansion solutions with effective stress soil

models have been proposed and concise reviews of these models are given in Cao *et al.* (2001) and Silva, 2005. In contrast, the ‘inverse’ problem of undrained cavity contraction has received considerably less attention.

Based on the cavity expansion solution in critical state soils of Collins & Yu (1996), Yu & Rowe (1999) present effective stress analyses of cylindrical and spherical cavity contractions in isotropic and axisymmetric conditions. They derive analytical and semi-analytical solutions using large strain formulation (*i.e.* with Eulerian stresses and Henky strains) for the simple case of linear-elastic perfectly plastic constitutive model, as well as for three different critical state models (original Cam-Clay with and without Hvorslev yield surface as well as modified Cam-Clay). Relationships linking the effective cavity pressure to the radial contraction were obtained by integration of the kinematical relations and for the yield criterion and flow rule of these three critical state models. Excess pore water pressure distribution is obtained by subtracting mean effective stress from the total stress distribution obtained from the radial equilibrium condition. The full derivation of this expression, as well as those for effective stresses and displacements around the contracting cavity can be found in Yu & Rowe.

Fig. 2.14 illustrates some of the results obtained by numerical integration of their semi-analytical solutions. Excess pore water pressure,  $\Delta u$ , and total cavity pressure,  $p$ , are normalised by the undrained shear strength,  $S_u$ , and plotted versus the ratio of initial to current cavity radius,  $a_0/a$ . The right hand-side figures show the cavity wall displacement,  $u$ , normalised by the current cavity radius, as a function of the current value of  $a/r$ , where  $a$  and  $r$  are the current radial coordinate and the cavity radius, respectively. The following remarks can be made:

- The choice of the soil model has an important effect on the predicted soil behaviour around the cavity, especially for heavily overconsolidated clays.
- Normally consolidated clays yield immediately at cavity wall and large amounts of positive excess pore water pressure ( $\Delta u/S_u > 1$ ) are generated at the beginning of the cavity unloading. As unloading proceeds, the trend reverses and excess negative pore water pressures are calculated after full unloading.
- As expected, pore water pressure remains constant during initial unloading of the cavity in lightly and heavily consolidated clays (or  $OCR > 1$ ), and this remains as long as the soil is elastic. Perhaps unexpectedly, Yu & Rowe obtain non-zero excess pore water pressure in the elastic zone.

- The ratio  $u/a$  varies linearly with  $a/r$ , except in *NC* clays where large strains are significant. This is in accordance with Mair & Taylor (1993).

The effects of the yield criteria and the non-associativity of the flow rule on the predicted displacement around tunnels are further discussed in Ogawa & Lo (1986). Although their analysis is presented for applications in rock mechanics, these conclusions remain applicable to constitutive models of soil. They study different flow rules in which the ratio of the principal plastic strain rates is a function of the dilatancy angle,  $\psi$ . They observed that the computed boundary wall displacement increases with increases angle of dilatancy,  $\psi$ , with which the flow rule is defined. Displacements were differing by a factor of 2 when varying  $\psi$  over the selected range. The computed results were found to be consistent with undrained convergences of tunnels in London Clay measured by Attewell & Farmer (1974) and Barratt & Tyler (1976).

Samarasekera & Eisenstein (1992) used a two-dimensional non-linear finite element analyses to predict stress changes around an unloaded cavity in undrained conditions. The results of their analyses showed that positive excess pore water pressures were generated around a significant region of an unsupported tunnel in normally consolidated clay, while negative excess pore water pressures were computed in overconsolidated clays. The effects of the proximity of the ground surface have also been discussed by Sagasetta (1987).

### 2.3.4 Consolidation around a contracting cavity

#### 2.3.4.1 Terminology

The transient behaviour of the cavity following the undrained excavation is sometimes referred to as ‘consolidation’ (*e.g.*: Yu, 1999), and sometimes as ‘swelling’ or ‘inverse consolidation’ (*e.g.*: Carter, 1988).

A clarification of the terminology associated with the effects observed as a result of excess pore water pressure dissipation is required before proceeding to their analysis. The term ‘consolidation’ usually refers to the gradual volume reduction ensuing dissipation of positive excess pore water pressures in a soil element. In contrast, the word ‘swelling’ is thought of as some kind of process giving rise to an increase in volume. The dissipation of pore water pressure around a contracting cavity is often said to be a consolidation problem, although it results in volume increase. And this is

where misrepresentation of the phenomenon can occur, mistaking cause of the observation for the effect.

'Consolidation' is alternately used to define the cause or the effect: the dissipation of positive excess pore water pressure, or the associated volume reduction. 'Swelling' should perhaps have the equivalent meaning(s) for opposed volumetric strains. However, it tends to be used to describe the *effect* resulting from two physically distinct causes, as well as one of this cause itself, but not the one that consists in the dissipation of negative pore water pressure (hence the need for the expression 'inverse consolidation'). The second phenomenon often labelled 'swelling' is physicochemical and relates to the hydration of clay minerals. This produces intercrystalline or osmotic swelling, both leading to the expansion of the clay lattices, and causing an increase in volume at the macro scale (Madsen & Müller-Vonmoos, 1989). This latter instance of swelling is well-known to rock tunnel builders and oil-well drillers who, as a result of hydration of anhydrite or smectites and the associated intercrystalline 'swelling' (the cause), observe 'swelling' (the effect). Although time-dependent, like consolidation, the word swelling used in this context does not refer to a consolidation phenomenon: the time dependency is due to time-dependent material behaviour rather than excess pore water pressure dissipation.

A clear distinction is necessary since many time-dependent solutions exist to describe swelling (or so-called squeezing) occurring in rock tunnelling. Constitutive models describing such material behaviour are essentially elasto-visco-plastic as they describe truly time-dependent material behaviour (*e.g.*: Fritz, 1984; Barla, 2000). Confusion arises when such models are applied to clay materials (*e.g.*: Ghaboussi & Gioda, 1977), where the effects of pore water pressure dissipation are questionably described by visco-plastic constitutive models as though the soil matrix had time dependent properties. As Muir Wood (2004) reaffirms, "it is worthwhile, when looking at features of soil response, to distinguish between time effects due to creep or ageing and time effects due to dissipation of pore water pressure". Therefore, whenever the time-dependency results from the finite permeability of the soil, transient volume changes are best described using principles of classical soil mechanics (*e.g.*: Atkinson & Mair, 1981). Pore water pressure should be coupled to changes in effective stresses from which deformation can then be calculated, rather than using artificial rheological properties of the soil skeleton. However, real aspects of material behaviour that can be ascribed to truly time-dependent soil response (secondary consolidations, or creep, rather than to a misinterpretation of transient consolidation), have to be described using visco-elastic models, since in such cases

deformation continues even in the absence of excess pore water pressure gradients (Muir Wood, 2004). Also, under certain circumstances, physicochemical swelling can occur simultaneously to consolidation causing coupling of hydro-mechanical and physicochemical effects. In such cases, combined hydro-mechanical and visco-plastic models might be appropriate (*e.g.*: Bellwald, 1987; Aristotenas, 1992 or Robinet & Tacherifet, 1996).

The approach taken in this section is one in which strains due to creep and physicochemical swelling are ignored and all time-dependent effects are regarded as being due to primary consolidation. With reference to the cause of the phenomenon, the negative volumetric strains occurring around the cavity will be referred to as consolidation.

#### 2.3.4.2 Semi-analytical consolidation solution for contracting cavities

Understanding excess pore water pressure dissipation is essential to assess the evolution of cavity deformation and the build-up of ground loading on the pipe. In pipe jacking, consolidation takes place following the undrained unloading of the cavity. If the overcut does not close in the undrained stage, drainage will cause further inward movement of the cavity wall, possibly until contact is made with the pipe. Consolidation then proceeds, however without further movement of the cavity wall; ground loading will gradually build up on the pipe, until hydrostatic conditions prevail. When contact is made between the clay and the pipe, the boundary conditions at the cavity wall are altered. Because the pipes are impermeable and rigid, the clay surface becomes a no-flux boundary and further radial displacements of the cavity boundary are restrained.

The problem of consolidation following the cavity expansion around driven pile foundations has been studied extensively (*e.g.*: Randolph & Wroth, 1979; Randolph *et al.*, 1979; Carter *et al.*, 1979; Burns & Mayne, 2002 or Silva, 2005). In contrast, the related situation in which (inverse) consolidation occurs around a contracting cavity such as a tunnel has received little attention. However, significant contributions have emerged from the oil and gas industry, where the issue of trapping drill strings as a result of wellbore diameter reduction may be, under certain aspects, considered analogous. However, most of these approaches take limited account of the logarithmic distribution of excess pore water pressure resulting from the initial undrained cavity contraction (equation 2.5). In addition, the elasto-plastic behaviour of clays is often not considered, and the transient problem has mostly been analysed with models based on Biot's theory of poroelasticity (*e.g.*: Detournay & Cheng,

1988) or models including mechanical as well as physicochemical effects (*e.g.*: Sherwood, 1993; Sherwood & Bailey, 1994 or Yu *et al.*, 2003).

Carter (1988) presents a semi-analytical solution for consolidation around an unloaded cavity. He assumes (1) that the original cavity unloading is sufficiently rapid for the soil to behave in an undrained manner, and (2), that the soil skeleton deforms elastically during unloading. Gradients of pore water pressures are assumed to be radial and therefore no flow occurs in the cavity axis direction (§ 3.2.5). Consequently, only radial movements may occur during consolidation and the transient problem may be treated in plane-strain conditions. Using Hooke's law (all the soil is assumed elastic during consolidation) to define the non-zero strain components,  $\varepsilon_\theta$  and  $\varepsilon_r$ , radial equilibrium in terms of total stress, as well as flow continuity, it may be shown (*e.g.*: Randolph & Wroth, 1979) that the consolidation problem in axisymmetric geometry is governed by the second-order partial differential equation:

$$\frac{\partial u}{\partial t} = c \left[ \frac{1}{r} \frac{\partial}{\partial r} \left( r \frac{\partial u}{\partial r} \right) \right] + g(t) \quad (2.7)$$

where  $r$  is the radial coordinate defined in Fig. 2.10. The bracketed expression denotes the scalar Laplacian of the transient excess pore water pressure relative to hydrostatic,  $u(r, t)$ . The term  $g(t)$  is a constant of integration depending on the boundary conditions, and  $c$  the clay's coefficient of consolidation:

$$c = 2G \left( \frac{1-\nu}{1-2\nu} \right) \frac{k}{\gamma_w} \quad (2.8)$$

in which  $G$  and  $\nu$  are the elastic shear modulus and the Poisson's ratio of the soil skeleton (drained),  $k$  the coefficient of hydraulic conductivity and  $\gamma_w$  the unit weight of water.  $G$ ,  $\nu$  and  $k$  are assumed to remain constant with time and radius; as though their value is not affected by changes of mean effective stress associated with the dissipation of excess pore water pressure.

The general form of the solution of equation (2.7) may be written as:

$$u(r,t) = \sum_{n=1}^{\infty} B_n \exp(-\lambda_n^2 ct) [J_o(\lambda_n r) + \mu Y_o(\lambda_n r)] \quad \text{for } r_o < r < r^* \quad (2.9a)$$

$$u(r,t) = 0 \text{ for } r > r^* \quad (2.9b)$$

where  $B_n$ ,  $\lambda_n$  and  $\mu$  are constants that may be integrated using the orthogonal properties of Bessel functions, and where  $J_o$  and  $Y_o$  are Bessel functions of the first and second kind, respectively. The radius  $r^*$ , beyond which pore water pressures can be assumed to be zero depends on the initial conditions and the subsequent distribution of pore water pressure (Randolph & Wroth, 1979).

Carter studied the effect of permeable and impermeable cavity walls partially supported with a total pressure of magnitude  $\lambda p_i$ , where  $p_i$  is the pore water pressure in the ground before cavity contraction and  $\lambda$  a positive quantity. This allows different set of boundary conditions to be established to account for the support pressure of a slurry column at the circumference of a vertical borehole. This slurry pressure could equally represent the lubricant pressure in the overcut excavated around the pipes.

The initial distribution of excess pore water pressure may be obtained from the undrained solution of the cavity contraction problem, which, for an elastic perfectly plastic soil model is expressed by equation 2.6. Assuming the support pressure at the boundary to act at  $t = 0$ , the initial distribution of excess pore water pressure is given by:

$$u_o(r) = 2S_u \ln\left(\frac{r}{r_o}\right) - \sigma_r + \lambda |p_i| \text{ for } r_o < r < R_p \quad (2.10a)$$

$$u_o(r) = 0 \text{ for } r > R_p \quad (2.10b)$$

and where  $R_p$  reduces with increasing cavity support pressure according to:

$$R_p = r_o \exp\left(\frac{\sigma_o - \lambda |p_i|}{2S_u}\right) \quad (2.11)$$

Equations 2.12a and b may be solved numerically using an algorithm proposed by Randolph (1977) and modified by Silva (2005).

Carter (1988) evaluated isochrones of excess pore water pressures for the initial logarithmic distribution of excess pore water pressure given by equation (2.6) and for

four sets of boundary conditions, combining a supported and unsupported borehole with a permeable and impermeable cavity wall. Fig. 2.15 shows the isochrones of excess pore water pressure for a stiff clays with  $OCR = 8$ , with an earth pressure coefficient of  $K_o = 1.6$  and a ratio of initial pore water pressure to initial vertical effective stress of unity ( $p_i/\sigma_v' = 1$ ). Case I and II correspond to dry boreholes, with zero internal total support, and case II and IV represent impermeable boreholes. Case III models a permeable borehole supported with a fluid pressure equal in magnitude to the hydrostatic pore water pressure prevailing before excavation of the borehole. The isochrones are presented in dimensionless quantities: excess pore water pressure,  $p$ , were normalised by the initial vertical effective stress,  $\sigma_v'$ , and the radial distance from the cavity axis,  $r$ , with the original cavity radius,  $r_o$ , and using the non-dimensional time factor  $T = ct/r_o^2$ . The following observations were made by Carter:

- In case II, III and IV the pore water pressure returns to hydrostatic and hence  $p = 0$  at equilibrium. In contrast, in the case of a 'dry' and permeable borehole (no total stress support) the fluid pressure at the boundary will always be zero and therefore  $p/\sigma_v' = -1$  (case I)
- The monotonically increasing excess pore water pressure in the case of an impermeable (case II) hole with zero pore water pressure at the boundary indicates that the pore water flow always occurs inwards from outer regions.
- The magnitude of generated excess pore water pressure during the unloading stage is larger when no support is provided to the cavity, and the provision of a support pressure reduces the size of the plastic zone.
- Excess pore water pressures around boreholes with groundwater support dissipate much faster when flow is allowed across the cavity boundary. As would be expected, the pore water pressure in the near cavity region rapidly returns to hydrostatic.

#### 2.3.4.3 Numerical analyses

Carter's semi-analytical solution assumed that the soil matrix deformed elastically during consolidation. Although providing powerful insight into the radial consolidation problem, the assumption from which this solution is derived bears some limitation. Indeed, the closed-form solution does not link the soil strength, permeability and shear modulus to the effective stress state (Yu & Rowe, 1999). Changes in mean effective stresses may be significant as the negative excess pore

water pressures around the cavity gradually dissipate and the resulting variations in strength, permeability and shear modulus should be taken into account.

Numerous FE analysis modelling pore water pressure dissipation around tunnels have been proposed. However, these analyses are often carried out to back-analyse case-studies and hence include the effect of a phreatic surface and that of a flexible lining installed a short time after the tunnel excavation. Possibilities for direct comparison with the semi-analytical solutions presented in the previous section are therefore limited. An extensive review of numerical methods accounting for hydro-mechanical coupling to analyse consolidation around tunnels in clay may be found in Atwa (1996).

Shin *et al.* (2002) present coupled hydro-mechanical FE simulations with a non-linear elastic perfectly plastic soil model and in which the equilibration period following the hydraulic perturbation due to tunnelling in clay (not steady state seepage) are modelled. The effects of the hydraulic boundary conditions on the transient lining loads are carefully examined. Finite lining permeability as well as fully permeable and impermeable linings are modelled to vary the flow regime at the boundary. In addition, the permeability of the clay surrounding the cavity is allowed to vary with time and radius. While Carter and Randolph & Wroth (1979) assumed constant permeability to derive their closed-form solution, the FE model proposed by Shin *et al.* may account for the effective stress dependency of the permeability and its potentially large variation in the period of time between the undrained cavity unloading and full equilibrium. Shin *et al.* emphasised the influence of the non-linearity of seepage flow on the time-dependent soil-lining interactions. To account for this non-linearity, they used the permeability model proposed by Vaughan (1989), in which the coefficient of permeability,  $k$ , is given by:

$$k = k_o e^{-Bp'} \quad (2.12)$$

where  $k_o$  is a reference permeability at zero mean effective stress,  $p'$ , and  $B$  a material property.

Qualitative conclusions from the analysis carried out by Shin and co-workers can be summarised as follows:

- The permeability of the soil adjacent to the tunnel reduces with time if the lining is permeable, while it increases in case of impermeable linings. Shin *et al.* do not

---

report analysis for a cavity which remains unsupported during the consolidation stage,

- Ground loading on an impermeable lining in a low-permeability soil is significantly higher than on a permeable lining. This contrasts with the conclusion of Atkinson & Mair (1983) who showed that, in case of a rigid lining, the permeability of the lining had no effects on the long-term lining load if seepage-induced stresses are taken into account.
- The analysis confirmed the large difference between prediction of steady-state pore water pressure distribution when using linear or stress-dependant permeability coefficient (Addenbrooke, 1996).
- The boundary conditions to the flow regime have a decisive effect on the rate of stress increase as well as on the magnitude of lining stresses at equilibrium. The permeability of the ground and its variations with effective stress also have a significant effect on the rate of stress build up.

### 2.3.5 Ground loading on the lining

#### 2.3.5.1 Introduction

The knowledge of the pore water pressure distribution around a freely contracting cavity is not sufficient to determine the pipe/soil interaction. In addition to the stress distribution in the ground, the deformation of the lining and the size of the overcut around the pipe influence the ground loading. In most cases, undrained conditions will not hold true for the duration of construction (weeks); however, equilibrium of pore water pressure does, in most cases where cavities are excavated in low permeability clay, take considerably longer than the construction time to return to equilibrium. Field measurements by Peck (1969) and Barratt & Tyler (1976), showed that large increase of lining loads can occur within a few weeks of constructions. It can therefore be anticipated that the jacking forces depend on transient radial pipe-soil stresses and that the rate of increase of the radial stresses is a critical factor controlling the jacking forces.

#### 2.3.5.2 Method of characteristic curves

Ground-lining interactions problems are usually approached using the so-called method of characteristic lines proposed by Peck (1969) and often referred to as the convergence-confinement method (Panet & Guenot, 1982). The underlying

principle of these methods is to determine a convergence vs. radial pressure relationship for both the soil and the lining independently (so-called ground and lining reaction curves). Using the assumption that the mode of deformation of both the lining and the ground is radial, and accounting for the radial convergence of the ground that has already occurred at the instant when the ground comes into contact with the lining, the solution for the short-term ground support interaction is given by the intersection of the reaction curves of the ground and the lining, as shown in Fig. 2.16.

Explicit closed-form solutions exist for ground reaction relationships in axisymmetric conditions with a variety of stress-strain models, yield criteria and plastic flow rules. These solutions express the radial convergence,  $\delta$ , in terms of soil parameters and total support pressure,  $\sigma_T$ . Excellent reviews of these work may be found in Brown *et al.* (1983), Mair & Taylor (1998), Barla (1999) and Gärber (2002). For the particular case of a linear elastic perfectly plastic soil model, such a ground reaction curve for undrained and axisymmetric conditions is given by combining equation 2.4 and 2.6 (*e.g.*: Mair & Taylor, 1993).

Because the majority of these ground reaction solutions were developed for application in rock mechanics, they are almost invariably restricted to monophasic media. Hence, hydro-mechanical effects are ignored. While it has been shown that solutions for monophasic elasto-plastic media remains valid for assessing the undrained response of porous elasto-plastic materials (Giraud, 1993), the time-dependant behaviour (“consolidation”, § 2.4.4.1) following the excavation cannot be captured with these approaches. Drained, or partially drained behaviour of porous material require consideration of the pore water pressure generation during the undrained phase and their subsequent dissipation. The determination of transient behaviour of elasto-plastic and porous materials is a complex problem and the estimation of the lining load after a given time is a laborious task if the problem is not unrealistically oversimplified.

A review of these approaches may be found in Gärber (2002). For example, solutions for characteristic lines of a poro-elasto-plastic medium in terms of effective stress have been proposed recently by Labiouse & Giraud (1998). They assumed the ground to be homogenous and isotropic and to behave according to a linear elastic-perfectly plastic soil model with Mohr-Coulomb failure criterion and plastic potential depending on the dilatancy,  $\psi$ . Closed-form solutions were obtained for conditions of axisymmetry and zero dilatancy  $\psi = 0$ . These solutions express the convergence of cavity wall as a function of the effective support pressure.

Contact between the pipe and the ground, in cases where the gap is small, can occur during the undrained unloading. In such cases, the equilibrium point may simply be found using the undrained ground response curve. Assuming the pipes to be infinitely rigid, no time-dependant convergence will arise and the effective stresses at the pipe-soil interface can be found by subtracting the transient pore water pressure from the total stress required for equilibrium. Such solutions combined with knowledge of the transient excess pore water pressure may allow calculating the gradual build-up of effective stresses on the pipes, but the approach may lack the merit of simplicity and the arduous mathematical expressions often require numerical integration. In addition, strain-hardening or softening soil behaviour cannot easily be taken into account, and the analytical or semi-analytical solutions are almost invariably restricted to axisymmetric conditions. This condition is rarely satisfied rigorously, either because of the proximity of the free ground surface or because of inhomogeneous ground conditions and anisotropic initial stress field. In addition, the proximity of a ground water also alters the assumption of radial flow conditions,.

### 2.3.5.3 Numerical analysis

For the reasons discussed in the previous paragraphs, as well as for the complexity of the displacement and hydraulic boundary conditions at the cavity wall the recourse to numerical methods is practically indispensable to assess the transient pipe-soil interactions. FE analysis of excess pore water pressure dissipation upon undrained unloading of a cylindrical cavity have been carried out by Anagnostou (1992), Giraud (1993), Atwa (1996), Benamard (1996), Addenbrooke (1999), Labiouse (1999), Vervoort & Van de Steen (2001), Gärber (2002) and Shin *et al.* (2002), amongst others. A critical appraisal of finite element analyses of ground response to tunnelling in clay may be found in Clough & Leca (1989). However, ground movements are usually the focus of such analyses and ground-lining interaction are not always carefully considered.

Gärber (2002) carried out extensive parametric studies using fully-coupled FE analyses to establish characteristic curves for a porous media in both undrained and partially drained conditions. Three-dimensional calculations were performed for a homogeneous and isotropic soil stratum under conditions of axisymmetry, using a linear elastic perfectly plastic soil model with a Mohr-Coulomb yield criterion and associated flow rule. Parametric studies allowed non-dimensional plots of ground reaction curves to be established for the short and long-term, as well as for the intermediate, transient conditions. They showed the influence of the hydraulic boundary condition at the cavity wall and related the time-dependant displacement of

a flexible tunnel wall to the gradual dissipation of excess pore water pressure. Fig. 2.17, for example, shows the short and long-term pore water pressure around a cylindrical cavity, both for the case of an impermeable (a) and a permeable (b) lining. Gärber's analyses demonstrated that for the short-term, *FE* analyses yield quantitatively similar distribution of excess pore water pressure around the cavity. Remarkably, in the case of the permeable lining, the numerical analyses predicted almost identical lining loads in the long-term as in the undrained short-term conditions.

### 2.3.6 Summary

- Upper and lower bound plasticity solutions for undrained unloading of cylindrical have been reviewed. Plasticity solutions give reasonable predictions for tunnels at a cover to depth ratio  $C/D < 3$ . As excess negative pore water pressure dissipates, the strength of overconsolidated clay deteriorates and instability may occur. In case of a permeable cavity supported with fluid pressure, dissipation of pore water pressure near the cavity occurs rapidly and undrained stability analyses should be used with caution.
- Stress and pore water pressure changes around a contracting cylindrical cavity in undrained conditions can be estimated with total stress models. The soil behaviour is idealised as linear-elastic perfectly plastic. The model under-predicts excess pore water pressures beyond the predicted plastic radius and is restricted to axisymmetric geometry and homogenous ground conditions.
- Effective stress models accounting for stress dependent material properties and effective stress history are scarce for cavity contraction problems. Semi-analytical solutions for critical state constitutive models require numerical integration. Little data is available to confirm the validity of the expressions proposed in the literature.
- The radial consolidation problem following undrained unloading of a cylindrical cavity has been studied analytically. The existing solutions assume that the soil matrix behaves elastically during unloading.
- *FE* analyses of unsupported contracting cavities have not been reported. An interesting analysis with non-linear seepage flow was reported by Shin *et al.* (2001), who also investigated the effect of lining behaviour.

- The problem of ground loading on a tunnel lining or on a pipe can be tackled analytically in the simplest case only. Undrained loading may be determined for a simple soil model, but in cases where the overcut around the pipe exceeds the undrained convergence, contact stresses will only occur during the consolidation stage. Determining transient ground loading needs to account for the change of displacement and flow boundary conditions.
- Many FE analyses of tunnelling problems are found in the literature, but the focus is usually on the ground movements rather than on the lining loads.

## 2.4 Physicochemical interaction near the excavation boundary

### 2.4.1 Introduction

Chemical components may be added to pipe jacking lubricants to alter the mechanical behaviour of the clay near the excavation boundary. Some success has been reported from the use of chemicals (*e.g.*: Alexanderson, 2001), but little is understood regarding the processes governing the interactions between the clay and these chemicals. This section reviews the application of such products in the oil and gas industry, where drilling engineering for hydrocarbon exploration has received and continues to receive immense attention. Considerable research concentrates on the development of more efficient drilling fluid and on the fundamental mechanisms involved in the shale-drilling fluid interactions. A search on the Society of Petroleum Engineers (*SPE*) literature database reveals the intensity of this continuous research effort: a query with the keyword “*drilling fluids*” returns over 4200 technical papers published since the beginning of the research presented in this dissertation (2001).

This proliferation of publication results from the commercial potential of the drilling industry, in which losses due to drilling related problems are estimated to amount to 1 billion USD per annum. In addition, the problem is complex: the several mechanisms involved are not only simultaneous, but also coupled, and there seems to be no consensus as to which ones are most significant under given circumstances. Gray *et al.* (1980) estimated that over 1400 trade-named drilling fluid components were marketed to perform one or several of sixteen separate functions, most of which are related to clay ‘swelling inhibition’. The number of generic chemical components was, in 1980, of the order of 25; which, combined with the natural variability of shale and drilling in pressure and temperature varying over orders of magnitude, explains the abundance of research projects.

A systematic review of such literature would generate more confusion than insight. Therefore, only the basic mechanisms by which drilling fluid components affect the mechanical behaviour of contracting well bore cavities are reviewed. The scope is limited to the effects which are potentially relevant for pipe jacking, and the emphasis is placed on the physical nature of the phenomenon. Both in well bores and in pipe jacking, the problem involves the alteration of chemical and hydro-mechanical conditions at the boundary of a soil element. The relevant processes therefore take place at the interface between the drilling fluid and the shale, and possibly in a small zone in which solvents seep and solutes are transported by diffusion and advection under the effect of hydraulic and chemical concentration gradients. The bulk properties of the soil/chemical mixtures are only of limited interest: instead, the problem is governed by rate at which the chemicals invade the pores, and by the stresses and strains induced as the soil-fluid system returns to chemomechanical equilibrium.

This section begins by discussing the analogies between the problems of pipe jacking and well bore drilling in order to appreciate the conditions under which the oil and gas industry experience is applicable to pipe jacking (§ 2.4.2). It then proceeds to give a concise description of the most important chemical components of drilling fluid and pipe jacking lubricant (§ 2.4.3). Finally, the physicochemical mechanisms by which they affect the transient behaviour of the unloaded wellbore are reviewed and experimental evidence substantiating or disproving the significance of each mechanism is discussed (§ 2.4.4). Again, the section is completed with a summary of observations (§ 2.4.5).

#### 2.4.2 Relevance of wellbore drilling fluids for pipe jacking lubrication

Hydrocarbon exploration and production involves drilling vertical holes with diameters in the range of 150 ('slimholes') to over 500 mm. Well bores often reach depths between 5 and 10 km where extreme temperature and pressure conditions are encountered. During drilling operations, *drilling fluids* are continuously pumped to the bottom of the hole through the hollow drill string, and then returned to the surface via the annulus around the drill string. The primary function of drilling fluids is to transport the soil cuttings from the drill bit to the ground surface (as in a slurry shield tunnelling TBMs, see section 1.3.1). Bentonite has been intensively used as a drilling fluid because its thixotropic behaviour helps suspend the cuttings during stoppages of fluid circulation, hence preventing their sedimentation to the hole bottom. The second function of drilling fluids is to maintain the borehole open for periods of days or weeks (Schlemmer *et al.*, 2003). A large proportion of the drilling is made through

shale formations, which tend to swell as they come in contact with aqueous mud and hydrate. As a result, borehole instability or excessive convergence of the cavity wall may occur, which causes constriction of the discharge flow path of the cuttings, drill string trapping, or even collapse of the wellbore (*e.g.*: Chapter 9, Gray *et al.*, 1980). This impedes further drilling as well as oil production and sometimes requires the well bore to be abandoned.

Continuous efforts are made to develop drilling fluids capable of improving borehole stability. Carefully engineered fluids are designed to reduce weakening of the shale formation and thus reduce the likelihood of instabilities and excessive contraction of the unloaded cavity ('shale inhibition'). This effort to support the borehole and prevent its closure is essentially the same as in pipe jacking, where the hole is initially unsupported and in contact with drilling fluid. While the well bore behaviour may be influenced by adapting the drilling fluid density and chemistry to the in situ conditions, the pipe-soil interactions may be equally controlled by altering the pressure and the chemistry of the fluid. Notably, drilling fluid components in the oil and gas industry and in tunnelling are essentially the same, and are often marketed by the same suppliers, albeit under different trade names.

Despite the similarities between well bore drilling and pipe jacking, a few differences must be kept in mind when converting the experience from shale/drilling fluid interactions into applications for pipe jacking. Firstly, pipe jacking lubricants are not used as a transport medium for cuttings, and therefore the lubricants do not have to flow over large distances or maintain soil cuttings in suspension; carrying capacity and thixotropic properties are not *a priori* essential. Secondly, the geotechnical properties of the formations through which oil wells are drilled differ considerably from the clay encountered at much shallower depths. The deep formations are often called 'shales'. This term designates a sedimentary rock formed by consolidation of clay- and silt-sized particles, often containing a large proportion of smectite of relatively large activity. The permeability and the voids ratio of shale are considerably smaller than that of clays at shallow depths. Thirdly, the stress level prevailing around deep well bores is two or three orders of magnitude higher than in pipe jacking, where the construction rarely takes place below depth of 30 m. Therefore, although the two processes are similar and the operative mechanisms are potentially the same, the different conditions are likely to affect their relative relevance: the governing processes may vary for different conditions of stress, mineralogy, fabric and geochemistry (Fam & Dusseault, 1998).

---

### 2.4.3 Composition and properties of drilling fluids and lubricants

#### 2.4.3.1 Generalities

As already mentioned, the different components of drilling fluids will be discussed from the standpoint of their effect on borehole stability. However, a brief description of the basic properties of the generic components is provided in this section. Although the experimental investigations reported in this dissertation only used partially hydrolysed polyacrylamide (*PHPA*), other generic components found in lubricants and drilling fluids are also discussed to provide an overview of the potential interactions between clay and chemicals.

Drilling fluids (or ‘muds’) are generally classified into oil-based muds (*OBM*) and water-based muds (*WBM*). Although *OBMs* provide highly effective shale inhibition and are thought to be the most efficient drilling fluids (primarily owing to their hydrophobic behaviour), awareness of lasting environmental impact of *OBMs* led to the development of legislation prohibiting their discharge. The elimination of *OBMs* in the 90’s imposed great technical difficulties for controlling wellbore instabilities. The need for alternative products triggered the resurgence of water-based muds (*WBM*) and the development of sophisticated additives to rival the outstanding properties of *OBM* (Bailey *et al.*, 1994). In addition to water, the three main components of water-based muds are bentonite, polymers and soluble inorganic chemicals. The composition of these products is briefly discussed in the following sections. More details on the chemical characterisation and proprieties of drilling fluids are provided by Gray *et al.* (1980), Fam & Dusseault, (1998) or Milligan (2000).

#### 2.4.3.2 Bentonite

The term bentonite refers to a range of natural clay minerals that occur in extremely small particles and in particular to sodium montmorillonite. The unit layers of the crystalline structure of montmorillonite comprise two tetrahedral silica sheets with a central alumina octahedral sheet. The several unit layers that form montmorillonite crystals are held together by exchangeable cations. The outstanding feature of montmorillonite is that water can enter between the unit layers, causing hydration and expansion of the mineral lattice. The ability of montmorillonite to adsorb large quantity of water is reflected by its liquid limit, which can exceed 500. This tendency to absorb intercrystalline water, and therefore to swell upon hydration, depends on the size and the valence of the interlayer cation; the divalent calcium

cation  $Ca^{2+}$  provides a stronger bond than the sodium cation  $Na^+$ , and therefore the sodium variety of montmorillonite more readily swells and absorbs water compared to potassium exchanged or *Ca*-Montmorillonite. Because of its small ionic radius, substitution with potassium ions  $K^+$ , the intercrystalline layers will be thinner and hold less intercrystalline water, and therefore will be less prone to swelling upon hydration. The relatively high negative charges on the montmorillonite platelets give rise to a number of engineering properties like aggregation, flocculation or a combination of both which are of great relevance to their application in tunnelling and pipe jacking. In addition, it is important to note that the engineering properties of dilute bentonite suspensions are greatly influenced by the presence of polymers and salts; these effects are discussed elsewhere (*e.g.*: Theng, 1979, Breen, 1998 or McRory & Ashmawy, 2005). Grim (1953), Gray *et al.* (1980), and Milligan (2000), amongst others, discuss the properties of bentonite in more detail.

#### 2.4.3.3 Polymers

Polymers are large molecules made up of repeating units. They are used in drilling fluids and lubricants as very dilute water-based solutions, either alone or in combination with other chemical components or bentonite. Polymers are varied and versatile substances, and a broad range of properties can be achieved by engineering synthesised polymers. The way in which a polymer interacts with clay mainly depends on its chemical composition, molecular weight, structure and ionic strength. Polymers used in drilling fluids are usually water-soluble and their behaviour in solution is strongly influenced by the pH and salinity of the water. The molecular weight may be varied over several orders of magnitude, typically between 300,000 and  $10^7$ , corresponding to chain lengths of the order of 1000 Å, which is one order of magnitude larger than the crystal thickness of montmorillonite and one order of magnitude smaller than the smallest particle of E-grade kaolin clay. These chains may be linear or branched, and both types may be cross-linked by covalent bonds. In solution, the polymer chains can create networks, giving rise to complex viscous behaviour. The length of the polymer chains and the cross-linking between them greatly influences their properties and interaction with clays. Synthetic polymers may be designed to ionize in solution, and any degree of ionisation can be attained, from fully ionic to fully anionic. Charged groups strongly affect behaviour and interactions with clays, other polymers and solvents.

Polymers may be broadly classified according to their origin; *natural* (starches, xanthan gum or guar gums), *semi-synthetic* obtained by the modification of natural polymers (carboxymethylcellulose), and purely *synthetic* (polyacrylates and

polyacrylamides). Carboxymethylcellulose (*CMC*) is a modified natural cellulose that may contain some amount of *NaCl*. It is an anionic polymer which is adsorbed on clay and which may sharply reduced filtration, especially when in high molecular weight form. It is therefore often used as a fluid loss reducer. (Gray *et al.*, 1980). Polyacrylamides are often used in the form of partially-hydrolysed polyacrylamide (*PHPA*), which may be ionic, cationic or non-ionic, depending on the degree of hydrolysis. Its molecular weight may range from 1 to 15 million. *PHPA* is believed to adsorb onto shale surfaces, thus creating a film that retards dispersion, disintegration and swelling of clay cuttings (Schlumberger). Therefore, *PHPA* is often used to inhibit the swelling of reactive shales. In addition, *PHPA* interacts with bentonite to link particles together and strongly affects the rheology, and may act as a flocculent. Polyanionic cellulose (*PAC*) is a cellulose derivative similar in structure, properties and usage in drilling fluids to carboxymethylcellulose (semi-synthetic polymer produced from natural cellulose), but contains substantially less *NaCl*.

The polymer interaction with clay particle surfaces strongly depends on the charge of the functional groups of the polymer (*e.g.*: Theng, 1979, Breen, 1999 or McRory & Ashmawy, 2005). Polycations are adsorbed on the negative clay surface as a result of coulombic attraction, and the adsorption capacity increases with the charge of the functional groups. Polymers of lower cationicity (*e.g.*: polyacrylamide with low degree of hydrolysis) form loops and tails around the particle, which leads to interparticle bridging (Breen, 1999). Due to repulsive electrostatic forces, polyanions are repelled by the electric charges on the clay particles; little adsorption takes places and polyanions can remain suspended in the diffuse layer. When the charge density is high, the polymers stretch and their chains become stiffer, which can promote bridging between clay particles. If the solvent contains salts, dissolved cations may shield the negatively charged functional groups and the polyelectrolyte chains may coil and collapse on the clay particle surface (Breen, 1999). Non-ionic polymers tend to remain in a random coil in solution and exhibit considerably less affinity with clay particles.

#### 2.4.3.4 Inorganic chemical solutions

A host of inorganic chemicals may be used in drilling fluids, mainly as additives rather than as the main constituents. Gray *et al.* (1980) lists the most common of these chemicals. Inorganic salt solutions of sodium or potassium, as well as potassium formate are the most commonly used of these chemicals. The effect of potassium is fundamentally different from other cation upon exposure to shale. The response of the shale strongly depends on the type of ion, and is not only controlled

by the fluid activity. Sodium and potassium silicate fluids have been the subject of a recent resurgence of interest and have been used as highly inhibitive water-based drilling fluids.

#### 2.4.4 Interaction mechanisms

The possible mechanisms of shale-drilling fluid interactions can be expressed through the fundamentals of conduction phenomena in porous media. These phenomena are summarised in Table 2.2 and discussed in Mitchell & Soga (2005).

##### 2.4.4.1 Permeability reduction near the cavity boundary

Drilling fluids are often formulated to delay their migration from the borehole into the shale formation. The chemical additives used for this purpose are referred to as fluid loss reducers. Two reasons justify the attempt to reduce fluid loss into the formation. Firstly, in a saturated formation, volumetric strain and cavity contraction only occur if a corresponding volume of water is drawn into the increasing pore volume of the swelling shale. This increase in void ratio is associated with the dissipation of the negative excess pore water pressure, and therefore, a reduction of effective stress around the cavity. This, in turn, causes further inward deformation and may lead to instabilities that could cause a collapse of the borehole. Reducing the water flow from the cavity into the formation therefore reduces the rate of volume increase and the rate of shear strength deterioration of the soil around the cavity. The second reason for reducing fluid loss is to minimise so-called *formation damage*. Formation damage refers to a variety of adverse mechanisms by which oil flow from the reservoir into the borehole will be significantly decreased during the production stage. This is of interest because it has been shown that a reduction of permeability of a thin annulus surrounding the borehole may cause significant reduction of hydrocarbon into the borehole, as a result of the radial flow geometry. Assuming linear seepage flow, Muskat (1949) showed that if the permeability of a region of radius  $r_d$  was reduced from  $k$  to  $k_d$  as a result of physicochemical “damage”, the flow from the formation is reduced according to:

$$\frac{Q_d}{Q} = \frac{\ln\left(\frac{r_e}{r_w}\right)}{\frac{k}{k_d} \ln\left(\frac{r_d}{r_w}\right) + \ln\left(\frac{r_e}{r_d}\right)} \quad (2.13)$$

where  $Q_d/Q$  is the productivity flow in the damaged formation normalised by the original productivity;  $k$  and  $k_d$  the permeability of the original and damaged formations, and  $r_w$ ,  $r_d$ , and  $r_e$  the radii of the well, the damaged zone and the drainage zone, respectively. Fig. 2.18 shows the flow reduction calculated with equation 2.13; it can be seen that for a 2 m diameter pipe jack, if the permeability of the soil in a 200-mm thick annulus around the excavation were reduced by an order of magnitude, seepage flow of the lubricant from the overcut into the soil would be reduced by over 30%. On the premise that the flow reduction predicted with equation 2.13 is proportional to the reduction of cavity contraction rate, it may be concluded that permeability reduction is an effective way of reducing the rate of consolidation and the build-up of ground loading on the pipes.

The permeability of an element of soil at the cavity boundary may be reduced by one or a combination of three mechanisms: (1) a reduction of the bulk permeability of the element; (2) the creation of an interface layer of low permeability at the boundary of the element, and (3) increasing the viscosity of the seeping pore fluid (filtrate). To minimise reservoir damage and optimise production, emphasis is placed on producing a thin, though and highly impermeable filter cake (Bailey *et al.* 1999). While bentonite suspensions are used in sand to provide a filtercake, bentonite does not form an effective filtercake on shale. Fam & Dusseault, 1998, amongst others, pointed out that no filtercake may form on shale because the permeability of the shale is several orders of magnitude lower than the permeability of the filtercake. The extent to which this conclusion is applicable to clays and fine silts seems not to have been investigated systematically. Permeability reduction of clays concentrates on the use of polymers and silicates and the way in which they affect the permeability in either of these ways is discussed in the following paragraphs.

### ***Polymers***

Polymer filtercake can form on clay or shale, just as bentonite cakes form on sand. The cake grows owing to the differential pressure between the drilling fluid and the pore water pressure in the well bore. A filtercake consists in a concentration of polymeric or colloidal particles that were dissolved or suspended in the drilling mud (Bailey *et al.*, 1994a). However, Bailey *et al.* (1994b) concluded from experimental evidence that the permeability of filter cakes produced by fluid loss polymers such as cellulose derivatives, xanthan gum and *PHPA* are typically one or two orders of magnitude higher than the permeability of the shale. As a result, fluid transport into

the shale is still controlled by the permeability of the shale, despite the formation of the cake, and water ingress is not appreciably reduced by these polymers. Shales have much lower permeability than the clays typically encountered during pipe jacking and there is little evidence as to the validity of this conclusion in soils of different void ratios.

Ballard *et al.* (1994) investigated polymer invasion into Oxford clay and a tertiary shale sample. They first carried out a series of benchmark tests using sea water plus 5% *KCl* as a percolating fluid. Four different polymers were then tested: *PHPA*, *PAC*, a polyamine and a glycol derivative with xanthan (an anionic polyelectrolyte), as well as starch. Each polymer was tested at two different concentrations and *PHPA* with two different molecular weights ( $7.0 \times 10^5$  and  $7.0 \times 10^6$ ) were investigated. The experimental procedure involved circulating the different fluid through a 10 to 20-mm thick natural sample under a constant pressure differential of 2.1 MPa. An overview of the tested combinations with the corresponding permeability reduction is given in Table 2.3.

No reduction in the invasion rate of the solution into Oxford Clay was observed when using (0.5-1.5 ppb) Xanthan, and only marginal reduction was apparent with approximately 0.1 and 0.5% *PAC* solutions. Flow rate reductions of approximately 30 and 20% were observed with starch solutions of 2.0 and 8.0 ppb, respectively, while polyamine halved the flow rate, irrespective of the solution concentration. High molecular weight *PHPA* reduced the water flow rate by 25%, while low molecular weight achieved a 40% reduction, perhaps inconsistently with what might be expected. Post-mortem analysis revealed that *PAC* did not invade the Oxford clay beyond a depth of 1 mm, while *PHPA* was found in the effluent, indicating that some proportion of *PHPA* did invade the clay. Starch was not detected beyond the first millimetre from the clay surface, while the low molecular weight (50,000) polyamine invaded the Oxford clay but was not detected in the effluent. This indicated that this cationic polymer was strongly adsorbed by the clay, although its small weight allowed invasion of the matrix. In contrast, for the range of concentration tested, glycol was transported through the clay sample.

Ballard *et al.* concluded from these observations and measurements that the maximum reduction of fluid invasion was achieved when the polymer chains were sufficiently small to penetrate the first millimetre of the clay but too large to be transported further. Permeability reduction would then result from pore clogging due to the adsorption or mechanical retention of the polymer in the clay; this mechanism leads to greater reduction of solution ingress rather than increasing the viscosity of

the filtrate. Post-mortem measurements confirmed the strong adsorption of polyamine, despite its relatively small molecular weight; being cationic, polyamine is readily adsorbed on the clay particles and is therefore retained in the clay although its small chains suggest that it could be transported through the clay. Experiments with *PAC* suggested that its chain size was too large to invade the clay, and as a result, *PAC* did not reduce water ingress significantly. If the polymer chains are sufficiently small to allow advective transport of the polymer through the clay, the reduction of water invasion appears to correlate with the viscosity of the filtrate, as was shown when using glycol solutions of different concentration.

Lal (1999) concurs with the idea that most polymers are too large to penetrate shales, but that low molecular weight products might achieve the desired permeability reduction. He further suggests that cationic polymers are strongly adsorbing and could (in the extreme) isolate the clay by creating an impermeable hydrophobic seal. Audibert *et al.* (1999) report core flow experiments on saturated sandstone samples with porosity of approximately 17%. The fluid loss polymers used were *PAC* (0.5-3g/l), starch (0.5g/l) and xanthan (1g/l). Retention and adsorption of the polymer was measured in all cases, and the associated plugging of the pores with polymer chains resulted in significant permeability reduction. They argued that starch performed better as a fluid loss reducer than *PAC*. These results show that while some polymers may not achieve the desired reduction of permeability in shale or in clay, they may prove efficient on coarser material like sandstone, which supports the conclusion of Ballard and co-workers.

A rationalisation of these contradicting observations was provided by Denys (2003). In a detailed study on dissolved polymer flow through porous media, Denys reviewed the mechanism of the permeability reduction due to adsorbed polyelectrolytes. The flow of polymer solution in porous media is governed by both physical and chemical interactions: dissolved polymer molecules may coil, cross-link, elongate and break as a result of the imposed flow conditions. Polyelectrolytes may stretch as a result of the repulsive forces between their functional groups, or in contrast, when in the presence of a small amount of multivalent cations (like  $\text{Ca}^{2+}$ ,  $\text{Mg}^{2+}$  and  $\text{Al}^{3+}$ ) the chains may cross-link with covalent bonds and form aggregates. The pH and salinity of the water in which the polymer is dissolved may thus have a marked effect on the hydrodynamic radius of the polymer, and, in turn, on the flow regime of polymer in porous media. Denys summarises the interaction mechanisms between polymer and porous media as follows: three different regimes of polymer flow in porous media may be distinguished depending on the relative magnitude of the characteristic pore

radius  $R_h$  and the hydrodynamic coil radius  $R_p$  of the polymer. Retention mechanisms differ for low permeability porous media, high permeability porous media, and intermediate permeability between these two regimes. The salient characteristics of the three regimes can be summarised as follows:

- If the pore size  $R_h$  is smaller than the polymer coil diameter  $R_p$ , the retention mechanism is called mechanical entrapment. If, as illustrated in Fig. 2.19, a layer of polymer has previously been adsorbed on the pore wall, mechanical entrapment can occur if  $R_p > 3R_h$ . This mechanism occurs at any flow rate, and the penetration depth of the polymer is relatively shallow if mechanical entrapment occurs and the retention may take place both under adsorption and non-adsorption conditions.
- In high permeability porous media ( $R_p < 50R_h$ ), experimental evidence suggests that mechanical retention by filtration in pores is negligible. Polymer retention may then only occur by adsorption, if the polymer has a tendency to adsorb on the porous medium. Adsorption may only proceed until complete saturation of the mineral surfaces, after which, stationary flow conditions prevail, hence without reduction of permeability. Newtonian, shear-thinning and shear thickening flow regimes are then observed depending on the shear rate and the viscosity of the polymer solution.
- A retention mechanism specific to intermediate permeability ( $3R_h < R_p < 50R_h$ ) has been identified by Zitha *et al.* (1998). Interestingly, permeability reduction is low at lower shear rate, but above a critical rate, the permeability to the polymer solution reduces steadily with time of injection. Fig. 2.20 depicts the mechanism that was proposed by Denys & Zaitoun to explain this observation: beyond a critical flow rate, the polymer coils begin to stretch and the elongated chains begin to bridge the pores by adsorption. The process proceeds as long as free adsorption surfaces remain, giving rise to the continuous permeability reduction with injection time. This mechanism was coined bridging adsorption. Higher plugging rates were observed with solutions of higher polymer concentration, the plugging rate decreases when decreasing the core permeability and, importantly, the phenomenon is absent under non-adsorbing conditions.

### *Silicates*

Recent research has indicated changes in the physicochemical nature of clays after exposure to high *pH* silicates (Bailey *et al.*, 1998). Soluble sodium or potassium silicates exist as metastable silicate monomere or oligomere in high *pH* solutions. When the solution invades the shale and mixes with the pore fluid, the solution *pH* drops and precipitation reactions as well as polymerisation occur. A silica gel may be formed, causing a reduction in permeability due to plugging of the shale pore, together with some strengthening of the formation as the precipitate cements grain contact. Bailey *et al.* (1991) also report ageing tests on a pure grade of kaolin (Supreme *ECC*) when exposed to silicate fluids. X-ray diffraction analysis revealed a redistribution of clay mineral species and the formation of aggregates which are believed to be responsible for the permeability reduction. Field experiences reported by Bailey *et al.* (1998) suggest that the silicate systems are efficient shale inhibitors and that well bore stability was excellent over long periods when using silicate systems. The drop in permeability/flow rate observed with silicate is slower, and a reduction of about 20% of the initial value is measured over a period of 70 days. The results are shown in Fig. 2.21. Silicates were reported to be superior to other water-based drilling fluids but comparatively little research and experimental evidence is available to encourage their application.

#### 2.4.4.2 Osmotic potential

The reduction of the shale permeability or the provision of an impermeable membrane at the shale/drilling fluid interface is not the only way in which the rate of water ingress into the shale formation may be reduced. In addition to increasing the resistance to the flow by reducing permeability, the actual gradient driving the pore water flow can be altered. As Mitchell *et al.* (1973) and Yeung & Mitchell (1993) pointed out, the hydraulic gradient (§ 2.3) is not the only force responsible for water movements in soil; Table 2.2 gives a summary of the direct and coupled flow phenomena that may occur in soil. While hydraulic gradient gives rise to (Darcy) flow of pore fluid, chemical gradient may, under certain conditions, induce a coupled flow of pore water (osmotic flow) or a direct flux of ions (diffusion). Chemical gradients across the cavity boundary can be created by varying the concentration of salts (*NaCl*, *KCl*, *CaCl<sub>2</sub>*) in the drilling fluid. If the salt concentration of the drilling fluid exceeds that of the pore water of the shale, the resulting chemical potential will drive water from the shale towards the drilling fluid to restore chemical equilibrium. If the flow is impeded, the osmotic potential will result in a pressure that will counterbalance the applied hydraulic pressure and contributes to stabilize the

wellbore (Chenevert, 1970). The osmotic potential may significantly reduce the water ingress into the cavity and, under extreme conditions, even promote fluid flow from the shale into the drilling fluid.

The processes leading to chemomechanical equilibrium depend on the ability of the ions to move through the pores of the clay. The clay is said to behave as an ideal semi-permeable membrane if solvent can flow through its pores while the ion transport is wholly restrained. Schlemmer *et al.* (2003) postulated that three types of membrane behaviour may be distinguished: (1) membranes allowing coupled flows between the drilling fluid and the shale; (2) membranes restricting the flow of both water and solute, and (3) membranes allowing the partial passage of solutes (a leaky membrane). The leakiness of a membrane is quantified by its efficiency,  $\sigma$ , where  $\sigma = 0$  characterises a membrane through which solute species may flow unrestrained, while  $\sigma = 1$  characterises an ideal semi-permeable membrane allowing only the passage of solvent. If ion transport is only partially impeded ( $0 < \sigma < 1$ ), ionic species will migrate from the dilute to the concentrated side of the membrane. When shale is in contact with a salt-based drilling fluid, this will result in counter-current flows of water and solute, hence with advective flow of solutes opposing diffusive transport. When cation exchanges occur simultaneously, the coupled processes become intricate and prediction of the net effect on cavity behaviour become difficult.

Two cumulative conditions must be fulfilled for the osmotic pressure to improve the stability of a well-bore. Firstly, a chemical concentration imbalance must exist between the shale pore fluid and the drilling fluid. Secondly, a membrane with efficiency greater than zero must exist between the dilute and concentrated fluids. The membrane may be either natural or formed by the interaction between the drilling fluid and the shale. The ability of clay to act as a membrane results from overlapping electrical double layers, and therefore depend on the pH and salinity of the pore water, as well as on the valence of the counter-ions and the voids ratio of the clay. Some authors presented evidence that clay acts as a semi-permeable membrane (Horsund, *et al.*, 1998), while others (Ballard *et al.*, 1994) argue that osmotic processes play no part in the control of water ingress.

The relative significance of ion and water transport depends on the ability of ions to move through the soil. When clays behave as leaky semi-permeable membranes, the two processes occur simultaneously and the attribution of the observed macroscopic effects to one of the cause only is difficult. For example, the change of chemical potential at the boundary of a soil element which does not behave as an ideal membrane will cause water to be expelled under the effect of osmotic potential and,

under certain circumstances a net diffusion of ions into the soil element. The ions will affect the clay minerals and cause further volume change as they affect the intra and interparticle forces.

The role played by osmotic effects in producing volume changes was measured by Barbour & Fredlund (1989). Samples of clay were preconsolidated to 200 kPa in a modified oedometer. Upon reaching equilibrium, the surfaces of the specimen were exposed to 4.0 molar NaCl solutions at atmospheric pressure. Clay specimens were prepared from slurries (water content 10-20% above liquid limit) of reconstituted natural soil (Regina Clay, predominantly a Ca-montmorillonite; IP: 51.2%) and a mixture of 20% montmorillonite clay and Ottawa sand. Following a total stress increment from 100 to 200 kPa, the upper surface of the clay was exposed to the electrolyte. The electrolyte caused a huge increase in the rate of consolidation, compared to the rate that prevailed following the application of the total stress increment.

Santamarina & Fam (1995) report similar observations on tests performed with kaolin and bentonite exposed to 4.0 molar KCl solutions at their drainage boundary. Exposing the surface of a saturated kaolinite (Peerless Clay, IP = 35%) specimen after equilibrium was reached under an effective stress of 610 kPa, caused the void ratio of the specimen to reduce from  $e_o = 0.95$  to  $e_f = 0.88$ . This effect was naturally more pronounced when using clay of higher reactivity, such as bentonite. When using bentonite, an excess pore water pressure front was observed, with magnitude in excess of two thirds of the effective stress, as a result of the change in chemical boundary conditions.

A recent study of shale-fluid interactions have been reported by Ewy & Stankovich (2002) and reinforce the conclusions made by others. They consolidated 12 mm-thick natural and saturated shale samples to hydrostatic effective stresses ranging from 10 to 30 MPa. Upon reaching equilibration (zero pore water pressure), the top surface of the sample was exposed to a combination of test fluids of different activities. Two of the four shale samples tested contained 40% kaolinite (the remainder was mixed illite/smectite) material and the test fluids were prepared at solutions of inorganic salts ( $NaCl$ ,  $KCl$  and  $CaCl_2$ ) in deionised water and in concentration ranging from zero to approximately 30%. The pressure of the test fluid at the boundary was generally 6.9 MPa. Pore water pressure was measured in the clay as well as radial and axial swelling. Although these pressures are beyond those attained in conventional tunnelling, some interesting conclusions may be drawn from their research. The main observation is that the pore water pressure measured at the bottom surface of the

sample at equilibrium was less than the applied fluid pressure at the top surface. This fluid pressure gradient across the 12-mm thick sample was sometimes sustained for a period of five days before gradually decreasing with time, and is thought to be a direct measure of the osmotic effects. This gradient was found to be dependent on the shale and fluid type, as well as on the cation concentration. No difference was measured when using deionised water as the pore fluid but up to 2 MPa was measured when using a 32% solution of  $CaCl_2$  in contact with a shale containing kaolinite as well as mixed layers of illite and smectite. Chemical analysis confirmed that the mode of transport of the cation was also diffusive and not only advective. The main conclusion from these tests is that osmotic forces can maintain shale pore water pressure at a value less than the applied fluid pressure for several days.

Reduction of water invasion by altering the activity of the drilling fluid was demonstrated in a wellbore simulator by Bailey *et al.* (1991). They measured a reduction in water invasion using KCl brines of different concentrations. Cations were found to invade the shale, hence demonstrating that the particular shale used does not behave as a perfect ion exclusion membrane.

The significance of chemical osmosis in clay materials has long been recognised (*e.g.*: Mitchell *et al.*, 1973 or Barbour & Fredlund, 1989) and recent reviews are provided in Keijzer (2000), Olsen (2003) and in chapter 9 of Mitchell & Soga (2005). Experimental evidence on stresses and strain changes in soil due to osmotic potential are presented in Barbour & Fredlund (1989), Santamarina & Fam (1995) and Fam & Santamarina (1996), and di Maio (1996), while the chemical effect on well-bore stability has been discussed by Hale *et al.* (1993), Mody & Hale (1993), Sherwood & Bailey (1994), Bailey *et al.* (1994), Hunag & Hale (1998), Fam & Dusseault (1998), Ewy & Stankovich (2002) and Schlemmer *et al.* (2003). Analytical contributions to the problem of chemo-mechanical coupling in well-bore stability are presented in Sherwood & Bailey (1994), Lomba *et al.* (2000), and Chen *et al.* (2003), amongst many others.

#### 2.4.4.3 Cation exchange processes and interparticle forces

When not impeded by an ideal semi-permeable membrane, ions may be transported into the shale by diffusion or advection. Ion migration affects their concentration in the pore water and, in turn, the electrostatic interactions between the clay particles. It has long been recognised that an increase in the pore water salinity may affect the electrical double layers and that exchanges of cations will greatly affect swelling characteristics of the clay (Ladd, 1960). Change of ion distribution in

the vicinity of the clay particle surfaces as well as cation exchange processes give rise to significant changes of the clay state and engineering properties. Volume change in clays may occur as a result of increased ionic concentration of the pore fluid. Permeability of the clay may be greatly affected, and changes of stiffness and strength have also been widely reported. The significance of such effects increases with the activity of the clay and the cation exchange capacity of the mineral, and while Mitchell *et al.* (1973) pointed out that they tend to be rather small in kaolin clay, some evidence showed that they are sometimes non-negligible. Osho (1970), for example, carried out an extensive study on kaolin samples initially mixed with electrolytes and reported “surprisingly” large influence of some electrolytes on the mechanical behaviour of kaolin.

Horsrud *et al.* (1998) report triaxial tests on a Palaeocene shale cored at 1870 m depth and containing 42.8% smectite. They measured undrained shear strength and volumetric strain as well as changes of permeability resulting from exposure to *KCl* solutions at concentrations ranging from 1 to 20%. Upon exposure to the *KCl* solutions (without hydraulic pressure gradient), the sample was found to shrink. For larger concentrations of *KCl*, the tests suggested that the final magnitude of volume change was independent of the salt concentration and that only the rate of shrinkage was affected by the salt concentration. This is attributed to substitution of potassium ion with other exchangeable cations initially adsorbed on the clay structure. The ions are usually sodium or calcium and because potassium ions are significantly smaller this causes the structure to shrink. Exposure to *CaCl<sub>2</sub>* and other salts showed negligible effects, indicating that the process is governed by the type of ion and not only their concentration in the solution. Tensile stresses in the microstructure are believed to cause some cracks and opening of channels at micro-scale as well as bond breakage. While the permeability of the shrunk shale specimen would be expected to reduce as it shrinks upon exposure to *KCl* solutions, the reverse is clearly observed. The permeability increases steadily upon exposure, reaching a final value 2.6 times the initial permeability. Horsrud *et al.* (1998) summarise: when exposed to *KCl* solution, the clay shrink and the cemented bonds are disrupted. Shrinkage has been shown to increase the permeability of the clay significantly, in turn increasing convective solvent flow and thus advective transport of ions, contributing to the enlargement of the influenced zone around the borehole. In addition, undrained triaxial test performed on the *KCl* exposed shale indicated a 30% reduction in peak strength compared to reference tests performed with deionised water as pore fluid. No semi-permeable membrane behaviour, nor osmotic transport and associated excess pore water pressure, was observed in these tests.

Bailey *et al.* (1998) carried out constant head (8 MPa) permeability tests on Oxford clay (30% Illite, 18% kaolinite) under an isotropic confining stress of 8.6 MPa. It was found that with 1.4M *KCl*, the permeability of the core increases by approximately 20%.

The net effects of *KCl* exposure on the stress distribution around a borehole have been discussed by Horsrud *et al.* (1998). While it has been recognised that time-dependent shrinkage (stabilising), strength reduction (destabilising) and permeability increase (destabilising) occur as a result of ion diffusion into the clay, there is no conclusive evidence as to the net effect on the transient cavity behaviour. They suggested, however, that ionic diffusion is expected to be slower than the consolidation process; however, advective ion transport may occur under hydraulic gradient, which may in turn affect the rate, the effects being due to ion exchange. Because *KCl* has both a stabilising and destabilising effect on the borehole, both depending on *KCl* concentration, it has been suggested that an optimum *KCl* concentration should exist to maximise benefits in terms of borehole stability.

#### 2.4.5 Summary

- The drilling fluids used for oil exploration are similar in composition to pipe jacking lubricants. One of the main function of these fluids is to ‘inhibit swelling’ of the shale/clay around the borehole.
- Basic components of water-based drilling fluids and lubricants are bentonite, polymers, salts and silicates. Among the huge number of existing components, *PHPA* and *PAC* are two of the most commonly used polymers. Salts such as *KCl*, *NaCl* and *CaCl* are often added to bentonite or to polymer-based drilling fluid. High pH sodium or potassium silicate drilling fluids have recently been used in drilling fluids but their application to pipe jacking has not been reported.
- Attempts to reduce swelling focuses on decreasing the rate of water ingress from the borehole into the pores of the soil in the near-cavity region. This can be achieved by increasing the viscosity of the filtrate, by reducing the permeability of the soil, by altering the gradient driving the flow into the pore water or by any combination of these mechanisms.
- Reductions of the clay permeability may be achieved with polymers and silicate fluids. Three mechanisms lead to the reduction of permeability due to polymer invasion into porous material, and there is substantial evidence showing that their

---

relative significance depends on the hydrodynamic radius of the polymer chain relative to the pore size of the clay, as well as on the adsorption potential of the polymer onto the clay particles.

- The main polymer properties governing their interaction with clay are the molecular weight (or chain length) and the charge distribution along the polymer chain. *PHPA*, for example, can therefore display a range of different behaviour when mixed with clay, depending on the degree of hydrolyses (which determines its ionic strength) and its molecular weight.
- Highly alkaline potassium or sodium silicate fluids were shown to precipitate and polymerise upon reduction of the solution pH. When this happens in the clay matrix, a gel may form and bond clay particles together in a way that decreases permeability. Although this process is slow, promising field experience has been reported from the oil industry.
- In addition to permeability reduction, the inhibition of shale swelling in well bore drilling focuses on the use of osmotic effects (so-called balanced activity drilling). High-salinity drilling fluids are used to induce a chemical potential or concentration gradient across the cavity wall. In cases where the clay or the clay-fluid mixture in the near-well bore region acts as a semi-permeable membrane restricting the migration of solute into the shale, osmotic flow will counteract hydro-mechanically induced Darcy flow, and hence reduce ingress of pore fluid into the cavity.
- In the absence of membrane behaviour, ions will diffuse into the clay by advection or diffusion. Cation exchange processes and changes in electrostatic interaction between the clay particles will often cause shrinking of the clay matrix, but this is usually accompanied by strength deterioration and significant permeability increase.
- Despite the wealth of data collected in physical experiments on clay-chemical interactions, no consensus has been reached as to the effect of a particular drilling fluid component on the behaviour of contracting cavities. The difficulty arises from the coupling of the different physicochemical and mechanical processes discussed in § 2.4.4. This is complicated by the fact that drilling fluids are almost invariably designed as a multi-component fluid. The effect of each component on the clay behaviour cannot be superimposed, because synergetic or antagonistic effects often arise when mixing two or more chemical components. The salinity

and the pH of the pore water and the solvent also influence the clay-chemical interactions.

## 2.5 Conclusions

This review of the mechanisms and processes by which lubricants affect the interactions between the soil and the pipe can be summarised as follows:

### Field observations (§ 2.2)

- Field experiences in pipe jacking lubrication are relatively seldom reported in the literature. The prominent observation when comparing jacking records from different projects is the wide scatter of unit jacking forces, with magnitude ranging from 2 to over 55 kN/m. A number of projects clearly demonstrated the potential benefits of effective lubrication: drives with length of 500 m or more have been jacked without the need of intermediate jacking stations or shafts and with production rates of 30-40 m per day.
- The variability of the operating variable over time and chainage renders the back-analysis of these jacking forces difficult. As a result, it is still unclear whether the small jacking forces observed under certain circumstances are a result of the lubricant composition, the injection location and frequency or the injection pressure. The legacy of these uncertainties is the lack of robust guidelines for the estimation of jacking forces accounting for the overcut magnitude around the pipes and for the lubrication schemes.
- Field or experimental evidence of the effect of polymeric lubricant or swelling inhibitor additives is almost inexistent. The net effect of such products is uncertain, and therefore, their use in practice remains sporadic. Similarly, the injection pressure of the lubricant is rarely documented and no confident conclusions can be drawn as to their effects.

### Ground response to cylindrical cavity contraction (§ 2.3)

- Because of the time-scale of construction, the pipe-soil interactions controlling the jacking forces are usually determined by the ground loading in partially drained conditions. The prediction of transient ground loading is particularly arduous to tackle theoretically as a result of the mixed boundary conditions that prevail during the consolidation around the pipes. The difficulty with the boundary conditions result from the initial gap around the pipe, from the variable

---

pressure of lubricant in the overcut and from the finite permeability of the cavity boundary.

- Accurate predictions of transient pipe-soil stresses require a correct estimation of both the initial excess pore water pressure distribution as well as the subsequent dissipation rate. The choice of a representative constitutive model was shown to be important; ideally, a model needs to deal with the ground in terms of effective stresses, accounting for strain-hardening/softening of the soil, and for large strains in the vicinity of the cavity. In addition, modelling nonlinear seepage flow with a stress-dependent coefficient of permeability was shown to yield more accurate predictions of the pore water pressure regime around the cavity.
- Some sophisticated 3D analyses (not reviewed here) modelling TBM advances can take a comprehensive list of factors into account, but there is still a lack of combination of simple physical and numerical modelling simulating the transient tunnel-lining stresses in plane-strain conditions. This is also true for the case where a gap initially surrounds the pipe or tunnel lining.

#### **Physicochemical interactions near the excavation boundary (§ 2.4)**

- A wealth of literature reports the effects of drilling fluid/lubricant components on a range of natural and reconstituted clay materials in the context of wellbore stability in the oil and gas industry. The response of clay samples to combined changes of hydraulic or chemical boundary conditions have been measured in permeability, swelling, triaxial or core-flow experiments. Contradicting effects have sometimes been reported, notably when measuring the permeability reduction of natural shale samples to different polymers. While abundant literature exists on the physicochemical interaction between clay and polymers, there is still a lack of understanding as to their implication on the engineering properties of the mixtures.
- Several interaction mechanisms have been identified and extensively studied, especially in the context of shale swelling inhibition around well bores. However, the relevance of each of the mechanisms for conditions beyond the range at which they were observed is still uncertain. In addition, the relative significance of each mechanism under different conditions of stress and clay mineralogy has not been established with confidence. In particular, the significance of the mechanisms of osmotic pressure and cation exchanges in pipe jacking is not fully

---

understood. The question of whether these processes are relevant at the pressure and the time-scale relevant to conventional tunnelling remains open.

- Swelling and permeability tests have sometimes generated contradicting results. This is thought to be the result of one or a combination of: (1) the variability of the test conditions and procedures, (2) the fact that the measured strains are often very small due to the large stiffness of the shale in unloading, (3) the variability of the natural shales on which tests are performed, (4) the wide range of test conditions, (5) the sensitivity of the clay mineralogy as well as the fluid and pore water pH and salinity.
- Models accounting for coupled hydromechanical and physicochemical processes of solvent and solute transport around the boreholes have been suggested. These models sometimes overlook the elasto-plastic nature of soil and the large gradients of pore water pressure that are generated around the cavity during undrained unloading. In addition, these approaches are never concerned with the stress build-up on a radial support, which is the problem at issue in pipe jacking.

Therefore, several aspects of the problem of stress build-up on pipes initially surrounded by an overcut containing drilling fluids require further investigation. The current state of knowledge does not allow reliable prediction (even qualitatively) of pipe-soil interactions when ‘lubricated’ with fluid of a given chemistry at different pressures.

Reference/ Project	Ground conditions	Pipe OD/ excavation diam.	Depth to axis m	Lubrication system	Lubrication	Unit jacking force: kN/m
Alexanderson (2001) Vibhavadi, Bangkok	Medium hard marine clay	3.04 3.20	12-14	Automatic, 3 ports every 15m	water	19 - 48
					bentonite	19 - 29
					polymer	4.8
Broomfield (2004) Minburi water pipeline, Bangkok	Soft Bangkok clay	1.625 n/a	approx. 5m	Automatic, 3 ports every 18m	bentonite	2.0 - 3.7
Milligan & Marshall (1998) Thurrock sewer system, UK	Soft to very soft silty/peaty clay	1.5 n/a	5.5 - 6.0	Second half of drive only	none	25
					bentonite	14
Milligan & Marshall (1998) Leytonstone sewer system, UK	Unweathered highly plastic firm to stiff London Clay	1.8 m	8.5	After 20m drive, but only at three occasions	none	12.7
					bentonite	
Milligan & Marshall (1998) Seaham sewer system, UK	Stiff glacial till (or clay)	1.8	7	n/a	none	48
					bentonite	15
Norris (1992) Honor Oak, UK	Stiff overconsolidated London Clay	2.27 n/a	11 - 21	none	none	54.4

Table 2.1. Summary of the reported pipe jacking projects

flow	gradient			
	hydraulic	temperature	electrical	chemical
fluid	hydraulic flow <i>Darcy's law</i>	thermo– osmosis	electro– osmosis	chemical osmosis
heat	convective heat flow	thermal conduction <i>Fourier's law</i>	Peltier effect	Dufour effect
current	streaming current	Seebeck effect	electric current <i>Ohm's law</i>	diffusion and membrane potentials
ion	streaming current	Soret effect	electro– phoresis	diffusion <i>Fick's law</i>

Table 2.2. Direct and coupled flow phenomena in soil  
(after Mitchell, 1993 and Keijzer, 2000)

POLYMER	CONCENTRATION (ppb)	SHALE	RATE BEFORE POLYMER (cm <sup>3</sup> hr <sup>-1</sup> )	RATE AFTER POLYMER (cm <sup>3</sup> hr <sup>-1</sup> )	RATE REDUCTION (%)
XANTHAN	0.5	OXFORD	0.254	0.262	
XANTHAN	1.5	OXFORD	0.215	0.222	
PAC	0.5	OXFORD	0.244	0.222	9
PAC	2.0	OXFORD	0.237	0.222	7
PHPA	2.0	OXFORD	0.287	0.214	25
PHPA (mw700.000)	2.0	OXFORD	3.01	0.180	40
PHPA	0.5	TERTIARY 8185'	0.0566	0.048	15
PHPA	2.0	TERTIARY 5790'	2.51	1.01	60
STARCH	2.0	OXFORD	0.304	0.209	31
STARCH	8.0	OXFORD	0.265	0.207	22
STARCH	2.0	TERTIARY 8185'	0.158	0.054	66
STARCH	3.5	TERTIARY 5790'	2.39	0.717	70
POLYAMINE	2.0	OXFORD	0.251	0.131	48
POLYAMINE	8.0	OXFORD	0.310	0.161	48
POLYAMINE	3.5	TERTIARY 8185'	0.0955	0.031-0.009	66-90
GLYCOL	3.0	OXFORD	0.284	0.203	26
GLYCOL	10.0	OXFORD	0.304	0.163	46
GLYCOL	10.0	TERTIARY 8185'	0.0496	0.033-0.016	34-67
GLYCOL	10.0	TERTIARY 5790'	2.68	1.8	32

Table 2.3. Test combinations and achieved permeability reductions  
(Ballard *et al.* 1994)

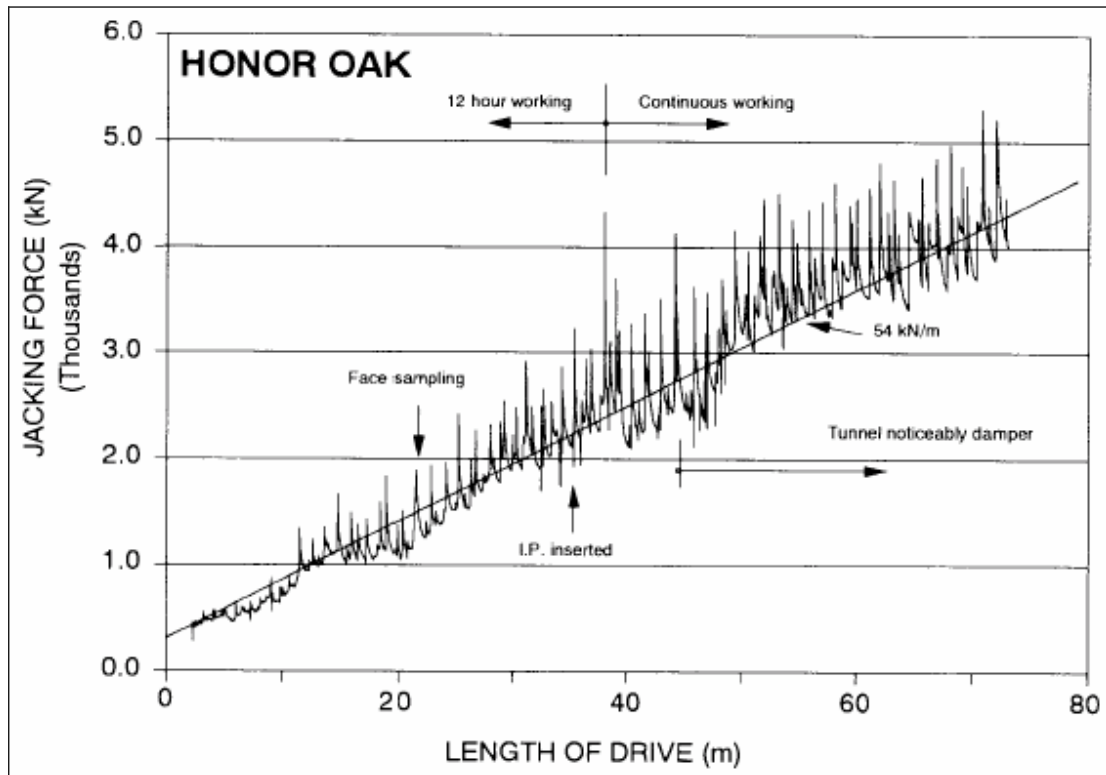


Fig. 2.1. Jacking record Honor Oak, London, UK (Norris, 1992)

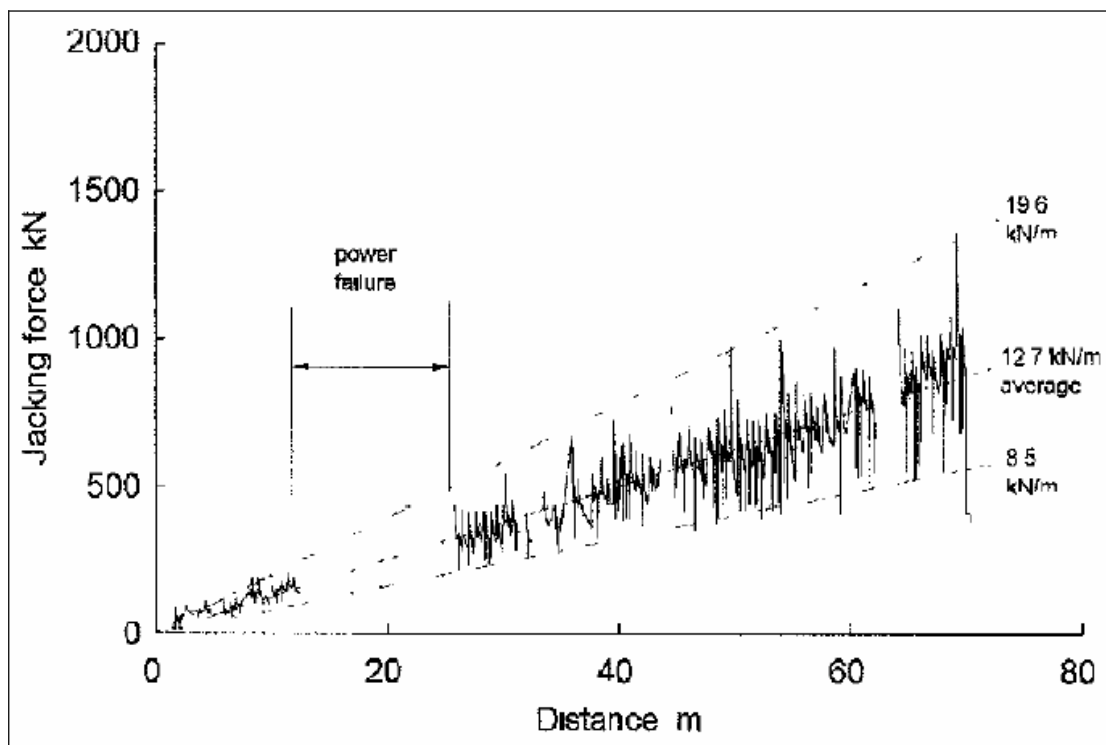


Fig. 2.2. Jacking record, Leytonstone, London, UK (Marshall, 1998)

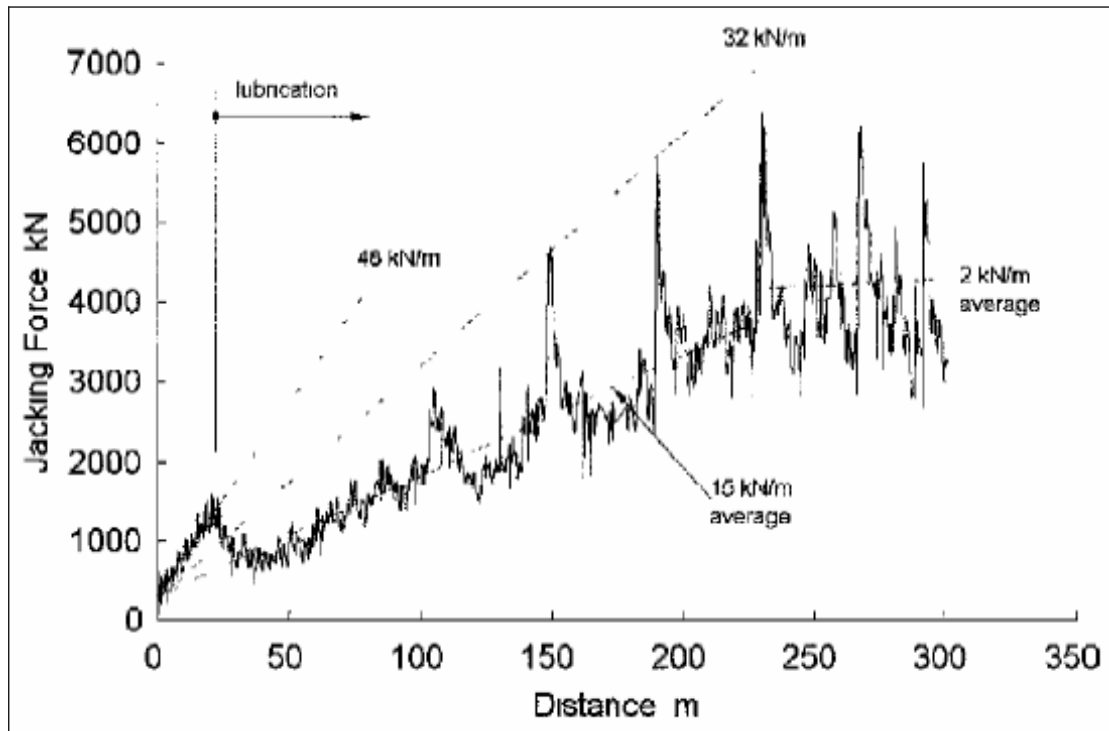


Fig. 2.3. Jacking record Seaham, UK (Marshall, 1998)

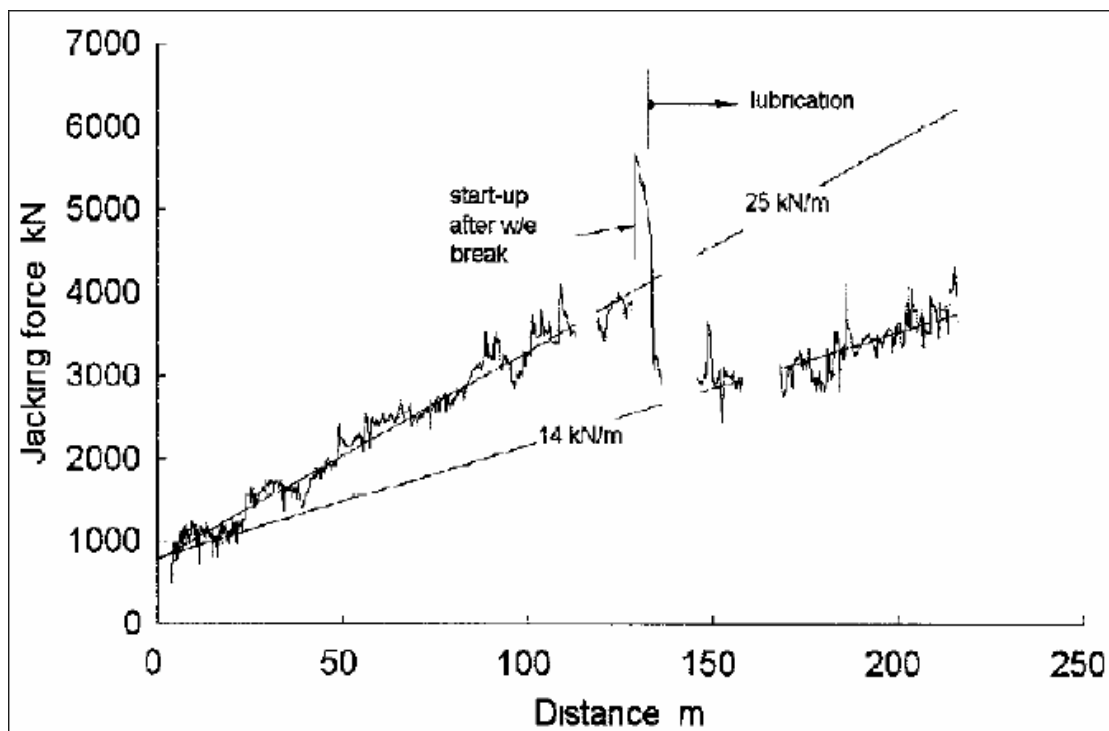


Fig. 2.4. Jacking record, Thurrock, UK (Marshall, 1998)

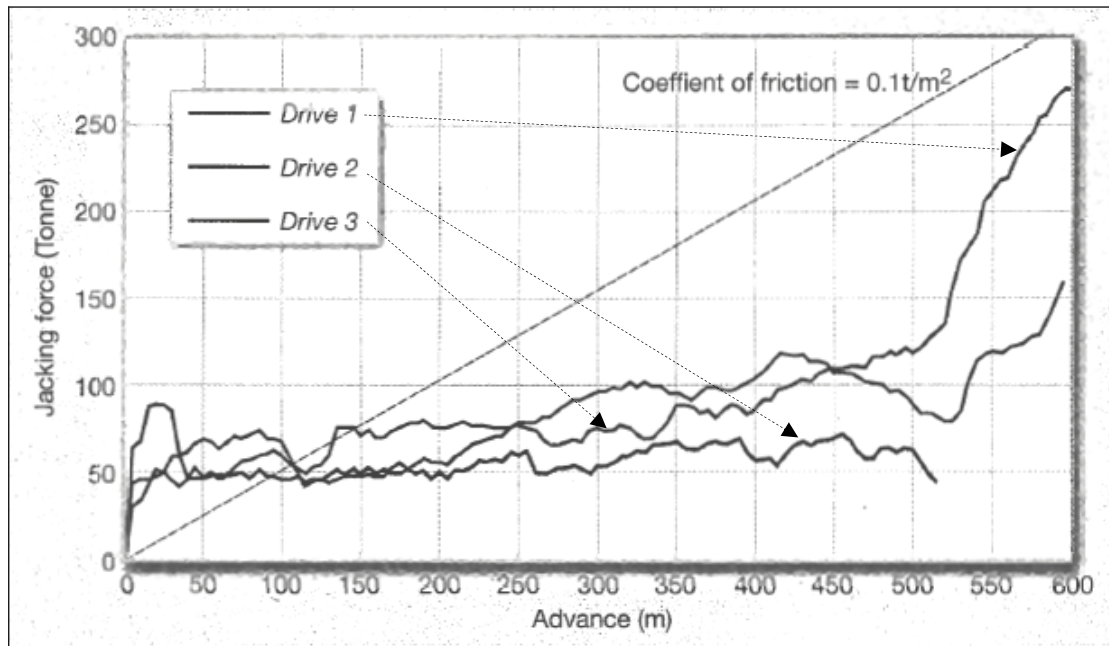


Fig. 2.5. Jacking record, Nimitmai, Thailand (Broomfield, 2004)



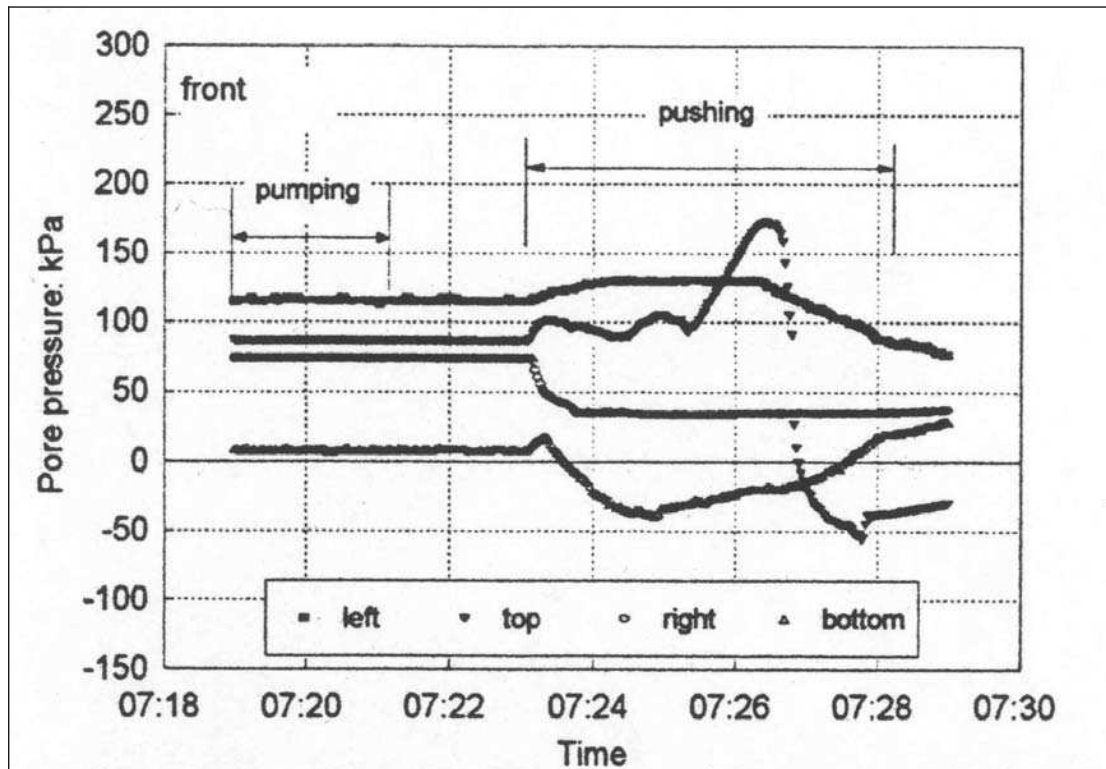


Fig. 2.7. Pore pressure variation at pipe front during lubricant pumping, Seaham, UK (Marshall, 1998)

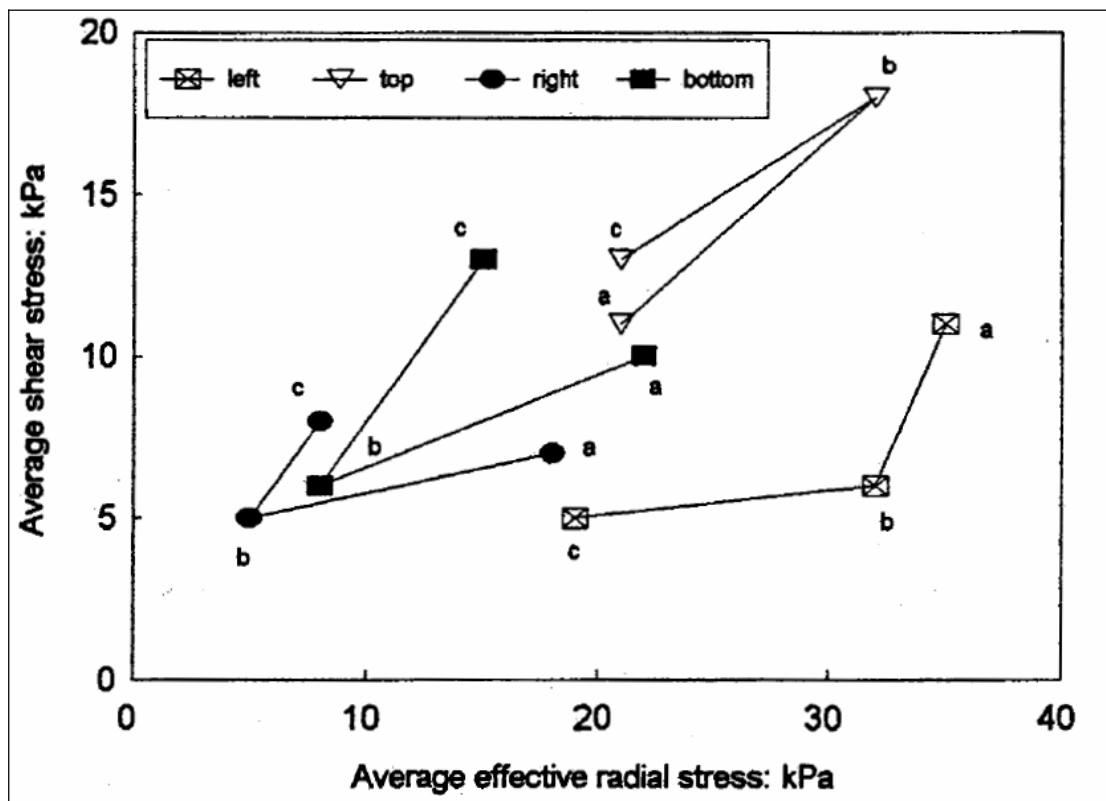


Fig. 2.8. Variation in average shear and effective stresses at the pipe centre, Seaham (Marshall, 1998)

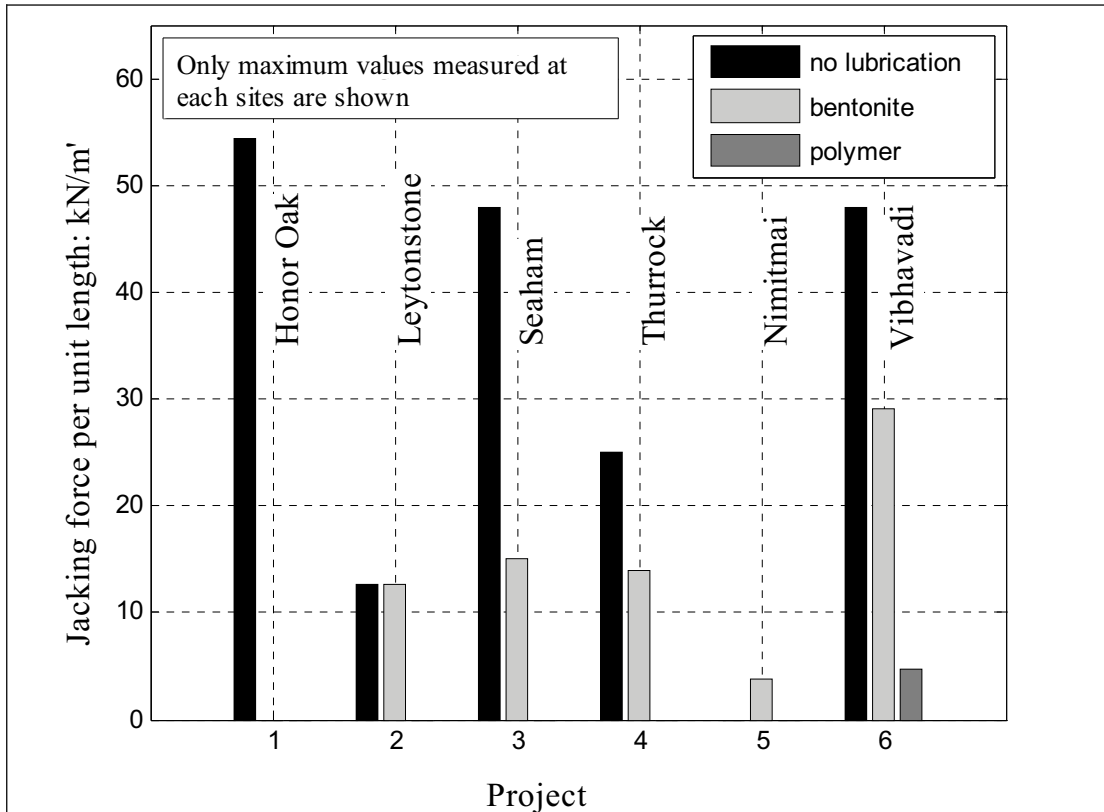


Fig. 2.9. Summary of unit jacking forces in different schemes

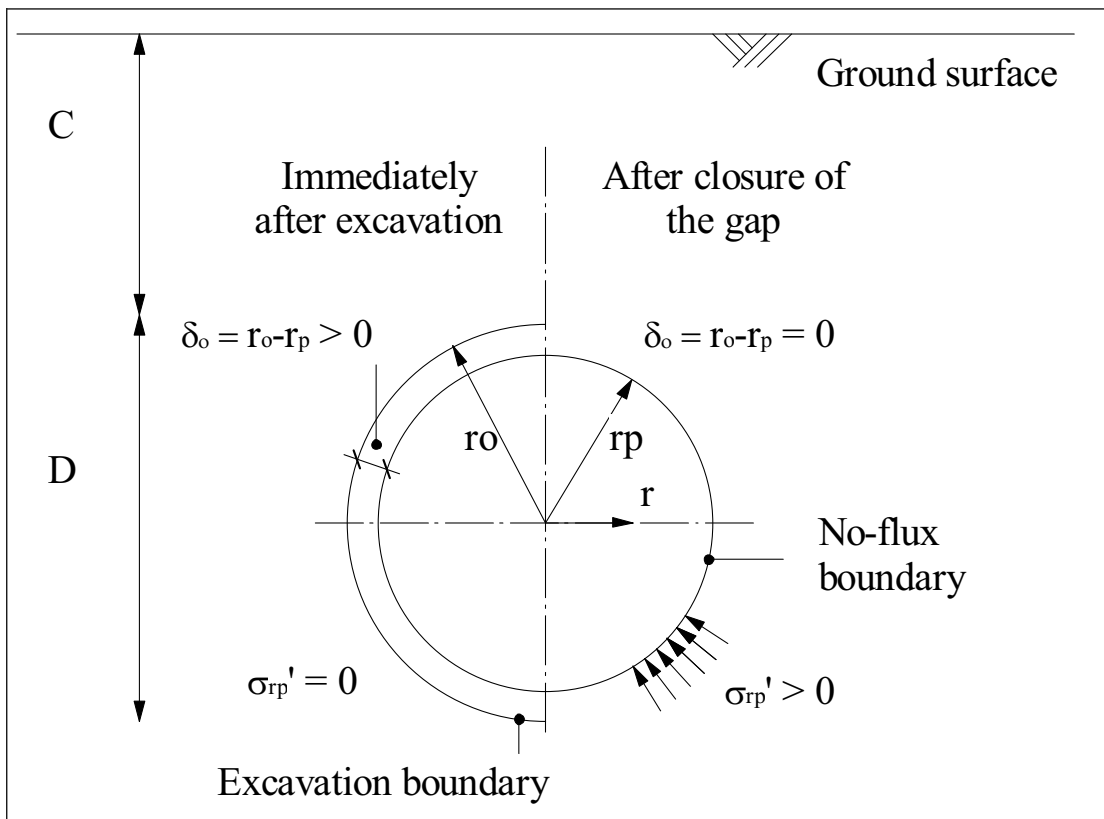


Fig. 2.10. Variable definition for cavity contraction

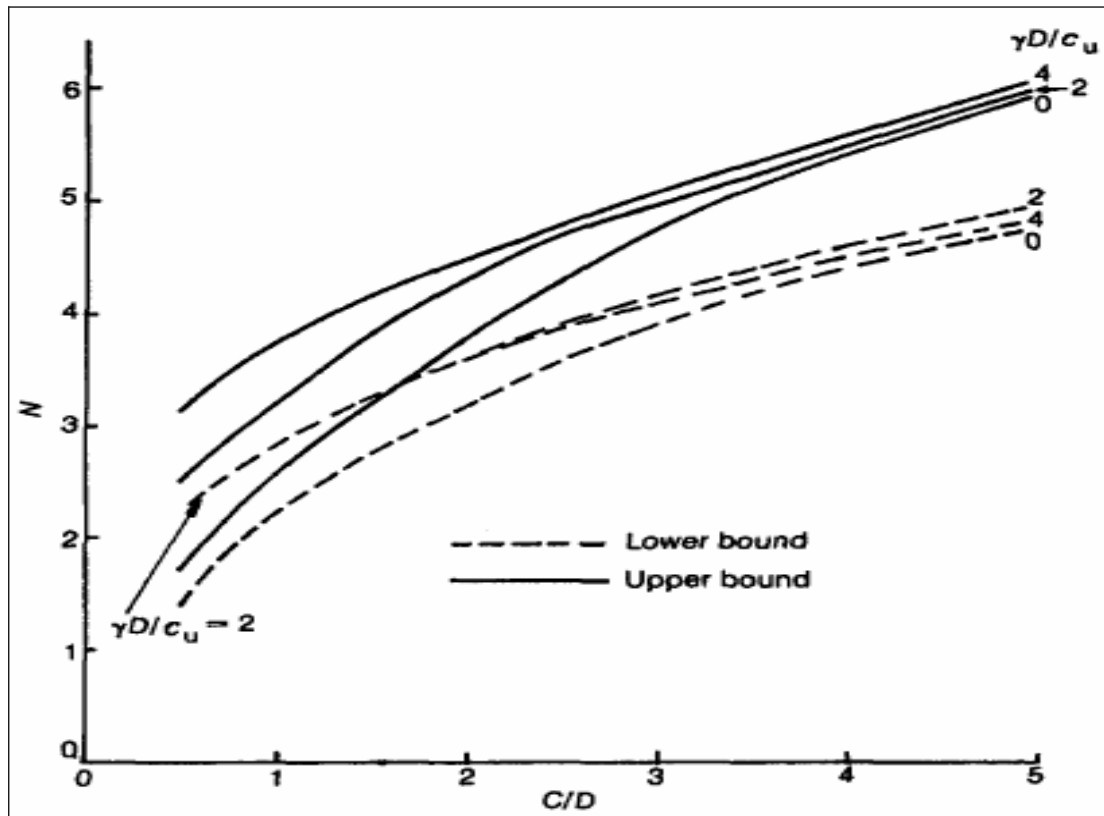


Fig. 2.11. Upper and lower bound stability ratios for plane strain circular tunnels (Davis *et al.*, 1980)

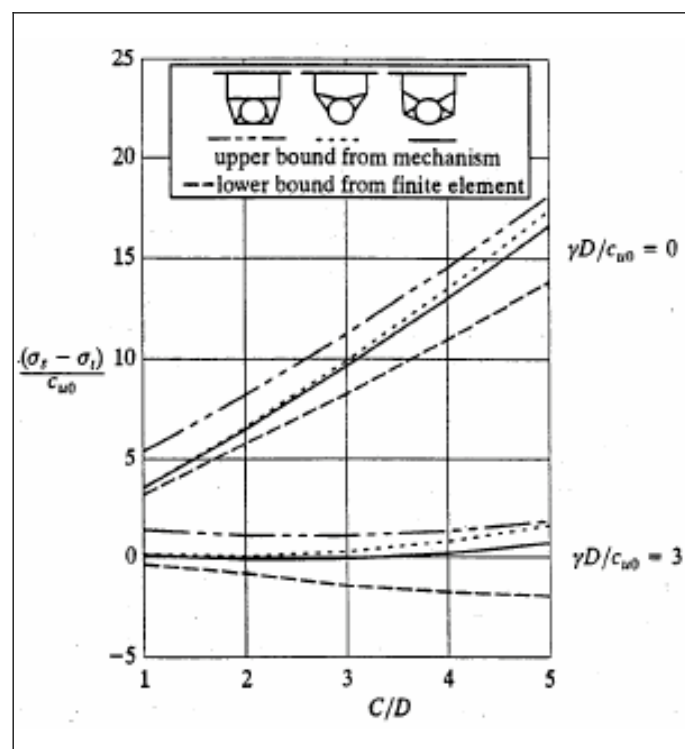


Fig. 2.12. Comparison of stability ratios for circular tunnels in soils whose undrained shear strength increases linearly with depth (Sloan & Assadi, 1993)

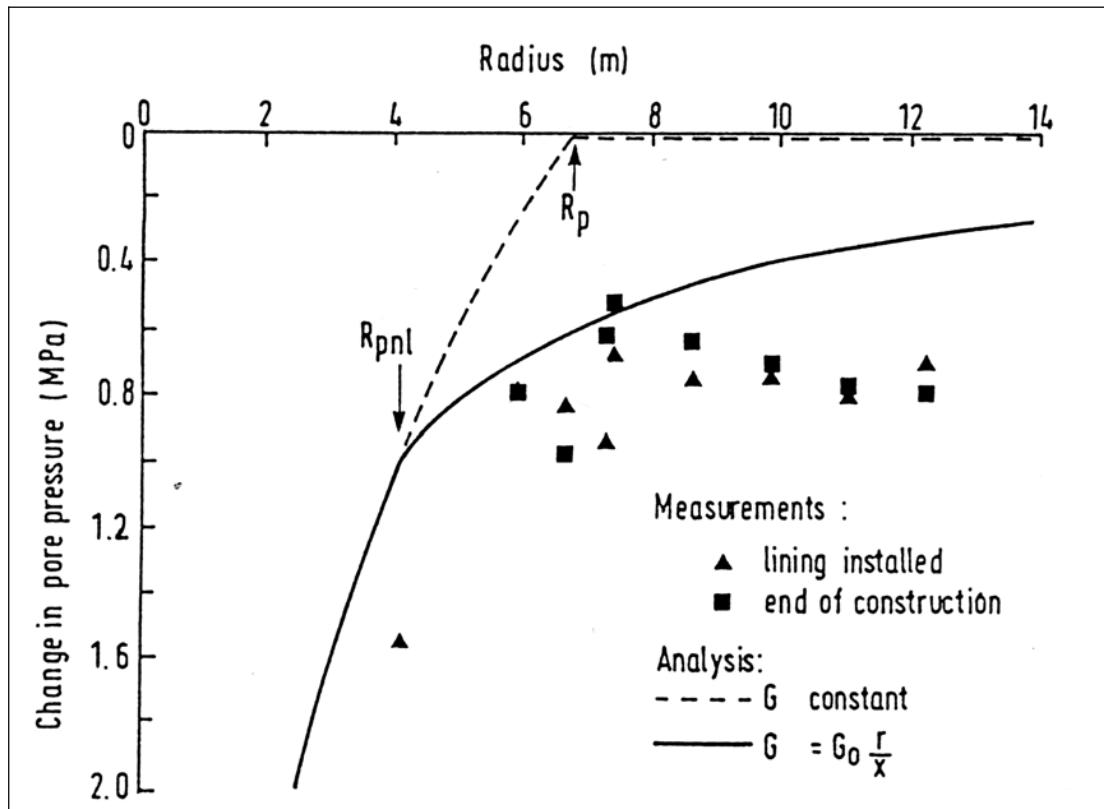


Fig. 2.13. Measured and predicted changes in pore water pressure around a deep tunnel in Boom Clay (Mair & Taylor, 1993)

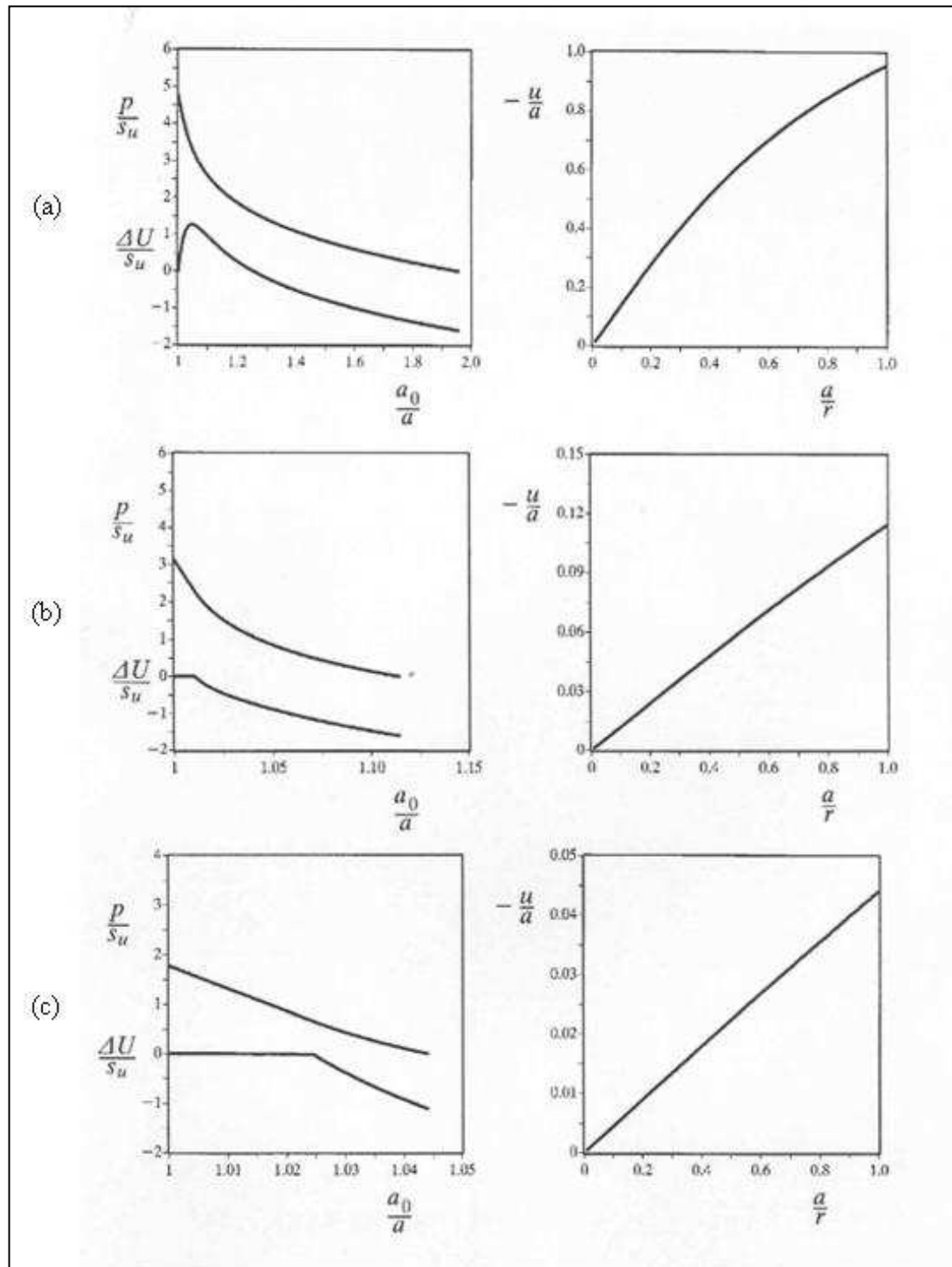


Fig. 2.14. Large-strain cylindrical cavity contraction solution for soil behaviour around tunnel in original Cam clay with OCR = 1.0 (a), 2.0 (b) and 5.0 (c) (Yu & Rowe, 1999)

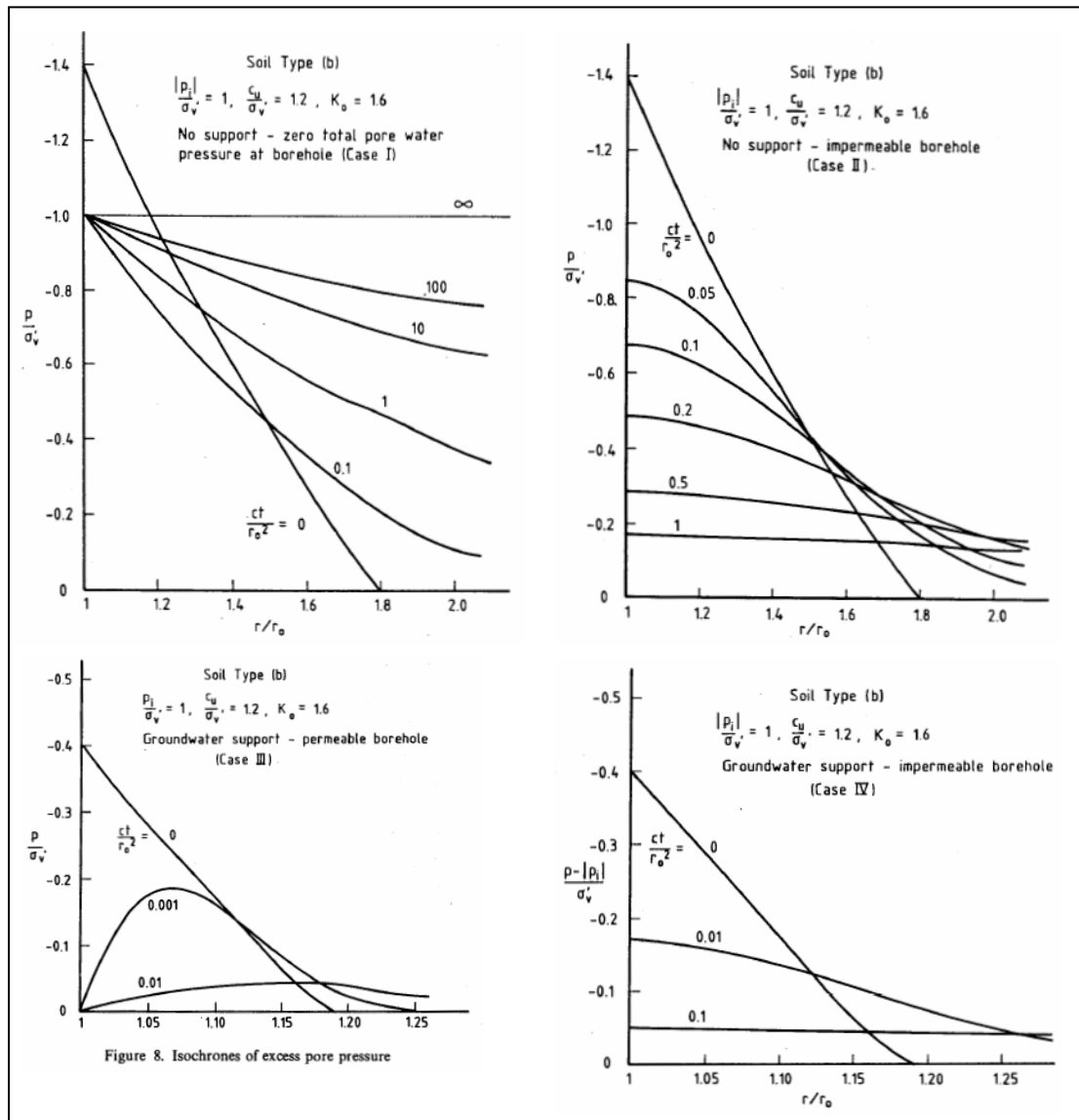


Fig. 2.15. Isochrones of excess pore water pressure for different sets of boundary conditions (Carter, 1988)

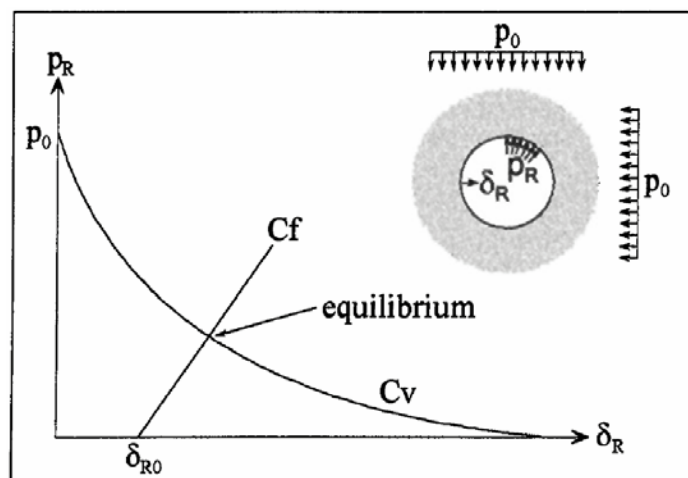
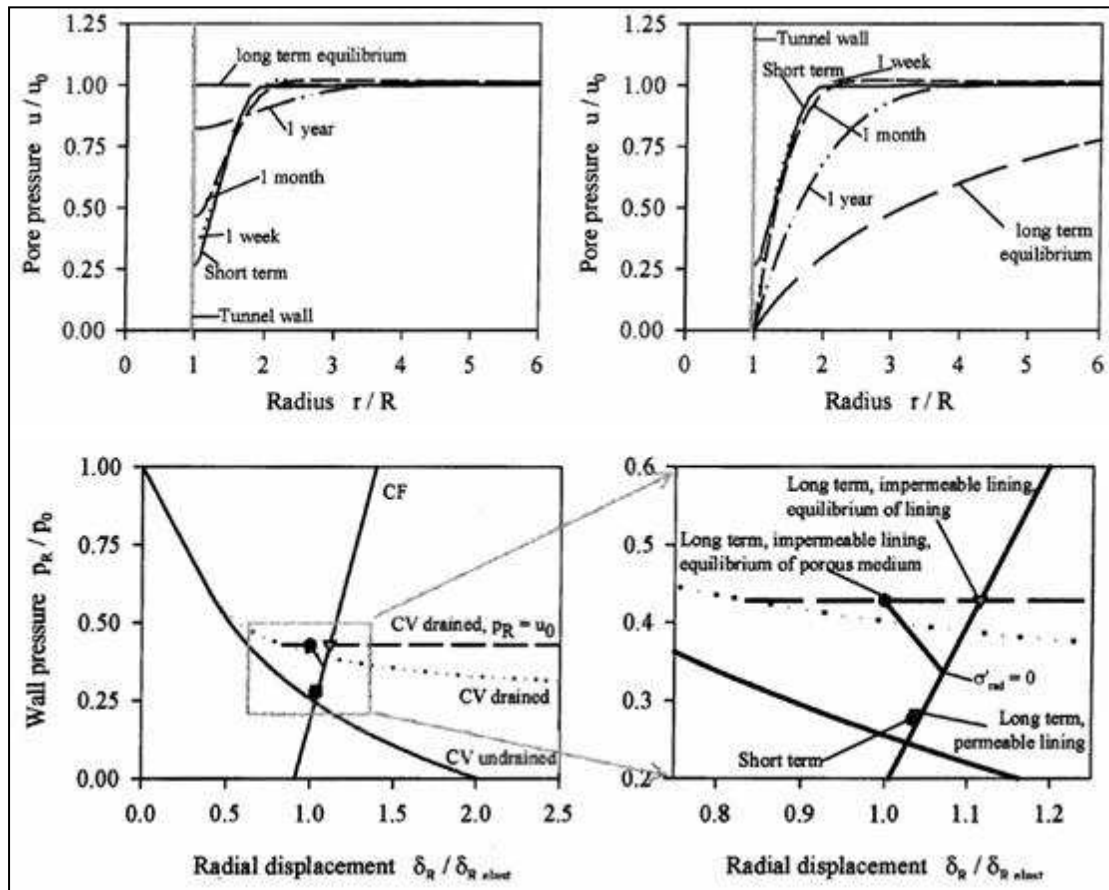


Fig. 2.16. Method of the characteristic curves (Panet & Guenot, 1982)



(a)

(b)

Fig. 2.17. Excess pore water pressure distribution and characteristic curves during transient ground loading; (a) impermeable lining; (b) permeable lining (Gärber, 2002).

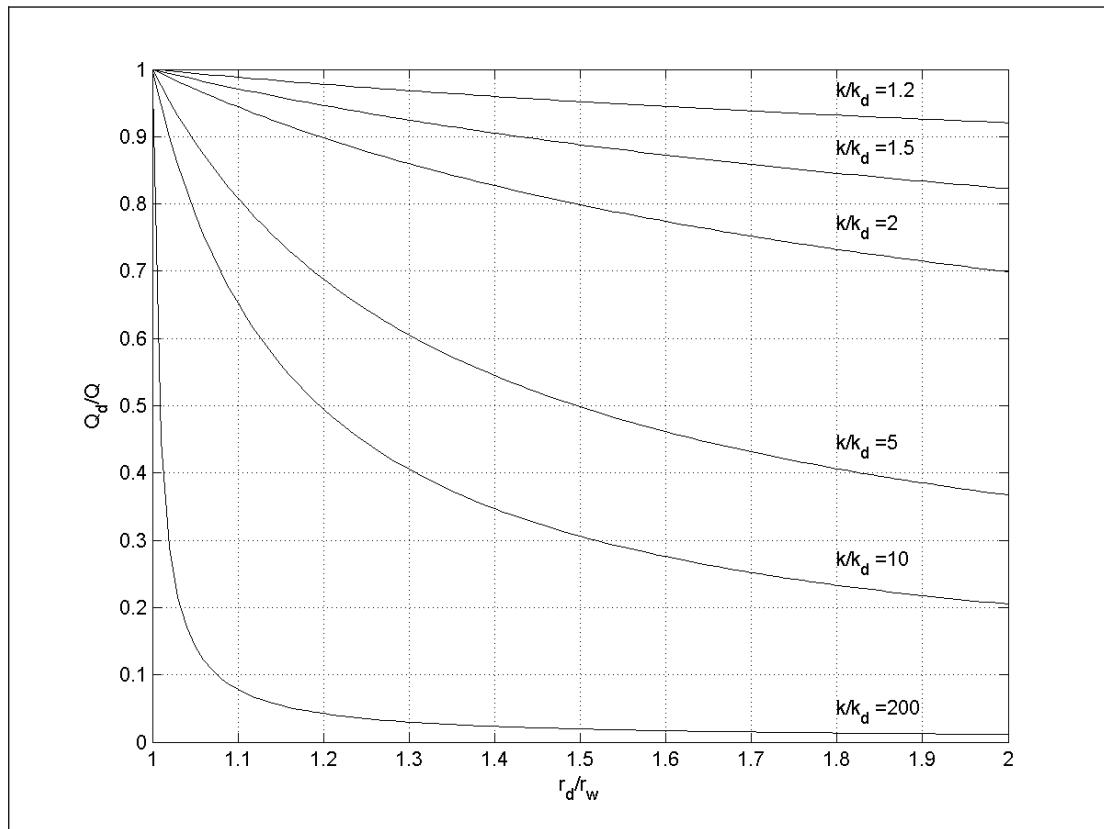


Fig. 2.18. Flow rate reduction  $Q/Q_d$  as a function of the permeability reduction  $k/k_d$  of an annulus of radius  $r_d$  around a cavity (after Muskat, 1947)

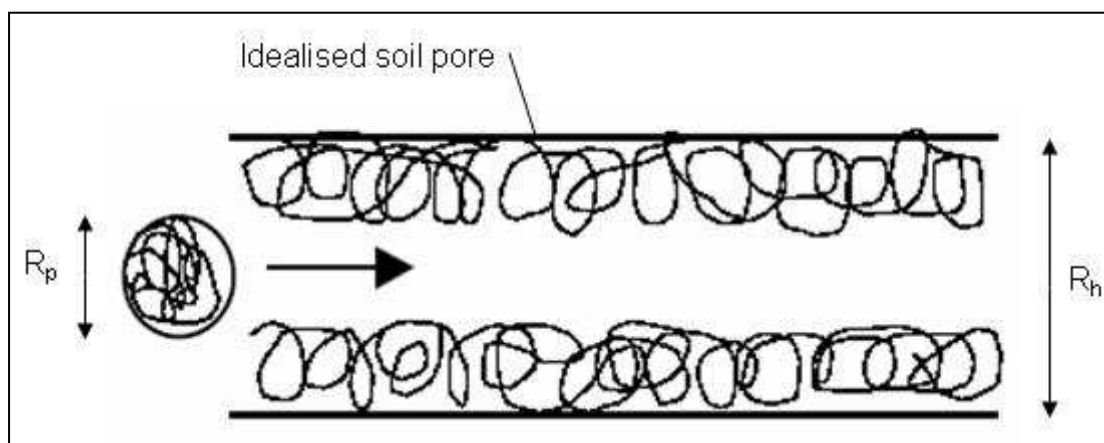


Fig. 2.19. A polymer coil entering a pre-adsorbed cylindrical pore (Denys, 2003)

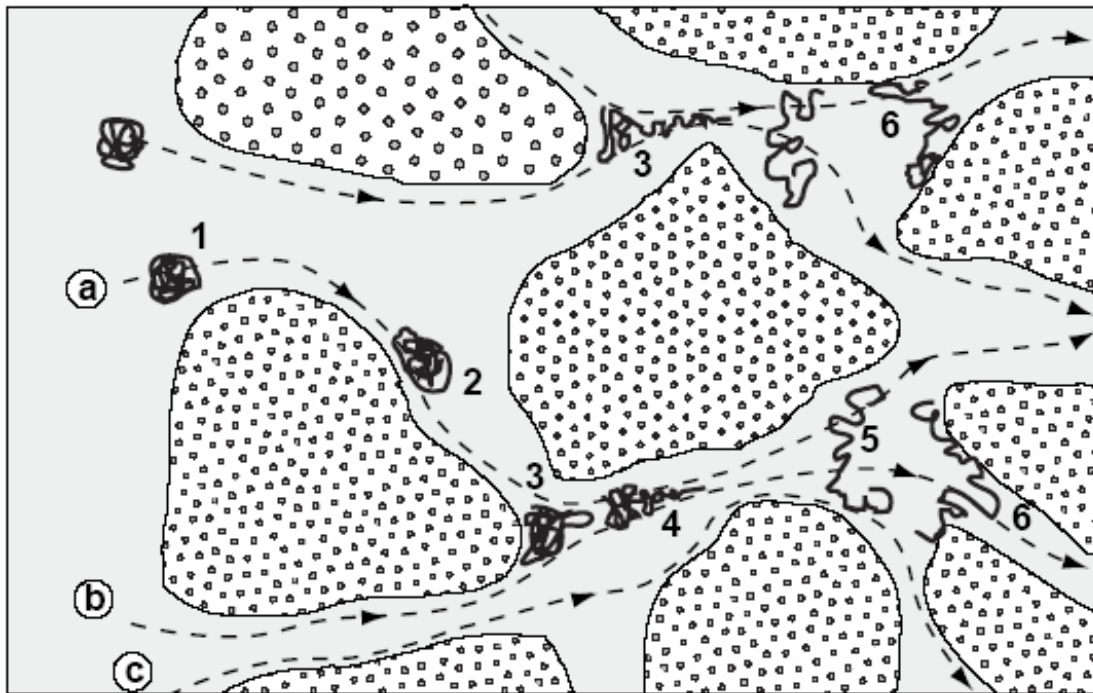


Fig. 2.20. The mechanism of polymer bridging adsorption (Denys & Zaitoun)

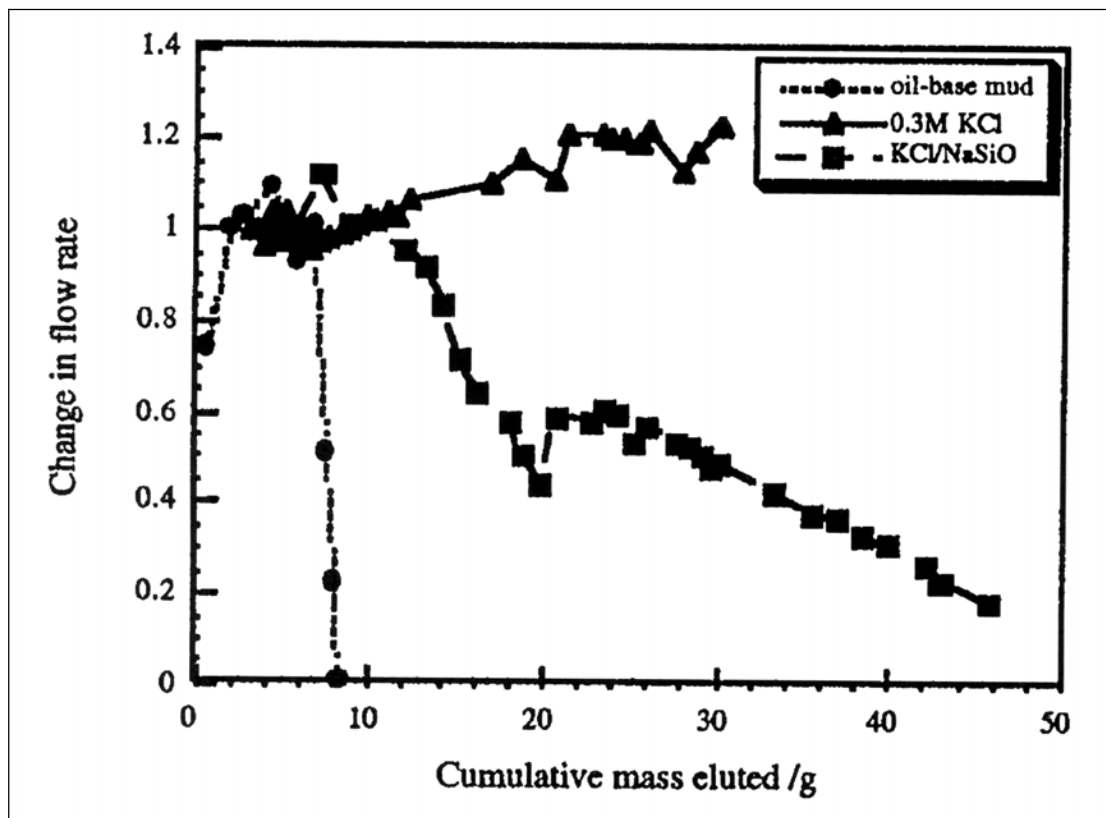


Fig. 2.21. Permeability reduction due to potassium silicate fluid (Bailey *et al.*, 1998)

## **CHAPTER 3: EXPERIMENTAL APPARATUS**

The present chapter discusses the research methodology and describes the experimental apparatus that was devised to investigate the effects of lubrication in pipe jacking. A photograph and a line diagram of this apparatus are shown in Figs 3.1 and 3.2.

Section 3.1 recapitulates the scientific objectives that motivated the development of the test apparatus. The selection of the modelling techniques is then discussed (§ 3.2), before presenting the design evolution of the experimental apparatus (§ 3.3), placing particular attention on the measures taken to ensure repeatable and quality-assured results. The remainder of the chapter then successively describes the material properties of the soil model and its preparation (§ 3.4), the instrumentation of the apparatus (§ 3.5), and the test procedure retracing the chronology of the preparation and execution of a typical test (§ 3.6). The test program is summarised in § 3.7, before concluding with a summary of the designed apparatus (§ 3.8).

### 3.1 Objectives

The foremost scientific objective that motivated the test series was to determine how the chemistry of lubricants and their injection pressure affect the short-term ground loading on a rigid pipe. The industrial incentive behind this objective is to change the current hit-and-miss approach to lubrication prevailing in the industry into a robust and controlled method for delaying the build-up of ground loading on the pipe, and in turn, the increase of jacking forces. This will allow both the performance and the reliability of the pipe jacking process to be improved, resulting in the significant benefits outlined earlier.

Such technological advance is currently restrained by the limited understanding of the fundamental interactions between the lubricant fluids and the clay. Reductions of swelling strains of the clay in the presence of certain chemicals have been conjectured, and even measured in idealised conditions (Merritt & Mair, 2002). However, these effects are less obvious in the conditions prevailing at the boundary of a contracting cavity, where the clay builds up pressure against a rigid boundary. Clay swelling inhibition, filter cake formation on the excavation boundary and reduction of interface friction angle are three mechanisms that may lead to the reduction of the shear force between the pipe and the soil. However, the fundamental mechanics and the effects of some operating variables are not yet understood with sufficient confidence.

The present research therefore proposes to focus on this problem by measuring the effect, of (1) different lubricant fluids and (2) different lubricant injection pressures on the transient radial stresses exerted by the soil onto the pipe. These experimental objectives have been broken down into the following tasks:

- To design and commission a laboratory-scale apparatus replicating the key aspects of the construction process of a pipe jack that are relevant to the problem of radial ground loading on the pipes;
- To develop a way of excavating a circular cavity by replicating a representative stress path experienced by the soil upon excavation and, subsequently placing lubricant fluids in contact with the boundary of the excavation thus created;
- To measure the ground loading on the pipe, both in terms of total and effective stress, as well as the shear stress acting between the pipe and the clay during jacking, and the pore pressure response in the soil surrounding the excavation.

## 3.2 Modelling technique

This section describes the methodology adopted to achieve the objectives defined in § 3.1. The simplifications that were introduced to idealise the construction process are first described in § 3.2.1, before examining the considerations that guided the choice of the modelling technique (§ 3.2.2 to § 3.2.5), and finally discussing the model dimensions and their implications (§ 3.2.6).

### 3.2.1 Idealisation of the construction process

#### 3.2.1.1 Excavation of a cavity

The essential aspect to be modelled is the unloading of a cylindrical cavity in a soil model, simulating the excavation taking place in pipe jacking. The stress paths imposed to the soil surrounding the cavity were given particular attention as they greatly influence the subsequent soil-pipe interactions. In its simplest form, an excavation may be considered as the instantaneous removal of the total radial stress acting on the excavation boundary. However, disturbances inevitably occur due to the three-dimensional nature of the excavation and the interaction of the cutting tools with the soil. These disturbances may result from unbalanced or over-balanced total stresses at the excavation face and from shearing along the shield of the boring machine. Should such disturbances become significant, then the stress regime in the vicinity of the excavation will be altered, and the simplifying assumption of cylindrical cavity contraction will no longer hold true. It is therefore important to control these disturbances in order to have a repeatable process and to limit them so that the mechanism is simplified to avoid disputable interpretation of the test results.

Simulating an excavation in a sand model is relatively straightforward; a rubber membrane buried in the model may simply be deflated to simulate the removal of the total radial stresses supporting the cavity. Clay models, on the other hand, are prepared from a slurry and undergo large volume reduction during their consolidation. For this reason, a membrane or another kind of temporary lining may not be placed in the soil model before it reaches its final consolidation state. The excavation has to be physically performed by removing the desired volume of clay in the fully consolidated model, a process which is usually carried out after having withdrawn the confining stress acting on the model (*e.g.*, Mair, 1979 or de Moor, 1989). Such temporary removal of the confining stress alters the pore pressure regime around the cavity, and unless equilibrium conditions are restored before the test, the effective stress path undergone by the soil in the field will not be correctly modelled. Therefore, a system allowing low disturbance drilling was to be developed to

excavate the cavity under the full overburden stress (§ 3.3.4). Low disturbance means that, for instance, excess pore pressures other than those due to the actual cylindrical cavity unloading as well as effects due to shearing between the soil and the excavation shield should be limited. If such an excavation process were achieved and if the excavation took place rapidly compared to the time required for the excess pore pressure around the cavity to dissipate, then the assumption of cylindrical cavity contraction may be assumed to hold true.

### 3.2.1.2 Lubrication

Lubrication is the key parameter of the present test series. Therefore, close control upon the injection procedure was required to ensure that the effects of lubrication are isolated from those of other variables. Also, the modelled lubrication process had to be representative (or at least, technically viable) of that in a prototype pipe jack. The essential parameters involved in lubrication are (a) the composition of the lubricant fluid, (b) its injection pressure, (c) the location of the injection ports, (d) the sequence of injection and, importantly, (e) the imposed hydraulic boundary conditions at the pipe-soil interface after injection.

There is no consensus or established practice in the industry for the choice of lubricant fluids for clay soils. While bentonite slurries, are still widely used, either as such or enhanced with chemical additives, there is a trend to move towards polymer-based products or other types of swelling inhibiting agents. These may be prepared as water solution and do not require bentonite to be added to the mixture. Injection routines vary significantly, often depending on the site operator and contractor practice. However, the lubricant is usually injected using positive displacement pumps. Two or three injection ports are typically arranged near the crown of specially equipped pipes, which may be included in the pipe string every five to ten pipes, depending on the need for lubrication. The lubricant is pumped around the pipes during the actual jacking of the pipe string. Pumping ceases during jacking stoppages and no provision is usually made to maintain the lubricant pressure in the overcut. The injection is therefore intermittent rather than continuous and is made in a volume-controlled manner rather than by maintaining a carefully selected lubricant pressure. While lubricants may be injected at pressures approximately equal to the total overburden pressure at pipe axis, the pressure in the overcut may rapidly return to lower values as the injection is interrupted during the intermittent stoppages. This is because the fluid may leak through the pipe joints, escape through discontinuities in the ground, or flow around the shield into the excavation chamber of the boring machine.

The range of lubricant chemistry selected for investigations was deliberately limited, placing more attention on the underlying mechanisms of the problem rather than on the comparison of the effect of several different products. Instead, the aim was to compare patterns of ground responses between a benchmark test series using plain water at different injection pressures, and a second series using a water-based polymer solution under otherwise identical conditions. The injection has to occur during excavation, because the large pore pressure gradient near the contracting cavity and the fast drainage time of the clay result in fast consolidation. Consequently, if the injection were delayed even by a few minutes, partial consolidation would occur before the lubricants are in contact with the cavity, and thus, their effects may not be fully captured. The intention was to inject the lubricant fluid immediately after excavation, continuously keeping the void between the pipe and the excavation saturated. Despite the fact that prototype lubrication is performed in a volume-controlled manner, the injection was modelled as a pressure-controlled process. This is because the injection pressure was a test variable, hence control of its magnitude was a requirement.

Another important consideration was the modelling of the post-installation hydraulic boundary condition at the cavity boundary, since it largely influences the consolidation process around the excavation and, in turn, the transient ground loading on the pipe. As depicted in Fig. 3.3, the problem of modelling this boundary may be clarified by considering three consecutive stages ensuing the onset of excavation: (1) the installation, involving lubricant injection under a constant pressure  $p_o$ ; (2) the cavity convergence, during which excess pore pressure dissipates while the cavity gradually converges towards the pipe, however without closing the overcut, and (3) the effective stress build-up stage, beginning when soil comes into contact with the pipe. While the lubricant pressure was controlled during the installation (stage 1), either pressure or flow control could be imposed at the pipe surface during the second and the third stages leading to equilibrium. If the pressure were to be controlled, recharge or discharge of lubricant would have been required to compensate for losses of lubricant absorbed by the swelling clay or excess of lubricant expelled by the converging ground onto the pipe. While this could have been easily achieved during stage 2, it would have required the provision of a permeable pipe soil boundary during stage 3 to allow the pore pressure boundary to be controlled uniformly along the pipe. Moreover, unless the lubricant injection pressure equalled the initial pore pressure, a steady state flow across the constant pore pressure boundary would have established in the long term. For instance, if the injection pressure were lower than the pore pressure, the injected lubricant would have been driven out of the overcut,

should flow not have been restricted through the pipe. This would have annihilated or failed to capture the effects of the lubricants. Therefore, the hydraulic boundary conditions at the pipe surface was modelled as an impermeable (no-flux) boundary during consolidation (stage 2 and 3), while a constant pressure was applied during the excavation (stage 1).

### 3.2.1.3 Model pipe

The string of pipes jacked from the launch to the reception shafts consists of several segments with length comprising between 1.5 to about 5.0 meters. Often, the segments are connected with special spigot-like joints allowing small rotations between the element axes, so that the pipes may be jacked along curved alignments. Because the pipes are designed to take the high compression loads caused by the jacking, they are thick-walled and therefore have considerable radial stiffness.

The diameter of the excavation created at the front of the pipe jack is invariably larger than that of the pipes. This leaves a so-called overcut, or gap around the pipes; this is a deliberate measure inherent to this construction method and which is aimed at temporarily reducing the radial stresses on the pipes to help maintain low jacking forces. The magnitude of this overcut varies greatly, but usually falls in the range of 10 to 25 mm, in terms of radial over-excavation. For a pipe of 2.0 m outer diameter, this corresponds, if full closure of the overcut occurs, to volume losses (see definition in § 6.3.3) in the range of  $\Delta A/A = 1.0$  2.5%, where  $\Delta A$  is the area of the overcut and  $A$  the cross-sectional area of the pipe.

The over-excavation ratio is a crucial aspect of the prototype and significantly influences the ground loading on the pipes. Therefore, this aspect was fully accounted for in the model. However, there was no need for modelling the segmental nature of the pipe string, which could simply be replaced with a monolithic cylinder of very high rigidity. The model pipe was to be instrumented to capture total and effective stress build-up on the pipe. Capturing the ground response upon excavation to obtain a full picture of the consolidation process required the immediate insertion of these instruments after the excavation, and in any case, before convergence of the cavity had reached the size of the overcut.

### 3.2.2 Modelling of ground conditions

This research focuses on the effects of lubrication in stiff overconsolidated plastic clay. The expected interactions between the lubricant fluids and the clay - the conjectured swelling inhibition - are more prominent in active clays, and therefore

more readily observed. Merritt & Mair (2001) showed that the range of chemicals tested as swelling inhibitors have a significantly more pronounced effect on clays containing illite or montmorillonite minerals, while the effects on the less active kaolin clays are rather more difficult to discern. However, kaolin is readily available as a processed material of controlled quality; it has been (in different varieties) the material of choice for geotechnical testing at Cambridge. Also, because more active clays usually have permeability orders of magnitude lower than that of kaolin, and hence also require unreasonably long periods to consolidate, they are therefore not suitable to prepare large models. Processed kaolin was also preferred to natural samples recovered from the field (*e.g.*: London or Gault Clay) in the interest of controllability and repeatability of the soil model properties.

The stress history and the initial state of stress of the clay model were chosen to represent those encountered at the depth where pipe jacks are typically installed, that is, approximately 10 m. Assuming the presence of a water table near the ground surface, and an average bulk density of the soil of  $20 \text{ kN/m}^3$ , a vertical effective stress  $\sigma_{vp}' = 100 \text{ kPa}$  and a pore pressure  $u_p = 100 \text{ kPa}$  were selected to represent field conditions. An overconsolidation ratio of  $OCR = 8$  was chosen as a representative value for London Clay or Gault Clay at 10 m below the ground surface.

### 3.2.3 Numerical or physical?

Numerical simulations of boundary value problems with either the finite difference or the finite element method require a robust knowledge of the constitutive behaviour of all materials of which the prototype consists. The processes occurring at the pipe-soil interface are of a complex nature, combining aspects of clay swelling, with progressive formation of a filter cake and absorption of the lubricant into the clay matrix. These phenomena are not well understood and would require intensive investigation before they can be incorporated in a numerical model. Unless these fundamental interactions between the soil and the different fluids are first understood, or if no validation of the results of the numerical analyses are available, little reliable conclusions may be gained from the straightforward numerical codes commonly used to investigate geotechnical engineering problems.

In addition, the problem of stress build-up on a rigid pipe from an initially over-sized cavity bears further difficulties in terms of numerical analyses. Depending on the size of the initial overcut, large deformations occur near the excavation boundary. Although methods exist to deal with such deformations in a numerical model, they represent added complexity. Furthermore, adaptive boundary conditions are required

at the excavation surface: free swelling takes place in the first instance with constant pore pressure before the ground touches the pipe. At this moment, a zero radial displacement condition is imposed to the soil. As a result of the soil's anisotropy and the non-symmetric stress boundary conditions, this change does not occur simultaneously around the circumference of the cavity. While some attempts were made to model these changes of boundary conditions in a finite difference model (Barla *et al.*, 2003), it was acknowledged that numerical methods suffer severe limitations to model the problem under investigation and that physical testing was a more reliable approach, as is usually the case when the modes of behaviour of a particular type of problem are not yet fully understood.

### 3.2.4 Centrifuge or 1-g?

In order to replicate the stress regime discussed in § 3.2.2 (*i.e.* approximately 200 kPa total stresses at the cavity axis level), the small-scale model had to be subjected to either a surcharge pressure or to centrifugal acceleration. Two fundamental differences result from the application of a surcharge pressure at 1-g and centrifuging a soil model. Firstly, while the stress gradient is approximately constant in a 1-g model, the increase between the top and bottom boundary being only due to the weight of the model under gravity, the gradient of stress in a model submitted to a gravity field enhanced by a factor of  $N$  is much greater, starting from a zero stress boundary at the surface and approximately increasing at a rate of  $N \cdot g$  kPa/m (ignoring variation of centrifugal acceleration with the centrifuge radius). Secondly, under surcharge pressure, the top boundary is evidently not a stress free boundary, and uniform vertical displacement is imposed to the surface of the model, quite the opposite of what may occur in a centrifuge model. Replicating the correct stress gradient and the free stress surface is only essential when studying boundary value problems in which the extent of the zone of influence reaches through regions of different stress level or indeed to the ground surface (White, 2002). This is the case when studying the behaviour of embankments, shallow pile penetration, collapse mechanisms or deformation patterns around shallow tunnels. However when the investigated mechanism does not require the replication of the stress gradient, as is the case for “deep” tunnels, the overburden may be replaced by an equivalent total stress.

In the present case, the nature of the problem consists of the interaction between the unloaded ground in the vicinity of the excavation with lubricant fluids and the model pipe. The investigated effect of polymer on the stress build-up on the pipes does not a priori depend on the vertical stress change between the crown and the invert of the

cavity, as would, for example, deformation patterns around a shallow tunnel. Assuming the cavity is sufficiently deep to exclude deformation mechanisms reaching to the ground surface, the proximity of the surface does not play a determinant role in the stress build-up on the pipe. In other words, the stress levels at the depth of the pipe-jack in the model can be replicated by the application of an equivalent surcharge pressure rather than by centrifugal acceleration.

In addition, the sequence of events required to simulate the construction process of the pipe jack (§ 3.2.1), namely the excavation of a cavity, the lubricant injection and the insertion of an instrumented model pipe, had to be performed “in-flight” without interruption of the gravity field. While these processes are technically feasible in the centrifuge, it would have attracted additional complication. Therefore, 1-g modelling was retained as the preferred methodology.

### 3.2.5 Stress and strain boundary conditions imposed to the soil model

The strain and loading conditions at the soil model boundaries as well as its geometry are discussed hereafter. They were chosen to reduce the dimensionality of the problem in view of subsequent analysis and to simplify the experimental set-up, while still modelling a typical prototype representatively.

An advancing pipe jack induces a three-dimensional strain and stress field around its excavation front. However, pipe jacks being long structures, plane-strain conditions can be assumed to approximately prevail in a cross-section sufficiently remote from the launch and reception shafts, as well as from the excavation face. This plane-strain assumption may also be valid for the transient stage leading to equilibrium if the excavation takes place so rapidly compared to the radial consolidation time, as to allow the component of water flow in the pipe axis direction to be neglected. In addition, if the depth to diameter ratio of the cavity is such that the difference of vertical stress between the crown and the invert of the pipe is small compared to the overburden at the pipe axis depth, and if  $K_o$  (coefficient of horizontal to vertical stress) approaches unity, then the radial consolidation problem may be modelled in an axisymmetric manner. This has the advantage of allowing relatively straightforward analytical solutions to be derived. Hence, the problem of cavity contraction occurring in pipe jacking possesses features of both axisymmetric and plane-strain problems and may therefore be modelled under different conditions; both approaches are bearing their own advantages and limitations.

Devising an axisymmetric model would have attracted technical difficulties, whether the confining stress was applied in the direction of the axis of symmetry or in the radial direction. In the former alternative, the excavation would have had to break through the piston that applies the total stress to the soil model, and required that the excavation be performed vertically. Given the size of the soil model, this solution attracted too much technical complication and was therefore discarded. Applying the confining stress in the radial direction would alleviate this sophistication, but because the model cannot be consolidated radially, this alternative requires that the soil model be first consolidated one dimensionally, before being pressurised in the radial direction. This also added many extra complications to the experimental procedure; modelling the problem in axisymmetric conditions was therefore abandoned. Instead, a plane-strain model with an initial geostatic stress field was preferred. While geostatic conditions have the disadvantage of introducing an additional variable in the problem,  $K_o$ , they represent field conditions realistically and are more conveniently reproduced in the laboratory, as they simply demand that the model be subjected to one-dimensional loading.

The strongbox containing the soil model was designed to be circular in plan, because hoop stresses provide lateral stiffness more economically than bending plates. However, a circular shape does not strictly impose plane-strain conditions to the model as would be the case for a rectangular strongbox. While symmetry nevertheless prevents out-of-plane-strains in the middle vertical cross-section, different displacement fields may result in the adjacent cross-sections due to their smaller lateral extent. However, the gradient of displacement in the pipe axis directions remains much smaller than that in the perpendicular directions. Similarly, at some distance behind the tunnel heading, the component of the hydraulic gradient in the pipe axis direction is negligible, so that consolidation around the pipe is predominantly governed by a planar flow regime. Again, these considerations neglect the 3D-effects resulting from the advancing tunnel heading, on the premise that the excess pore pressure caused by the advancing face is much smaller than that due to the unloading of the cavity and that the excavation occurs in such a small time, that negligible flow is induced the longitudinal direction. Pore pressure measurements in different cross-sections along the excavation are presented in § 4.5.2.2 to corroborate this assumption. In conclusion, quasi-plane-strain conditions are approached in the median vertical plane of the cylindrical strongbox and out-of-plane effects may be ignored to reduce the dimensionality of the problem.

### 3.2.6 Selection and implications of model dimensions

#### 3.2.6.1 Side-boundary effects

Understanding the effects of the lateral limitation of the soil container is essential to assess the validity of the test results. In cases where the observed phenomenon is influenced, or even governed, by boundary effects rather than by the test parameter, the experimental results may not allow meaningful conclusions to be drawn from the experiment. The philosophy of the present experiment was to compare the magnitude of stress redistribution in different experiments, in which the lubricant process was varied. Therefore, some interferences of the boundary effect with the observed phenomenon were acceptable, on the premise that the proximity of the boundary would affect the results in similar mode and magnitude regardless of the chosen test parameter.

However, this assumption is not valid if the effect of the boundary does not only affect the model behaviour quantitatively, but also qualitatively. This may be the case, if stress changes in the model result in the formation of a gap between the soil and the side-wall of the container. Water may then drain between the soil and the side-walls of the strongbox, providing a free-flow boundary along the vertical boundaries of the soil model. This would fundamentally modify the flow regime and the consolidation around the model pipe. Under certain conditions, such a mechanism could occur only for a range of test parameters, perhaps when no support pressure was offered to the contracting cavity, while stress changes might be insufficient to allow the soil to depart from the tank if larger lubricant pressure are applied to the contracting cavity. Such uncontrolled boundary effects may rule out the prospect of meaningfully comparing results from different tests.

Therefore, limiting boundary effects was important to ensure that such mechanisms would not occur for the range of test parameters. Because experimental evidence with respect to boundary effects for 1-g model tunnels in clay is limited, two criteria were defined to select the container dimensions. For a cavity in an infinite and isotropic soil model of otherwise identical properties, the radial stress at the radius equal to the strongbox radius should not reduce to zero, and, secondly, the radius of the plastic zone should not exceed the strongbox radius. Closed-form solutions of cylindrical cavity contraction in linear-elastic perfectly plastic material were used to calculate the radius of the plastic zone of a contracting cavity with zero internal support under axisymmetric and isotropic stress and strain conditions. The undrained shear strength of the clay was estimated using the Cam-clay relation and the parameters summarised in Table 4.1.

### 3.2.6.2 Selection of the model dimensions

The key dimensions of the model, namely the height  $H$  and diameter  $D$  of the cylindrical soil model, as well as the diameter of the pipe  $D_p$  and that of the excavation  $D_o$ , are illustrated in Fig. 3.4. They were selected so as to (a) allow the instrumentation for total stresses and pore pressures, as well as the excavating device to be accommodated in the model pipe, (b) to limit boundary effects, and (c) to achieve similarity between the model and a typical prototype. In addition, the overall size of the model was minimised in order to limit the soil model preparation and the consolidation time, which scales with the square of the model height.

The minimal diameter  $D_p$  of the model pipe is limited by the space required to accommodate the instrumentation, the excavation tools and the discharge path of the clay cuttings. As explained in § 3.3.3, an existing device with a diameter  $D_p = 83.1$  mm was used to model the pipe, so that the diameter was given and the other dimensions had to be chosen as a function of  $D_p$ . On the basis of the considerations discussed in § 3.2.6.1, a minimum strongbox to pipe diameter ratio of 4 was respected to avoid significant lateral boundary effects, and the distance from the pipe axis to the top boundary was kept greater than 3.5 pipe diameters.

The overcut ratio around the model pipe may either be expressed as the radial thickness of the annular gap or in terms of corresponding volume loss  $\Delta A/A$ , where  $\Delta A$  is the area of the overcut and  $A$  the cross-sectional area of the pipe. As already mentioned, overcut ratios of  $\Delta A/A = 2.5\%$  or more are not uncommon in the field. The ratio in the model was selected to compromise between similarity requirements and technical limitations. Unless the radial overcut was less than the combined undrained and time-dependent radial convergence of the contracting cavity prior to the insertion of the pipe into the soil model, the instruments would not be inserted before ground closure on the pipe. This would not only result in a loss of information in the early stage of the consolidation, but would also have involved shear stresses between the ground and the pipe during installation of the latter, possibly to a different extent when using different lubricant products. These would have combined different effects on the stress build-up (smearing of excavation surface, excess pore pressure dissipation due to shearing or pipe misalignments), and would have exposed the experiment to potentially inconclusive results in terms of fundamental mechanisms. The overcut was therefore slightly “exaggerated” compared to the range relevant to prototype situations, with a radial gap of  $\Delta r = 3.5$  mm, corresponding to a value of  $\Delta A/A = 8.5\%$ .

### 3.2.6.3 Scaling laws

Practical value to design and analysis can only be derived from reduced-scale experiments if the response observed through the model can be confidently extrapolated to full-scale prototypes. Establishing scaling relationships relating the measured physical quantities in models of different dimensions and at full-scale requires an understanding of how the model size affects the measured quantities. Physical phenomena occurring in the model as a mere result of the selected scale should be identified, as they may otherwise distort our understanding of the investigated problem. Because model test are usually carried out when the modes of behaviour in a physical problem are not yet recognised, the scale invariance of the investigated phenomenon must be assumed in a first instance. “Modelling of models” (the repetition of tests on geometrically self-similar models at different scales) is then required to confirm this assumption and to propose scaling relationships for processes of yet unexplained nature.

When all linear dimensions of a prototype are reduced by a factor  $n$ , all stresses in the model are, if the model size captures a sufficient representative volume of clay to eliminate particle-size effects, scale-independent. Geometrical similarity would have required the overcut ratio  $\Delta A/A$  to be equal in the model and prototype. However, for reasons that will become clear later, the ratio was exaggerated in the model, hence violating geometrical similarity and potentially introducing significant scale-effects. Therefore, extrapolation of the results to situations of varying  $\Delta A/A$  will require prior determination of the effect of this factor, especially with respect to the pipe-soil stresses. The magnitude and the radial distribution of excess pore water pressure generated in the undrained unloading are not *a priori* sensitive to the model scale (see § 4.2.2 for a discussion). However, the rate of dissipation of excess pore water pressure is affected by the model scale. Seepage velocity is  $n$  times larger as a result of larger hydraulic gradients, and drainage distances are reduced by a factor of  $n$ . Using Darcy’s law, it can easily be shown that if linear dimensions are reduced by a factor  $n$ , the consolidation time in the model is  $n^2$  times faster that at prototype scale. Hence, 1 minute at the model scale represents, for an excavation of 3.5 m diameter, just over 1 day. In other words, one year consolidation around a 3.5 m excavation may be observed in just over 6 hours in a 1/33 model.

The installation speed affects the ratio of longitudinal to radial flow at a given distance behind the tunnel face. To achieve rigorous similarity (assuming consolidation to be the dominant processes of the time-dependant behaviour) the installation speed in the model should be increased by a factor  $n^2$ , this would ensure

an identical degree of consolidation to have occurred at a given distance,  $x/D$ , behind the excavation. The selection of the pipe installation speed in the model restricted by technical considerations (§ 3.3.4), and an adequate value was found to be approximately 1.5 mm/s. For a pipe jack of 3.5 m diameter, this corresponds to an installation time of 3 m/days. As discussed in § 2.2.2, production rates in the field sometimes exceed 35 m/day (Broomfield, 2004), so that the selected model speed is an order of magnitude lower than in a typical prototype. Therefore, the overcut ratio  $\Delta A/A$  was slightly exaggerated in the model, so that the installation of the model pipe instruments in the soil could be completed before closure of the ground occurred onto the pipe.

The interaction between the lubricants and the clay are likely to be affected by the model scale. The depth of diffusion or seepage of chemicals from the cavity boundary into the clay may not scale with the size of the cavity radius. As a result, the effects of the lubricant, such as the temporary or the permanent reduction of pipe-soil stresses, may vary with the model scale, but the description of these effects would require the interactions between the clay and the chemicals to be better understood. Other, perhaps less obvious, scale effects may arise from strain-rate sensitivity and seepage-induced effective stresses. In particular, the interface shear stresses between the pipe and the clay may be affected by the model scale, especially when shear-rate effects are likely to play a significant role. Such effects may be amplified at reduced scale, where the thickness of shear layers reduces and shear rates increase. It is therefore appropriate to treat these aspects of the model behaviour with caution when attempting to link the experimental results to the response of full-scale pipe jacks.

### 3.2.7 Summary

The construction process of pipe jacking was replicated at small scale in an 800-mm diameter by 600-mm high cylindrical soil model of saturated E-grade kaolin. This soil model is one-dimensionally consolidated to an OCR of 8 and subjected during the experiment to a geostatic stress field by applying 200 kPa total vertical stress and 100 kPa of water pressure to its top surface. A 90-mm diameter cylindrical cavity is excavated under these confining stresses using a low-disturbance drilling system, while lubricant fluids are injected under controlled pressure around the 83-mm diameter rigid model pipe. At the end of the excavation, the fluid boundary condition at the excavation surface is changed to a no-flow boundary, as shown in Fig. 3.3. The selected dimensions and the geometry of the physical model, are summarised in Fig. 3.4.

### 3.3 Apparatus design

This section presents the design evolution of the apparatus that was devised to simulate the construction process of pipe jacking under the boundary conditions discussed above. This section only addresses the mechanical components of the test equipment; the instrumentation of the model is discussed separately in § 3.5. The new strongbox and consolidation system are first presented (§ 3.3.1 and § 3.3.2), before detailing of the model pipe and the excavation technique (§ 3.3.3 and § 3.3.4). The method of lubricant injection is then discussed (§ 3.3.5) before finally describing the equipment allowing the controlled and repeatable installation of the pipe into the soil model (§ 3.3.6).

Details of the main mechanical components were extracted from the text and gathered in Table 3.1. Each component is annotated in the text with a numeral subscript which refers to the corresponding row of Table 3.1, where the part number and manufacturer details are tabulated.

#### 3.3.1 Strongbox design

A new strongbox was commissioned, in which clay models could be both consolidated and tested. The shape and the overall dimensions of these models were discussed in § 3.2.5 and § 3.2.6, respectively. The 800-mm diameter and 1200-mm high strongbox was designed to be fully impervious and sustain an internal hydrostatic pressure of 1.0 MPa. Its components, shown in Figs 3.5 and 3.6, comprise a cylindrical side-wall with an extension, a base plate and a piston to applying pressure on the clay. The bolted assembly was dismountable in order to ease the model preparation, the post-mortem recovery of the soil specimen, and the exhumation of the instruments buried in the soil model.

The side-wall and its extension were fabricated by rolling and steam-welding steel sheets (grade BS EN 10025 5275). An assembly flange was welded on both end of the side-wall and its extension, before heat treatment and accurate boring to the required diameter of 800 mm, leaving a minimum wall thickness of 10 mm. An ‘O’-ring groove was machined in the bottom flange of these two components. The extension was used for the first stage of the consolidation to accommodate the originally high volume of slurry, and was later removed to ease the installation of the pore pressure transducers through the piston. It proved important to accurately align the side-wall and the extension with pin dowels before bolting them together, in order to avoid damage to the piston seals during consolidation. A chamfer was machined in the upper edge of the strongbox to further reduce the risk of damaging the piston

‘O’-rings. The side-wall was bolted onto the 25-mm thick base plate shown in Fig. 3.6. Radial ribs were welded under the base plate to leave sufficient space to accommodate drainage pipes.

The two diametrically opposed orifices were bored through the side-wall to allow insertion of the model pipe at a vertical distance of 300 mm above the base plate. The diameter of these circular holes was 100 mm, leaving a gap of 5 mm around the cutting edge of the model pipe. Steel collars extending 60 mm outside the strongbox were fitted with a flange on which the model pipe assembly could be firmly connected during the test, as shown in Fig. 3.7. Steel plugs mounted flush to the inner surface of the strongbox blanked these two apertures during consolidation.

The piston shown in Fig. 3.5 imparts the surcharge pressure and a uniform displacement field to the top surface of the soil model, both during the consolidation and the test. The piston is 799 mm in diameter, thus leaving a 0.5 mm clearance between its outer diameter and the strongbox. This close fit as well as the 60-mm high steel ring welded on the piston helped restrain rotation of the piston about horizontal axes. Despite this effort, tilting of  $1.1^\circ$  could occur with this geometry, permitting a maximum “differential settlement” of over 15 mm between two diametrically opposed points under the piston. This has caused a number of problems, as will be discussed later. In order to resist a water pressure of 100 kPa in the strongbox, two ‘O’-rings were accommodated in a pair of grooves machined in the steel ring around the piston, as shown in Fig. 3.5. A mesh of interconnected radial and circumferential ducts was machined in the bottom face of the piston to allow horizontal circulation of the water to and from the four drainage holes in the piston. In addition, 37 ports were provided to insert the pore pressure transducers at the positions shown in Fig. 3.5. Finally, the piston was fitted with a load bearing plate accurately machined so as to be perfectly parallel to the surface of the piston that comes in contact with the clay.

### 3.3.2 Provision of consolidation and surcharge pressure

A consolidation system was devised to provide the force of approximately 400 kN required to consolidate the 800-mm diameter soil model to a pressure of 800 kPa. The system comprised a hydraulic cylinder<sup>1</sup> with an active surface area of 158 mm diameter and which was mounted in the load frame photographed in Fig. 3.1. Because pressures of the order of 20 MPa were necessary to reach the desired load, the pneumatic pressure systems otherwise used in the laboratory were discarded in the interest of safety. A hydraulic pressure system was designed to provide a maximum consolidation force of 500 kN with 2.5% accuracy at full-scale.

A simplified line diagram of this system is shown in the upper right-hand corner of Fig. 3.2. Hydraulic pressure is generated with a 1:40 Haskell pump<sup>2</sup>, to which both the pilot and the driving pressure were supplied by the laboratory air compressor. The generated oil pressure is then regulated with two medium-resolution hydraulic pressure regulators<sup>3</sup> before being supplied to the top and bottom chamber of cylinder upper chamber of the cylinder. A 50-mm diameter flexible hose connected the pressure system to the upper chamber of the cylinder in order to reduce the impact resulting from the pressure blows inherent to the Haskell pump operation.

Research progress having been impeded by insufficient accuracy and precision of this hydraulic pressure control, an alternative system was devised to improve the control of the total stress imparted to the soil model during the actual test. The poor performance of the first system is thought to be due to a combination of insufficient regulator resolution, inadequate pilot pressure in the Haskell pump, as well as malfunctioning of the regulators as a result of contamination of the oil medium. In the second system, a diagram of which is shown in the top-left corner of Fig. 3.2, the pressure was provided by compressed nitrogen. The pneumatic (rather than hydraulic) pressure was regulated and applied to an interface chamber where it was transmitted to the oil medium via a rubber bag interface. The actuation cylinder and the pressure line connecting the interface chamber to the piston were saturated with oil so that the volume of compressed air in the system was restricted to a couple of litres, hence limiting the stored energy. Because it is more straightforward to control pneumatic rather than hydraulic pressure, this hybrid system allowed accurate pressure control of the test pressure, while complying with safety requirements. However, because of the small volume of the interface chamber, the ram stroke was limited to about 100 mm and the maximum force was not sufficient to complete the full consolidation. The more accurate hybrid system could therefore not be used for consolidation.

A test cycle hence required the use of the two different pressure systems: one for the consolidation, and one for the test itself. Full consolidation was achieved in the first instance, before decreasing the pressure to atmospheric to allow changing the hydraulic system to the pneumatic one. The full test pressure of 200 kPa was then immediately reapplied and the test carried out as soon as equilibrium conditions were measured in the soil model. The effects of this additional pressure cycle on the geomechanical properties of the soil model were considered to be negligible.

A better control of surcharge pressure could be achieved with the hydro-pneumatic pressure system, as discussed in § 4.4.1.1.

### 3.3.3 Model Pipe

The model pipe had to provide a rigid and impermeable support to the excavated cavity, and was to be instrumented to measure the radial ground loading acting on its surface, both in term of total and effective stress. It was necessary that the pipe be inserted immediately after the excavation of the cavity, and in any case before radial convergences of the cavity reached the magnitude of the overcut.

Instead of designing a novel piece of equipment, it emerged that the pipe could conveniently be modelled using an existing device. Indeed, the so-called load cell pressuremeter (*LCPM*), which is an instrument that was designed in the 70's as an alternative to self-boring expansion pressuremeters, is instrumented to measure total lateral stress and pore pressures acting on its shaft. In addition, it is equipped with a self-boring mechanism which excavates a cavity of the same diameter as the device, while continuously recording the stresses acting on its shaft. Measurements are therefore made, at least theoretically, of the total horizontal stress in the ground (Darley *et al.*, 1996 and 1999). While it is intended that the *LCPM* be installed vertically in the ground, it may be used in the laboratory to drill horizontally and act as the required model pipe.

An overview of the *LCPM* is shown in Fig. 3.9; its main components and dimensions are summarised in Fig. 3.10. It consists of an 83.1-mm diameter by 1000-mm long brass body with a 30 mm hollow central bore where a drill rod can be accommodated and the soil cuttings circulated to the rear of the instrument. Six load cell clusters are equally spaced around the *LCPM* circumference, approximately 450 mm behind its nose. As detailed in § 3.5.2, each of the six instrument cluster comprises a load cell measuring direct stress as well as a pore pressure transducer. Examples of field data obtained with the *LCPM* have been reported by Darley *et al.* (1996 and 1999) and, more recently, by Gourvenec *et al.* (2005).

The *LCPM*, kindly made available by Cambridge Insitu Ltd<sup>4</sup> for the present research, was modified to (a) allow low-disturbance horizontal drilling in kaolin clay, (b) excavate an overcut of 3.5 mm around its nominal diameter, and (3) to inject lubricant at a close distance behind the excavation face. These modifications are described in the following sections.

### 3.3.4 Self-boring mechanism

#### 3.3.4.1 Principles of low disturbance drilling

The excavation mechanism used by the Cambridge type pressuremeter was developed by Hughes (1973). It consists of a tapered cutting edge into which the soil is extruded as the instrument penetrates into the ground. Once the soil has moved sufficiently far into the taper for the extrusion force to balance the total stresses in the soil, a cutter excavates the soil and the cuttings are flushed using an appropriate drilling fluid. Theoretically, zero-disturbance drilling may be achieved if the cutter is set in such a position that forces at the leading edge of the cutting shoe are balanced. The optimal cutter position depends on the undrained shear strength of the clay, the taper angle of the cutting edge and on the total stress acting in the direction of the excavation axis. Clarke (1981) proposed a set of equations to optimise the cutting edge shape and the cutter position to minimise ground disturbances during drilling. If the cutter is set closer to the taper edge, so-called over-drilling occurs; total stresses are not fully balanced, which causes stress relief and negative excess pore pressure around the advancing face. On the other hand, placing the cutter too far back into the taper increases the extrusion force and causes positive excess pore pressure as well as outward soil movement ahead of the excavation.

#### 3.3.4.2 Design of a new cutting tool

A new set of components was designed to adapt the self-boring mechanism to the present experiment. These components are shown in Figs 3.11 to 3.13; they comprise (a) a cutting edge carrier, (b) a cutting edge, (c) a cutter, as well as a drill rod with its bearings. The function and the design of these parts are discussed below, highlighting the modifications that were necessary to excavate through the kaolin clay used in this research.

The cutting edge carrier drawn in Fig. 3.11 provides an interface between the cutting edge and the *LCPM* body; it accommodates the front bearing of the drill rod and the injection ports for the lubricant. It consists of a 70-mm long brass cylinder with the same diameter as the *LCPM*. Two threads are cut in the carrier for assembly with the *LCPM* and the cutting edge. Three slots are machined at 60° angle to push-fit the three-leg rod bearing into the front end of the carrier. At the rear, the three hypodermic capillaries carrying the lubricant are glued in cylindrical fittings, themselves glued in radial orifices through the *LCPM*. A groove is machined in the intrados of the carrier, so that it locates above the ports of the cylindrical units that deliver the lubricant. Four diagonal holes then distribute the lubricant in another

groove located immediately behind the cutting edge. This way, the lubricant was injected immediately behind the recess at the rear of the cutting edge (in tests T2 to T5 only; § 3.7).

The geometry of the cutting edge shown in Figs 3.11 and 3.12 as well as the cutter position in the taper was not based on Clarke's design recommendations. Instead, the final design evolved from a combination of Cambridge Insitu's expertise with four excavation trials on kaolin. The selected outer diameter of the cutting edge is 89.1 mm, therefore leaving a radial gap of 3.5 mm around the model pipe. The taper angle was 15° and the overall length of the cutting edge 90.0 mm. During excavation, shearing therefore occurred between the oversized cutting edge and the clay, causing some disturbance in the vicinity of the excavation boundary. Having this 90 mm contact area between the edge and the clay did, on the other hand, prevent loss of lubricant from the annular overcut to the excavation face.

A series of four excavation trials were carried out by excavating a cavity along the axis of a 250-mm diameter cylindrical tube in which kaolin had been normally consolidated to a vertical effective stress of approximately 400 kPa. The first excavation trial was carried out with a standard cutter used on the *LCPM* in the field. This cutter consisted in a single 8.0-mm thick steel blade leaving a 1.0 mm clearance between its lateral edges and the taper of the cutting edge in order to prevent accumulation of clay at this location. The distance from the cutter apex to the front of the cutting edge was 7.0 mm. Water was injected at tap pressure through the inside of the 28-mm *OD* drill rod and deflected laterally by a bowl-shaped disk located 30 mm behind the front of the cutter. The drill rod was loaded on two nickel-bronze-aluminium bearings: one on the pipe carrier unit (§ 3.3.6.2) and in the cutting edge carrier (three-leg bearing). The reaction to the axial thrust on the rod was taken by a washer soldered on the drill rod and reacting on the three-leg bearing.

This first cutter proved inadequate to excavate the kaolin. After the cutting edge had penetrated a distance of approximately 100 mm into the clay, the angular speed of the cutter gradually decreased and the cutter eventually jammed among cuttings that had re-compacted into a stiff mass at the rear of the cutting edge. As a result, excavation of the clay stopped and further advancement of the *LCPM* caused positive excess pore pressure of the order of 1 MPa in the soil model, which was not acceptable. This failure to excavate the clay was attributed to the following factors. Firstly, the 28-mm *OD* drill rod left a mere 5-mm thick annulus in 38-mm diameter bore of the *LCPM* for the clay discharge, and bottlenecks as well as sharp angles remained, where the accumulation of clay cuttings could potentially initiate. Secondly, the clay's ductility

prevented it being broken up in discrete chips that could be flushed readily with the drilling fluid. Thirdly, the ‘drilling fluid’ was not used efficiently: insufficient water flow and pressure were delivered at the face. A higher flow was necessary to produce sufficient velocity to drag the clay cuttings towards the discharge outlet and higher pressure was required at the point of injection to have a dispersing effect on the clay. Also, the bowl-shaped disk deflected the lubricant injection radially, causing large loss of energy at the impact with the cutting edge. Directing a high pressure flow in the actual direction of the discharge path, as shown in Fig. 3.11, was required to help in removing the clay and preventing its accumulation in the cutting edge.

The first design was therefore modified as follows: the cross-sectional area of the discharge flow path was increased by reducing the drill rod diameter by a factor of two. The three-leg bearing located at the front of the cutting edge carrier was chamfered to reduce the resistance it provided to the clay discharge, and all sharp angles inside the cutting edge and its carrier were eliminated. Finally, larger openings were machined in the rear bearing of the drill rod. These corrections proved insufficient, as the second excavation trial resulted in similar clogging as that observed in the first trial.

The third generation of cutting tools had evolved into a system comprising the double-blade cutter photographed in Fig. 3.13. Four 1.5-mm diameter injection nozzles were soldered on the cutter so the drilling fluid would be injected at high velocity towards the discharge path. The cruciform cutter reduced the thickness of the clay chip by a factor of two (at same angular/linear velocity ratio), which eased their discharge. As an additional measure, the water used to flush the cutting was injected using a high pressure pump, resulting in much higher discharge flow velocity. While these changes allowed the excavation to proceed notably further than with the previous system, the cutter still eventually clogged, preventing the successful zero-disturbance excavation that had been the intention. Further changes mitigating these difficulties are described in the next section.

#### 3.3.4.3 Drilling fluid

In addition to the modifications discussed above, low-disturbance drilling into the kaolin was only successfully achieved when using an appropriate drilling fluid injected at sufficiently high pressure. Plain water, used in the first three excavation trials, proved inadequate, and was replaced by a water-solution of a 0.3% water-based solution of a polymer marketed by *Cetco*<sup>5</sup> under the trade name *Insta-pac 425*. This polymer is a partially hydrolysed polyacrylamide (*PHPA*), and is anionic

(Cetco, 2006). The molecular weight of *Insta-Pac 425* was not disclosed by its supplier. This drilling fluid prevented the remoulding of the clay after it had been cut and greatly eased its transportation to the discharge outlet by dispersing the clay into a fine almost cohesionless mixture with a texture similar to that of fine saw dust in water. It has to be noted that the drilling fluid does not come in contact with the excavation boundary and does not interact with the lubricant injected in the overcut annulus.

A submersible borehole pump<sup>6</sup> was used to propel the drilling fluid from a tank where it was mixed at the required concentration prior to the test. An average flow rate of approximately 8 l/min was achieved throughout the installation of the model pipe yielding a flow velocity of approximately 140 mm/s inside the model pipe. This flow was found to be very important to keep the clay cutting in motion and maintain a sufficient gradient for the discharge of the clay. The flow rate delivered by the pump was very sensitive to the polymer concentration of the drilling fluid. Initial trials revealed that the pump could not pump the polymer solution when prepared at concentrations in excess of 0.7%. A compromise was thus to be met to take advantage of both the mechanical and physicochemical effects of the drilling fluid: a high concentration of polymer was desired to disperse the kaolin cuttings, but too high a concentration would have increased the fluid viscosity so much that the delivered flow and pressure would be too small to provide the required carrying capacity to flush the cuttings. A polymer concentration in the range 0.2-0.25% was found to be adequate to excavate through E-grade kaolin.

### 3.3.5 Lubricant injection

#### 3.3.5.1 Injection method

As discussed in § 3.2.1.2, the lubricant fluids were to be injected at constant pressure around the model pipe so as to be in contact with the clay as soon as the cavity unloading occurred. In the first four tests, the lubricant was therefore injected from the rear of the cutting edge, rather than from the strongbox wall, at the rear end of the cavity. This ensured that the overcut would be saturated even if full closure of the ground onto the pipe occurred at some distance behind the cutting edge before the installation was completed. The lubricant injection ports were located in the cutting edge carrier, as shown in Fig. 3.11, at the point where the cavity is unloaded. The lubricant was lead to the front of the model pipe with three parallel hypodermic tubes of 1.5 mm internal diameter. There, the hypodermics were connected to the injection ports via three diagonal 1.5 mm holes. After the first four tests, the installation time

was reduced to approximately 10 minutes and it had been observed that ground closure did not occur during installation. It was therefore simpler to inject the lubricant directly from the tank collar, at the location indicated in Fig. 3.7. This second method was used in tests T5 to T8.

In tests T2 and T3, a peristaltic pump was used to pump the lubricant from the supply reservoir to the injection points. Peristaltic pumps have the advantage of delivering a constant flow regardless of the resisting pressure, and allow flow regulation to a high resolution and accuracy. This way, constant flow of lubricant was thought to be delivered for both water and polymer, despite their different viscosity and flow resistance. As it became apparent that the injection pressure was extremely sensitive to the rate of increase of the overcut volume relatively to the lubricant flow, a pressure relief valve was included between the pump and the injection ports to try to provide a more accurate injection pressure. This method did not allow repeatable results, although the pressure relief valve considerably improved the control of the lubricant injection pressure. Improvement of the fluid boundary condition control at the excavation surface required this system to be replaced by a more straightforward pressure-controlled injection system.

An interface chamber pressurised with pneumatic pressure was therefore used in all subsequent tests (T4-T8), as depicted in Fig. 3.2. The vessel was filled with approximately 8 l of lubricant and compressed air was applied to the top of the vessel. The air pressure, regulated to give the required injection pressure, drove the lubricant into an immersed pipe and through the 8-mm diameter pipe to the injection ports.

#### 3.3.5.2 Lubricant fluids

The main parameter that was varied in the different tests was the type of lubricant. A first benchmark test T1 was performed without injecting any lubricant. Partially de-aired tap water was used in tests T2 to T6 and a water-based solution of anionic polymer was used in tests T7 and T8. The lubricant was prepared as a 0.3%-solution of the polymer *Insta-pac 425* (§ 3.3.4.3). The chemical characterisation and some properties of *PHPA* were discussed in § 2.4.3.3.

#### 3.3.6 Model pipe assembly and driving equipment

##### 3.3.6.1 Guiding cylinder

Accurate alignment of the pipe relative to the strongbox was essential to ensure repeatable and symmetrical positioning of the *LCPM* instruments in excavated

cavity. Quality-assured alignment in the vertical and horizontal plane was achieved by steering the model pipe within a guiding cylinder, which was accurately positioned relative to the soil model by means of a bolted assembly with the mounting flange of the strongbox collar, as shown in Fig. 3.1 and 3.7. An interface flange was located in the guiding cylinder via a spigot joint, fastened with radial bolts and bolted to the strongbox to provide a rigid assembly. The opposite end of the guiding cylinder was blanked with another flange provided a mounting surface for the hydraulic ram actuating the model pipe. The model pipe was fixed to the wheeled platform described in § 3.3.6.2, and this whole assembly could translate within the guiding cylinder in the direction of the cylinder axis. The model pipe was loaded on three steel rollers mounted on the interface flange, as represented in Fig. 3.7. These two bearings restrained movement of the model pipe in the plane perpendicular to its axis, while allowing a degree of freedom in the axis direction.

The guiding cylinder was supported by a purpose-built truss mounted on four adjustable casters, by means of which the height of the guiding cylinder could be adjusted to bring the model pipe into line with the strongbox. The cylinder rested on two pairs of synthetic wheels, so it could be rolled about its axis to ease manoeuvring and access to the instruments around the model pipe. Five 110-mm diameter holes were machined along the length of the guiding cylinder to provide access to the model pipe assembly and discharge of the clay during the excavation.

### 3.3.6.2 Pipe carrier unit

The insertion of the model pipe involved four concurrent actions; (1) rotating the clay cutter, (2) injecting the drilling fluid at the excavation face to disperse and carry the kaolin cuttings, (3) pushing the model pipe forward, and (4) injecting lubricant into the annulus around the model pipe. The mechanical components required to perform these operations were mounted on the wheeled platform, or pipe carrier unit, shown in Figs 3.14 and 3.15. This unit consists of a carriage to which the *LCPM* was fixed by means of a 50-mm diameter cone clamp, and is mounted on two sets of three synthetic wheels arranged at an angle of 60° around the circumference to allow the carriage to roll inside the guiding cylinder. A small tolerance between the wheels and the cylinder, as well as tight assembly of the guiding cylinder with the strongbox ensured accurate and repeatable alignment of the model pipe relative to the targeted excavation.

The cutter rotation was powered by a 620-W air motor<sup>7</sup>, which delivered a torque of 50 N·m at 60 rpm. An air motor was selected for this application in wet and confined

environment because they do not require electric components and are self-cooling. As drawn in Fig. 3.14, the transmission of the driving torque from the drive end of the motor to the drill rod was ensured by two pairs of spur gears mounted on two parallel shafts in order to circumvent the water swivel mounted at the extremity of the drill rod. The torque transfer between the pinions and the shafts was ensured by radially expanding couplers<sup>8</sup>. These couplers failed on two occasions, interrupting the torque transmission to the cutter and, in turn, causing stoppages of the excavation. A water swivel<sup>9</sup> was mounted on the end of the rod to transmit the drilling fluid from the supply line into the hollow drill rod.

### 3.3.6.3 Jacking actuation

The force driving the model pipe from its initial position through the 800-mm diameter strongbox had to overcome the frictional resistance between the cutting edge and the soil, the extrusion force of the clay into the tapered cutting edge, the thrust on the cutter, as well as the friction between the *LCPM* body and the lip seal. Since a gap was excavated around the model pipe, little or no friction developed between the clay and the *LCPM*. The selection and the control of the installation speed was important to ensure low-disturbance drilling, because, for a given rotation speed of the cutter, it controlled the required driving torque and the thickness of the clay chips. Excessive speed increases the penetration of the cutter, which causes the resisting torque to be higher, and in turn, the cutter angular speed to reduce. This, in turn, further increases the penetration depth of the cutter, and, as evidenced by the pilot test series, gradually leads to the standstill of the cutter as the maximum torque of the motor is reached. In addition, the speed had to remain constant, to maintain steady excavation regime and ensure repeatability of the effects due to the excavation in the different tests.

The driving force was provided by thrusting behind the wheeled carriage with a hydraulic ram. The hydraulic cylinder was mounted on the rear flange of the guiding cylinder so that the reaction to the driving force was transmitted in tension through the walls of the cylinder and then to the strongbox via the collar flange. The hydraulic pressure was generated by an electric motor<sup>10</sup> and, in tests T1 and T2, the installation speed was adjusted by means of a needle valve which altered the oil flow on the high-pressure side of the piston. This system proved extremely poor in maintaining a constant driving speed, as the oil flow through the valve was extremely sensitive to the driving resistance. Several readjustments of the needle valve setting were necessary during the installation and the resulting installation speed was extremely erratic (§ 4.4.2).

To remediate this problem, a two-way flow control valve<sup>11</sup> was introduced on the high-pressure side of the oil supply to maintain a constant flow of oil into the piston, and, in turn, a constant installation speed. This device does not require electrical input and allows maintaining the oil flow into the hydraulic cylinder within tight limits independently of the pressure and temperature of the oil medium. As shown in Fig. 4.6b, the installation speed was then successfully maintained throughout the installation of the model pipe within a control band of 0.2 mm/s, or 2% of the target installation speed (0.75 mm/s in test T3 and 1.25 mm/s in all subsequent tests).

#### 3.3.6.4 Pipe-strongbox interface

Particular attention was given to the design of the joints between the model pipe and the strongbox. The function of these components was to seal against the lubricant pressure in the overcut and prevent leakage of the soil's pore fluid during and after the installation of the model pipe.

Since the model pipe was fitted with a cutting edge that was 3.5 mm larger in diameter than its shaft, the seal between the strongbox and the pipe had to accommodate for this reduction in diameter during the installation. To overcome this difficulty, the system shown in Fig. 3.7 and 4.17 was devised. It consists of a sleeve leaving a 2.0-mm clearance around the main body of the *LCPM*. This sleeve may slide back and forth on a distance equivalent to the length of the cutting edge, so it can be mounted behind this edge at the beginning of the installation and gradually move forward as the excavation proceeds. In its final position, it rests flush to the soil model surface and prevents clay from being squeezed into the gap between the *LCPM* and the inside of the strongbox collar. In its initial position, the retracted position of the joint allowed the cylinder and tank flanges to be bolted together, with the front end of the cutting edge being slightly protruding into the clay, as shown in Fig. 3.7. As shown in this figure, two 'O'-rings and a lip seal ensured the water tightness between the flanges, the strongbox collar, and the sliding joint. It has to be noted that difficulties were encountered to slide the joint in place after installation (due to misalignment) and that the joint was therefore left with its front end at some distance between the collar flange and the clay surface. Despite this difficulty, the joint arrangement proved effective: the pore pressure was withheld throughout the 24 h equilibration stage and no lubricant escaped from the annulus around the pipe.

Another seal was required to prevent flow of water through the inside of the model pipe in its final position. Because it was not feasible to seal off the excavation face from the inside of the pipe (as, say, in a closed-face tunnel boring machine), the pipe

was driven throughout the strongbox so that its cutting edge would protrude on the opposite side. There, the difficulty was the potential misalignment of the pipe as it emerged into the collar: a deviation of  $0.2^\circ$  between the *LCPM* and the targeted excavation axis would cause over 2.5 mm lateral deviation of the cutting edge. The use of conventional seals, such as ‘O’-rings or lip seals, would have required severe tolerances on the alignment of the *LCPM*. Therefore, an alternative solution was devised in order to obviate the anticipated complications.

The joint where the *LCPM* protrudes from the strongbox was made by driving the cutting edge approximately 20 mm into a solidified paraffin wax block, which was cast into the strongbox collar prior to the model pipe installation. The paraffin wax sealed both the excavation face, preventing pore pressure flow inside the model pipe, and around the cutting edge, keeping the lubricant into the overcut annulus. Low melting point paraffin wax was used; as it is more ductile and cracks formation resulting from the cutting edge penetration into the paraffin was reduced. The preparation of the blanking plug is shown in Fig. 3.17: the steel plug was first removed, rotated and bolted back on the flange to blank of the cylindrical cavity within the strongbox collar. The wax was then melted, slowly poured into the collar via a port in the collar and allowed to set for several hours. The integrity of the wax plug was verified by removing the steel cover and, when necessary, the operation was repeated by pouring additional paraffin wax in the collar.

### 3.4 Soil model preparation

This section discusses the properties of the soil model. The material selection is first discussed (§ 4.4.1), before reviewing some of its engineering properties (§ 4.4.2) and describing the soil model preparation technique (§ 4.4.3).

#### 3.4.1 Material selection

Soil models of repeatable properties are best achieved when prepared using industrially processed raw material rather than natural samples recovered from the field. Kaolin clays (so-called China clays) are readily available commercially, and their properties are controlled within well-defined limits. Different varieties of kaolin have been used as the standard clay material for geotechnical modelling at the University of Cambridge. While the fine-graded Spestone and Spewhite were used by many researchers until about 1990s (*e.g.*: Mair, 1979), Polwhite E (so-called E-Grade) has replaced these varieties in recent years. This variety, supplied by Richard Backer Harrison Group<sup>12</sup>, is a medium particle size kaolin that may be classified as a

low plasticity, silty clay. It has recently been used by Evans (1994), Potter (1996), Barker (1998), Carrier (2000), Garribo (2003), Take (2003), Merritt (2004) and Thushyanthan (2005). The fundamental and mechanical properties of E-Grade kaolin determined or compiled by these researchers are summarised in Table 4.1 and are discussed further in § 4.3.

### 3.4.2 Soil Model Preparation

#### 3.4.2.1 Slurry preparation

The soil samples were prepared by mixing dry E-grade kaolin powder with tap water. In order to guarantee uniformity of the slurry, it was mixed at a minimum of 100% water content, which approximately corresponds to twice the liquid limit of this clay material. Two batches of 450 kg were mixed mechanically for approximately 6 hours under a partial vacuum of -100 kPa below atmospheric pressure to ensure initial saturation of the slurry.

The use of de-ionised or distilled water involved too much effort with regard to the required quantities. Knoyle (1979) showed that the Cam-clay parameters  $\lambda$ ,  $\kappa$ , and  $\Gamma$  of Speswhite kaolin were not perceptibly affected when preparing the clay with de-ionised water instead of the tap water.

After having carefully greased the sidewalls of the strongbox with water-resistant grease, the slurry was transferred from the mixer into the strongbox using a diaphragm pump. The inlet of the pump was placed in the mixer, well below the surface of the slurry, while its outlet was kept submerged under the slurry in the strongbox. This way, no air was trapped during this process and the slurry retained its initial saturation.

#### 3.4.2.2 Top and bottom boundary drainage

A two-way drainage was provided to allow faster consolidation. The horizontal boundaries of the soil model were covered with filter paper and a 5-mm thick porous polypropylene sheet (Vyon) to filtrate the pore water expelled from the consolidating clay. Tissue paper was carefully placed around the Vyon sheets to prevent oozing of the clay between the sidewalls of the strongbox and the Vyon. A woven mesh with 5x5 mm weaves was placed directly on the base of the strongbox to increase horizontal permeability between the clay and the strongbox and allow excess water to drain through the outlets provided in the base plate. At the top boundary,

lateral permeability was achieved by a mesh of circumferential and radial grooves machined in the piston.

#### 3.4.2.3 Consolidation procedure

The clay model was consolidated to an OCR of 8, and tested under a vertical effective stress  $\sigma_{v0}' = 100$  kPa. The maximum consolidation pressure of  $\sigma_{vp}' = \sigma_{vp} = 800$  kPa was reached in two stages, as shown in Fig. 3.18. A preliminary consolidation to a vertical effective stress of 400 kPa was first carried out, before reducing the vertical stress to zero and installing the pore pressure transducers.

The preliminary consolidation stage occurred by increasing the vertical load incrementally, approximately doubling the load after each increment. Each increment of stress was maintained until the measured rate of vertical compression had reduced to small values of the order of 1 mm/h. This typically resulted in a consolidation time of 48 hours for each loading steps below 25 kPa, progressively reducing to about 18 hours at larger pressure increments.

Upon reaching the maximum pre-consolidation stress, the vertical stress was decreased to zero in several increments of no more than 100 kPa to prevent cavitation of the pore fluid. During unloading, water was fed to the drainage lines to avoid air being sucked in the model. Approximately 24 hours were allowed for dissipation of excess pore pressure after removal of the last total stress increment, and the pore pressure transducers (*PPTs*) were then installed into the soil model as described in § 3.5.3.6.

Consolidation resumed immediately after the installation of the *PPTs*: the strongbox was reloaded into the consolidation frame, carefully aligned under the cylinder ram and a total stress of 100 kPa was reapplied to the clay. The load was then doubled until the maximum stress of 800 kPa was reached. More time was allowed for the last increment to equilibrate so that the effective stress profile in the vertical direction would not be affected by residual excess pore pressure.

After reaching equilibrium under a vertical stress of 800 kPa, the load was reduced in steps of 50 kPa, while feeding water into the sample from both drainage boundaries. In tests T1 to T4, the unloading stopped at 200 kPa. A back-pressure of 100 kPa was then applied by pressurising a 10 l air-water interface, which connected to the drainage line. The effective stress acting at the boundary thus reduced to  $\sigma_{vp}' = 100$  kPa. After full equilibrium was reached, the model was ready for testing. In tests T4 to T8 the total stress was completely removed to allow the hydro-

pneumatic pressure system to be connected. Total stress and back pressure were then applied to the model and, when necessary, readjusted to reach the required equilibrium.

### 3.5 Apparatus instrumentation

#### 3.5.1 Summary

Essentially, the instrumentation of the pipe jacking apparatus consists of six earth pressure and six pore pressure cells measuring total stress and fluid pressure on the pipe, as well as eight pore pressure transducers measuring the pore pressure in the soil model. Another ten instruments were used to monitor and control the boundary conditions before, during and after the installation of the model pipe.

A schematic of the model pipe instrumentation and the position of the pore pressure transducers are shown in Figs 3.19 and 3.30, respectively, while Fig. 3.2 shows a synoptic diagram of the instrument used to measure the boundary conditions. The main characteristics as well as the calibration data of the model pipe instrumentation, the *PPTs* and the ancillary instrumentation are summarised in Table 3.2 and 3.4. This section focuses on the description and the calibration method of the model pipe instruments and the *PPTs*. The calibrations of the other instruments are relatively straightforward and are therefore only described briefly.

#### 3.5.2 Model pipe instrumentation

##### 3.5.2.1 Earth pressure cells

As depicted in Fig. 3.19, the model pipe (*LCPM*) described in § 3.3.3 is instrumented with earth pressure cells measuring the total radial stress at six equally spaced locations around its circumference. A photograph of the load cell clusters that house the instruments is shown in Fig. 3.20. These earth pressure cells, which are similar in design to the Cambridge-type contact stress transducer of Arthur and Roscoe (1961), consist of a top plate with an active area of 5 cm<sup>2</sup> supported by four slender strain-gauged webs. Strain gauges are arranged on the webs, so as to be sensitive to normal stresses and compensate for bending moment resulting from load eccentricity. The shear stress acting on the load platen as a result of the friction between the soil and the pipe may not be measured with these instruments.

In addition, six pressure transducers measure the internal gas pressure in each of the sealed load cell compartments when operating in the so-called active or null-sensing

mode. This allows the deflection of the load cell platen to be controlled by the internal gas pressure so that the load platen remains flush to the pipe surface regardless of the load to which it is subjected. Zeroing the platen movement and measuring the gas pressure required to do so allow the effective stress to be derived indirectly. If used in direct mode, *i.e.* without internal gas pressure counteracting the soil pressure, the instrument may be subjected to error owing to the small movements of the top plate. Although this movement is small, about 16  $\mu\text{m}$  at 2 MPa pressure, it significantly reduces the readings due to arching effects around the plate. The magnitude of this under-registration depends on the relative stiffness of the cell and the soil (Carder & Krawczyk, 1975). While it is intended that the load cells be used in active mode to minimise under-registration effects, this was thought to be an unnecessary complication for the present study. Indeed, several additional components would have been required, adding to the complexity of the system and its susceptibility to failure.

The direct stress cells were calibrated by applying pneumatic pressure in a sealed collar placed over the load cell clusters. The applied pressure was measured with a Druck digital pressuremeter and recorded manually. The calibration showed linear output over the range of zero to 200 kPa, and the average sensitivity obtained in the eight calibrations of the load cell were comprised between 740 and 883 kPa/V for the six instruments, as summarised in Table 2.

#### 3.5.2.2 Pore pressure cells

The pore pressure transducer on the *LCPM* will be referred to as “cells” (or *PPC*) rather than “transducers” (or *PPT*) to avoid confusion with the miniature transducers buried within the soil and described in § 3.5.5.

The *LCPM* is fitted with six pore pressure cells (*PPC*) located a distance of 49 mm to axis behind each direct stress cells. They measure the value of the hydraulic boundary condition at the pipe surface and therefore allow the derivation of the ground loading on the pipe in terms of effective stresses. The *PPCs*, shown in Fig. 3.21, consist of a 5-mm diameter filter elements mounted flush with the pipe surface and which separates the soil from the water reservoir of the *PPC*. A 350- $\Omega$  rosette strain gauge measures the deflection of the circular diaphragm at the base of this reservoir when water is driven through the filter as a result of pore pressure changes in the soil.

Saturation of the pore pressure cells required a special procedure to ensure high-quality response of these instruments. The main motivation for careful saturation was

to mitigate evaporation-driven desaturation before the insertion of the model pipe into the soil causing growth of air bubbles in the reservoir and biased response. The difficulty in saturation was due to the fact that, although the filter element was easily detachable, the *PPCs* reservoir cannot be removed from the *LCPM* body for saturation. Using the technique described in § 3.5.3.3 by which the cells are saturated under vacuum is therefore limited by the manoeuvrability of the *LCPM*.

In the first experiments (T1 to T4), the *PPCs* were therefore, for simplicity, “saturated” by submerging the porous elements in a water bowl and bringing it to ebullition. Immediately before the insertion of the model pipe, the reservoir above the diaphragm was filled with de-aired water using a pipette. The cap with the filter element was then mounted, while a 1.5 mm aperture through the cap allowed air remnants to vent out of the reservoir. The vent was finally blanked off with a grub screw and the porous element covered with saturated clay slurry to delay air-entry and avoid de-saturation before the insertion of the model pipe into the soil model. The *LCPM* was then rotated by 60° and the operation repeated until all *PPCs* were saturated.

Clearly, this procedure did not ensure a high degree of saturation because some air was inevitably trapped in the reservoir during this process. Therefore, an improved technique was devised for the second half of the tests (T5 to T8), using a procedure similar in principle to that used for the saturation of the miniature *PPTs* (see § 3.5.3.3). Figs 3.22 and 3.23 show the set-up that was adopted to allow initial saturation under vacuum. The oven-dried filter elements were mounted on the model pipe (the air vent blanked off) and sealed in a sleeve leaving a small annulus around the *LCPM* and the intrados of the sleeve. A partial vacuum nearing -100 kPa was applied to the cylindrical sleeve via a connection port at its apex. The bottom of the sleeve was connected to the dip pipe of an air-water interface, itself subjected to the same vacuum of -98 kPa. Tap 1 initially isolated the water reservoir from the sleeve, and the vacuum was left for a minimum of 30 min to de-air the water, the sleeve, the pore pressure cell filters and their reservoirs. After this de-airing stage, tap 1 was opened and the pressure on the air-water interface slightly increased (to about -93 kPa), so as to induce a slow and controlled flow of water from the chamber into the annulus between the sleeve and the *LCPM*. This way, the pore pressure cells were gradually submerged under a partial vacuum of about -95 kPa. Once fully submerged, taps 1 and 2 were closed to retain the water within the sleeve, and the rest of the system was disconnected to prepare for the installation of the pipe. The sleeve was removed a few minutes before the installation begun to allow the *LCPM* to be retracted within the guiding cylinder and the cutting edge to be mounted at its

extremity. After the sleeve had been removed, the filter elements were coated with kaolin slurry to delay evaporation-driven de-saturation before the end of the *LCPM* installation into the soil model.

### 3.5.2.3 Displacement transducers

Due to technical difficulties and time restrictions, the devices described below could not be incorporated in the tests. However, their design is briefly described in the interest of future development for similar application.

The existing instrumentation on the *LCPM* did not allow measurements of the deformation of the contracting cavity. Although the time at which ground closure occurs may be determined by looking at when the pore pressure departs from the total stress (effective stress becomes non zero), knowledge of the radial convergence of the cavity was desired to derive time-convergence relationships in the presence of difference lubricants. Therefore a device was designed to measure the radial convergence of the cavity at a location close to the earth and pore pressure cells.

Several constraints limited the choice of design option for the instrument measuring the cavity convergence:

- The instrument was to be under up to 1 bar fluid pressure either in water or in polymer lubricant. Water-tightness of the load cell clusters had to be guaranteed throughout the tests, to protect the electronic components in the instruments cluster;
- No irreversible modifications could be made to the *LCPM*;
- The installation of additional wiring for power and signal was unreasonably complicated. The device was therefore designed to operate at the same excitation as the other instruments so that the existing power and signal transmissions could be used;
- The lip seals shown on Fig. 3.7 restricted the design in that the instrument could not initially protrude from the model pipe shaft or be sensitive to the shearing against the lip seals when penetrating into the soil container.

The design concept that was developed to meet with these constraints consisted in removing three of the six pore pressure cells and uses the space, mounting holes and

power supply thus provided to accommodate a displacement transducer. The design of the instrument is shown in Fig. 3.24, and its main components are photographed in Fig. 3.25. The device comprises a base plate of identical geometry as that of the main body of the *PPCs* and a retractable piston that could move in the radial direction. This piston was initially flush to the pipe surface to allow insertion of the *LCPM* into the soil model. After the pipe installation, the piston could be pushed radially until its cylindrical face came in contact with the excavation boundary. The piston was actuated using the pneumatic pressure supply available in the load cell clusters for the operation of the earth pressure cell in active mode. After the piston was deployed in this position, the air pressure below the piston was released from the back of the probe so as to leave the piston free to retract. The piston would then be held into position by friction in the ‘O’-ring between its shaft and the main body of the instrument, and could be retracted to its initial position under the effect of the converging cavity. The friction resistance to be overcome when retracting the piston was marginal, and therefore, the support pressure applied to the converging cavity was negligible.

The movement of the piston, and, hence the convergence of the cavity, is measured by connecting the piston to a beryllium copper cantilever, which deflects as the piston moves between the initial to its expanded position. The cantilever is strain-gauged with a full Wheatstone bridge and wired to measure its bending deformations while compensating for temperature effects. The connection between the piston and the strain-gauged element was achieved using a cantilever arm (Fig. 3.25) on the “dry side” of the ‘O’-ring that seals the gap between the moving shaft and the main body of the transducer. This part of the instrument was machined to the most severe tolerances so that the ‘O’-ring compression would be just sufficient to ensure water tightness. Thus the friction between the piston shaft and the ‘O’-ring could be minimised and the piston could be actuated in the radial direction with reasonably small pneumatic pressures.

Because no seal was provided between the shaft and the piston, air leaked into the instrument chamber, failing to build up sufficient pressure to overcome the friction acting on the piston shaft and provoke its outward motion. To prevent air from escaping, the thin annulus (0.1 mm thickness) between the piston and the shaft was filled with high viscosity grease. This proved sufficient to seal against air pressures and allow the piston to be effectively pushed outwards by means of pneumatic pressure.

### 3.5.3 Pore pressure measurements in the soil

#### 3.5.3.1 Generalities

Detailed measurements of the excess pore pressures resulting from the unloading of the cavity and their dissipation during the transient stage leading to equilibrium were desired. This is because the ground loading on the pipe is a consolidation problem, for which mechanisms may only be fully explained if the pore fluid response is understood.

Therefore, a series of miniature pore pressure transducers (*PPTs*) were installed at the pipe axis level, in the median vertical plane perpendicular to the model pipe. In order to obtain the radial distribution of pore pressure, the devices were located at a range of horizontal distances from the pipe axis varying between 1.3 and 8.0 pipe radii, *i.e.* 55 and 332 mm from the pipe axis, as depicted in Fig. 4.8. The distance between the devices was smaller in the vicinity of the excavation, where larger pore pressure gradients were expected, and gradually increased away from the pipe. Some *PPTs* were arranged at equal distance on either side of the pipe axis to establish the symmetry of the pore pressure response and assess the relevance of the pipe misalignment. A pair of devices was also installed in another cross-section in order to measure how the circular shape of the box (§ 3.2.5) affects the pore pressure generation and dissipation in a cross-section where the side boundary is significantly closer to the excavation than in the equatorial cross-section of the strongbox. The *PPT* layout was slightly varied in the different tests, and the position of each transducer is summarised in Fig. 4.8.

Measuring the pressure of the pore fluid in saturated clay is a task that requires particular attention, since many factors may compromise the reliability of the measurements. Firstly, difficulties may arise with the actual installation method of the transducers within the soil: the homogeneity and the properties of the soil model should not be altered by the installation and the presence of the *PPTs*, hence the need for miniature devices and an adequate installation method. Miniaturised devices are patently fragile and susceptible to electronic and mechanical malfunction. Secondly, the nature of the device requires careful techniques of saturation and calibration as their response to pressure change is significantly affected by the presence of even the merest quantity of air within the instrument. This section describes the methodology that was adopted to ensure the highest possible confidence in the measurements of pore water pressures within the soil model, successively describing the transducer technology (§ 3.5.3.2), the saturation and calibration techniques (§ 3.5.3.3 and

3.5.3.4, respectively), the quality-control of the transducer responses (§ 3.5.3.5) and the insertion methods (§ 3.5.3.6).

### 3.5.3.2 Transducer technology

Two families of miniature *PPTs* - the Druck *PDCR-81* and the modified Entran *EPB-C1* -, were used in the present study. These two types of transducers both have similar dimensions with a diameter in the region of 7 mm, and a nominal pressure range of 700 kPa. They both operate on the same principle: a filter element sufficiently fine to retain soil particles but coarse enough to be permeable to water separates the soil from a small reservoir, the base of which consists of a flexible strain-gauged diaphragm. Changes of pressure in the pore fluid cause a hydraulic gradient across the filter, which induces a flow of the pore fluid into, or out of the reservoir. If the reservoir is initially saturated, the diaphragm is forced to deflect, returning an output from which the pressure may be accurately inferred if the device has previously been calibrated carefully. Owing to the tensile strength of water, the diaphragm may be “pulled outwards” as the pore pressure in the soil becomes negative. However, any occurrence or emergence of air bubbles in the reservoir or in the filter instantaneously destroys the tension of the water. As a result, tension of the pore fluid in the soil may no longer be transmitted to the diaphragm and the measurements become untrustworthy. Saturation techniques extenuating this undesired behaviour are detailed in the following section. The key features of the Druck and Entran *PPT* are given hereafter; more details of their design and a discussion of their performance may be found in Take (2003) and Take & Bolton (2002).

The Druck *PDCR-81*, fabricated by Druck Ltd<sup>13</sup>, is the current standard for measurement of positive pore water pressures. It has been widely used at Cambridge University since the 90's and its design and performance are discussed in Ridley & Burland (1993), König *et al.* (1994) and Take (2003). The outer body of the *PPT* is a cylinder of 6.35 mm diameter by 12.20 mm length, including the filter element. As shown in Fig. 3.26, the Druck *PDCR-81* consists of a 0.13 mm thick strain-gauged silicon diaphragm mounted on a glass cylinder, leaving a small gap between the outer steel body of the device to avoid sensitivity to lateral soil pressures. A ceramic filter element can be push-fitted at the extremity of the steel casing, leaving a 0.13 mm gap between the filter and the instrumented diaphragm. The average sensitivity measured with a nominal excitation of 10 V DC was 46.35 kPa/V, after signal amplification by a gain of 100. Owing to its silicon diaphragm, this device usually displays good performance in terms of thermal sensitivity. While the *PDCR-81* performs

remarkably well under positive pressure, it has been found to have limitations when it comes to measuring large tensions (Ridley & Burland, 1999). The design features limiting the sustainable tension are discussed in detail by Take (2003).

Limitation of the Druck *PDCR-81* in measuring pore water tension recently prompted the design of a new device at the University of Cambridge (Take, 2003). Take collaborated with Entran to develop a so-called pore pressure and tension transducer (*PPTT*) that could reliably measure large suctions. The novel instrument is based on the commercially available Entran *EPB-C1*<sup>14</sup>. The detailed design evolution of the *PPTT* and its resulting aptitude for large suction measurements are discussed in Take (2003). The pressure sensitive element of this device consists of a stainless steel welded diaphragm. As shown in Fig. 3.26, a stainless steel ring is mounted on the *EPB-C1* chassis, leaving a deliberated gap around the diaphragm to eradicate cross-axis sensitivity. The ceramic filter element is bonded to the edge of this stainless ring using a high-strength adhesive, and may be conveniently replaced without damaging the *PPT*. The Entran body is 6.98 mm in diameter, and about 40% shorter than the Druck device with a total length of 7.04 mm. When powered with a 10 V *DC* supply, the average sensitivity was slightly higher than that of the Druck instrument, with 52.38 kPa/V, after signal amplification by a gain of 100. Considerable zero drifts were observed and it was found that for long-term measurements, the device was only adequate to measure relative pressure changes. The average range of zero offset for all the Entran devices was as high as 227.56 kPa, while the offset of the Druck transducers only drifted over a range of 50.55 kPa. The average sensitivity and its standard deviation as well as the average offset and maximum zero drift are tabulated in Table 4.4.

### 3.5.3.3 *PPT* saturation

Meticulous saturation routines were implemented to thoroughly de-air the transducer reservoirs and their porous stones. Impeccable saturations were required because poorly de-aired *PPTs* become vulnerable when subjected to pressures below atmospheric. Remnants of air in the transducer filter or reservoir (cavitation nuclei) may form bubbles, which then grow, and eventually lead to cavitation as the pressure is reduced towards absolute negative pressures (Take, 2003). Further increments of pressures then result in gas expansion or contraction in the transducer. This adversely affects the response time of the transducer, the magnitude of the measured pressure, the repeatability of the output, and prevents the measurement of pore suction. The output of a poorly saturated instrument is simply unreliable.

Although the unloading of the cavity causes a rapid drop of pore pressure, possibly as far as atmospheric pressure, no pressures significantly inferior to atmospheric were expected during the actual test. However, the *PPTs* experience large pressure decrements during their lifetime, potentially reaching absolute negative pressures. These increments may occur during consolidation, as the maximum consolidation pressure (800 kPa) applied on the soil model is reduced to the test pressure (200 kPa). Each decrement of total stress at the model boundary causes an equivalent reduction of pore pressure in the soil model. If the model is at equilibrium before a total stress reduction of, say, 100 kPa, the pore pressure drops from hydrostatic, *i.e.* close to atmospheric, to -100 kPa gauge pressure (or close to absolute negative). *PPTs* may also be subjected to pressures well below atmospheric after their insertion into the soil model. This is the case when equilibrium is not fully achieved at the time of insertion; residual negative pore pressure in the soil combined with the possible presence of air trapped during the insertion process may expose the *PPTs* to sufficiently large tension to provoke air-entry in the transducer, if they are poorly saturated.

If air bubbles are present or if they grow as a result of poor saturation, the response time of the transducer will be adversely affected as more flow of water through the ceramic filter will be required to make up for the gas expansion or contraction in the *PPT*. Therefore, capturing the rapid pore pressure drop (of the order of 80 kPa), which occurs upon excavation of the cavity required a well-saturated instrument. Therefore, in addition to the limitation of consolidation pressure decrements and sufficient dissipation of excess negative pore pressure before the insertion of the *PPT*, impeccable saturation was necessary to ensure high-quality pore pressure measurements. In addition, this carefulness reduced the risk of putting the effort of saturating, calibrating and carefully inserting the pore pressure transducer to jeopardy by triggering cavitation with an accidentally large pressure drop on the soil model.

Saturation techniques have become more sophisticated over time, resulting in much higher measurable suctions for a given type of transducer. Traditionally, saturation took place by simply immersing the transducers in de-aired water and subjecting the submerged devices to several pressure cycles between atmospheric pressure and -90 kPa in glass desiccators (*e.g.* Mair, 1979). Porous filters were submerged in boiling water until air ceased to escape from their pores (*e.g.* König *et al.*, 1994). Recently, Take (2003) showed that initial saturation under vacuum significantly reduced the theoretical pressure required to fully dissolve air remnants in the transducer. Considerably higher degrees of saturation could therefore be achieved by saturating the transducer under a partial vacuum, followed by pre-pressurisation to a

pressure nearing the permissible over-range of the transducers to force remnants of air into solution, which stabilised cavitation nuclei by reducing the radius of air bubbles at a given pressure. The theoretical justification of this method using Boyle's and Henry's law as well as comparison of its performance with that of other techniques are discussed extensively in Take's dissertation.

The entire contingent of *PPTs* was saturated before each of the eight tests with a technique essentially similar to that proposed by Take & Bolton (2003). The saturation set-up is shown in Fig. 3.27: an oven-dry *PPT* is sealed in a fully impervious cylindrical Perspex chamber. The Perspex cylinder is originally kept horizontal and filled with thoroughly de-aired water in such a way that the *PPT* would remain above the surface of the water. A partial vacuum of approaching zero absolute pressure is then applied in the chamber via a port located above the water level and maintained for a minimum of 20 minutes. The Perspex cylinder is then slowly rotated until the *PPT* is fully submerged. After another 30 minutes, the vacuum is reduced and saturation proceeds under atmospheric pressure. The freshly saturated *PPT* is then transferred to the calibration manifold where it is subjected to a large pressure of the order of its permissible full load (700 kPa) in order to force remnants of air into solution.

#### 3.5.3.4 *PPT* calibration

The eight *PPTs* were calibrated at least once before each test, using the calibration set-up depicted in Fig. 3.28. Eight *PPTs* were sealed simultaneously into the manifold, which had previously been carefully de-aired by applying several pressure cycles between -100 kPa and 1000 kPa. The *PPTs* were pressurised by applying pneumatic pressure to an air-water interface connected to the manifold. Pressure increments below atmospheric were applied by connecting the interface chamber to a vacuum line. The applied pressure was measured with a Druck digital pressure indicator and recorded manually, while the output of the *PPTs* was logged at 5 Hz throughout the calibration. A 10-bar range pressure transducer also measured the pressure inside the manifold continuously. The pressure recorded manually was used to derive the calibration factors of the pressure transducer, which was then used to calculate the calibration factors of the *PPTs*.

The calibration procedure consisted in increasing the pressures from atmospheric to 100 kPa in pressure increments of approximately 10 kPa, each increment being maintained for a minimum of 30 to 60 seconds. Upon reaching 100 kPa, the pressure was reduced in steps of -10 kPa, until about -80 kPa. A second cycle of positive-

negative pressure was then applied to assess the repeatability of the response. The second cycle also permitted inappropriate saturations to be revealed, because approaching absolute suction in the first cycle often triggered partial de-saturation, should the device be improperly saturated. The average sensitivity and its standard deviation as well as the average offset and maximum zero drift are tabulated in Table 3.3.

#### 3.5.3.5 Quality control of *PPT* measurements

Quality-control of the *PPT* saturations was systematically performed before inserting the transducers into the clay model. Poor saturation was detected by scrutinising the response of the transducers in the pressure range between atmospheric and -80 kPa gauge pressure: bubble growth would be detected by suspiciously large response time and non-linear or sometime unstable output. Whenever poor saturation was suspected, the *PPT* was re-dried in the oven, and re-saturated until the desired high-quality response was achieved as a badly saturated device not only returns unreliable measurements but is also prone to failure.

The loading history and the measured response of an unsuccessfully saturated transducer is shown in Fig. 3.29. The calibration curve was subdivided in four segments corresponding to the different loading stages. The first two segments correspond to the loading and unloading from atmospheric to approximately 200 kPa gauge pressure, while the third and the fourth segments represent the unloading from atmospheric to -50 kPa and the subsequent reloading to about 60 kPa, respectively. The sensitivity of the transducer was calculated by segment-wise linear regression of the calibration data.

This detailed analysis of the calibration data reveals that the *PPT* responses to loading and unloading in positive gauge pressure is linear and differ by just over 1%. However, the slope of the calibration curve for unloading below atmospheric pressure is 25% larger than the average sensitivity measured for the first pressure cycle in the positive pressure range. On reloading, the *PPT* response is barely discernible to that in the first pressure cycle; it recovers its “original” sensitivity. Therefore, the response of poorly saturated *PPTs* is affected by considerable hysteresis, and stiffer response in unloading below atmospheric pressure.

In contrast, the behaviour of another transducer of the same type (Entran EPB) is shown in Fig. 3.30. It can be seen that the slope of the calibration lines as calculated for the different segments defined above all fall within 1% of their average value.

This falls within the margin of error that has to be allowed for the accuracy, stability and measurement of the applied pressure.

#### 3.5.3.6 *PPT* insertion into the soil model

The main challenge of the *PPT* installation was to accurately position the *PPTs* into the soil without de-saturating the transducers or the clay and by causing minimal disturbance to the soil model. An installation method allowing accurate positioning was required, since the target position of some *PPTs* was as close as 5 mm from the excavation boundary; slight deviation from this position would have resulted in the destruction of the *PPT* during the excavation of the cavity.

The *PPTs* were installed from the consolidation piston, through the ports described in § 3.3.1 and shown in Fig. 3.5. Downward vertical holes, 8 mm in diameter, were sunk to the depth of the excavation axis. Horizontal installation from the side wall of the tank was discarded because drilling would have had to be made at a different angle to the tank wall or a different distance from the side-wall for each transducer in order to install them along a straight line. Vertical installation, in contrast, could be done at right angle to the piston and to the same depth for each transducer, which was more convenient. Also, vertical insertion from the top of the sample eased the dismantling of the tank after the test, allowing the strongbox to be disassembled by lifting the sidewall so as to expose the soil sample with the *PPTs* trapped through the piston. The transducers could then be conveniently excavated from the side of the model, and a new model could be prepared and consolidated before the excavation of the previous model finished, thus allowing a reduction of the test cycle time.

The *PPTs* were installed in a pre-consolidated soil model. The consolidation stress applied before the *PPT* installation was selected so that the clay was sufficiently consolidated to restrict displacement of the *PPTs* in the subsequent consolidation stage and deviation from their targeted installation position. However, this pre-consolidation stress had to be limited to ensure that the slurry used to backfill the hole through which the *PPT* were installed would consolidate to the same degree than the adjacent clay and yield an homogenous model without preferential drainage paths along the *PPT* cables. It was found that pre-consolidating to a stress of  $\sigma_{vp}' = 400$  kPa was adequate to satisfy these two requirements: on excavating the *PPT*, their position was found to be within 3 mm of the targeted position and no noticeable difference of consistency was observed between the backfill and the surrounding clay matrix. A post-mortem impression of the *PPT* array is shown in Fig. 3.31.

---

The installation was made using the method developed by previous researchers at Cambridge. The plugs blanking the ports through the piston were first removed. An 8-mm diameter hole was sunk to the depth of the excavation axis by gently pushing a thin brass casing while removing the plug of soil in the latter with a hand auger. On reaching the desired installation depth, the casing was removed and the saturated *PPT* inserted using a half-pipe guide. The *PPT* was pushed approximately 5 mm into the soil below the bottom of the excavation. Finally, the hole was back-filled with E-grade kaolin slurry at approximately 70% water content using a dedicated clay-syringe.

#### 3.5.4 Monitoring of boundary conditions

A synoptic overview of the instrumentation described in this section is shown in Fig. 3.2, while the characteristics of each device are recapitulated in Table 3.4. The tag in brackets appearing in the section title refers to the label of the corresponding instrument in Fig. 3.2

##### 3.5.4.1 Total stress boundary condition (*LI*)

The total stress applied at the top boundary of the soil model during both the consolidation and the test was monitored with a load cell located between the hydraulic cylinder ram and the piston. The load cell was a bespoke column-type compression load cell<sup>15</sup>, with a nominal range of 50 t. The load cell was specified to feature linearity and repeatability characteristics above the usual datasheet standards. This helped improve the precision of the measurements of the small increment of stress applied in the early stage of the consolidation. The load cell was calibrated by the manufacturer who quoted a sensitivity of 18.79 kN/V for an excitation of 10 V and after signal amplification of 100. A spigot located the instrument through a hole in the loading plate of the piston, and although the load cell was compensated for bending moments, its loading surface was originally dome-shaped to eliminate bending moments in the load cell. This dome was later machined to a flat surface after recurrent problems due to tilting of the piston had occurred. This helped prevent the rotation of the piston discussed in § 3.3.1.

##### 3.5.4.2 Hydraulic boundary condition (*PTI*)

The back pressure was measured with a 700-kPa range Druck pressure transducer. The transducer was connected to the top drainage line. It was recalibrated under pneumatic pressure on several occasions, though not after each tests.

### 3.5.4.3 Height of the soil model (*DWI*)

The vertical position of the piston applying the total stress to the soil model was monitored, in order to derive the value of the soil's voids ratio during consolidation and to indicate the height of the soil sample. This allowed, on the one hand, to estimate the consolidation ratio and decide when to increase the consolidation pressure and, on the other hand, to derive soil model properties such as the consolidation coefficient  $c_v$ , and the Cam-Clay parameters  $\lambda$  and  $\kappa$ . The piston position was measured by means of a 750-mm range cable actuated high-precision potentiometer<sup>18</sup> (draw wire transducer). The housing of the potentiometer was clamped on the consolidation frame while the cable was attached to the piston. The draw wire transducer was calibrated once at the beginning of the test series by fastening it on a bench and pulling the cable to different positions measured to a precision of  $\pm 1$  mm, as described in Merritt (2004).

### 3.5.5 Monitoring of lubricant injection

#### 3.5.5.1 Lubricant pressure (*PT2* and *PT3*)

The injection pressure of the lubricant is an important parameter, since it corresponds to the hydraulic boundary condition at the excavation boundary prior to the closure of the overcut onto the pipe. The lubricant pressure was measured by the pore pressure cells on the *LCPM*, but because the injection of lubricant was to begin before these instruments had penetrated into the soil model, an independent measure was required. A pressure transducer was therefore connected to the injection line, close to the actual injection port. In test T1 to T4 the ports were located on the actual model pipe behind the cutting head. Dynamic losses in the hose carrying the lubricant from the tank to the injection points caused the measured pressure to slightly overestimate and the actual pressure in the overcut. In tests T5 to T8, the lubricant was injected immediately into the overcut through a port in the strongbox collar, as shown in Fig. 3.7. In this case, the pressure gauge was located adjacent to this port, at the level of the pipe axis, so that the measured value matched the pressure of the lubricant at the excavation boundary. No particular saturation procedure was adopted for the pressure gauges: their reservoir was simply submerged in a water container before being push-fitted in the previously saturated injection line. The pressure gauges were regularly calibrated as described in § 3.5.4.2.

### 3.5.5.2 Lubricant volume (*L2*)

The flow rate of lubricant injected around the model pipe was monitored throughout the installation. This was achieved by hanging the lubricant reservoir to a high resolution load cell which measured the weight of the assembly. The mass flow rate of lubricant was then obtained by differentiation of the reservoir weight with respect to time. A bi-directional 400-N range load cell<sup>16</sup> with off-axis load compensation was used for this purpose. Because the total weight of lubricant injected in a test was of the order of 10 N, the output resolution was relatively poor and required filtering before the data could be used.

This load cell was shared with other researchers and because the data it measured was not crucial, no independent calibration was performed and the calibration factors were obtained from a fellow researcher.

### 3.5.6 Monitoring of pipe insertion

#### 3.5.6.1 Model pipe position (*DW2*)

During installation, the model pipe was out of sight, within the guiding cylinder. Therefore, the pipe position had to be monitored during installation to control its final position and to derive its installation speed. The position was measured with a 1500-mm range draw-wire transducer<sup>19</sup>. This transducer operates on the same principle as the draw-wire described in § 3.5.4.3. The potentiometer housing was attached on the flange blanking the rear of the guiding cylinder, while the extremity of the draw-wire was connected to the pipe carriage. The calibration was made by moving the model pipe assembly to different positions and recording the draw-wire transducer output.

#### 3.5.6.2 Jacking force (*L3*)

The jacking force was measured to infer the average shear stress acting on the model pipe, not so much during installation, but rather during the post-equilibrium jacking events. A bi-directional 15-kN range load cell<sup>17</sup> was used for this purpose. Despite the bending compensation of the load cell, misalignment between the hydraulic ram, the model pipe carriage and the guiding cylinder were thought to influence the measured jacking force. Therefore, a special adaptor was devised so the load cell could be connected between the ram and the carriage with a loose fit. This way, misalignments would be compensated automatically and both tension and

compression can be transmitted. The calibration factors supplied by the manufacturer were used.

### 3.5.7 Signal conditioning, data acquisition and raw data processing

#### 3.5.7.1 Model Pipe instrumentation

All instruments on the model pipe were powered and logged with the dedicated system provided by Cambridge Insitu Ltd. This data acquisition system comprised the electronic compartment for signal conditioning located on the model pipe, immediately behind the cutting edge carrier and the junction box. The signals from the transducers are amplified in the electronic compartment, before being multiplexed and connected to a junction box via a 16 bit silver wire. The signals are de-multiplexed and converted from analogue to digital signals in the junction box. An RS232 cable connects the junction box to a laptop where the data is logged by a bespoke data acquisition software. After the test, the raw data may be retrieved in *comma separated value* (\*.csv) or *text* (\*.txt) format. The sampling frequency of the *LCPM* data is limited to 1/12 Hz.

#### 3.5.7.2 PPT and ancillary instrumentation

The remaining 16 instruments were connected to the standard junction box allowing differential amplification of the signals. The data was logged on a mobile PC with a 16 channel data card and the data acquisition software DasyLab<sup>20</sup>, which is at present the standard software used by researchers in Cambridge for data acquisition in 1-g and centrifuge testing. The data logger was set to store the data on *ascii* format (\*.asc). The sampling rate for all these instruments was normally 5 Hz, although 10 Hz was used in test T3.

## 3.6 Testing procedure

This section describes the test procedure by summarising the key activities of the test preparation and execution in chronological order. The previous sections focused on the detailed design evolution of the mechanical, electronic and geomechanical components of the experimental apparatus. The present section deliberately repeats some of the material discussed earlier in order to give a clear overview of the actual procedure. The numbers in parentheses refer to the section where each item is described in detail.

### 3.6.1 Soil model preparation

The sidewalls of the strongbox were coated with water-pump grease and the bottom drainage was prepared by placing successively a woven mesh, a Vyon sheet, and filter paper on the base of the strongbox. A volume of  $0.565 \text{ m}^3$  of E-Grade kaolin slurry at 100% water content was mixed under vacuum for approximately six hours before being transferred into the strongbox using a diaphragm pump. The slurry was then left to consolidate under its own weight for two days. Filter paper was then placed directly on the clay surface, followed by a Vyon sheet and tissue paper to prevent oozing of clay between the Vyon and the strongbox. The piston was then inserted into the strongbox, having previously cleaned and greased the 'O'-ring grooves. The strongbox was finally lifted into the consolidation frame and carefully centred under the ram. The consolidation then begun as described in § 3.4.3.3.

On reaching equilibrium under a total stress of 400 kPa, the stress was reduced to zero in steps of 100 kPa, while continuously feeding water to the drainage lines. After sufficient time had been allowed for pore pressure equilibration, the strongbox was placed on the laboratory floor, its extension removed and the ports through the piston were opened to allow insertion of the *PPTs*. The previously saturated (§ 3.5.3.3) and calibrated (§ 3.5.3.4) devices were then inserted into the clay (§ 3.5.3.6). Care was taken to prevent air from being drawn into the soil model by maintaining a hydraulic pressure above atmospheric under the piston. The strongbox was then reloaded in the load frame and consolidation resumed immediately so that the *PPTs* were not subjected to negative gauge pressures for a prolonged period of time.

The consolidation program was resumed until reaching a vertical effective stress of 800 kPa, at which point the pressure was kept constant for a minimum of three days to achieve full equilibrium. The pressure was then decreased to zero in steps of no more than 50 kPa to limit the suction in the *PPTs*, while feeding water to the top and bottom drainage lines. Each increment required approximately one day of equilibration time.

During the unloading from 800 kPa to atmospheric pressure, the blanking plug of the orifice into which the cutting edge protrudes at the end of the installation was removed, and rotated  $180^\circ$  so as to leave cylindrical cavity between the collar flange and the clay surface ("reception chamber for *LCPM* cutting edge"). Paraffin wax was melted and poured into the collar so as to form a plug inside this cavity (§ 3.3.6.4).

Once all the consolidation pressure had been removed, the hydraulic pressure line feeding the top chamber of the cylinder of the consolidation system was then

disconnected and connected to the oil-air interface chamber for the reasons described in § 3.3.2. Compressed nitrogen was used to reapply a total stress of 200 kPa to model and time allowed for equilibrium. A water back-pressure of 100 kPa was applied to the horizontal boundaries of the model and this hydraulic boundary condition maintained throughout the experiment.

The load applied to the piston, its vertical movement, the hydraulic back-pressure as well as the response of the *PPTs* buried in the soil model were then carefully observed for a period of 12 to 24 hours to ensure that equilibrium conditions prevailed before the test commenced. On several occasions, readjusting the total stress proved necessary to bring the boundary condition values within 2% of their target value, each time calling for a one-day equilibration period. Once this criterion was satisfied, the soil model was ready for testing.

### 3.6.2 Preparation of the model pipe assembly

The driving equipment assembly shown in Figs 3.1 and 3.16 was dismantled after each test, in order to carry out essential maintenance, modifications, and to clean the clay spoil accumulated at the rear of the model pipe and in the guiding cylinder during excavation. Gearings were thoroughly cleaned and the expanding couplers connecting the drill rod and the air motor were tightened up to avoid their failure during the excavation. The model pipe assembly with its driving equipment was then inserted in the driving cylinder and the flanges bolted on the ends of the cylinder. The model pipe was maintained in its fully extended position (pulled outwards).

The direct stress and pore pressure cells could then be calibrated under pneumatic pressure (§ 3.5.2.1), and after having verified that all instruments responded satisfactorily, the pore pressure cells were saturated (§ 3.5.2.2). To this effect, the caps were dried for a minimum of one hour at 105°C and mounted on the model pipe before being sealed into the saturation sleeve.

The lubricant mixture was prepared according to its specified composition for each test. The tap water was de-aired under a partial vacuum of approximately -100 kPa. The air-lubricant interface tank was then suspended from the load cell, pressurised with the required injection pressure, and connected to the injection line feeding the liquid in the annulus around the model pipe. The injection line was saturated by circulating the lubricant fluid through it before the test commenced. In addition, 200 l of drilling fluid were prepared as a 0.25% water solution of the *PHPA Insta-pac 425* (§ 3.3.4.3).

The plug blanking the orifice through the strongbox was removed, while keeping the total stress and the back-pressure on the model. The aluminium sleeve keeping the pore pressure cells saturated was then removed and the ceramic filter of the *PPCs* coated with kaolin slurry to delay evaporation-driven desaturation. The clay cutter and the cutting edge were mounted as the model pipe was retracted in its initial drilling position. The flange of the guiding cylinder was approached towards the strongbox collar and the height and polarity of the cylinder was adjusted to align the strongbox and the guiding cylinder. After the cylinder and the strongbox had been firmly connected, the assembly was ready for ‘launching’ and excavation could begin.

### 3.6.3 Insertion of model pipe

The cutting edge was initially pushed 5 mm into the clay to prevent leakage of the lubricant fluid from the overcut into the inside of the model pipe. Lubrication then begun by releasing a valve on the pressurised lubricant vessel. The void between the model pipe and the strongbox collar was saturated, and air remnants were expelled from a vent near the apex of the collar. Because the vent was not exactly at the highest point of the collar, some amount of air was inevitably trapped in the annulus. After this initial saturation, excavation begun by successively switching on the air motor driving the clay cutter (§ 3.3.6.2), the submersible pump supplying the drilling fluid to the excavation face (§ 3.3.4.3), and the hydraulic pump actuating the model pipe assembly (§ 3.3.6.3).

Installation proceeded at the constant rate of 1.25 mm/s until the cutting edge had penetrated approximately 20 mm into the wax plug previously cast into the strongbox collar. This provided a barrier around the cutting edge through which the pore fluid could not escape to the inside of the model pipe. On reaching this final position, the model pipe instrument would be positioned in the middle vertical plane of the strongbox. The driving equipment (hydraulic ram, cutter motor, and submersible pump) was switched off and a valve was closed on the lubricant line to prevent the injected lubricant from being forced back into the tank as the fluid pressure in the annulus became larger than that in the lubricant reservoir.

An equilibration period of approximately 24 hours was then allowed for the pore pressures in the clay to return to their nominal value and for the ground loading onto the pipe to reach a steady value. The steel plate blanking the wax plug was then removed and the model pipe was jacked forward by approximately 50 mm. After digging out the wax that had been forced in the model pipe, the cutter and the cutting

edge could be removed to allow the model pipe to be retracted without expanding the existing cavity to the diameter of oversized cutting edge. Several cycles of back and forth jacking on a distance of 100 mm were then performed in alternating direction while measuring the pore pressure response and the jacking force. Eventually, the model pipe was fully retracted.

#### 3.6.4 Post-mortem proceedings

In test T8, the undrained shear strength was measured with a 16-mm diameter hand-vane through the ports of the piston whilst the total stress was still applied on the soil model. The fluid back pressure was, however, removed as water would otherwise have leaked through the port through which the shear vane was inserted. A first set of measurements was taken, before reducing the total stress by 50% and then performing another set of measurements under this new confining pressure.

The load was then removed from the soil model and the strongbox placed on the laboratory floor. The sidewall of the strongbox was disconnected from its base and could then be lifted while the soil sample remained on the base plate. This required that a -90 kPa vacuum be applied to the top and bottom drainage boundary, so that the piston, the clay and the base plate would hold together. This was required since the piston was not allowed to detach from the clay, as this would have torn the *PPT* cables going through the piston.

Having exposed the sample as shown in Fig. 3.31, the post-test procedures could be carried out conveniently. The height of the sample and its moisture content were measured, and shear vane tests were performed at different locations with a 16-mm diameter hand shear vane inserted approximately 250 mm into the soil sample. The relevance of the removal of the total stress on the measured shear strength value is discussed in § 4.3.5. The *PPTs* were then excavated and their positioned measured.

### 3.7 Test programme

The equipment described above was originally intended to be used for a series of six tests, using three different lubricant fluids, each of them injected at two different pressures. A second series of test in which the size of the radial overcut around the pipe would be varied was also planned.

However, several technical difficulties required iterative improvement of the test apparatus before high-quality data could be obtained. The test program could therefore not be followed as planned and, out of a total of eight experiments, as shown in Table 3.5, only three tests (test T5, T6 and T8) using two different lubricants (water and water-based solution of *PHPA*) were completed fully to the expected standards.

The main characteristics and parameters of the eight tests that were performed are recapitulated in Table 3.4. The value of the boundary conditions are summarised in this table, each time giving their target value, as well as the average and standard deviation of the actual value measured during the test.

A succinct description of the technical difficulties encountered throughout the test series may be found in Table 3.5, where the successive improvements of the test equipment are also tabulated.

### **3.8 Final remarks**

The control of boundary conditions was the source of many of the refinements of the experimental procedure. The accuracy, precision and repeatability that could be achieved is presented in detail in § 4.4. The limitations and the potential sources of errors associated with the modelling idealisations as well as with the experimental procedure are discussed in § 4.7, after the presentation of the experimental data.

Item	Description	Manufacturer	Type	§
1	Hydraulic jack	Enerpac New Romney, UK www.enerpac.com	RR-15032	3.3.2
2	Pneumatic to hydraulic pressure amplifier	Haskell Pump		3.3.2
3	Hydraulic pressure regulator	Hale Hamilton		3.3.2
4	Load cell pressuremeter	Cambridge Insitu Ltd Little Eversden, UK www.cambridge-insitu.com	-	3.3.3
5	Drilling fluid (PHPA)	Cetco Europe Ltd www.cetco.com	Insta-pac 425	3.3.4.3
6	Submersible pump	Sumo		3.3.4.3
7	Air motor	Atlas Copco	LBZ 42A0020-11	3.3.6.2
8	Couplers	Ringspann Bedford, Bedfordshire, UK www.ringspann.co.uk		3.3.6.2
9	Rotary union	Deublin Ltd		3.3.6.2
10	Electric motor	Laftert	LMR71LR	3.3.6.3
11	Flow control valve	Bosch Rexroth Ltd St. Neots, Cambridgeshire, UK www.boschrexroth.com	2FRM 6	3.3.6.5
12	Kaolin clay powder	Richard Baker Harrison Group Ltd Ilford, UK www.rbhltd.com	Polywhite E	3.4.1
13	Miniature pore pressure transducer	Druck Ltd www.druck.com	PDCR-81	3.5.3.2
14	Miniature pore pressure transducer	Entran Devices Ltd www.entran.com	EPB	3.5.3.2
15	Load cells	Novatech Measurements Ltd Hastings, UK www.novatechuk.demon.co.uk	F218-Z	3.5.4.1
16			F256-Z3154	3.5.5.2
17			F214 Loadstud	3.5.6.2
18	Draw wire transducers	Automation Sensorik Messtechnik Ltd Moosinning, Germany www.asm-sensor.com	WS42	3.5.4.3
19				3.5.6.1
20	Data acquisition software	DasyLab Ltd Monchengladbach, Germany www.dasylab.net	Version 6	3.5.7.1

Table 3.1. Mechanical components of the experimental apparatus and manufacturer details

Measured parameter	Instrument type	Designation	Sensitivity		Offset	
			Mean kPa/V	Standard deviation kPa/V	Mean kPa	Max. drift kPa
Radial total stress on pipe (see § 3.5.2.1)	Earth pressure cell	LC1	755.18	56.03	-243.60	1963.20
		LC2	797.73	14.51	-506.90	2475.00
		LC3	787.95	10.26	-22.90	94.10
		LC4	883.82	38.18	1684.90	2746.30
		LC5	740.81	35.92	-42.80	178.80
		LC6	788.02	28.94	-79.50	260.90
Fluid pressure on pipe (see § 3.5.2.2)	Pore pressure cell	PPC1	536.32	112.51	612.00	396.80
		PPC2	676.62	187.49	1140.60	228.80
		PPC3	541.85	116.84	752.00	835.90
		PPC4	677.48	232.77	231.70	663.90
		PPC5	546.65	111.22	554.80	560.90
		PPC6	624.45	189.21	108.70	719.30

Table 3.2. Calibration factors of model pipe instrumentation

Measured parameter	Instrument type	Manufacturer	Serial Number	Nominal range	Sensitivity		Offset		Ref.
					Mean	Stand. dev.	Mean	Max. drift	
Pore pressure in soil model	Miniature pore pressure transducers	Entran	02F02F03-D11	700 kPa	54.67	0.55	171.70	367.50	3.5.2.2
			02F02F03-D14		55.47	2.99	371.30	241.00	
			02F02F03-D15		55.17	1.59	-38.30	206.40	
			02F02F03-D16		51.10	1.76	103.50	114.50	
			02F02F03-D19		45.50	3.79	11.00	208.40	
			00H00H15-D02		49.66	3.38	-147.00	171.70	
		02K02J09-D05	52.01		7.38	-77.10	46.40		
		02K02J25-D05	55.19		0.20	-78.10	78.40		
		PPT-024	43.37		-	16.70	-		
		PPT-026	42.12		-	-12.70	-		
		PPT-057	50.27		-	0.10	-		
		PPT-10053	42.94		-	-3.20	-		
		PPT-11055	43.68		0.34	12.00	3.10		
		PPT-11058	43.00		0.57	-3.20	1.80		
		PPT-11060	43.64		-	-17.60	-		
PPT-11066	43.95	1.75	0.40	1.90					
Soil model height	Draw wire transducer	ASM	WS42	750 mm	111.496	-	588.8	-	3.5.4.3
Model pipe position			WS12	1500 mm	165.353	-	14.8	-	3.5.6.2
Lubricant pressure / back-pressure	Pressure transducer	Druck	S/N 105 25 03	700 kPa	70.68	0.21	8.90	2.00	3.5.4.2
			"orange"	10.16	0.08	-0.50	0.50		
			S/N 103 44 49	10.18	0.11	-1.00	1.50		
			S/N 154 43 42	100 kPa	71.07	-	4.10	-	
Total stress			F218-Z	500 kN	373.80	-	-0.30	-	3.5.4.1
Lubricant volume	Load cells	Novatech	F256-Z3154	0.4 kN	-2	-	0	-	3.5.5.2
Jacking force			F214 Loadstud	15 kN	13.43	-	-0.10	-	3.5.6.2

Table 3.3. Calibration factors of *PPTs* and ancillary instrumentation

Test	Total stress				Back pressure		Installation speed				Lubricant pressure				
	Pressure system	Target value kPa	mean: kPa	std: kPa	mean: kPa	std: kPa	Control system	Target value mm/s	mean: mm/s	std: mm/s	Injection method	Type	Target value kPa	mean: mm/s	std: mm/s
T1	Hydraulic	200.0					Needle valve				No lubrication				
T2	Hydraulic 2		234.4	21.1	4.3	23.1			1.07	0.32	Flow control (peristaltic pump)	De-aired water	50.0	69.1	43.4
T3			170.5	20.6	-1.0	0.0	Rexroth flow control unit	0.00	0.00					-3.8	3.1
T4			266.0	13.6	88.5	0.2		1.16	0.08	Volume control (presurised vessel)	39.5			2.7	
T5	Hydro-pneumatic system		206.7	1.5	96.7	0.1		1.32	0.17		4.4	1.9			
T6			204.1	1.5	99.5	0.2		1.32	0.11	50.3	5.4				
T7			191.9	5.7	94.6	4.4	1.25	0.30	Polyanionic cellulose	51.6	1.1				
T8			201.5	1.0	99.1	0.1	1.33	0.15		39.0	1.2				

Table 3.4. Test parameters

Test	Date	Problem description	Cause	Mitigation measure	Ref.
T1	05/05/03	Erratic installation speed, stoppages	Inappropriate regulation of the oil flow into hydraulic cylinder	Replace needle valve by a servo flow control unit	3.3.6.3
T2	31/10/03	Uncontrollable lubricant injection pressure	Inappropriate injection method (peristaltic pump)	Inclusion of a pressure relief valve to control injection pressure	3.3.5.1
		Stoppage of clay cutter rotation, causing blockage of discharge path and generation of large positive pore pressure in soil model	Failure of the expanding couplers (cone clamps) transmitting torque to drill rod	Replace couplers with new unit and improve adhesion on drill rod using screw grab and high strength adhesive	3.3.6.2
T3	30/01/04	Failure of hydraulic seal around consolidation piston after pipe installation, loss of water back-pressure into the soil model	Damaged O-rings and/or excessive tilt of the consolidation piston, causing insufficient compression in the O-rings	Replace O-ring; machine a chamfer in upper edge of extension to prevent damages to the O-rings when inserting piston	3.3.1
		Insufficient lubricant pressure control	Pressure relief valve too sensitive to fluid viscosity	Replace peristaltic pump with interface chamber to allow pressure-controlled injection	3.3.5.1
T4	31/10/04	Malfunctioning instruments on LCPM, signals partly noisy and partly lost	Leak through the instrument cluster lid, causing gradual failure of electronic components of some instruments	Replace joint and damaged electronic components in the LCPM instrument cluster	
		Total stress control not sufficiently accurate. Large pressure fluctuations induced by the cavity excavation	Malfunctioning hydraulic pressure regulators, variation of pilot pressure controlling Haskel pump	Devise an alternative hydro-pneumatic system with improved characteristics. Pressure supplied by compressed nitrogen	3.3.2
T5	02/12/04	Lubricant injection system failed	Lubricant line connection in the LCPM failed	Location of lubricant injection changed to the rear end of the cavity, near strongbox collar	3.3.5.1
T6	23/12/04	Test objectives achieved			
T7	12/01/05	Hydraulic seal failure (s. T3)	Excessive tilt of consolidation piston	Machine a flat on the dome-shaped load bearing face of the load cell	3.5.4.1
		Failure of expanding couplers (s. T2)	see T2	Replace old couplers and adhesive	
T8	20/02/05	Test objectives achieved			

Table 3.5. Summary of technical difficulties and remediation measures



Figure 3.1. Overview of experimental apparatus

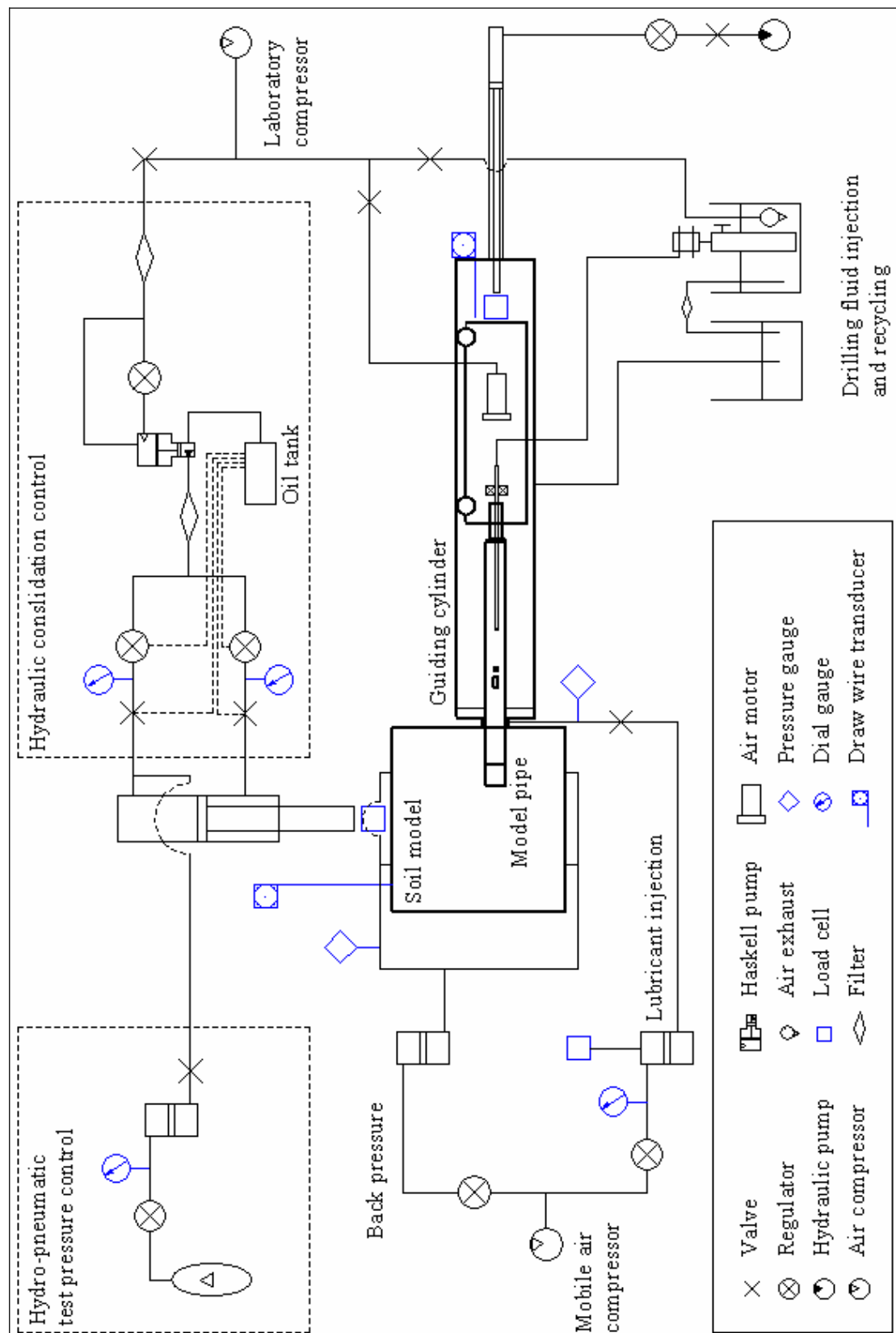


Figure 3.2. Line diagram of test set-up

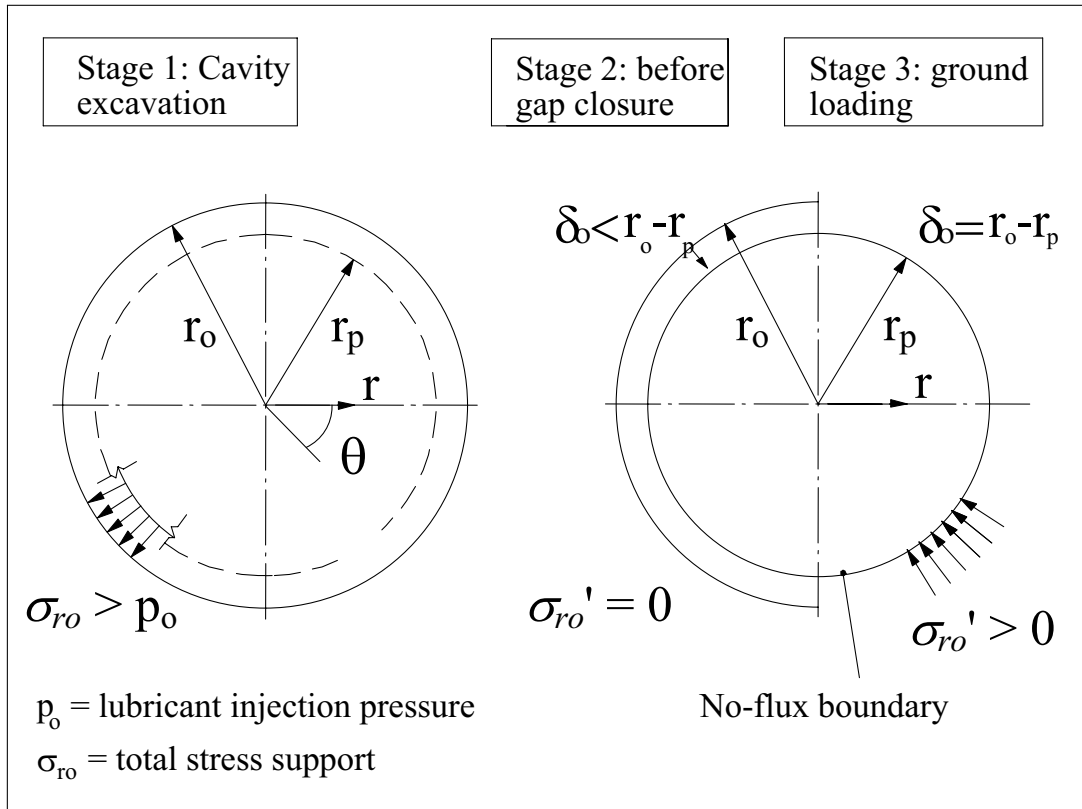


Figure 3.3. Boundary conditions at the cavity wall

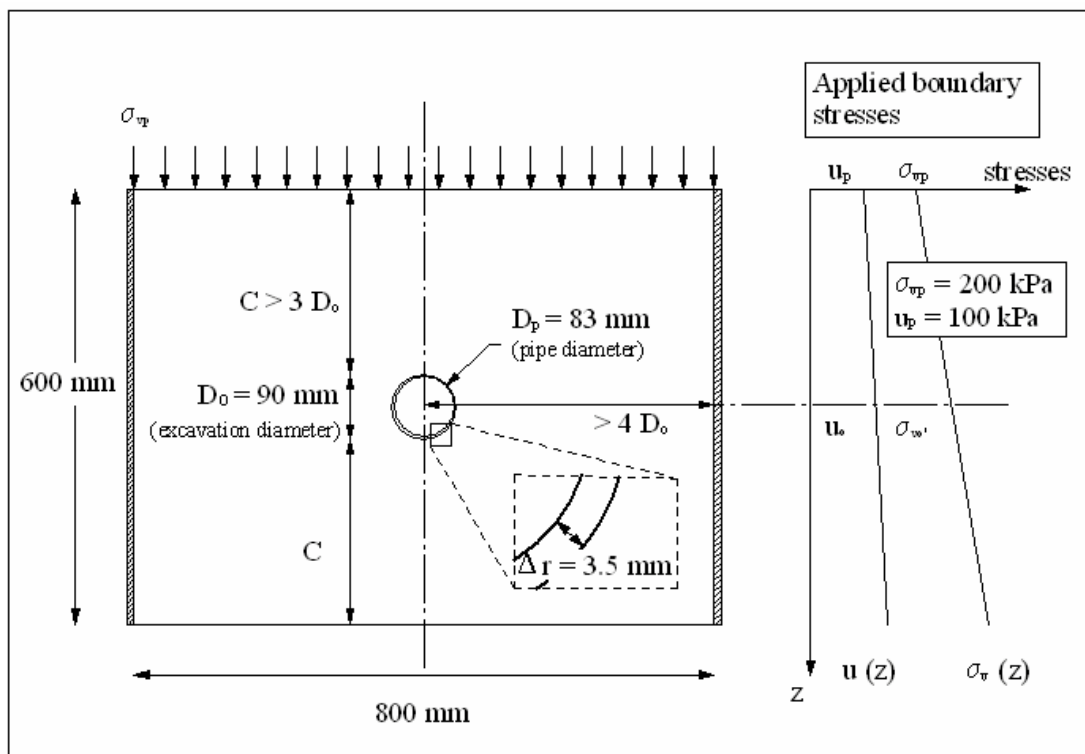


Figure 3.4. Soil model dimensions and initial stress conditions

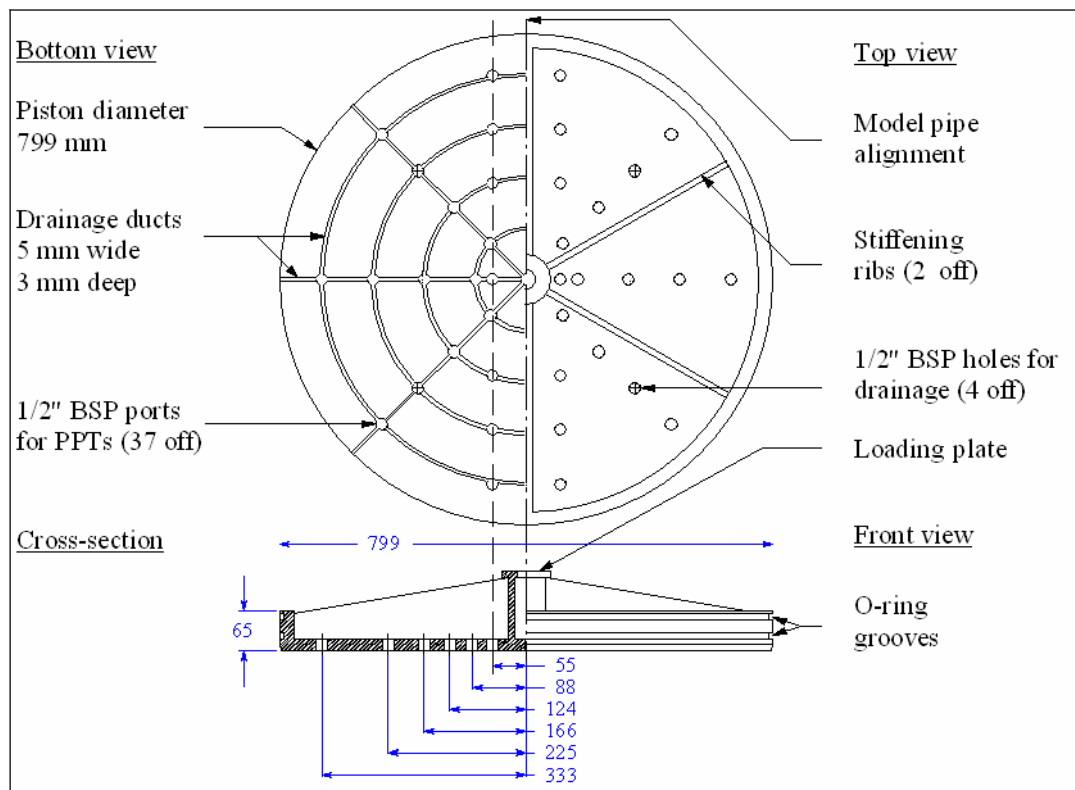


Figure 3.5. Strongbox piston; cross-section, top, bottom and side view

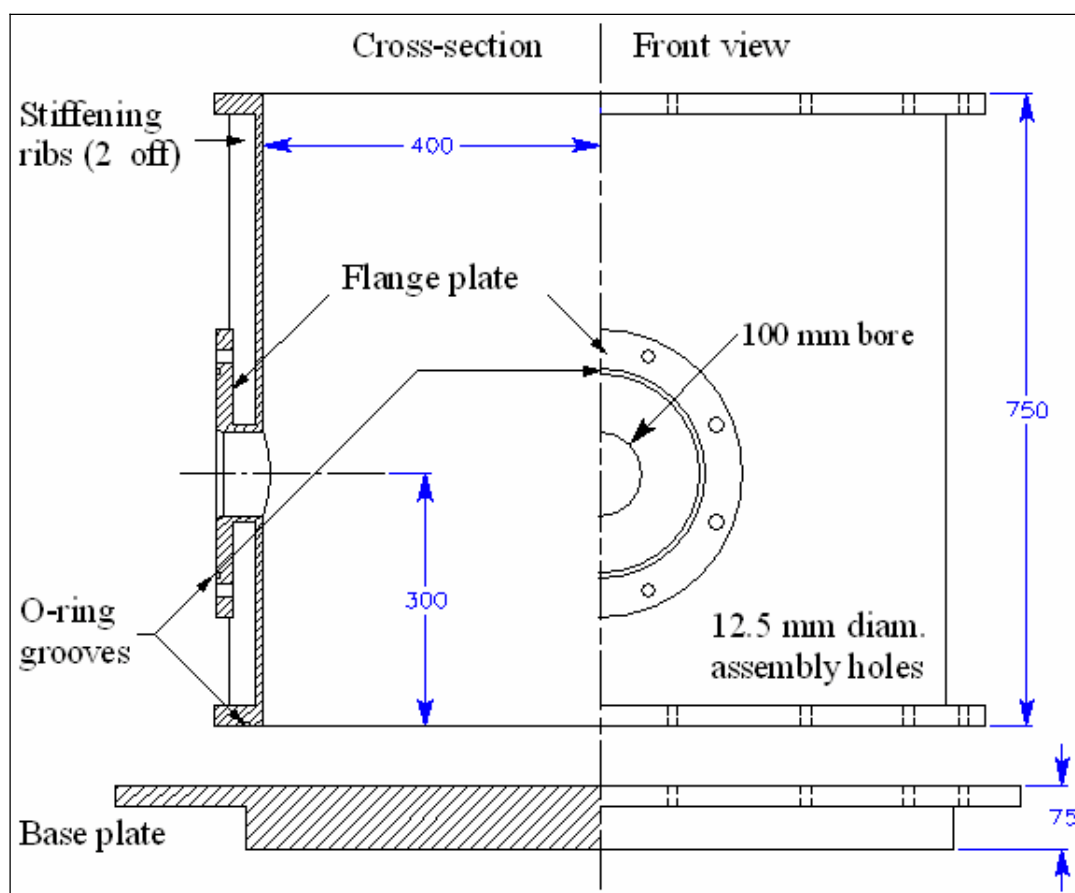


Figure 3.6. Strongbox cross-section and side view

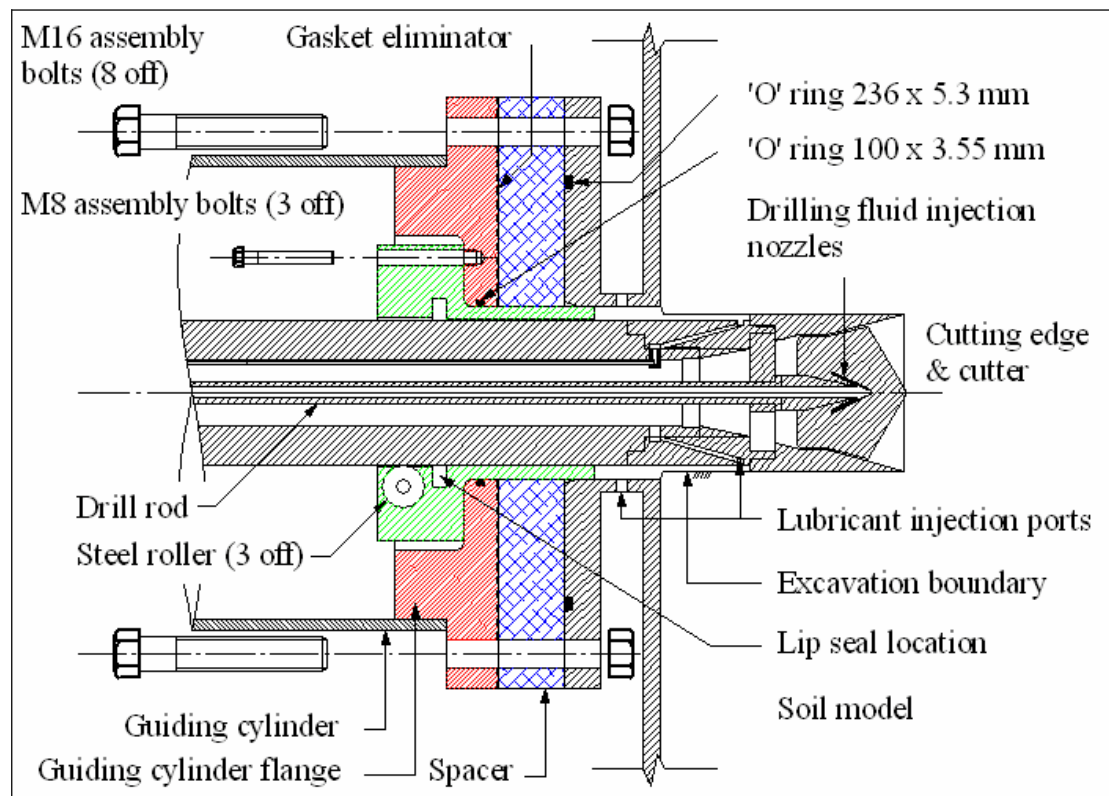


Figure 3.7. Guiding cylinder-strongbox assembly



Figure 3.8. Photograph of the pipe-strongbox interface (without spacer)



Figure 3.9. Overview of the load cell pressuremeter (courtesy Cambridge Insitu Ltd)

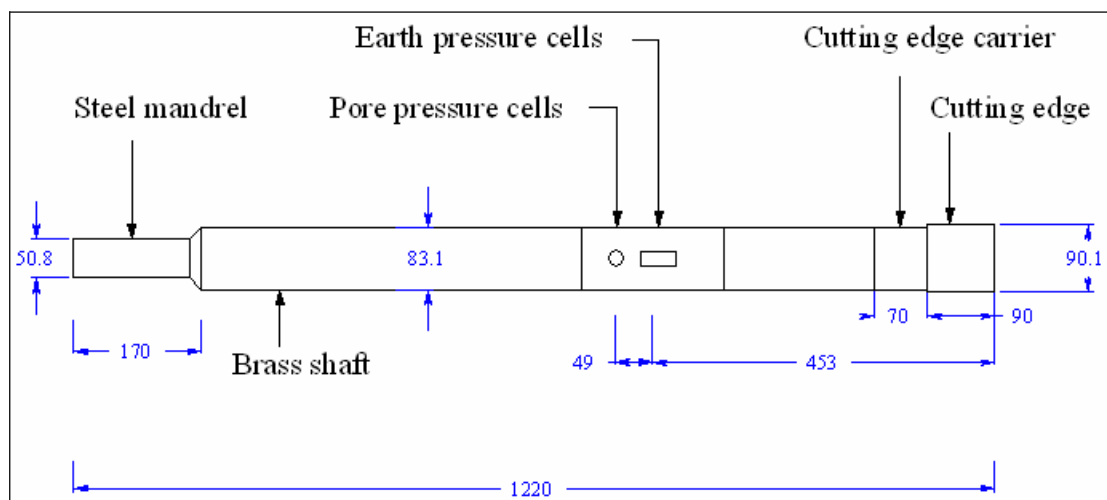


Figure 3.10. Overall dimensions of the load cell pressuremeter

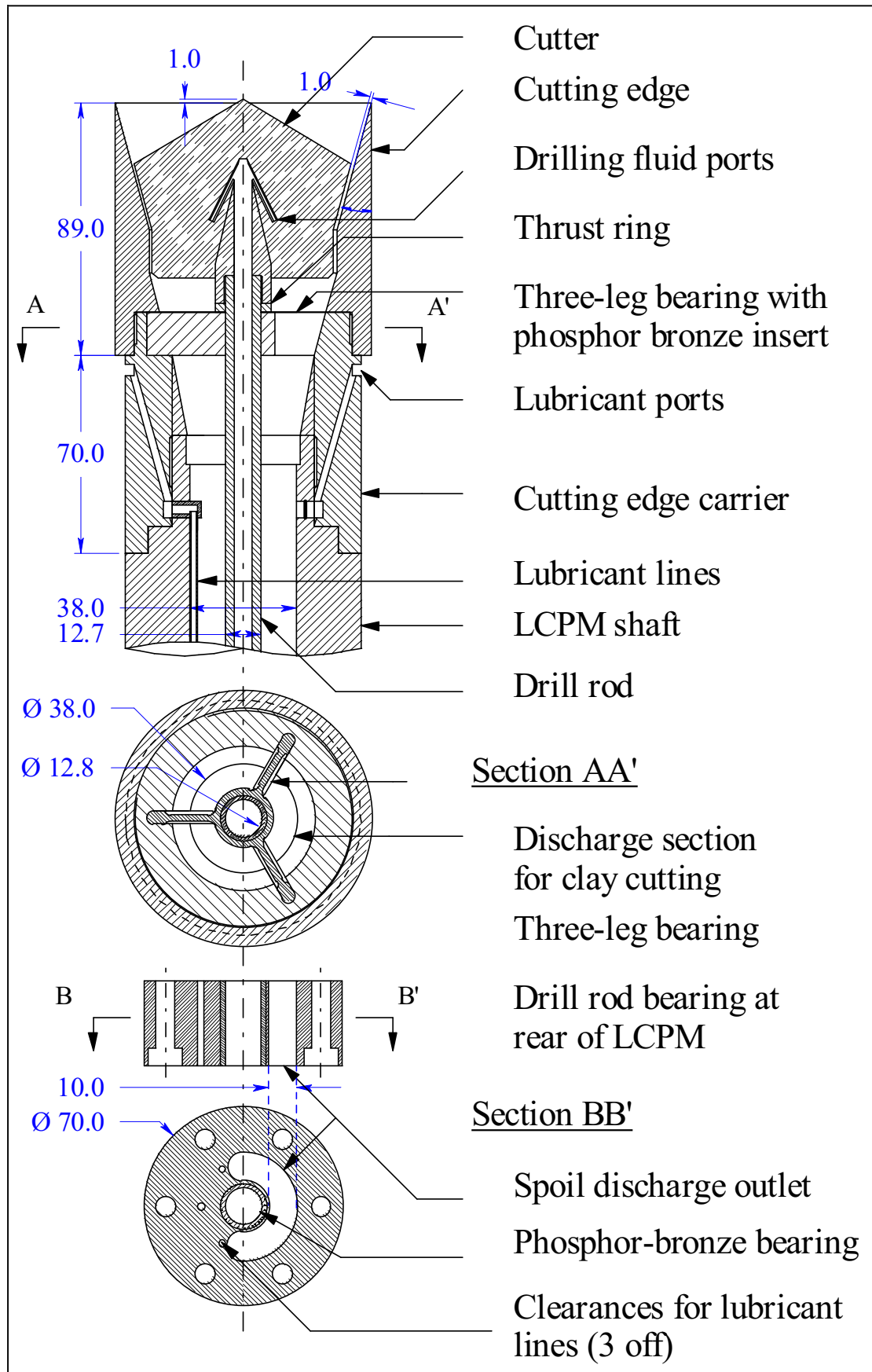


Figure 3.11. Design details of the low-disturbance drilling system



Figure 3.12. Components of the excavation tools



Figure 3.13. Clay cutter with injection nozzle for drilling fluid

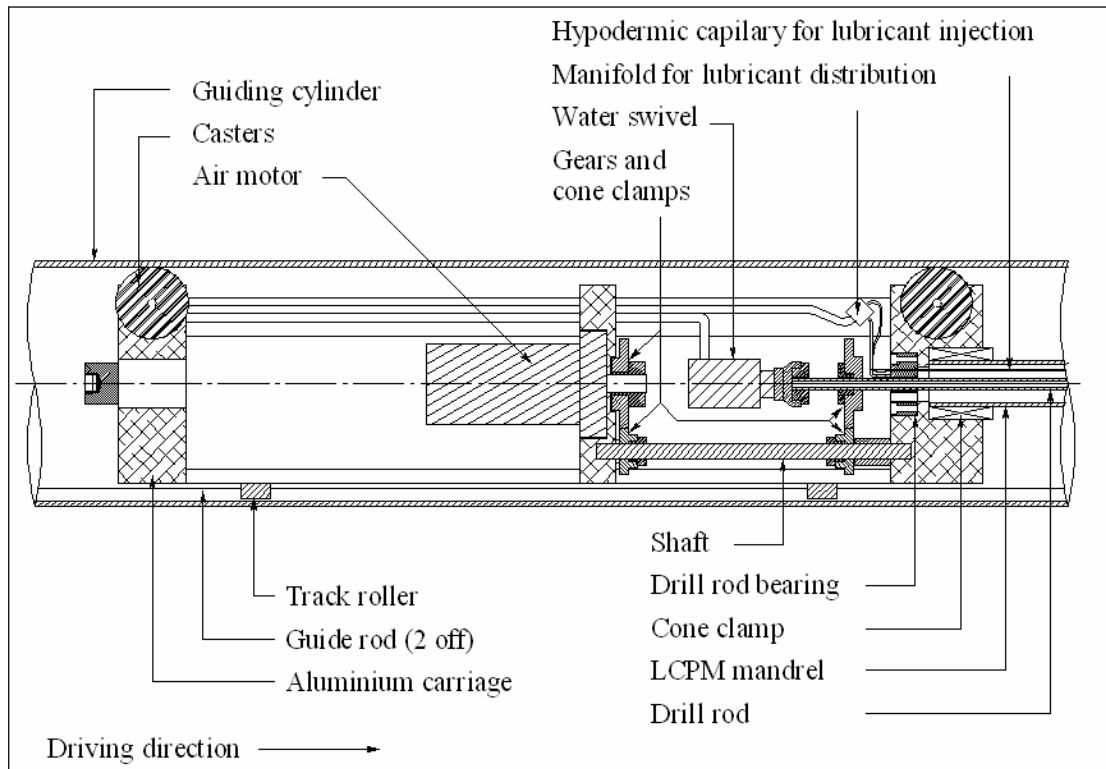


Figure 3.14. Pipe-carrier unit; longitudinal section

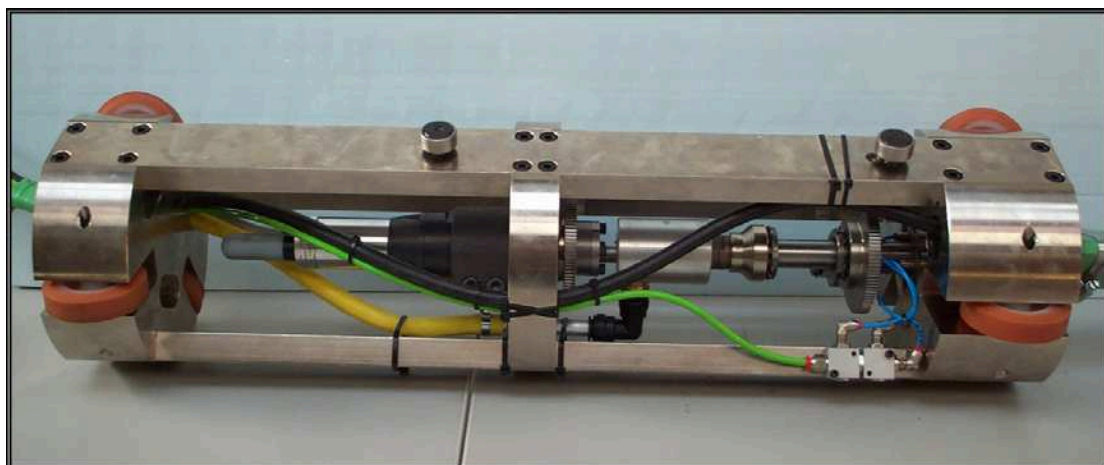


Figure 3.15. Pipe carrier unit

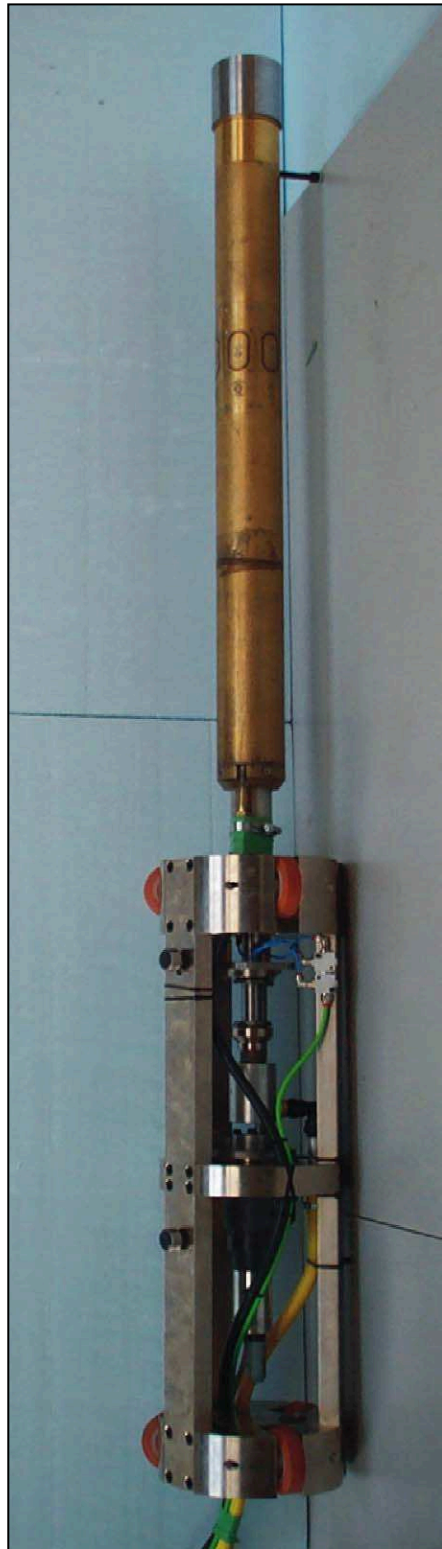


Figure 3.16. Model pipe assembly



Figure 3.17. Paraffin wax seal (*top left*: clay surface before pouring wax; *top right*: after setting of wax; *bottom middle*: cutting edge break through after end of test)

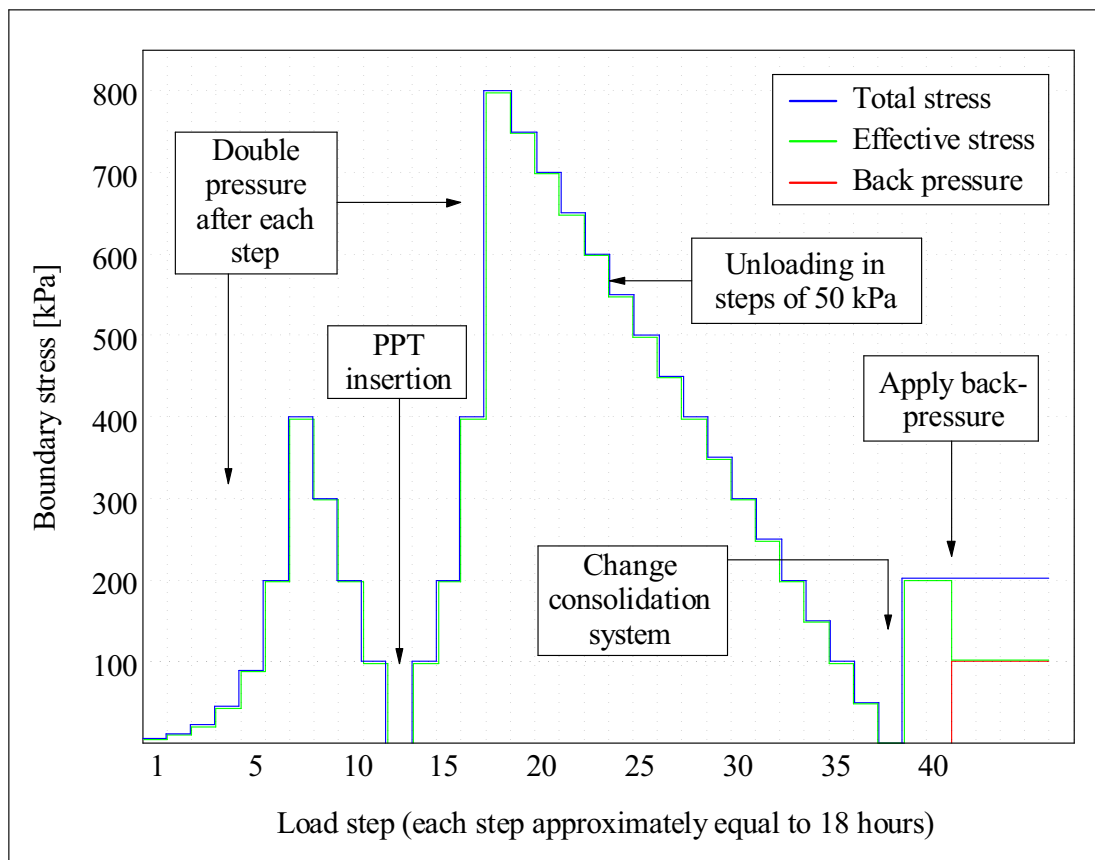


Figure 3.18. Consolidation history of the soil model

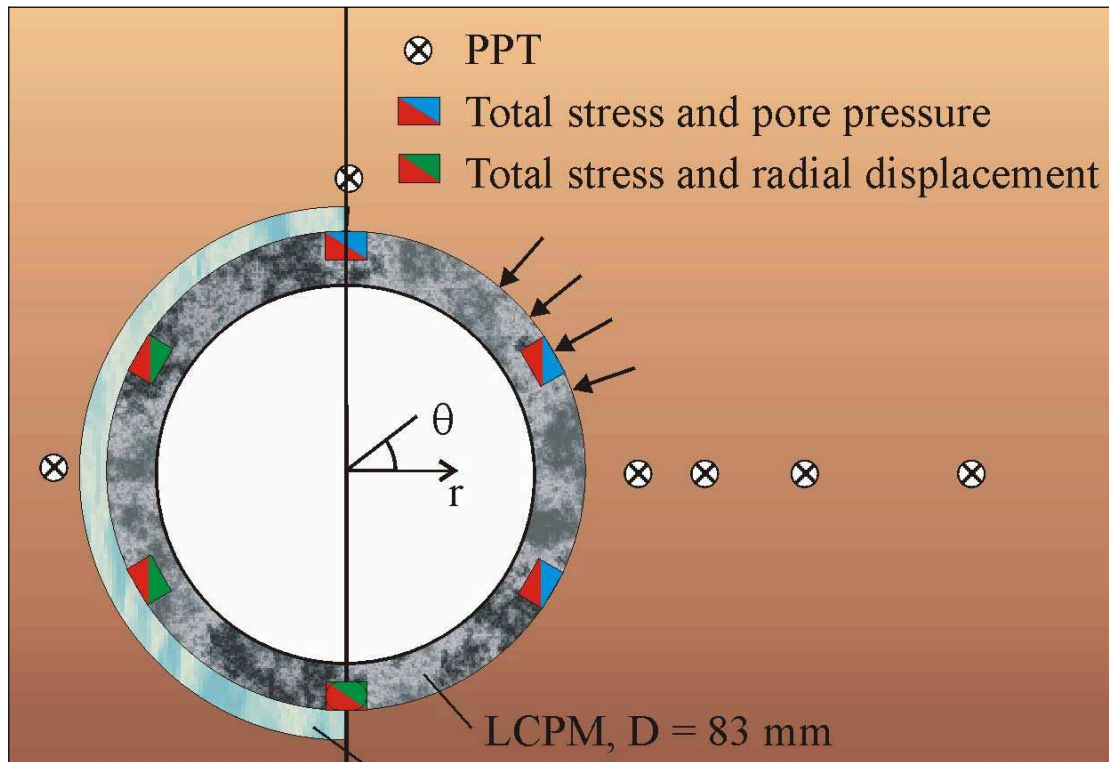


Figure 3.19. Synoptic diagram of *LCPM* instrumentation

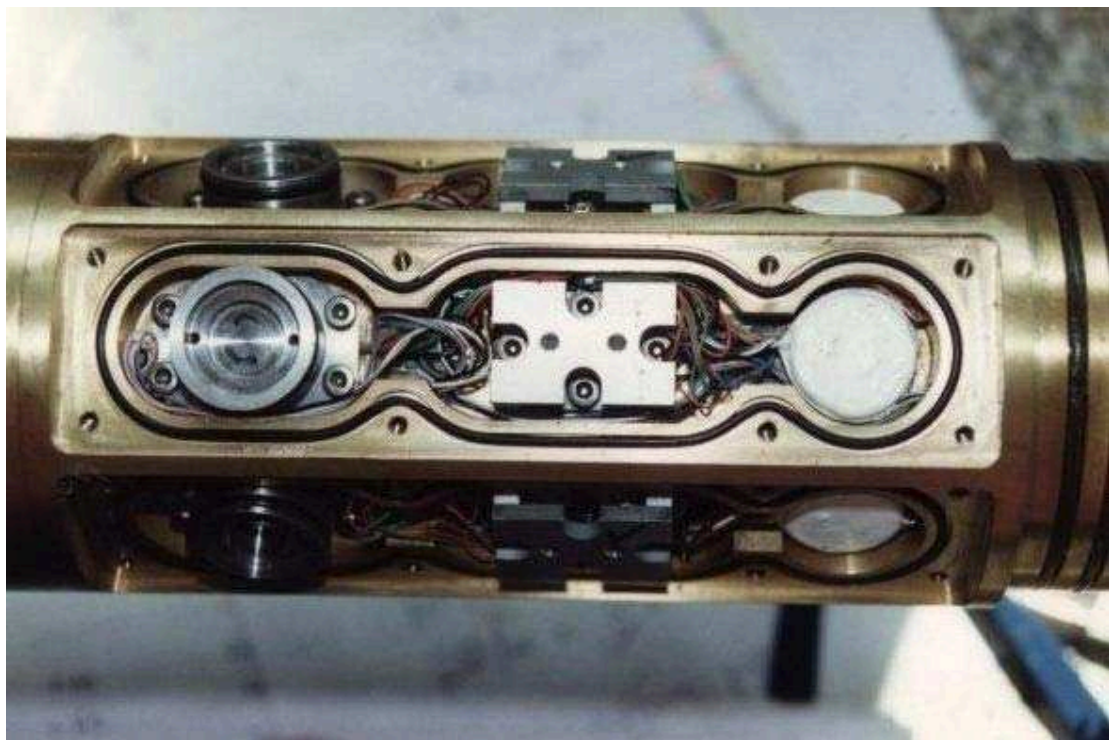


Figure 3.20. Instrument compartments on the *LCPM*



Figure 3.21. Pore pressure cell (PPC) on the *LCPM*

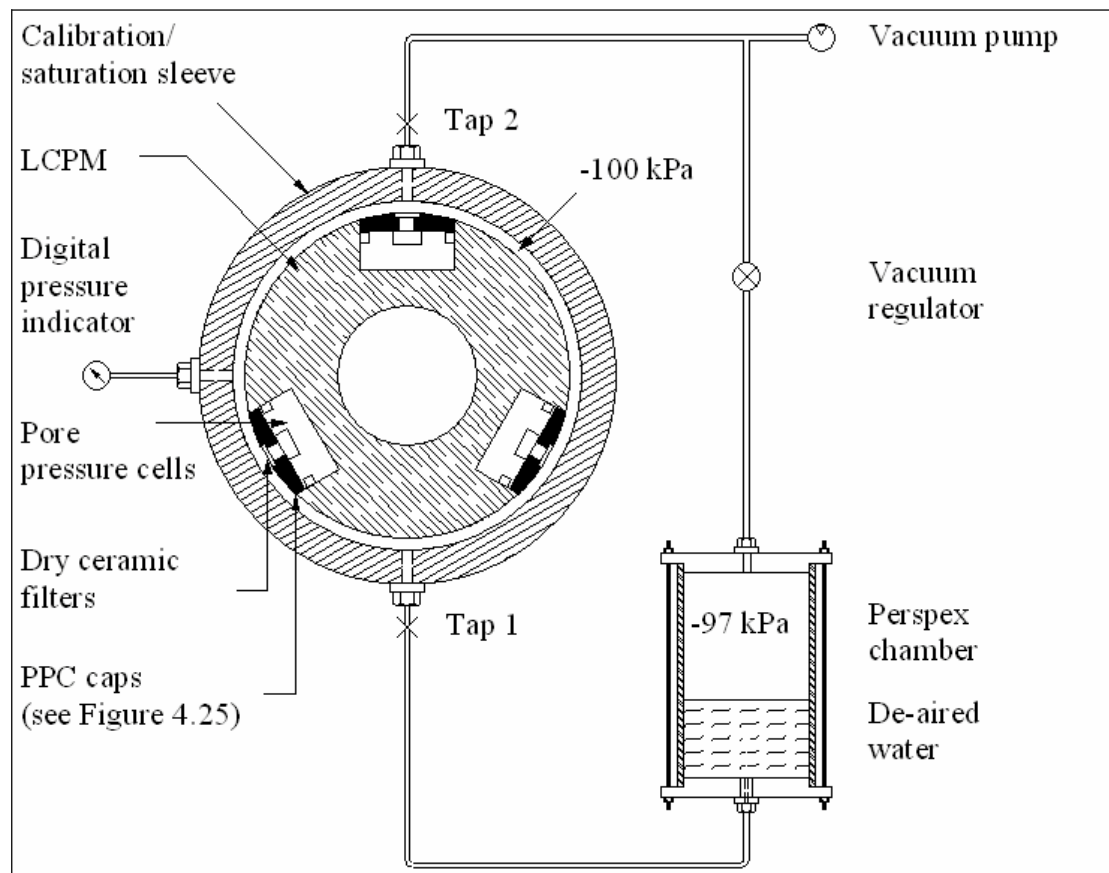


Figure 3.22. Set-up for the saturation of the pore pressure cells (PPCs)

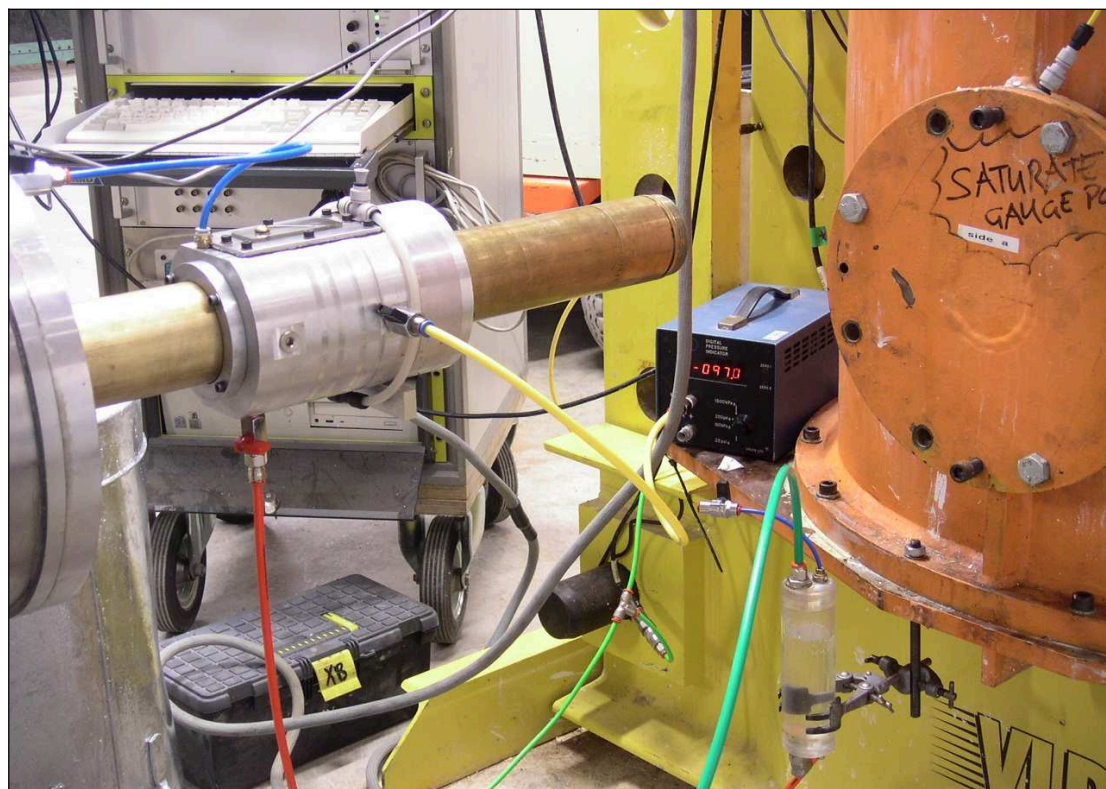


Figure 3.23. Overview of the pore pressure cells (PPCs) saturation set-up

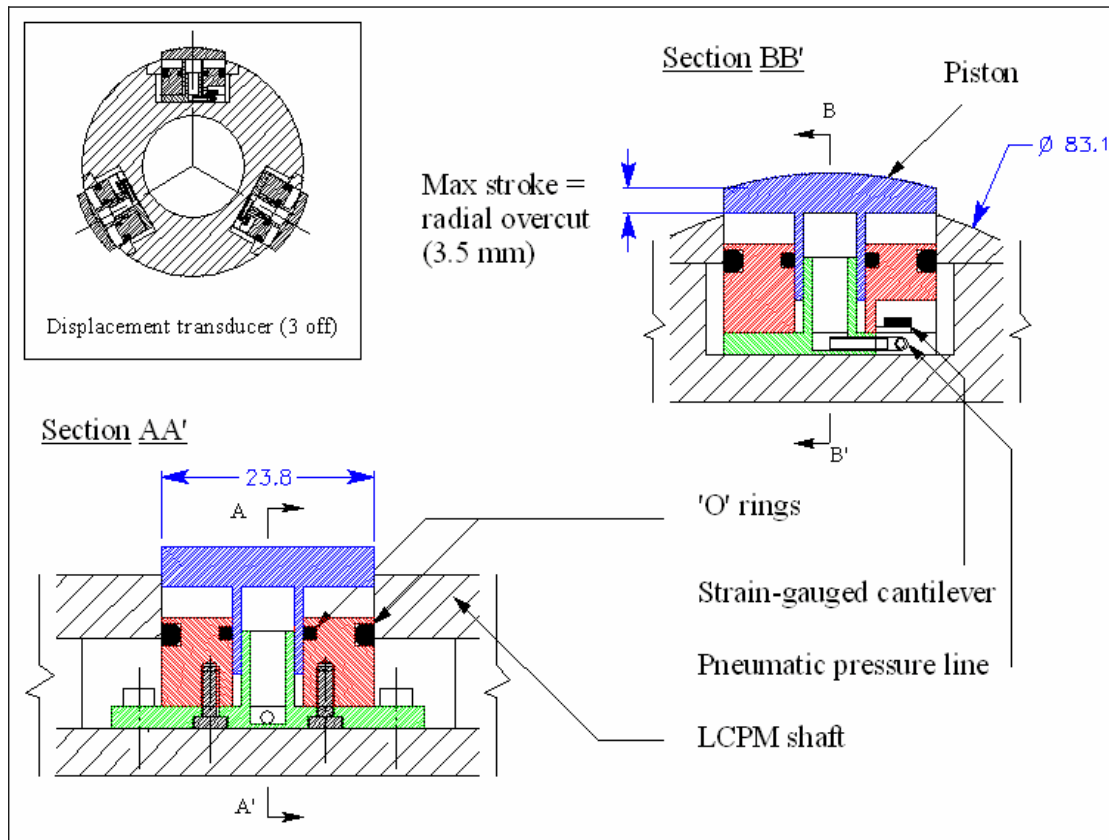


Figure 3.24. Displacement transducer design



Figure 3.25. Displacement transducer components

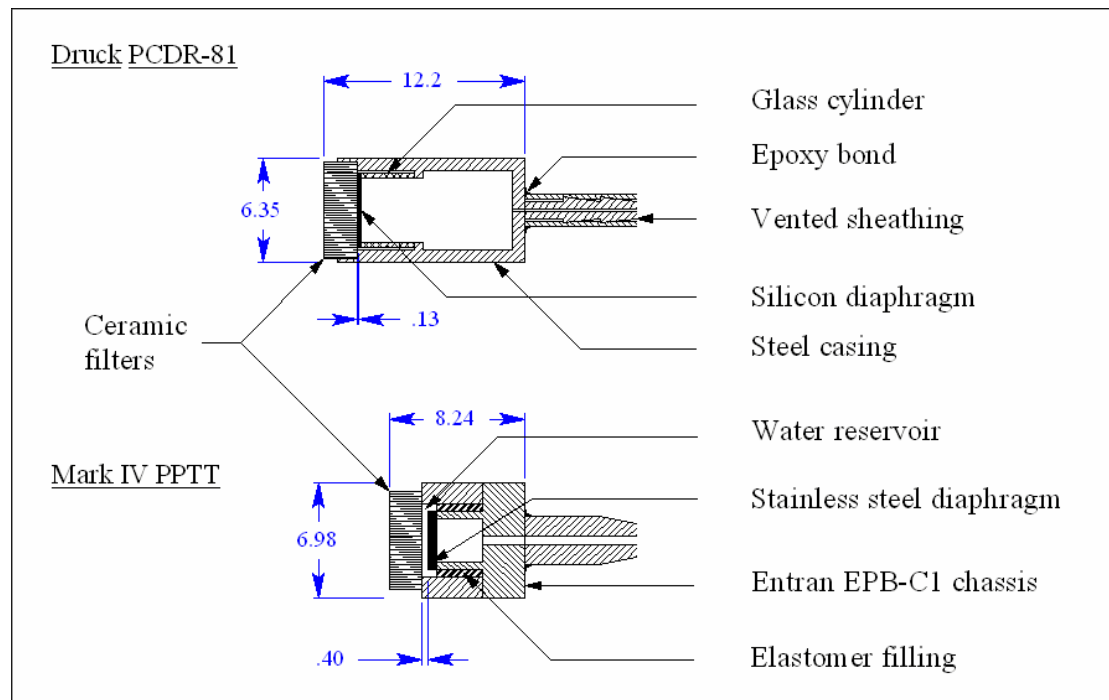


Figure 3.26. Miniature Druck and Entran *PPTs*

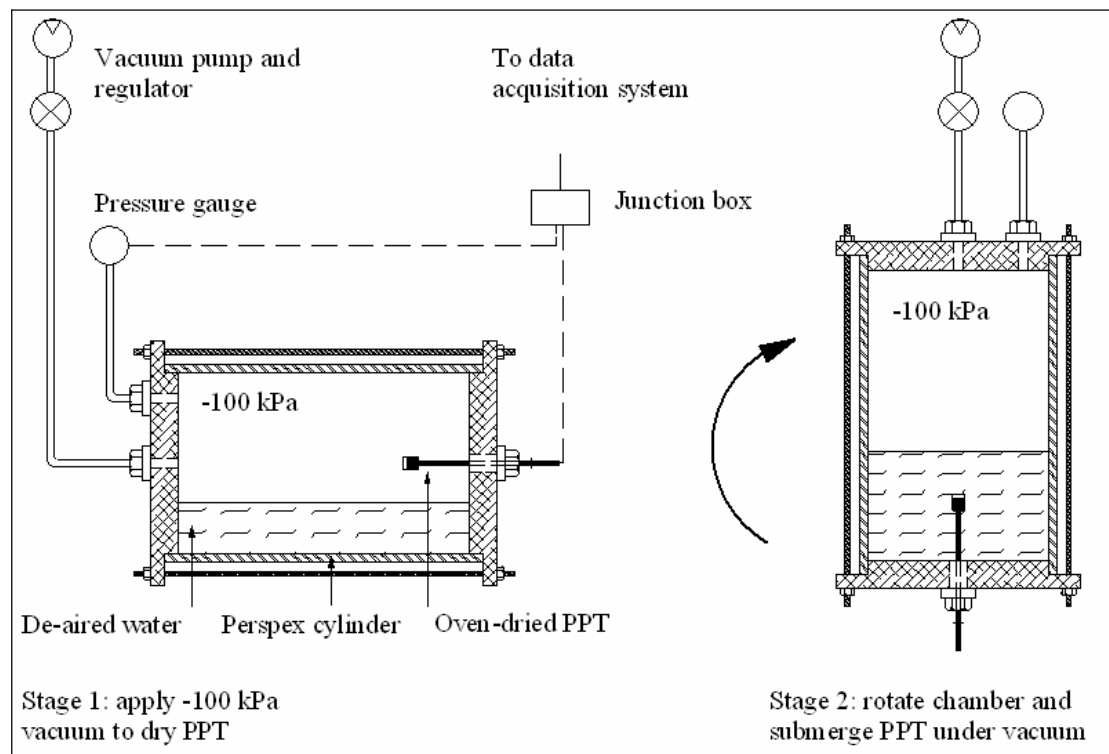


Figure 3.27. Saturation set-up for miniature *PPTs*

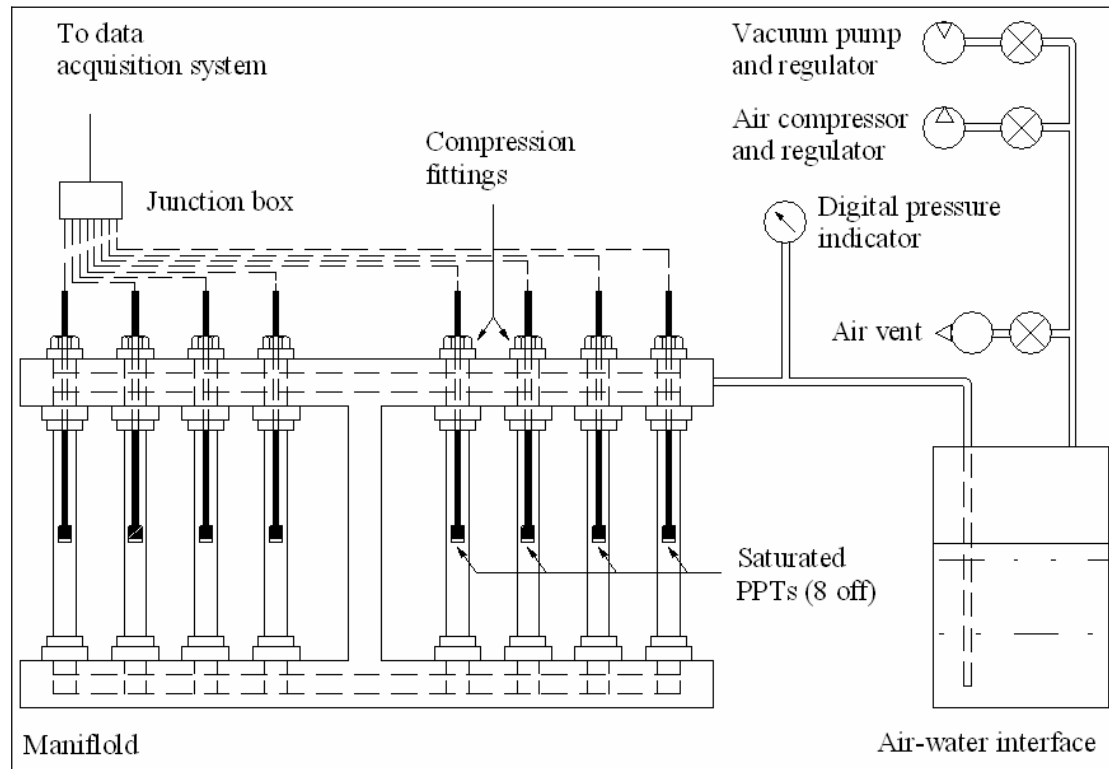


Figure 3.28. Calibration set-up for miniature *PPTs*

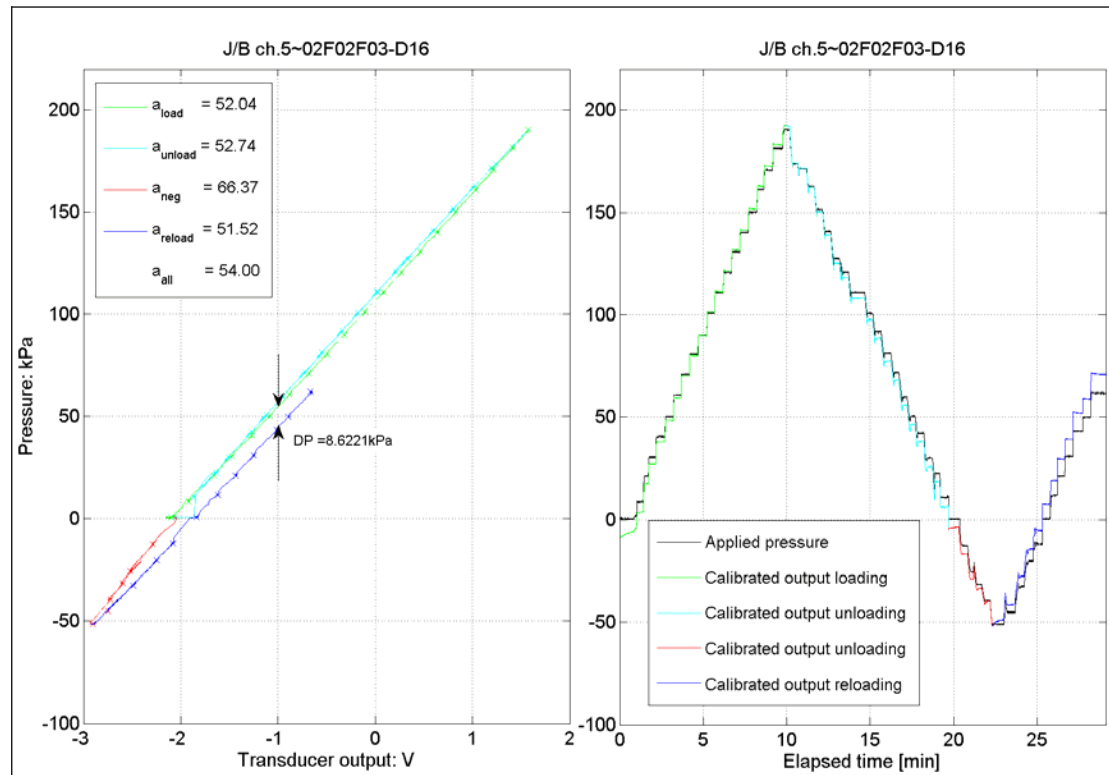


Figure 3.29. Typical response of a poorly-saturated (Entran) *PPT*

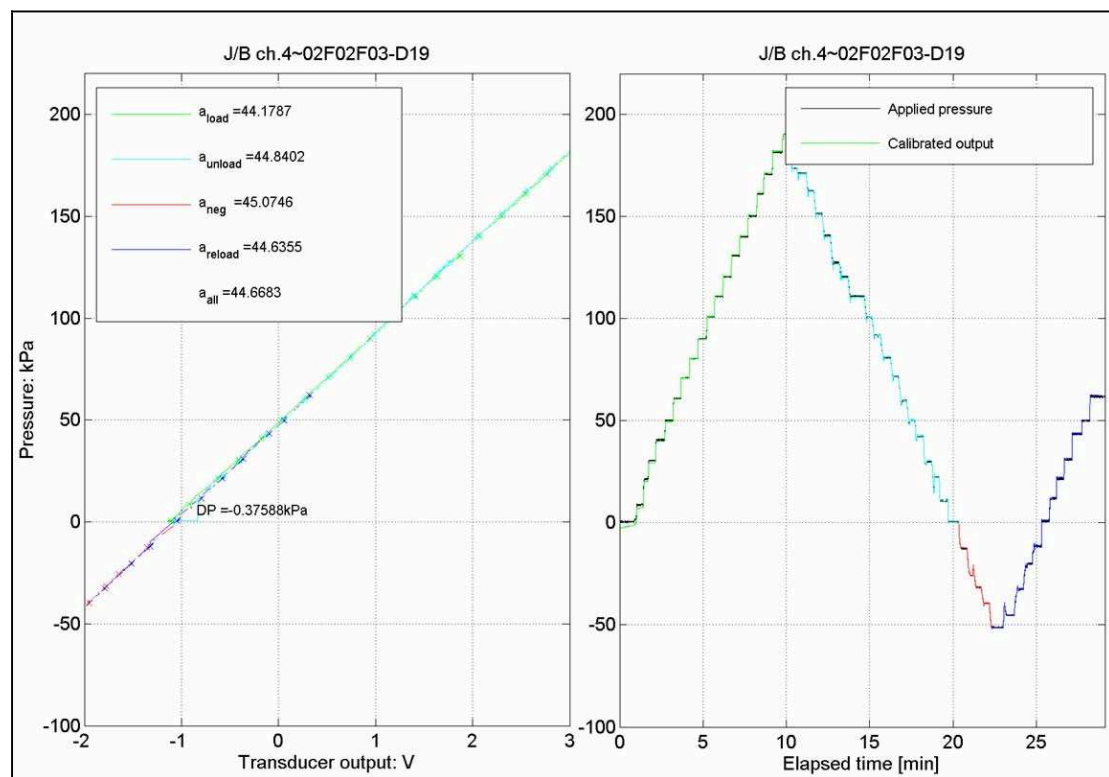


Figure 3.30. Typical response of a well-saturated (Entran) *PPT*



Figure 3.31. Post-mortem view of the exposed *PPTs*

## CHAPTER 4: EXPERIMENTAL RESULTS

### 4.1 Introduction

#### 4.1.1 Scope and objectives

This chapter presents the experimental data gained from the series of test performed with the apparatus described in Chapter 3. Its objective is to report factual observations: all relevant features of the data in relation to the test procedure are examined before discussing the effects of the test variables on the results. An interpretation of these observations is provided in Chapter 5, along with a discussion suggesting practical implications of the test results.

While a total of eight experiments was performed (Table 3.4), three tests only are reported in detail. These tests, in which the experimental objectives were either fully or at least partially achieved, are referred to as tests T5, T6 and T8 throughout this thesis, and their main characteristics are summarised in Table 3.4 and 3.5. It was intended that the three tests presented herein be carried out under identical boundary conditions, except for the pressure and chemical composition of the fluid (also called “lubricant”) injected in the annular gap surrounding the model pipe during its installation. While this fluid consisted of de-aired water in test T5 and T6, a 0.3% water-solution of (anionic) partially hydrolysed polyacrylamide (*PHPA*) was used in test T8. The water was injected under near-zero pressure in test T5, while injection pressures of approximately 50 and 40 kPa were used to inject the water and polymer in test T6 and T8, respectively. The objective of this chapter is to describe the effect of these two variables on the pipe-soil interactions.

### 4.1.2 Chapter layout

The chapter first describes the way in which the raw data was processed prior to its analysis (§ 4.2). It then discusses the geotechnical properties of the soil model, as measured during its preparation and in the post-mortem investigations (§ 4.3). The boundary conditions imposed on the soil model during each experiment are then compared to assess the repeatability of the test conditions (§ 4.4). The core of the data is presented next: excess pore water pressure generated by the excavation of the cavity and their subsequent dissipation are analysed in detail (§ 4.5), before examining the transient build-up of fluid and earth pressure on the model pipe (§ 4.6). This is followed by a discussion on how potential sources of errors may have affected these results (§ 4.7) and, finally, by a summary of the key observations made in this series of experiments (§ 4.8).

## 4.2 Presentation and processing of test data

### 4.2.1 Definitions, conventions, and references

The variables used in this chapter are defined in Fig. 2.10, and the main dimensions of the model components are summarised in Fig. 3.4. The adopted sign convention is one in which compressive stresses as well as fluid and pore water pressures above atmospheric are taken as positive. The frame of reference is defined by a cylindrical coordinate system,  $\{r, \theta, x\}$ , where the abscissa  $x$  coincides with the axis of the model pipe. The origin of this coordinate system is positioned at the centre of the strongbox, with  $x$  increasing in the direction of the pipe installation, as shown in Fig. 4.1. The radial direction,  $r$ , is taken perpendicular to  $x$  and the azimuthal coordinate,  $\theta$ , is defined as the clockwise angle with the vertical.

The origin of time was chosen as the instant when the rear of the oversized cutting edge passed through the plane  $x = 0$ , as depicted in Fig. 4.1. This way,  $t = 0$  represents the time at which radial unloading of the cavity occurred in the middle vertical plane of the strongbox and may be taken as the beginning of the consolidation process around the cavity.

### 4.2.2 Scaling of test results

The applicability of the observed model behaviour at engineering scale depends on the conditions of similitude between the model and a prototype. Model tests results are normally presented in terms of dimensionless groups of parameters so that they may be directly extrapolated to different scales. However, this requires

rigorous dimensional analysis to be carried out or systematic investigation of geometrically similar models at different scale. Neither was carried out in the present study and hence, simple non-dimensional groups are used to present the data. As a result, extrapolation of the results to scales relevant to engineering applications must be done with caution. The non-dimensional charts presented in this chapter might be misleading as they do not incorporate all parameters influencing, say, the ground loading on the model pipe. For example, the overcut ratio  $r_o/r_p$  and the effects pertaining to the physicochemical interaction of lubricant with the cavity are not yet fully understood and therefore, their effect should not be extrapolated beyond the scale at which the model test was carried out.

Linear dimensions are normalised with the initial radius of the cavity,  $r_o$ , and sometimes, to respect some implicit convention when presenting tunnelling data, with its diameter  $D_o$ . Time-dependant effects associated with the diffusion of pore water pressure are naturally affected by the scale of the model. The expression for the time factor  $T = c_v t / r_o^2$  proposed by Soderberg (1962) is often used to render the time dimensionless. In this expression,  $t$  represents the physical time,  $c_v$  the consolidation coefficient of the clay and  $r_o$  the initial cavity radius. The reason for using the factor  $T$  is that, as may be shown assuming that the seepage occurring during consolidation obeys Darcy's law (*e.g.*: De Moor, 1989), identical degrees of consolidation occur after a given  $T$  at geometrically similar points around excavations of different radii  $r_o$ .

The consolidation coefficient used in  $T$  is usually that measured in virgin one-dimensional (anisotropic) compression (Terzaghi, 1943). However, the coefficient  $c_v$  is not an intrinsic soil parameter and depends on the direction of loading, as well as to the mean effective stress and its history. In addition, Al Tabaa & Wood (1987) argue that the use of  $c_v$  as a parameter to describe transient pore water pressures has limitations because considerable changes of  $c_v$  occur upon yielding. They propose that the coefficient of permeability,  $k$ , is a more fundamental factor and that an approach in which  $k$  is linked to the mean effective stress,  $p'$ , should produce a better description of consolidation phenomena. This was substantiated by experiments on model tunnels of different diameters (modelling of models) performed by de Moor (1989). She showed that around cavities of different radii, excess pore water pressure as a function of the dimensionless time  $T$  failed to produce similar relationships. In other words, the rate of time-dependant variables did not appear to depend on the dimensionless group  $T$ , which suggests that extrapolating the test results obtained at small-scale using the time factor  $T$  entails a certain degree of approximation. Because  $p'$  and, in turn,  $k$ , greatly vary with time and radius around a contracting cavity (see § 2.3), using the permeability to normalise data is not straightforward. Therefore, the

simple expression proposed by Soderberg to express the physical time as a dimensionless group is adopted to present the physical time in a dimensionless form.

#### 4.2.3 Raw data processing

The test data was recorded using two separate data acquisition systems operating at different sampling frequencies. All signals from the model pipe instrumentation (§ 3.5.2) were logged at a frequency of approximately 1/12 Hz, while those from the remaining instruments (§ 3.5.3 to 3.5.6) were recorded by the software DasyLab at a rate of 5 Hz. As a result, the length of the data files acquired with DasyLab was 60 times longer than the other and, the sampling of the signals obtained with the two separate systems were not equally spaced in time. In order to enable mathematical operations between these two sets of data, the raw data was manipulated so as to produce data vectors of identical lengths with synchronised signal sampling. Also, because 24 hours worth of data at 5 Hz was recorded in each tests, relatively large data file were generated. Hence, after the elimination of noise affecting the signals, the size of the data files was reduced so that all the different tests could be simultaneously manipulated with minimal processing power and memory capacity. The Matlab routine used to process the raw data and convert it into a form convenient for subsequent analyses is reproduced in Appendix A.

For each tests, the file obtained from DasyLab was cropped 300 seconds before the precise moment at which excavation begun, so that data from corresponding events in different tests were found in the same rows of each data matrix. Undesired noise emanating from both electrical and mechanical sources was then partially eliminated. A Savitzky-Golay smoothing algorithm was chosen to filter the signals because of its ability to track narrow features of the data while wiping out isolated peaks typical of undesired electrical noise or mechanical vibrations. The Savitzky-Golay algorithm operates by fitting an interpolating polynomial of degree  $p$  through a frame of  $N$  successive data points, and uses this polynomial to evaluate the middle point of the frame. The frame is then shifted forward by one row and the operation is repeated until the entire vector has been treated. The characteristics of the filtered data strongly depend on the choice of the frame length,  $N$ , and the degree of the polynomial,  $p$ . The filter parameters  $N$  and  $p$  were selected by trial and error to eliminate features of the data confusing its interpretation, while retaining those reflecting relevant behaviour of the physical model. After filtering, the size of the data file was then reduced by retaining every  $n^{\text{th}}$  row of the data matrix. After having verified that changes of all relevant variables remained inferior to 2% per log cycle of time after 6 hours, the data files were cropped to retain a total of 6 hours of data only and saved in a matrix  $A$ .

The data from the LCPM instrumentation was then evaluated at the intervals defined by the time domain of  $A$ . The value of the LCPM data at each time steps defined was calculated by linear interpolation between consecutive sampling points. Each time series was then converted into engineering units using the calibration coefficients measured before each test. The data corresponding to the position of the model pipe as well as the origin of time were shifted to conform to the time and space references defined in § 4.2.1, but the offset of all other instruments was kept as determined by the calibration coefficient. The way in which some readings were later manipulated to rectify instrument drift that occurred between the calibration and the test execution will be detailed in each case along with the presentation of the corresponding data. Finally, a unique variable name containing the name and location of the measured variable as well as the test number was assigned to each variable. This pre-processing of data produced a compact database in which the reading of each instruments appeared in engineering units in vectors of identical length and at synchronous sampling time.

Figs 4.2 and 4.3 compare the unfiltered signal of a relatively noisy *PPT* with the smoothed signal obtained with two different combinations of the parameters  $N$ ,  $p$  and  $n$ . A cubic interpolating polynomial ( $p = 3$ ) was used in both cases; the filtered data in the upper and lower figures were generated with frame lengths of  $N = 31$  and  $61$ , and reduction factor  $n = 5$  and  $10$ , respectively. The noise corrupting the raw data is believed to have emanated from mechanical rather than electrical sources. Potential sources of such noise were vibrations created by the advancing excavation and the rotating cutting head ( $\sim 4$  Hz). As expected, the filtered data becomes smoother with increasing frame length ( $N$ ), but it does so at the cost of greater amplitude loss of the data peaks. While this is the desired effect when peaks are due to random noise, excessive trimming of peaks should be avoided when they result from processes relevant to elucidate the experimental data. In order to quantify the difference between the raw and the filtered data, and help select the filter parameters  $N$ ,  $p$  and  $n$ , the absolute differences between the raw and filtered data were computed and are represented in bar charts in Figs 4.2 and 4.3. As shown in Fig. 4.3, the difference between the raw and the data filtered using  $N = 31$  and  $n = 5$  falls just above  $0.3$  kPa for 95% of the data points ( $5.6$  kPa when filtering using  $N = 61$  and  $n = 10$ ), with some errors ranging from  $5$ - $10$  kPa in isolated cases. Hence, the combination of parameters used in Fig. 4.3 was considered appropriate to filter the data and was used for all tests.

### 4.3 Soil model characterisation

#### 4.3.1 Stress history of the soil model

Interpretation of the experimental results requires the initial stress state and the mechanical properties of the soil model to be known. This section retraces the stress history undergone by the clay during the model preparation and estimates the strength parameters of the clay in the initial condition. The consolidation history of the soil model preparation is outlined in Fig. 3.23. One-dimensional compression progressed stepwise up to  $\sigma_{vp}' = 400$  kPa, and was followed by unloading to zero total vertical stress, and stepwise reloading to the maximum consolidation pressure  $\sigma_{vp,max}' = 800$  kPa. This was followed by another complete unloading to allow changing the consolidation system. The test pressure of  $\sigma_{vp}' = 200$  kPa was then restored, before applying the back-pressure of  $u_p = 100$  kPa. The surcharge pressure was measured by an external load cell placed between the cylinder ram and the piston imparting the pressure onto the clay. The total stress at pipe axis depth was determined as follows:

$$\sigma_{vo}(t) = \frac{F(t)}{A} + \gamma \cdot (C + D/2) \quad \text{eq. 4.1}$$

where  $F(t)$  is the force measured by the load cell,  $A$  the surface area of the piston (Fig. 3.5),  $\gamma$  the average saturated unit weight of the clay at the end of the consolidation, and where  $C, D$  are as defined in Fig. 2.10. In determining  $\sigma_{vo}$ , the weight of the piston (0.93 kN) and the friction between its 'O'-ring and the container wall were assumed to roughly cancel each other. In addition, friction against the side wall of the container is known to cause a loss of vertical effective stresses over the depth of the model. Measurements by Mair (1979) during centrifuge model tests using Spestone kaolin showed that less than 10% vertical stress was lost in friction for a rectangular model with an aspect ratio of  $H/D \approx 1$  and whose sidewalls had been coated with lithium-based water pump grease. The loss of vertical stress in friction is often estimated using the relationship (*e.g.*: Merritt, 2004):

$$\frac{\sigma_{vo}'}{\sigma_{vp}'} = \exp\left(-4 \tan(\delta) K \frac{H}{D}\right) \quad \text{eq. 4.2}$$

in which  $\sigma_{vp}'$  is the vertical effective stress immediately under the surcharge piston,  $\delta$  the angle of residual shearing resistance between the clay and the greased strongbox wall,  $K$  an appropriate coefficient of earth pressure, and  $H/D$  the height to diameter

ratio of the strongbox. For  $\delta = 5^\circ$ , equation 4.2 predicts  $\sigma_{vo}'/\sigma_{vp}' = 0.85$ , which means that the vertical effective stress at pipe axis depth is approximately 15% lower than it would be if the strongbox wall were frictionless or if the H/D tended towards zero. However, the stiff response of the soil model on the reload loop after loading to  $\sigma_{v,max}'$  and unloading to zero produces small relative displacement between the clay and the strongbox wall. Therefore, it was considered unlikely that values of  $\delta = 5^\circ$  could be fully mobilised and, in the absence of supporting measurements, the effect of wall friction on vertical stress distribution were ignored and the total stress at pipe axis depth estimated with equation 4.1.

The overconsolidation ratio (*OCR*) of the clay may vary with depth because of fluctuating total stresses during consolidation. The *OCR* could be slightly smaller in the middle horizontal plane of the model, away from the drainage boundary, where the largest excess pore water pressures remain after any consolidation time. The erratic patterns of total stresses during equilibration of the last consolidation increment do not allow the *OCR* profile with depth to be estimated accurately. The last increment of total stress was maintained for a prolonged period of four to seven days to ensure full dissipation of excess pore pressure, but fluctuations of the total stress  $\sigma_{vp}$  of up to 40 kPa over periods of over 12 hours were measured. This caused constant changes of pore water pressure across the model. While the extent to which these excess pore water pressure dissipated remains difficult to estimate, an estimate of the *OCR* can nevertheless be attempted: in each cycle, faster dissipation of excess pore pressure would occur near the drainage boundaries, and therefore, excess pore pressure at pipe axis depth are likely to have returned to near hydrostatic conditions after a few days. Although this could not be verified, it is likely that the deviations of the *OCR* from its target value of 8 are actually between 5 and 10%.

#### 4.3.2 Compression and consolidation parameters.

The Cam-Clay parameters obtained by other investigators are summarised in Table 4.1. The values reported by Elmes (1985), Evans (1994) and Potters (1996) reflect the difficulties in obtaining accurate measurements of the Cam-Clay parameters. Because of difficulties encountered during the consolidation of the model in the present tests series, the consolidation data was not exploited to derive further estimations of the slope of the normal consolidation,  $\lambda$ , and swelling line,  $\kappa$ . The consolidation coefficient  $c_v$  is used in the analysis to describe the excess pore pressure dissipation around the cavity. The coefficient of consolidation for one-dimensional virgin loading may be written in terms of fundamental parameters:

$$c_v = \frac{k(1+e)\sigma_v'}{\kappa\gamma_w} \quad \text{eq. 4.4}$$

where  $k$  is the coefficient of permeability,  $e$  the voids ratio and where the other parameters are as defined previously. Clearly,  $\kappa$  must be replaced by  $\lambda$  for consolidation due to unloading or reloading beyond the maximum pre-consolidation pressure. Al-Tabbaa & Wood (1987) showed that the permeability of overconsolidated kaolin was relatively insensitive to the  $OCR$  and was primarily a function of its voids ratio. For Spestone kaolin, they proposed the following empirical relation for vertical and horizontal permeability:

$$\begin{aligned} k_v &= 0.53e^{3.16} \times 10^{-9} \text{ m/s} \\ k_h &= 1.49e^{2.03} \times 10^{-9} \text{ m/s} \end{aligned} \quad \text{eq. 4.5}$$

Permeability measurements on samples recovered from the soil model of test T5 were performed by Mascagni (2005). The samples were trimmed to cylinder of 100 mm diameter by 100 mm height, confined under a hydrostatic pressure of 200 kPa (Mascagni, 2006). The tests were performed by imposing three different fluxes of water ( $< 0.12$  ml/min) through the samples (in the direction of the consolidation stress  $\sigma_{vp}$ ) and measuring the hydraulic gradient upon reaching steady state flow. The permeability measurement was repeated on four different samples recovered from the same model and the mean value calculated from the measurement was  $k_v = 6.28 \cdot 10^{-9}$  m/s with a standard deviation of  $1.7 \cdot 10^{-9}$  m/s. This value is one order of magnitude higher than that proposed by Al-Tabbaa & Wood (1987) for Spestone kaolin and confirms the expected larger permeability for the coarser E-Grade variety of kaolin.

Using the average coefficient of permeability measured by Mascagni, the average moisture content measured in all tests (§ 4.3.4) and  $\kappa = 0.02$  (Table 4.1), equation 4.4 yields  $c_v = 6.15$  mm<sup>2</sup>/s at the initial vertical effective stress  $\sigma_{vo}' = 100$  kPa. This value compares well with  $c_{v,iso} = 5$  mm<sup>2</sup>/s ( $= 1.57 \cdot 10^2$  m<sup>2</sup>/year) reported by Elmes (1985) for isotropic rebound.

#### 4.3.3 Horizontal-to-vertical stress ratio

The earth pressure coefficient at rest for normally consolidated soil,  $K_{0nc}$ , may be estimated by calculating one-dimensional plastic compression with the the critical state soil model Cam Clay. The slope,  $\eta_{Knc}$ , of the one-dimensional

compression line in the  $p':q$  plane may be estimated numerically using the following expression (e.g.: Wood, 1990):

$$\frac{\eta_{Knc}(1+\nu')(1-\Lambda)}{3(1-2\nu')} + \frac{3\eta_{Knc}\Lambda}{M^2 - \eta_{Knc}^2} = 1 \quad \text{eq. 4.6}$$

in which  $M$  and  $\Lambda (= (\lambda - \kappa) / \kappa)$  may be calculated with the Cam-Clay parameters summarised in Table 4.1 and where data from Wroth (1975) may be used to estimate the drained Poisson's ratio  $\nu'$  as a function of the plasticity index  $I_p$ . A few iteration steps lead to  $\eta_{Knc} = q/p' = 0.405$ , and the value of  $K_{0nc}$  can be found by combining its definition with that of  $p$  and  $q'$ :

$$K_{0nc} = \frac{3 - \eta_{Knc}}{3 + 2\eta_{Knc}} = 0.68 \quad \text{eq. 4.7}$$

In comparison, a value of  $K_{0nc} = 0.50$  is found when using Jâky's (1944) original expression:

$$K_{0nc} = (1 - \sin \phi'_{crit}) \frac{1 + \frac{2}{3} \sin \phi'_{crit}}{1 + \sin \phi'_{crit}} = 0.50 \quad \text{eq. 4.8}$$

with  $\phi'_{crit} = 26.5$ . Although equation 4.5 was derived to represent an at-rest stress state by using a stress fields in limit state (Michalowski, 2005), data by Mayne & Kulhawy (1982) support the validity of its predictions for normally or lightly consolidated clays. Hence, theoretical values of  $K_{0nc}$  fall in the range  $0.50 < K_{0nc} < 0.68$ .

Overconsolidation results in higher values of horizontal-to-vertical effective stress ratio. Empirical correction to estimate this ratio, denoted  $K_{oc}$ , were originally proposed by Schmidt (1966) and later modified (Mayne and Kulhawy) to surrogate  $\sin(\phi'_{crit})$  to the at-rest rebound parameter  $a$  (eq. 4.9). For  $OCR = 8$ , and the values of  $K_{0nc}$  predicted with equations 4.3 and 4.5, earth pressure coefficient  $K_{oc}$  in the initial state before the test falls in the following range:

$$K_0 = K_{0nc} (OCR)^a \approx K_{0nc} (OCR)^{\sin \phi'_{crit}} = 1.3 - 1.7 \quad \text{eq. 4.9}$$

By rearranging equation 4.4, the stress ratio  $\eta_{Knc} = q/p'$  in the overconsolidated state is found to be  $\eta_{Knc} = -0.50$  to  $-0.25$ .

#### 4.3.4 Moisture content and voids ratio

The moisture content of the clay model was measured after the end of the test. Between 5 and 7 samples were taken from various locations in the clay. The measurements were extremely consistent: negligible variations in moisture content were measured in samples recovered from clay close the top boundary, close to the strongbox wall, well within the bulk of the sample or near the cavity boundary. The average measured moisture contents were  $w = 35.2, 35.5$  and  $35.4\%$ , for T5, T6 and T8, respectively. The degree of pore saturation was not measured, but the meticulous procedure followed to prepare the clay model (§ 3.4.3) implies that the  $S_r$  was in fact close to unity. The specific weight of E-Grade kaolin quoted by Elmes (1985),  $G_s = 2.6$ , yields an average voids ratio of  $e = w \cdot G_s = 91.9\%$ .

#### 4.3.5 Undrained shear strength

##### 4.3.5.1 Shear-vane measurements

The undrained shear strength,  $S_u$ , of the model was measured after the tests with a 20-mm diameter hand shear vane. Between 9 and 27 measurements were taken in each test, both by shearing a cylinder of soil whose axis was parallel (vertical) and perpendicular (horizontal) to the direction of the applied consolidation stress. All measurements were done by inserting the shear vane at a depth of 120 mm. In test T5 and T6, measurements were performed after having extracted the soil model from the strongbox, and hence, under zero confining total stress. The influence of the total stress on shear strength measurements was shown to be significant when cavitation limits the maximum attainable suction in the pores of the clay (Knogle, 1979 and Rose, 1978). In order to determine if the measurements on the unconfined sample were affected by the prior removal of total mean stress, a series of measurements (T8-vertical-confined) was performed in test T8. There, the shear vane was inserted vertically through ports in the piston while still applying the surcharge pressure to the clay model. The back-pressure was reduced to zero a few seconds before the first measurement was taken, so that the pore pressure at 120 mm depth is unlikely to have changed significantly at the time at which the measurements were performed.

The average of all measurement performed amounted  $S_u = 69$  kPa. The range of values as well as the average obtained for each test and direction of measurement are summarised in Fig. 4.4. Also indicated in this figure is the number of measurements performed in each case and with which the average value was calculated. In some cases the range of measurement is relatively spread out. In test T5 for examples, the measured undrained shear strength covers a range of 17 kPa, which correspond to

30% of the mean value (60 kPa). The standard deviation was comprised between 1.8 and 5.6 kPa in each set of measures. Considering the rudimentary character of hand-shear vane measurement, this can be deemed acceptable. No trend could be discerned with location of the measurement or indeed with the direction of shearing, although a slightly higher average seems to emerge for measurements performed in the direction perpendicular to the consolidation direction. As may be seen in Fig. 4.4, the undrained shear strength measured under confined conditions does not depart significantly from that measured on the unconfined sample and the difference is well within the variability of the measurement obtained from each series. The sensitivity of the measurement to excess pore water pressure generated during the insertion of the shear vane was assessed by allowing dissipation to occur in the vicinity of the shear vane after its insertion. Five measurements were taken, allowing 6 different equilibration times geometrically progressing between zero and 8 minutes. No trend could be discerned.

#### 4.3.5.2 Undrained shear strength prediction

Also shown in Fig. 4.4 is the undrained shear strength predicted with the relationship derived from the critical state model Cam-Clay:

$$S_u = \frac{M}{2} \exp\left(\frac{\Gamma_{CLS} - v}{\lambda}\right) \quad \text{eq. 4.10}$$

in which the parameters  $M$  and  $\lambda$  are as those defined previously and recapitulated in Table 4.1. The intercept of the critical state line,  $\Gamma_{CSL}$ , in the volume space  $v:lnp'$  can be estimated according to the relationship:

$$\Gamma_{CSL} = \Gamma_{ISO} - \lambda + \kappa \quad \text{eq. 4.11}$$

Using the Cam-clay parameters reported by Elmes (1985), equation 4.10 yields  $S_u = 84$  kPa, which, considering the sensitivity of  $S_u$  to the value of the exponent,  $(\Gamma_{CSL} - v)/\lambda$ , agrees remarkably well with the measured undrained shear strength ( $S_u = 69$  kPa).

## 4.4 Boundary conditions

### 4.4.1 Applied stresses at the soil model boundaries

#### 4.4.1.1 Total stress

The total vertical stress applied at the upper boundary of the clay model was measured and calculated as described in § 4.3.1. In all tests, its target value was  $\sigma_{vp} = 200$  kPa. As shown in Fig. 4.5a, difficulties were experienced to control  $\sigma_{vp}$  in test T3 and T4: while the total stress was constant before the test, sharp reductions were triggered by the excavation, followed in both cases by a gradual recovery to the initial pressure. A further reduction then occurred, albeit at a slower rate, and such cycles of total stresses, sometime with amplitudes exceeding 40 kPa continued throughout the equilibration period following the pipe installation. The fluctuating total stress at the soil model boundary caused constant changes of excess pore water pressures, which added to those induced by the excavation. This prevented the effects of the test variables to be isolated. Therefore, the consolidation system used for tests T1 to T4 was hardly apt to deliver repeatable test results and a refined version was devised to enhance the repeatability of the test conditions. The new pressure control (§ 3.3.2) allowed much improved precision and accuracy of the total stress control in tests T5, T6 and T8. While fluctuations persisted during the pipe installation, their magnitude was significantly reduced: the standard deviation of total stress throughout each test ranged from 1.0 to 1.5 kPa, and the deviation of the mean value from the target pressure of 200 kPa fell in the range of 0.75 to 3.5%, as shown in Fig. 4.5a.

#### 4.4.1.2 Back-pressure

A target water back-pressure of  $u_o = 100$  kPa was to be applied at the horizontal boundaries of the soil model to simulate the effect of a water table. However, technical complications were encountered to control the water-tightness of the gap between the piston and the strongbox wall: in tests T2 and T7, the 'O'-ring seals located in this gap failed, probably following damage during consolidation. This resulted in an immediate loss of back-pressure for the remainder of the test. Measurements illustrating this problem in test T7 appear in Fig. 4.5b: the effect of the seal failure on the back-pressure may be clearly seen to occur 25 minutes after the beginning of the test. The failure allowed water to circulate through the drainage pipes and to be expelled via leakage paths between the strongbox and the piston. While the transducer in the drainage line still measured a pressure close to 100 kPa, the pore water pressure is likely to have reduced to much lower values almost instantaneously, creating a propagating front of negative excess pore water pressure

thought the model with an associated increase in effective stresses. This additional component of pore pressure affected the test result in the way described in the previous paragraph and was therefore undesired. As may be seen in Fig. 4.5b, the standard deviation of  $u_o$  throughout the duration of tests T5, T6 and T8 was negligible, and the mean back-pressure deviated by a maximum of 3.3% from the target value of 100 kPa. The standard deviation of back-pressure throughout each test remained below 0.2 kPa, and the deviation of the mean value from the target pressure was about 3%. The effect of these slightly different back-pressure affect the hydraulic gradients causing flow of water towards the cavity, but these small differences are not expected to have a significant effect on the test results.

#### 4.4.1.3 Effective stresses

Effective stresses immediately below the upper boundary of the soil model were calculated by subtracting the back-pressure  $u_p$  from the total stress  $\sigma_{vp}$ . Fig. 4.5c summarises the boundary effective stresses throughout the tests. The average effective stress applied immediately under the piston during the excavation was  $\sigma_{vp}' = 106.6, 101.5, \text{ and } 101.3$  kPa for tests T5, T6 and T8, respectively. The average effective stress over the entire consolidation period are  $\sigma_{vp}' = 109.8, 103.8, \text{ and } 103.0$  kPa for T5, T6 and T8 respectively.

#### 4.4.2 Model pipe installation

An accurate control of the model pipe installation speed was desired to generate repeatable amounts of disturbance to the soil model during the excavation. This is because the installation speed largely determined the magnitude of over or under-balanced stresses at the excavation face during the pipe installation and, in turn, the excess pore water pressures generated ahead of the advancing excavation face. Fig. 4.6a shows the trajectory of the rear of the oversized cutting edge of the pipe during its installation, while the rate of advance obtained by differentiation of the model pipe position appears in Fig. 4.6b. The installation time of the pipe in test T5, T6 and T8 amounted to approximately 10 minutes and the final pipe position in the  $x$ -direction fell, in all tests, within a band of 4 mm. The computed installation speeds are remarkably constant throughout all tests and varied by 0.1 mm/s only. The overlapping trajectory  $x(t)$  of the pipe in all the tests results from the defined time origin and frame of reference as well as the constant and repeatable installation speed. This repeatability implies that events such as the cavity unloading and the change of boundary condition after the end of the installation occur concurrently and the

constant time elapsed between these events allow direct comparison of the test results.

#### 4.4.3 Lubricant injection

##### 4.4.3.1 Method and monitoring

The injection of lubricant into the annulus was performed under controlled pressure, as explained in § 3.2.1.2. After completion of the excavation, the annular gap was sealed, confining the fluid so that it could only escape by seeping into the pore space of the clay. Sealing of the gap induced a change of fluid boundary condition which is best described by considering the situation both before and after the closure of the cavity onto the model pipe. Before closure, lubricant flow across the cavity wall and fluid pressure variation at the cavity wall could occur without restriction. After closure, however, the pipe-clay interface became a no-flow boundary, while the boundary fluid pressure remained free to vary. During contraction of the cavity, continuity of flow implies that every increment of volumetric strain in the soil was accompanied by a reduction of the fluid volume in the gap.

The lubricant pressure in the annulus was measured by a transducer that communicated with the annulus (PT2 in Fig. 3.2). Fig. 4.7a shows the evolution of lubricant pressure during the pipe installation. While the lubricant was injected from behind the advancing cutting edge of the model pipe in test T5, the injection ports were moved to a stationary location in the strongbox collar in test T6 and T8 (Fig. 3.16). The injected volume of lubricant was measured by monitoring the changing weight of the lubricant supply tank during injection, and the cumulated volume of injected lubricant is plotted versus time in Fig. 4.7b, where the initial volume (assuming zero convergence) of the annular void excavated around the pipe is also indicated. Details of the lubricant injection in each test are discussed next.

##### 4.4.3.2 Test T5

In test T5, injection of the lubricant was affected by the failure of the fitting connecting the lubricant supply line to one of the three capillary tubes used to conduct the lubricant to the rear of the cutting edge (Fig. 3.12). The broken connection was located approximately 1000 mm behind the injection ports and the failure only affected one of three supply pipes. The apparent increase in lubricant flow rate shown for test T5 at  $t = -1$  min (Fig. 4.7b) indicates the leak in the injection line. Insufficient evidence is available to determine if the measured injection volume was in actual fact

injected into the annulus, but the plateau reached just after  $t = 2$  min attests that the lubricant supply ran empty and that no lubricant was injected from this instant onwards. While the measured lubricant volume cannot be relied upon in test T5, the pressure measurements shown in Fig. 4.7a are in close agreement with the fluid pressure measurements on the model pipe (§ 4.6.1). These pressures require further clarification in order to understand the fluid boundary condition at the cavity wall imposed in test T5.

The intricate pattern of lubricant pressure shown in Fig. 4.7a may be tentatively explained by unpacking the sequence of events that occurred during the excavation: the instant at which a loose connection on the supply line caused erratic pressure, and eventually, a drop to atmospheric pressure. The reason for the pressure then reducing below zero is due to the advancing pipe leaving an under-pressurised cavity behind the cutting shield. While the broken connection should vent the annular gap via the capillary tubes through which lubricant were injected, the temporary sub-zero pressure is likely to have been caused by capillary rise in the 1000-mm long tubes. After the water filling the capillary at the time of the connection failure was sucked into the annular gap, air could vent into the annulus and the pressure around the pipe hence returned to zero. The peak of fluid pressure measured after the end of the installation is likely to be due to the contraction of the cavity, which confines the water in the annulus and forced it through the capillaries, essentially reversing the preceding process. The observed pressure relates to the pressure required to impose water flow through the 1-mm ID capillaries. Because the resistance to flow is a function of the flow rate, cavity pressure decreases with the rate of cavity convergence. As a result of the broken pipe connection, sealing of the gap upon completion of the pipe installation was ineffective in altering the fluid boundary condition. However, as shown in Fig. 4.7a at  $t = 5$  min, a discontinuity in the lubricant pressure evolution was measured shortly after the end of the excavation, after the gap was tentatively sealed. This may be due to the closure of the annulus, effectively imposing a no-flux condition across the pipe-soil interface. The reasons for the opposite trend compared with test T6, where the lubricant was also water, will be explained later.

#### 4.4.3.3 Test T6

As in test T5, plain water de-aired under vacuum for several hours was used as a lubricant in test T6. The injection pressure in test T6 was within approximately 3 kPa of the targeted pressure  $p_o = 50$  kPa, and remained constant throughout the excavation. The irregularities observed in the time interval  $t = [-4, -2]$  were caused

when repairing a malfunctioning bleed valve on the injection system. These manipulation caused some loss of fluid, but the volume of lubricant plotted in Fig 4.7b was corrected by adjusting the injection rate during the time interval  $t = [-4, -2]$ . Because the lubricant pressure stayed well-above atmospheric pressure at all time, there is a high probability that the annulus remained saturated and that this temporary incident did not affect pore water pressure measurements in the soil.

At the end of the installation, the annulus was, again, isolated, and an immediate drop of pressure in the annulus was measured as a result. As will be discussed later, this is because the water was absorbed into the clay under the effect of the large hydraulic gradients away from the cavity. The volume of lubricant injected into the gap was found to match exactly the initial volume of the gap, calculated assuming zero convergence. However, this match is thought to be merely fortuitous: convergence of the cavity wall is likely to have occurred during the excavation, hence reducing the volume of the annulus, while lubricant was simultaneously seeping into the clay. The close agreement between the annulus volume and the injected lubricant volume suggests that these two effects roughly cancelled each other to produce the overlapping curves observed in Fig. 4.7b.

#### 4.4.3.4 Test T8

The lubricant used in test T8 was a 0.3% water-based solution of the *PHPA Insta-pac 425* (hereafter: ‘polymer’). Although identical injection pressure was targeted in test T6 and T8, the average pressure measured during the pipe installation in test T8 was 39 kPa, i.e. 22% lower than that in T6. The immediate drop observed at  $t = -6$  min coincides with the beginning of the excavation and relates to dynamic losses caused by the high viscosity of the polymer.

In contrast with the drop of lubricant pressure observed at  $t = 4.8$  in T6 upon alteration of the boundary condition at the end of the excavation, sealing of the annulus in T8 produced a marked increase of polymer pressure. This increase is believed to be the superposition of two effects, namely an immediate pressure increase relating to the elimination of dynamic losses in the supply system and a time-dependant increase arising from the confinement of the polymer solution in the annulus. This latter effect occurs as a result of the reduced permeability of clay to polymer, compared to that of water: little or no seepage into the clay occurs, and the converging cavity confines the remaining volume of polymer in the gap. This observation will be described in more detail in the following section. Fig. 4.7b further indicated that the volume of injected polymer in T8 is smaller than that of water in

T6, which substantiates the hypothesis that a smaller volume of lubricant seeps into the clay when substituting water with polymer.

## 4.5 Pore water pressure measurements

### 4.5.1 Preliminary remarks

#### 4.5.1.1 Labelling of instruments

The designation of the pore pressure transducer (*PPT*) location is shown in Fig. 4.8. The letter ‘A’ and ‘B’ refer to the installation plane  $x = 0$  and  $x = -157$  mm, respectively, while the following numeral refers to the radial order of the transducers, and increases with the distance from the cavity. The lower-case letter ‘a’ and ‘b’ indicate *PPTs* that were installed at symmetrical position for control purposes and the prefix T5, T6 or T8 are added to the *PPT* name to identify the test number.

#### 4.5.1.2 Normalisation of pore water pressure data

Measurements of excess pore water pressure in clay are commonly normalised by the undrained shear strength of the clay,  $S_u$ , as proposed by Butterfield & Johnson (1973). However, the post-test measurements of  $S_u$  were affected by some variability (Fig. 4.4), and it was therefore considered inappropriate to introduce error inherent to the crudeness of hand-vane measurement into the high-quality pore water pressure data. Alternative candidates to normalise excess pore water pressure data are the total or the effective stress. In order to select the normalisation factor, let us consider a stress plane with an arbitrary yield locus such as that depicted in Fig 4.9. The effective and total stress path depicted in Fig. 4.9 show that, for a given preconsolidation pressure  $p_c'$ , during a given total stress path, the excess pore water pressure generated depends on the initial effective stress  $p'$ . The hydrostatic pore pressure  $u_o$  merely shifts the total stress path to the right of the stress plane and does not affect the magnitude of the excess pore water pressure. However, a shift of initial effective stress along the  $p'$  axis before subjecting the soil element to the same changes in total stress produces different amounts of excess pore pressure. Therefore, an effective stress parameter was considered to be more appropriate than total stress to normalise the measurements of pore water pressure. Because  $K_{onc}$  was not measured,  $\sigma_{vo}'$  could be estimated more reliably than the corresponding mean effective stress  $p_o'$ , and the ratio  $\Delta u/\sigma_{vo}'$  will be used to describe excess pore water pressure in the non-dimensional form. The value of effective stress used as a normalisation factor was calculated as follows:

$$\sigma_{vo}' = \sigma_{vp}' + \gamma'z = (\sigma_{vp} - u_p) + \frac{G_s}{1 + wG_s} \gamma_w (C + D/2) \quad \text{eq. 4.12}$$

where all variables are as defined previously and where both  $\sigma_{vp}$  and  $u_p$  are taken as their average value during the 5 min preceding the excavation.

#### 4.5.1.3 Hydrostatic conditions before excavation

Drift of the *PPT* output voltage prevented direct measurements of absolute pore water pressure from being obtained reliably. Fig. 4.10 summarises the mean pore water pressure measured during the 5 minutes immediately preceding the beginning of test T5, T6 and T8, respectively. In this figure, the deviation between the calculated hydrostatic pressures expected under equilibrium conditions and the pore water pressure measured by each *PPT* is indicated above the corresponding bar. For each test, the hydrostatic pore water pressure at pipe axis depth is indicated by a horizontal line. Light and dark shades are used for the measurements taken by the Entran and the Druck transducers, respectively.

While *PPT* measurements depart less than 5 kPa from the expected pore water pressure in 7 cases, the mean deviation was as high as 43 kPa, with maximum values of up to 390 kPa. The device exhibiting 390 kPa drift did not respond satisfactorily during the unloading of the cavity (see Fig. 4.13: T5\_PPT\_A1) and hence, the data obtained from this transducer was therefore disregarded. Assuming that the sensitivity remained constant between the calibration and the test, the average output drift during the soil model consolidation was calculated to be 59 and 26 kPa for the Druck and the Entran devices, respectively. While such large drifts are usually expected in case of poor *PPT* saturation, all calibrations indicated that a high degree of saturation had been achieved. Therefore, the most probable cause of drift is of electrical origin. Thermal sensitivity is most likely to have originated the drift since the instruments were powered for prolonged periods of time (several weeks).

Since offset drift affected the long-term measurements, the *PPTs* were exclusively used to measure excess pore pressure. The value measured during the 5 minutes preceding the beginning of the model pipe installation was subtracted from the measured gauge pressure in order to obtain excess pore water pressure relative to the equilibrium conditions prevailing before the test. For practical reasons, the *PPTs* were not recalibrated after the experiment and their sensitivity was assumed to have remained unchanged. Table 3.3 shows that the sensitivity of the instruments did not

vary appreciably in successive calibrations, so that this assumption of constant sensitivity is unlikely to produce significant errors.

#### 4.5.2 Generated excess pore water pressure

An overview of the measured ratio  $\Delta u/\sigma_{vo}'$  during the excavation and during the subsequent equilibration period appears in Figs 4.11 and 4.12, respectively. In these figures,  $\Delta u/\sigma_{vo}'$  is presented versus the physical time,  $t$ . In accordance with the reference system defined in § 4.2.1,  $t = 0$  corresponds to the instant at which the rear of the oversized cutting edge passes through the middle vertical plane of the strongbox (Fig. 4.1). While the data obtained from T5\_ppt\_A1 and T6\_ppt\_B1 was disregarded following malfunction of these instruments, the remaining 22 instruments appear to have responded properly.

In test T8, the ratio  $\Delta u/\sigma_{vo}'$  returned to zero after a consolidation time of approximately 2.5 hours (Fig. 4.12c), hence indicating the restoration of hydrostatic conditions. However, such full recovery of pore water pressure was not observed in test T5 and test T6. Perhaps surprisingly, average values of  $\Delta u/\sigma_{vo}' = -0.20$  remained in the long-term (Fig. 4.12a and b), despite the unchanged back-pressure at the soil model boundary (§ 4.4.1.2). While this ‘under-reading’ could have been caused by a change in the *PPTs* sensitivity following the large unloading increment (§ 3.5.3.5), relatively close agreement between all *PPTs* suggest that the measured difference is not due to instrumental error. In addition, when negative  $\Delta u/\sigma_{vo}'$  persist in the long-term, a larger spread of pressure was apparent indicating the presence of small hydraulic gradients in the soil model and suggesting that steady state seepage sets up in the long-term.

The effect of the changing fluid boundary conditions (§ 3.2.1.2 and § 4.4.3) in test T6 and T8 clearly affected the measured pore water pressures, as may be seen in Figs 4.11 and 4.12. While, as a result of the failure of the injection system, no such change was effected in T5, discontinuities in the rate of dissipation nevertheless occurred, albeit somewhat later. As already discussed, this observation hints at the closure of the cavity and the associated change of flow condition across its boundary.

##### 4.5.2.1 Symmetry of pore water pressure measurements

In order to assess the precision and the reliability of the measurements, a number of *PPTs* pairs were installed at symmetrical positions about the pipe axis. The symmetry of the measured  $\Delta u$  about the cavity axis may be affected by the response

of the *PPTs* as well as by errors in their installation position. The selected installation method was such that deviation of the *PPT* guide by  $1^\circ$  from the vertical caused a 5 mm error in the horizontal location of the *PPT* at the pipe axis depth (300 mm). In regions of steep gradients of pore water pressure, such ‘misplacement’ of the transducer produces significant errors in the estimation of the radial distribution of  $\Delta u$ . In addition to these factors, the symmetry of *PPT* readings may be affected by the deviation of the model pipe axis from its installation direction, causing the cutting edge of the pipe to exert more pressure against the excavation wall on one of its hemisphere.

Figs 4.13 to 4.17 compare the ratio  $\Delta u/\sigma_{vo}$  obtained from pairs of *PPTs* installed symmetrically about the pipe axis. The data presented in these figures was not manipulated other than to shift the measured  $\Delta u$  by the value shown in Fig. 4.10. In most cases, the difference between symmetrically installed pairs of transducers was less than 5 kPa, and sometimes almost indiscernible (Figs 4.14 and 4.16). This indicates a high reliability of the pore water pressure measurement technique. Two pairs of transducers T6\_pptA1/a1 and T8\_pptA1/a1, temporarily measured diverging trends, as shown in Figs 4.16 and 4.17. Although these trends occurred in different tests, they were both measured by *PPTs* installed at  $r/r_o = 1.8$  and similar patterns were observed. The pore water pressure measured by T6\_ppt\_a1 and T8\_ppt\_A1 reduced by 50 kPa as the pipe reached the position  $x/D = 0.5$ . The trend then reverted and  $\Delta u/\sigma_{vo}$  increased by 0.35 0.45 kPa before reducing again at  $x = 0$ . In both cases, the minimal values measured by the transducers which underwent this saw-blade behaviour are approximately 10 kPa lower than that of the symmetrical transducer. As shown in Fig. 4.11 (T6\_ppt\_A2/a2), this trend was not observed in the adjacent pair of *PPTs* installed at  $r/r_o = 1.8$ . Although this observation could not be fully explained, it is believed to derive from small deviations between the axis of the pipe and that of its installation.

#### 4.5.2.2 Effect of container shape on excess pore water pressure

In tests T5 and T6, a second row of *PPTs* was installed in the plane  $x = -157$  mm. Fig. 4.14 and 4.16 show that, for constant distance between the pipe and the corresponding *PPT*, slightly larger  $\Delta u/\sigma_{vo}$  were measured in plane B than in plane A. While the ratio  $\Delta u/\sigma_{vo}$  reached approximately equal magnitudes in both plane at  $x = 0$  and  $x = -157$  mm, the pattern of dissipation following cavity unloading differs in both cross-sections. Transducers installed in plane B indicated rapid dissipation of the excess pore water pressure: more than a third of the generated

negative pore water pressure was recovered while the pipe was advanced a further 0.5D, i.e. in about 30 seconds. The diverging trends in test T5 and T6 that were measured upon this recovery pertain to the difference in fluid boundary condition and will be discussed later. In addition to the factors affecting the symmetry of the readings, the difference in generated pore water pressures at different locations may result from fluctuations in balance forces at the excavation face, as explained in § 3.4.3.1.

Comparison of pore water pressure reading in plane A and B clearly indicates that the plane-strain condition is violated by the varying distance from the excavation to the lateral boundary. The extent to which the circular plan of the container affects the measured pore water pressure in the middle plane compared to an equivalent rectangular strongbox cannot be evaluated directly. However, because all tests were performed under identical boundary conditions, the error produced by the strongbox shape should remain equal in all tests and hence, should not affect the conclusions derived from the results.

#### 4.5.2.3 Initial distribution of excess pore water pressure

The excess pore water pressures generated during the excavation process appear in Figs 4.18 to 4.23. In these figures, the generation of  $\Delta u/\sigma'_{vo}$  at  $r/r_o = 1.8$  (*PPT\_A2*, see Fig. 4.8) as a function of the normalised pipe position ( $x/D$ ) is compared for all tests in the left-hand plot. The right-hand plot shows the radial distributions of  $\Delta u/\sigma'_{vo}$  with  $r/r_o$  at times corresponding to different values of  $x/D$  during the excavation. The radial isochrones were obtained by shape-preserving interpolation between the pore water pressure measurements. In order to allow the isochrone to be drawn all the way to the cavity radius, the ratio  $\Delta u/\sigma'_{vo}$  at the cavity boundary was calculated using the following relationship:

$$\left. \frac{\Delta u}{\sigma'_{vo}} \right|_{r=r_o} = \frac{p_o - u_o}{\sigma'_{vo}} = \frac{p_o - u_b - \gamma_w (C + D/2)}{\sigma'_{vo}} \quad \text{eq. 4.11}$$

in which  $p_o$  is the lubricant pressure in the annulus or at the pipe-soil interface,  $u_b$  the initial back-pressure and all other parameters as defined previously. Since the pressure  $p_o$  was not measured for  $x/D < 0$ , the isochrones for  $t < 0$  ( $x/D < 0$ ) are only drawn for the range  $r/r_o \geq 1.2$ . When plotting the isochrones for values of  $t > 0$ , i.e. after the passage of the cutting edge at  $x/D = 0$ , the cavity wall was assumed to remain at  $r/r_o = 1$  and the reduction in radius due to convergence was ignored.

Fig. 4.18 shows that hydrostatic conditions prevailed when the pipe was at the position  $x/D = -4$ . In test T5, no excess pore pressures were generated ahead of the excavation until the cutting edge reached the position  $x/D < -2$ . Test T6 saw the development of marginal positive excess pore water pressures at a distance of approximately 3 diameters ahead of the face, as shown in Fig. 4.19a. While this technique had proven difficult at first, these results show that the successive refinements described in § 3.3.4 were effectively allowed, in test T5 and T6, the insertion of the model pipe without causing significant stress changes in the clay. In test T8, however, positive excess pore water pressures were measured as the excavation face reached  $x/D = -4$  and continued rising until reaching  $\Delta u/\sigma_{vo}' = 0.2$  at  $x/D = -1.5$  (Fig. 4.19a). The generation of excess pore pressure ahead of the shield in test T8 is likely to be the result of over-balanced face pressure resulting from a slower angular speed of the clay cutter.

In all tests, the ratio  $\Delta u/\sigma_{vo}'$  began to reduce sharply as the excavation face reached  $x/D = -1.75$ . Excess pore pressures continued to increase as the cutting edge passed through the instrumented section until reaching a maximum. While Fig. 4.18 shows that the maximal excess pore pressure at the radius  $r/r_o = 1.8$  occurred when the rear of the cutting edge reached, in all tests,  $x/D = 0.5$ , Fig. 4.11 reveals that in test T6 and T8, the time at which the minima of pore water pressures occurred increased with the distance from the cavity. In test T6, the minimum pore water pressure was measured before the rear of the cutting edge reached the instrumented section at  $x = 0$ , and while  $\Delta u$  began to recover at  $r/r_o = 1.2$ , it continued decreasing at larger radii.

The radial distribution of excess pore pressure is typical of that around a permeable borehole with a ground water support (*e.g.*: Fig. 2.15: case III). The pore water pressure in the vicinity of the cavity reduced below the lubricant pressure at the cavity boundary (Fig. 4.21 to 4.23). It is interesting to see, that despite the higher lubricant pressure in test T6 than in T8, the pore water pressure is lower in T6. However, the positive pore water pressures induced in test T8 ahead of the excavation face are most probably the cause for this difference and if this initial amount of  $\Delta u$  were subtracted from the isochrone of pore pressure shown in Fig. 4.22, initial excess pore water pressure distribution would be very similar in all tests, with magnitude reducing with the lubricant pressure. The magnitude of the pore water pressure reduction near the cavity boundary ( $p_{pt\_A1/a1/B1/b1}$ ) during the passage of the cutting edge ranged from 80 kPa, in test T8 to 115 kPa in test T5, hence reaching values below zero atmospheric pressure.

The isochrone plotted in Fig. 4.21 reveals that large hydraulic gradients prevailed immediately after the excavation. The average gradient of the isochrones near the cavity boundary (corresponding to the rate of outward seepage) is of the order of 4000 kPa/m, thus yielding positive (radial) hydraulic gradient of about 400. The direction of the hydraulic gradient reverses at a radius of between  $r/r_o = 1.2$  and 2. The hydraulic gradient near the cavity when the pipe reached  $x/D = 0$  was of similar magnitude in test T6 and T8, and somewhat smaller in test T5 where the lubricant pressure at the cavity boundary was considerably smaller (Fig. 4.21).

#### 4.5.3 Dissipation of excess pore water pressure

##### 4.5.3.1 Presentation of excess pore water pressure dissipation

The consolidation of the clay around the contracting cavity is described by Figs 4.25 to 4.31, where the dissipation and the distribution of  $\Delta u/\sigma_{vo}'$  in test T5, T6 and T8 are compared for different times. In the left-hand graph of Figs 4.25 to 31,  $\Delta u/\sigma_{vo}'$  measured at  $r/r_o = 1.2$  (*PPT\_A1/a1*: Fig. 4.8) is plotted for each test versus the dimensionless time factor  $T = c_v t/r_o^2$  on a semi-logarithmic scale ( $\log_{10}$ ). A value of  $c_v = 3 \text{ mm}^2/\text{s}$  ( $= 95 \text{ m}^2/\text{year}$ ) was used to calculate  $T$ . For selected time factors  $T$ , in each case represented by a vertical line in the left-hand graph, the radial isochrones of  $\Delta u/\sigma_{vo}'$  measured in all three tests are compared in the right-hand graph. The value of  $r/r_o$  at the cavity wall is taken as unity throughout the consolidation period, and its reduction towards its ultimate value  $r_p/r_o = 0.92$  due to the contracting cavity is ignored.

The evolution of the fluid pressure at the cavity boundary during consolidation is discussed, before analysing the pore water pressure in the clay. The consolidation is described by distinguishing two main phases, namely before and after sealing of the gap (§ 4.5.3.3 and 4.5.3.4, respectively). Finally, some comments are made on the pore water pressure measured in the long-term (§ 4.5.3.5).

##### 4.5.3.2 Evolution of fluid pressure at cavity boundary

The evolution of the fluid pressure at the cavity boundary throughout the tests is plotted in Fig. 4.39, where  $p_o$  has been normalised by the initial hydrostatic pressure at pipe axis depth,  $u_o$ . During the model pipe installation, the lubricant pressure,  $p_o$ , was controlled and, therefore, remained constant (§ 4.4.3). At the end of the installation, an alteration of the boundary condition occurred. In test T6 and T8 the annulus was deliberately sealed at  $T = 0.4$  ( $t = 4.5 \text{ min}$ ), hence preventing further fluid transport into or out of the annulus via the supply system. In test T5, the gap was

also sealed in the same manner as in the other test, but this operation was expected to have remained ineffective as a result of the damaged injection system (§ 4.4.3.2). The trend followed by the fluid pressure at the boundary nevertheless suggests an alteration of the boundary condition at  $T = 0.55$  ( $t = 6.5$  min).

The effect of this change of fluid boundary condition on the fluid pressure  $p_o$  may be clearly seen in Fig. 4.39. In test T6, the fluid pressure,  $p_o$ , immediately began to reduce upon sealing of the gap. The reduction was rapid and large, with a drop of over 25 kPa in 5 minutes (from  $T = 0.4$  to  $T = 0.8$ ). In test T5, a drop of approximately 15 kPa was measured after  $T = 0.55$ . This behaviour observed in test T5 and T6 was in contrast to that in test T8, where no reduction of fluid pressure at the cavity boundary was measured after the gap was sealed. On the contrary, as soon as the annulus was sealed (thus, confining the polymer solution in the annulus) the lubricant pressure immediately increases (Fig. 4.39). As has already been mentioned, a small component of this immediate increase in pressure might relate to the recovery of dynamic losses in the lubricant system as the injection comes to a halt. However, this immediate increase is followed by a significant increase of the fluid pressure at the pipe-soil boundary, causing a fast and monotonic recovery of fluid pressure towards hydrostatic conditions.

After the initial reduction of fluid boundary pressure measured in test T5 and T6 after sealing of the gap, the trend reverted at  $T = 0.8$  ( $t = 9$  min), when pore water pressures reached minima. After reaching these minima, a monotonic stage of recovery took place until steady-state conditions were reached approximately 2 hours after the unloading of the cavity. In test T8, the increase of the fluid pressure at the pipe-soil interface continued monotonically at a gradually reducing rate until equilibrium was reached. As was also observed for the pore water pressure (Fig. 4.12), the fluid pressures at the pipe-soil interface in test T5 and T6 do not return to the hydrostatic pressure measured before excavation took place. Instead, the pore water pressure remained about 30 kPa inferior to the back-pressure applied at the upper boundary of the soil model. This behaviour is unexpected when the cavity boundary is impermeable, thus imposing no-flux conditions across the excavation wall. The cause for this deficit of pore water pressure at 'equilibrium' could not be identified with certainty. Visual inspection at either end of the pipe during consolidation suggested that possibilities of leakage could be ruled out, but the data nevertheless imply that the model pipe acted as a sink.

#### 4.5.3.3 Dissipation of $\Delta u/\sigma_{vo}'$ before sealing of the gap ( $0 < T < 0.4$ )

A first phase of pore water pressure dissipation may be distinguished during the pipe installation, from the unloading of the cavity at  $x = 0$  until sealing of the gap ( $0 < T < 0.4$  or  $0 < t < 4.5$  min). During this interval, the lubricant pressure,  $p_o$ , was controlled and remained constant, as described in § 4.4.3. Although this time interval is small in relation to the entire consolidation period ( $0 < T < 30$ ), a few observation may be pointed out.

Immediately after reaching their minimum value at  $x/D = 0.5$  (Fig. 4.22a), a rapid dissipation of  $\Delta u$  was measured near the cavity boundary (while  $p_o$  remained constant). As shown in Fig. 4.11b, this trend was more pronounced in test T6 than in test T8. Immediately after unloading of the cavity, a sharp dissipation of  $\Delta u$  was measured by T6\_ppt\_A1 near the cavity boundary ( $r/r_o = 1.2$ ). While this dissipation was also measured at  $r/r_o = 1.8$ , albeit at a reduced rate and magnitude, this feature disappeared at larger radii (Fig. 4.11b: T6\_PPT\_A3/A4). This sudden dissipation of  $\Delta u$  near the cavity may also be discerned in test T8 (Fig. 11c), but at a much smaller rate and magnitude and only at the location  $r/r_o = 1.2$ . This rapid initial dissipation can be partially attributed to the large hydraulic gradient in the direction of the cavity axis. An isochrone showing the distribution of  $\Delta u/\sigma_{vo}'(x, r)$  in the horizontal plane through the pipe axis appears in Fig. 4.32, giving an impression of the three-dimensional nature of the problem around the advancing excavation face. The contours of constant  $\Delta u/\sigma_{vo}'$  are shown in Fig. 4.33. It may be seen that the longitudinal component of the hydraulic gradient,  $i_x$ , is larger than the radial hydraulic gradient,  $i_r$ . As the face moves away from a given section, the hydraulic gradient in that section gradually becomes dominated by its radial component, and the rate of dissipation is then comparatively smaller. As a result, the dissipation of  $\Delta u$  immediately behind the cutting shoe is rapid, as a result of pore water flow in the direction of the pipe axis and gradually reduces as the longitudinal hydraulic gradient vanishes and the flow conditions become two-dimensional. A comparison of test T6 and T8 also show that the recovery is more pronounced in case where water is used as a lubricant than when the annulus was filled with polymer. Because the polymer flow through the clay is expected to be much slower than that of water, this suggests that, in test T6, water ingress from the cavity wall also accounted for the fast recovery of pore water pressure in the vicinity of the cavity.

#### 4.5.3.4 Dissipation $\Delta u/\sigma_{vo}'$ after sealing of the gap ( $T > 0.4$ )

The second, quite distinct phase of excess pore water pressure dissipation occurs after sealing of the gap around the model pipe ( $t > 4.5$  min,  $T > 0.4$ ). The effect of the change of boundary condition on the lubricant pressure  $p_o$  was discussed in § 4.5.3.2, where it was pointed out that clearly diverging trends were followed by the lubricant pressure depending on its composition (water or polymer). The pore water pressure response in the clay upon sealing of the gap is discussed next.

Fig. 4.26 shows that before the gap was sealed, the hydraulic gradient was directed outward from the cavity, i.e. the high fluid pressure at the cavity boundary would induce outward flow towards zones of lower pore pressures. Under these conditions, the pore water pressure in the immediate vicinity of the cavity could have been expected to rise as a result of fluid ingress from the annulus outward, so that the drop of fluid in the annulus observed in test T5 and T6 would be accompanied by an increase in pore water pressure in the adjacent clay. This did not occur. The fluid pressure reduction measured at  $r/r_o = 1$  occurred at all radii, with rates and magnitudes slightly decreasing with distance from the cavity. In test T8, the response of the pore water pressure near the cavity boundary was opposite, with a sharp and monotonic increase of pore pressure at  $r/r_o = 1.2$  and a somewhat smaller increase at  $r/r_o = 1.8$  (Fig. 4.11c, 4.26 and 4.27). The initiated rate of pore water pressure recovery reached about 15 kPa/min at  $r/r_o = 1.2$ . Interestingly, the trend reverted at radii of  $r/r_o = 2.8$  and beyond. The reduction of pore water pressure increased with the radius away from the cavity, and reaches approximately 15 kPa (Fig. 4.11c: T8\_ppt\_A5/a5) at  $t = 40$  min ( $T = 2.7$ ), before dissipation of  $\Delta u$  resumes until reaching hydrostatic conditions at about  $t = 150$  min ( $T = 13$ ).

In test T5 and T6, a further change of behaviour was measured following the initial drop of pore water pressure. At  $t = 9$  min ( $T = 0.8$ ), the decaying pore water pressure measured at  $r/r_o = 1.2$  reached a minima (Fig. 4.11b). This may be seen in Fig. 4.27a, where  $\Delta u$  measured at  $r/r_o = 1.2$  is shown together with a radial isochrone of pore pressure at  $T = 0.8$ . The pore water pressure at larger radius all followed the same trend, however with the minima. The second derivative of  $\Delta u/\sigma_{vo}'$  in T8 also changes sign at  $T = 0.5$ ; the falling rate of dissipation then increases again, perhaps suggesting a change of mechanism at this time. Despite their differences until the change of boundary condition, the isochrones of radial  $\Delta u/\sigma_{vo}'$  distribution are surprisingly parallel for  $0.5 < T < \infty$ , indicating nearly identical radial hydraulic gradients. However, the magnitude of pore pressure is higher in T8, and a difference of between

15 and 30 kPa subsists when comparing the pore water pressure of test T6 and T8 at steady-state.

#### 4.5.3.5 Pore water pressures at steady state ( $T > 30$ )

Except for test T8, where all *PPTs* buried in the clay measured excess pore pressure departing less than 3% from the hydrostatic pressure, excess pore pressure did not dissipate fully in the long-term in test T5 and T6. Radial isochrones shown for  $T = 30$  in Fig. 4.31 suggest that hydraulic gradients subsist towards the zone of soil near  $r/r_o = 1.2$ . These long-term measurements of low  $\Delta u$  in T5 and is confirmed by all the *PPTs* installed symmetrically at position  $r/r_o = 1.2$  and 2.0. Although not shown in the figures, data was logged well beyond the scale considered here and it could be verified that the changes of pore pressure at the pipe-clay boundary between  $T = 30$  to  $T = 60$  are less than 2% (however, interesting to see that band of pore water pressure spread becomes narrower and all instruments come to approximately the same value, perhaps suggesting the absence of electrical drift for the duration of the test). As already discussed in § 4.5.3.2, this suggests that the model pipe acted as a sink, allowing steady-state flow from the horizontal model boundary towards the model pipe. While this was unexpected and could not be supported by visual observation during the tests, this possibility cannot be ruled out.

## 4.6 Ground loading on pipe

### 4.6.1 Preliminary remarks

Six earth pressure cells (§ 3.5.2.1) measured the total radial stresses exerted on the model pipe by the clay and three pore pressure cells (*PPCs*, § 3.5.2.2) measured the fluid pressure on the pipe. The sensitivity and the offset of these instruments varied considerably during their successive calibration as well as between each calibration and the corresponding test. Although the calibration of the LCPM instrumentation was systematically carried out the same day as the test, deviations of the total stress measurements from the expected values were recorded before the beginning of the test, while the instruments were still all subjected to atmospheric pressure.

The average stress measured by the earth pressure cells during the 5 minutes immediately preceding the excavation was -0.7 kPa in test T5, indicating excellent instrument stability between the calibration and the excavation. In test T6, this error was still within the range of tolerance of such instruments with a measured stress of

-4.8 kPa. However, this was no longer the case in test T8 where the average initial drift of the earth pressure cell was as high as -265 kPa, with one instrument measuring a total pressure of 1 MPa (instead of zero). These considerable output drifts are believed to have arisen from extreme hygro- and thermosensitivity of the strain gauges, whose protective coating could have suffered damage as the test series progressed. Indeed, changing humidity and temperature conditions occurred after calibration, when the instrument clusters were submitted to a vacuum-pressurisation cycle under water to saturate the *PPCs*. The detailed responses of the earth pressure cells during their installation into the strongbox are documented in appendix A (Fig. A.1, A.3 and A.5). The average values for each test are compared in Figs 4.36 and 4.38 for the installation and the consolidation period, respectively. As indicated in these figures, peaks of pressure occur as a result of the interaction of the earth pressure cells with the joint drawn in Fig. 3.15.

The output of the pore pressure cells were also affected prior to the beginning of the tests. In test T8, the fluid pressure measured by instrument ‘ppc5’ before entering the strongbox decayed by approximately 5 kPa over a period of 5 minutes (Fig. 4.35), while the other transducers measured constant pressure. The difference of pressure between ppc5 and the two other instruments persisted throughout the remainder of the test and may even be observed even in the long-term. The pore pressure cells could not be kept underwater to ensure their continuous saturation in the 5 minutes preceding the excavation and thus, this gradual pressure decay is believed to derive from incipient desaturation of the *PPCs*. As a result of these significant changes in offset before or during the installation of the instruments, zeroing the instrument reading immediately before the beginning of the test was not a reliable method to determine the absolute value of total stress and pore pressure on the pipe. Therefore, particular attention was given to the offset manipulation and the way in which the baseline readings were determined in each case is outlined hereafter, along with the discussion of the corresponding data.

#### 4.6.2 Fluid pressure on the pipe

This section further details the way in which the fluid pressure at the cavity boundary was measured and how the instrument offset was determined. The average pressure in each test appears in Fig. 4.39. The evolution of the fluid pressure at the cavity boundary during the pipe installation and the subsequent consolidation was discussed in § 4.5.3.2 and is not repeated here.

Fig. A.7, A.9 and A.11 (Appendix A) show the three fluid pressure measurements normalised by the initial pore water pressure at pipe axis depth,  $u_{ro}/u_o$ , during the pipe installation in test T5, T6 and T8, respectively. Fig. 4.35 compares the average values of  $u_{ro}/u_o$  for each test. The offset of the *PPC* was shifted by correlating their reading with reliable measurement of the annulus pressure at a time when they were known to be the same. The annulus pressure was also measured by a Druck transducer at the location indicated in Fig. 3.15. The measurement from this instrument proved extremely stable and repeatable (Table 3.2), and it was considered appropriate to use it as a reference to determine the base-line fluid pressure measured by the *PPCs*. Before closure of the annulus, the pressure transducer communicated with the *PPCs* via the saturated gap, hence, as soon as the *PPCs* had penetrated into the annulus and their reading had stabilised, the instrument offset could be calculated so that their measurements matched the pressure indicated by the Druck transducer. The position of the model pipe at the instant when the offset was calculated was  $x/D = -1$ , at which time it was reasonable to assume that ground closure had not occurred, and hence, that the fluid filling the annulus communicated with both the transducers and the *PPCs*. This way, the drift of the *PPCs* prior to the test, as well as other effects pertaining to the test procedure and affecting the base-line reading of the *PPCs*, were eliminated.

Fig. 4.35 as well as Figs A.7 to A.12 (Appendix A) indicates good agreement between the Druck transducer as well as all *PPCs* during the remainder of the pipe installation, confirming the constant pressure of lubricant in the annulus. Because the lubricant pressure was measured near the strongbox wall and the *PPC* gradually penetrated into the strongbox until reaching their final position in the middle vertical plane of the tank, the close agreement between the measured fluid pressures at all locations indicate that, in all tests, the annular gap around the pipe remained open throughout the installation process.

#### 4.6.3 Total stress on the pipe

Figs 4.37 and Fig. A.1 to A.6 (Appendix A) show the total stress on the pipe ( $\sigma_{ro}$ ) during the pipe installation, normalised by the initial vertical stress at pipe axis depth ( $\sigma_{vo}$ ). Following the procedure described in the previous section, the total stress measurements were offset in order to match the fluid pressure in the annulus immediately after all the instruments had penetrated the strongbox.

Six independent measurements of total radial stress were made. Mechanical constraints restrained the azimuthal orientation of the LCPM during installation, so

that an earth pressure cell could not be installed rigorously at the pipe crown. Instead, the LCPM was installed so that the axis normal to the surface of earth pressure cell LC1 formed an angle of  $5^\circ$  with the vertical. As a result, measurements of pairs of pressure cells lying in a symmetrical configuration about the model pipe axis cannot be directly compared to assess the symmetry of the measurements. The uniform distribution observed after the test indicates that the total stress is entirely due to fluid pressures, and that variations thereof at a given time around the pipe only result from the hydrostatic pressure difference, i.e. less than 1 kPa. Total stress distributions at larger values of  $T$  become gradually less uniform. Because the model pipe movements were restricted, the free displacement boundary at the upper model surface caused larger total stresses on the crown than on the invert of the pipe. While this difference was observed in all tests, it reduced with increasing effective stress as the pore water pressure was found to equalise all around the pipe. Because the fluid pressure distribution is uniform before closure of the overcut, the closure may be determined as the instant when the distribution of  $\sigma_{ro}/\sigma_{vo}$  with  $\theta$  becomes non-uniformity.

A temporary drop of total stress is measured slightly before the end of the excavation. As shown in Figs 4.35 to 4.37,  $\sigma_{ro}/\sigma_{ro}$ , reduce by up to 17 kPa over a period of time of 1 minute ( $0.3 < T < 0.4$ , before sealing the annulus). The total stresses then recovered to the pressure measured before the drop. The drop in total stress was observed in all tests, albeit with a different magnitude, and was consistently accompanied by a simultaneous reduction of fluid pressure on the pipe. However, the reduction of the fluid pressure was much smaller than the reduction in total stress. No negative effective stresses may of course occur; and in cases where the annulus is saturated with fluid, any change in fluid pressure is expected to be recorded simultaneously as a change in total stress. The difference arising in this case is thought to be a result of signal conditioning; low sampling frequency meant that the signal from each transducer was recorded at large time intervals ( $\sim 12$  sec). Hence, fast events like a sudden and temporary pressure drop may not be reconstructed fully from the low frequency signal. The large spread of values measured around the pipe supports this hypothesis. The drop in total stress is therefore likely to have been induced by a drop in fluid pressure of similar magnitude. However, the reduction measured by the *PPCs* does not agree with the measured lubricant injection pressure, which remains constant until sealing of the annulus. This effect could not be fully explained, but the pore pressure measurement in the soil did not follow the same trend as the *PPCs*, which suggest that this drop is related to some phenomenon taking place in the gap or an effect affecting the output of the LCPM instrumentation.

In test T5 and T6, the sealing of the gap gave rise to a reduction of total stress following the same trend as the reduction of pore water pressure (§ 4.6.2). Upon reaching minima at  $T = 0.65$  and  $1.3$  in T5 and T6, total stresses began to increase until reaching a steady value of approximately  $\sigma_{ro}/\sigma_{ro} = 0.5$  at  $T = 20$  ( $t = 3$  hours). Remarkably, the final total stress on the pipe reached the same magnitude in tests T5 and T6, differing by less than 1.5%. This is in contrast with total stresses in test T8, where  $\sigma_{ro}/\sigma_{vo}$  increased immediately after the annulus was sealed. This increase continued monotonically until reaching a steady value of  $\sigma_{ro}/\sigma_{ro} = 0.57$ , i.e. 11% higher than in tests T5 and T6. While the rate of total stress increase in tests T5 and T6 reduced steadily after  $T = 2$  and  $3$  ( $t = 23$  and  $24$  minutes), respectively, a discontinuity in the rate of stress changes may be observed in test T8. At  $T = 5.2$ , a noticeable increase of rate of total stress build-up is observed. While the increase rate of  $\sigma_{ro}/\sigma_{ro}$  before this discontinuity suggested that an equal value was going to be reached in all three tests, some event seems to have triggered a further increase of total stresses on the pipe. A scrutiny of the boundary condition (Fig. 4.5a) reveals that a small change of the total stress,  $\sigma_{vp}$ , acting at the model boundary occurred simultaneously ( $t = 60$  min). However, this sudden variation of surcharge pressure  $\sigma_{vp}$  was smaller than 2% of its nominal value of  $\sim 200$  kPa and cannot, alone, explain the observed discontinuity in the rate of ground loading on the pipe.

#### 4.6.4 Effective stresses at the pipe-clay interface

Large relative error affected the determination of the effective stresses,  $\sigma_{ro}'$ , acting on the model pipe. This is because they were obtained by subtracting fluid pressure,  $u_{ro}$ , from the total stresses,  $\sigma_{ro}$ , therefore adding the absolute errors affecting the subtrahend and the subtrahend. Because the offset of both the earth pressure cells and the *PPCs* were determined using the known annulus fluid pressure at  $x/D = -1$ , the offset of effective stress was not manipulated in any other way. In addition, the precision of the effective stress determination is affected by the relatively low sensitivity of the LCPM instrument. Also, the low sampling frequency prevented signals from events occurring faster or at a higher frequency than the period of sampling of 12 seconds from being reconstructed.

The dimensionless time,  $T_c$ , at which contact is made between the pipe and the clay can be determined as the time at which effective stresses become non-zero. However, because of the significant relative error in effective stresses, as well as their small rate of increase and the non-uniform convergence of the ground with  $\theta$ , the moment at which the annulus closed cannot be determined with precision. However, the

incipient pipe-clay contact can also be inferred from the distribution of total stress around the model pipe. As long as total stresses are due to fluid pressure only, a uniform distribution is expected; when effective stresses arise, i.e. when pipe-clay contact occurs, total stresses become non uniform, as may be seen for test T8 at around  $T = 3$  (Fig. A.6, Appendix A).

The time,  $T_c$ , at which the closure of the gap occurred in tests T5 and T6 may be relatively clearly discerned in Fig. 4.41. In addition to the effective stress becoming non-zero, a point of inflexion in the  $T:\sigma_{ro}'$  relationship marks the onset of effective stress build-up. As shown in Fig. 4.41, the gap closure occurs at an earlier stage in test T5 than in test T6, where it happens at  $T_c = 1$  and 1.3 ( $t = 10$  and 14 minutes), respectively. As a result of the smaller effective stresses measured in test T8, the determination of  $T_c$  is more difficult. While the data presented in Fig. 4.41 suggest immediate closure upon sealing of the annulus at the end of the excavation, the rate of effective stress increase following the initial step is marginal, with a gradient of approximately 2 kPa in 30 minutes, i.e. 20 times lower than the increase of effective stress in test T5. A point of inflexion may also be discerned in test T8, at  $T = 2.5$  (Fig. 4.41). Because total stresses were also remarkably uniform around the pipe circumference until this value of  $T$  (see Fig. 4.55), it was considered more accurate to establish the closure of the gap at this stage rather than immediately after the end of the excavation. The small effective stresses observed in test T8 before  $T_c = 2.5$  are believed to fall within the cumulated instrumental error of the earth and the pore pressure cells.

As can be seen from Fig. 4.41, the average radial effective stresses in test T5 increased sharply until reaching a ratio  $\sigma_{ro}'/\sigma_{vo}' = 0.17$  at  $T = 2$  ( $t = 22$  minutes). Perhaps surprisingly, the effective stresses on the pipe then ceased to increase and begun to reduce significantly until returning to a ratio of between  $\sigma_{ro}'/\sigma_{vo}' = 0.11$  and 0.14 where they stabilised in the long-term. This behaviour was not observed in test T6, where effective stresses increased monotonically, albeit at a slightly lower rate, until reaching a maximum value of  $\sigma_{ro}'/\sigma_{vo}' = 0.28$ , i.e. twice the magnitude measured in test T5. The use of a polymer-based lubricant in test T8 resulted in much lower rate of radial effective stress increase on the model pipe. In addition, the long-term effective stresses were also much lower than in both other tests where water was injected at different pressures in the annular gap. A maximum ratio of  $\sigma_{ro}'/\sigma_{vo}' = 0.08$  was measured in T8. This ratio corresponds to about 1/3 of the effective stress ratio measured in T6, and 2/3 of that recorded in T5.

## 4.7 Model limitations and sources of errors

Factors that could potentially have affected the experimental results presented above are briefly discussed in this section. The sources of errors may be classified in two categories: those due to the simplification that were deliberately introduced by the modelling technique (§ 4.7.1), and those caused by inaccuracies inherent to the test execution and the measurement techniques (§ 4.7.2). The significance of the former type of errors needs to be appreciated so that recommendations for engineering applications may be derived from the experimental data. The second kind of errors affects the reliability of the results; understanding them is crucial to provide a robust commentary on the data and avoid attributing the observed behaviour to erroneous causes.

### 4.7.1 Errors related to modelling

The physical model introduced several simplifications of the problem to allow a repeatable test procedure. The experimental philosophy was to isolate the processes influencing the interactions between the lubricant fluid and the radial ground loading on the pipes. The aim of the experiment was to measure patterns of response in different conditions rather than to predict the behaviour of a specific prototype. The sources of error therefore pertain to the relevance of the processes included in the model, as well as to the selection of model geometry and boundary conditions imposed on the model. The principal modelling decisions likely to have an effect on the relevance of the test results may be summarised as follows:

- The intensity of ground loading on pipes reduces with increasing overcut ratio  $r_o/r_p$ . This ratio was considerably larger in the model than in a typical field situation. The influences of the overcut size as well as the way in which the results scale with it are not fully understood. Therefore, care ought to be exerted when extrapolating the experimental results to engineering scale, especially with respect to the effect of  $r_o/r_p$ .
- The intermittent jacking and lubrication sequence typical for pipe jacking was idealised as a two-stage operation. The construction process was modelled by (1), the excavation and installation of a pipe under a well-defined and constant hydraulic boundary condition and (2), a consolidation stage. This differs to the situation in a real pipe jack where the ground closure usually occurs before the completion of the pipe-jack. While still undergoing radial consolidation, certain sections of soil are subjected to intermittent shearing, and shear-induced excess

pore water pressure add to the residual transient pore water pressure resulting from the cavity unloading. This extra component of pore water pressure affects the pipe-soil stresses and, in turn, the jacking forces. This is an important effect that contractors are well aware of, and there is some anecdotal evidence suggesting that the lubricant composition may affect the modes of shearing and the magnitude of shear-induced pore water pressure, and hence the jacking forces.

- The hydraulic boundary condition at the excavation wall was idealised as described in § 4.4.3.1. Pore water pressure measurements have shown the striking effect of altering the hydraulic boundary condition after the test. It would be a valid point to question the effect of lubricants composition under constant-pressure fluid boundary condition, not only during the pipe installation, but also throughout the consolidation. Some insight into this important question is provided in Chapter 5.
- During jacking, the pipe string may snake horizontally in the oversize bore (itself sinuous as a result of driving corrections) and, also, rise as the upward thrust of the lubricant exceeds the weight of the submerged pipe. The lateral degrees of freedom mainly result in a symmetrical stress distribution on the pipe about the horizontal and vertical axes. In the model experiment, movements of the pipe in the plane perpendicular to its axis were restrained to avoid technical complications at the pipe-strongbox interface. As a result, the ground loading on the model pipe does not satisfy vertical and horizontal equilibrium because resulting forces at the pipe-strongbox interface compensates for the difference in the up and downward ground loading on the pipe.

#### 4.7.2 Errors related to test execution

A number of problems may have affected the repeatability of the test conditions and the accuracy of the measurements. The factors that are considered to have had the most significant effect may be summarised as follows:

- The total vertical stress applied to the soil model fluctuated considerably during the consolidation. The maximum overconsolidation pressure could not be maintained at the targeted value of 800 kPa. Variations of over 40 kPa remained, hence preventing a constant and repeatable *OCR* profile to be achieved for the soil models in test T5, T6 and T8.

- The actual value of overburden pressure  $\sigma_{vo}$  at the depth of the pipe axis was not measured directly. Discrepancies between the measurements of the load over piston surface area may result from three different sources. Firstly, the weight of the ram and the piston, the friction in the hydraulic cylinder and in the ‘O’-rings around the piston were assumed to compensate each other. Secondly, losses of total stress by friction along the side-wall of the strongbox were ignored. This simplification may result in an underestimation of the normalised ground loading on the pipe  $\sigma_{ro}/\sigma_{vo}$ . The related effect of stress non-uniformity below the rigid piston (or indeed the tilt of the piston) was also ignored.
- The finite distance to the lateral boundary affects the stress redistribution and consolidation process around the contracting cavity. While the horizontal earth pressure was not measured at the side-wall, detailed pore water pressure measurements near the lateral boundary were made, allowing some conclusions to be drawn with regard to the side boundary effects. The consequence of having a strongbox with a circular plan, rather than rectangular, was discussed in § 3.2.5 and pore water pressure measurements at different cross sections of the strongbox are compared in § 4.5.2.2.
- The pore pressure cells (*PPCs*) on the LCPM were calibrated prior to their saturation. This procedure is not ideal but it was imposed by technical imperatives and improvements would have required substantial modification of the test equipment. Importantly, the effect on the measured fluid pressure at the pipe-soil interface due to contact between the polymer and the porous element of the *PPC* was not tested under controlled conditions. Under-reading resulting from clogging of the filter by the polymer was hypothesised, but the pore water pressure measurements discussed in § 4.5.3.4 suggested the absence of such effects. Being initially saturated, the polymer cannot penetrate sufficiently deep into the ceramic stone to create a cake preventing the full transmission of fluid pressure from the pipe-soil boundary into the reservoir of the instrument. This effect would be expected if considerable flow was allowed across the porous element, such as, for example, in a permeability test.

#### 4.8 Summary of observations

The data presented in this chapter may be summarised as follows:

---

**Boundary conditions (§ 4.4)**

- The successive improvement of the test equipment allowed three tests (T5, T6 and T8) to be carried out under repeatable boundary conditions. The boundary stresses applied to the soil model to simulate in-situ stresses could be maintained within 1% of their nominal value throughout the test. Their mean value deviated less than 3.5% (total stress) and 3% (fluid back pressure) of their target values of 200 and 100 kPa, respectively.
- The model pipe installation occurred under extremely repeatable conditions. After improving the excavation tools and introducing a polymer-based drilling fluid to disperse the clay cuttings behind the excavation face, the pipe could be inserted into the clay without causing significant stress changes ahead of the advancing face. The installation rate of the pipe was identical in all three tests analysed in this chapter, with almost indiscernible variations of speed and final position from one test to the other.
- The injection procedure of the lubricant was also satisfactorily controlled. De-aired water was used as a lubricant in test T5 and T6, and a water solution with 0.3% polymer was used in test T8. Although identical lubricant pressure were targeted values of  $p_o = 50$  and 39 kPa were measured in tests T6 and T8, respectively. In test T5, the lubricant was injected near atmospheric pressure, as a result of damage of the injection system.

**Pore water pressure measurements (§ 4.5)**

- High quality measurements of pore water pressure in the clay surrounding the excavation were obtained. All but two *PPTs* (out of 25) responded satisfactorily during the tests and were able to measure the abrupt drop of pressure after having been buried in the model for several weeks. The accuracy of the pore water pressure measurements could be demonstrated by remarkable agreement between pairs of transducers installed symmetrically about the model pipe axis.
- During the pipe installation, large drop of pore water pressure were measured as the cutting edge of the model pipe was one diameter before and after the plane in which the *PPTs* were installed ( $-1 < x/D < 1$ ). Negative excess pore water pressures of up to -100 kPa were measured in test T5 after passage of the cutting edge. This magnitude as well as the initial distribution of excess pore water pressure in the radial direction varied slightly in each tests, probably as a result of different lubricant pressure in the annulus.

- The dissipation of excess pore water pressure around the excavation was differed fundamentally depending on the composition of the lubricant injected into the annulus. When water was used as a lubricant, the fluid pressures at the boundary and the pore water pressure in its vicinity were found to reduce markedly upon sealing of the annulus. The opposite effect was measured when polymer solution was used as a lubricant: fluid pressure and pore water pressures increased sharply upon sealing of the gap, and then continued to recover monotonically until reaching hydrostatic pressure under equilibrium conditions.
- Pore water pressures were expected, in all cases, to return to hydrostatic pressure at equilibrium. While this could be measured in test T8, it did not occur in test T5 and T6 where pore water pressures of approximately -30 kPa were sustained in the long-term. Agreement between all the instruments as well as small hydraulic gradients towards the model pipe suggest that, in these tests, the model pipe acted as a sink and provided a leakage path, thus allowing steady-state seepage. The polymer may have prevented this in test T8, by effectively reducing the permeability of an annulus of clay around the pipe.

#### **Ground loading on the pipe (§ 4.6)**

- The ground loading on the model pipe was clearly affected by the composition and the injection pressure of the lubricant. The lubricant composition and pressure not only affected the transient build-up of effective stresses on the model pipe, but also, perhaps unexpectedly, their final magnitude. Large differences in effective stress at equilibrium were measured. The dimensionless effective stress reached  $\sigma_{ro}' / \sigma_o' = 0.28$  at equilibrium in test T6, where water was injected under 50 kPa as a lubricant. Contrastingly,  $\sigma_{ro}' / \sigma_o' = 0.08$  was measured in test T8, hence showing that the ground loading in terms of effective stress had reduced by over 65% when using polymer as a lubricant, even though the lubricant pressure was approximately 25% lower in test T8 (compared to test T6).

<b>Granulometry</b>			
Specific Gravity	$G_s$	2.6	-
Mean particle size	$d_{50}$	0.005	mm
<b>Plastic limits</b>			
Plastic Limit	$w_l$	30	%
Liquid Limit	$w_p$	51	%
Plasticity Index	$I_p$	21	%
<b>Cam-Clay Parameters (average of values quoted in literature)</b>			
Gradient of compression line	$\lambda$	0.15	-
Gradient of swelling line	$\kappa$	0.03	-
Ordinate of isotropic compression line	$\Gamma_{iso}$	2.44	-
Ordinate of one dimensional compression line	$\Gamma_{1D}$	2.44	-
Ordinate of critical state line	$\Gamma_{cs}$	2.04	-
Critical state frictional constant	$M$	1.05	-
<b>Consolidation parameters</b>			
Coefficient of consolidation (virgin consolidation)	$c_v$	1.00	mm <sup>2</sup> /s
Coefficient of consolidation (isotropic rebound)	$c_v$	5.00	mm <sup>2</sup> /s

Table 4.1. Summary of properties and engineering parameters of E-Grade kaolin (after Barker, 1998; Merritt, 2004)

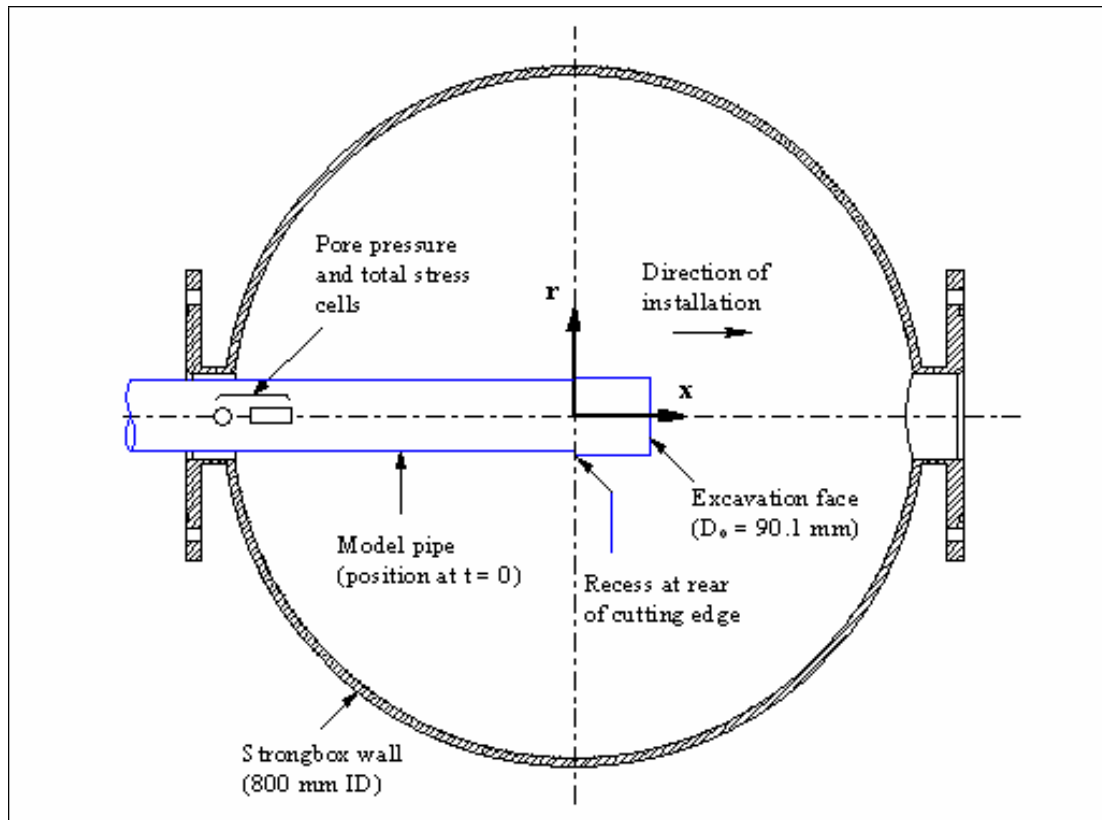


Figure 4.1. Spatial reference frame

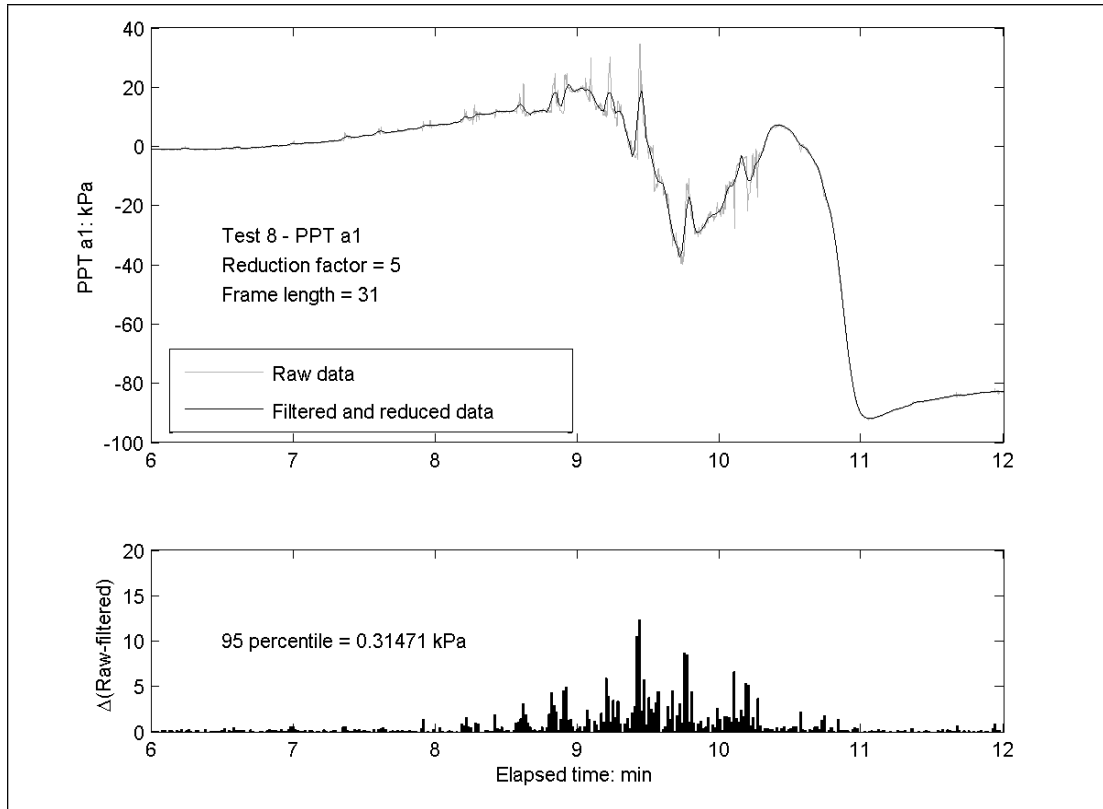


Figure 4.2. Raw and filtered data ( $N = 61, n = 10$ )

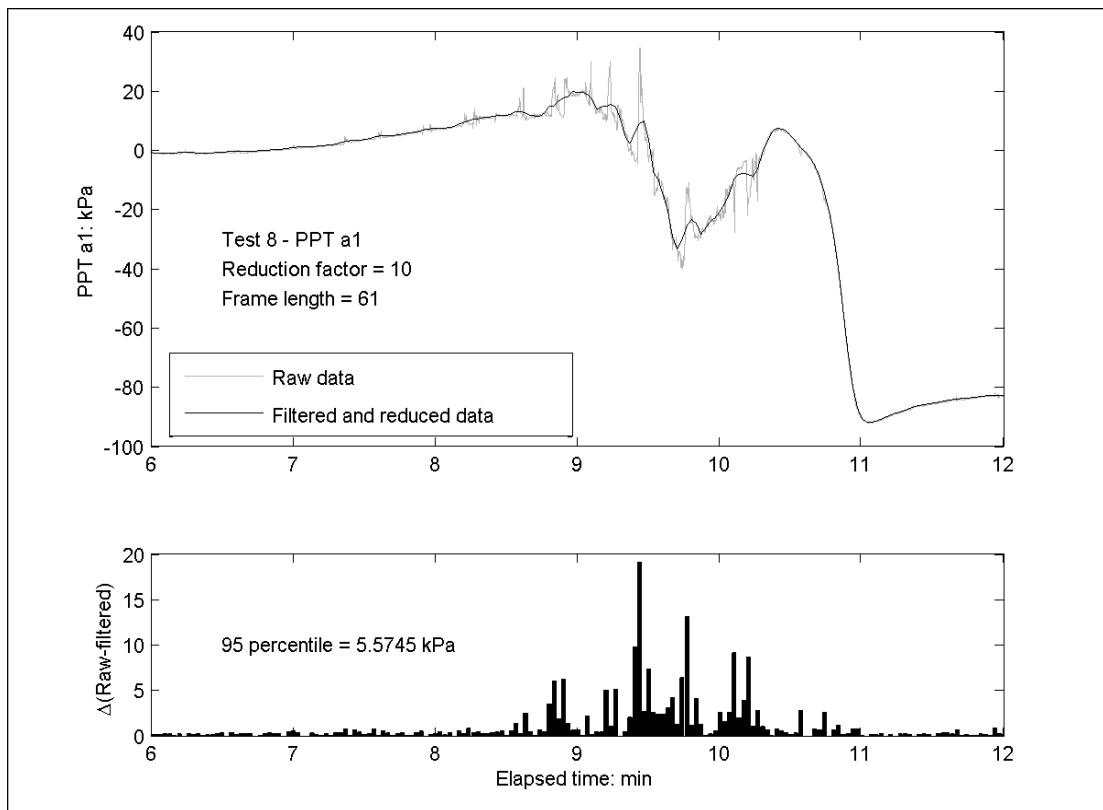


Figure 4.3. Raw and filtered data ( $N = 31, n = 5$ )

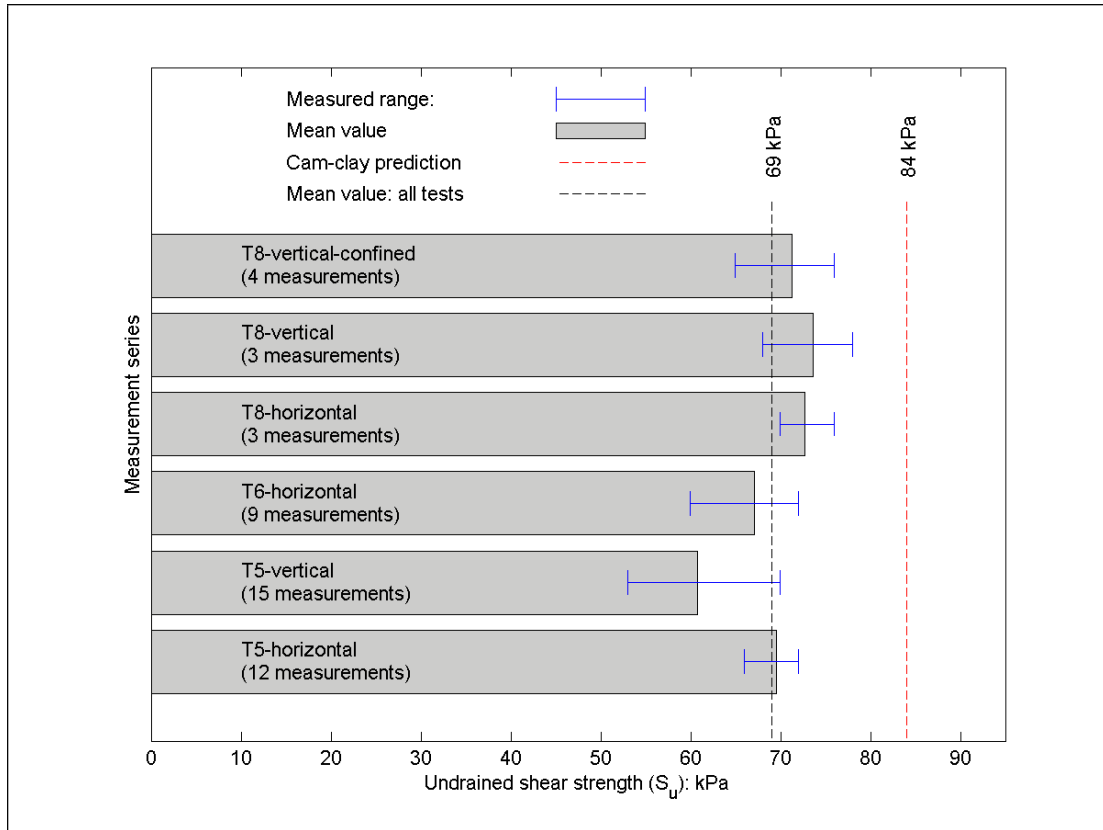


Figure 4.4. Undrained shear strength measurements

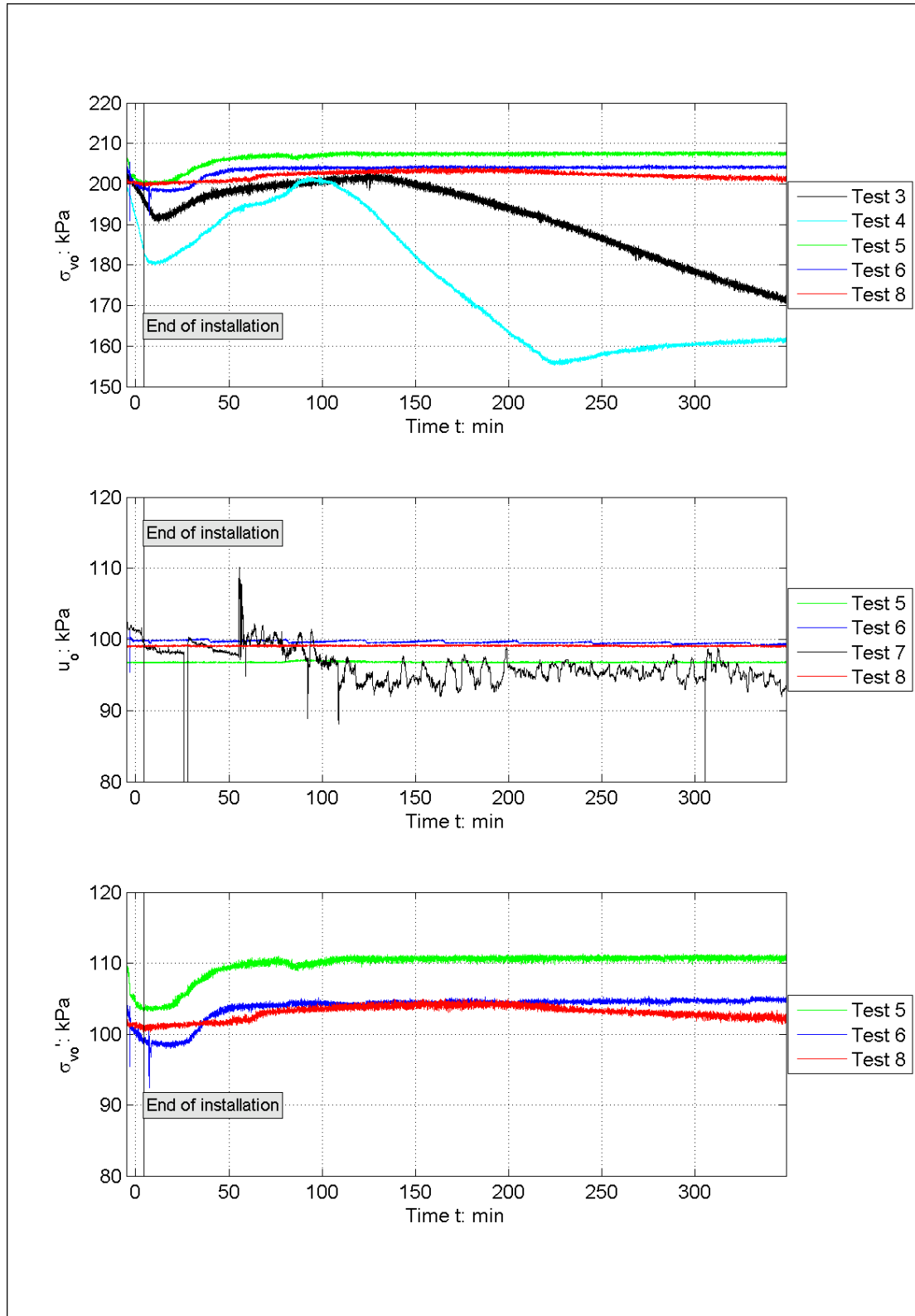


Figure 4.5. (a) Total stress; (b) back-pressure; and (c) effective stress at boundary

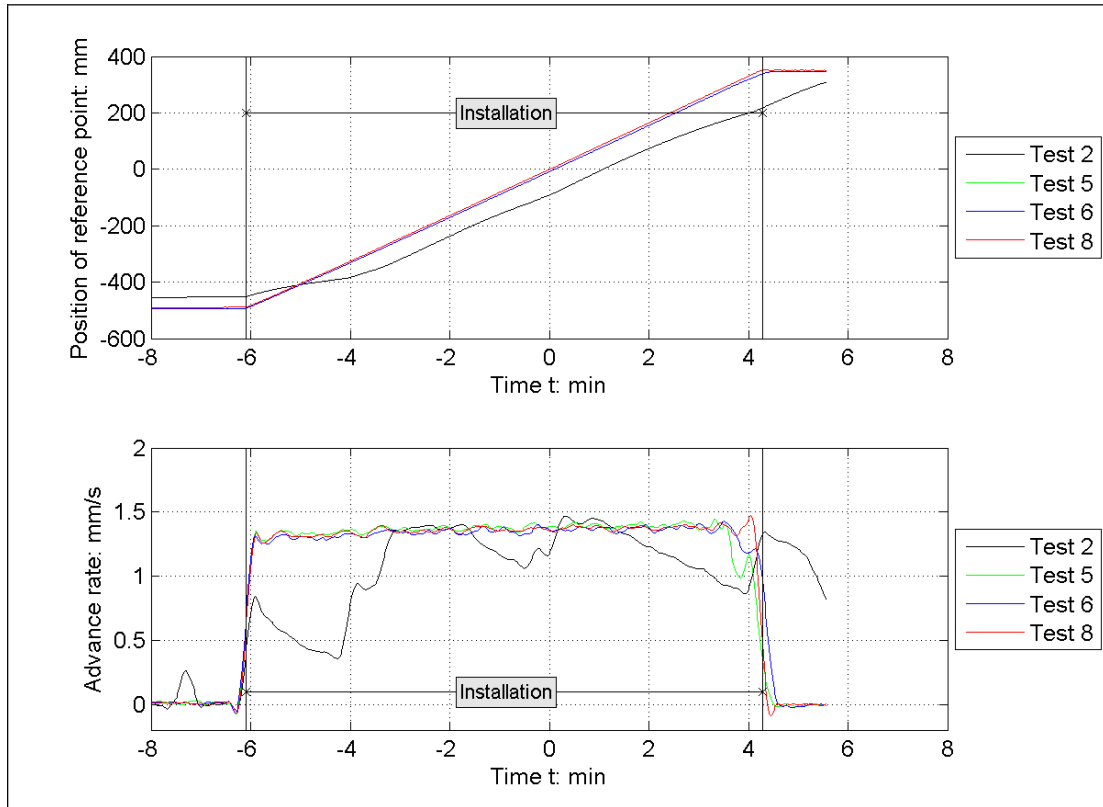


Figure 4.6. (a) Trajectory and (b) advance rate of model pipe

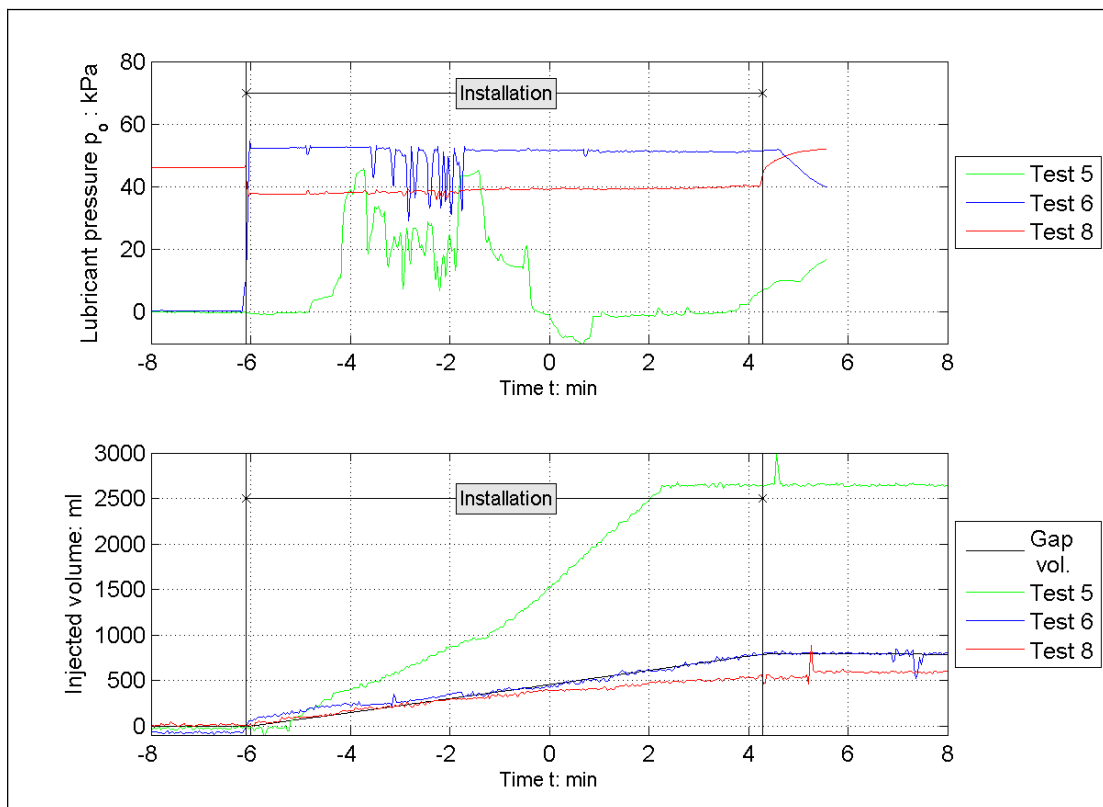


Figure 4.7. (a) Lubricant pressure; (b) lubricant volume

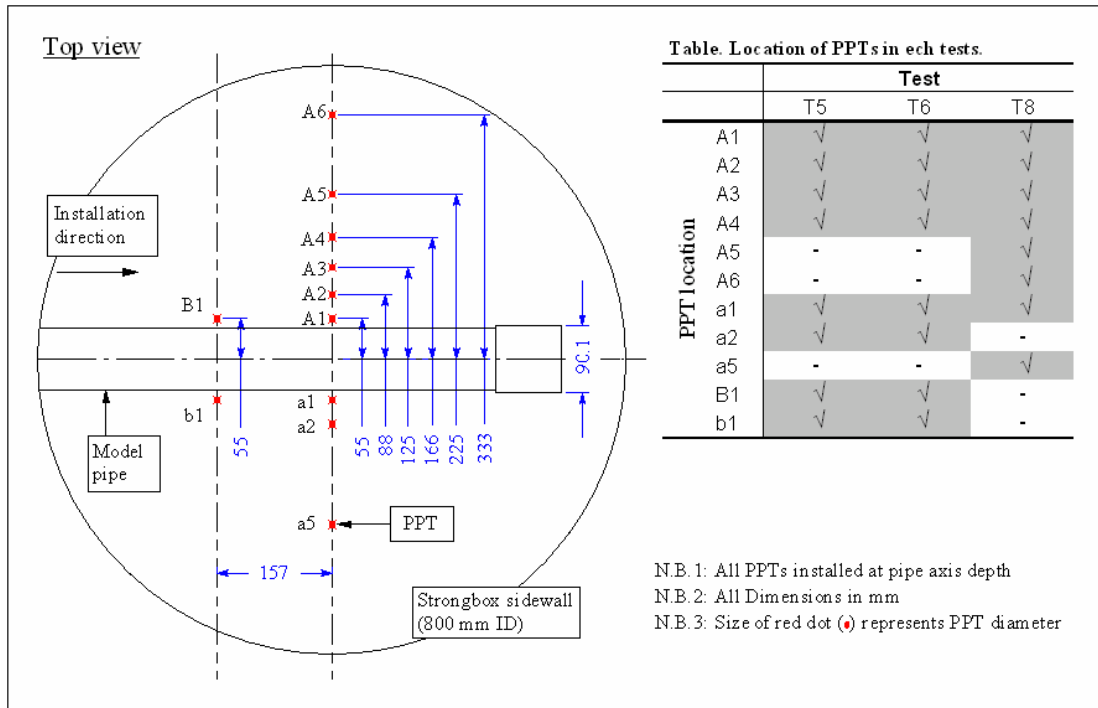


Figure 4.8. Position and designation of PPTs

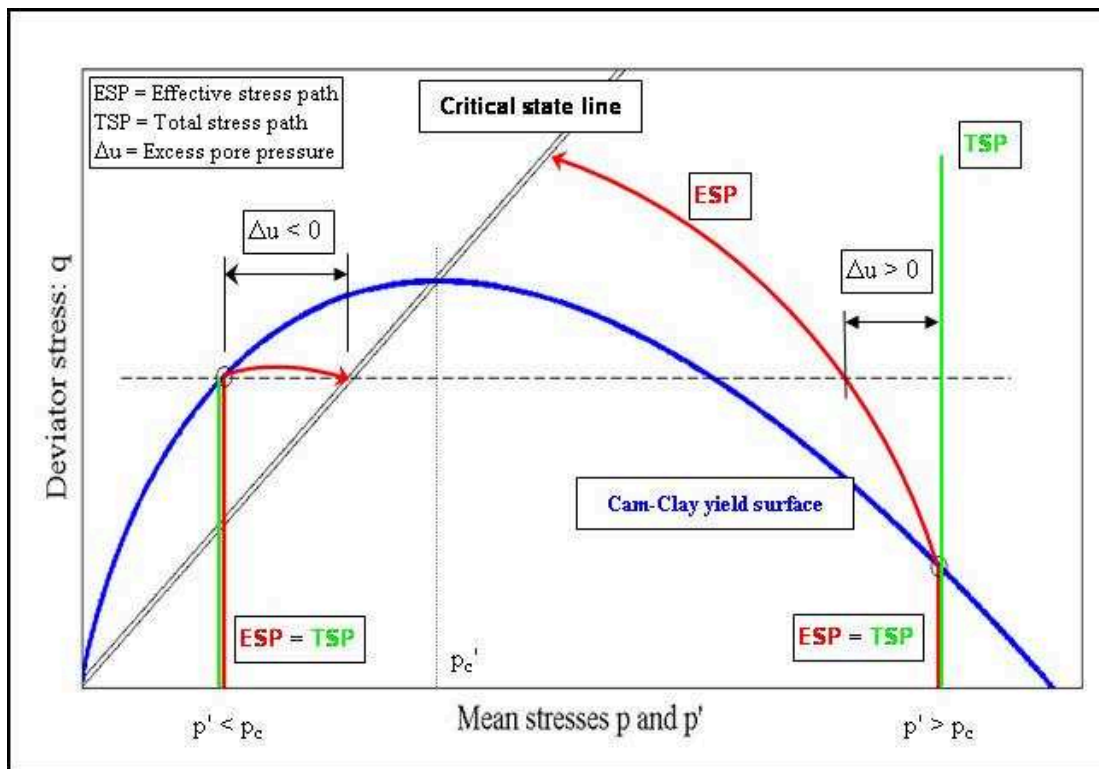


Figure 4.9. Excess pore water pressure due to changes in deviator stress

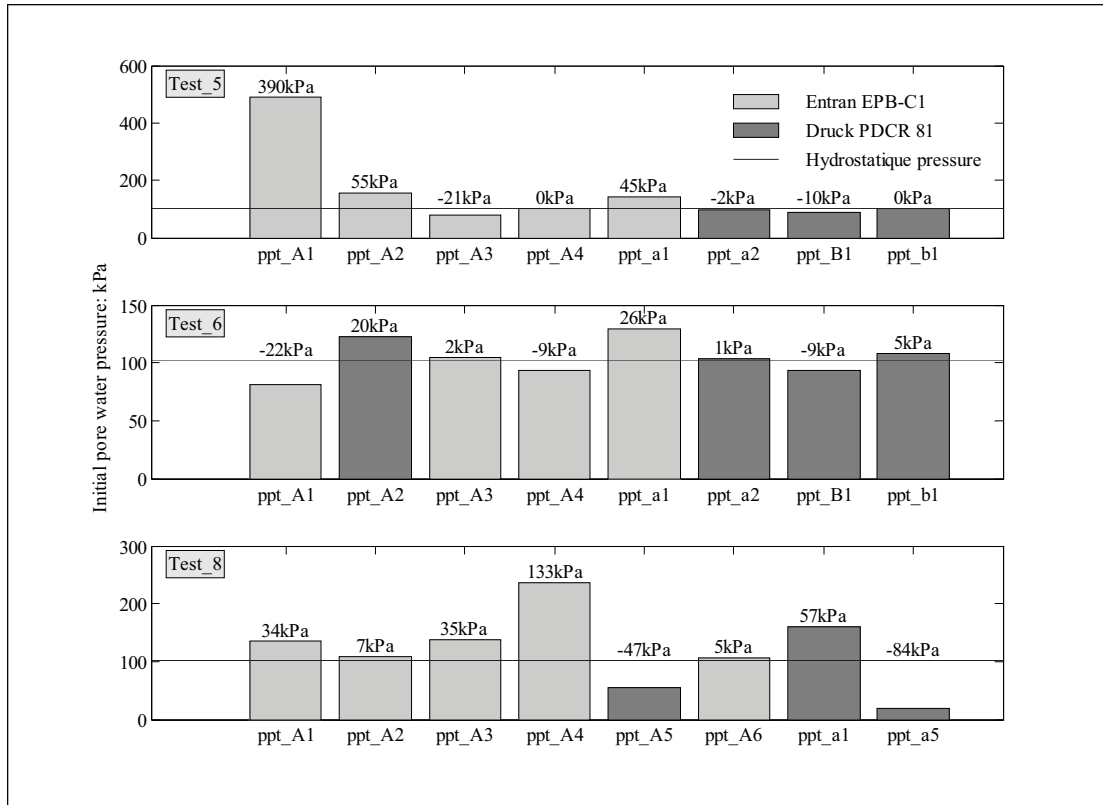


Figure 4.10. Measured pore water pressure at equilibrium

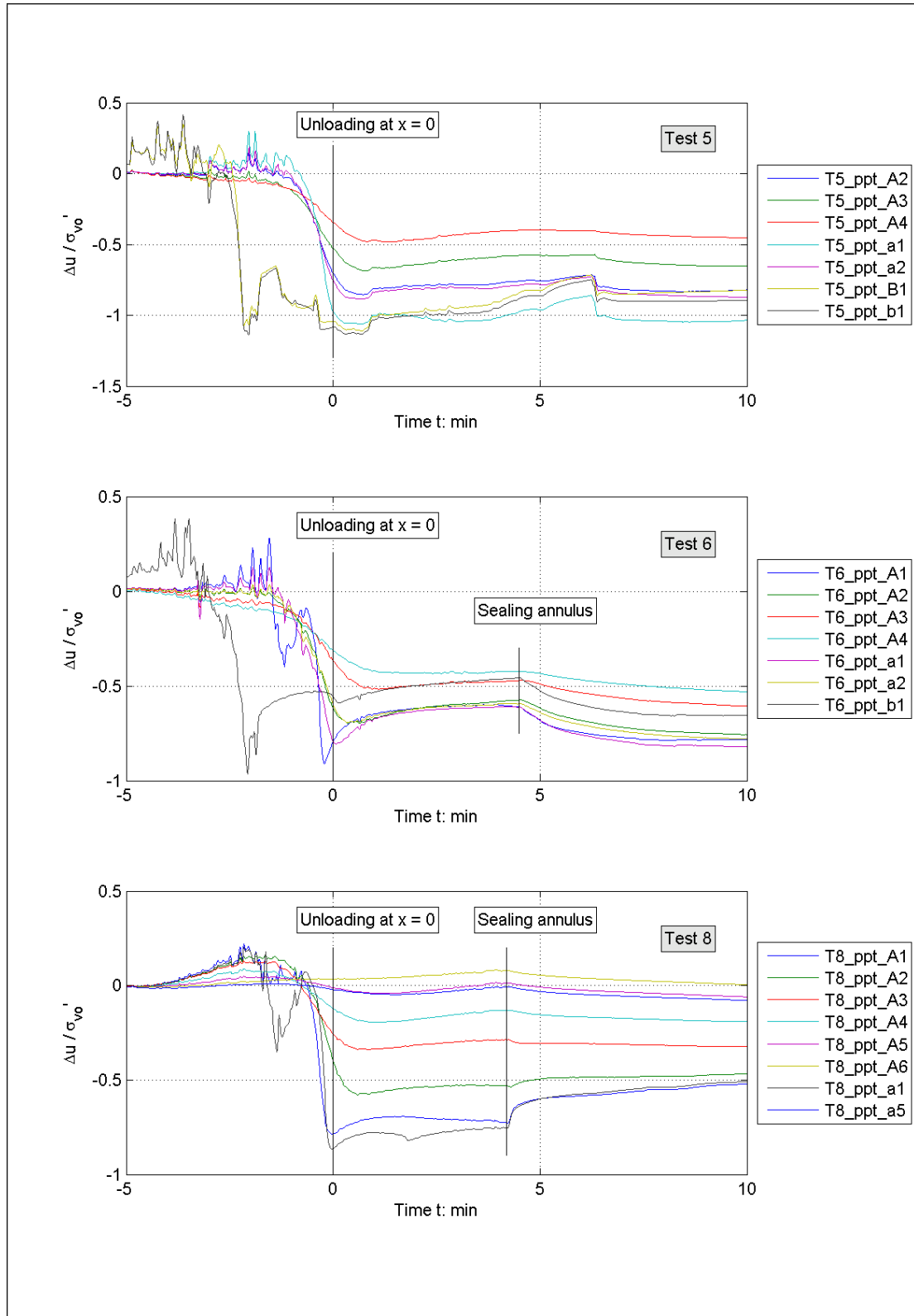


Figure 4.11. Overview of excess pore water pressure measurements during excavation

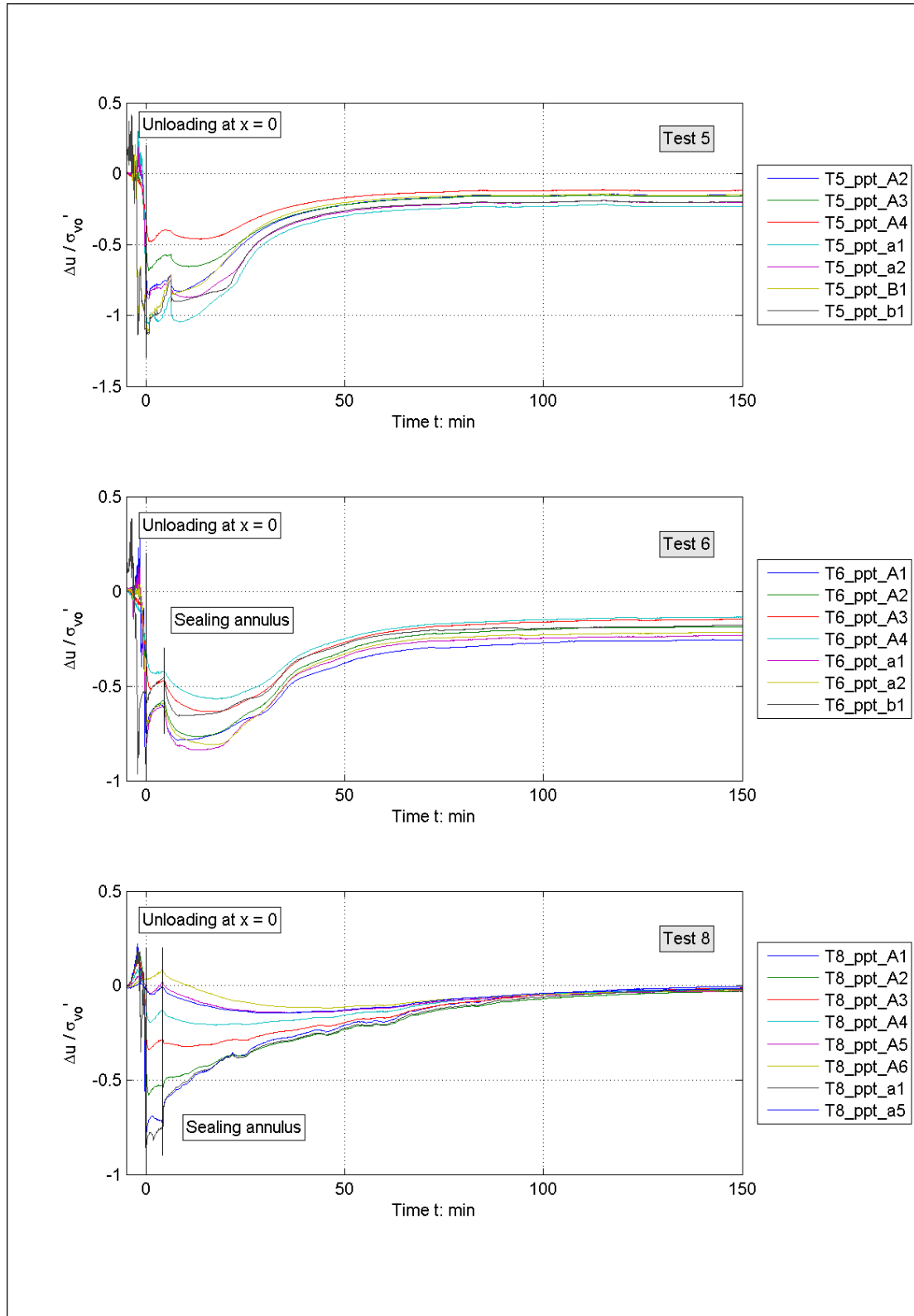


Figure 4.12. Overview of excess pore water pressure measurements during equilibration period

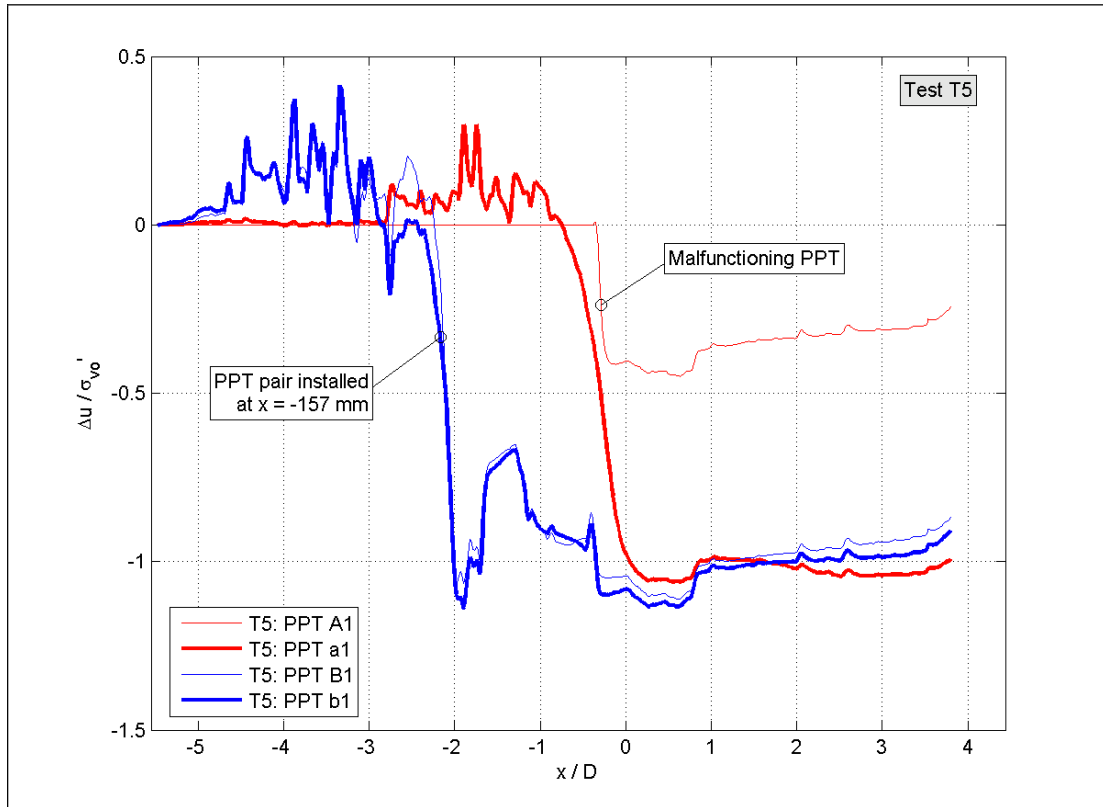


Figure 4.13. Symmetry of pore water pressure T5 PPT\_A

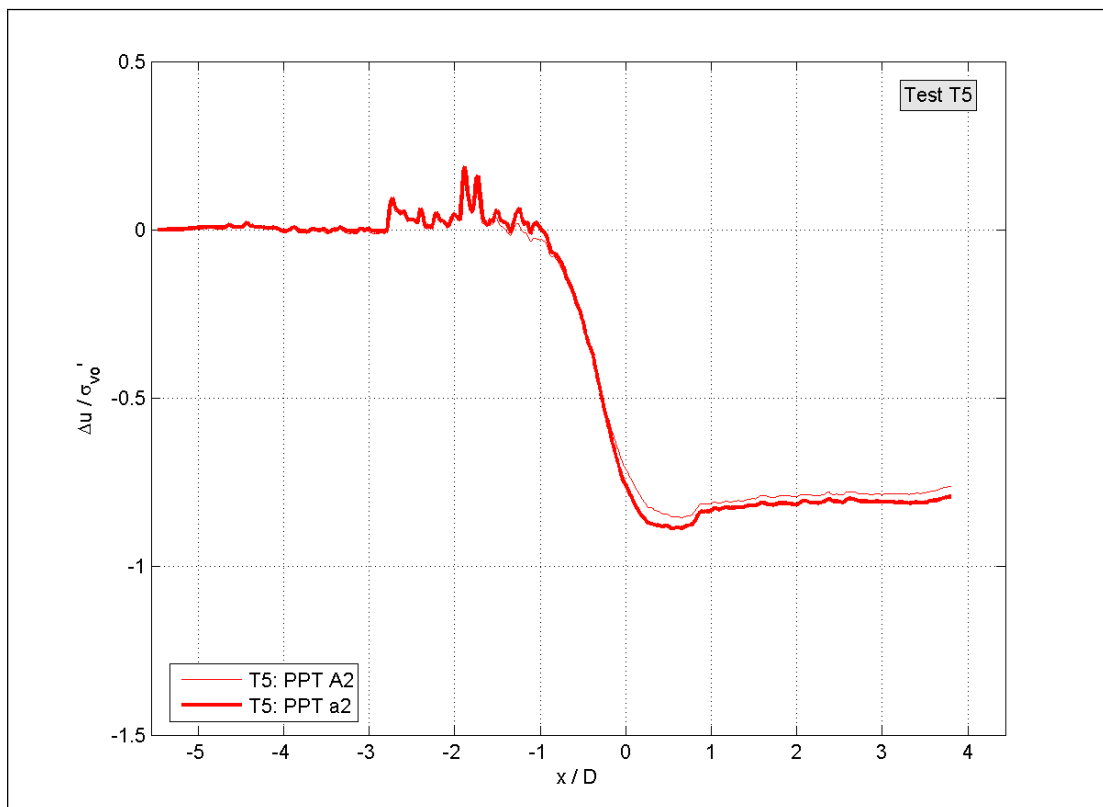


Figure 4.14. Symmetry of pore water pressure T5 PPT\_B

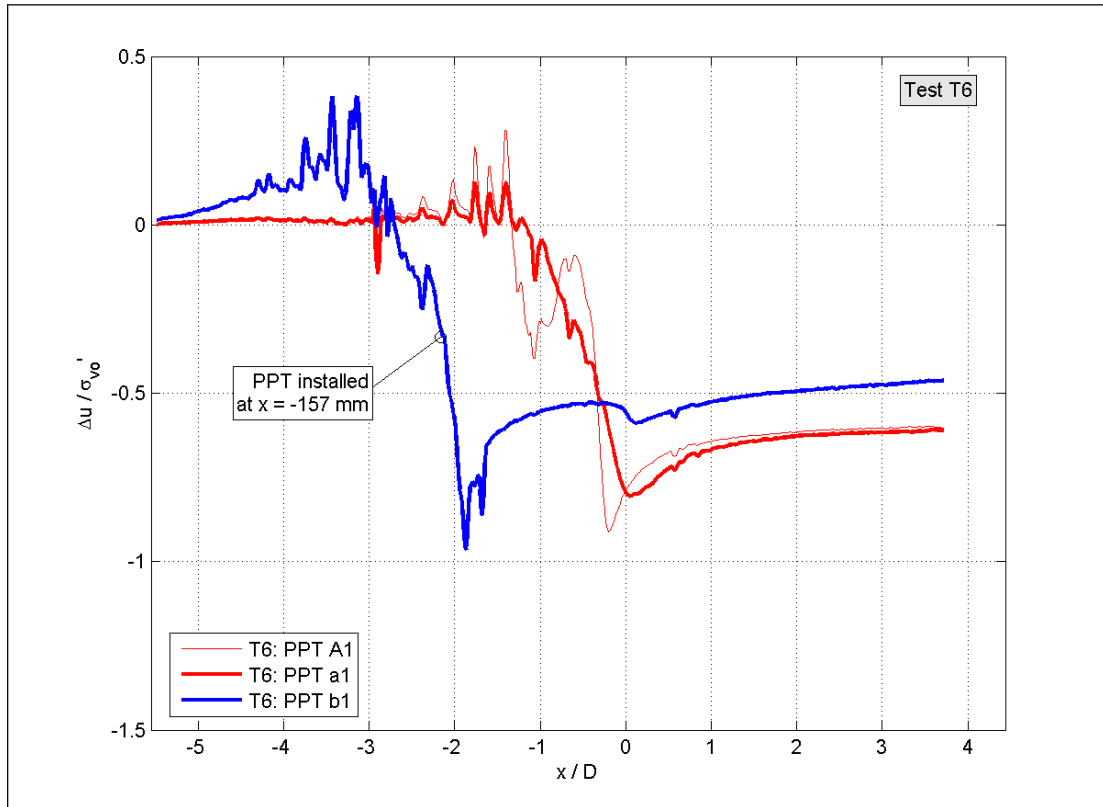


Figure 4.15. Symmetry of pore water pressure T6 PPT\_A

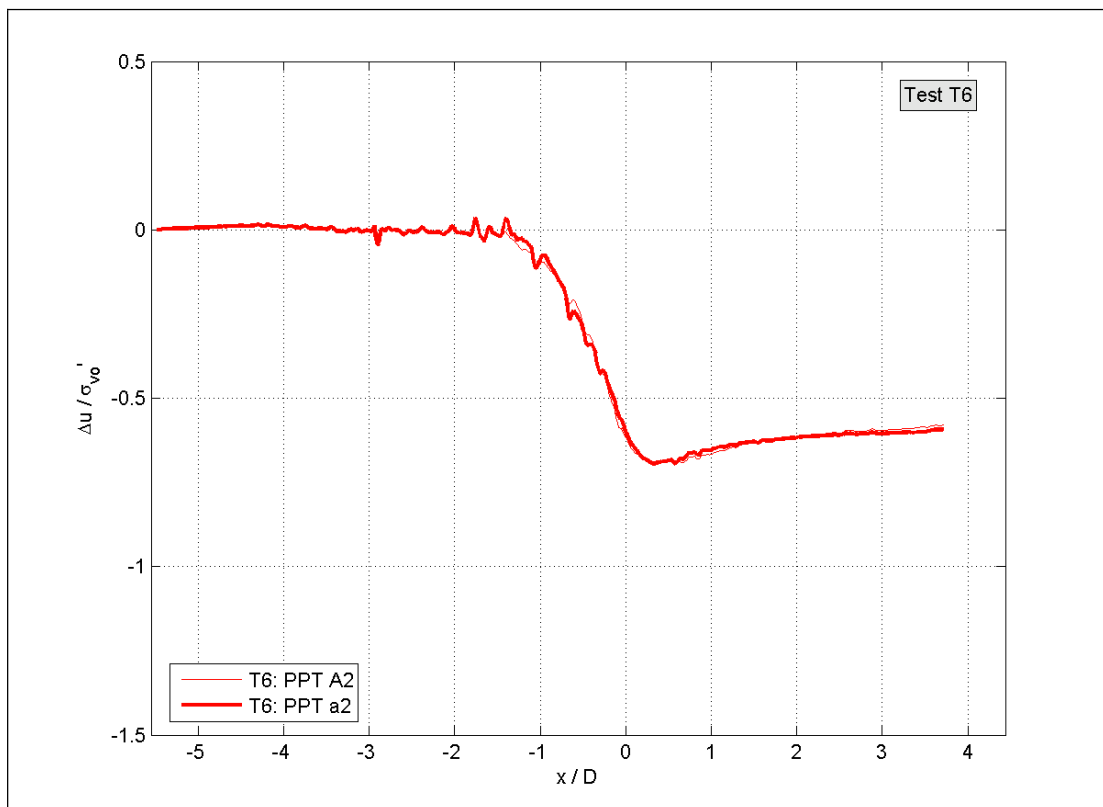


Figure 4.16. Symmetry of pore water pressure T6 PPT\_B

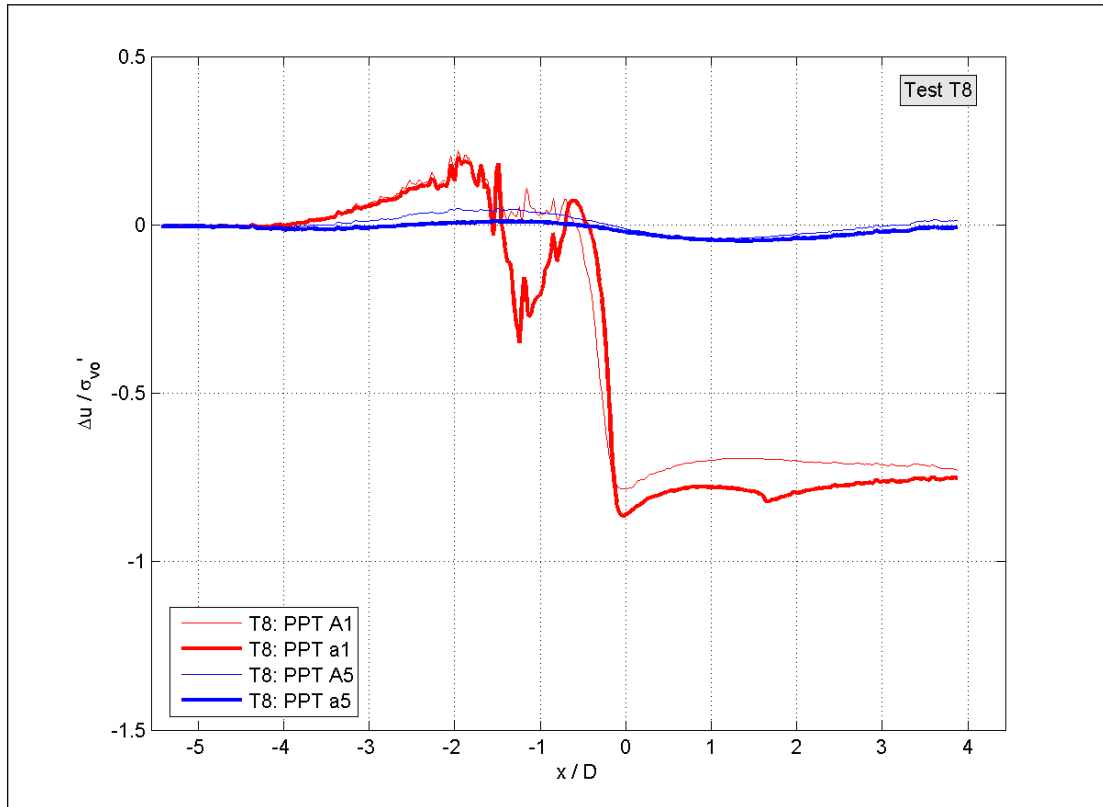


Figure 4.17. Symmetry of pore water pressure T8 PPT\_A

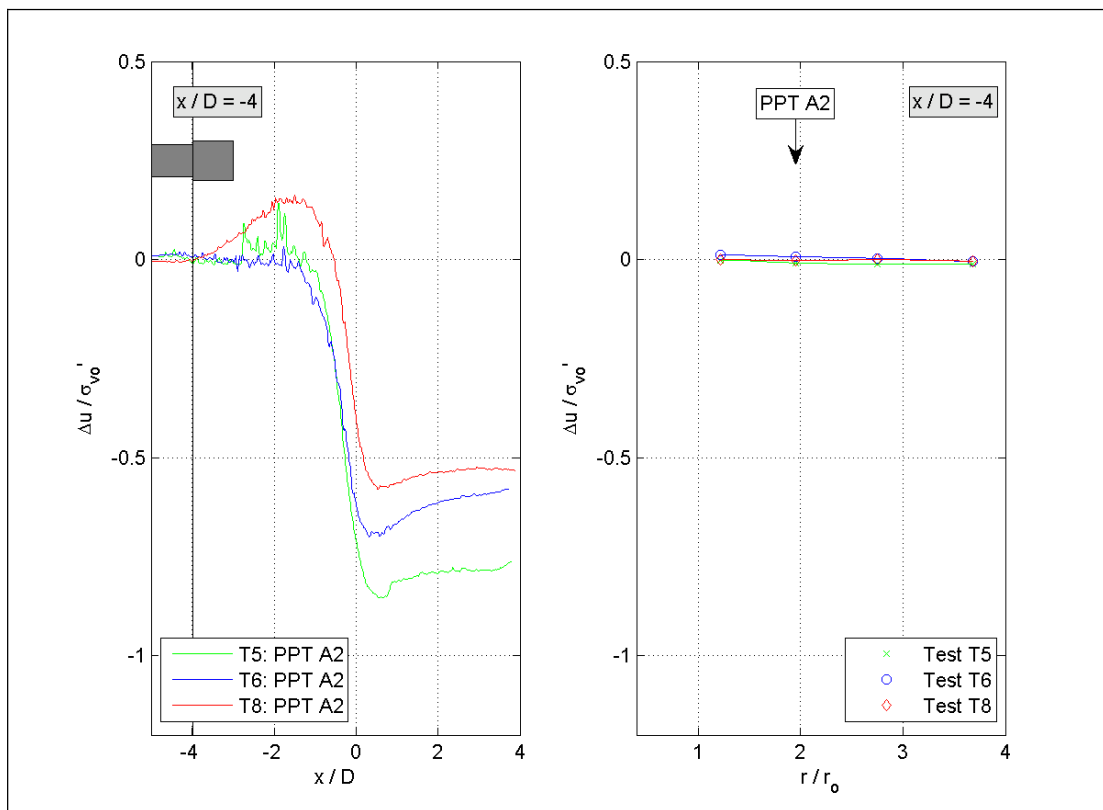


Figure 4.18. Generated pore water pressure and isochrones  $x/D = -4$

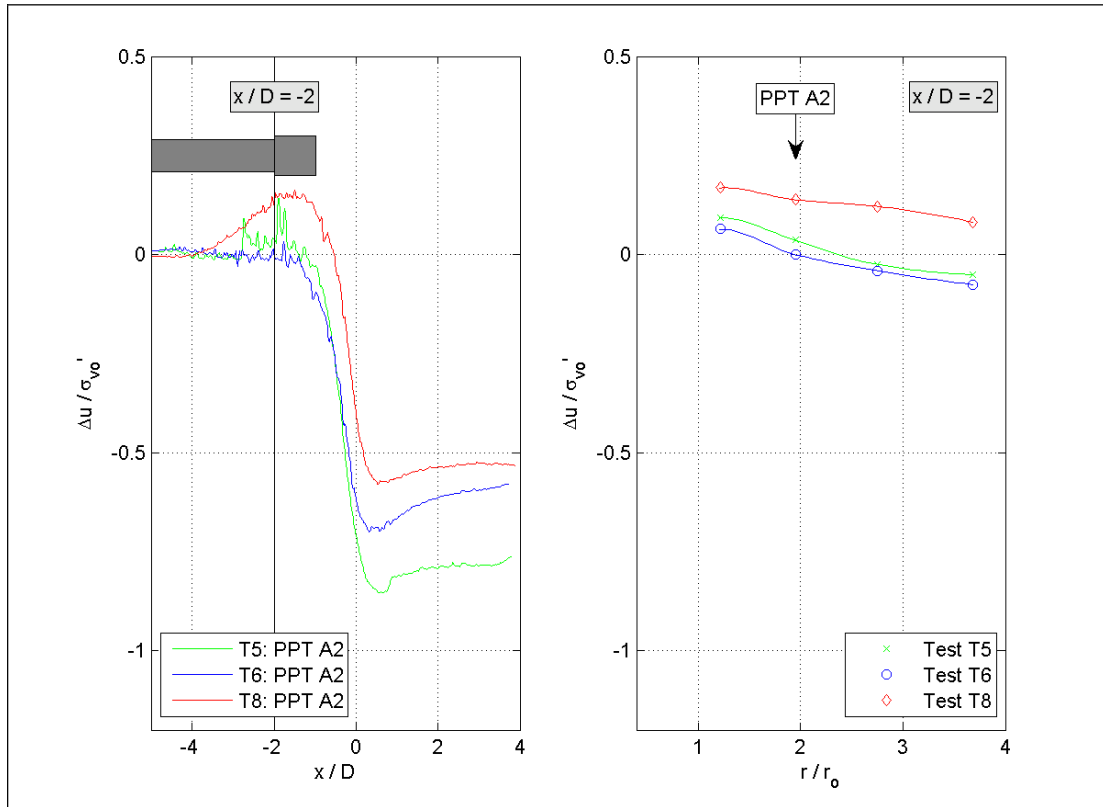


Figure 4.19. Generated pore water pressure and isochrones  $x/D = -2$

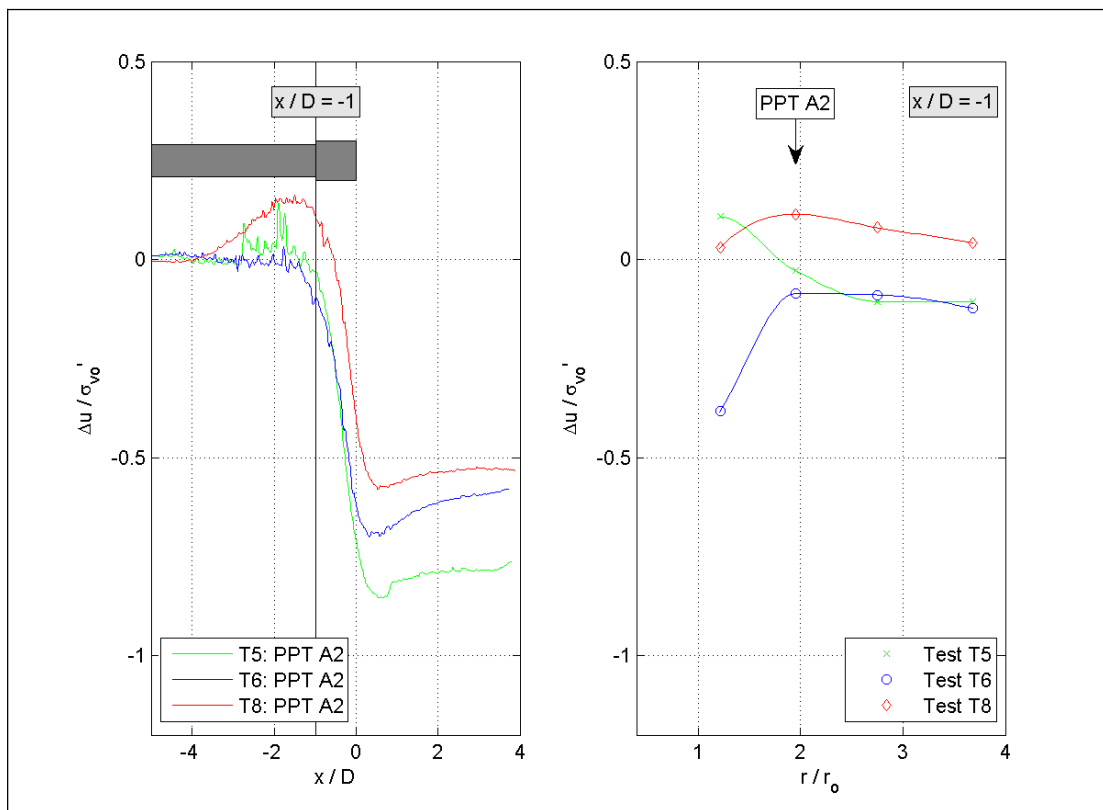


Figure 4.20. Generated pore water pressure and isochrones  $x/D = -1$

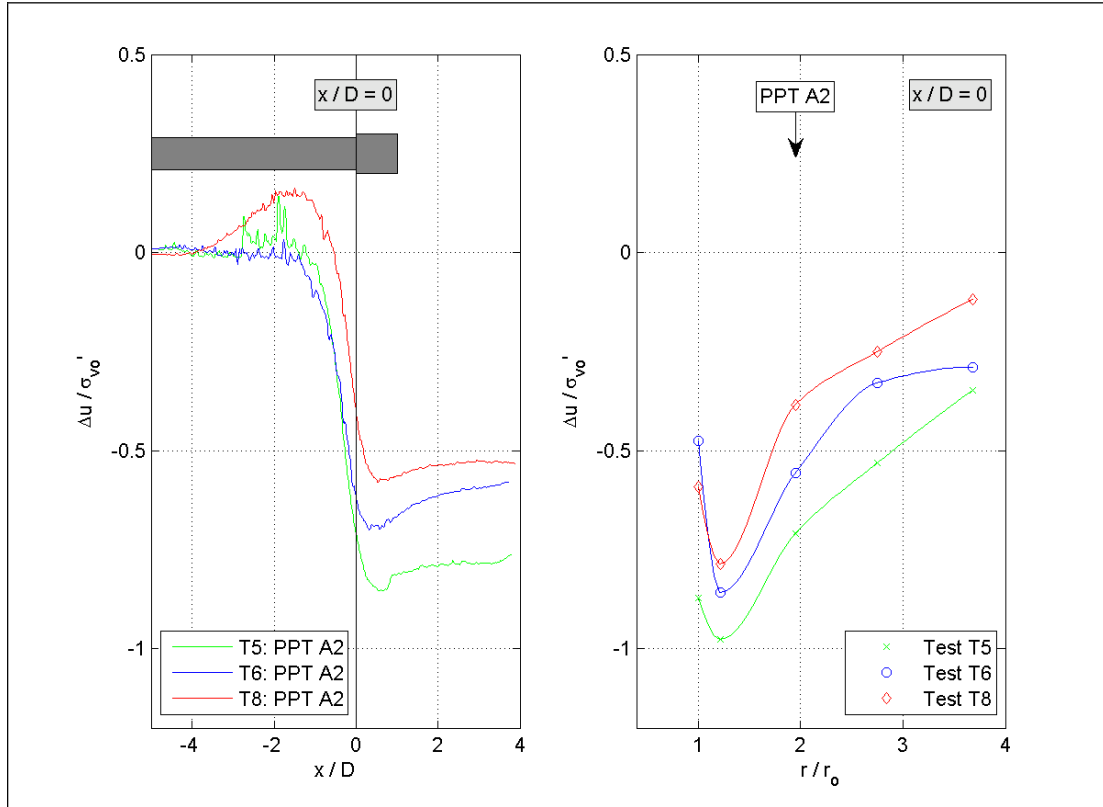


Figure 4.21. Generated pore water pressure and isochrones  $x/D = 0$

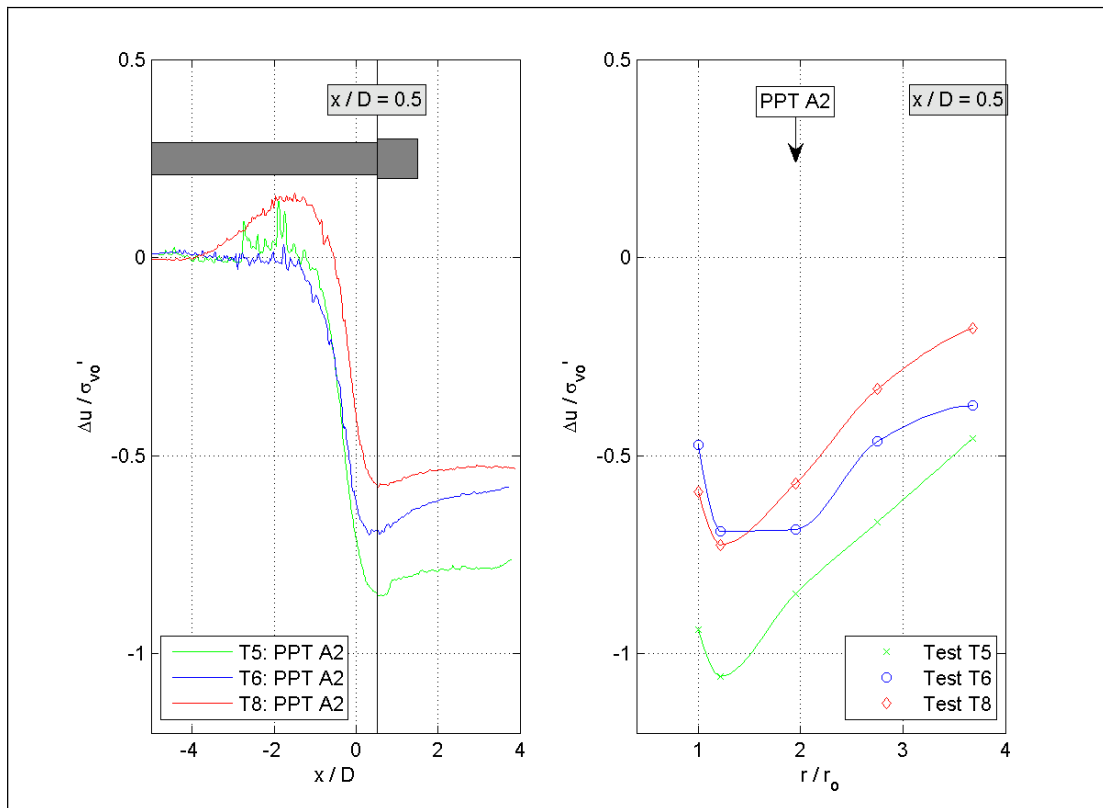


Figure 4.22. Generated pore water pressure and isochrones  $x/D = 0.5$

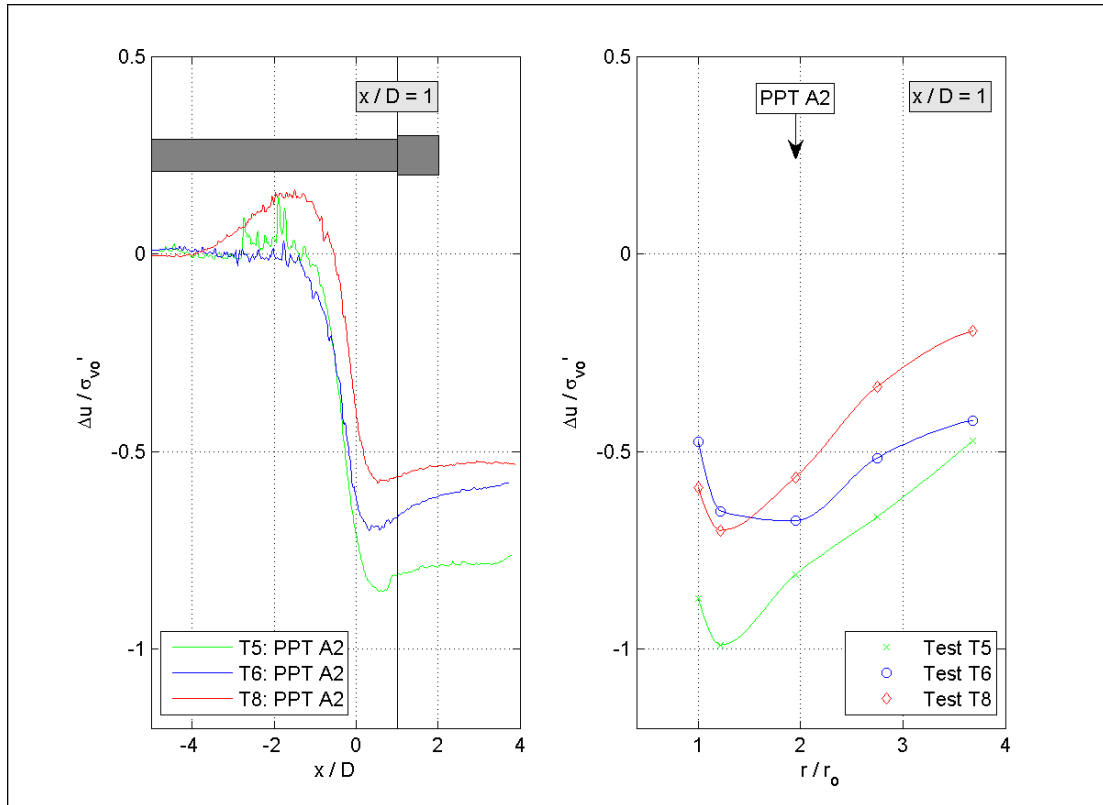


Figure 4.23. Generated pore water pressure and isochrones  $x/D = 1$

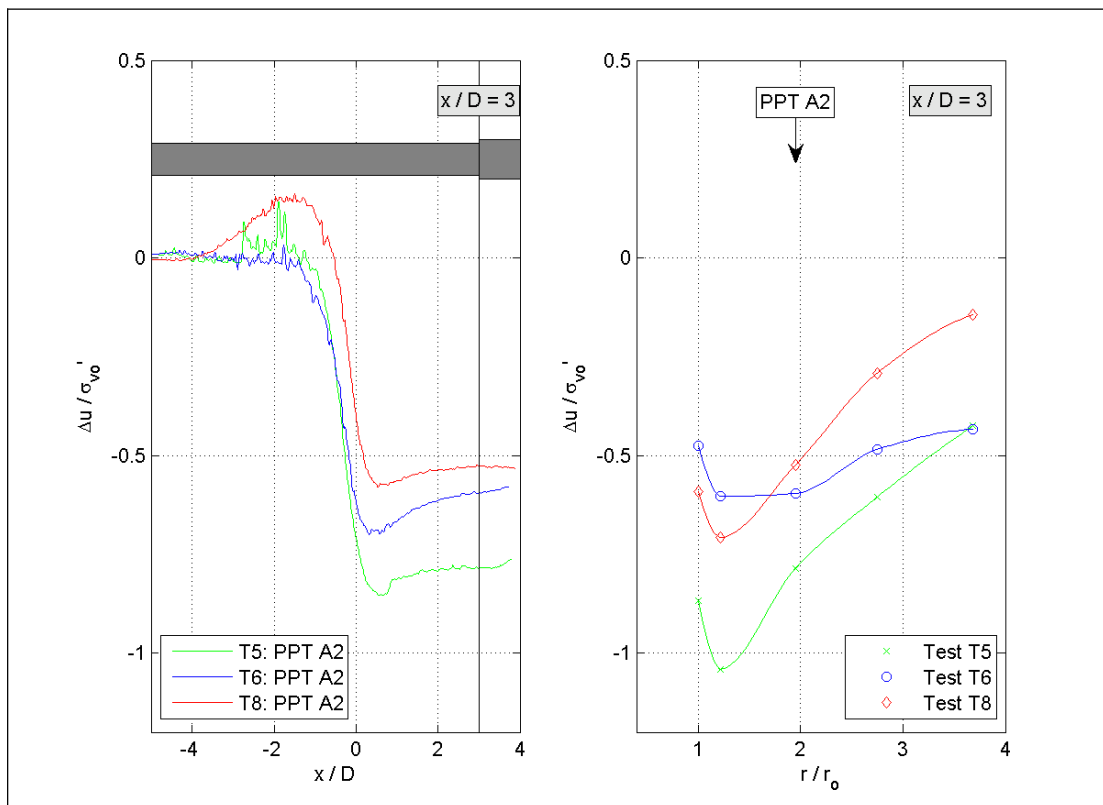


Figure 4.24. Generated pore water pressure and isochrones  $x/D = 2$

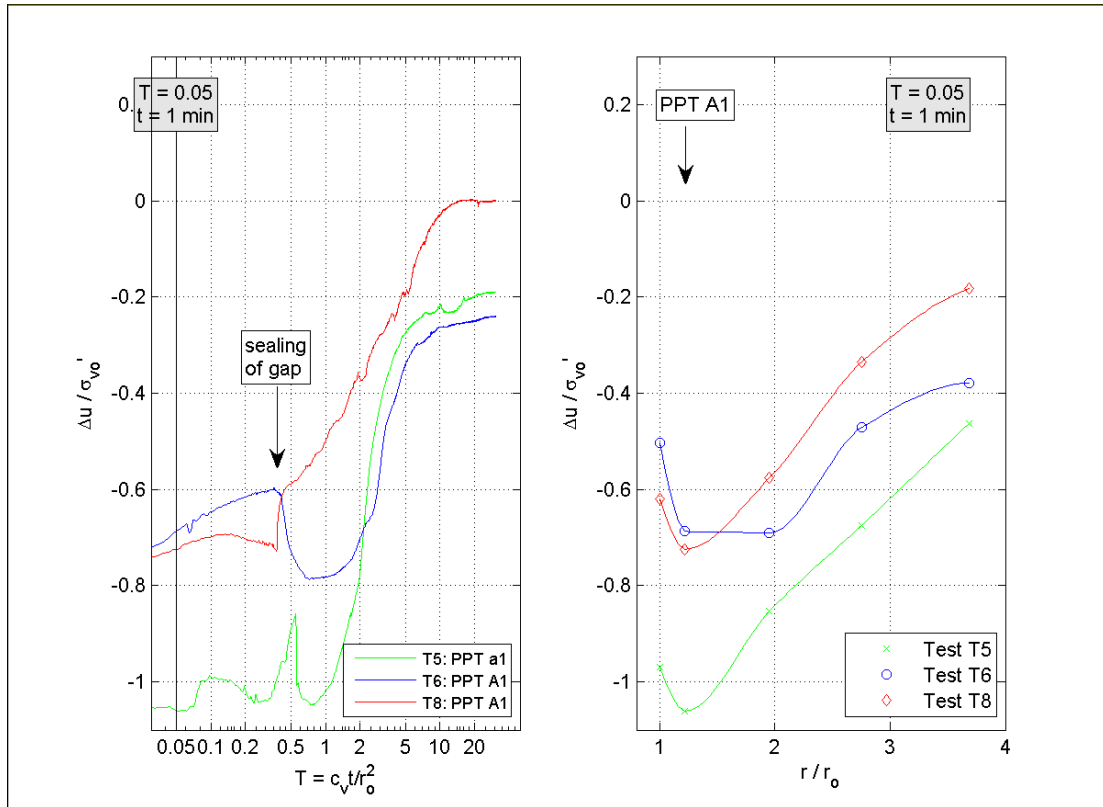


Figure 4.25. Dissipation of excess pore pressure  $T = 0.05$

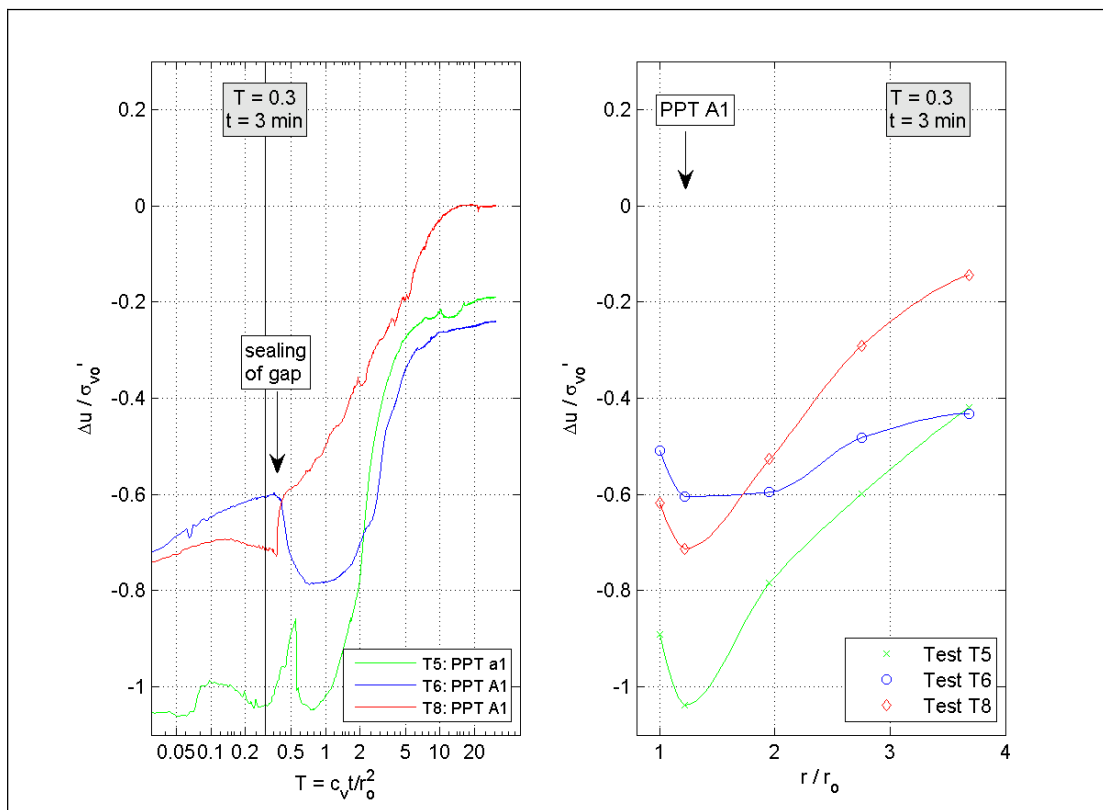


Figure 4.26. Dissipation of excess pore pressure  $T = 0.3$

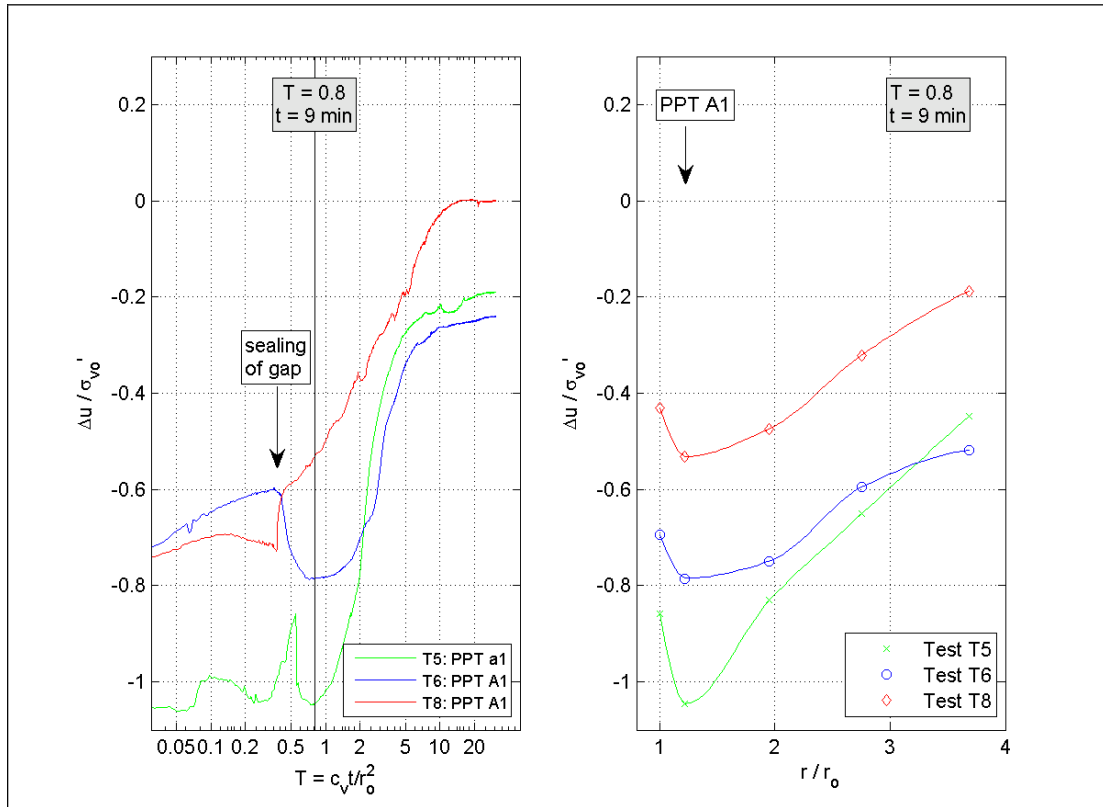


Figure 4.27. Dissipation of excess pore pressure  $T = 0.8$

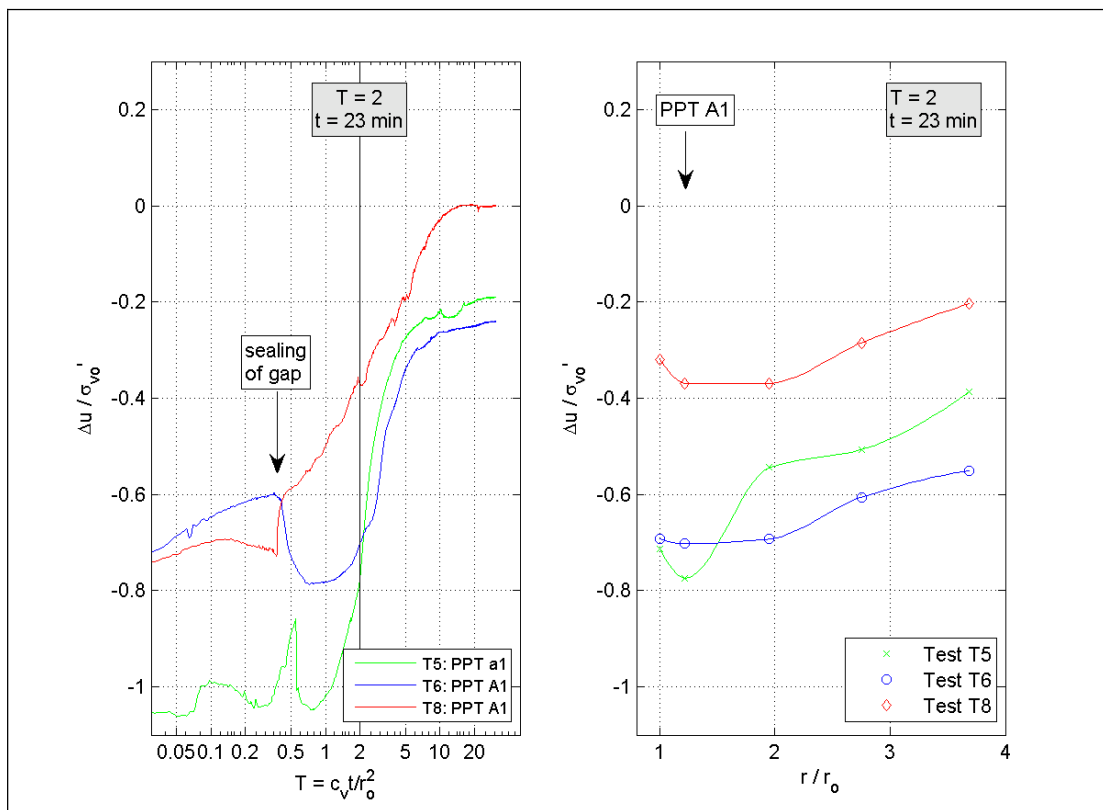


Figure 4.28. Dissipation of excess pore pressure  $T = 2$

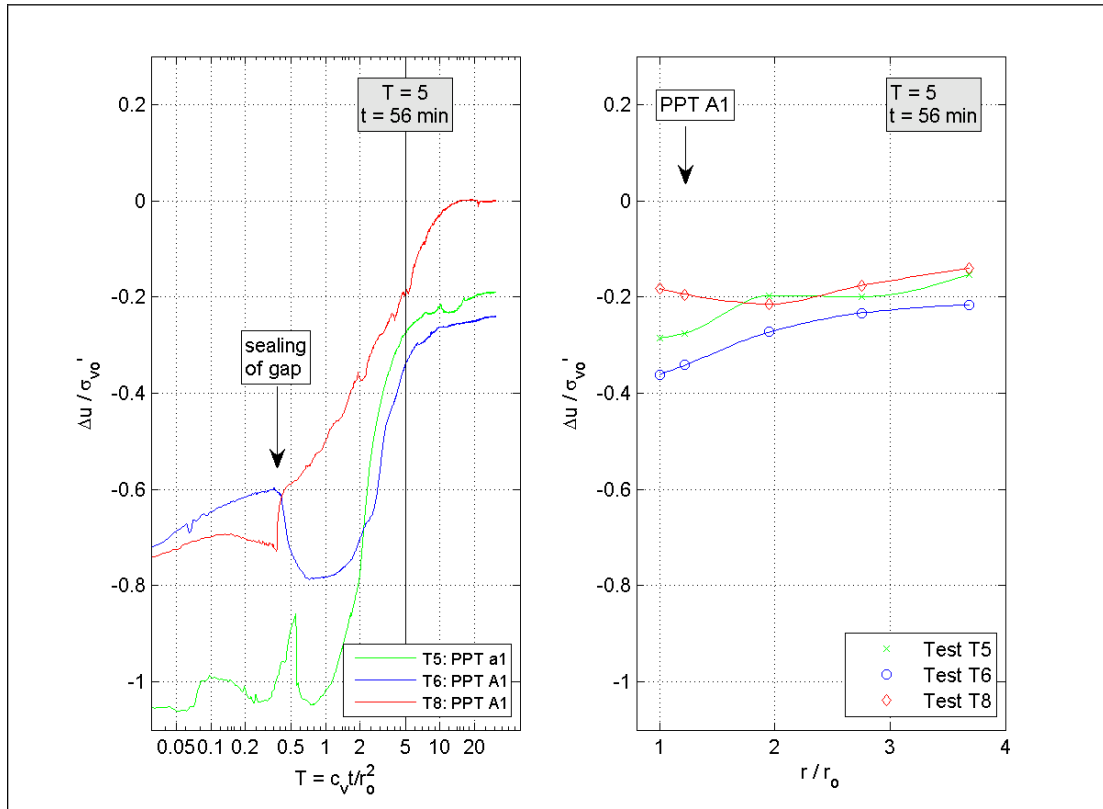


Figure 4.29. Dissipation of excess pore pressure  $T = 5$

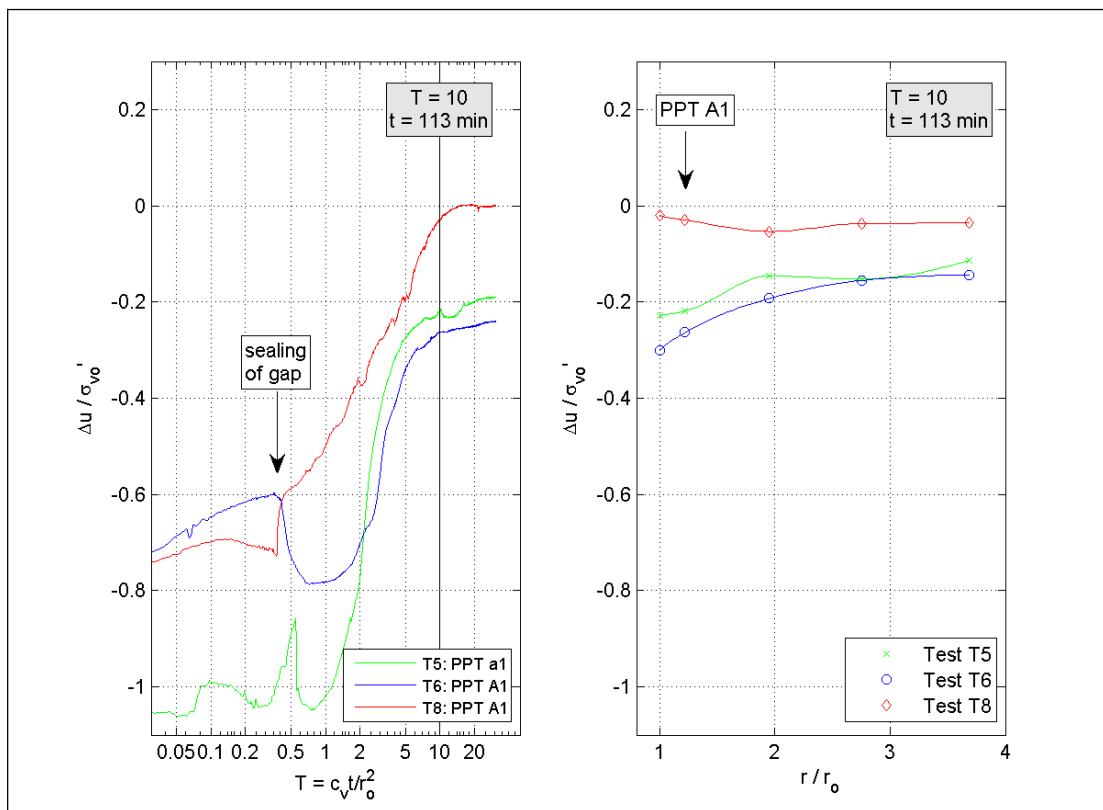


Figure 4.30. Dissipation of excess pore pressure  $T = 10$

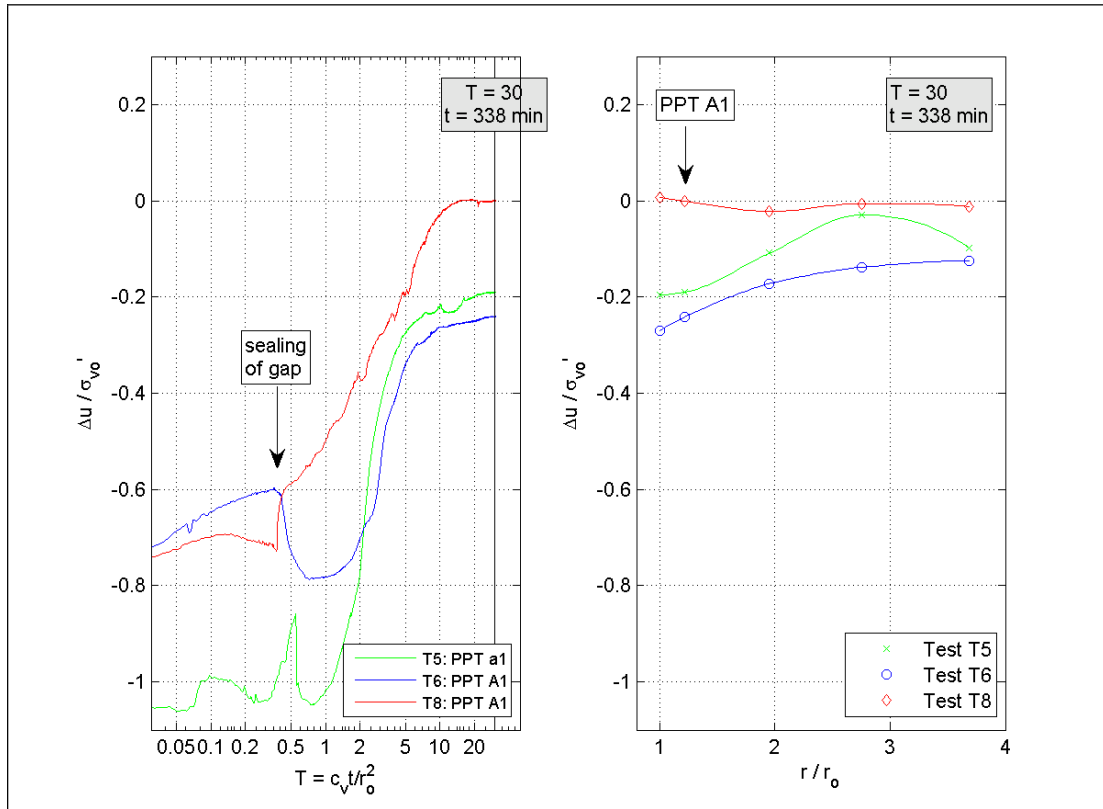


Figure 4.31. Dissipation of excess pore pressure  $T = 30$

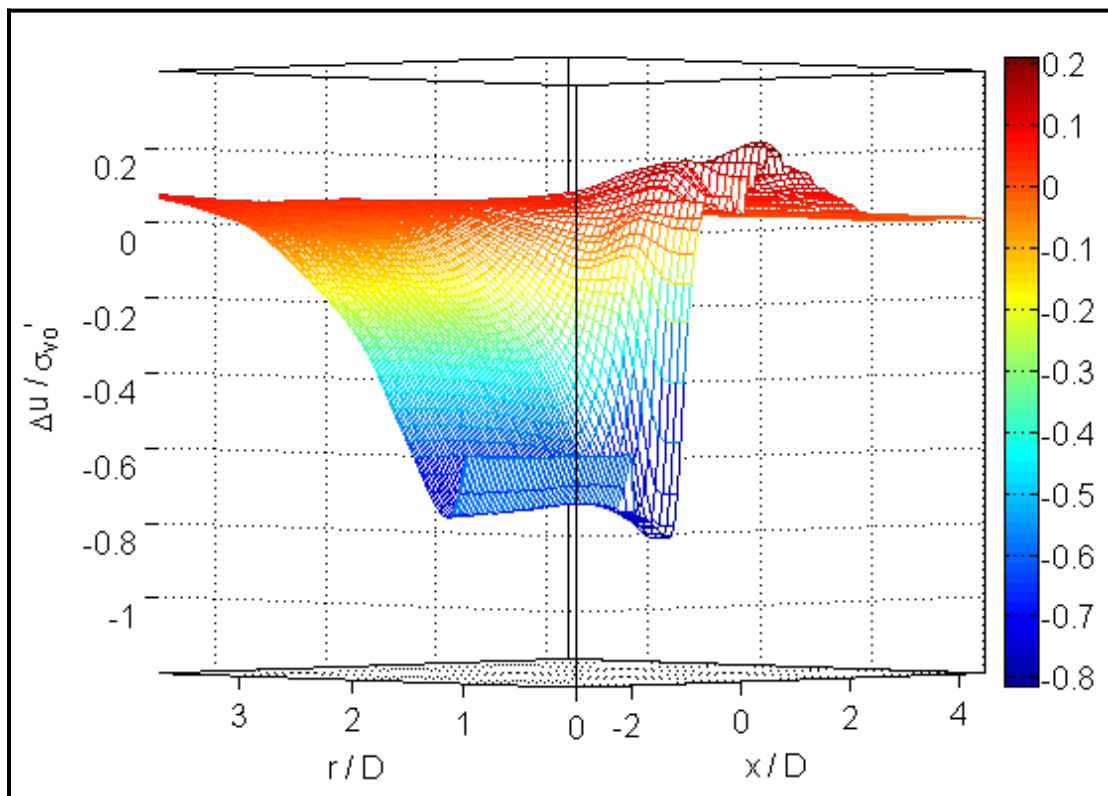


Figure 4.32. Two-dimensional pore water pressure isochrone ( $T = 0.03$ )

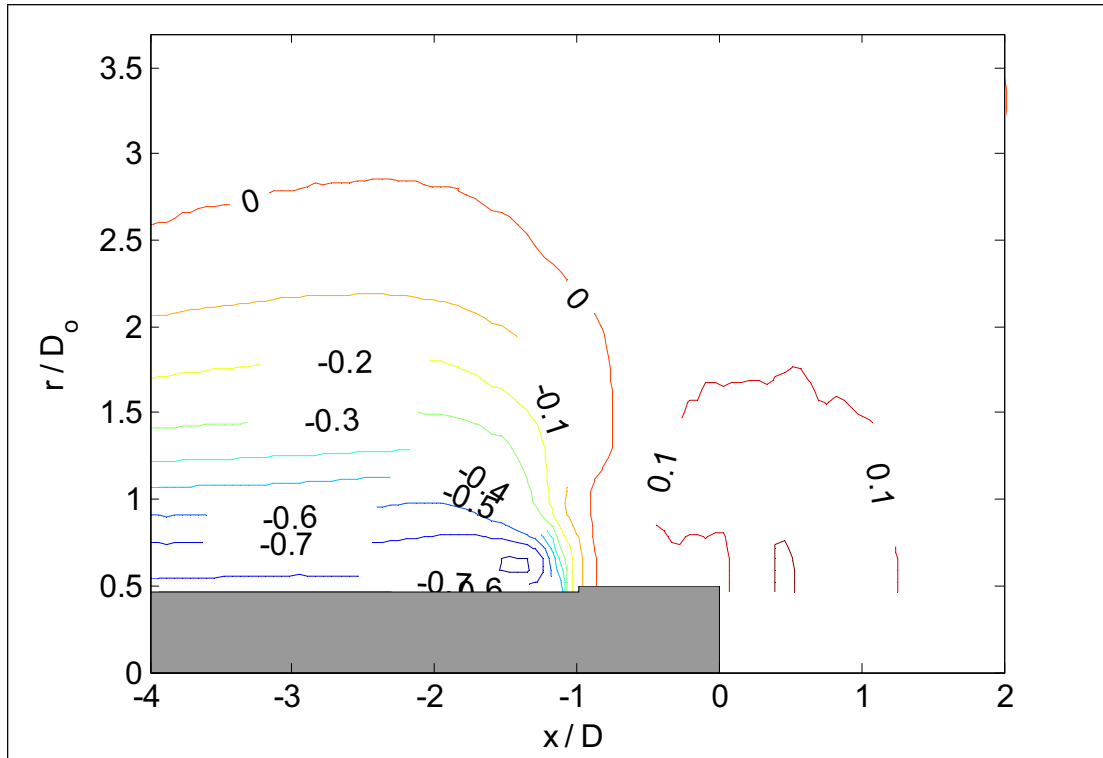


Figure 4.33. Pore water pressure contour around the advancing excavation face in T8

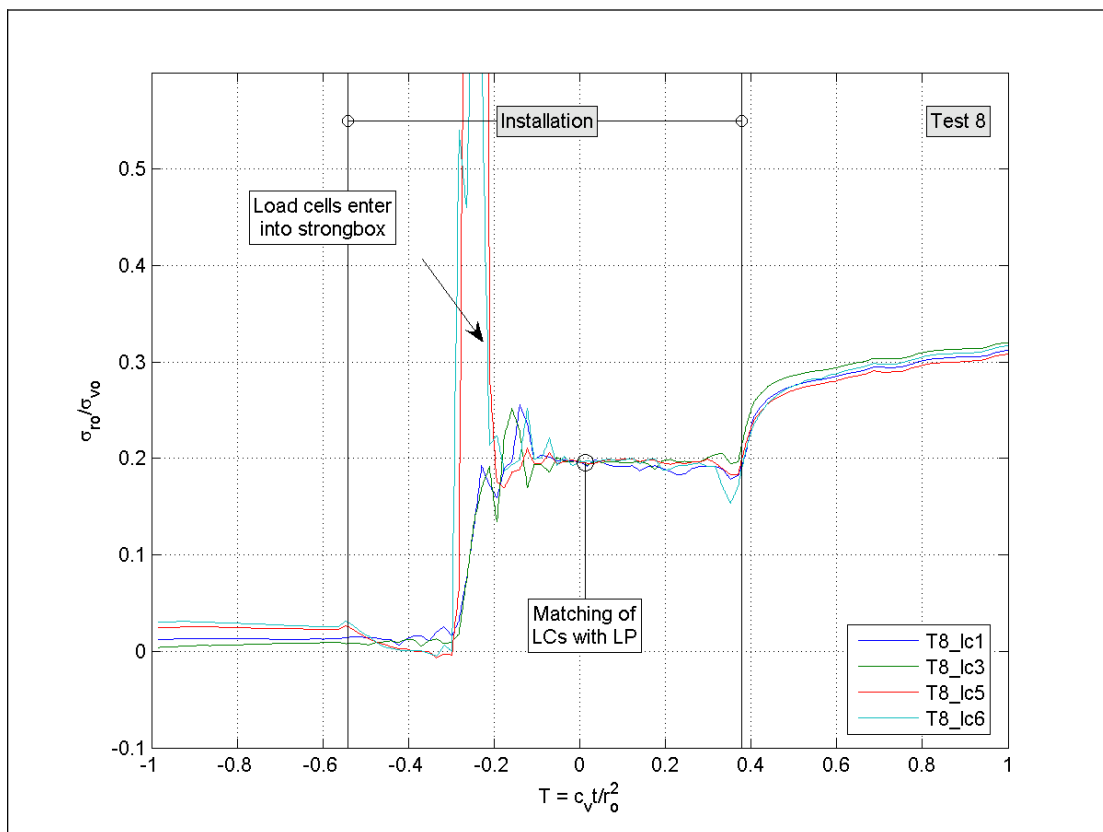


Figure 4.34. Total stress on pipe during installation test T8

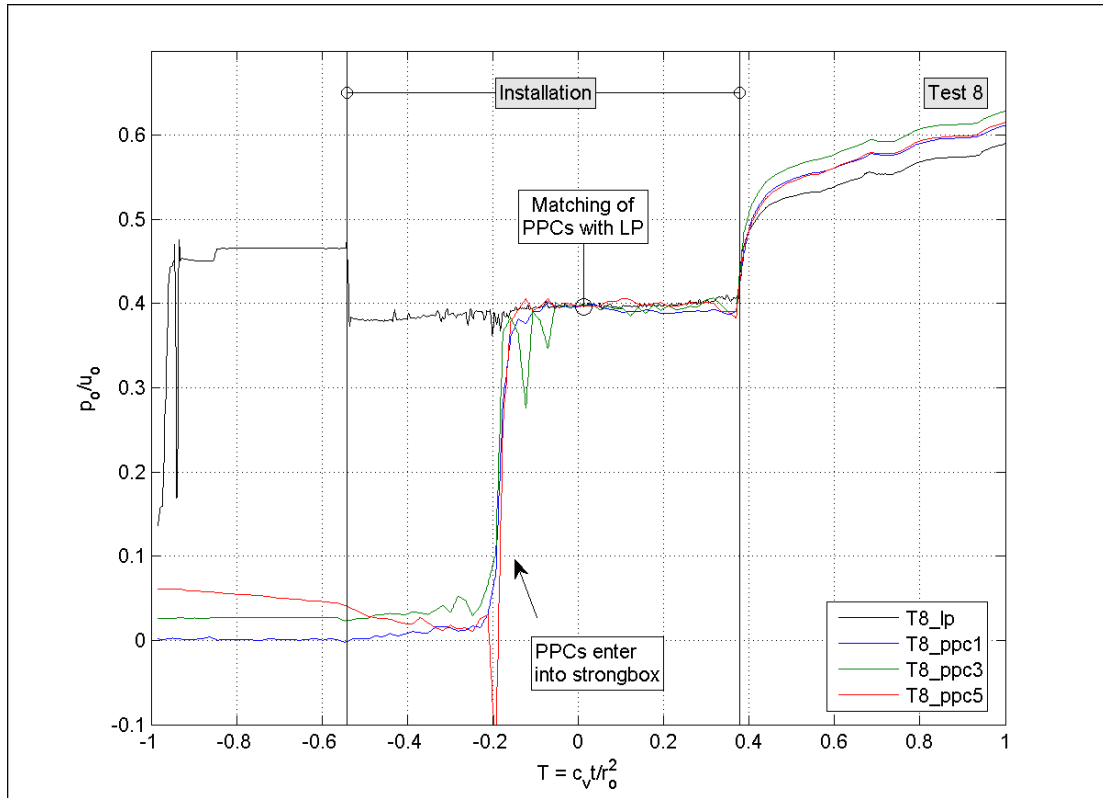


Figure 4.35. Fluid pressure on pipe during installation test T8

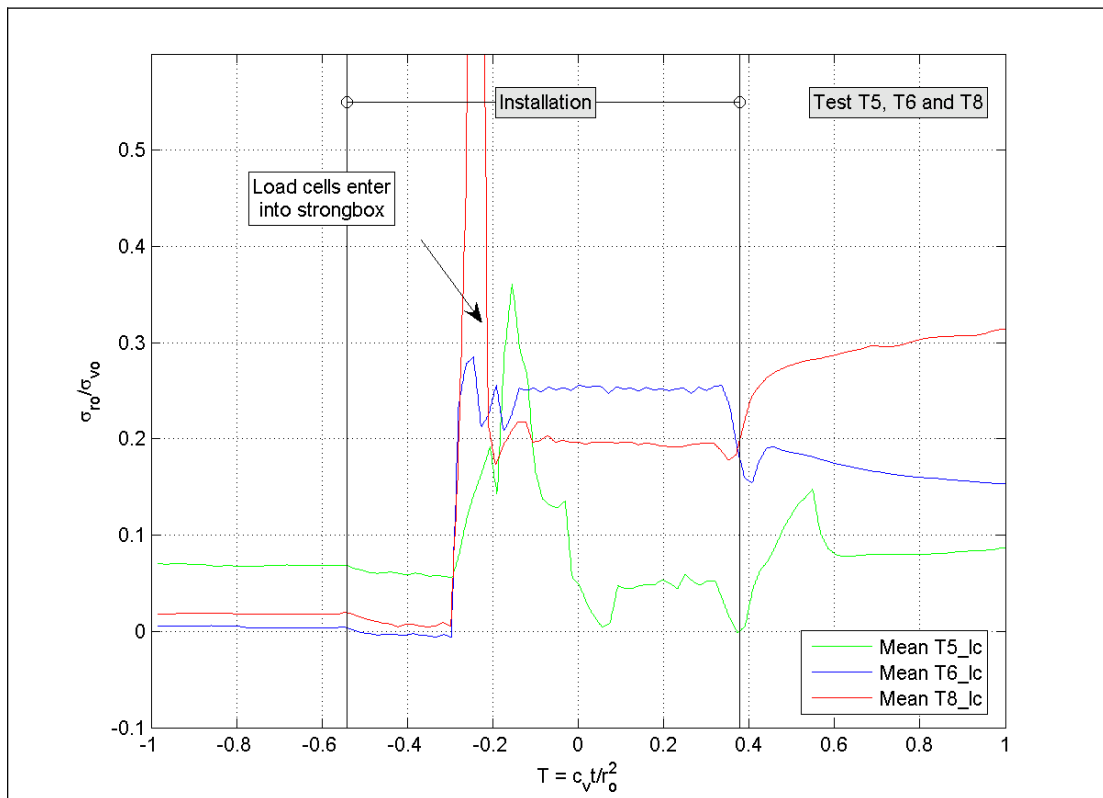


Figure 4.36. Comparison of total stresses during pipe installation (T5, T6 and T8)

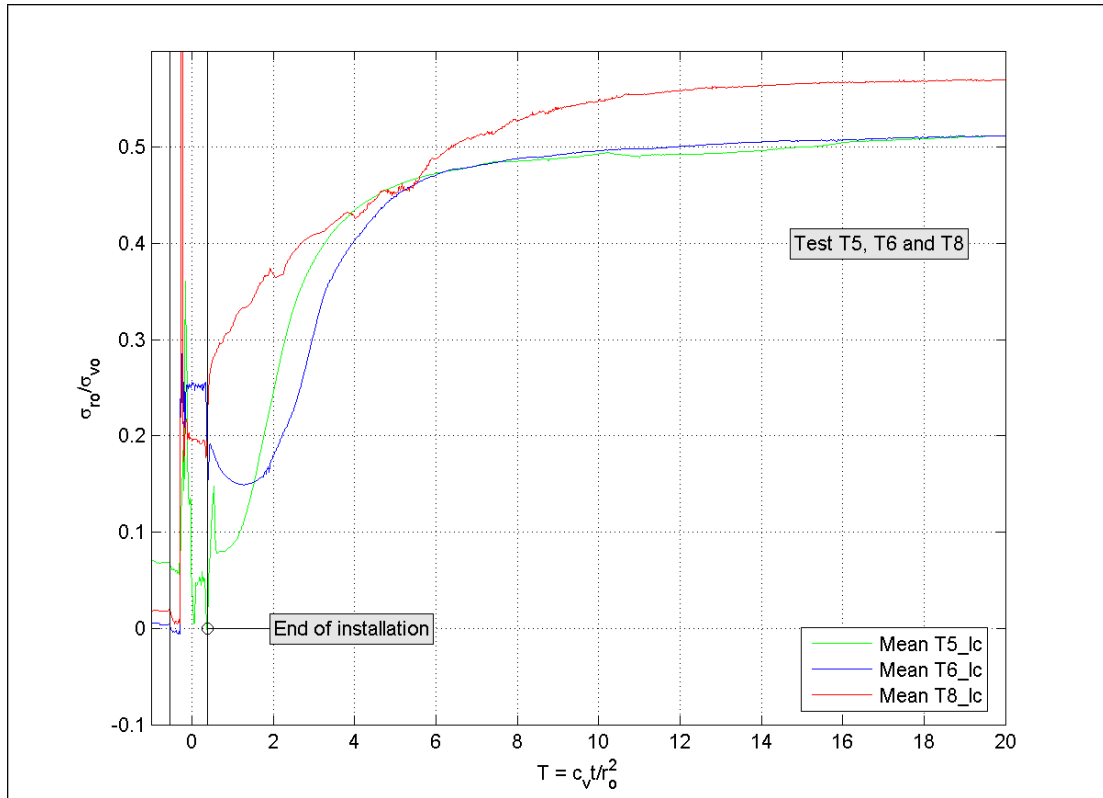


Figure 4.37. Comparison of total stresses during consolidation (T5, T6 and T8)

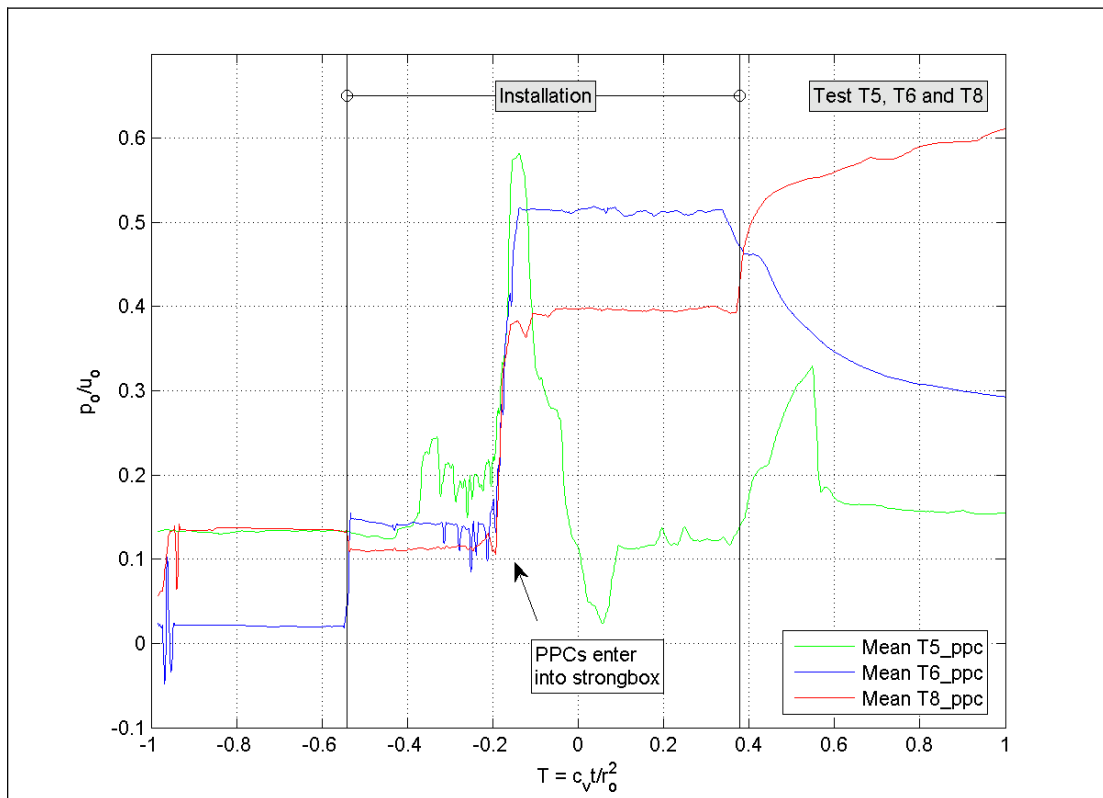


Figure 4.38. Comparison of fluid pressure during pipe installation (T5, T6 and T8)

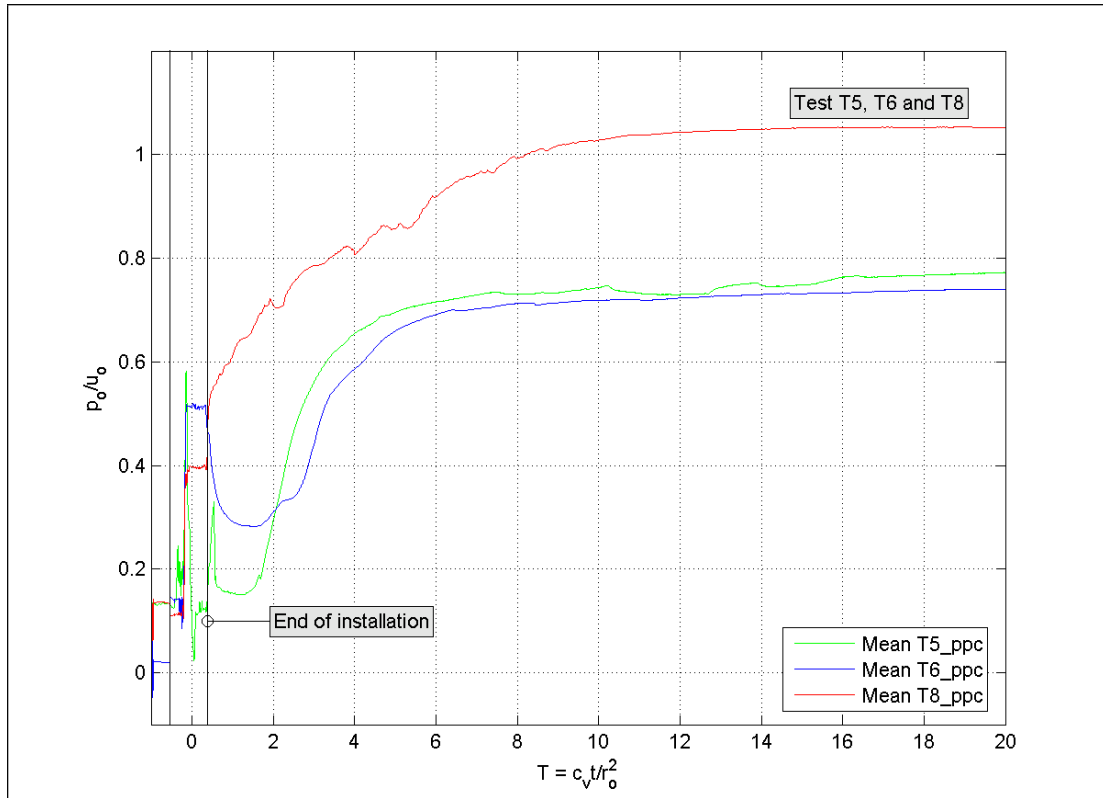


Figure 4.39. Comparison of fluid pressure during consolidation (T5, T6 and T8)

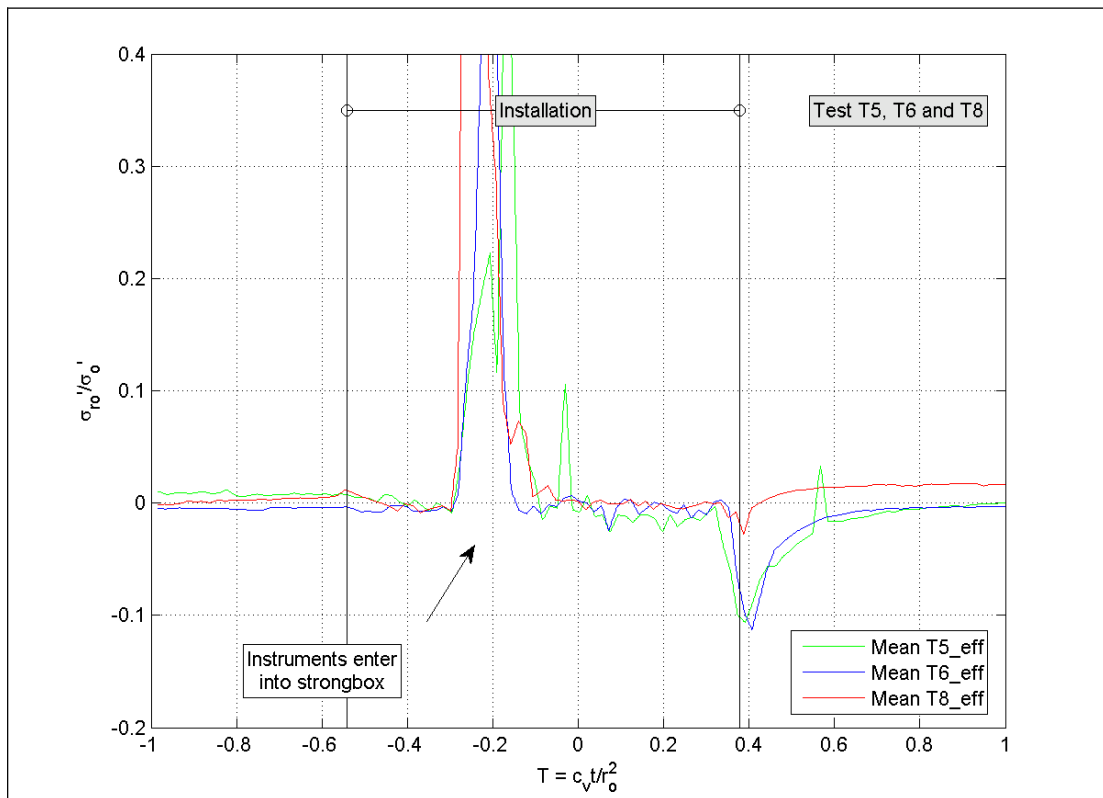


Figure 4.40. Comparison of effective stresses during pipe installation (T5, T6 and T8)

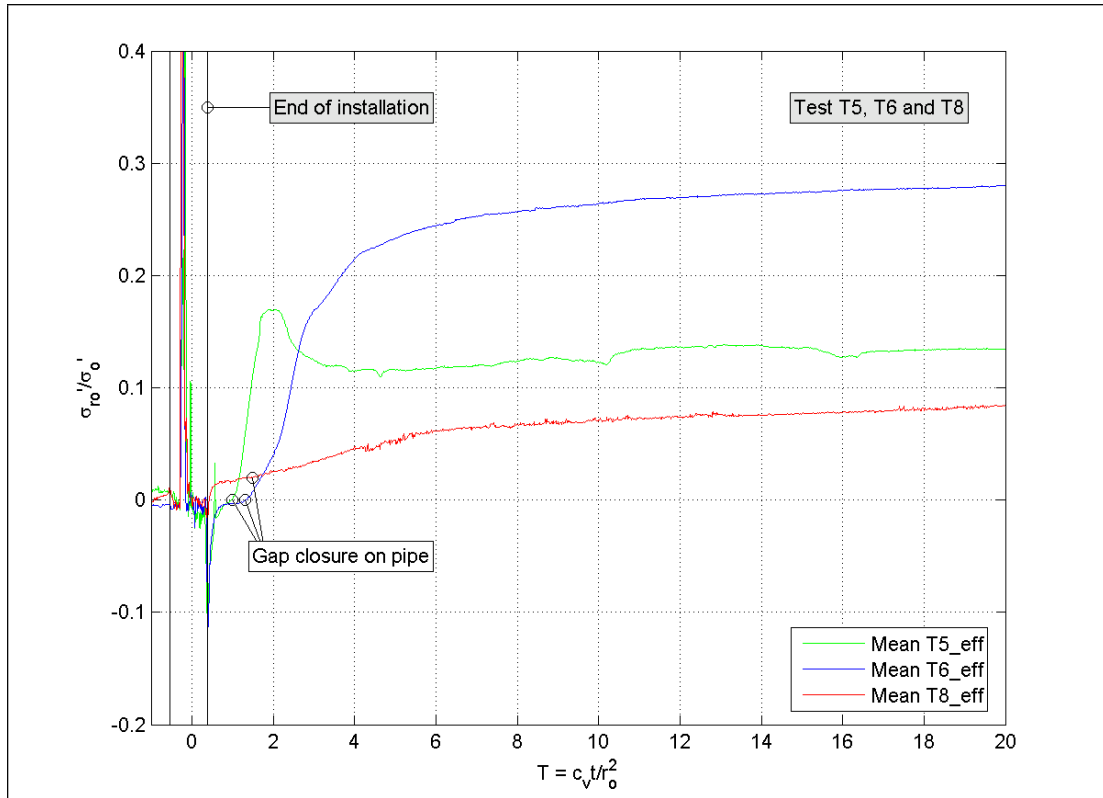


Figure 4.41. Comparison of effective stresses during consolidation (T5, T6 and T8)

## **CHAPTER 5: DISCUSSION OF EXPERIMENTAL RESULTS**

### **5.1 Introduction**

#### 5.1.1 Scope and objectives

The experimental results presented in chapter 4 revealed a significant effect of the lubricant composition on radial effective pipe-soil stresses. Under the boundary conditions imposed in the model experiment, substituting water with a polymer lubricant resulted in a 65% reduction of the radial effective pipe-soil stresses. This chapter uses simple concepts of soil mechanics to explain the mechanisms responsible for the contrasting response observed in test T6 (water lubricant) and T8 (polymer lubricant). The objective of this chapter is, on the one hand, to identify the key mechanisms responsible for the measured reduction of effective stress and, on the other hand, to discuss the implications of the experimental results for the applications of pipe-jacking lubrication in the field.

### 5.1.2 Chapter layout

A model of soil behaviour based on concepts of Critical State Soil Mechanics is first reviewed to highlight features of soil response influencing cavity contractions in saturated, overconsolidated clay (§ 5.2.1). Key interactions between the polymer lubricant *PHPA* and kaolin clay are then summarised to help understand the processes occurring at the cavity boundary (§ 5.2.2). The successive stages of soil response taking place during the unloading of the cavity unloading and the consolidation are then dissected and explained using the ideas outlined in § 5.2. The sequence of events is first described for test T6 (water lubricant), and is then compared to the process of cavity contraction in test T8 (polymer lubricant) (§ 5.3). Finally, repercussions for the selection of lubricant products and injection procedure in the field are discussed in light of the interpretation of the experimental data (§ 5.4.1).

## 5.2 Elements of soil behaviour and of clay-polymer interactions

### 5.2.1 Model for the behaviour of overconsolidated clay

A model of soil behaviour is required to help analysing the different stages of soil response caused by stress changes around the contracting cavity. As the cavity is unloaded, stress changes give rise to elastic unloading and swelling around the cavity. As unloading proceeds, plastic yielding may propagate from the cavity wall towards outer zones of soil, possibly leading the soil to failure. The partially undrained character of the problem results in the generation of significant pore water suction. As a result, large hydraulic gradients arise and drainage of pore water during consolidation leads to further stress changes, possibly causing additional yielding. Understanding these different aspects of soil behaviour is essential to explain the experimental observations.

*Original Cam-Clay* (Schofield & Wroth, 1968) is a soil model which brings many important aspects of general soil response under one roof. For any increment of stress, the model allows predicting elastic and plastic strains, both in compression and shearing, excess pore water pressure, as well as changes of strength and stiffness due to hardening or softening. While *Original Cam-Clay (OCC)* allows a reasonably accurate description of the behaviour of normally or lightly consolidated clay, it was acknowledged by its authors that it performs less well when predicting the response of overconsolidated clay. As described in the following paragraphs, it can nevertheless be used to provide a qualitative description of the behaviour of overconsolidated clay.

The formulation of *OCC* employs the mean effective and deviator stress component  $p'$  and  $q$ . These two stress variables may be written in terms of the radial ( $\sigma_r$ ), circumferential ( $\sigma_\theta$ ), and longitudinal ( $\sigma_x$ ) total stress component used in the cylindrical coordinate system (§ 4.2.1):

$$p' = \frac{1}{3}(\sigma_r + \sigma_\theta + \sigma_x) - u \quad \text{eq. 5.1 and 5.2}$$

$$q = \sigma_r - \sigma_\theta$$

where the pore water pressure,  $u$ , is the sum of the hydrostatic component  $u_o$ , and the excess pore pressure, denoted  $\Delta u$ . Cam-Clay predicts that the response of an element of soil remains elastic as long as the effective stress paths undergone by this element as a result of total stress changes at its boundary remains inside the yield surface defined in the  $p':q:v$  space. If the stress vector reaches the yield surface at any point, irrecoverable plastic strains are produced, and the plastic deformations are accompanied with hardening, softening, or with flow at constant volume. The *OCC* yield surface is best visualised by considering its intersection with the compression plane at  $q = 0$ , in which the intersection with the yield surface defines the line of plastic spherical compression shown in Fig. 5.1b and described by:

$$v = \Gamma_{iso} - \lambda \ln p' \quad \text{eq. 5.3}$$

where the gradient of the compression line,  $\lambda$ , and its ordinate  $\Gamma_{iso}$  are material constants. Unloading from and reloading to the maximum spherical compression previously attained by a soil element causes changes of specific volume defined by the isotropic swelling and recompression line

$$v = v_\kappa - \kappa \ln p' \quad \text{eq. 5.4}$$

where the gradient  $\kappa$  is a material constant and  $v_\kappa$  depends on the isotropic preconsolidation pressure  $p_v = e \cdot p_c'$ . The intersection of planes of constant specific volumes with the yield surface in the  $p':q:v$  space produce geometrically similar yield curves satisfying the equation:

$$\frac{q}{Mp'} + \ln \left( \frac{p'}{p_c'} \right) = 1 \quad \text{eq. 5.5}$$

in which  $M$  is the critical state friction constant and  $p_c'$  the preconsolidation pressure characterising the size of the yield locus. The underlying idea of the Cam-Clay

concept is that there exist a locus of points in the  $p':q:v$  space at which the soil yields at constant volume. This line, the critical state line, may be located in the compression and in the stress plane by following expressions:

$$\begin{aligned} v &= \Gamma_{CLS} - \lambda \ln p' \\ q &= Mp' \end{aligned} \quad \text{eq. 5.6 and 5.7}$$

In OCC, when the stress state of a soil element is brought to the yield surface, any further increment of stress leads to plastic volumetric and shear plastic strain increments obeying an associated flow rule, as depicted by the vectors of dilatant and contractile plastic flow in Fig. 5.1a. Therefore, yielding on the right ('wet') side of the critical state line produces contractile plastic straining (hardening), while yielding on the 'dry' side of the critical state line is associated with dilatant yielding (softening). However, Cam-Clay fails to accurately predict the yielding of overconsolidated soil elements on the left side of the critical state line, which are found to undergo brittle failure before reaching the yield surface. Data obtained by Hvorslev (1937) led Roscoe *et al.* (1958) to correct the Cam-Clay yield surface on the dry side of critical state with a peak strength rupture envelope. However, this 'Hvorslev surface' being only a local "correction" of the Cam-clay surface, it is not necessary to introduce this refinement to provide a qualitative description of soil behaviour.

### 5.2.2 Permeability reduction of kaolin in the presence of *PHPA* solutions

The model of soil behaviour needs to be complemented with an understanding of the properties of the boundary layer at the cavity wall, where the polymer is likely to have affected the clay. In a theoretical model, these effects may be accounted for by changing the properties of the clay in the boundary layer near the cavity wall or by considering the manner in which the processes at the cavity wall affect the boundary conditions. The fluid boundary condition was anticipated to play a decisive role in the build-up of ground loading on the pipe. Because the interactions between the clay and the polymer were not fully understood, a series of tests was devised to measure the permeability of E-Grade kaolin to the lubricant used in the model experiment Mascagni (2005).

The permeability was measured on samples taken from the soil model used in test T4, where the model preparation process was identical to that in test T5, T6 and T8. Block samples were trimmed on a lathe to cylindrical shapes of 100 mm diameter and 100 mm height, before being reconsolidated to an isotropic total pressure of 100 kPa in an apparatus similar to a triaxial cell. The sample was coated with a latex membrane and a sintered polypropylene disc was placed on its horizontal drainage

boundaries. Constant flow permeability tests were performed by imposing a flow of de-ionised water through the sample (in the direction of the consolidation pressure) and measuring the reduction of fluid pressure between the top and the bottom of the sample. The permeability of the E-Grade to water was first measured by imposing four different flow rates in the range of 0.01 to 0.12 ml/min. In the second stage of the test the water permeant was replaced with a 0.3% solution of *Insta-pac 425*, i.e. the *PHPA* used as a lubricant in test T8.

Mascagni (2005) measured a reduction of the pore fluid flow through the sample when substituting the water permeant with the *PHPA* solution. The average permeability of the stratum of kaolin invaded with polymer reduced sharply when replacing water with polymer. The reduction proceeded for approximately 5 minutes, at which time the permeability reached a plateau at  $k = 1.47 \cdot 10^{-11}$  m/s, i.e. 400 times smaller than the permeability to water (§ 4.3.2). Chemical analyses on the sample recovered after the test showed that a layer of 20 mm thickness contained a polymer concentration of 0.2%, and that this concentration reduced to zero at 40 mm depth. The test was repeated four times all gave consistent results.

### 5.3 Interpretation of the model behaviour

#### 5.3.1 Preliminary remarks

This section clarifies the patterns of soil response resulting from cavity unloading and from the subsequent consolidation. Mapping accurate stress paths requires a knowledge of the stress components  $\{\sigma_r, \sigma_\theta, \sigma_x, u\}$ , which must at all time satisfy (1) equilibrium of total stress around the cavity, (2) compatibility of strains and (3) satisfaction of an appropriate constitutive behaviour. In the absence of direct measurement of soil stresses, average stress paths based on simple assumptions are used here to illustrate representative soil response. Stress paths will be represented for an element of clay at the spring line of the cavity, as depicted in Fig. 5.2.

The complex boundary condition at the cavity wall makes it difficult to clarify the pore pressure response around the cavity. Dissipation of excess pore water pressure during consolidation is accompanied with rapidly changing cavity pressure and flow conditions across the cavity wall. In order to simplify the problem, it seemed worthwhile to idealise the evolution of the total cavity pressure during the different stages of the excavation and subsequent consolidation. Fig. 5.3 shows an *idealisation* of the total radial stress  $p_o$  at the cavity boundary. Four successive stages have been identified, each corresponding to either a change of cavity pressure under undrained

conditions, pore water pressure dissipation under constant cavity pressure, or a combination of both. In test T6 and T8, the first two stages of cavity unloading and pore pressure dissipation occur under qualitatively similar, although not rigorously equal, cavity pressure. The soil response in T6 and T8 only departed significantly at the end of stage II, when the annular gap was sealed. For reasons that will become clear later, this change of boundary conditions, caused a reduction of cavity pressure in test T6, and an increase of cavity pressure in test T8. These changes were not instantaneous, but in order to simplify the discussion, they will nevertheless be treated as though they occurred under undrained conditions.

The initial stress state of the clay (§ 4.3) may be expressed in terms of mean and deviator stress components using equations 5.1 and 5.2. According to these definitions, and using a  $K_{oc}$  value above unity (§ 4.3.3), the initial deviator stress is negative, as shown in Fig. 5.4a, where point  $O$  and  $O'$  denote the total and effective stress states before excavation of the cavity. The horizontal distance between  $O$  and  $O'$  represents the hydrostatic pore water pressure. The initial size of the yield surface is determined by the maximum consolidation pressure applied during the model preparation. As a result of the repeatable model preparation process, the size of the yield surface as well as the location of the initial stress states were identical in test T6 and T8.

### 5.3.2 Undrained cavity unloading (stage I)

The excavation of the cavity causes large reductions of total stress at the cavity wall. As the rear of the cutting edge progresses beyond the soil element section, the total radial stress at the spring line reduces from the initial horizontal stress ( $K_{oc} \cdot \sigma_{vo}' + u_o \approx 260$  kPa) to the lubricant pressure ( $p_o \approx 45$  kPa, Fig. 4.7a). This reduction of radial stress is accompanied by an increase in hoop stress  $\sigma_\theta$ . While the increase in hoop stress is equal to the reduction of radial stress for cavity contraction in elastic materials, the finite shear strength of the clay limits the increase of  $\sigma_\theta$  in plastic material. After the element reached yielding at the cavity boundary, further reduction of cavity pressure cannot cause additional increase of hoop stress, and hence, mean total stress must decrease. Unloading of the cavity causes large increase in deviator stress ( $q = \sigma_\theta - \sigma_r$ ), while the mean stress reduces, and hence, the total stress path due to the excavation may therefore be assumed to take the direction  $OA$ , as shown in Fig. 5.4a. However, if the clay behaved elastically, the initial direction of the total stress path would be vertical until  $OA'$  reaches the yield surface. It would then deviate towards point A.

Because the change of stress occurs rapidly (Fig. 4.21), it is reasonable to assume undrained conditions during unloading. This condition of constant volume dictates that the mean effective stress remains constant within the yield surface, and therefore the effective stress path will initiate along the line  $O'A'$  (Fig. 5.4a). Immediately before reaching point  $A'$ , the soil element is on the verge of yielding and has mobilised peak strengths ( $q > Mp'$ ). Any further increment of deviator stress or reduction of spherical pressure causes irrecoverable shear straining and negative plastic volumetric strains (dilation). The soil state moves to a shorter  $\kappa$ -line in the volume space (Fig. 5.4b), while the yield surface shrinks as a result of softening. Unless the stresses applied to the boundary of the soil element reduce to satisfy the new yield surface, further yielding will occur and shrinkage of the yield surface will accelerate until the element fails explosively. Since further increase of deviator stress cannot be supported by the soil element, the load will be shed to the surrounding material until a new equilibrium of total stress is achieved. Dilatant yield under undrained conditions produces negative excess pore water pressure and hence prevents the rapid failure of the element along the path  $A'F'$ . The stress path takes the direction  $A'F'$  and is limited to the right by the deviator stress imposed on the element. If shearing proceeds, the effective stress path reaches the critical state line at  $F'$ , where excess pore water pressure would have taken the value  $\Delta u$ .

Except for differences in lubricant pressure  $p_o$  and differences in excess positive pore water pressure generated ahead of the excavation, the model tests revealed similar behaviour during this stage. The shape, as well as the magnitude of the excess pore water pressure  $\Delta u$  immediately after passage of the cutting edge at  $x/D = 1.5$  were similar in both tests. Also, the large suction that developed during unloading indicates that a zone of soil of radius  $r > 5r_o$  had yielded. It is likely that the soil in the vicinity of the cavity has reached point  $F'$  at the end of the excavation.

### 5.3.3 Consolidation under constant cavity pressure (stage II)

The reduction of mean stress and the dilatant shearing caused significant suction in the clay. The resulting distribution of excess pore water pressure with the cavity radius appears in Fig. 4.21. Because the fluid boundary condition was maintained above the pore water pressure in the clay near the cavity boundary, hydraulic gradients were directed away from the cavity. This caused ingress of fluid from the annulus around the pipes into the clay surrounding the cavity. As drainage is allowed, fluid ingress into zones of high pore water suctions causes dissipation of the excess pore water pressure and hence, a reduction of the mean effective stress. However, because the effective stress point at  $F'$  is already on the verge of plastic

yielding (at critical state), any reduction of mean effective stress under unchanged deviator stress cannot be sustained by the softened element. Again, unless the total stress path retreats towards, say,  $I'$ , the element will shear at constant volume and load will be redistributed to zones of soil at larger radii. The soil state in the volume space (Fig. 5.4b) will move upwards along the critical state line to a shorter  $\kappa$ -line at a higher voids ratio. As the soil swells, the yield locus shrinks and the clay softens, therefore reducing its shear strength. Full dissipation of suction would cause the effective stress point to progress towards point  $D'$  (assuming the total stress path is parallel to  $OA$ ), at horizontal distance of the total stress line equal to the initial hydrostatic pore pressure. During the journey from  $F'$  to  $I'$ , the clay softens and dilates.

In test T8, little dissipation of pore water pressure occurred during stage II, even near the cavity boundary where rapid loss of suction was measured in test T6 (Fig. 4.12b). This was expected and results from the different flow boundary at cavity wall: while also under constant pressure, ingress of pore fluid from the cavity wall into the soil is impaired by the composition of the lubricant. As discussed above, the permeability of the kaolin to the polymer solution used in this experiment was (when measured under 100 kPa isotropic total stress) 400 times lower than that to water, hence resulting in 400 time smaller rates of lubricant seepage into the clay. While some excess pore water pressure dissipated during stage II in test T6, little or no loss of suction occurred during for the corresponding period in test T8 (Fig. 4.25). As a result, the effective stress path due to consolidation will extend further towards  $I'$  in test T6 than in T8 at the time when the consolidation process was 'interrupted' by the alteration of the boundary condition at  $T = 0.4$  (Fig. 5.2).

#### 5.3.4 Change of cavity pressure after sealing of the gap (stage III)

As was discussed in § 4.5.3.4, sealing of the gap effected a change of support pressure at the cavity boundary. The soil-lubricant interactions were seen to be fundamentally different depending on whether water (test T5 and T6) or polymer (test T8) was used as a lubricant. The decrease (T6) and increase (T8) of cavity pressure are depicted in the idealised plot of Fig. 5.3, and the total and fluid pressure measured in the model experiments are compared in Fig. 4.37 and 4.39, respectively. No pipe-soil contact had occurred before the beginning of stage III ( $T = 0.4$ , Fig. 4.41).

#### ***Mechanism of cavity pressure reduction in test T6***

At the outset of stage III, significant suction remained around the excavation and transient contraction of the cavity wall was still ongoing. Had the total cavity pressure

be held constant, convergence would have continued until full dissipation of excess pore water pressure had been achieved (impermeable pipe). Under these circumstances, a confinement of the lubricant fluid by the converging cavity wall could have been anticipated. This would have caused the lubricant pressure to increase, and the rate of cavity convergence to reduce. This, however, did not happen. On the contrary, the cavity pressure (fluid pressure) immediately began to reduce after the gap was sealed ( $T = 0.4$ ).

In order to clarify this observation, the flux of lubricant across the cavity boundary must be considered. The isochrones of Fig. 4.25 show that large hydraulic gradients exist around the cavity. For radii of between 1.2 and  $1.5 \cdot r/r_o$ , the hydraulic gradients are such that fluid flow occurs from the cavity towards outer zones of soil, while at larger radii, the hydraulic gradient induce pore water flow towards the cavity. Elements of clay located in the region of  $r/r_o = 1.5$  must therefore swell substantially and lubricant must be adsorbed into the clay to accompany its volume change. Since no recharge of fluid occurred around the pipe after sealing of the gap, seepage of lubricant into the clay reduces the volume of 'free' liquid in the annulus. Concurrently, the thickness of the annulus reduces as the cavity wall converges towards the pipe (Fig. 5.6). The change of lubricant pressure in the annulus is governed by the rate of volumetric strain of the soil, in relation with the rate at which water can ingress into the soil. If the rate of seepage into the clay exceeds the volumetric strain rate of the clay around the cavity, the pressure of lubricant must reduce. The relatively high permeability of the clay and the large hydraulic gradients observed near the cavity wall suggest that this mechanism must indeed have been responsible for the measured reduction of cavity pressure in test T6.

#### ***Effects of cavity pressure reduction in test T6***

Fig. 4.27 demonstrates that the reduction of fluid pressure at the cavity wall is not associated with an increase of pore pressure at  $r/r_o = 1.2$ , as would be the case if the process was due to consolidation (pore water pressure equalisation) only. Instead, the reduction of cavity pressure induces negative excess pore water pressure. As may be seen in Fig. 4.12b, suctions were measured at all PPT locations, and are likely to have occurred throughout the model. The simultaneous reduction of pore water pressure in the clay and at the cavity boundary had the effect of maintaining, at least temporarily, the initial hydraulic gradient, and hence the seepage of lubricant and the associated reduction of cavity pressure persisted. As hydraulic gradients then reduced ( $T = 2$ , Fig. 4.28), the seepage rate of water into the clay reduced and further convergence of the cavity resulted in a gradual pressure increase in the annulus.

At the end of stage (II), the total stress state of an element of clay at the spring line was at point  $I$  and its effective stress state at the apex of the shrunk yield locus at  $I'$ . The reduction of cavity pressure after sealing of the gap causes further unloading of the clay. If the clay were able to carry further increments of deviator stress, the total stress path would resume its journey in the direction of point  $F$  (Fig. 5.4). However, the clay is at critical state and cannot carry additional deviator stress. The total stress path therefore has to move to the left as further cavity unloading occurs. If the unloading were sufficiently rapid to allow generation of excess pore water pressure (stage III, Fig. 5.3) suction will develop, leaving the mean effective stress unchanged and allowing the total mean stress to reduce at constant deviator stress towards point  $S$ . If undrained conditions indeed prevailed, point  $S'$  would locate as shown in the volume space of Fig. 5.5b.

As drainage then occurs, pore water flows into the soil element and suction dissipates. The mean effective stress therefore reduces, hence causing further plastic shear and volumetric distortion. The effective stress state moves down the critical state line towards  $T'$  (Fig. 5.5a), and, in the volume space (Fig. 5.5b), point  $S'$  ascends along the critical state line as plastic dilation occurs. As already discussed above, the new, looser state of the soil is associated with a smaller yield surface, and the soil will have softened considerably. As the clay of the element at the spring line softens, the total stress path moves downwards in a direction that may only be estimated by considering equilibrium of total stresses and compatibility of strains around the cavity. The likely direction is, however, that shown in Fig. 5.5a. As a result, unloading of the cavity after the annular gap was sealed (stage III) is therefore likely to have produced considerable softening of the clay.

### ***Mechanism of cavity pressure increase in test T8***

As discussed above, the evolution of the cavity pressure depends on the rate of seepage into the clay and the rate of cavity contraction. The cavity pressure is maintained constant if the rate of lubricant ingress into the soil matches the rate of volume change of the annulus. While a reduction of pressure was measured in the presence of water in the annulus (test T6), the opposite occurred when polymer was used as a lubricant. As was the case in T6, the cavity wall is converging towards the pipe at the outset of stage III. Sealing of the gap prevents the polymer from being expelled from the annulus through the injection ports and therefore the cavity confines the lubricant in the gap. Seepage of the polymer into the clay cannot occur sufficiently fast to prevent pressure increase in the cavity. This is because the permeability of the clay is drastically reduced by the polymer (§ 5.2.2). Mascagni

(2005) measured that the permeability to *PHPA* gradually reduced to a value approximately 400 lower than the hydraulic conductivity. Continuity of fluid volume shows that if the cavity fully converged onto the pipe and that if the confinement of lubricant was effective so it was forced to penetrate into the clay, the volume of solution would have invaded the clay up to a radius of the order of  $r_p/r_o = 1.1$ . Under these circumstances, Fig. 2.18 shows that a tenfold reduction of seepage rate across the cavity wall occurs when a layer of outer radius  $r_d$  suffered a permeability reduction  $k/k_d = 200$ . This supports the hypothesis that the rate of polymer seepage into the clay must indeed have been insufficient to prevent the polymer pressure from increasing under the confinement imposed by the converging cavity, and that the permeability reduction is responsible for the large increase in cavity pressure measured in test T8 at  $T = 0.4$  (Fig. 4.35).

### ***Effects of cavity pressure increase in test T8***

Section 5.3.3 argued that the state of a clay element at the spring line of the cavity would have lain nearer to point  $F'$  than in test T6 as a result of the small loss of suction observed during stage II. The increase of cavity pressure that occurs at  $T = 0.4$  (Fig. 4.35) and then continues throughout stage III (Fig. 5.2) causes the total stress path in test T8 to move to the right, say from point  $J$  to point  $R$ , without significant changes of deviator stress. The immediate increase of pressure observed at  $T = 0.4$  was sufficiently fast to be taken as an undrained event. Therefore, the increase in mean total stress caused an increment of positive pore water pressure, which caused rapid loss of suction near the cavity, as shown by the measurements of PPT A1 (located at  $r/r_o = 1.2$ ) in Fig. 4.26 and 4.27. The increase of cavity pressure is likely to have left the mean effective stresses unchanged, since the increase of total pressure was accompanied by an increase of similar magnitude of the pore water pressure.

Again, as drainage occurred, mean effective stress reduction from the point  $J'$ , on the verge of yielding, caused plastic dilation and softening: the state  $Q'$  moves down the critical state line and the voids ratio increases as shown in Fig. 5.6a and b, respectively. However, since the cavity pressure gradually increased throughout stage III, the total stress path may take the direction  $RQ$ , as shown in Fig. 5.6a the suction would dissipate without the large softening, as in test T6.

### 5.3.5 Build up of pipe-soil stresses (stage IV)

The flow regime around the contracting cavity is altered during stage IV as contact occurs between the pipe and the cavity wall. This is the second change of

boundary condition during consolidation, after that triggered by the sealing of the gap. At the time of pipe-soil contact, the soil near the cavity boundary had softened in both test T6 and T8, but the extent of the softening was considerably larger in test T6 (water lubricant), where the cavity pressure reached lower values during stage III and where flow of pore water into the clay could occur from the cavity boundary. The plastic dilation and softening reduces the shear strength of the clay, and as a result, causes redistribution of load to neighbouring soil elements and the propagation of the zone of softened soil.

The effect of a softened zone of soil around a cavity were investigated by Alonso *et al.* (2003) and Wang & Dusseault (1994), they showed that the distribution of radial and circumferential stresses is greatly affected by softening around the cavity, in turn altering the radial effective stress at the boundary. Closed-form solutions and numerical analyses presented by these authors show that the radial effective stress on a rigid lining increases with the degree of softening, or indeed with the radius of the zone of soil affected by strength loss. This is in line with the hypothesis adopted in this discussion and suggests that the mechanism of radial effective stress reduction in test T8 (polymer lubricant) relates to the limitation of strain-softening resulting from the increased supporting pressure at the cavity boundary.

## **5.4 Repercussions for field application of lubrication**

### **5.4.1 Effect of lubricant composition**

The model experiment showed that polymer lubricant greatly reduced the radial effective stresses acting on the model pipe, which confirms that polymer would perform better than water in reducing jacking forces. The test results demonstrate that, under the boundary conditions imposed in the model test, polymer ‘lubricants’ do not solely act by reducing interface shear friction between the ground and the pipe. In addition to ‘lubrication’, polymers significantly reduce the ground loading onto the pipe. In cases where the pipe-soil behaviour obeys a friction law, the 65% reduction of normal stresses onto the pipes will result in an equally large reduction of jacking force. If, in addition, the angle of shear resistance between the clay and the pipe is reduced by the action of the polymer, jacking forces might drop to a fraction of what they would have been using water as a lubricant.

Section 5.3 showed that the polymer reduces radial effective stress by two concomitant actions. Firstly, it provided total radial stresses to support the cavity during its contraction; these stresses were much greater than in the case of water.

Secondly, the polymer greatly reduced water ingress from the cavity wall, thus reducing the rate of consolidation compared to test T6, where water supply in the cavity could be absorbed by the surrounding swelling clay. A mechanism of loading reduction by alteration of the clay properties due to polymer infiltrated can almost be ruled out in view of the minute depth of penetration of the polymer (~5 mm). Although no experimental evidence exists as to the effects of products such as potassium brines ( $K^+$ ), often used in oil well drilling and pipe jacking to inhibit swelling and, in turn, reduce ground loading. It seems unlikely, at least in the case of kaolin, to obtain a similar reduction with such kind of products used individually. Indeed, solutions of potassium cation are known to reduce swelling by processes altering the mineralogical properties of the clay (substitution of the interlayer cations); this will have a marginal effect in kaolin, which has a relatively small cation exchange capacity. In addition, substantial evidence show that  $K^+$  increases the permeability of the clay through which it is allowed to seep or diffuse. Such an increase of permeability would exacerbate the effects observed in test T6, and hence act counterproductively.

Bentonite is effective in granular material (sand and gravels), where it forms a filtercake and allows a support pressure to be imparted to the cavity wall. In clay, although bentonite is often (almost systematically when a lubricant is used) used, its benefits are not yet fully understood. Some authors ruled out the possibility that bentonite formed a low permeability barrier on the clay surface. If the bentonite does not help reduce the permeability at the cavity wall, then its benefits are likely to be limited to that of reducing interface pipe-soil friction. In addition, bentonite being a dispersion (rather than a solution), the suspended particles may be filtrated by mechanical action and therefore provide free water for the clay to swell and soften, as observed in test T6. Also, space restriction on pipe jacking construction sites often limit the size of mixing tanks for bentonite. When large volumes of bentonite are required, it is sometimes insufficiently hydrated before injection around the pipes. Under boundary conditions such as those in the model test, *i.e.* if the annulus is a sealed and lubricant cannot escape from it other than by seeping into the ground, poorly hydrated bentonite may develop swelling pressures as it continues to hydrate in the annulus. Hydraulic gradients will increase and unless a low permeability boundary is formed on the cavity wall, the seepage rate of free water into the clay will increase. This, once again, would act counterproductively, in that it may accelerate swelling (stage II) and softening of the clay surrounding the cavity. Because pipe jacking drives in clay often encounter lenses of granular material or fissured clay, bentonite is required to “seal off” these zones of greater permeability. The ability of

the polymer to reducing the permeability of coarser material has been suggested (§ 6.3.3), but direct comparison with bentonite and polymer-enhanced bentonite would be required to address this issue.

Since the hypothesised mechanism of effective stress reduction on the pipes is one in which the lubricant must prevent fluid ingress into the clay, it is a valid point to question the necessity of injecting lubricant (at all). If no lubricant at all were injected, no free water would be available for the clay to swell and consolidation might take correspondingly longer, with associated benefits in terms of ground loading reduction. However, a 'dry' drive also means zero total stress support at the cavity boundary, and hence, more softening in early stage, with in turn, larger pipe-soil stresses at equilibrium. This may be a valid strategy in clays whose permeability is so low, that the suction generated during unloading will not dissipate during the time of construction. Secondly, for the portion of drive where the overcut remains open, lubricant causes full or partial buoyancy of the pipe and therefore eliminates or decreases the sliding friction of the pipe on the base of the hole. Sliding friction can be significant, and therefore the effects of partial buoyancy are often of great advantage. In addition, the 'benefit' of not providing free liquid that can be absorbed by the swelling clay is, in most cases, annihilated by ground water ingress at some location along the pipe jack (sand lenses, fissures, loss of face support liquid in slurry shields).

#### 5.4.2 Effect of injection procedure

The injection pressure affects the fluid boundary condition imposed at the cavity wall. While lubricant pressures may be relatively well controlled in model experiments, field situations often do not allow or aim for such control. Much more, the lubricant is injected intermittently, often by controlling its volume per 'push' (number of pipes inserted) and monitoring the lubricant pressure is not carried out systematically. Also, lubrication is usually introduced partway through the drives, after a certain percentage of the available jacking capacity is reached and sometimes days or weeks after launching of the pipe jack. Some authors (*e.g.*: Marshall, 1998) suggested that because introducing lubrication partway into the drive helps reduce the interface shear stresses on the entire length of the pipe, lubricant need not be injected before the capacity of jacking load is approached. Perhaps lubrication from the beginning of the drive would result in even lower jacking forces, as in the projects reported in § 2.2.2.5 and 2.2.2.6.

The pressure of the lubricant during the installation determines the magnitude of radial unloading and, in turn, the magnitude of shearing imposed to the soil around

the cavity, as well as the generated suction. The lower the lubricant pressure during the excavation, the farther the stress state will move along the total stress path OA of Fig. 5.4. If the lubricant pressure were maintained so as to balance the initial stress state, then no changes of total stress would occur around the cavity and little or no convergence of the cavity wall would occur. The pipes would be buoyant in the saturated cavity and jacking forces would be marginal. The problem is to prevent fluid loss into the ground, either by seepage through the pore space or via discontinuities, *i.e.* discontinuities in fissured clay or pockets of high permeability material like sand or gravels. Smearing effects along the TBM shield as well as increase of hoop stresses around the cavity as a result of small reductions of radial stresses may be sufficient to ‘heal’ fissures and cracks in the clay and prevent fluid loss via such discontinuities. Potentially more problematic are the higher permeability materials that may occur on one or more portion of the drive and which may require the use of bentonite to seal them off.

Anecdotal evidence suggests that pressurising the ‘wrong’ lubricant product may be counterproductive. Some experimental evidence of this hypothesis is provided when comparing the effective stresses that built up on the pipe in test T5 and in test T6, both conducted with water as lubricant. Despite the poor control of lubricant pressure in test T5 (water lubricant), the lubricant pressure was on average much lower than in test T6 (water lubricant), *i.e.* approximately 5 kPa, compared to 50 kPa in test T6. Since all other factors were kept constant in the two tests, the higher pipe-soil stresses in test T6 (50 kPa lubricant pressure) compared to test T5 (~5 kPa lubricant pressure), can only be attributed to the difference in cavity pressure (during stage I and II). As expected, a higher water pressure in the annulus acts counterproductively. However, while the rate of pressure build-up was expected to increase with the lubricant pressure, the opposite was measured. In addition, the final magnitude of pipe-soil stresses were anticipated to coincide in the long term, the experimental results showed that that a marked difference remained. The final pressure is 50% lower in case of low injection pressure of the water lubricant (T5) than in case of high injection pressure of water (T6), and the reasons behind this observation require further investigations.

## 5.5 Final remarks

The validity of the conclusions drawn from the experimental data with respect to the ‘deficit’ of pore water pressure measured at equilibrium in test T5 and T6 can be questioned. It may be asked whether the reduction of effective stress

measured in test T8 is partly merely the result of the higher pore water pressure that acted at the pipe-soil interface in test T8. Test data suggested the existence of steady state seepage towards the model pipe. Comparison of Fig. 4.37 and 4.38 shows that the difference of fluid pressure measured between T5, T6 and T8 at equilibrium (30 kPa) is the same as the different of total stress. It may be anticipated, although no evidence is available to confirm this conclusion, that if the fluid pressure at the boundary had recover to hydrostatic pressure, then the total stress on the pipe would have increased accordingly, hence leaving the effective stresses unchanged.

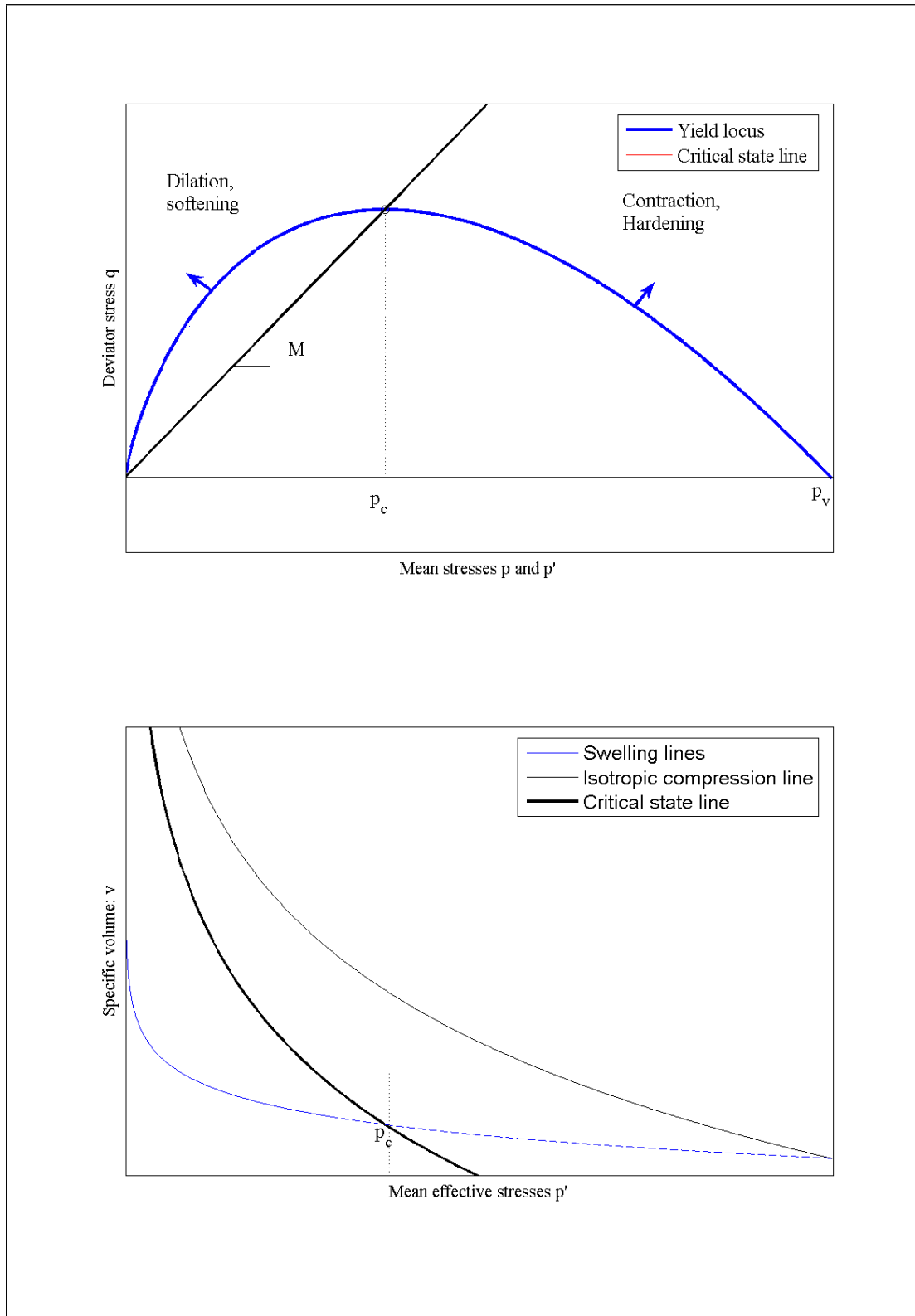


Figure 5.1 Cam-Clay yield model: (a) stress plane, (b) compression plane

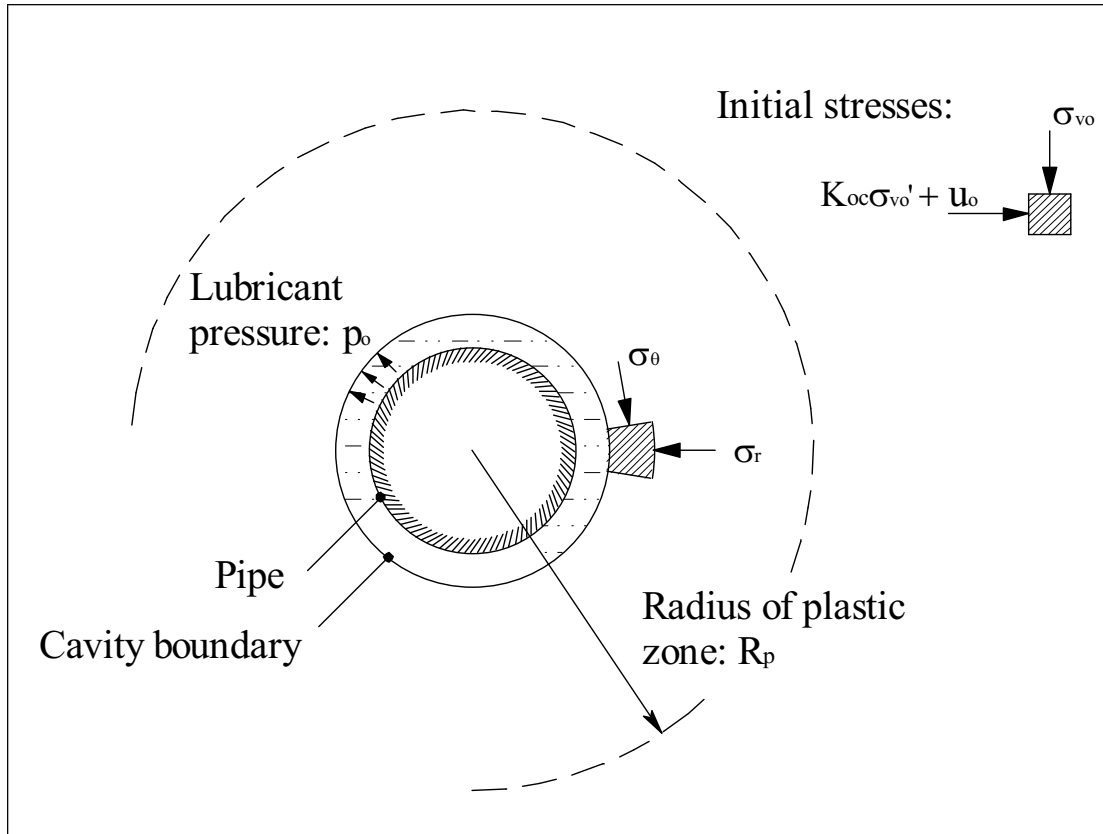


Figure 5.2 Stress components on an element of soil at the spring line

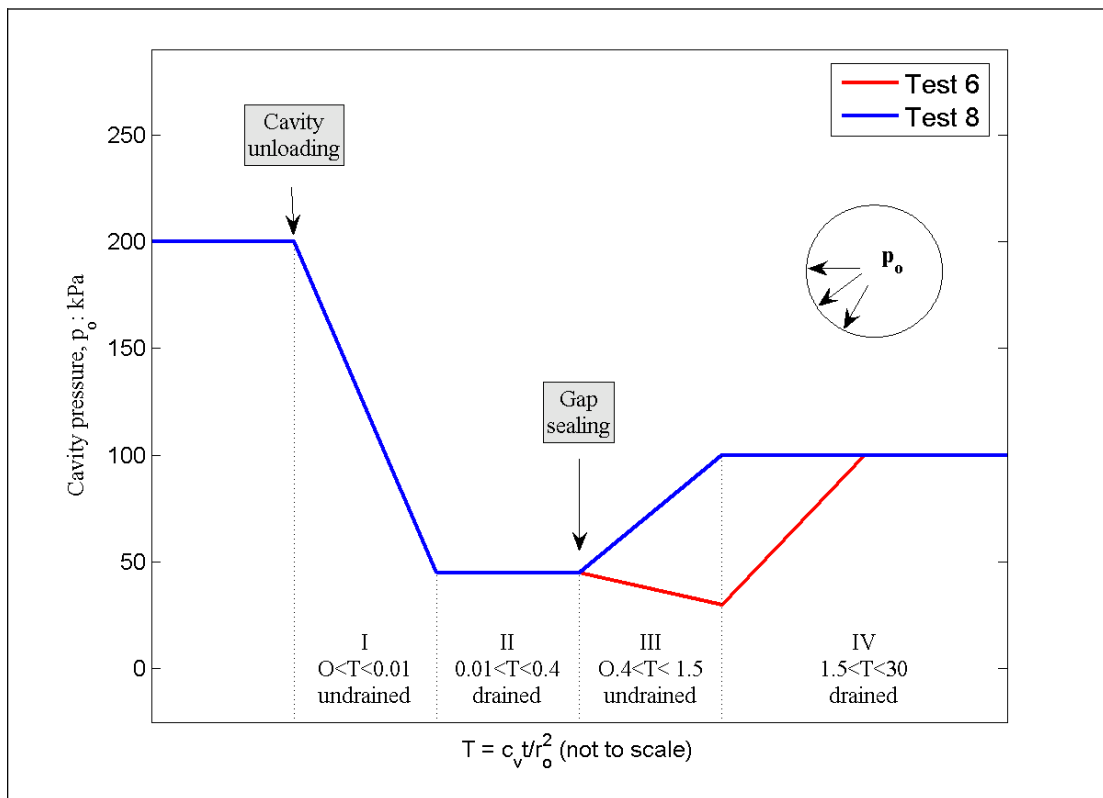


Figure 5.3 Idealised cavity pressure evolution in test T6 and T8

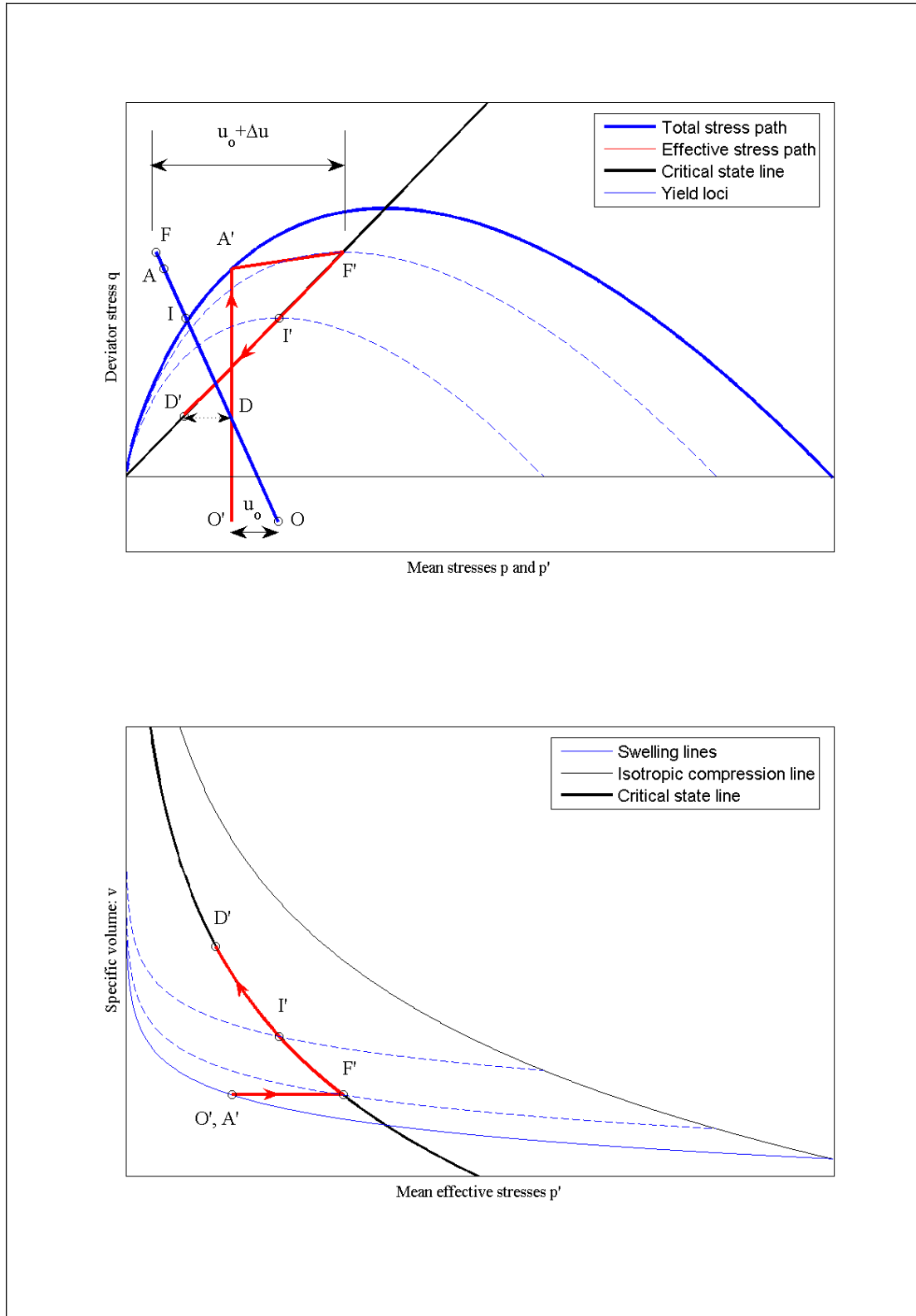


Figure 5.4 Stress paths for undrained unloading (stage I and II) (test T6 and T8)

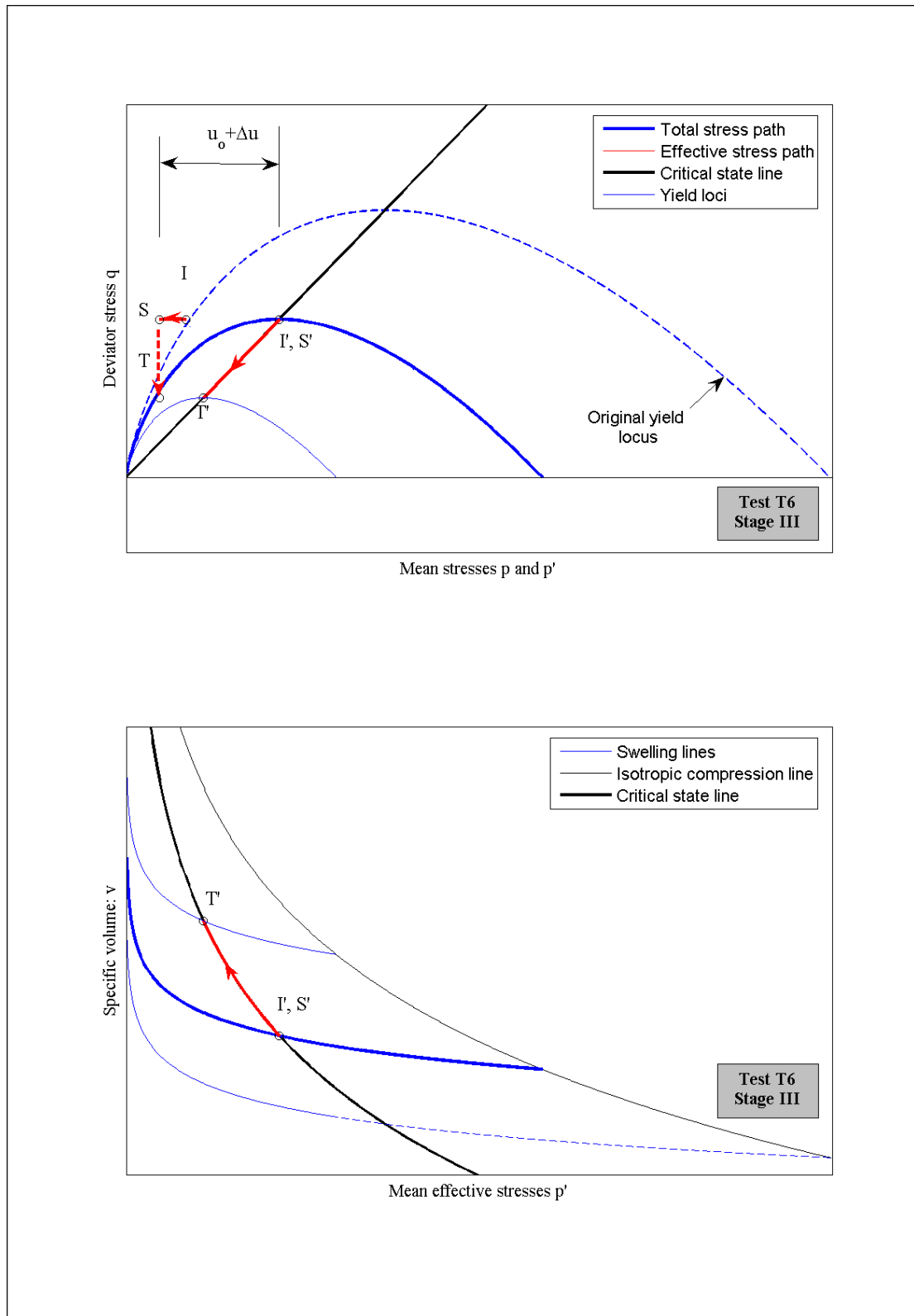


Figure 5.5 Stress paths during stage III and IV (test T6)

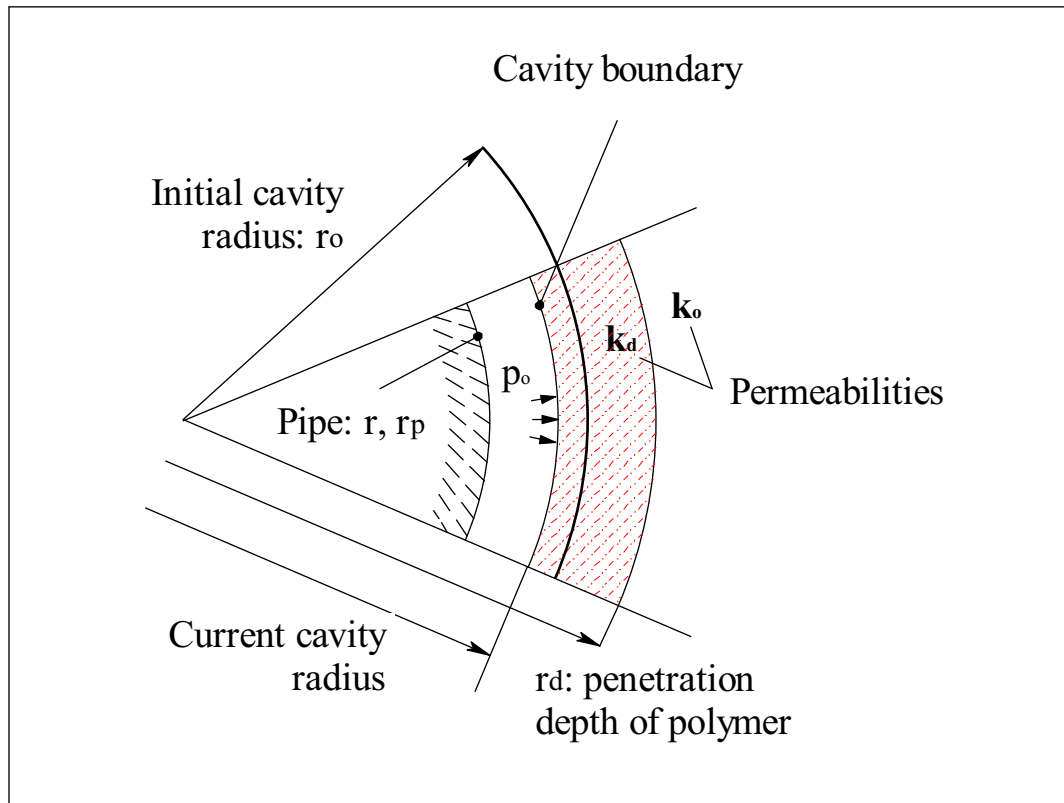


Figure 5.6 Zone of polymer invasion and permeability reduction

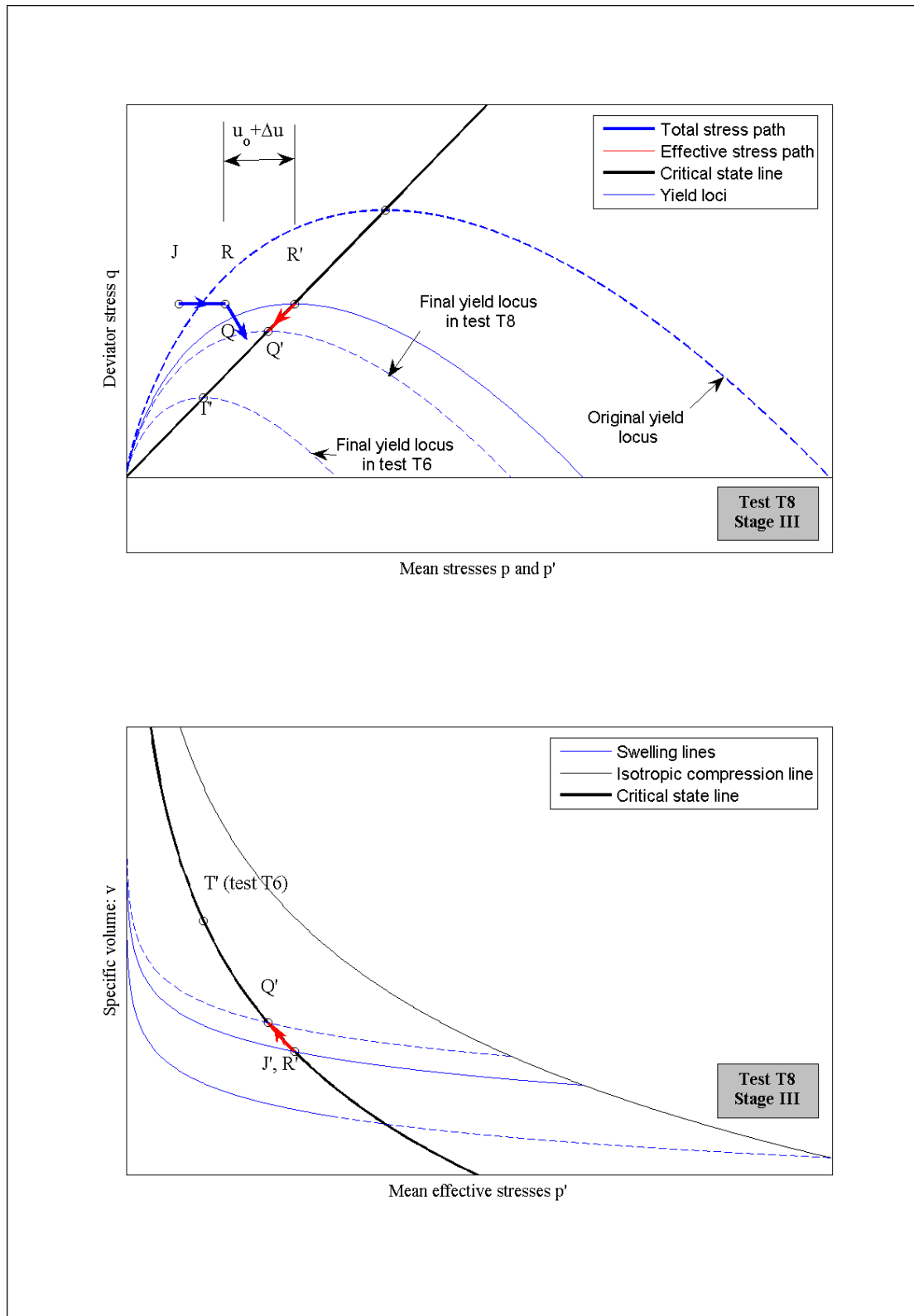


Figure 5.7 Stress paths during stage III and IV (test T8)

## **CHAPTER 6: LITERATURE REVIEW: SOIL CONDITIONING IN EARTH PRESSURE BALANCE MACHINES**

### **6.1 Scope and objectives**

This chapter is the counterpart of the literature review of lubrication in pipe jacking presented in chapter 2. Here, the related problem of soil conditioning in earth pressure balance (*EPB*) machines is addressed with the same objective. The current state of knowledge is summarised and lessons learned from field experiences are discussed in order to substantiate the needs for research highlighted in the introduction (§ 1.3.4). This review complements and updates the recent reviews of Milligan (2000) and Merritt (2004), to which it will refer extensively, and focuses on the material relevant for the discussion of field data presented in chapter 7.

The chapter first gives an outline of the *EPB* machine technology: it discusses how the pressure to the tunnel face is provided and controlled (§ 6.2). It then summarises the current practice and understanding of soil conditioning in *EPB* machines: the effects of foams and polymers on different types of ground are reviewed and guidelines for the application of soil conditioning are discussed (§ 6.3). Finally, the impact of *EPB* tunnelling is addressed by delineating the problems of face stability and ground movements induced by the operations of *EPB* machines (§ 6.4).

## 6.2 Earth pressure balance machine technology

### 6.2.1 Provision of face pressure

The principles of *EPB* machines technology were described in § 1.3. While slurry shields use high-density bentonite slurry, *EPB* machines rely on the excavated ground as a support medium for the excavation face. The excavated ground is confined between the tunnel face and a pressure bulkhead arranged at a distance of between 1 and 3 m behind the face, as shown in Fig. 1.2. A screw conveyor (typically about 1 m in diameter and 10 m in length) is used to extrude the soil confined in the excavation chamber, thus allowing advance of the machine. The shield is jacked forward by thrusting on the lining with hydraulic rams arranged around the circumference of the machine. The rams have a stroke slightly larger than the length of the lining segments, so the machine can be advanced by the length of one lining segment while excavation proceeds. Upon reaching a stroke of typically 1500 mm, the rams are retracted to allow erection of a new lining ring, on which the machine thrust will then react to complete its next ‘shove-build’ cycles.

As shown in the free body diagram of Fig. 6.1, the forward thrust applied to the machine is reacted by three components: (1) friction around the shield, (2) normal total stresses  $p_2$  between the bulkhead and the soil in the excavation chamber, and (3) normal total stresses,  $p_1$ , between the cutting wheel and the in-situ soil. Item (1) may be of the order of 1 MN, but is usually small compared to the total thrust, because an overcut (or “bead”) is excavated around the shield to improve its manoeuvrability. Item (2) reduces to negligible values when the excavation chamber is not filled with the support medium. This is the case when machines are operated in so-called ‘open-mode’ or when the chamber is improperly filled as a result of excessive rate of soil extraction by the screw conveyor. For a given thrust, item (3) increases with reducing pressure in the excavation chamber, but must always be greater than zero for excavation to proceed. It provides horizontal (as well as shear) stresses between the cutting wheel and the tunnel face, and the resulting force depends on the total thrust, the pressure in the excavation chamber, as well as the opening ratio of the cutting wheel. Fig. 6.2 compares the openings in the cutting wheels of two *EPB* machines used on the construction of the *Metrosur* (Madrid) and the *CTRL* (London). The excavated diameters were similar (9.4 m and 8.15 m), but the ratio of opening in the cutting wheel differed significantly in these two machines. The openings of the cutting wheels were approximately 30 and 57%, in the machines used in Madrid and London, respectively. Clearly, a much larger proportion of the thrust will be transmitted directly between the cutting wheel and the tunnel face, compared to the machine in Fig. 6.1b, where control of the face pressure will depend more on the

confinement pressure of the soil in the excavation chamber. The friction (and hence the torque) acting on the cutting head will also be correspondingly larger. Hence, the support pressure to the excavation face is provided partly by the thrust from the cutting wheel and partly by the confinement pressure of the soil in the excavation chamber. For a given thrust on the shield (easily controllable by the machine driver), the proportions of item (1) and (2) largely depend on the pressure of the support medium in the excavation chamber.

### 6.2.2 Control of pressure in the excavation chamber

The pressure of the support medium in the excavation chamber is controlled by the mass flow rate of soil entering the excavation chamber and that discharged at the outlet of the screw conveyor. The bulk modulus of the spoil governs the pressure fluctuations induced by differences in soil masses contained in the excavation chamber. In order to maintain a constant pressure, a rate of soil mass equal to that entering the excavation chamber (plus the injected conditioning agents) must be discharged by the screw conveyor. If the machine advances steadily, a reduction in the extraction rate causes an increase of the pressure in the excavation chamber, and vice versa. Because of the relative incompressibility of the soil in the excavation chamber, differences in the rate of discharge and the rate of excavation result in pressure fluctuations of large magnitude in the excavation chamber. Therefore, it is crucial that the rate of soil discharge by the conveyor be controlled accurately in order to maintain a constant face pressure.

The rate of discharge of the screw conveyor depends on the geometry and angular velocity of the screw. In addition, the pressure gradient along the screw, the interface shear stresses between the screw conveyor (flights and shaft) and its casing, the shear strength of the soil, as well as the geometry of the screw outlet significantly affect the discharge process. When the shear strength of the spoil reduces below a critical value, the pressure gradient between the inlet and the outlet of the conveyor might suffice to cause extrusion without rotation of the conveyor. This leads to uncontrolled extrusion of soil, which causes rapid loss of the face pressure and can lead to face instabilities or excessive ground movements. When, on the contrary, a critical spoil strength is exceeded, the spoil-conveyor stresses rise to such high values that the conveyor might fail to discharge the soil, bringing the machine to a halt and requiring time-consuming 'unclogging' of the machine. The discharge rate is further affected by the intense shearing of the soil near the inlet and the outlet of the screw, as well as arching mechanisms around the inlet of the screw conveyor (Anagnostou & Kovári, 1994, Bezuijen *et al.*, 2005).

### 6.2.3 Mechanics of screw conveyors

Theoretical models describing the mechanics of screw conveyors have been proposed by Yoshikawa (1996a, b and c), Talmon & Bezuijen (2002) and Merritt (2004). These models relate the pressure drop and the discharge rate of screw conveyors, mainly as a function of the screw geometry as well as the shear components between the soil and the screw flight, casing and barrel. Measurements on full-size and model-scale screw conveyors were also obtained by these authors. A review of these theoretical models and of the experimental measurements is provided by Merritt (2004). In addition, Merritt performed model experiments on a 100-mm diameter by 1-m long screw conveyor. The following observations were made for steady-state extrusion of normally consolidated E-Grade kaolin, natural London Clay cuttings, as well as Lambeth Group clays mixed in various proportions of foams and polymers:

- The shear stress acting between the screw conveyor casing and the mixture being discharged is constant along the conveyor and is approximately equal to the average undrained shear strength of the mixture (as measured with a hand shear vane).
- A thin layer of soil coated the inside of the screw casing after each test, suggesting that the interface shear behaviour is controlled by a soil-on-soil mechanism.
- The torque required to operate the screw increased linearly with the shear stresses between the clay and the casing of the screw conveyor.
- The normal total stress between the soil and the casing decreased linearly along the conveyor, while effective stresses remained constant.
- The dissipation of total pressure along the screw reduces with increasing screw pitch, while the discharge flow rate increases with the screw pitch.

### 6.2.4 Monitoring and operation of *EPB* machine

*EPB* machines are heavily instrumented for real-time monitoring of their key parameters. This allows the machine operation to be controlled and adjusted continuously, mainly to steer the machine and control the pressure in the excavation chamber, while keeping the torque of the cutting wheel and the screw conveyor below predefined threshold levels. The main machine parameters that may be altered are the thrust applied by each group of hydraulic jacks, the angular velocity of the screw

conveyor as well as the gates or valves that may be deployed to fully or partially restrict the outlet of the screw conveyor. Additional control of the machine is often achieved by varying the injection rate of soil conditioning agents or switching the injection from one point of the machine to another, as will be discussed in § 6.3.

### 6.3 Soil conditioning in *EPB* machines

#### 6.3.1 Aim and methods

The material in the excavation chamber should allow uniform transmission of earth pressure from the chamber to the tunnel face. In addition, it should be of low permeability to resist ground water pressures and have a consistency allowing its controllable discharge by the screw conveyor. Natural soils seldom possess such properties. Therefore, the properties of the excavated soil have to be altered by the injection of soil conditioning agents. This occurs by injecting water, foam, polymer and sometimes bentonite or a combination of these products from nozzles located on the cutting wheel of the machine. The conditioning of the soil aims to alter its properties so that a soft and compressible soil mass of low permeability, low internal friction (or shear strength), and controlled adhesion characteristics may be created. Ideally, the soil then has the appearance of a soft plastic paste, with a consistency index,  $I_c$ , ranging from 0.40 to 0.75 (Maidl, 1995), corresponding to undrained shear strengths,  $S_u$ , of between 5 and 25 kPa (Milligan, 2000). In addition, the support medium should be compressible to limit the pressure fluctuations resulting from differences between the excavated and the discharged soil volumes, and its permeability should be lower than  $k = 10^{-4}$  m/s so that ground water pressures may be withstood (Maidl, 1995).

Injection nozzles of soil conditioning agents are often located in the excavation chamber or in the screw conveyor. However, injection at the point of cut (on the cutting wheel) improves mixing of the additives with the excavated soil and helps create a homogenous mixture in the excavation chamber (Milligan, 2001). The injection plant usually comprises five to ten injection nozzles for conditioning agents, most of which are usually arranged at different radii on the cutting head and a pair of them at different locations in the casing of the screw conveyor. The injection rates are monitored continuously during the operation of the machine and can be altered during the operation by the machine driver. Changing the product type or its chemical composition is normally not possible during a ‘shove’ and can only be carried out during ring build time.

The foam, the polymer and the bentonite slurries used as conditioning agents are generic names for products possessing a wide range of physicochemical properties. Foam is produced in the tunnelling machine by dispersion of compressed air in a water-based solution of surfactant. The properties of foam that are believed to play a significance role in soil conditioning mainly “depend on the solution chemistry, the relative air and liquid phase volume (the foam expansion ratio, *FER*), and the foam bubble size” (Merritt, 2004). Polymer is prepared as a low concentration (typically 0.2 to 2%) water-based solution. While polymer solution can be used independently, it is mostly used as an additive to foam and bentonite. These conditioning agents are discussed in detail by Milligan (2001). Some physical properties of foam, with and without polymer additives, were investigated by Maidl (1995) and Quebaud (1996). Basic properties of polymers and bentonite used in drilling fluids and soil conditioning were summarised in § 2.4.3, where further references are provided.

### 6.3.2 Parameters involved in soil conditioning

*EPB* machines require conditioning of the excavated soil in almost all ground conditions. Conclusions from basic research into the effects of chemical treatment (§ 6.3.3) showed that the properties of the soil-chemical mixtures strongly depend on the type and quantity of the product, or combination of products, mixed with the ground. These different properties may significantly affect the operation of the tunnelling machine, and the soil conditioning treatment required in different ground conditions have to be defined in each particular case. The parameters that have to be selected comprise the type of product (water, foam, polymer, bentonite or a combination of any of those) as well as their quantities. The quantity of soil conditioning agent are usually expressed as a volume ratio of conditioning agent relative to the volume of ground in situ (before excavation). Injection ratios of foam (*FIR*) and polymer (*PIR*) solutions are hence defined as follows:

$$FIR = \frac{V_f}{V_s} \cdot 100 \quad \text{eq. 6.1}$$

$$PIR = \frac{V_p}{V_s} \cdot 100 \quad \text{eq. 6.2}$$

where  $V_f$  is the volume of foam at atmospheric pressure,  $V_p$  the volume of polymer solution, and  $V_s$  the volume of soil. The properties of the foam strongly depend on its proportion of air and surfactant solution, which is characterised by the foam expansion ratio (*FER*):

$$FER = \frac{V_f}{V_{fl}} \cdot 100 \quad \text{eq. 6.3}$$

where  $V_{fl}$  is the volume of foaming liquid solution and  $V_f$  the volume of foam. In addition, the concentration of surfactant and polymer ( $c_s$  and  $c_p$ , respectively) used in the preparation of the foaming liquid and the polymer solution are defined as:

$$c_s = \frac{V_{surf}}{V_{fl}} \cdot 100 \quad \text{eq. 6.4}$$

$$c_p = \frac{V_{pol}}{V_p} \cdot 100 \quad \text{eq. 6.5}$$

where  $V_{surf}$  and  $V_{pol}$  are the volume of surfactant and polymer, respectively.

### 6.3.3 Effects of conditioning agents on engineering properties of the soil

The effects of conditioning agents on soil properties are varied and complex. The interactions relevant to the operation of EPB machines are those which can affect the properties of the soil in the short-term: under normal operating conditions, the soil only remains for a period of 10 to 15 minutes in the excavation chamber before being discharged by the screw conveyor. Long-term effects are only pertinent to the transport and disposal of the spoil and are therefore not relevant to the machine operation. The mixture in the excavation chamber of a tunnelling machine is highly heterogeneous, since only limited mixing power is provided. In clay, discrete lumps may be produced by the drag teeth or bite cutters of the cutting head, the mixture being likely to consist of soil cuttings which may range from a few millimetres to approximately 400 mm in diameter, depending on the properties of the in situ ground. As a result of the short mixing time, injection of soil conditioning agents can only have a limited effect on the bulk properties of aggregates formed by large lumps of soil. The action of foam, polymer or bentonite may only alter the interface properties of the lumps by lubricating their interface and binding them together to reduce the macro pores of the cut material. This reduces the shear strength of the entire mixture and prevents a recompaction of the lumps under the effect of the large confinement pressure in the excavation chamber (up to 300 kPa). In coarse grained soil, on the contrary, a much more homogeneous mixture may be obtained because of the higher permeability and the cohesionless nature of granular soil. Foam is believed to integrate the sand matrix to produce a relatively homogeneous mixture of sand grains and foam bubbles. In mixed face conditions, for example when a sand lens is

encountered within a clay formation, the heterogeneity of the material in the excavation chamber will be exacerbated, and the characterising the properties of the material contained in the excavation chamber is difficult.

While some systematic research into the properties of conditioned soil was initiated in the mid 90's, the majority of published work dealing with the effects of soil conditioning is related to specific tunnelling projects. In addition, the majority of the research focused on soil conditioning of granular soils. This perhaps reflects that soft and medium stiff clays needed not much conditioning to attain a suitable consistency for *EPB* machines, while stiffer clays could in most cases be excavated in open-mode, hence obviating the use of soil conditioning. As tunnel diameters increase and tolerances on volume loss reduce ( $V_L < 1\%$  is often specified), closed-mode operation has become necessary, even in stiff clays. In response, some research on the effects of foam and polymers on clayey material were carried out recently. The salient observations that emerged from different laboratory index tests may be summarised as follows:

*Effects of conditioning on sand:*

- The stability of foam is considerably increased when mixed with sand. The foam bubbles in the sand matrix were found to survive for several days, while the foam on its own would degrade within hours (Maidl, 1995; Houlsby & Psomas, 2001).
- When penetrating through high permeability sand and gravels, foam fully displaces the pore water and the foam bubbles remain intact. Test results suggest that foam can penetrate several centimetres into the excavation face and prevent ingress of ground water into the excavation chamber (Maidl, 1995).
- Sand ( $d_{50} = 0.2$  mm) with permeability of the order of the order of  $k = 4 \cdot 10^{-4}$  m/s can be made 'impermeable' to water for over 40 minutes under a hydraulic gradient of  $i = 20$  when previously flushed with a foam generated from a surfactant solution containing 0.7% carboxymethylcellulose polymer (Maidl, 1995).
- The addition of a structuring biopolymer to foam can prevent the segregation of fines in coarse sands or sandy gravels. Foam alone cannot prevent flow of water and washout of fines, and the resulting matrix of coarse grains is too stiff and its shear strength too high to allow *EPB* operations.

- The stability of foam in a sand matrix was found to be independent of the relative air and water content in the foam (*FER*), but was significantly increased when 0.7% carboxymethylcellulose (*CMC*) was added to the foaming solution (water and surfactant). Higher concentrations of *CMC* did not improve the stability of the foam.
- Non-ionic polymers of sufficiently large molecular weights can adsorb onto electrically neutral soil particles; a gel may arise around the particles to form a ‘cohesive matrix’ with reduced friction between the sand grains (Babendererde, 1993) and “binding together coarse grained soils” (Boone *et al.*, 2005).
- The compressibility of granular materials is considerably increased when mixed with foam (Maidl, 1995; Houlsby & Psomas, 2001).

*Effects of conditioning on clay:*

- The Atterberg limits of E-Grade kaolin and reconstituted London Clay prepared with water and water-based solutions of *PHPA* polymer were determined by Merritt (2004). He found that the liquid limit,  $w_l$ , increased from 50 to 90% and from 70 to 120% when adding 0.5% *PHPA* to E-Grade kaolin and London Clay, respectively.
- The bulk shear strength of an aggregate of natural London clay cuttings conditioned with various combinations of foam and polymers was investigated by Merritt *et al.* (2003) and the results may be found in Merritt (2004). Clay cuttings passing a 25 mm mesh were mixed with foams or polymer solutions under atmospheric pressure in a drum mixer for approximately 30 to 60 seconds. The polymer was found to increase the shear strength of the mixtures compared to that measured when water only was added to the clay (at identical water content).
- Clay-foam mixtures were found to behave in a fundamentally different manner than sand-foam mixtures. While the shear strength of conditioned sand rapidly reduces to extremely small values (< 5 kPa) as the injected quantity of foam is increased, this is not observed when foam is added to clay cuttings (under atmospheric pressure). For foam injection ratios (volume ratio of foam to soil, *FIR*) of up to 60%, the foam was found to break down as the foaming liquid was adsorbed by the clay. Only when large foam quantities (*FIR* > 200%, measured at atmospheric pressure) were injected, could the shear strength of the clay mixture be reduced to values in the region of 25 kPa (Merritt *et al.*, 2003).

- 
- Slump tests on different soil types mixed with a range of *FIR* are reported in Leinala *et al.* (2000). Fig. 6.3 shows results consistent with those of Merritt *et al.*: *FIRs* of over 300% were necessary to reduce the slump values to that obtained of sand mixed with considerably smaller quantities of foam (about one third).
  - When conditioning London Clay cuttings, the addition of *PHPA* polymer to the foam cuttings was shown to prevent breakdown of the foam. This is probably as a result of the polymer coating the clay lumps, which in turn reduces the adsorption of the foaming liquid by the clay. In such instances, foam could be seen in the macro pores of the clay matrix and the shear strength of the mixtures was (at identical water content) lower than when foam, water or polymer were added separately (Merritt *et al.*, 2003).
  - Polymers influence the adsorption potential of water onto the clay surfaces and are therefore thought to prevent the clay from recompacting in the excavation chamber. Polymers are also said to reduce the ‘stickiness’ of plastic clays, therefore reducing the adhesion of the clay onto the metal surfaces (Maidl, 1995).
  - In addition, polymer coating around the clay cuttings lubricates their interface and reduces the shear strength of the mixture in the excavation chamber, essentially leaving a conglomerate of stiff to hard clay lumps separated by a soft and slippery interface with the appearance of a soft paste of low shear strength (Maidl, 1995).
  - In groundwater with high salinity or contaminated with electrolytes, solutions of anionic polymer help neutralise cations that would otherwise tend to disperse the clay and prevent the formation of a plastic paste (Maidl, 1995).
  - Solutions of anionic polymer of small molecular weight reduce adhesion of plastic clay to metal surfaces (Maidl, 1995).
  - Interactions with polymers of small molecular weight are predominantly governed by the ionic strength of the polymer and hence the electrical interactions with charged clay minerals (Maidl, 1995).
  - Anionic surfactants are best used for foam generation as their negative charge is not absorbed by the clay particles (Maidl, 1995).

#### 6.3.4 Recommendations for selection of soil conditioning parameters

The primary source of recommendations for the selection of product type, their dosage rate ( $c_s$  and  $c_p$ ) and injection quantities ( $FIR$  and  $PIR$ ) are those provided by the suppliers of conditioning products. These recommendations, which may be found in trade literature of each supplier, are usually based on qualitative description of the average soil type, but often take limited account of the engineering properties of the soil. For each marketed product available, a series of benefits are usually quoted and a range (usually quite large) of dosage and injection rates is suggested.

A special guideline for the use of “specialist products for soft ground tunnelling” was published in 2001 by EFNARC and reedited in 2005. This more recent version of the EFNARC guidelines provides specifications for product qualities, and suggests the parameters to be obtained in geological investigations in view of selecting soil conditioning products. The EFNARC recommendations for the selection of product type and dosage rate are summarised in Table 6.1. It can be seen that a combination of foam and polymer are recommended in every type of ground. Different foam types are recommended as a function of the soil grading, but no distinction is made regarding the type and concentration of the polymer to be used in different ground conditions. In addition, although the quality of each foam type is described, their chemical composition is not revealed, hence making the correlation with fundamental research difficult. These guidelines further recommend that the concentration of surfactant be in the range of 0.5 - 5% and that the foam should be prepared to an  $FER$  of 5 to 30 (calculated at working pressure, *i.e.* the pressure in the excavation chamber). Although the EFNARC guidelines recognise the need to measure the engineering properties of the soil, their recommendations for soil conditioning are based on its particle size distribution only.

Alternative and complementary recommendations may be found in the technical literature, but these are usually based on the experiences acquired on a limited number of specific tunnelling projects rather than on systematic research. These contributions are nevertheless invaluable and are summarised in Maidl (1995), Milligan (2000 and 2001), as well as in Merritt (2004). Jancsecz *et al* (1999) advised on the need of soil conditioning as a function on the grading curve of the soil, as showed in Fig. 6.4. A summary of soil conditioning needs in different ground conditions was compiled by Milligan (2001) and is reproduced in Table 6.2, in which the difficulties that might be encountered in each type of soil and the proposed conditioning treatment to mitigate these problems are also summarised. Milligan (2001) reports that the  $FIR$  should be chosen so that the foam volume corresponds to the void content of the cut material after the material has bulked up in the excavation

chamber. Limited evidence suggests that this would yield *FIRs* of between 20 and 30%, but evidently, the difficulty resides in the determination of the volume of voids in the excavation chamber. Kusakabe *et al.* (1997) proposed a formula to calculate an adequate *FIR* as a function of the particle size distribution of the soil, while Maidl (1995) suggested that the foam volume should be such that the cumulated volume of fines (< 0.06 mm), pore water and foam matches the pore volume of the loosest possible packing of the coarse grain matrix (> 0.06 mm). These two methods give similar results, but they are not applicable to determine foam dosage in clayey ground conditions. For clayey ground conditions, Maidl (1995) reports that the ideal properties of conditioned mixtures should be of low to intermediate plasticity ( $I_p = 10 - 20\%$ ) and at such a water content that their consistency index falls in the range  $I_c = 0.4 - 0.75$ , corresponding to a very soft clay undrained shear strength of between 5 to 25 kPa. The consistency of clay soil may be increased by adjunction of water, and the Atterberg limit tests reported in § 6.3.2 showed that the polymer solutions may greatly affect the plastic and liquid limit of the clay, and hence, its consistency index. However, no specific guidelines are currently available to indicate the product type and quantities required to achieve a clay-conditioning agent mixture with the consistency recommended by Maidl.

### 6.3.5 Field observation of soil conditioning effects

Published case-studies of soil conditioning are scarce in comparison to the large number of worldwide tunnelling projects where *EPB* machines are employed. The majority of these case-studies describes the properties of the excavated ground and gives average injection rates of soil conditioning agents. Importantly, anecdotal evidence of the machine behaviour is often documented, giving invaluable information as to the problems encountered and the effect of conditioning agents. Milligan (2000 and 2001) summarised some of the reported case-studies, and Boone *et al.* (2005) tabulated the different conditioning treatment used on eight different projects (Table 6.3). Relevant information from other published case-studies are summarised in Table 6.4. This table highlights the problems encountered in driving the *EPB* machine and, when available, gives details of the soil conditioning treatments. The key lessons and observations learned from the case studies condensed in Table 6.4 may be summarised as follows:

- The main difficulties encountered were related, in clay soil, to the ‘stickiness’ of plastic clays, and in coarse granular soil, to the segregation or ‘wash out’ of fine particles from the matrix of coarse grains. Both ‘symptoms’ resulted in high

cutter head torque, difficulty in controlling the face pressure, and in coarse granular soil, poor control the water inflow through the screw conveyor.

- Conditioning ‘sticky clays’ with large quantities of foams ( $FIR > 100\%$ ) often successfully eliminated or reduced clogging problems. The segregation of fines from the matrix of coarse granular soils could be prevented by the addition of a water binding polymer to the surfactant solution. The use of such polymer-enhanced foam allowed control of groundwater pressure in coarse soils by temporarily reducing their permeability.
- Geotechnical characterisation of the muck in the excavation chamber was only reported in one of the projects summarised in Table 6.4: Bezuijen *et al.* (2005) found that saturated sand conditioned with foam remained, under the conditions encountered in the excavation chamber (*i.e.*  $\sim 300$  kPa total stress), above its maximum density (in the absence of foam). The shear strength of the mixture was measured in the laboratory and values of the order of 1 kPa are reported.
- Bentonite or crushed limestone were injected in a few cases to increase the fines content of gravely soils.

## 6.4 Impact of *EPB* machines

### 6.4.1 Face stability

Pressurising the excavated soil in the excavation chamber of *EPB* machines aims to prevent instability of the tunnel face and to reduce ground movements around the excavation. The determination of adequate face pressure to guaranty the stability of the face is discussed by Krause (1987), Anagnostou & Kovári (1994) or Jancsezc & Steiner (1994), amongst many others. This section avoids repeating their conclusions but focuses instead on the relation between face stability and the operating parameters of the *EPB* machine, in particular the “face pressure” and the pressure in the excavation chamber. The previous sections showed that the provision of satisfactory face pressure is only possible when soil conditioning is used to alter the properties of the mixture in the excavation chamber. The interactions between these properties, the control of face pressure as well as the operation of the machine are crucial to the determination of soil conditioning treatments.

In slurry machines, the properties of the support medium in the excavation chamber are relatively homogenous and well understood, and the total support stress imparted to the tunnel face solely depends on the slurry pressure. In contrast, the mixture of

soil and conditioning agents in the excavation chamber of an *EPB* machine is highly heterogeneous. The ‘earth pressure’, usually measured on the bulkhead at the rear of the excavation chamber, is often assumed to act as a supporting pressure to the excavated face, in addition to the stress imparted to the tunnel face by the cutting head, as discussed in § 6.2.1. However, as emphasised by Anagnostou & Kovári (1994), the pressure in the excavation chamber is transmitted to the face as a fluid as well as an effective pressure in proportions that mainly depend on the properties of the conditioned soil. The heterogeneity of the material makes the independent control of one or the other of these two components difficult. In addition, the strength of the material, which may vary between 1 to 30 kPa, means that during rotation of the cutting wheel, the intense shear distortions, the mixing process and the possible arching of stress between the openings of the cutting wheel may prevent the pressure in the excavation chamber from being fully transmitted to the face. The transmission of pressure from the chamber to the face depends on the properties of the conditioned soil, the geometry of the excavation chamber and the cutting wheel, as well as the operating condition of the machine. Little or no research on these different interactions has been published to date.

While a high consistency of the material in the excavation chamber of an *EPB* machine makes the control of the face pressure difficult, it prevents substantial collapse of the ground into the tunnelling machine. However, as reaffirmed by Feng (2004), “true *EPB* drives require that the working chamber is always filled with earth”. Only under this condition may instabilities be prevented, in particular local collapses of the face. The stability of the tunnel face in granular soils also requires the control of the ground water pressure. In *EPB* machines, this occurs by maintaining a fluid pressure in the excavation chamber in order to at least resist the pore water pressure of the ground. This can be achieved if the permeability of the bulk material is sufficiently low to prevent seepage flow through the screw conveyor and therefore uncontrollable water ingress into the tunnel.

#### 6.4.2 Ground movements

While face stability is normally guaranteed when *EPB* machines are operated in closed-mode, *i.e.* when the excavation chamber is continuously filled with a soil mixture of the intended consistency, ground movements often remain a source of concern. A large proportion of the volume loss caused by shield tunnelling is due to stress relief at the face of the tunnel (face loss). This component of volume loss predominantly depends on the magnitude of the pressure supporting the face during the excavation.

Shirlaw *et al.* (2002 and 2003) reported back-analyses of face pressure measurements in relation to measurements of the volume loss induced by the tunnelling process on the North East Line in Singapore, where 20 km of tunnels were excavated with *EPB* machines. The 6.5-m diameter tunnels were driven through the *Kallang* formation, (which predominantly consists of normally consolidated clays of  $S_u \approx 30$  kPa), alluvial sands and clays, as well as other geological units as detailed by Shirlaw *et al.* (2003). Measurements of surface settlement indicated a volume loss smaller than 0.5% along most of the route, which is usually deemed acceptable in terms of ground movement and impact on existing structures. However, “20 incidents of very high, local ground loss or sinkholes” were reported. In three cases, the volume of the depression caused by the tunnelling machine reached 30 m<sup>3</sup> and two larger depressions of 50 and 67 m<sup>3</sup> were also measured. A water main was also reported to break as the *EPB* machine passed beneath it. The high volume losses occurred in all the soil formations encountered. No consistent trend was discerned between the volume loss and the face pressure (probably principally equal to the pressure in the excavation chamber) normalised by the total overburden pressure. However, Shirlaw and his co-workers concluded that all the sinkholes and other cases of excessive settlements were “related to the use of inadequate face pressure”, and that the use of *EPB* machines in varying mixtures of rock and granular soils below the water table remains problematic. Soil conditioning treatments and further operational factors of the *EPB* machines were not reported in detail. Surface depressions and sinkholes similar to those that occurred on the North East Line in Singapore were also caused by *EPB* machines on the construction of the Jubilee Line Extension in London (Withers, 2001).

## 6.5 Conclusions

This chapter has addressed the operation of *EPB* machines in relation with the provision of face support and its impact on face stability and ground movements induced by the tunnelling process. The following conclusions that can be derived from the material reviewed in each section may be summarised as follows:

### **Earth pressure balance machine technology (§ 6.2)**

- *EPB* machines have been used in a wide range of ground conditions, from stiff and highly plastic clays to coarse gravelly sands, both above and below the water table.

- 
- *EPB* machines can excavate large tunnels of over 9 m diameter under safe conditions and with acceptable impact on the surrounding ground and structures. Large pore water pressure in highly permeable grounds may, under certain conditions, be withstood.
  - The control of face pressure is often difficult when the ground conditions depart from the ‘optimum’ conditions for which *EPB* machines were originally intended.

### **Soil conditioning in *EPB* machines (§ 6.3)**

- Detailed reports of soil conditioning treatments, including the chemical type, as well as the dosage and injection rates are scarce. Soil conditioning treatments are predominantly selected on a trial-and-error basis and existing guidelines do not account systematically for the engineering properties of the ground.
- The effects of some foam and polymers on reconstituted and natural clay have been investigated, but the mechanisms that make each conditioning agent a successful additive and the implication of the results for practical applications are not yet fully understood.
- Little research only has been carried out on the way in which the operation of *EPB* machines is affected by soil conditioning and, in turn, how the ground response to the tunnelling operation is influenced by improved control of the machine operation.

### **Impact of *EPB* machine (§ 6.2)**

- Large sinkholes and excessive ground movements still occur, especially when difficulties in controlling the pressure in the excavation chamber are encountered.
- Multi-variable regression analysis of the *EPB* machine data was performed (Leinala *et al.*, 2000) to assess the effect of its operational parameters on the mining rate. While such analyses are useful in identifying trends, it is not clear whether the mining time is a consistent indicator of the machine performance. A physical description of the interactions between the machine, the conditioned ground and the ground movement should be sought to complement statistical approach.

***Endnote***

<sup>1</sup>The dimensionless volume loss,  $V_L$ , is defined as the volume ratio expressed as a percentage of  $V_s$ , the volume of the settlement trough due to tunnelling, and  $V_T$ , the excavated volume of the completed tunnel.

Soil	Foam Type				Polymer additive
	A	B	C	FIR	
Clay				30-80	Anti clogging polymer
Sandy clay - silt				40-60	
Sand - clayey silt				20-40	Polymer for consistency control
Sand				30-40	Polymer for cohesiveness and consistency control
Clayey gravels				25-50	
Sandy gravels				30-60	
Foam type A:	High dispersing capacity (breaking clay bond) and / or good coating capacity (reduce swelling effects).				
Foam type B:	General purpose, with medium stability.				
Foam type C:	High stability anti segregation properties to develop and maintain a cohesive soil as impermeable as possible.				

Table 6.1 Guideline for the application of soil conditioning (EFNARC, 2005)

Soil type	Mining characteristics	Treatment	
Plastic clays	Tend to reconstitute with little loss of strength in machine chamber.	High dosage of foam at head to keep excavated material as separate pieces.	
Laminated, silty or sandy clays	Break up better, but still tend to reconstitute, slightly abrasive, form plug.	Possibly none other than water to reduce shear strength to acceptable value; in stiffer clays, medium dosage of foam at head. Possibly add lubricant to foam to reduce abrasion.	
Clayey sands and gravels.	Flow easily, may form plug if fines content in excess of 10%; highly abrasive.	Add lubricant polymer at head to reduce wear; add water-absorbing polymer at screw if required to form plug and control water inflow.	
Silty fine sands	Do not flow, do not form plug, allow ground water inflow, highly abrasive; problems increase with larger particle sizes.	Foam with polymer additive to stiffen foam and provide lubrication; approximate dosage rates for polymer:-	0.1%
Sand/gravel			0.25%
Gravel and cobbles			1 - 3%
Cobbles and boulders	Tend to congregate in clumps in head and/or jam screw.	Large dosages of additive to keep cobbles separate in head and provide water control and lubrication.	

Table 6.2 Soil conditioning application in *EPB* machine  
(Milligan, 2001)

Soil	Conditioning Agents	C <sub>F</sub> or C <sub>P</sub> (%)	FIR (%)	FER	Performance Notes	Reference
sand	N <sub>a</sub> -polyacrylate powder	0.5 to 3 (P)	55 to 60		20 to 10 cm slump, viscosity of polymer-water mix 1x10 <sup>4</sup> to 2x10 <sup>4</sup> (cp), mixing time increased slump	Tamai et al. (1989)
	N <sub>a</sub> -polyacrylate powder	0.5 to 3 (P)	55 to 60		15 to <1 cm slump, viscosity of polymer-water mix 1x10 <sup>2</sup> to 5x10 <sup>4</sup> (cp), mixing time increased slump	
	Vinyl acetate-acrylic acid copolymer	0.5 to 3 (P)	55 to 50		12 to 4 cm slump, viscosity of polymer-water mix 1x10 <sup>3</sup> to 1x10 <sup>4</sup> (cp), mixing time increased slump	
	isobutylene-maleic acid copolymer	0.5 to 3 (P)	55 to 50		16 to 2 cm slump, viscosity of polymer-water mix 1x10 <sup>4</sup> to 2x10 <sup>4</sup> (cp), mixing time increased slump	
soft clay	Mix A	3 (F)	20	8	Mix to achieve "plastic flow" but to avoid creating a "state of mud"	Kodama & Yamaguchi (1990)
sand & clay	Mix A	3 (F)	30	8		
sand & gravel	Mix B	1 (F) 2 (P)	60	6		
hard clay	Mix A	3 (F)	40	8		
gravel, sand	anionic surfactant, synthetic polymer	1.5 (F) 0.7 (P)	40 to 80	5 to 8	above water table, FIR adjusted to maintain slump between 5 and 15 cm	Peron & Marcheselli (1994), CT (1994)
Gravel	anionic surfactant, synthetic polymer, bentonite	1 (F) 2 (P) 7 (B)	15 to 22, with 12 to 18 of B	6	bentonite slurry consisted of sand, water, and bentonite (sand content ?), slump maintained between 4 and 8 cm	Kanayasu et al. (1995)
clay & sand	surfactant	5 (F)	50 to 150	10 to 15	used to prevent clogging of TBM	World Tunneling (1996)
sand, gravel, fines	anionic surfactant, synthetic polymer	0.7 (F)	25 to 35	10		Wallis (1995), Herrenknecht & Maidl (1995)
silty sand	anionic surfactant	1 to 5	5 to 15	10	for a slump of 12 cm	Quebaud et al. Henry (1998).
silty sand & gravel	anionic surfactant, CMC polymer	3 (F)	30	10	for primarily granular soils with fines	Williamson et al. (1999)
sand & gravel	anionic surfactant, CMC,	1 (F) 2 (P)	30	8	for coarser-grained soils	
sand, gravel, cobbles	anionic surfactant, CMC, acrylic polymer, bentonite	1 (F) 2 (P) 100 (AP) 10 (B)	30 0.8 45	8	mix of foam (with CMC), direct addition of acrylic polymer, and bentonite slurry for mining under high water pressures, 8 l/m <sup>3</sup> of AP used directly in slurry	
uniform sand	synthetic polymer foaming agent and PHPA with VCP oil and other polymers, bentonite	3 (P) 0.7 (AP) 3 to 4 by dry mass (B)	20 to 50	9 to 40	multiple protein-based polymers were used with similar behavior, foam sustained high voids ratios in foam/sand mix at relatively high stresses in Rowe-cell compression tests, most important variable was FIR rather than agent type, polymer with excessive water had negative affect on foam stability	Psomas & Houlsby (2002)

C<sub>F</sub> = concentration of foaming agent by weight in water; C<sub>P</sub> = concentration of polymer by weight in water; FIR = foam injection ratio; CMC = carboxyl methyl cellulose; (F) = foaming agent, or surfactant; (P) = polymer; (AP) = additional polymer; (B) = bentonite

Table 6.3 Case-studies of soil conditioning (Boone *et al.*, 2005)

Project/Tunnel diameter	Ground conditions	Problems encountered	Conditioning treatment	Remarks	Reference
WMATA, Washington, US - 5.7m	Clay / Clayey sand / gravelly sand.	High plasticity stiff to very stiff clays sticking in head chamber.	Adjunction of water made clay too slippery for belt conveyor.	Problems to control face pressure in mixed face conditions with layers of sand and clay.	Clough & Leca (1993)
Passante Ferroviario, Milan, Italy - 8.0 m	Alluvial sandy and gravelly soils (<20% fines), above GWT <sup>1</sup> .		FIR = 60-80% FER = 5-8% c <sub>f</sub> = 1.5% c <sub>p</sub> = 0.7% (cellulose)	5% water was added in dry sections, and FIR was reduced to 50-60% in the water bearing ground.	Perron & Marcheselli (1994)
Metro Line 5, Valencia, Spain - 6.5 m	Alluvial sands and gravels (<15% fines), lenses of stiff silty clay, below GWT.	Bentonite injection only, but difficulties due to incompressibility of mixture.	FIR = 20-30% Foam gave better results, more compressible material.	Permeability up to 10 <sup>-3</sup> m/s, too high for slurry shield.	Wallis (1995), Herrenknecht & Maidl (1995)
West Seattle Tunnel, Seattle, US - 3.4 m	Clay, silt, sands and gravel.	Partial collapse of sand into head chamber when foam was used. Bentonite was therefore introduced.	Foam, bentonite, and polymer (c <sub>p</sub> = 0.5-2%)	Foam did not seem to reduce torque and wear.	Webb & Breeds (1997)
Metro, Lille, France - 7.7m	Flanders clay.	Clay caused clogging in the head chamber	Foam	12 injection nozzles in head chamber, 6 on the cutting wheel, 2 on screw conveyor.	Mauroy (1998), Babendererde (1998)
Storebaelt, Danemark - 8.7m	Glacial till with water-bearing lenses (220kPa), hard fissured clays.	Control of low plasticity water content. Machine wear.	Foam and polymer.	Mechanical stirring should be arranged to stir polymer in the head chamber.	Doran & Athenoux (1998)
South Bay Ocean Outfall, San Diego, US - 4.0m	Marine sediments: OC clays - silt, sands, gravels, cobbles and boulder. High permeability.	When only foam used, fines and foam were washed out gravel matrix, and gravel then clogged conveyor.	FIR = 25-35% (average) BIR <sup>2</sup> = 50% in gravels	Chamber pressures >700kPa: dealt with by adding an anionic acrylamide polymer to	Williamson <i>et al.</i> (1999)

Table 6.4. Summary of EPB machine case-studies with soil conditioning



Project/Tunnel diameter	Ground conditions	Problems encountered	Conditioning treatment	Remarks	Reference
Light Rail Transit System, Izmir, Turkey - 6.5m	Gravelly and silty sands / clayey and sandy silts / clay with water content above liquid limit	Screw conveyor worn down on 140mm.	No foam necessary in silty soil with sand layers. FIR>200% in clay with $I_c=0.65$ , $S_u=74\text{kPa}$ .	Laboratory test showed that polymer may reduce permeability of clayey silt as much as bentonite.	Janscecz <i>et al.</i> (1999), Langmaack (2000)
Aviles, Spain - 4.0m	Gravelly beach sand <sup>1</sup>	Washout of foam and fines from the coarse grain matrix.	Foam with 2-4% water binding polymer (Meyco Fix SLF P1).	Polymer additives strongly reduced segregation of fines from gravel matrix.	Langmaack (2000), Feng (2004)
Sheppard Subway Twin Tunnel, Toronto, Canada - 5.9m	Glacial silty sand / clays / soft and hard tills, below GWT with water pressure of 150kPa.		Foam in all types of ground FIR > 100% in hard till.	Statistical analysis correlating machine data (FIR, FER, torque, thrust, etc.) to mining time.	Leinala <i>et al.</i> (2000)
Metrosur, Madrid, Spain - 9.3m	High plasticity 'Tosco' with 80% clay and silt.	Foam did not prevent clogging of cutterhead and head chamber: frequent stoppages for cleaning.	Polymer was added to the foam and solved clogging problems.		Maynar <i>et al.</i> (2000), Feng (2004)
Botlek Rail Tunnel, The Netherlands - 9.5m	Saturated sand with tunnel axis 23m below water table.		Foam only, muck density above maximum sand density and shear strength around 1kPa.	Pore water pressure measured in head chamber. 20 muck samples retrieved from head chamber.	Bezuijen <i>et al.</i> (2005)
Lot 5 Turin Subway, Turin, Italy - 8.0m	Glacio-fluvial gravel, sand and cobbles with 15% clay and silt. Partially below GWT	Muck too liquid for belt conveyor / difficulty in controlling face pressure	Anionic surfactant with a guar-gum polymer. FIR = 40%, FER = 8	Fine crushed limestone injected to increase fine content (5-10% of excavated volume).	Boone <i>et al.</i> (2005)

<sup>1</sup>Ground water table<sup>2</sup>Bentonite injection ratio

Table 6.4. Summary of EBP machine case-studies with soil conditioning (continued)

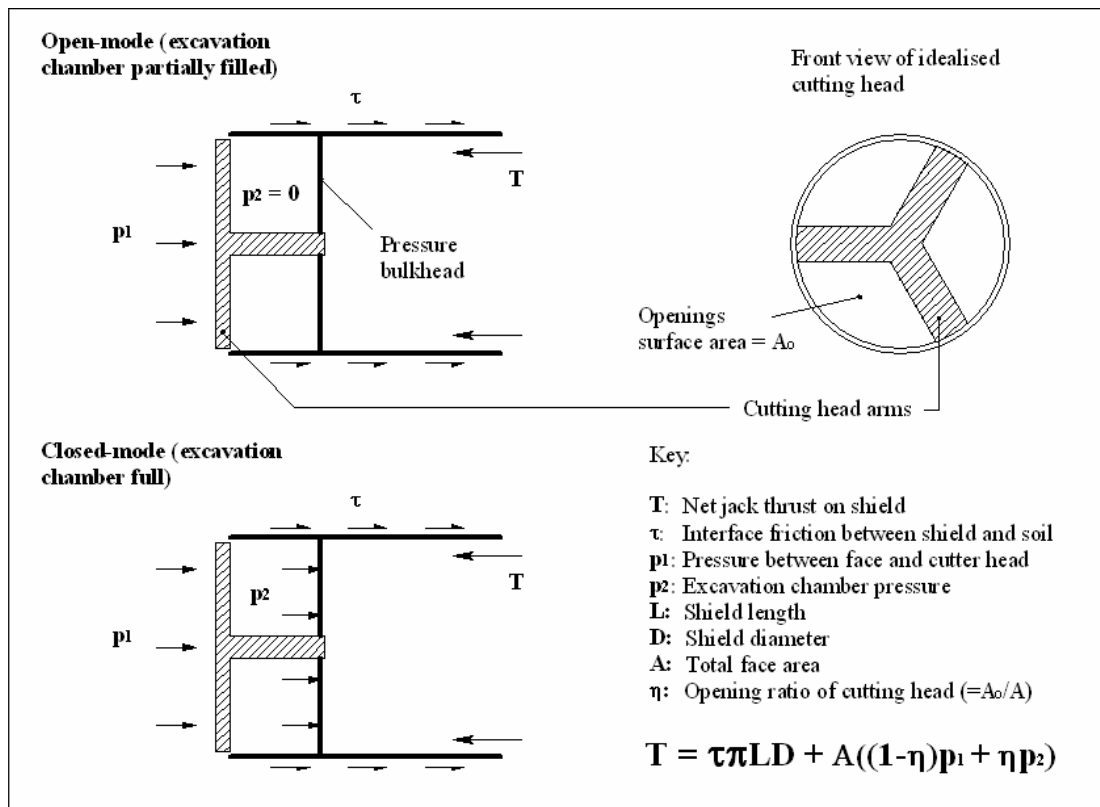
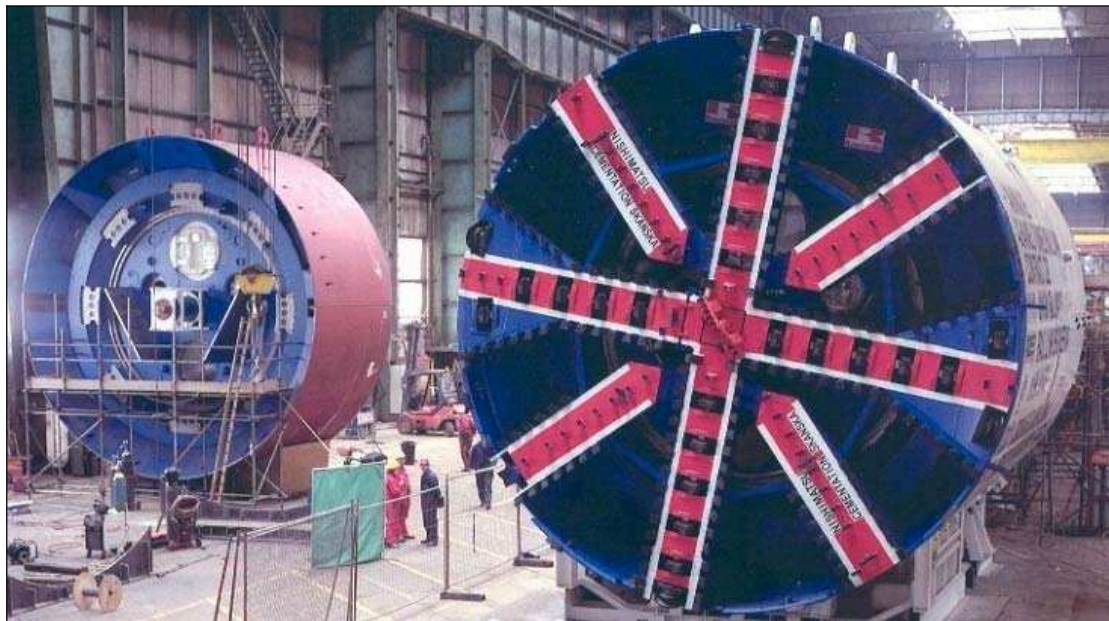


Fig. 6.1. Horizontal forces acting on an idealised EPB machine



(a)



(b)

Fig. 6.2. Example design of cutting wheel of EPB machine: (a) Herrenknecht machine (Metrosur, Madrid, Spain), 9.4 m diameter, 31% face opening (Maynar *et al.*, 2000); (b) Kawasaki (CTRL, London, UK), 8.5 m diameter, 57% face opening (courtesy Rail Link Engineering).

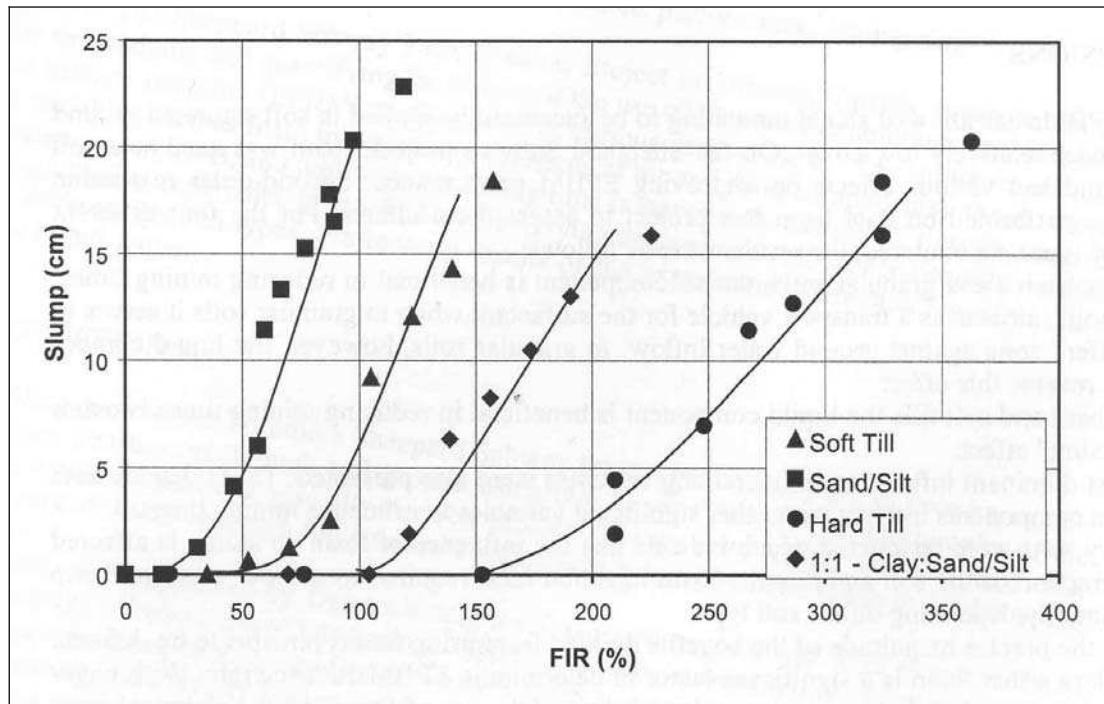


Fig. 6.3. Foam injection ratio (*FIR*) versus slump test results (Leinala *et al.*, 2000)

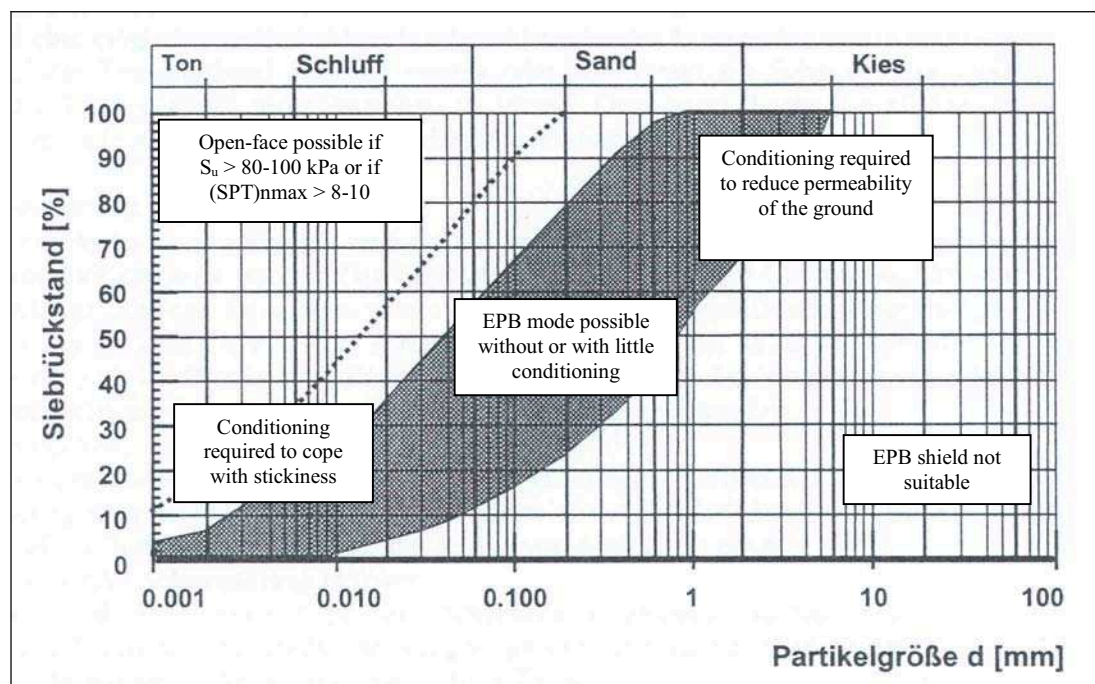


Fig. 6.4. Soil conditioning *needs* in different types of ground (Jancsecz *et al.*, 1999).

## **CHAPTER 7: FIELD DATA OF EPB MACHINES**

### **7.1 Introduction**

#### 7.1.1 Background and objectives

The objective of this chapter is to answer some of the questions raised in chapter 6. Monitoring data from the earth pressure balance (*EPB*) machines used on the Channel Tunnel Rail Link (*CTRL*) project are back-analysed to investigate the interactions between soil conditioning, the machine behaviour, and the ground movements induced by their operation. The *CTRL* tunnels were excavated in a wide range of ground conditions, and a series of laboratory experiments was carried out prior to the tunnelling works to assess the effects of conditioning on the main types of ground that had to be excavated. This chapter compares the soil conditioning applied in this project to the recommendations suggested by the laboratory tests and by the guidelines discussed in § 6.3.4. The effects of soil conditioning on the control of the *EPB* machines are also analysed.

### 7.1.2 Chapter layout

Some background to *Contract 220* of the *CTRL* project is first given, followed by a summary of the ground conditions and a description of the *EPB* machines (§ 7.2). The machine and the ground movement data are then analysed and presented in a way that mirrors the structure of chapter 6: the application of soil conditioning and the machine behaviour are analysed first (§ 7.3), before considering its impact on the ground volume loss (§ 7.4). In each section, the data of the entire tunnel route is summarised in tabular form, but detailed analyses focus on the three main types of ground conditions, namely the Thanet Sand, the Lambeth Group and the London Clay. This is followed by a discussion of the results: the conditioning required in the soil strata encountered in London is compared to existing recommendations and the control of face pressure as well as its effects on the ground movements are then discussed (§ 7.5).

## 7.2 Channel Tunnel Rail Link Project; *Contract 220*

### 7.2.1 Project overview

Eighteen kilometres of twin-bore tunnels were excavated in London between late 2002 and early 2004. This work was commissioned by Union Railways (North) Ltd and formed part of the *CTRL* project, a 109 km high-speed railway line between London's St Pancras station and the Channel Tunnel.

This chapter focuses on *Section 2* of the *CTRL*, and in particular on *Contract 220*, constructed by the contractor Nishimatsu/Cementation/Skanska. The tunnelling works of *Contract 220* comprised 7.5 km twin-bore tunnels excavated westwards from Stratford Box to Gifford Street Portal near St Pancras station and two ventilation shafts at Graham Road and Corsica Street, as shown in Fig. 7.1. The excavation diameter was 8.11 m, and the temporary lining of the tunnels consisted of nine gasketed, fibre-reinforced concrete segments forming a ring of 7.85 m outer diameter, therefore leaving a 130-mm thick tail void. The tunnel depth to axis increased from about 8 m at Stratford Box to approximately 40 m at Graham Road, before reducing to 5 m as the tunnel ascended towards the west portal. The structures overlying and surrounding the tunnels comprised 5 km of retaining walls, 28 bridges, several gas and water mains, as well as the North London Flood Relief Sewer and the four tunnels of the Victoria Line and the Great Northern & City Line. The closest of these existing tunnels is about 10 m, and the flood relief sewer just a couple of meters above the crown of the *Contract 220* tunnels, and hence required the ground movements caused by the new tunnels to be rigorously controlled. Further details of

the tunnelling works of *Section 2 CTRL* are described in the literature (*Tunnels & Tunnelling*, vol. 35(9), 2003).

### 7.2.2 Ground conditions

The difficulty, and hence the significance, of *Contract 220* to the present research lies with the wide range of ground conditions encountered at the tunnel horizon. The typical geological sequence encountered along the route is summarised in Table 7.1. As shown on the longitudinal profile reproduced in Fig. 7.2 and Table 7.2, the tunnels were excavated through the full sequence of geological formations summarised in Table 7.1. Upon launching from Stratford Box, the tunnelling machines first went through 80 m of mixed face conditions of Upnor sands and the basal beds of the Lambeth Group clays. The proportion of Lambeth Group soil then gradually reduced for the next 140 m, while Thanet Sand appeared in the invert until reaching full face conditions Thanet Sand after 560 m of drive. For 1500 m, the tunnel crown then intermittently encountered the Upnor formation, which typically made up 30% of the excavation face. Chalk then appeared in the invert, reaching a maximum content of 50% near the Graham Road shaft. As the alignment then ascended towards the west portal, the tunnel crossed the full sequence of tertiary deposits, starting with the Thanet and Upnor sands and followed by the full sequence of the Lambeth Group units. Approximately 700 m were mined in rapidly changing mixed face conditions when the Harwich formation was encountered at the interface between the upper units of the Lambeth Group and the London Clay. The remainder of the drives continued in full face London Clay until 200 m before the west portal, where superficial soils increasingly appeared in the crown until forming 90% of the tunnel face.

The geological and hydrogeological conditions along the route of *Contract 220* were reported in a geotechnical design basis report based on 32 boreholes (Union Railways, 1997). This chapter focuses on the three sections (3, 8 and 10, Table 7.2) that were excavated in full face Thanet Sand, Lambeth Group and London Clay, respectively. The main features of these three formations may be summarised as follows:

#### **London Clay**

The London Clay stratum, usually overlain by Thames Gravel and made ground, is 40 m thick in the west portal regions and thins eastward to approximately 6 m. The upper few meters are weathered, firm to very stiff and extremely closely fissured (< 20 mm fissure spacing). It contains occasional silt or sand partings. The underlying

unweathered London Clay is also very stiff and extremely closely fissured but contains only rare silt and sand partings. Towards its base, the London Clay becomes sandier and siltier with more frequent partings. It may contain 100 to 300-mm thick beds of moderately strong mudstone. The London Clay was described as being of high to very high plasticity and firm to very stiff. Its undrained shear strength increases linearly with depth, from about 40 kPa at the top of the stratum to 250 kPa or more at its base.

### **Lambeth Group**

The Lambeth Group, formerly known as the Woolwich and Reading Beds, has historically led to problems in tunnelling due to groundwater problems and to the extraordinary lateral and vertical variability of the formation. The Lambeth Group strata are 15 to 25 m thick and comprise the Woolwich and Reading, and the Upnor formations. The main units of the Woolwich and Reading formation are described in Table 7.1 and more details on the lithology on the Lambeth Group may be found in Page & Skipper (2000) and Hight *et al.* (2001). The Lambeth Group clay formations (Upper Mottled Clay and Lower Shelly Clay, Table 7.1) comprise very stiff with intermediate to high plasticity clay, which is intermediately to extremely fissured and is usually sand free. The measured plasticity indices vary between 12 and 68% and the liquid limit between 30 and 95%. The Lambeth Group clays are very stiff and its undrained shear strength was measured at around 300 kPa.

The basal unit of the Lambeth Group is formed by the 3 to 12-m thick Upnor formation, which consists of silty sand. Continuous horizons of gravel or pebble beds in thicknesses of up to 3 m occur throughout the unit. They contain medium to coarse rounded flint gravel in a clay, sandy clay or sand matrix. Lenses of water bearing silt and dense sands may be encountered in both the London Clay and Woolwich and Reading Beds.

### **Thanet Sand**

The Thanet Sands consist of structureless fine and medium silty sand and are very consistent over the entire route of the tunnels. The unit is approximately 15 m thick to the west of Stratford Box, and thins to about 4 m at Corsica Street vent shaft. The permeability of the Thanet Sand was measured between  $5 \times 10^{-8}$  to  $1 \times 10^{-5}$  m/s. The Thanet Sand is underlain by the 300 mm to 1 m thick Bullhead Beds, consisting of flint gravel and nodular flints contained within a sandy clay or clayey sand matrix. The Upper Chalk is found immediately below the Bullhead Beds and the Thanet Sand. It is moderately weak and may contain large flints with unconfined

compressive strengths of up to 600 MPa. When excavated, the brittle flint leaves sharp fragments, which are believed to form a paste with the chalk and greatly affect the operation of the cutting wheel.

### Hydrology

Two aquifers were encountered within the tunnel area: the lower chalk aquifer and the upper superficial aquifer. The lower aquifer comprises the chalk, the overlying Upnor and Thanet Sands, and the basal beds of the Woolwich and Reading formation. The upper aquifer comprises the recent deposits of the superficial strata, namely the Terrace, Alluvial and Flood Plain Gravels, and is perched upon the underlying low permeability clay formations. In March 1996, the piezometric levels were measured at 70% and 50% of hydrostatic pressure in the London Clay and the Woolwich and Reading Beds, respectively. In addition, the ground water table in the lower aquifer (Thanet Sand) was lowered by pumping prior to the tunnelling work in order to reduce the water pressures of up to 330 kPa to ease the tunnelling works and, in particular, the construction of the cross passages.

#### 7.2.3 Design and instrumentation of the *EPB* machines

The ground conditions summarised above dictated the use of closed-face tunnel boring machines. The tunnels of *Contract 220* were excavated with two identical *EPB* machines designed by Kawasaki Heavy Industries. The shield of the machine had a diameter of 8.15 m and a total length of 11.3 m. The excavation chamber was conical and reduced to a diameter of 4.8 m at a distance of 2040 mm behind the tunnel face, where the pressure bulkhead was located.

The machine was equipped with a central shaft screw conveyor, whose characteristics are summarised in Table 7.3. The conveyor inlet was located approximately 1500 mm below the tunnel axis where it protruded 1285 mm into the excavation chamber. The conveyor was fitted with a double guillotine gate near the discharge point at the rear of the conveyor. Two earth pressure cells were located at the third points of the screw, and two injection nozzles for soil conditioning were arranged near these load cells. The screw drive consisted of four hydraulic motors, each delivering a rated torque of 12.1 kN·m, as detailed in Table 7.3. The angular speed of the screw was controlled by altering the engine oil pressure, rendering the accurate setting of a selected rotation speed difficult.

The cutting wheel of the machine was fabricated as an eight-arm open-star with a thin outer rim and a central shaft bearing. The opening ratio of the wheel was

approximately 57% of the excavated area (Fig. 7.5 and 7.6. No shutters were provided to close the free area between the cutting arms, so that support to the face had to be provided by the confined soil in the excavation chamber. The cutter arms were fitted with about 250 bite cutters, 20 disc cutters and two pairs of copy cutters to over-excavate around the shield when required. Seven injection nozzles for soil conditioning were distributed along the wheel radius and two additional ports were located in the screw conveyor, as mentioned above.

Both *EPB* machines were instrumented with about 130 instruments. The foam injection and expansion ratio (*FIR* and *FER*), as well as the polymer injection ratio (*PIR*) were monitored automatically, while the foaming liquid and polymer solution concentrations were logged manually by the tunnel crew. The total pressure in the excavation chamber was measured at 5 locations, distributed from -600 to 2000 mm vertical distance from the tunnel axis. The load cells were located on the pressure bulkhead, *i.e.* 2040 mm behind the excavation face. The locations of the load cell are shown in Fig. 7.7. Other parameters relevant to this chapter are tabulated in Table 7.4. All data was logged continuously for the entire duration of the construction at a data acquisition rate of 0.2 Hz and the data files were stored on a PC in *comma separated value* (\*.csv) files, each containing one day worth of data. These data files were separated into smaller files, each containing one ring worth of data, hence forming a data base of approximately 10,000 files which could be easily manipulated with *Matlab*.

### 7.3 Application and effects of soil conditioning

#### 7.3.1 Definition and presentation of data

The parameters that were introduced to describe the monitoring data of the *EPB* machines are defined in this section. The machine data in each of the eight ground conditions encountered at the tunnel axis depth are summarised by their average and standard deviation. The shove-build cycle corresponding to a 1500 mm excavation followed by the construction of a segmental lining ring will be referred to as “*ring*”. Between the excavation cycles, the cutter head and the screw conveyor come to a halt, and the thrust on the machine is reduced to allow the lining to be erected. Therefore, the data during that period of time are treated as independent experiments. Average values of machine parameter per ring have been extracted from the data. While average and standard deviation of all parameters were calculated for all the *rings* in each of the eight types of ground conditions, the data is only described

in detail for the three sections of excavation in full face Thanet Sand, Lambeth Group, and London Clay, respectively.

The soil conditioning applied in the different ground conditions will be described by four parameters, namely the *FIR*, the *PIR* and the *FER* defined in equations 6.1 to 6.3, and the total liquid injection ratio (*LIR*). Using the previous definitions (§ 6.3.2), the *LIR* can be written as follows:

$$LIR = \frac{V_{fl} + V_p}{V_s} = \frac{FIR}{FER} + PIR \quad \text{eq. 7.1}$$

where  $V_{fl}$  and  $V_p$  are the volume of foaming liquid and polymer solution, respectively, and  $V_s$  the volume of excavated soil. These four parameters were calculated for each ring, whereby  $V_s$  was taken as the volume of soil excavated (8.15 m OD by 1.5 m length) construction. Table 7.5 summarises the soil conditioning parameters in the eight different types of ground conditions encountered around the tunnel route, broadly classified as granular, cohesive and mixed granular and cohesive. For each type of face condition, Table 7.5 shows the average and the standard deviation of the values measured for all rings of the corresponding section (Table 7.2). The distribution of *FIR*, *FER*, *PIR* and *LIR* are plotted in Fig. 7.8 to 7.11 for the tunnel section in Thanet Sand, Lambeth Group, London Clay, and the section of mixed ground condition with Lambeth Group/Harwich Formation/London Clay. The injected quantities of soil conditioning agent and their effect on the machine behaviour are discussed for each of the three full face conditions in § 7.3.2 to 7.3.4.

Average machine parameters per ring and per section were also calculated. Following the definitions introduced in Fig. 6.1, the face pressure is carefully distinguished from the pressure of the conditioned material in the excavation chamber. The chamber pressure will be referred to as  $p_2$ , as defined in Fig. 6.1. This pressure undergoes large variations during each ring excavation, and because these variations are believed to (1) be a measure of the effectiveness of soil conditioning and control of the machine, and (2) be strongly related to the ground movements induced by the machines, several parameters were introduced to quantify these variations. These parameters are defined in Fig. 7.12, where the time series of chamber pressure (in full face London Clay) for the five earth pressure cells in the excavation chamber are plotted in Fig. 7.12a.

- $p_{2,range}$  characterises the uniformity of the pressure in the excavation chamber and is calculated as the average difference between the maximum and the minimum measurement of chamber pressure during the excavation and ring build.

- $p_2$  is the average reading from the five instruments (Fig. 7.12c) and is used to describe the other chamber pressure components.
- $p_{2,drop}$  quantifies the decay of chamber pressure that may occur between two excavation events and is defined as the difference between the maximum and the minimum chamber pressure during the build time.
- $p_{2,excav}$  and  $p_{2,mean}$  represents the average of  $p_2$  during the excavation, as well as during the combined excavation and the build time of a ring.
- $p_{2,min}$  was introduced to represent the lowest of the five pressure measurements in the excavation chamber (marked as “Up” for the case presented in Fig. 7.12a).
- $p_{2,IQR}$  quantifies the fluctuation of chamber pressure during each ring. In order to provide a descriptor not affected by instrumental errors or narrow pressure peaks, the fluctuation was described by the interquartile range rather than the standard deviation or by the full range of the data. As shown in Fig. 7.12b, it is defined as the difference between the first and the third quartile of the measurement distribution.
- Finally,  $p_{2,10\%}$  was chosen as a measure of the low face pressure occurring during a given period of time. This variable was introduced because certain authors pointed out that the ground volume loss may depend on the lowest rather than the average face pressures (e.g.: Shirlaw *et al.*, 2003). The parameter  $p_{2,10\%}$  was therefore defined as the 10%-percentile of the distribution of  $p_2$ , i.e. the value of face pressure below which 10% of the data points were measured (Fig. 7.12b).

Each of these components (except  $p_2$ ) yield one data point per ring, and hence approximately 5,000 data points for each of the upline and downline tunnels. In order to provide an overview of this data, the average values of these components and other relevant machine parameters were calculated for each different type of ground conditions. This was done separately for the upline and downline tunnels and the results are tabulated in Tables 7.6 and 7.7.

Correlations between machine parameters are often sought to elucidate the mechanical interaction governing the EPB machines behaviour, especially in relation to the ground conditioning parameters (e.g.: Leinala *et al.*, 2000). Because of the large number of parameters potentially affecting the machine, and because these

parameters are often altered simultaneously (with no identifiable pattern), it is notoriously difficult to identify insightful relationships. Before embarking into detailed analysis of the machine data, it is useful to rationalise the data by trying to identify trends between the different parameters. In order to identify trends between the soil conditioning parameters and the machine parameters, pair-wise relationships were plotted as in Fig. 7.13 and the correlation coefficient between the two data sets was computed to indicate the existence or the absence of a relationship. While correlation coefficients of -1 or 1 indicate perfect association between the two variables (with the negative sign showing that one variable decreases as the other one increases), values near or equal to zero implies total absence of correlation. The significance of the coefficient of correlation has limitations because of the simultaneous variation of variables which may have a combined effect on the machine parameters. One such variable is the ground condition and in order to eliminate its effect, matrices of correlation coefficients were computed for each of the three types of full face ground conditions. The three matrices reproduced in Table 7.8 show, for both the upline and the downline, the correlation coefficients between the *FIR*, the *FER*, the *PIR* and the *LIR* with a range of machine parameters that were expected to be affected by the soil conditioning.

Scrutiny of Table 7.8 reveals little or no correlations. While some trends correspond to what could have been expected, the inconsistency of the obtained correlation coefficient between the two tunnel lines in the same type of ground conditions emphasises the limitation of such approaches. However, large values of correlation in Table 7.8 may hint at insightful messages. Three examples of relatively large correlation and one where the correlation was close to zero are plotted in Fig. 7.13. Fig. 7.13a shows that, in Thanet Sand, increasing *FIRs* seemed to be associated (quite unexpectedly) with reducing advance rate of the machine, while the shield thrust can be increased when larger amounts of liquid (*LIR*) are injected (Fig. 7.13b). Fig. 7.13c reveals that in London Clay, the uniformity of the chamber pressure improves as the *FER* increases, and that, interestingly, the range of pressure ( $p_{2,range}$ ) is never less than 50 kPa when the *FER* is less than about 2.5. Fig. 7.13d illustrates the significance of a correlation coefficient approaching zero: no trend may be discerned between the *LIR* and the screw torque, even though the liquid injection was varied over a wide range. However, as already explained, little or no conclusions may be derived from such observation. This is because, in this last example for instance, the screw torque may depend on other parameters than just the *LIR*, and these may have been varied as a result of the higher *LIR*. In this last example, a change of discharge rate or a partial

restriction of the screw outlet may well have affected the conveyor torque, hence leading to the observed scatter in Fig. 7.13d.

In order to gain further insight into the machine behaviour, the following sections provide a more detailed description of the machine behaviour in each different type of ground conditions.

### 7.3.2 Tunnelling in Thanet Sand

#### 7.3.2.1 Soil conditioning

The distribution of the quantities of soil conditioning agents injected in the 376 rings excavated in full face Thanet Sand are plotted in the histograms of Fig. 7.8 and their average values are summarised in Table 7.5. The left-hand charts of Fig. 7.8 (a to d) correspond to the upline, while the same data is plotted in the right-hand figures (e to h) for the downline. It may be seen that the distribution of average quantities injected in both machines were almost identical: the foam was injected at a rate of about  $FIR = 50\%$  (Fig. 7.8a/e) with an expansion ratio  $FER = 10$  (Fig. 7.8b/f), while polymer solution was injected at  $PIR = 7\%$  (Fig. 7.8c/g). For both lines, this represented a total liquid injection ratio  $LIR = 10\%$ , hence a cumulated volume of foam and polymer solution of approximately  $8 \text{ m}^3$ . On average, the  $FIRs$  used in the Thanet Sand were slightly above the range recommended by the EFNARC (30-40%, Table 6.1). Peña (2003) reported index tests carried out on mixtures of foam and Thanet Sand. He measured that Thanet Sand conditioned with foam alone at  $FIR = 50\%$  had shear strengths of the order of 10 kPa, and a slump of 120 mm, hence falling within the recommended range of 100 to 150 mm suggested by Quebaud (1995). In addition, Peña showed that a  $PIR$  of 20% produced a mixture with a slump of about 100 mm, but no results for combined foam and polymer treatment were reported.

#### 7.3.2.2 Effect of the liquid injection ratio ( $LIR$ )

In order to identify the effect of the total liquid injection ratio, the machine data are compared for a series of six consecutive rings in which the  $LIR$  was significantly varied. The machine data corresponding to these six rings (555 to 560) are plotted in Fig. 7.14 and their average values are summarised in Table 7.9. Fig. 7.14a shows that while the  $FER$  was held relatively constant for the six rings, the  $FIR$  was nearly doubled in the last three rings and the  $PIR$  increased from zero to about 9%, hence causing the total liquid injection ratio to increase from 2.9% in ring 555 to 14.7% in ring 560. Fig. 7.14b shows the mean and the range of the chamber

pressure  $p_2$ . The average values summarised in Table 7.9 indicates that the mean earth pressure during the excavation ( $p_{2,exc}$ ) remained relatively constant for the entire series of rings, hence allowing direct comparison of the other machine parameters. The excavation-build cycles may be seen in Fig. 7.14b from the jack position increasing from zero to 1500 mm as the shield is pushed forward during excavation and retracted to zero during ring build. The thrust on the shield and the cutter head torque are shown in Fig. 7.14c, while the torque and the angular speed of the screw conveyor are plotted in Fig. 7.14d.

A 30%-reduction of the cutter head and of the screw torque was measured in ring 559 and 560 compared to the preceding four rings (Table 7.9). As could perhaps have been expected, this reduction was not apparent in ring 558, despite the much larger amount of polymer solution that was injected in this ring. While this could perhaps have been expected for the screw conveyor torque (since the material conditioned at the cutter head needs to flow through the machine), the reasons why it did not occur for the cutter head torque are not clear. It has to be noted, however, that the reduction of cutter head and screw conveyor torque can, in addition to the increased  $LIR$ , also be attributed to the increased shield thrust and the reduced angular speed of the screw conveyor.

Although not easily observed in Fig. 7.14b, the averages of  $p_{2,drop}$  and  $p_{2,iqr}$  both reduced in the last two rings (559 and 560), the reduction of  $p_{2,iqr}$  being due to that of  $p_{2,drop}$ . While this was at first attributed to an improved stability of the foam, and hence a lower rate of pressure decay during the time of the ring erection, a closer look at Fig. 7.14b reveals that the larger pressure decay in ring 555 to 557 is more likely to be associated with larger ring build time, thus allowing the pressure decay to continue for a prolonged period of time. However, the generic pattern of exponential pressure decay during ring build is less recognisable in the last few rings, perhaps suggesting some positive effect of the polymer.

### 7.3.2.3 Effect of the foam injection ratio ( $FIR$ )

A similar comparison was performed to identify the effects of the  $FIR$  on the machine parameters in Thanet Sand. The machine data of ring 491 to 496 are plotted in Fig. 7.15 and their average values are summarised in Table 7.10. After two rings where the  $FIR$  was well above the average, the  $FER$  was reduced by about 70%, and then gradually increased until ring 496, where a similar amount of foam as in ring 491 was injected. Table 7.9 reveals that the  $PIR$  was not changed significantly in these five rings, so that the reducing  $LIR$  is in large proportion due to the variations in  $FIR$ .

It is interesting to note that while the average advance rate of the machine and the thrust applied to it was 20 and 25% lower than for the series of rings appearing in Fig. 7.14, whereas the torque of both the cutter head and the screw conveyor was 13 and 50% larger, respectively. This occurred despite a lower pressure  $p_{2,exc}$  measured in the chamber during excavation.

Reducing the *FIR* from 84.3 (ring 491) to 19.5 (ring 493) clearly resulted in a 40% higher screw conveyor torque. As high *FIRs* were restored, the screw conveyor torque returned to the values initially measured in ring 491. A trend of decreasing pressure drop during ring build ( $p_{2,drop}$ ), with reducing *FIR* may also be discerned in Fig. 7.15. Although the severe rate of pressure drop measured during the erection of ring 491 was also measured in the other rings, the rate seemed to decrease after some time, thus leading the pressure to stabilise. This may indicate that the foam, when added in such high proportion to the sand, rapidly breaks down, which leads to large drops of pressure during the machine standstill.

Finally, in Figs 7.14 and 7.15, it is interesting to compare rings 491-492 with rings 555-554, for which the *PIR* was also zero but the *FIR* was approximately half the value used in the first pair of rings. When the *FIR* was doubled, the advance rate of the machine reduced by about 15-30%. This may be a result of the larger thrust applied in the first case (the chamber pressure was comparable in both cases).

### 7.3.3 Tunnelling in the Lambeth Group

#### 7.3.3.1 Soil conditioning

The soil conditioning parameters used for the 580 rings excavated in the Lambeth Group formation are summarised in Fig. 7.9 and Table 7.9. For the upline tunnel, the total amount of liquid injected in the Lambeth Group was on average 80% higher than in the Thanet Sand. For the downline tunnel, the average *LIR* was only 30% higher than in the Thanet Sand, but this might be due to a large number of rings (3225 to 3418) where almost no conditioning was used. In these rings (corresponding to chainage 4228 to 3939 in Fig. 7.21), the chamber pressure was close to 10 kPa, hence indicating that the *EPB* machine was driven in open-mode (probably as a result of mechanical damage of the rotary joints of the cutter head). This indicates that, in the absence of soil conditioning, the chamber pressure could not be maintained at the required levels. Unfortunately, while Bowers & Moss (2006) report volume loss measurements in several sections on the upline between chainage 4228 and 3939, the

equivalent is only provided for one monitoring section on the downline where excavation occurred in open-mode.

The mean *FIR* used in the upline was equal to that used in the Thanet Sand, however with a wider scatter. *FIRs* in excess of 100% were used for over 30 rings, while extremely low values of 5% have also been used (Fig. 7.9a and b). While the average *FIR* was approximately equal to that used in the Thanet Sand, the *FER* was lower, hence an indication of larger volumes of foaming solutions. In addition, the *PIR* was 4% higher on average. The in situ moisture content of the Lambeth Group ranged from 8-13% to the east of Graham Shaft, to 15-21% further west. The moisture content of the spoil (measured in 105 rings) in the Lambeth Group ranged from 16 to 41%, with an average value of 29%. The addition of the average in situ moisture content (18%) and the average *LIR* (18%) yields a value which lies about 7% higher than the average moisture content of the spoil. This indicates that the clay-conditioner mixture does not mix into a homogeneous paste, and that some significant proportion of free liquid remains in the head chamber.

#### 7.3.3.2 Effect of the liquid injection ratio (*LIR*)

As for the Thanet Sand, machine data corresponding to a series of rings in which large changes of soil conditioning parameters occurred are analysed to identify the effect of the conditioning agents. As shown in Fig. 7.16a, extremely high foam quantities ranging from *FIR* = 122 to 245% were injected in rings 3726 to 3728. In the following four rings, the *FIR* was reduced to marginal values comprised between 7 and 10%. This was due to a reduction of the *FER* from about 13 to 1. Except for the first ring of the series (ring 3726), the *LIR* was almost constant at around 20%, with small variations of *PIR* only, therefore allowing the effects of the *FER* to be isolated. The corresponding machine data are plotted in Fig. 7.16b to d and their averages are summarised in Table 7.9.

The reduction of the *FER* from ring 3729 seems to have resulted in a 30% increase of the advance rate of the machine, for relatively constant torque and pressure in the excavation chamber. The average torque of the cutter head increased by about 10%, but no consistent trend was observed by the screw conveyor torque in relation to the *FER*. Most notably, the pressure drop during ring build was, on average, more than halved when the *FER* was reduced from 13 to 1, and in turn, the volume of the air phase in the foam. While the intermittent thrust applied during ring build helps prevent large drop of chamber pressure, the effect of reduced compressed air injection into the face seems clear. In addition, the spatial and temporal fluctuation of chamber pressure ( $p_{2,range}$  and  $p_{2,iqr}$ ) seems not to have been adversely affected by the reduced

quantity of foam, hence suggesting that the benefit of conditioning in the Lambeth Group were derived from effects associated with the *LIR* rather than the physical properties of foam.

### 7.3.3.3 Effect of the foam injection ratio (*FIR*)

Fig. 7.17 shows the machine data for a series of 10 rings through which both the *FIR* and the *PIR* were progressively increased, thus resulting in *LIRs* gradually increasing from 9 to about 20%. The variations in *FIR* were, this time, due to increasing foam solution volume, and the *FER* was held reasonably constant.

The striking feature revealed by a first inspection of Fig. 7.17 is that the increased volume of foams injected in the second half of the series of rings considered, did not result in a smoother control of the machine, as could perhaps have been expected. Instead, the amplitude of chamber pressure fluctuations increased, as observed in Fig. 7.17b and indicated by the increasing values of  $p_{2,iqr}$  tabulated for ring 3608 to 3617 in Table 7.9. Interestingly, the advance rate of the machine reduced as the *FIR*, and thus *LIR*, were increased. This was a result of a reduced thrust on the machine. Surprisingly, the cutter head torque did not reduce with the thrust and this despite increasing *FIR* and *LIR*. The screw torque showed no consistent trend with the *FIR*, but did not appear to be reduced as the *LIR* was doubled from ring 3608 to 3617. Once again, increased quantities of soil conditioning agents, and in particular, foam volumes, did not appear to be associated with significant benefits in terms of performance (advance rate) or control ( $p_{2,iqr}$ ) of the machine.

## 7.3.4 Tunnelling in London Clay and Harwich Formation

### 7.3.4.1 Soil conditioning

London Clay is a more homogenous material and its engineering properties, although variable, may be more easily described than that of the highly heterogeneous and variable Lambeth Group Formation. The average moisture content of the London Clay was measured at about 24%, the plasticity index at 47% and the plastic limit at 23% (Union Railways, 1997). Therefore the consistency index,  $I_c$ , of the natural London Clay can be assumed to have lain at about unity, *i.e.* much higher than the ideal value for *EPB* machine operation ( $I_c = 0.4$ ; Maidl, 1995). In addition, the undrained shear strength of the London Clay at tunnel axis depth ranged from 150 to 250 kPa or more, hence one order of magnitude higher than the strength deemed appropriate for *EPB* machine operation in closed-mode.

As shown in Fig. 7.10a, the total volumes of foam used in the London Clay, were on average half that injected in the Thanet Sand and the Lambeth Group. However, the *FER* was also reduced to half the value used in these other ground conditions, so that the volume of foaming liquid was approximately identical to that injected in the Thanet Sand and the Lambeth Group. The injected quantity of foam fell below the recommended range of *FIR* of 30 to 80% (EFNARC, 2005). In the upline tunnel, the volume of polymer was approximately 30% higher than in the Lambeth Group, with *PIR* = 13%, but the amount of polymer was reduced to half this value in the downline tunnel. These quantities correspond to total liquid injection ratios (*LIR*) of 19 and 13% for the upline and downline tunnels, respectively. For the upline tunnel, the moisture content of the spoil was measured for 44 rings, and an average of 43% was calculated. This exactly matches the sum of the natural moisture content (24.3%; Union Railways, 1997) and the average *LIR* (19%). Assuming that the conditioning agents left the Atterberg limits of the London Clay unchanged, the moisture content of the spoil corresponds to a consistency index  $I_c = 0.42$ , *i.e.* just within the range recommended by Maidl (1995).

Index tests were performed in advance of tunnelling to assist the contractor in selecting soil conditioning parameters (Merritt *et al.*, 2002). London Clay samples were recovered from Corsica Street ventilation shaft, and fall cone as well as shear vane tests were performed to determine the bulk undrained shear strength of London Clay cuttings mixed with a range of foam and polymer combination. Fig. 7.20 shows how the undrained shear strength of the mixture relates to the *LIR* for different combinations of foam and polymer. As may be seen in Fig. 7.20, for *LIR* in the region of 20% (as for the upline tunnel in London Clay), the undrained shear strength of the conditioned London Clay is smaller when polymer solution is used instead of foam, and little or no difference was noted when varying the polymer concentration in the range of 0.2 to 1%. The *FIRs* required to achieve a shear strength of  $S_u = 25$  kPa were, for an expansion ratio of 10, as high as 200%, and the effect of the foam was, in the case of London Clay, attributed to its liquid phase. Combinations of foam with polymer yielded, at identical *LIR*, considerably lower shear strength than when the two products were used independently. For the average parameters used in the upline tunnel, Fig. 7.20 suggests that the undrained shear strength of the London Clay conditioned with both foam and polymer might have lain in the region of 12 kPa, corresponding to a tenfold reduction compared to the *in situ* value. The relatively small quantities of foam reported in Fig. 7.10a confirm that the London Clay can be remoulded into a material of sufficiently low shear strength to allow closed-mode *EPB* machine operation by the addition of relatively small quantities of foam. This is

in contrast to *FIRs* in excess of 100, or sometimes 200% reported in other projects in stiff clay (*e.g.*: Langmaack, 2000 or Leinala *et al.*, 2000). The addition of polymer is believed to reduce the adsorption of the foam by the clay cuttings. As a result, the lubricating effect of the polymer is combined with that of foam, therefore leading to the small shear strengths reported in Fig. 7.20.

#### 7.3.4.2 Effect of the liquid injection ratio (*PIR*)

Fig. 7.18 and Table 7.10 document the machine parameters for a series of rings in which the *PIR* was considerably varied, while the *FIR* and *FER* were held approximately constant. *PIRs* of about 16% were used in first three rings (4393 to 4395), before being reduced to 4% in the following four rings. Both the chamber pressure  $p_2$  and the advance rate of the machine were relatively constant for the entire series, thus allowing the effects of the *PIR* on the other machine parameters to be determined.

Upon reducing the *PIR*, the cutter head and the screw torque increased by 20 and 35%, respectively. In the London Clay, the screw conveyor torque was, at comparable angular speed, approximately 30% lower than in the Lambeth Group. The reduced *PIR* had little or no noticeable effects on the control of chamber pressure, as may be seen in Fig. 7.18b and deduced from the absence of trend between the *PIR* and the spread of the face pressure data  $p_{2,iqr}$ . The Interquartile range was also much lower in the London Clay than in the Lambeth Group, indicating lower fluctuations and hence a better control of the chamber pressure, as can also be seen by comparing the chamber pressure data in Fig. 7.17b and 7.18b.

#### 7.3.4.3 Effect of the foam injection ratio (*FIR*)

Fig. 7.19 and Table 7.10 show the machine data for a series of rings (rings 4777 to 4782) in which the *FIR* used in the first three rings (5%) was more than trebled for the subsequent three rings. The advance rate of the machine and the chamber pressure were constant throughout the six rings. However, the chamber pressure above 200 kPa, *i.e.* about 60% larger than in the rings whose data appear in Fig. 7.18. The advance rate was approximately halved. The outstanding feature about this series of rings is that the chamber pressure was accurately controlled while maintaining a pressure in excess of 200 kPa throughout the excavation (Fig. 7.19b): the values of  $p_{2,iqr}$  tabulated in Table 7.10 indicate that 50% of the average chamber pressure data points fell within a band of 10 kPa, which is quite remarkable. A comparison of Fig. 7.19d with 7.18d indicates that the screw conveyor speed did not have to be altered significantly throughout each shove, hence indicating that steady

state operation had been reached. In addition, little loss of pressure occurred during ring build, perhaps reflecting the benefits of lower *FIRs*. However, although this demonstrates the ability of the machine to operate in stiff plastic clays while maintaining a high face pressure, the lower operation speed that was achieved during these rings has to be noted (Table 7.10).

A further difference of behaviour noticed for rings 4777 to 4782 was the reduced screw speed in relation to the advance rate of the machine. While the ratio of machine advance rate to screw angular speed (ignoring the inconsistency in the units) ranged from 9.7 to 10.5 in all the ring series discussed in the previous paragraphs, this ratio was as high as 15 in rings 4777 to 4782, indicating that a larger discharge rate per screw revolution was achieved. This is consistent with the models of Merritt (2004), which predicts that the angle of soil flow increases with the pressure difference in the chamber and at the discharge outlet of the conveyor. A larger angle of soil flow corresponds to increased discharge rates (and hence advance of the machine) and reduced torque. The reduction of screw conveyor torque as the chamber pressure increases may be seen when comparing ring 4393 to 4399 with the series from 4777 to 4782. Some of the difference of the screw torque might be a result of varying soil conditioning parameters, but scrutiny of Table 7.10 reveals that a trend of decreasing screw torques with increasing chamber pressure can be observed (perhaps unexpectedly).

## 7.4 Effect of machine parameters on ground volume loss

### 7.4.1 Definitions and presentations of data

This section relates the machine parameters to the ground volume loss that was caused by the construction of the upline tunnel. The ground volume loss was determined from arrays of transverse surface settlement measurements at 43 sections along the tunnel route (Wongsaroj *et al.*, 2006). These sections were grouped in three categories, corresponding to where the tunnel face was in Thanet Sand or Upnor and Thanet Sand (§ 7.4.2), in the Lambeth Group Formation (§ 7.4.3) and in London Clay or in mixed face conditions with London Clay, Harwich and Lambeth Group Formation (§ 7.4.4). The total volume loss was separated into three components, by analogy with the three components of maximum surface settlement  $S_F$ ,  $S_S$  and  $S_T$  shown in Fig. 7.21. Accordingly,  $V_{L,face}$  was defined as the volume loss that has occurred when the tunnel face lies in the monitoring section, and  $V_{L,shield}$  and  $V_{L,tail}$  were used to denote the additional volume loss that develop over the shield and the tail of the machine, respectively. As depicted in Fig. 7.21, zones of influence were

chosen on the simplifying assumption that the face pressure  $p_f$  only influences the measured ground movements as the face approaches the monitoring section, while subsequently occurring volume losses are marginally influenced by the face pressure and rather more by the grouting processes around the shield and behind the tail void.

This work focuses on the effect of the face pressure on the total and the face component of the volume loss. The face pressure  $p_f$  is assumed to be a function of the two components  $p_1$  and  $p_2$  depicted in Fig. 6.1, and it is not solely equated to  $p_2$  as is often suggested in the literature. The 10%-percentile of  $p_2$  was introduced (Fig. 7.12) in response to the suggestion that the magnitude of the face volume loss may be significantly related to the temporary minimum pressures  $p_2$  rather than to its mean value only (e.g.: Shirlaw *et al.*, 2003). In the absence of measurements allowing accurate estimation of the three components  $\tau$ ,  $p_1$  and  $p_2$  (Fig. 6.1), no attempt was made to calculate  $p_1$ . Instead, the volume loss at the face was correlated to the total thrust acting on the shield, expressed with the dimensions of a stress by division by the total area of the tunnel face. Each face pressure component was rendered dimensionless by normalisation with the total overburden stress at tunnel axis depth.

An overview of the ground volume loss along the entire route of *Contract 220* is provided for both the upline and the downline tunnel in Fig. 7.22 (both tunnels were driven from chainage 9000 towards chainage 1500). The mean and the range of total and face loss caused by the tunnelling operation in each of the eight types of ground conditions are summarised in Table 7.11. The following sections relate the total as well as the face component of volume loss to the face pressure components in the three main types of ground conditions.

#### 7.4.2 Ground volume loss in Thanet and Upnor Sands

Fig. 7.24 shows the total and face volume loss components as a function of the mean chamber pressure  $p_2$ , the 10%-percentile of  $p_2$  and the normalised thrust  $T/A$ , each of them normalised by the total overburden stress at pipe axis depth. In this figure, the values of  $p_2$  and  $T$  were calculated as the average in zone 1 (fig. 7.21), which was taken to extend a distance equivalent to five rings (7.5 m) ahead of the excavation face. Fig. 7.24d shows that the mean chamber pressure  $p_2$  was generally between 10 and 30% of the total overburden pressure at tunnel axis depth. With chamber pressures such as these, the face component of the volume loss never exceeded 0.2%. For a tunnel diameter of 8.15 m, a trough width parameter  $K_y = 0.4$  and a tunnel axis depth of 25 m, this corresponds to a maximum surface settlement,  $S_{max}$ , of no more than 1.7 mm. Larger volume losses at the face were measured in two

sections, with a maximum value of 0.6% ( $S_{max} = 5.9$  mm) at chainage 8885. Fig. 7.24a reveals that the total volume losses was approximately three times larger than the face loss  $V_{L,face}$ , although the large face loss measured in one instance (0.6%) resulted nearly 3% total volume loss ( $S_{max} = 29$  mm). Fig. 7.23 indicates that the volume loss occurring over the shield and the tail increase with the face volume loss. This suggests that the effects of stress relief at the tunnel face may be delayed until the machine has advanced beyond the monitoring section.

The relationship between  $p_2$  and  $V_{L,face}$  failed to produce an unambiguous trend, hence indicating that parameters other than the average face pressure may influence the face component of the volume loss. Fig. 7.24b/e and 7.24c/f show the relation between the 10-percentile chamber pressure and the thrust expressed as  $T/A$ . In all cases, it can be seen that low values of  $p_{2,10\%}$  and  $T/A$  are associated with high face volume losses, and high values consistently produce small volume losses at the face. However, while some trend can be distinguished, large differences in volume losses are sometimes observed in cases where both the average  $p_2$  and  $p_{2,10\%}$  were almost identical. In order to identify the cause of these contrasting face volume losses under identical face pressures, the history of chamber pressure and thrust for the machine drive in zone 1 were analysed in detail. Fig. 7.27 and 7.28 compares two sections in mixed face conditions (Upnor and Thanet Sand) through which the average values of  $p_2$  were approximately equal, but the resulting face volume losses differed by a factor of 6. The two sections are compared in the following paragraphs, and the components of face pressure and volume loss are summarised in Table 7.12. Again,  $p_2$  and  $T$  were taken as the average during the drive through zone 1 (Fig. 7.21), *i.e.*, including the measurements during both the excavation and the build time.

For the two sections driven in the Upnor and Thanet formation compared here, the face volume loss differed by a factor of 6, and total volume loss amounted to 1.23 and 2.85%. As shown in Fig. 7.24d, the average face pressures were nearly equal in both cases. However, lower values of  $p_2$  were measured for rings 1211-1217 approximately 2 hours before the tunnel face reached the monitoring section (Fig. 7.28a), possibly causing the larger ground surface movements at this location. Also, the average shield thrust was considerably lower in the section where large volume loss was measured, and while this may partly result from reduced friction  $\tau$  on the tunnel shield (the tunnel was 10 m shallower at this location), it is likely that the smaller thrust also resulted in a smaller face support pressure component  $p_1$ .

Figs 7.29 and 7.30 compare the same data for two sections in full face Thanet Sand and where the face volume loss differed by a factor of 2. The average face pressure as

well as  $p_{2,10\%}$  were, in this case, lower for the section which experienced the smaller volume loss. This unexpected trend was also observed for the average thrust, which was 10% smaller in the section of lower volume loss. A more detailed comparison of Fig. 7.29 and 7.30 does not reveal features in the machine data which helps explain the measured difference in volume loss. It has to be kept in mind, however, that the difference in face volume loss between the two sections corresponds to a difference of maximum surface settlement  $S_{max}$  of only 0.5 mm.

#### 7.4.3 Ground volume loss in the Lambeth Group

The relationship between the volume loss components induced by tunnelling in the Lambeth Group formation and the machine parameters are plotted in Fig. 7.25. As in the Upnor and Thanet Sand, the average face volume loss was 0.2%, which corresponds to about 20% of the total volume loss (Table 7.11). No volume losses above 1% were measured in the Lambeth Group, where the average chamber pressure  $p_2$  was 126 kPa for the Upline tunnel (Table 7.6).

#### 7.4.4 Ground volume loss in London Clay and London Clay/Harwich Formation/Lambeth Group

The relationship between the volume loss components induced by tunnelling in the London Clay and London Clay/Harwich Formation/Lambeth Group formation and the machine parameters are plotted in Fig. 7.26. Fig. 7.26d shows that chamber pressure of about 30% of the total overburden stress where sufficient in maintaining the face volume loss below 0.3% and the total volume loss below the contractual limit of 1%. As summarised in Table 7.7, the average chamber pressure in the London Clay was 184 kPa. In the mixed face condition with London Clay, Harwich Formation and Lambeth Group, the volume loss was marginally lower, probably reflecting the larger chamber pressure maintained in this critical section of the drive in which the machines were under-crossing existing tunnels (Fig. 7.3). While clear trends cannot be identified in these figures, it may be seen that when different volume losses are produced at identical chamber pressure parameters  $p_2$  and  $p_{2,10\%}$ , the difference can be attributed, in some cases, to a clearly different thrust.

Table 7.12 compares the average components of face pressure for two sections in which the face volume loss differed by a factor of 3 and for which the average value of  $p_2$  was approximately equal. The magnitude of the average thrust applied to the shield in the five rings preceding the monitoring section was 26% lower in rings 3974-3980, where the larger face volume loss was measured. As may be seen in Fig. 7.32, the chamber pressure reduced from an average of 250 kPa to about 100 kPa

before the tunnel face reached the monitoring section. In addition, a steadier control of the thrust was achieved before reaching the monitoring section where lower volume loss was measured.

A similar comparison is made in Table 7.12 and Figs 7.33 and 7.34 for two sections in full face London Clay. The higher volume loss was induced in the section where the higher chamber pressure and thrust were applied, once again suggesting that other parameters than  $p_2$ ,  $p_{2,10\%}$  and  $T/A$  are likely to have played a significant role in causing the volume loss.

## 7.5 Discussion

### 7.5.1 Effect of soil conditioning parameters

The clear identification of the effects of the soil conditioning parameters has been found to be difficult as a result of the concomitant variation of several machine parameters. In addition, the location of the injection was not recorded by the monitoring system. Polymer was often injected directly into the screw conveyor, usually intermittently as the trigger levels for the oil pressure in the screw conveyor drive were approached. This occurred by diverting the flow of polymer from the cutter head into the screw, but this information was not logged by the monitoring system.

With  $FIR = 50\%$  and  $FER = 10$  in the Thanet Sand, the parameters of foam injection fell within the range of recommendation available in the literature (*e.g.*: EFNARC, 2005). However, while these guidelines suggest that polymer solutions be injected in addition to the foam, no recommendations as to the determination of suitable volumes are suggested. The excavation of both tunnel lines in the Thanet Sand was done with  $PIRs$  of between 7 and 7.5%, and the total volume of liquid injected was, on average, about 10%. While no evidence exists to treat these figures as “optimum” quantities, the safe and efficient excavation of over 1,000 m in full face Thanet Sand indicates that these values may be taken as a robust guidance.

While some  $FIRs$  in excess of 200% were sometimes used in the stiff clays of the Lambeth Group, no direct benefits of such large quantities of foams were observed. On the contrary, the data presented in Fig. 7.14 to 7.19 and summarised in Table 7.9 and 7.10 consistently show a reduction of advance speed with increasing  $FIR$ . While the cutter head and the screw conveyor torque usually reduced as a result of increased  $FIR$ , the fluctuations of chamber pressure were never reduced in a noticeable manner.

Over 1,500 m were excavated in full face London Clay with an average chamber pressure during excavation close to 200 kPa. While the feasibility of closed-mode operation in stiff plastic clays was sometimes been questioned, the data presented herein clearly demonstrates that carefully selected soil conditioning scheme allows the London Clay to be remoulded into a mixture that can be extruded in a controllable manner by the screw conveyor. Shear-vane measurements on 300 mm diameter lumps of London Clay at the discharge of the screw conveyor suggested undrained shear strengths in the range 20-30 kPa. For the moisture contents obtained from measurements on the discharged material, these strengths correspond to those measured in the laboratory tests by Merritt *et al.* (2002).

The *FIR* used in the London Clay fell below the range recommended by the EFNARC (30-80%), and contrasted with the need for “large” quantities of 100% and beyond sometimes reported in the literature. Analysis of machine data revealed that the effect of the foam in clay is that of its liquid phase, and that the reasons which makes foam a suitable additive in sand, cannot be extrapolated to clayey material. Observation of London Clay discharge at the outlet of the screw conveyor revealed poor mixing when large quantities of foam were used. Intermittent discharge of clay lumps alternated with gushing of fluid and blow out of compressed air. In cases where the injected foam breaks due to sorption of the foaming liquid into the clay, its benefits are compromised and the large quantities of compressed air injected into the excavation chamber are likely to have counterproductive effects. Most notably, larger pressure drops will occur during the machine stoppages and fluctuation of chamber pressure will be exacerbated as a result of discontinuous discharge rate due to the heterogeneity of the soil mixture. Fig. 7.19b shows outstanding control of high chamber pressures of about 200 kPa, with little reduction during build time. The shield thrust and the screw rotation speed plotted in Fig. 7.19c and d, respectively, indicate that steady state operation of the machine was achieved in these rings. For rings 4777-4779, the *FIR* was no higher than 6% and the *FER* close to unity (Table 7.10) indicated that negligible quantities of compressed air were injected in these three rings, and hence, that polymer alone was sufficient to ensure “optimal” operation of the *EPB* machine.

### 7.5.2 Soil-machine interactions and control of face pressure

The pressure imparted to the tunnel face was shown to be a function of both the chamber pressure  $p_2$  and the direct pressure  $p_1$  between the cutter head and the face. For a given thrust  $T$ , the resultant of  $p_1$  and  $p_2$  depends on the shear component,  $\tau$ , around the shield of the machine. The value of  $\tau$  may vary significantly depending

on the ground conditions, but also as a result of the overcut excavated by the scrapers and the injection of bentonite around the shield. The operation of the machine is usually done by the application of a constant thrust, the value of which is chosen to limit the torque requirement of the cutter head. This determines the advance rate of the machine, and the chamber pressure is then regulated by altering the oil pressure of the screw conveyor drive. The regulation of the face pressure is not a linear problem, in that a reduced screw speed will increase the chamber pressure, and hence the drop of pressure along the conveyor. In turn, the angle of soil flow will increase (Merritt, 2006) and hence the discharge rate. Injection of polymer into the screw conveyor is believed to dramatically change the interface friction between the soil and the conveyor casing, thus causing immediate alteration of the screw regime and hence the fluctuations observed in Figs 7.14d to 7.17d. This prevents steady state operation and causes large fluctuations of chamber pressure (e.g.: ring 3715, Fig. 7.17b and d at  $t = 8$  h).

The sensitivity of the screw conveyor operation to the material properties suggests that the excavated soil should best be conditioned as early as possible in order to maximise the mixing time and hence improve the homogeneity of the material in the head chamber. Conditioners should be injected directly in the cutting head and the material should only be injected into the screw conveyor as a last resort measure to reduce the driving torque.

### 7.5.3 Effect of machine parameters on ground volume loss

The salient lesson from the monitoring exercise is that face pressures of the order of 10 to 30% the total overburden pressure were sufficient to maintain total volume losses below 1%. No clear trend were discerned between the face pressure components and either the total or the face component of the volume loss. This may be partly due to the influence of parameters that were not taken into account. These include the overcut ratio (“bead”) as well as the steering correction of the machine, both of which have a direct influence on the total amount of soil excavated. However, the absence of trend is also due to the small range within which the chamber pressure was varied and to the small volume losses that were measured, often corresponding to maximum settlements of the order of 1 mm. Under such circumstances, errors in the determination of the volume loss may have just as much effect as variations of the chamber pressure in the range of, say, 100 to 200 kPa.

In clay, the dependence of the face volume loss on the temporary low chamber pressure component did not produce the expected relationship. It was expected that a reduction of face pressure for a short period of time, possibly a few minutes only,

would be sufficient to affect the volume loss significantly. No such trend could be identified. This was attributed to the small load factor  $LF$  prevailing in the stiff Lambeth Group and London Clay.  $LF = N/N_c$ , (where  $N$  is the stability ratio defined in equation 2.1 and  $N_c = 8.5$ ; Mair, 1979) was estimated in the range 0.2 and 0.3. As may be seen in Fig. 7.35, the volume loss measured for tunnels in clays is well described by an exponential function of the load factor  $LF$ . Reductions of face pressure by  $S_u/10$  will increase  $LF$  by a tenth, which, in regions of low  $LF$ , say from 0.25 to 0.35 will increase the volume loss from 0.7 to 0.9%. This explains why the variations of chamber pressures in the stiff to very stiff Lambeth Group and London Clay did not result in significant differences in the measured volume losses.

## 7.6 Summary

The field data presented in this chapter allowed explaining crucial interactions between the soil conditioning, the *EPB* machine operations and their impact on the ground volume loss. The key points of this chapter may be summarised as follows:

- The experience of *Contract 220 CTRL* showed that *EPB* machines can be driven efficiently in a wide variety of ground conditions. In particular, appropriate soil conditioning allowed the machines to be operated in closed-mode in the stiff and very stiff clays of the Lambeth Group as well as in the London Clay.
- Remarkably well-controlled face pressure have been achieved in London Clay. This was achieved by injection of about 15% of polymer solution, and little or no foam was required to allow the clay to be remoulded to an undrained shear strength of  $S_u = 20\text{-}30$  kPa. This confirmed the conclusions drawn from the index tests performed by Merritt *et al.* (2002) and which suggested limited benefits to the use of foam in stiff clays.
- The operations of the machine in the Lambeth Group showed more fluctuations of the chamber pressure, and steady state operations could hardly be achieved. The revolution speed of the screw conveyor and the thrust on the machine had to be altered frequently, which often resulted in large variations of the chamber pressure.
- Volume losses of below 1% were achieved throughout most of the drive, with only a few instances of larger volume loss. For the 30 m deep tunnels sections in

---

the London Clay, the volume loss was not significantly affected by the magnitude of the chamber pressure  $p_2$ , or indeed by the temporary low values of the chamber pressure. This was attributed to the relatively small dependency of the volume loss when the load factor  $LF$  is in the region of 0.2-0.3%.

- However, in order to minimise the risk due to unexpected zones of locally high permeability or granular material, it is crucial to maintain a full excavation chamber at all times, and therefore, a chamber pressure. It is important not to associate the measurement of large chamber pressures as necessarily meaning a “full” excavation chamber. This is because the pressure may merely result from the compressed air injected with the foam, and excessive amounts of foams in the chamber may not allow partial collapses of the face to be prevented.
- The machine behaviour and its effects on the ground movements is highly operator dependant. Different driver may chose to control the machine with different parameters. The different “driving-style” may have a significant impact on the control of the chamber pressure and, in turn, on the impact of the tunnelling operations.

Formation	Unit	Code	Lithology
LONDON CLAY	LONDON CLAY	LC	Stiff and very stiff grey to brown fissured CLAY. Sometimes very silty or slightly sandy in basal 10m. No glauconite, no gravel.
HARWICH FORMATION		HF	Variable lithology, grey to grey brown, fine SAND +/- shells. Fissured CLAY as London Clay. Shelly CLAY +/- impure shelly LIMESTONE.
	BLACKHEATH BEDS	HFBB	Rounded black fine and medium flint GRAVEL with clay, sandy clay or sand matrix. Blackheath Beds present as a subdivision of the HF.
WOOLWICH AND READING	UPPER MOTTLED CLAY	WRUMC	Stiff and very stiff red brown and brown mottled grey CLAY +/- fissuring.
	(UPPER SAND)	WRUS	Brown or grey fine SAND, silty SAND or sandy SILT. No bedding.
	LAMINATED BEDS	WRLB	Interlaminated grey brown grey fine SAND, SILT and CLAY in variable proportions. Occasional claystone lamina. Rare shells.
	LOWER SHELLY CLAY	WRLSC	Stiff and very stiff grey clay with shelly lamina and shell beds. Occasional shelly sands.
	LOWER MOTTLED BEDS	WRLMB	Very stiff red brown, brown and grey mottled CLAY. Burrowed top. Occasional calcareous nodules up to 500mm. Brown and grey medium SAND, sometimes clayey. Occasional calcareous nodules.
UPNOR FORMATION		UP	Brown medium SAND +/- glauconite; bedding.
			Rounded black or brown fine and medium flint GRAVEL in a clay, sandy clay or sand matrix.
			Dark grey or dark greenish grey fine or medium glauconite SAND, often silty. +/- grey clay lamina. +/- scattered rounded fine and medium flint gravel +/- thin pebble beds, +/- beddings
THANET SAND	THANET SAND	TS	Grey fine and medium silty SAND, finer and siltier with depth. Generally no bedding, no pebbles, no clay and no glauconite, although all rarely present. Sometimes with discontinuities.
	BULLHEAD BED	BUL	Gravel or cobble sized flints sometimes white rinded in a matrix of green grey clay or sand.
UPPER CHALK (Seaford Chalk)	HAVEN BROW	UCK	White medium dense, weak to moderately weak chalk with +/- flint.
	CUCKMERE		
	BELLE TOUT		

Table 7.1. Stratigraphic formation and unit names (Union Railways, 1997)

Section	Ring n <sup>o</sup> / chainage	Length m	Axis depth: m	Face conditions	Remarks
1	1 - 55 9065 - 8983	83	12-20	UPNOR AND LAMBETH GROUP	Initially 50%, each, then gradually more UPNOR
2	56 - 323 8981 - 8581	401	20-25	UPNOR AND THANET FORMATION	WRB disappears after ring 139. Initially 2/3 UPNOR, gradually reducing to FULL FACE THANET.
3	324 - 700 8579 - 8015	564	25-35	FULL FACE THANET SAND	Analysed in § 7.3
4	701 - 1663 8014 - 6571	1443	32-35	UPNOR AND THANET FORMATION	UPNOR starts appearing in crown at ring 700- 1663 (up to 50%, but often 30%).
5	1664 - 2690 6569 - 5030	1539	35-42	THANET AND CHALK	Max. 50% chalk between ring 2050 and 2200.
6	2691 - 2748 5029 - 4943	86	35	UPNOR AND THANET FORMATION	At first, full face THANET from 2691- 2748, then progressively more UPNOR until full face UPNOR
7	2749 - 3280 4942 - 4145	797	35	UPNOR AND LAMBETH GROUP	Increasing proportion of WRBLMC in invert until full face conditions reached.
8	3281 - 3860 4144 - 3275	869	32-35	FULL FACE LAMBETH GROUP	Analysed in § 7.4
9	3861 - 4327 3274 - 2575	699	25-35	LAMBETH GROUP / HARWICH / LONDON CLAY	Up to 20% HARWICH, LAMBETH GROUP decreases as LONDON CLAY increases.
10	4328 - 4888 2573 - 1733	840	12-25	FULL FACE LONDON CLAY	Analysed in § 7.5
11	4889 - 5025 1732 - 1528	204	10-12	LONDON CLAY AND ALLUVIUM	Alluviums appear in invert and increase to 90% near portal.

Table 7.2. Ground conditions at tunnel level along the route  
(based on 32 boreholes)

<b>Screw conveyor characteristics</b>		
<b>Geometry</b>		
Overall screw length	15000	mm
Auger diameter	1120	mm
Casing diameter	1190	mm
Central shaft diameter	267	mm
Auger pitch	900	mm
Screw axis inclination	13.5	°
<b>Drive</b>		
Number of motors	4	-
Rated oil pressure	24.5	MPa
Rated torque	12.11	kNm
Rated speed	110	rpm
Gear ratio	7.4	-

Table 7.3. Screw conveyor characteristics – Kawasaki machines  
Contract 220 *CTRL*

Parameter	Description
Ring number	Number of ring being constructed (from 1 to 5000)
Date Time	Real time and date
Net Jack stroke	Stroke of shield jack
Face Pres (centre)	
Face Pres (down)	
Face Pres (left)	Chamber pressure $p_2$ measured at location shown in Fig. 7.7
Face Pres (right)	
Face Pres (up)	
Screw EP (front)	Earth pressure in screw conveyor at location shown in Fig. 7.4
Screw EP (rear)	
Screw Pres	Oil pressure of screw conveyor drive. May be used to calculated screw torque
Screw Rev Speed	Angular speed of screw conveyor
Gate Open (front)	
Gate Open (rear)	Position of front and rear screw conveyor gates
Jack Spd Avg	Advance rate of the shield
S_Jack Thrust	Total thrust on the shield
Cut Rote Speed	Angular speed of the cutting head
Cutter Torque	Cutting head torque
Foam injection ratio ( <i>FIR</i> )	
Liquid injection ratio ( <i>LIR</i> )	Soil conditioning parameters
Excavating	Binary code: 1 during excavation, 0 during ring build

Table 7.4. Selection of monitored machine parameters

		FOAM		WATER/POLYMER		TOTAL LIQUID			
		FIR (%)	FER (%)	PIR (%)	LIR (%)				
		Mean	Std.	Mean	Std.	Mean	Std.	Mean	Std.
*Tunnel section according to Table 7.2									
<b>PREDOMINANTLY GRANULAR SOIL</b>									
*3	THANET SAND								
	upline	52.4	21.8	10.3	0.7	7.1	3.4	10.3	4.9
	downline	50.4	20.9	12.4	5.2	7.5	5.9	10.2	5.2
2/6	UPNOR SAND / THANET SAND								
	upline	69.8	32.9	11.9	1.6	10.1	3.9	15.9	5.1
	downline	50.5	27.8	14.1	4.1	10.5	6.1	13.9	6.4
5	THANET SAND / CHALK								
	upline	48.0	24.6	12.7	2.5	2.4	2.9	5.3	3.9
	downline	21.9	18.0	11.3	3.7	4.1	2.6	5.2	3.4
<b>PREDOMINANTLY COHESIVE SOIL</b>									
8	LAMBETH GROUP								
	upline	54.6	29.6	8.1	3.3	10.9	4.5	17.9	5.5
	downline	38.6	32.1	7.0	4.3	8.0	11.6	13.2	12.6
10	LONDON CLAY								
	upline	24.8	11.3	4.3	1.3	13.2	4.1	19.0	4.7
	downline	26.6	13.8	3.9	1.9	6.3	3.1	13.3	2.6
<b>MIXED COHESIVE AND GRANULAR FACE CONDITIONS</b>									
1/7	UPNOR SAND / LAMBETH GROUP								
	upline	49.0	38.8	7.8	2.9	8.7	9.3	12.9	6.2
	downline	41.8	23.7	10.7	2.7	12.5	4.9	14.9	6.7
9	LAMBETH GROUP / HARWICH / LONDON CLAY								
	upline	12.7	9.4	2.4	1.8	10.1	5.1	15.6	7.5
	downline	47.9	37.1	5.2	3.7	3.5	3.8	12.5	4.6
11	LONDON CLAY / ALLUVIUM								
	upline	7.9	5.1	3.9	1.5	7.4	3.3	9.4	3.7
	downline	n/a	n/a	n/a	n/a	n/a	n/a	n/a	n/a

Table 7.5. Summary of soil conditioning parameters in different ground conditions

	Advance rate mm/min		p <sub>2,mean</sub> kPa		Thrust MN		Cutter torque MNm		Screw torque kNm		Screw speed rpm	
	Mean	Std.	Mean	Std.	Mean	Std.	Mean	Std.	Mean	Std.	Mean	Std.
*Tunnel section (Table 7.2)												
<b>PREDOMINANTLY GRANULAR SOIL</b>												
*3 THANET SAND												
upline	58.5	11.7	90.0	17.4	24.2	4.7	6.9	1.1	97.3	21.2	5.9	1.3
downline	52.8	13.5	84.5	10.3	23.1	4.5	5.6	1.7	83.9	20.4	4.5	1.2
2/6 UPNOR SAND / THANET SAND												
upline	59.8	17.3	98.0	26.0	21.5	4.9	7.1	1.3	111.0	27.8	6.8	2.0
downline	57.6	18.9	104.8	27.0	27.4	4.8	6.7	1.4	84.8	19.7	4.4	1.4
5.0 THANET SAND / CHALK												
upline	69.1	17.9	114.2	19.7	20.4	3.5	6.9	1.5	113.7	26.4	7.7	1.8
downline	69.3	17.4	108.6	29.2	28.5	4.5	6.5	1.4	83.6	19.0	4.6	1.2
<b>PREDOMINANTLY COHESIVE SOIL</b>												
8.0 LAMBETH GROUP												
upline	36.1	13.2	126.3	58.6	16.4	3.8	7.6	0.8	101.3	30.1	5.2	5.2
downline	38.6	17.5	135.5	80.0	18.0	4.3	6.6	1.6	109.1	33.6	3.6	2.8
10.0 LONDON CLAY												
upline	30.8	7.5	182.1	47.1	19.6	3.3	7.5	1.1	63.7	18.4	2.6	1.0
downline	35.7	9.1	189.8	45.3	18.1	2.7	7.4	1.1	88.0	18.1	3.4	1.5
<b>MIXED COHESIVE AND GRANULAR FACE CONDITIONS</b>												
1/7 UPNOR SAND / LAMBETH GROUP												
upline	56.3	19.5	100.8	26.8	21.9	5.5	7.2	1.3	107.1	29.3	6.4	2.3
downline	55.2	19.2	101.5	29.6	27.1	6.0	6.8	1.4	85.5	20.0	4.4	1.5
9.0 LAMBETH GROUP / HARWICH / LONDON CLAY												
upline	24.8	8.3	224.7	46.8	26.1	4.2	8.1	0.7	78.2	26.1	1.9	1.0
downline	21.3	6.6	192.9	56.5	21.2	3.6	7.1	1.3	99.8	27.3	1.5	0.6
11.0 LONDON CLAY / ALLUVIUMS												
upline	34.0	8.7	84.8	36.4	12.2	2.9	6.2	1.7	59.9	14.4	3.5	1.6
downline	45.2	7.8	109.0	38.7	10.5	3.1	4.4	1.9	78.2	16.5	5.5	1.7

Table 7.6. Summary of average machine parameters in different ground conditions

	<b>p<sub>2,mean</sub>: kPa</b>		<b>p<sub>2,exc</sub>: kPa</b>		<b>p<sub>2,iqr</sub>: kPa</b>		<b>p<sub>2,10%</sub>: kPa</b>		<b>p<sub>2,drop</sub>: kPa</b>		<b>p<sub>2,range</sub>: kPa</b>	
	Mean	Std.	Mean	Std.	Mean	Std.	Mean	Std.	Mean	Std.	Mean	Std.
*Tunnel section (Table 7.2)												
<b>PREDOMINANTLY GRANULAR SOIL</b>												
*3 THANET SAND												
upline	90.0	17.4	94.7	12.1	20.8	12.5	73.8	16.9	55.6	31.4	53.8	5.5
downline	84.5	10.3	92.6	7.1	14.8	7.4	73.4	12.0	35.0	13.1	46.5	7.9
2/6 UPNOR SAND / THANET SAND												
upline	98.0	26.0	101.7	22.8	23.4	15.0	79.0	24.0	60.3	32.0	39.3	14.4
downline	104.8	27.0	114.9	25.9	20.3	18.7	88.9	30.4	47.0	32.2	51.0	17.9
5.0 THANET SAND / CHALK												
upline	114.2	19.7	119.7	12.9	27.2	16.3	91.9	21.0	67.0	32.4	29.3	7.1
downline	108.6	29.2	125.0	26.4	30.3	22.9	86.2	34.5	64.7	36.7	53.5	21.7
<b>PREDOMINANTLY COHESIVE SOIL</b>												
8.0 LAMBETH GROUP												
upline	126.3	58.6	127.0	55.0	30.5	23.6	98.6	49.5	75.9	60.1	28.0	9.2
downline	135.5	80.0	143.4	82.6	34.6	32.2	104.7	68.6	91.4	74.7	65.2	40.0
10.0 LONDON CLAY												
upline	182.1	47.1	184.0	46.3	26.6	20.6	156.8	47.8	60.3	53.9	43.9	9.6
downline	189.8	45.3	197.8	40.1	41.4	26.7	153.4	44.3	109.2	69.4	107.2	33.3
<b>MIXED COHESIVE AND GRANULAR FACE CONDITIONS</b>												
1/7 UPNOR SAND / LAMBETH GROUP												
upline	100.8	26.8	104.5	23.5	22.7	15.4	82.3	25.3	59.3	34.6	36.5	15.1
downline	101.5	29.6	110.9	29.2	19.4	18.0	86.0	32.0	46.1	31.9	46.9	19.2
9.0 LAMBETH GROUP / HARWICH / LONDON CLAY												
upline	224.7	46.8	217.1	38.5	42.9	31.3	187.2	39.7	127.2	100.2	44.0	21.4
downline	192.9	56.5	203.2	48.3	45.8	27.7	155.2	58.9	130.1	67.1	84.4	29.2
11.0 LONDON CLAY / ALLUVIUMS												
upline	84.8	36.4	84.7	34.0	16.3	11.5	70.9	33.9	34.9	26.2	51.2	12.6
downline	109.0	38.7	111.1	37.9	22.6	15.2	88.6	37.2	64.6	35.8	142.7	66.6

Table 7.7. Summary of average face components in different ground conditions (see Fig. 7.12)

<b>Machine operation in full face Thanet Sand</b>						
<b>Parameter</b>	<b>Symbol</b>	<b>FIR</b>	<b>FER</b>	<b>PIR</b>	<b>LIR</b>	<b>Line</b>
Advance rate		-0.44	-0.04	-0.31	-0.42	Upline
		-0.24	-0.04	-0.19	-0.15	Downline
Cutter head torque		-0.20	-0.18	-0.03	-0.04	Upline
		-0.41	-0.10	0.14	0.22	Downline
Screw torque		-0.01	0.14	0.02	0.04	Upline
		0.04	0.06	-0.14	-0.35	Downline
Shield thrust		0.15	-0.08	0.39	0.44	Upline
		-0.20	-0.13	0.30	0.36	Downline
P <sub>2,IQR</sub>		0.14	-0.04	0.09	0.10	Upline
		0.02	-0.04	0.12	0.15	Downline
P <sub>2,range</sub>		0.20	-0.03	-0.04	0.10	Upline
		0.13	0.09	-0.43	-0.40	Downline
P <sub>2,drop</sub>		0.22	-0.06	0.07	0.10	Upline
		0.11	0.20	0.00	0.04	Downline

<b>Machine operation in full face Lambeth Group</b>						
<b>Parameter</b>	<b>Symbol</b>	<b>FIR</b>	<b>FER</b>	<b>PIR</b>	<b>LIR</b>	<b>Line</b>
Advance rate		-0.24	0.17	0.08	-0.03	Upline
		-0.49	0.80	-0.06	-0.54	Downline
Cutter head torque		-0.15	0.04	-0.02	-0.04	Upline
		0.41	-0.45	-0.05	0.32	Downline
Screw torque		-0.22	-0.11	0.19	0.17	Upline
		-0.24	0.12	-0.09	-0.28	Downline
Shield thrust		-0.32	-0.24	0.31	0.28	Upline
		0.42	-0.64	-0.02	0.46	Downline
P <sub>2,IQR</sub>		-0.21	-0.24	0.41	0.37	Upline
		0.50	-0.64	-0.05	0.44	Downline
P <sub>2,range</sub>		-0.13	-0.13	0.18	0.21	Upline
		0.39	-0.56	0.09	0.49	Downline
P <sub>2,drop</sub>		-0.11	-0.19	0.30	0.30	Upline
		0.36	-0.54	-0.06	0.32	Downline

<b>Machine operation in full face London Clay</b>						
<b>Parameter</b>	<b>Symbol</b>	<b>FIR</b>	<b>FER</b>	<b>PIR</b>	<b>LIR</b>	<b>Line</b>
Advance rate		-0.31	0.20	-0.22	-0.42	Upline
		0.12	0.50	0.34	-0.07	Downline
Cutter head torque		0.13	0.16	-0.06	-0.07	Upline
		0.07	0.14	-0.28	-0.35	Downline
Screw torque		-0.08	0.23	-0.29	-0.40	Upline
		-0.08	-0.22	-0.05	0.05	Downline
Shield thrust		0.35	0.26	0.19	0.30	Upline
		-0.01	-0.05	-0.40	-0.36	Downline
P <sub>2,IQR</sub>		0.09	-0.09	0.15	0.22	Upline
		-0.17	-0.28	-0.38	-0.28	Downline
P <sub>2,range</sub>		-0.38	-0.69	-0.05	-0.01	Upline
		-0.33	-0.40	-0.30	-0.29	Downline
P <sub>2,drop</sub>		0.15	0.03	0.17	0.22	Upline
		-0.16	-0.22	-0.14	-0.01	Downline

Table 7.8. Summary of correlation coefficient between soil conditioning parameters and machine parameters (the data corresponding to the shaded parts are plotted in Fig. 7.13)

	Ring no.	FIR	FER	PIR	LIR	Speed	Thrust	Torque	Screw torque	Screw speed	P <sub>2,mean</sub>	P <sub>2,exc</sub>	P <sub>2,iqr</sub>	P <sub>2,10%</sub>	P <sub>2,drop</sub>	P <sub>2,range</sub>
		%	%	%	%	mm/min	MN	MNm	kNm	rpm	kPa	kPa	kPa	kPa	kPa	kPa
Fig. 7.14	555.0	31.1	10.6	0.0	2.9	61.8	26.0	6.5	95.1	5.9	102.0	108.3	15.8	90.2	71.8	56.9
	556.0	38.9	10.9	0.0	3.6	63.5	24.4	6.0	87.1	6.0	95.3	110.0	26.2	75.8	51.6	51.0
	557.0	30.6	10.8	0.0	2.8	68.3	27.0	5.8	90.2	6.4	92.4	106.8	23.8	74.2	68.0	52.2
	558.0	24.3	10.1	7.5	9.9	60.9	29.0	6.4	92.7	6.0	87.7	113.4	37.6	67.0	42.4	56.3
	559.0	51.7	10.3	9.5	14.5	51.3	26.0	4.1	69.8	5.1	98.4	104.4	14.2	86.4	28.8	51.9
	560.0	56.9	10.4	9.2	14.7	52.1	25.7	4.2	57.6	4.8	95.0	106.6	20.1	81.6	37.4	52.6
Fig. 7.15	491.0	84.3	10.0	0.0	8.4	53.8	20.0	6.8	101.4	5.4	147.7	97.3	89.8	86.8	184.6	59.0
	492.0	73.8	10.3	0.0	7.2	42.8	20.9	4.8	121.9	4.5	86.6	102.7	22.9	58.8	65.4	52.9
	493.0	19.5	9.1	1.2	3.4	43.8	19.3	6.7	144.7	4.2	75.3	84.1	18.8	62.2	55.0	47.8
	494.0	39.0	10.9	0.5	4.1	47.5	19.2	6.4	131.8	5.0	77.3	90.9	23.0	62.6	45.8	51.3
	495.0	48.9	10.9	1.4	5.9	47.2	20.0	6.3	137.2	5.6	60.6	79.0	33.8	37.0	82.2	77.1
	496.0	80.5	11.4	2.5	9.6	51.5	19.0	6.6	101.1	5.6	71.7	66.8	13.8	60.6	36.6	71.5
Fig. 7.16	3726.0	244.8	13.3	11.6	30.0	26.1	13.6	7.3	107.3	2.2	112.4	113.2	35.9	65.8	110.6	29.6
	3727.0	144.6	13.7	8.7	19.3	37.1	13.4	7.0	104.5	2.9	115.5	127.1	34.3	81.7	96.4	35.7
	3728.0	121.7	11.9	8.5	18.7	36.6	12.9	7.0	147.7	3.4	106.3	121.4	53.9	73.8	115.2	34.9
	3729.0	9.7	1.0	10.1	20.2	34.9	14.3	7.4	124.0	3.3	94.0	123.6	73.6	43.4	166.2	27.6
	3730.0	5.5	0.6	9.7	19.4	47.9	13.7	7.9	92.9	4.3	123.7	129.6	16.8	109.2	56.6	34.8
	3731.0	6.8	0.7	10.3	20.7	45.6	15.5	7.9	150.6	4.3	147.9	146.9	12.6	130.5	43.4	35.6
	3732.0	6.9	0.6	11.0	22.0	43.0	17.6	6.9	139.3	3.6	164.0	164.0	42.2	120.3	194.2	33.3

Table 7.9. Summary of average soil conditioning and machine parameters for the rings plotted in Fig. 7.14 to 7.16

	Ring no.	FIR %	FER %	PIR %	LIR %	Speed mm/min	Thrust MN	Torque MNm	Screw torque kNm	Screw speed rpm	P <sub>2,mean</sub> kPa	P <sub>2,exc</sub> kPa	P <sub>2,iqr</sub> kPa	P <sub>2,10%</sub> kPa	P <sub>2,drop</sub> kPa	P <sub>2,range</sub> kPa
Fig. 7.17	3608.0	41.3	9.8	4.9	9.1	47.1	22.7	7.1	92.1	4.5	96.3	101.0	11.8	83.1	43.2	31.1
	3609.0	45.2	10.1	4.4	8.9	55.0	22.6	7.4	114.0	6.0	99.6	103.8	19.4	81.8	40.4	35.3
	3610.0	49.7	12.1	5.2	9.4	69.4	22.6	7.1	132.3	6.8	107.5	119.6	30.3	83.0	54.4	33.5
	3611.0	57.8	9.7	6.1	12.1	67.5	21.9	6.4	97.5	5.8	122.5	121.2	37.6	77.6	171.2	33.0
	3612.0	63.0	12.4	7.5	12.6	55.0	20.0	7.7	140.3	4.8	86.7	96.6	28.8	60.0	59.6	37.3
	3613.0	87.3	12.8	8.6	15.4	n/a	n/a	n/a	n/a	n/a	36.9	n/a	14.3	28.2	38.0	18.8
	3614.0	92.2	13.1	7.8	14.8	35.5	19.4	7.7	112.3	3.4	101.7	112.4	54.6	54.3	124.2	36.4
	3615.0	84.1	14.0	8.4	14.4	40.7	18.3	8.1	133.8	3.5	88.7	103.6	45.0	50.2	60.4	28.8
	3616.0	90.4	13.5	11.5	18.2	31.4	15.0	6.7	104.9	3.4	95.6	99.9	54.6	55.4	182.8	41.0
3617.0	158.2	12.5	7.2	19.8	16.1	15.3	7.1	90.3	1.7	61.6	91.7	78.0	16.6	164.6	35.8	
Fig. 7.18	4393.0	29.5	7.1	14.9	19.0	46.2	17.9	6.4	64.1	4.1	120.3	117.9	7.2	109.5	12.4	28.2
	4394.0	25.4	6.6	17.4	21.2	42.7	18.3	6.9	61.8	3.7	130.2	122.9	28.2	104.0	34.2	33.1
	4395.0	27.0	6.4	15.1	19.3	44.4	19.0	6.3	68.5	4.0	130.2	119.2	24.6	108.5	16.8	28.5
	4396.0	22.1	5.9	3.8	7.5	47.4	19.5	6.9	86.4	4.3	116.4	125.2	13.0	102.4	46.2	28.0
	4397.0	18.7	5.7	3.3	6.5	47.8	19.4	8.3	89.1	4.8	122.8	125.1	6.8	118.2	26.6	30.4
	4398.0	21.6	5.4	4.0	8.1	42.3	19.0	8.2	83.8	4.4	122.1	123.9	15.9	106.0	37.8	31.1
	4399.0	23.8	5.8	4.1	8.2	43.5	19.0	8.1	90.8	4.6	123.4	116.6	13.8	111.0	13.4	30.1
Fig. 7.19	4777.0	6.1	1.4	10.6	15.0	27.2	22.2	8.3	68.0	1.8	220.1	222.1	12.4	205.7	19.8	64.3
	4778.0	5.4	1.3	12.0	16.1	24.6	21.0	8.2	51.1	1.7	218.6	209.2	36.0	197.0	35.6	54.1
	4779.0	3.8	1.2	11.6	14.9	26.9	22.5	8.3	64.1	1.9	208.6	207.6	10.4	195.2	20.0	64.6
	4780.0	19.5	2.5	10.2	18.1	24.3	21.2	8.2	40.5	1.6	203.0	205.1	17.6	187.0	34.2	55.8
	4781.0	18.1	2.2	10.2	18.6	24.5	20.3	6.0	48.2	1.8	210.8	206.4	25.9	178.6	95.8	57.4
	4782.0	16.4	2.4	5.9	12.7	31.5	20.3	6.5	67.3	2.5	201.1	202.1	11.1	188.0	17.2	57.3

Table 7.10. Summary of average soil conditioning and machine parameters for the rings plotted in Fig. 7.17 to 7.19

Face conditions	Total volume loss: %		Face volume loss: %		$V_{L,face}/V_L$ %
	Mean	Range	Mean	Range	
Lambeth Group and Upnor Formation	0.6	0.3 - 0.7	0.1	0.0 - 0.2	20.1
Upnor Formation and Thanet Sand	0.7	0.2 - 2.9	0.2	0.1 - 0.6	21.3
Thanet Sand	0.4	0.2 - 0.8	0.1	0.0 - 0.2	23.7
Thanet Sand and Chalk	0.3	0.2 - 0.5	0.1	0.1 - 0.1	21.5
Lambeth Group	0.7	0.5 - 1.0	0.2	0.1 - 0.3	22.4
Harwich Formation and Lambeth Group	0.7	0.7 - 0.7	0.2	0.2 - 0.2	24.3
London Clay, Harwich and Lambeth Group	0.5	0.4 - 0.5	0.1	0.1 - 0.1	20.9
London Clay	0.7	0.6 - 0.8	0.2	0.1 - 0.3	32.4

Table 7.11. Mean and range of total and face volume loss in different ground conditions (Upline tunnel)

Chainage (rings)	Face conditions	Tunnel axis depth m	$V_{L,face}$ %	$V_L$ %	$p_{2,mean}/\sigma_{vo}$ %	$p_{2,10\%}/\sigma_{vo}$ %	$T/(A\sigma_{vo})$ %	Figure
7247.5-7240 (1211-1217)	Upnor Formation and Thanet Sand	31.60	0.10	1.23	9.8	6.7	21.3	Fig. 7.27
8892.5-8885 (114-120)		21.00	0.60	2.85	9.4	4.9	11.1	Fig. 7.28
8477.5-8470 (392-398)	Thanet Sand	24.00	0.05	0.30	16.7	11.7	34.6	Fig. 7.29
8377.5-8370 (458-464)		24.30	0.10	0.23	20.9	16.4	37.1	Fig. 7.30
3037.5-3030 (4018-4024)	London Clay, Harwich and Lambeth Group	33.60	0.05	0.47	41.4	30.0	51.8	Fig. 7.31
3102.5-3095 (3974-3980)		33.00	0.14	0.44	38.7	25.3	37.6	Fig. 7.32
2492.5-2485 (4382-4388)	London Clay	33.00	0.14	0.80	30.7	24.6	39.0	Fig. 7.33
2297.5-2290 (4511-4517)		31.00	0.25	0.72	36.2	31.0	47.2	Fig. 7.34

Table 7.12. Comparison of average face pressure components in four pairs of sections with high and low face volume losses.



Fig. 7.1. Tunnel route of CTRL Section 2 (Brown, 2003)

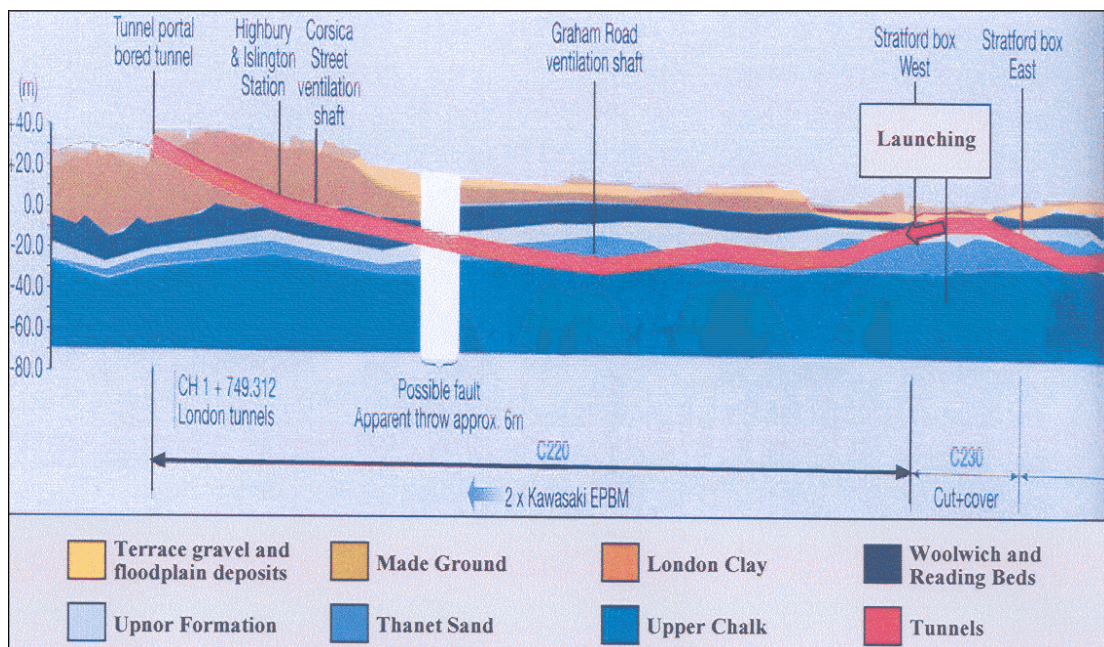


Fig. 7.2. Longitudinal geological section of Contract 220 (after Woods, 2003)

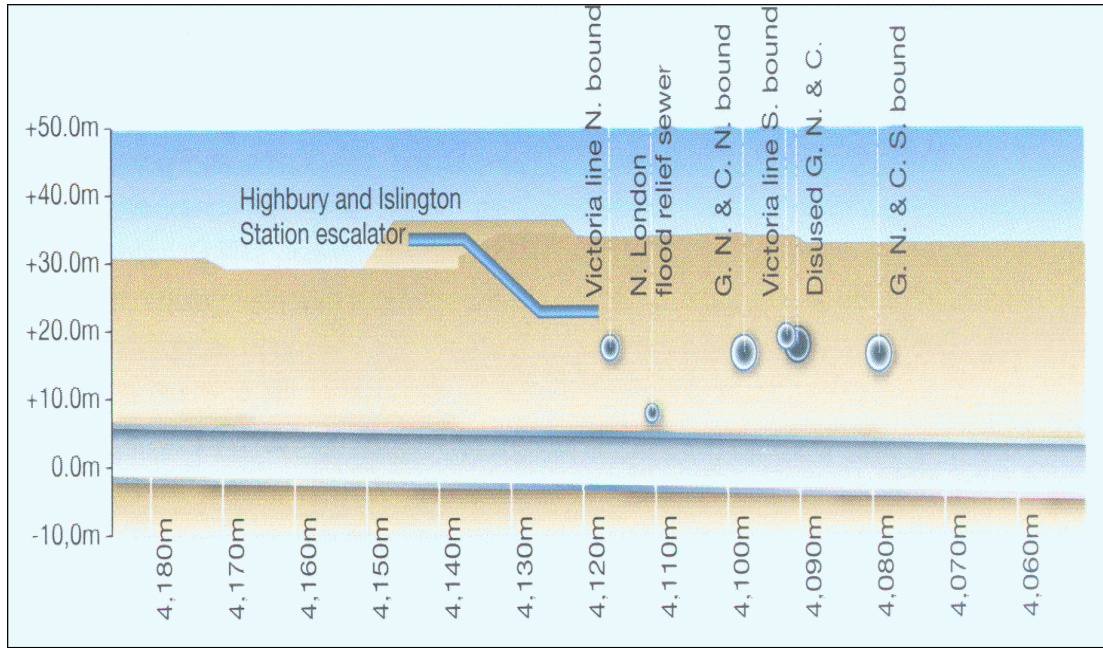


Fig. 7.3. Under-crossing of the Tube lines and sewer in the Highbury Corner area (Ano, 2003)

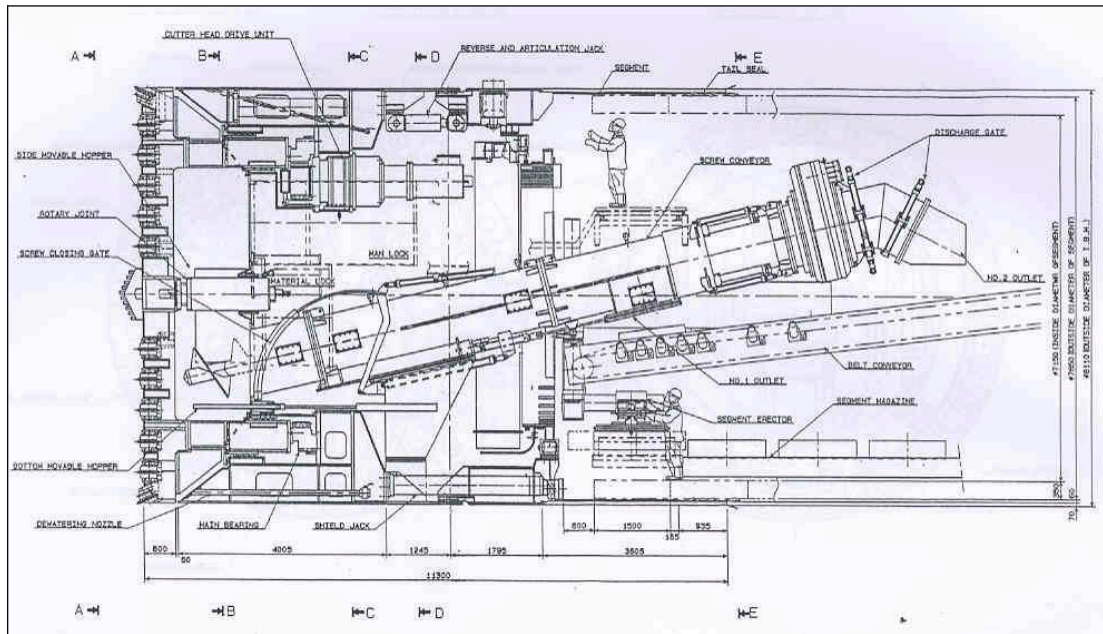


Fig. 7.4. Cross-sectional view of the Kawasaki EPB machine (by courtesy of Nishimatsu Construction Ltd)

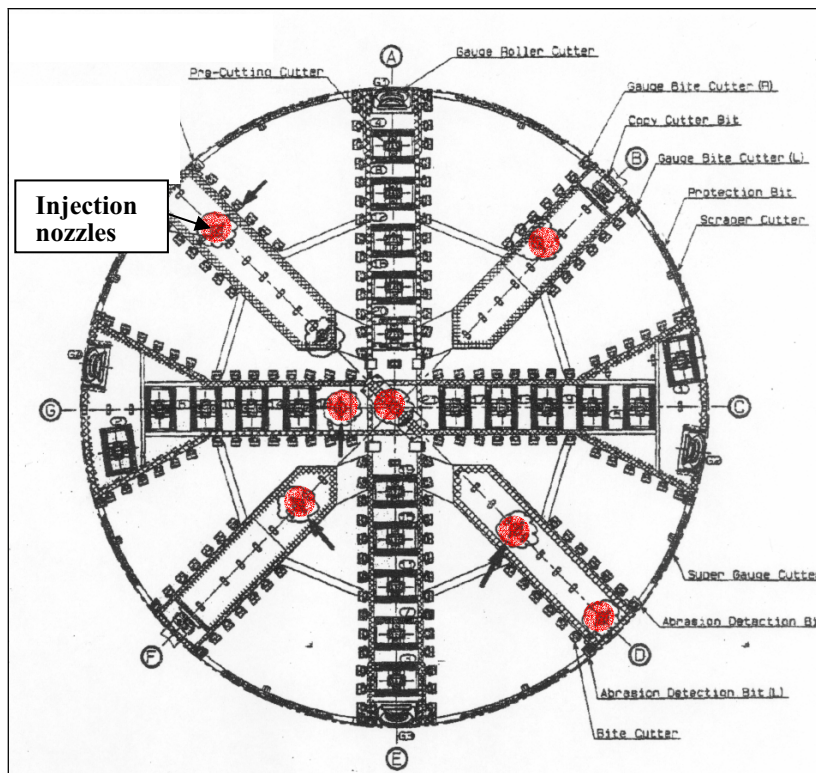


Fig. 7.5. Front view of cutter head (by courtesy of Nishimatsu Construction Ltd)



Fig. 7.6. Photograph of cutter head (by courtesy of Rail Link Engineering)

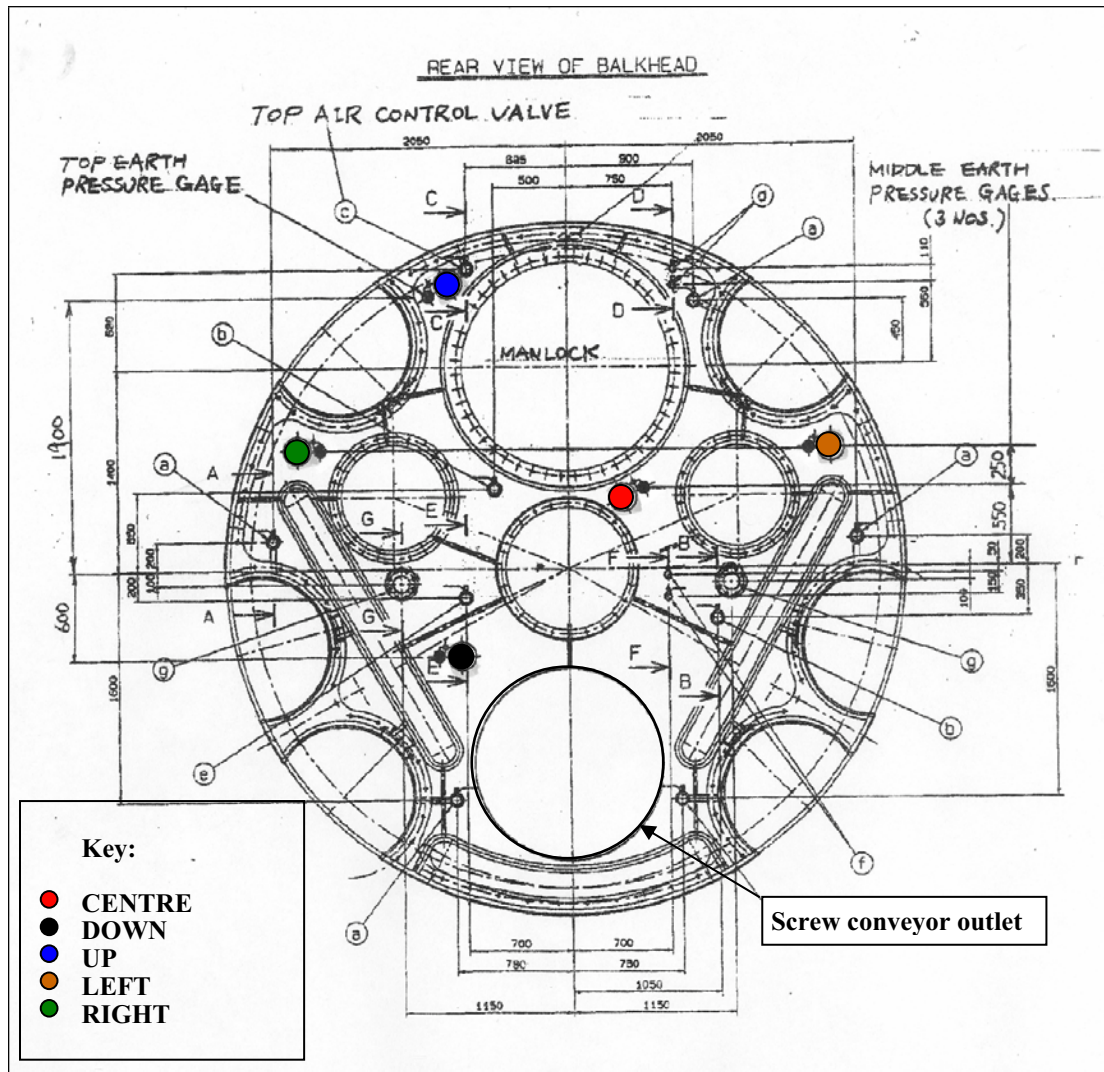


Fig. 7.7. Cross-sectional view of the machine bulkhead (by courtesy of Nishimatsu Construction Ltd)

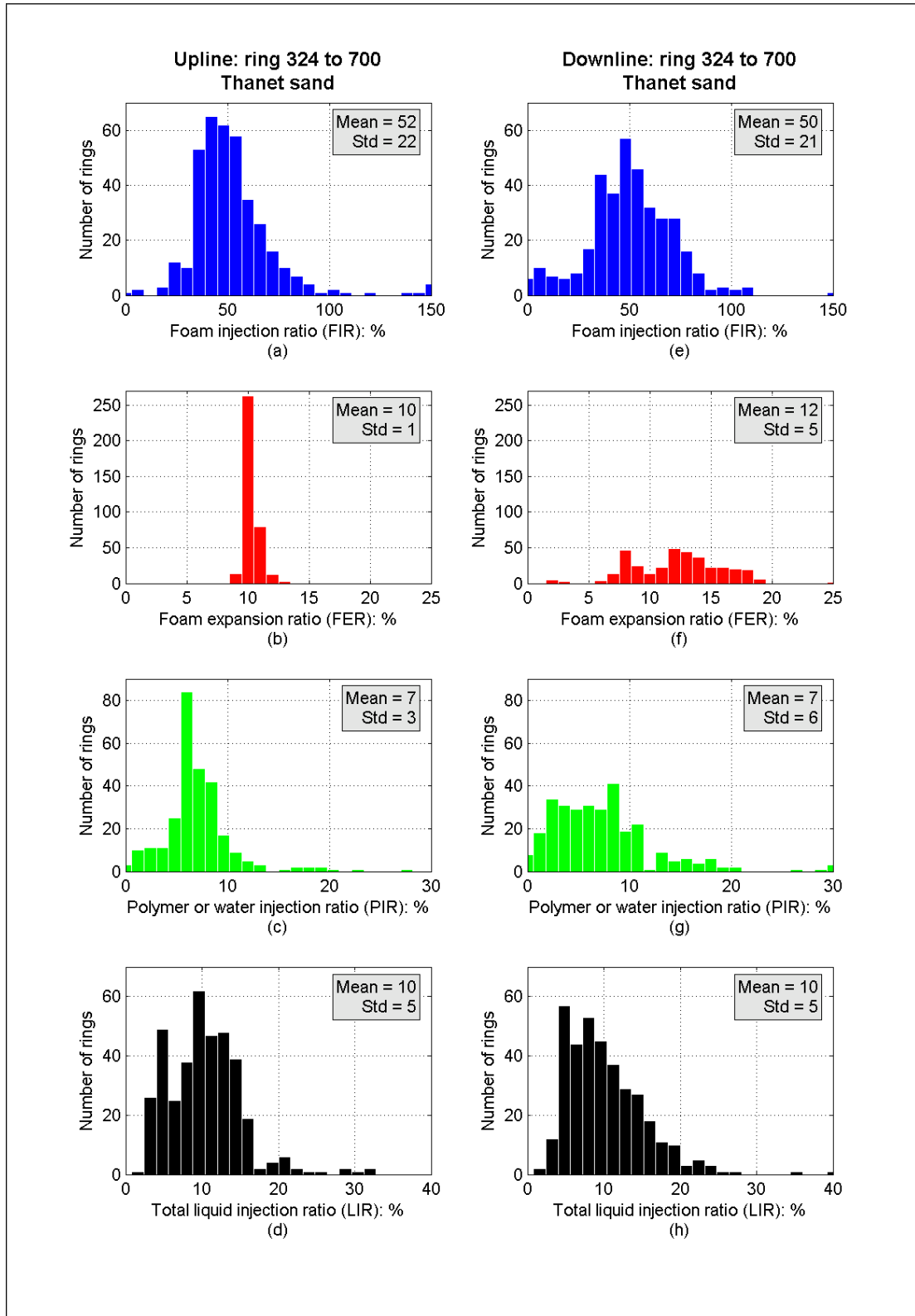


Fig. 7.8. Distribution of soil conditioning parameters in Thanet Sand

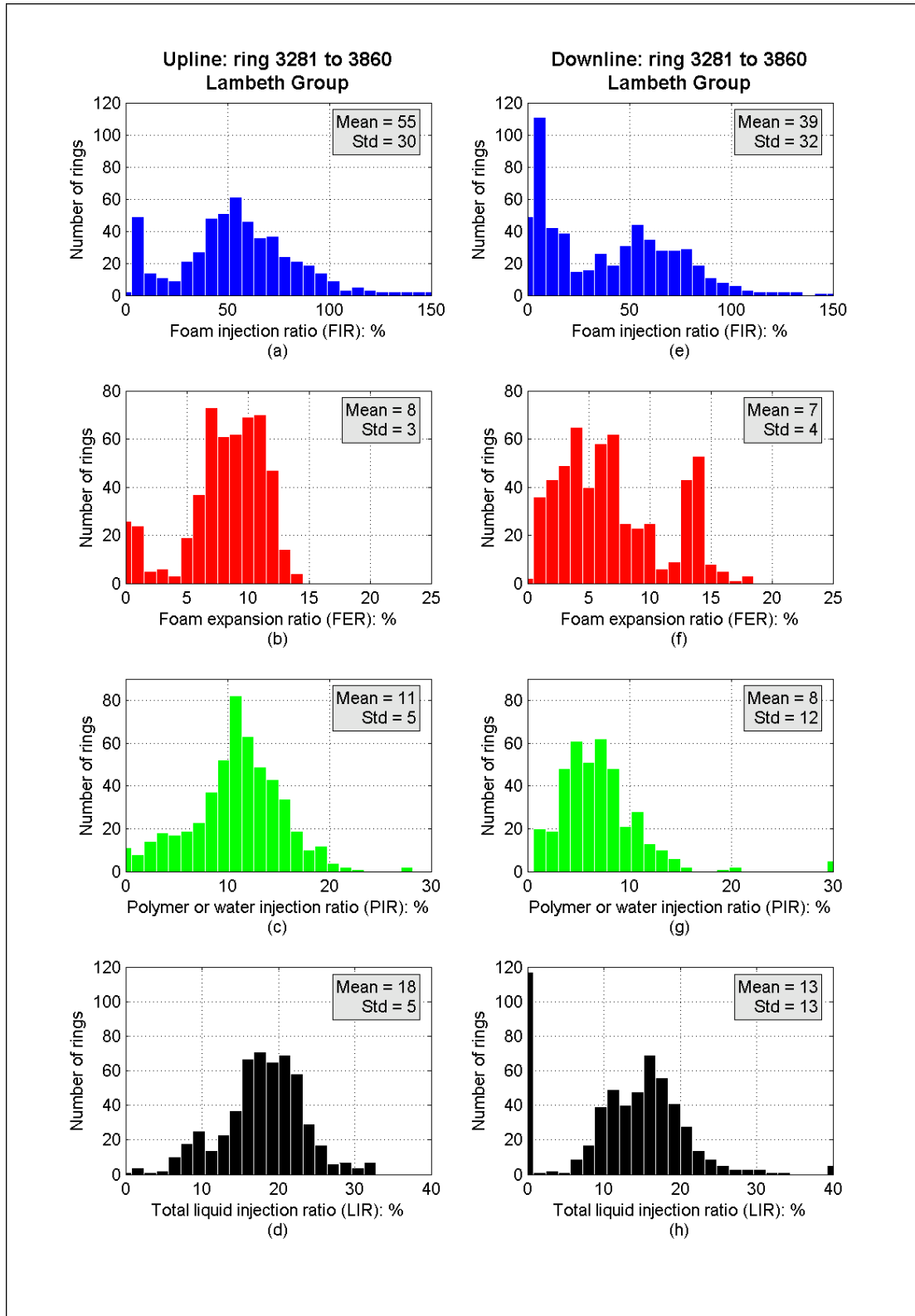


Fig. 7.9. Distribution of soil conditioning parameters in the Lambeth Group

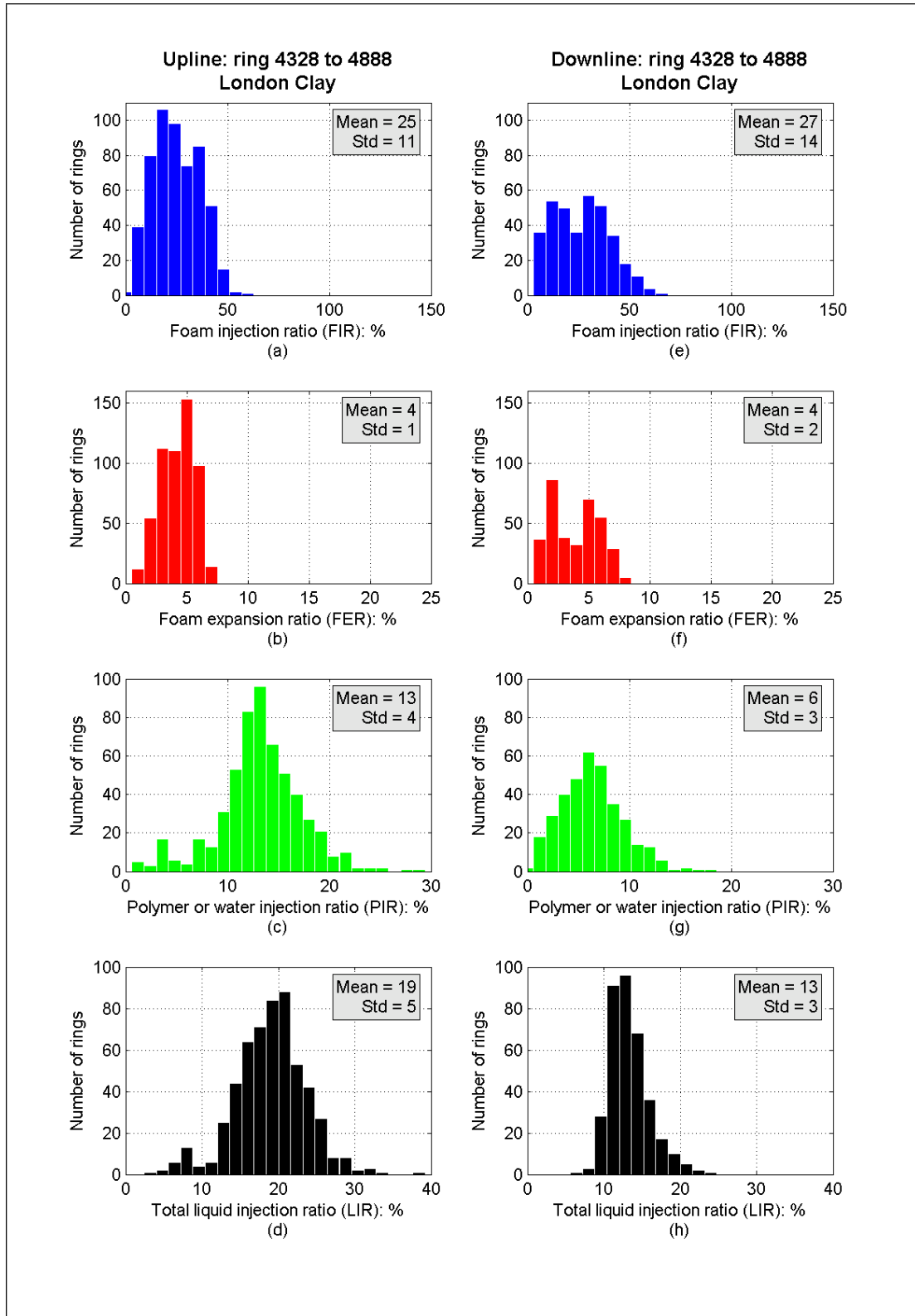


Fig. 7.10. Distribution of soil conditioning parameters in London Clay

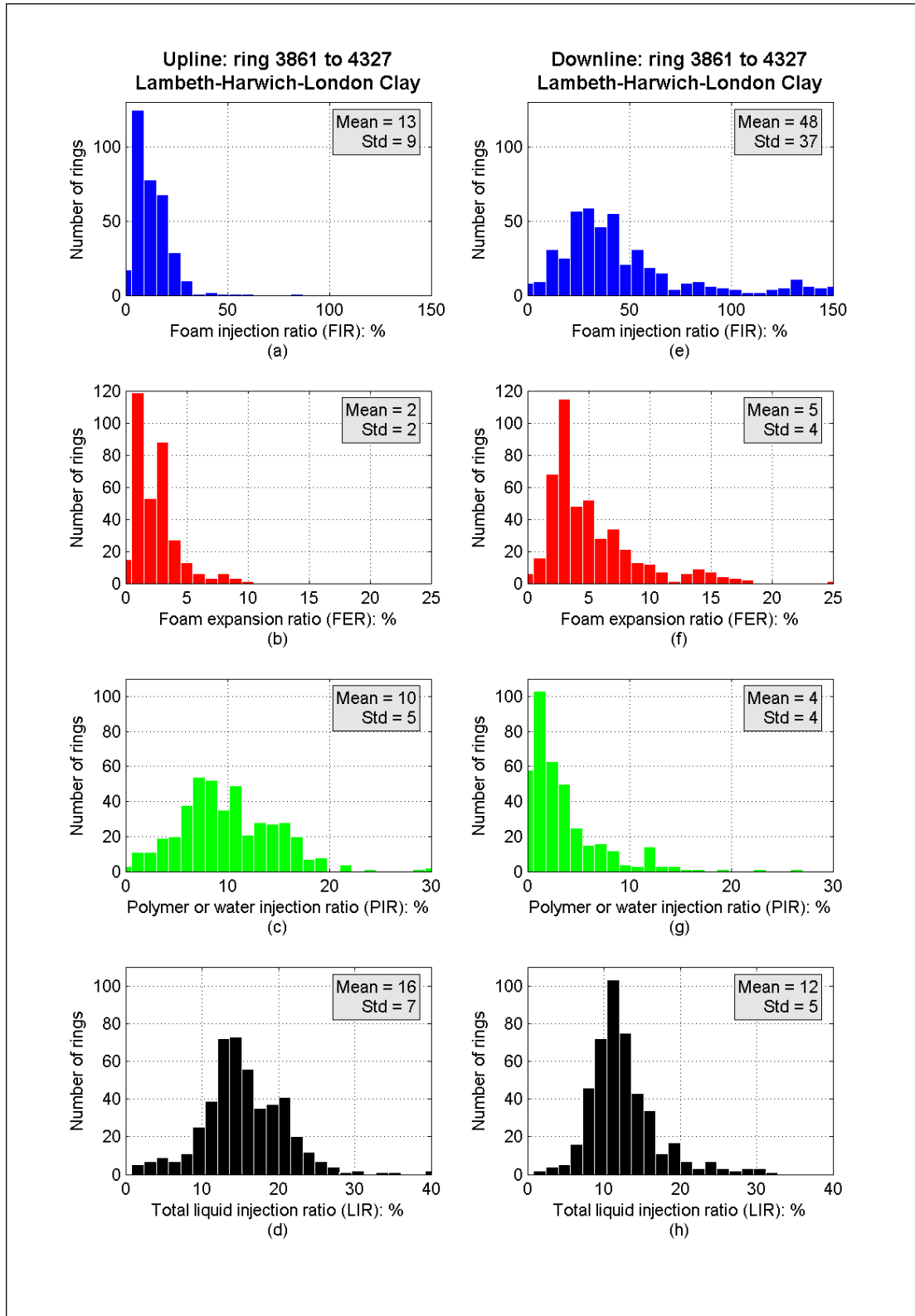


Fig. 7.11. Distribution of soil conditioning parameters in mixed face conditions Lambeth Group / Harwich Formation / London Clay

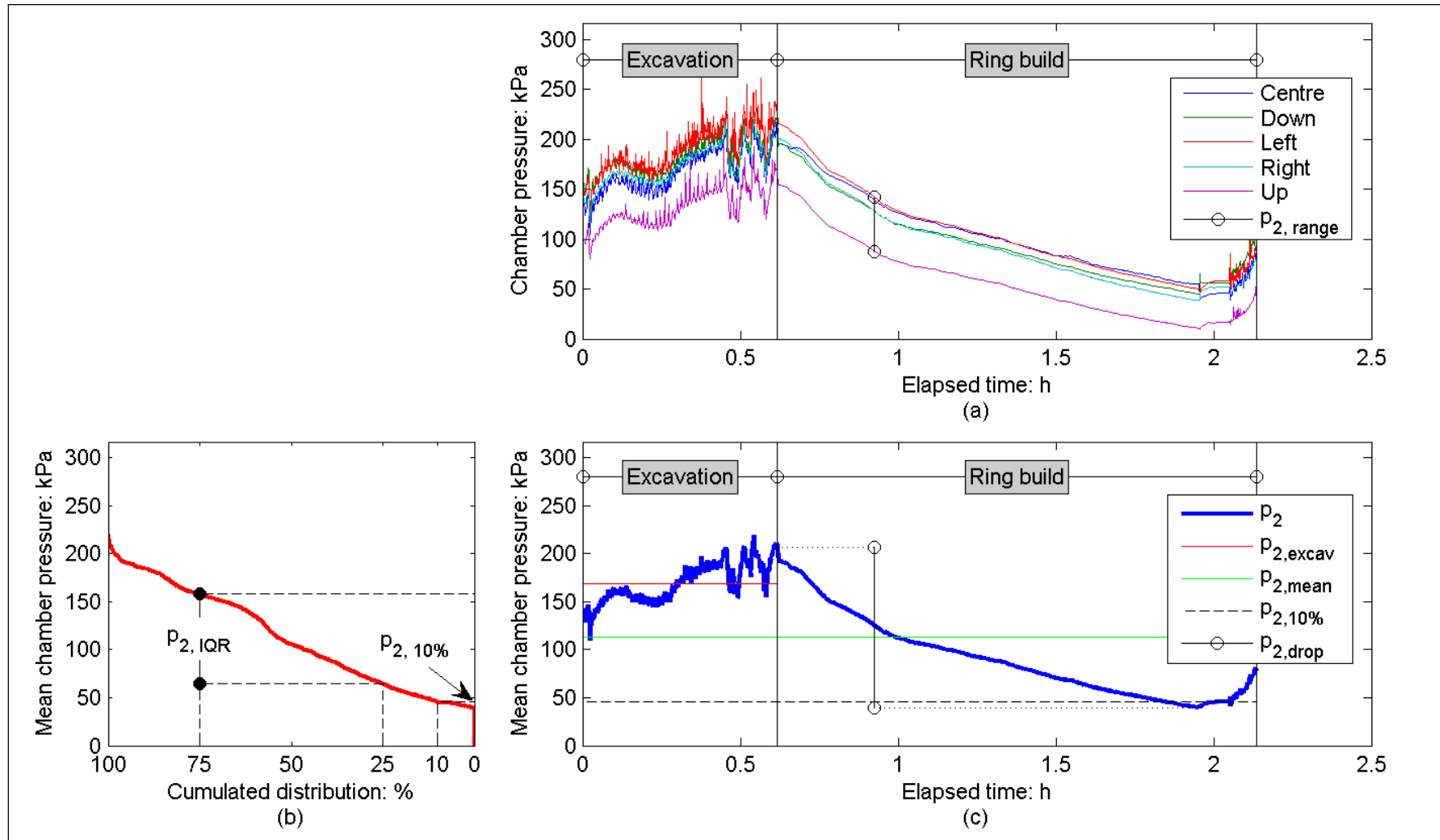


Fig. 7.12. Definition of the chamber pressure components

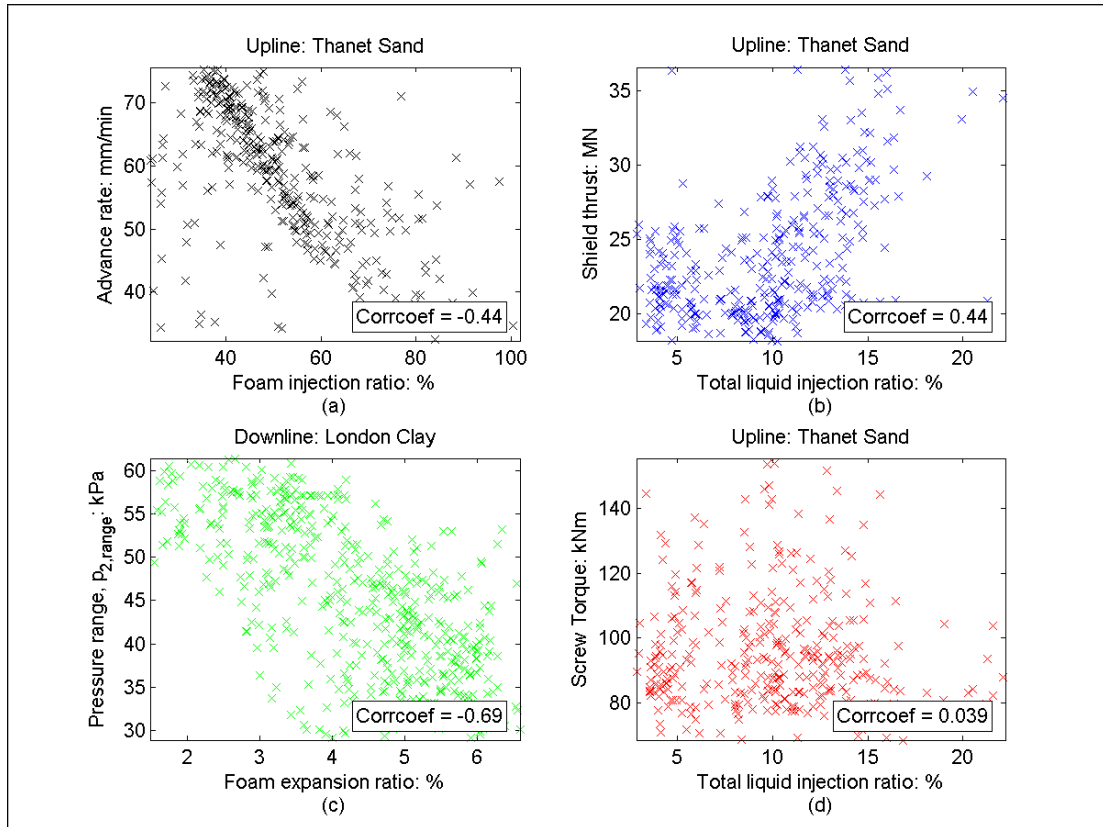


Fig. 7.13. Correlation between soil conditioning and machine parameters (see Table 7.8)

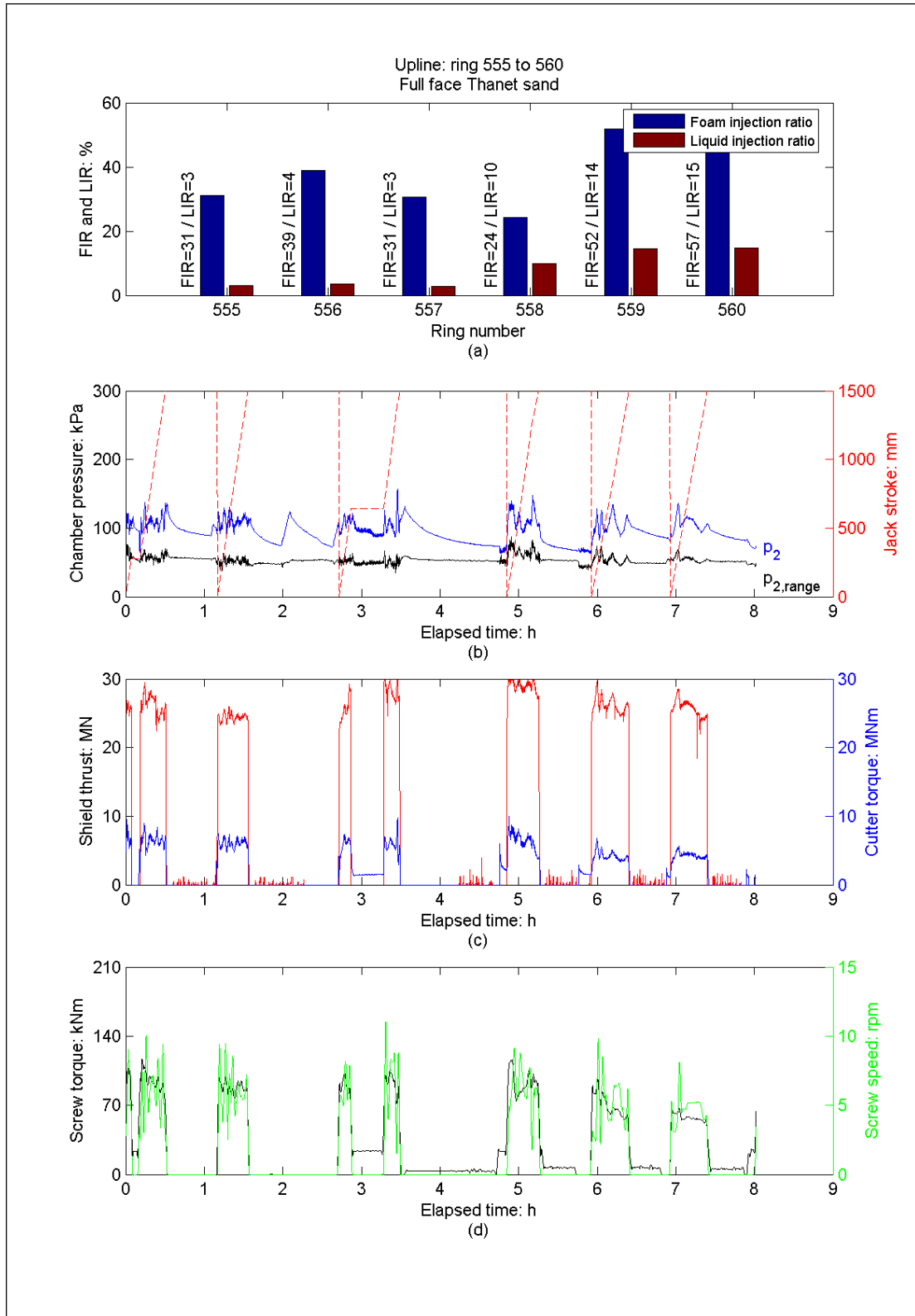


Fig. 7.14. Machine parameters in relation to soil conditioning parameters: effect of total liquid injection ratio (*LIR*) in Thanet Sand

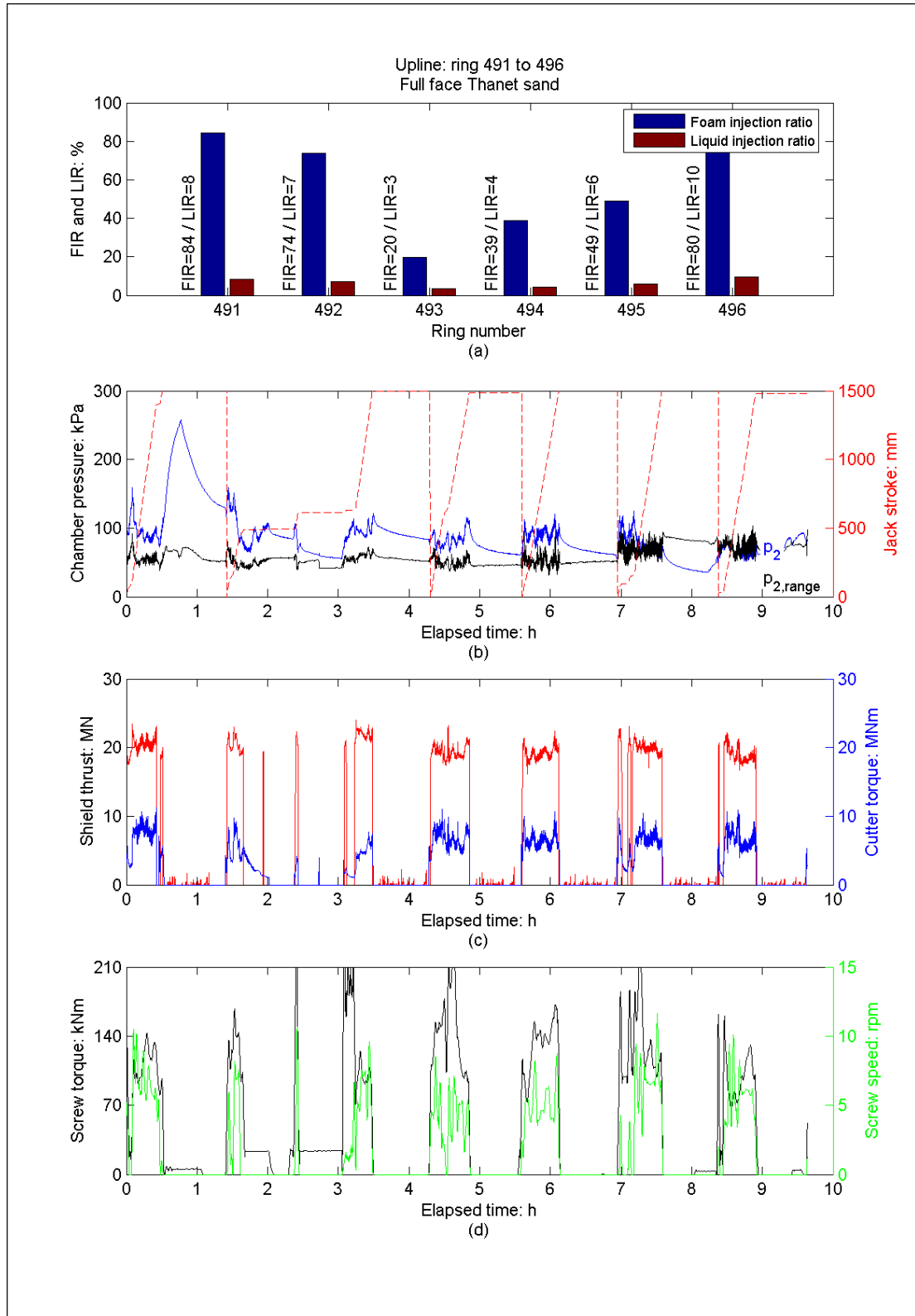


Fig. 7.15. Machine parameters in relation to soil conditioning parameters: effect of foam injection ratio (FIR) in Thanet Sand

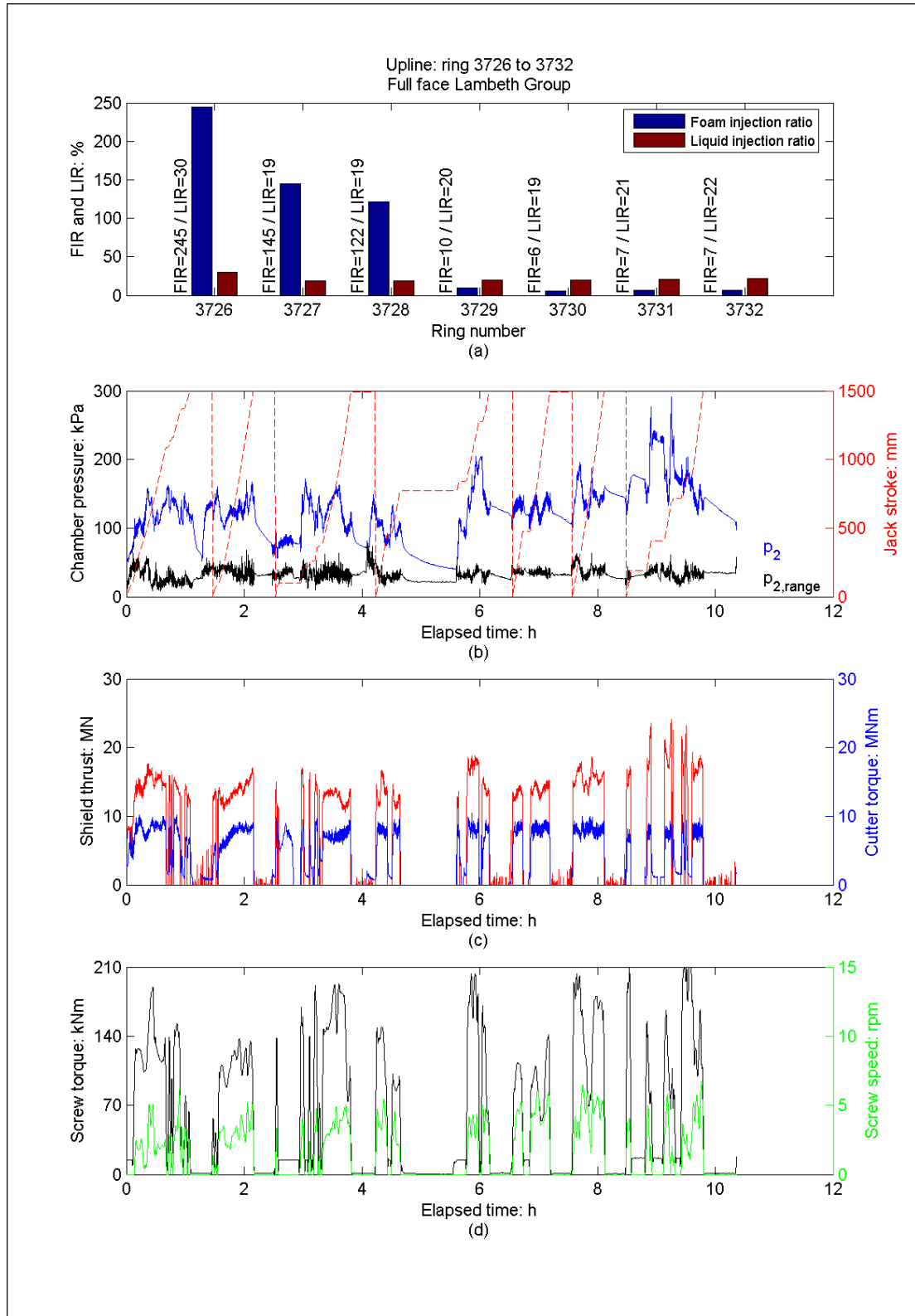


Fig. 7.16. Machine parameters in relation to soil conditioning parameters: effect of foam injection rate (*FIR*) in the Lambeth Group

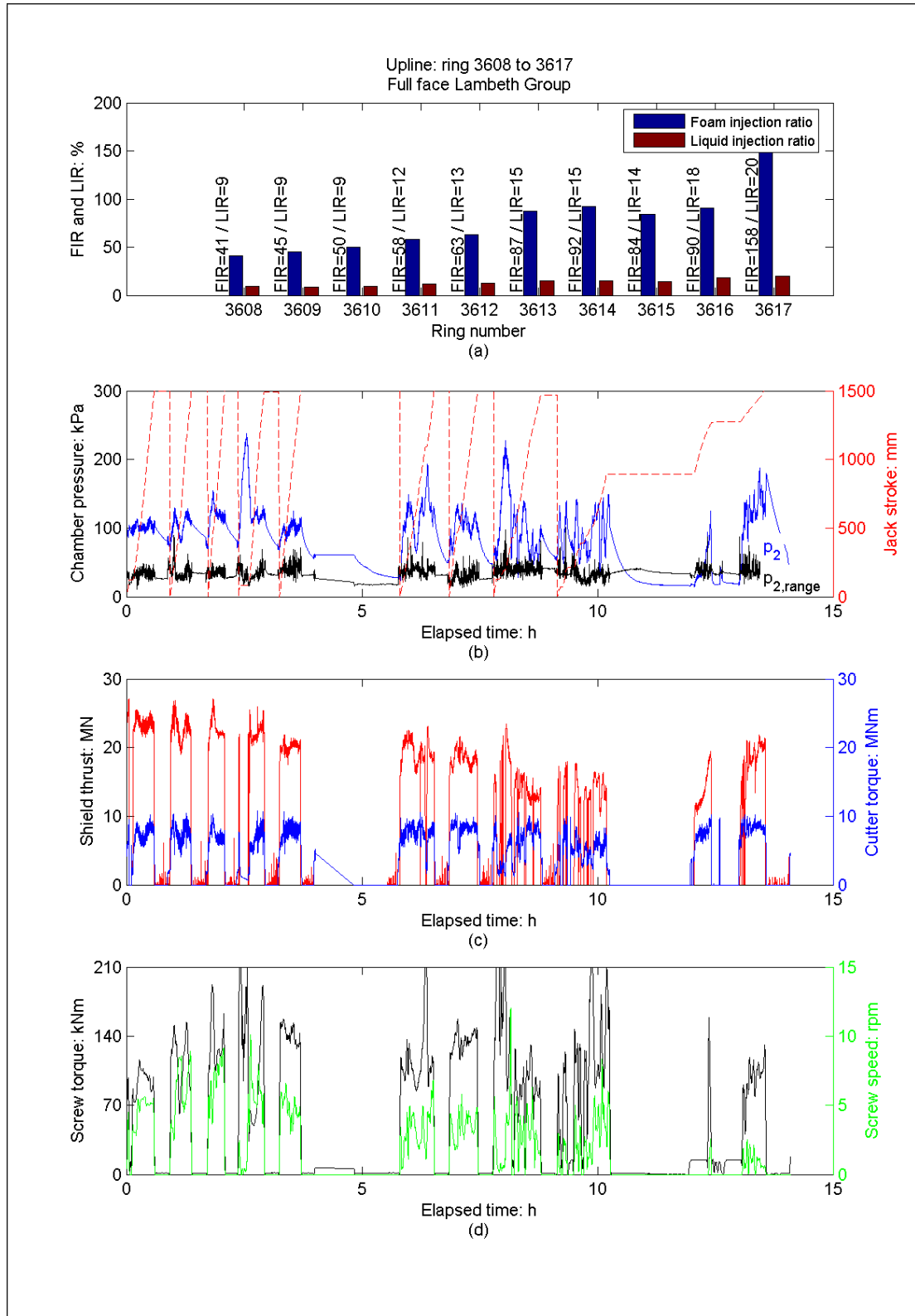


Fig. 7.17. Machine parameters in relation to soil conditioning parameters: effect of Total liquid injection ratio (*LIR*) in the Lambeth Group

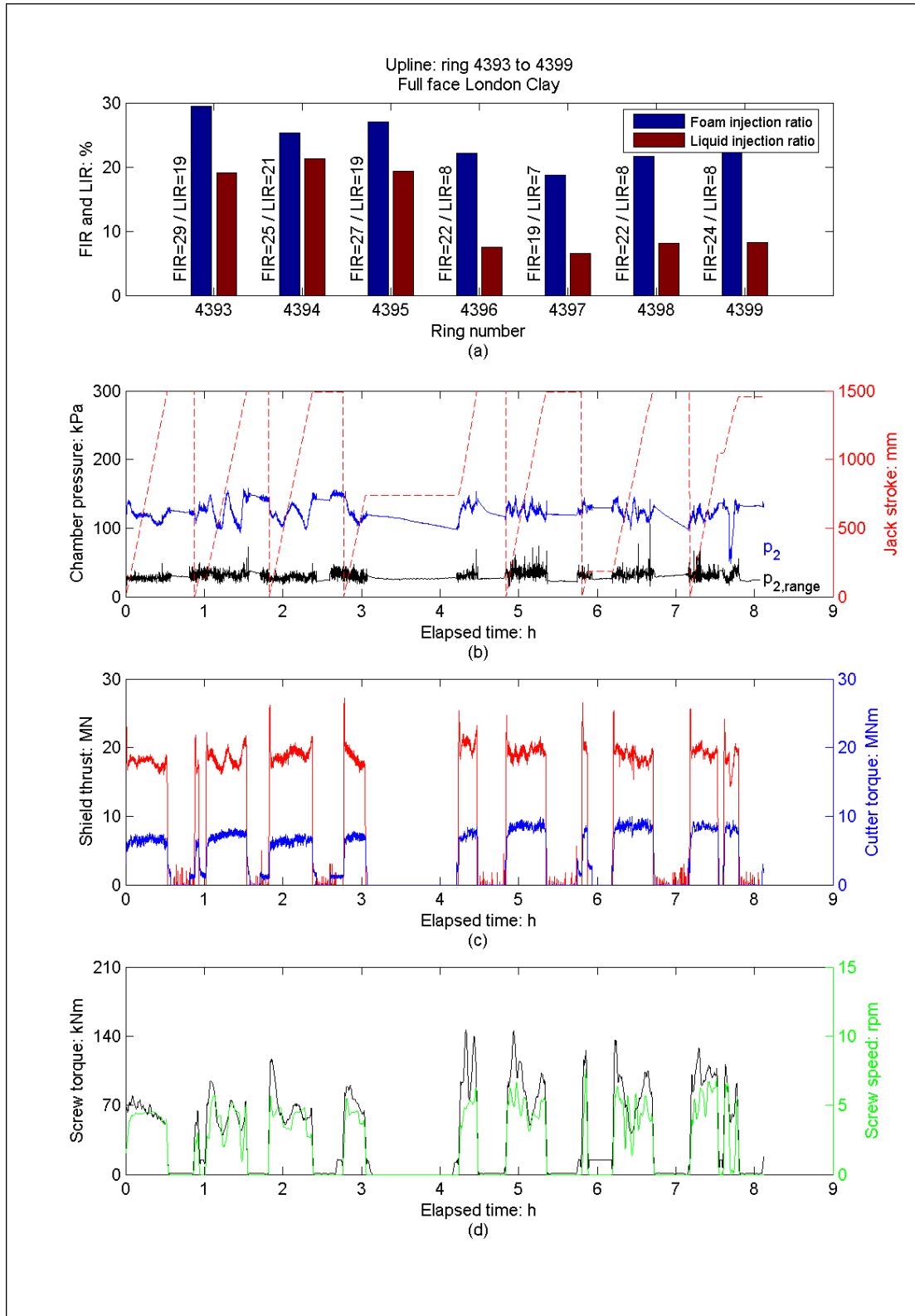


Fig. 7.18. Machine parameters in relation to soil conditioning parameters: effect of liquid injection ratio (*LIR*) in London Clay

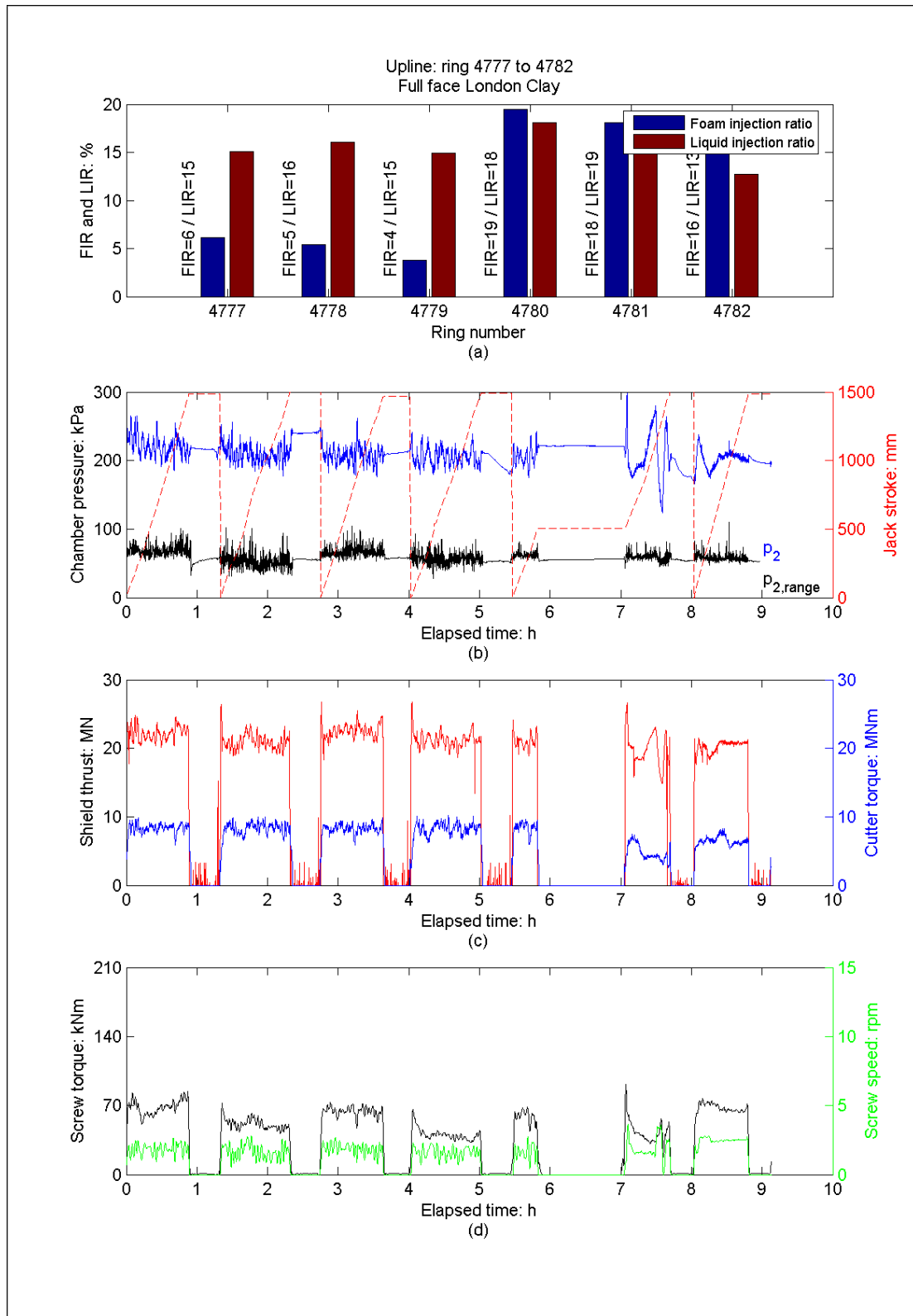


Fig. 7.19. Machine parameters in relation to soil conditioning parameters: effect of foam injection ratio (FIR) in London Clay

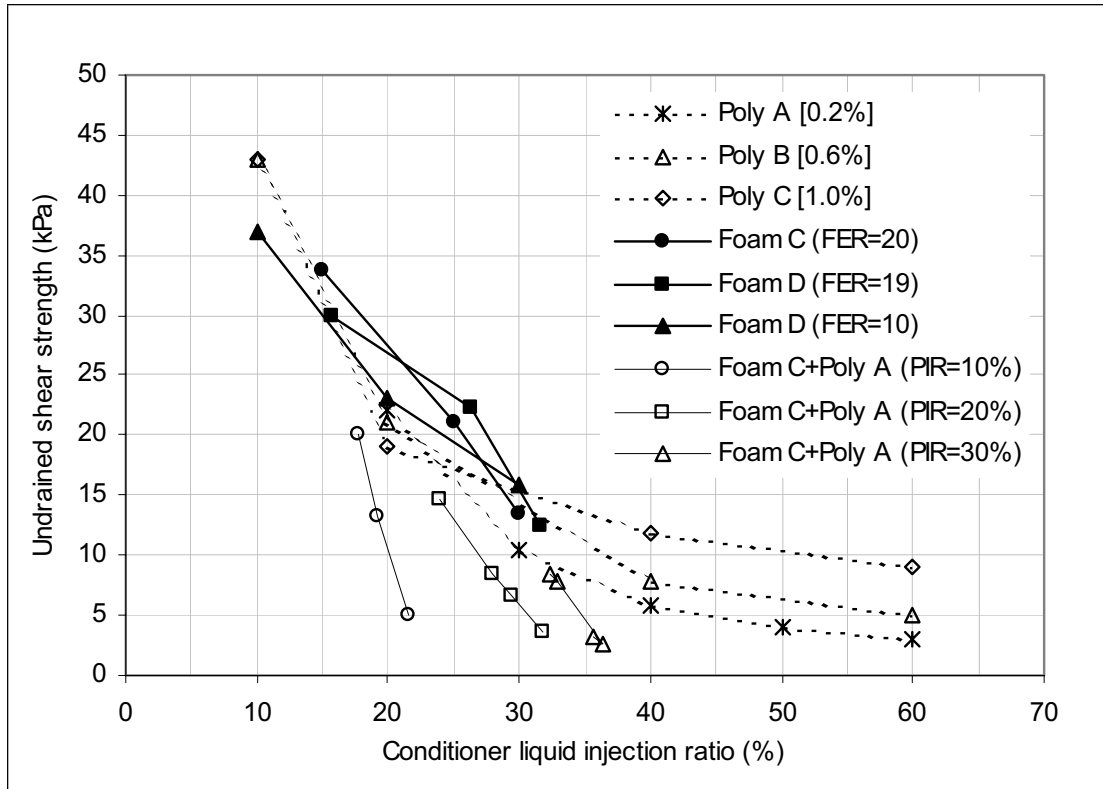


Fig. 7.20. Conditioned London Clay sample strength and liquid injection ratio (Merritt *et al.*, 2002)

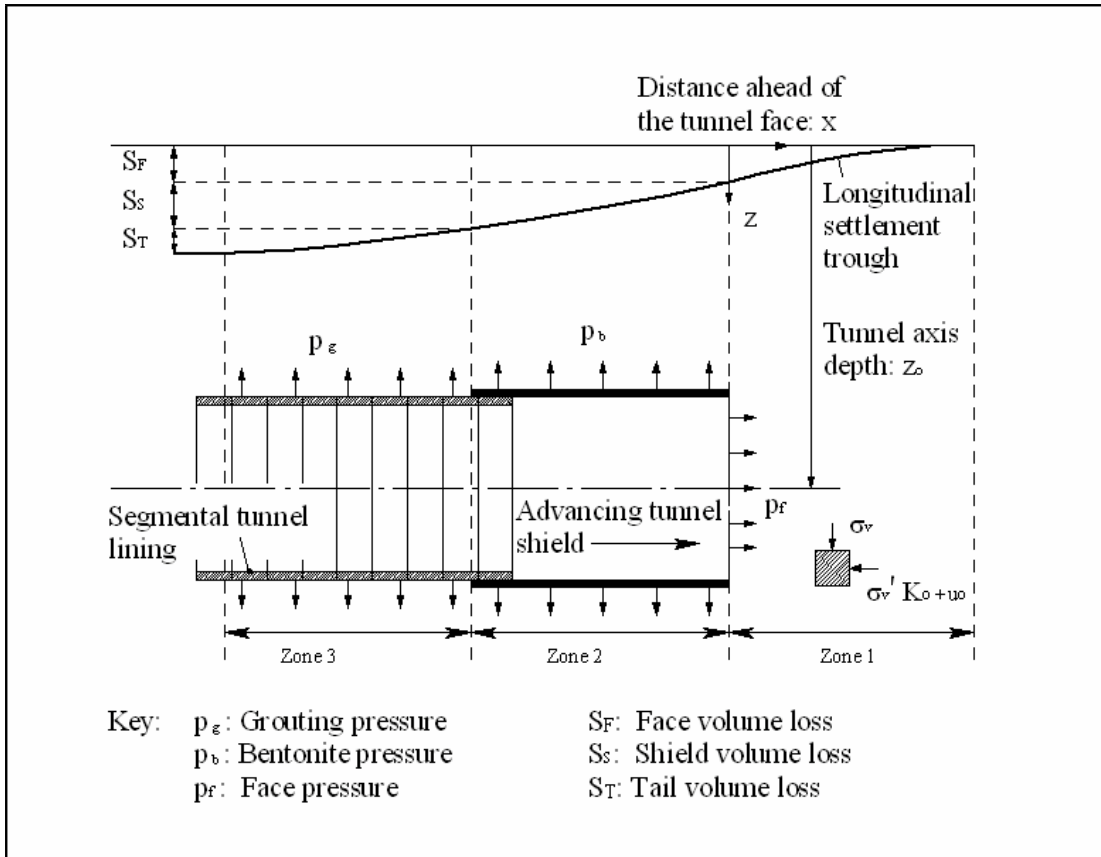


Fig. 7.21. Definition of volume loss components and related machine parameters (after Wongsaroy *et al.*, 2006)

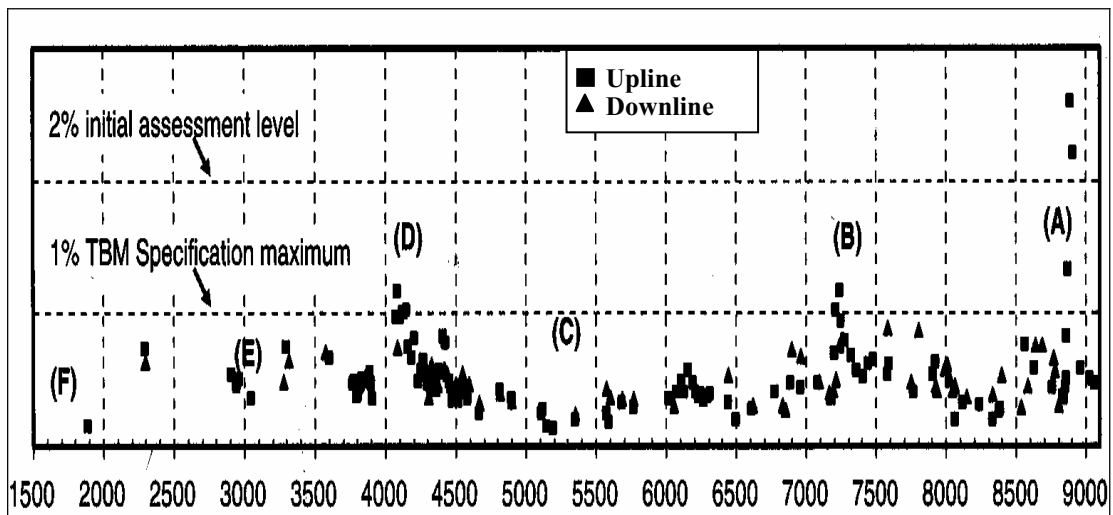


Fig. 7.22. Volume loss along Contract 220 derived from transverse ground surface settlement monitoring profiles (Bowers & Moss, 2006)

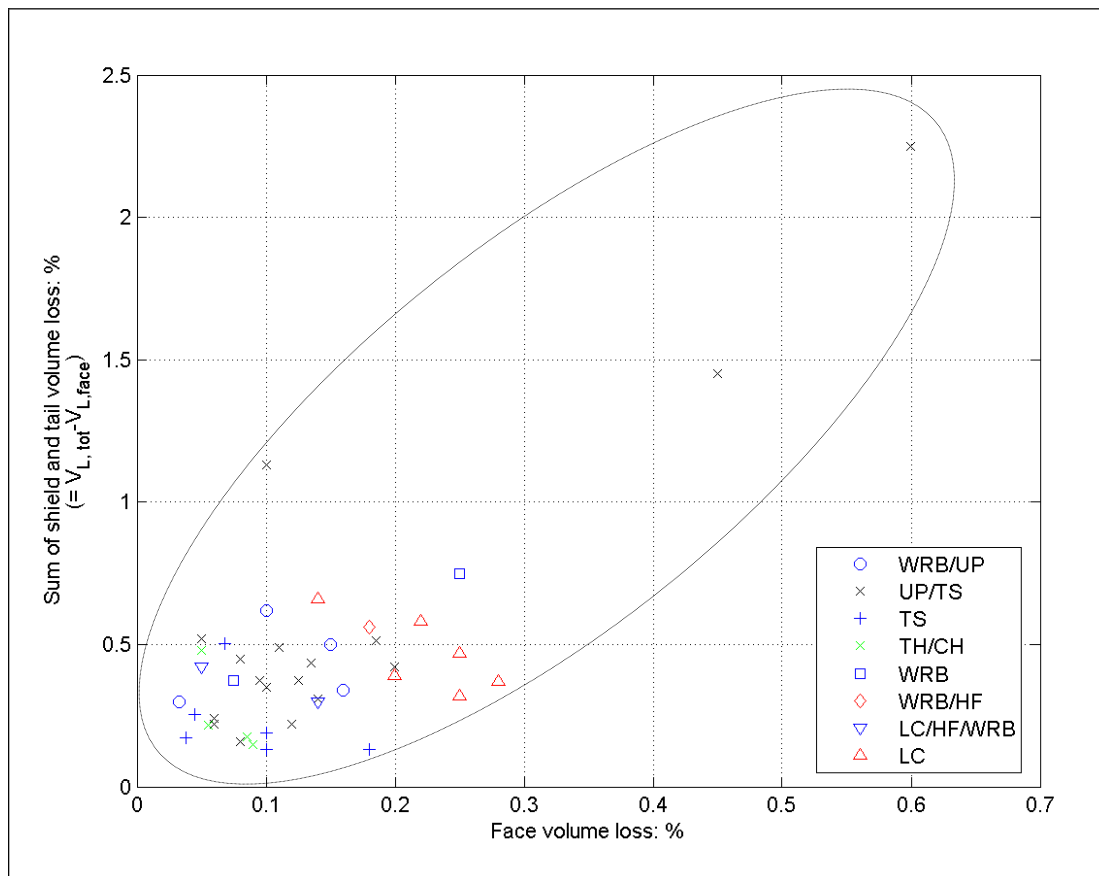


Fig. 7.23. Relationship between face volume loss and sum of shield and tail volume loss components

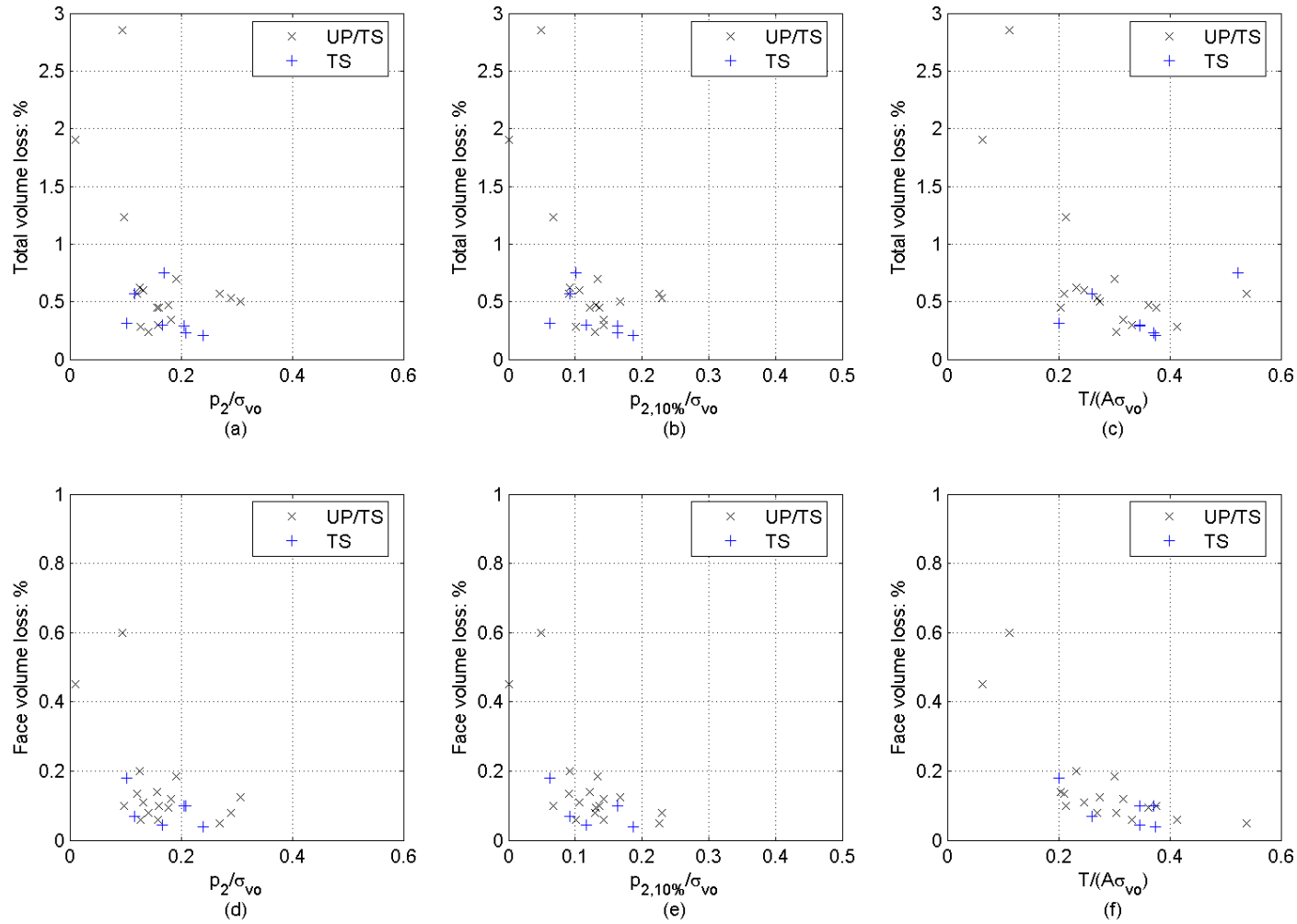


Fig. 7.24. Relationships between face pressure and volume loss components Thanet Sand and Upnor/Thanet Sand

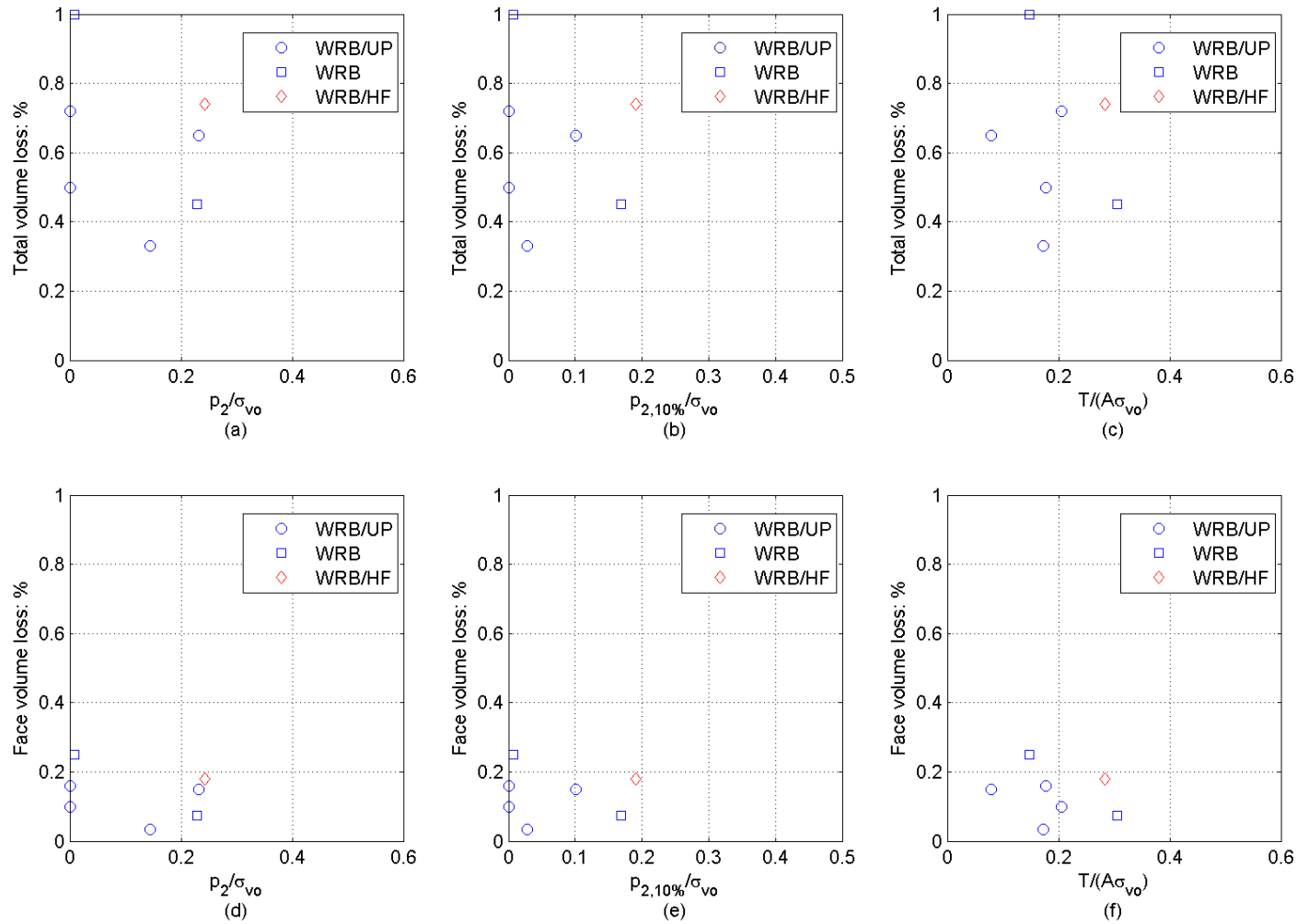


Fig. 7.25. Relationships between face pressure and volume loss components in Lambeth Group and Lambeth Group/Harwich Formation

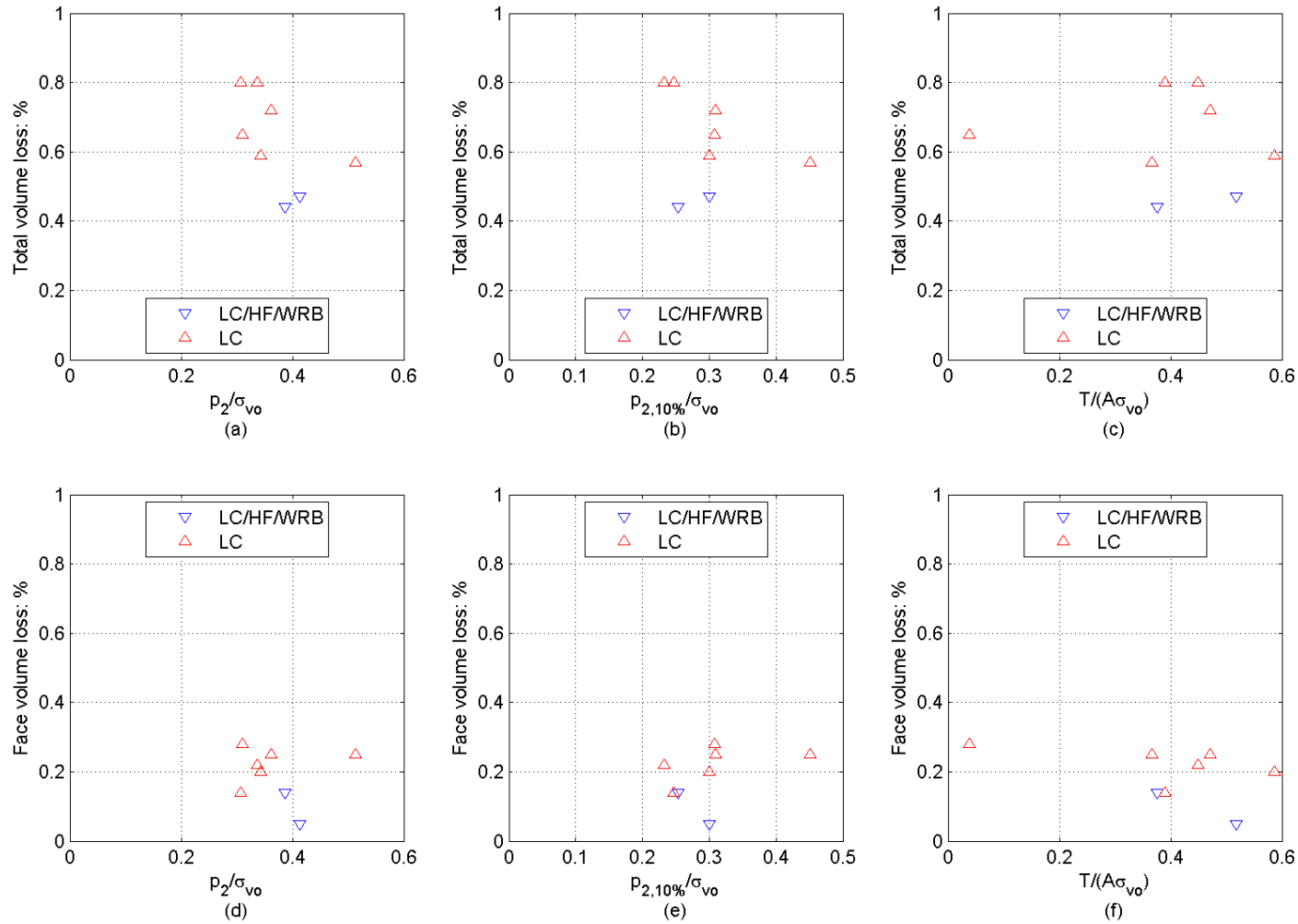


Fig. 7.26. Relationships between face pressure and volume loss components London Clay and London Clay/Harwich/Lambeth Group

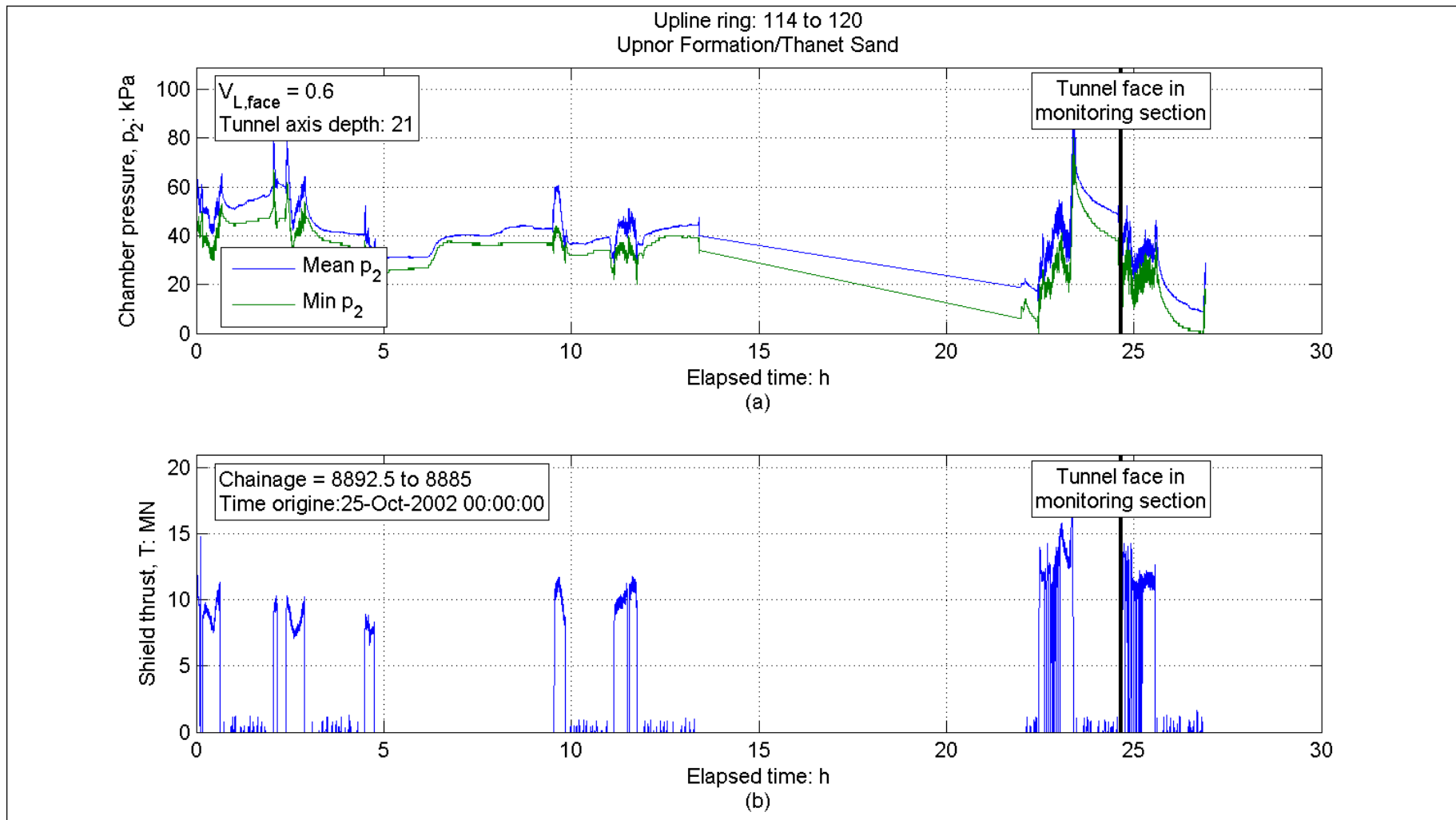


Fig. 7.27. Chamber pressure (a) and total thrust (b) during excavation face progress through the 7.5 m preceding monitoring section

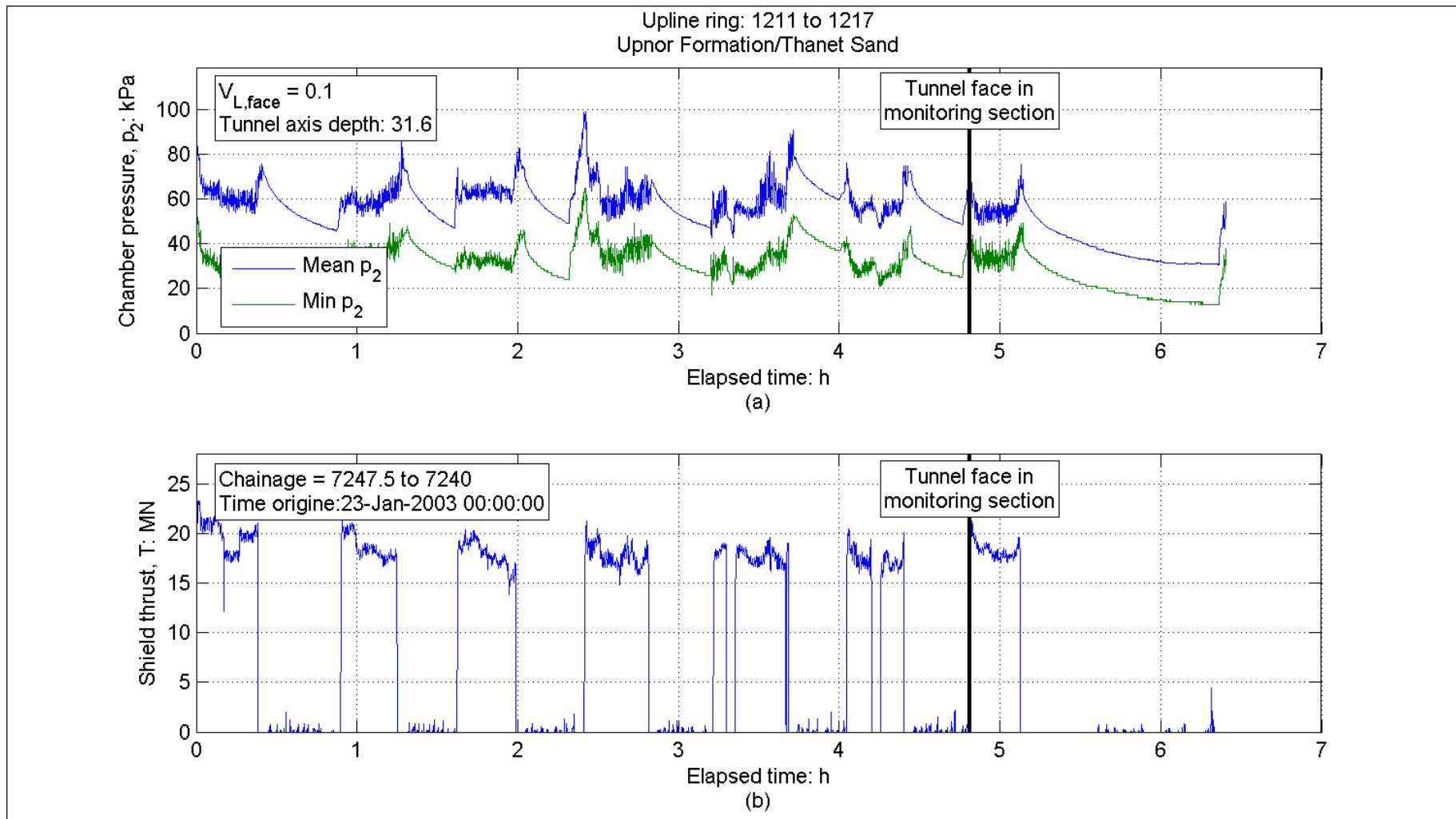


Fig. 7.28. Chamber pressure (a) and total thrust (b) during excavation face progress through the 7.5 m preceding monitoring section

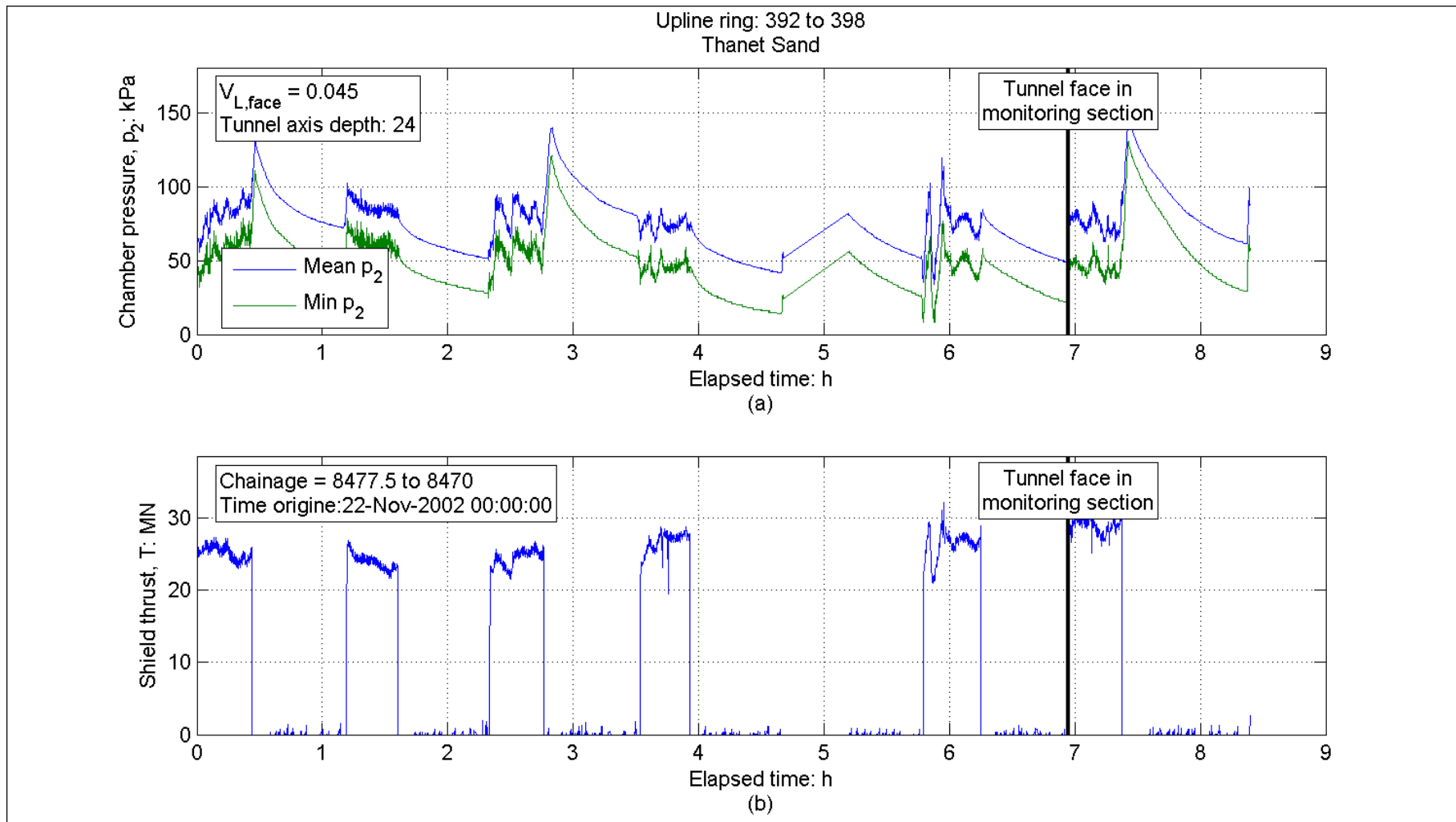


Fig. 7.29. Chamber pressure (a) and total thrust (b) during excavation face progress through the 7.5 m preceding monitoring section

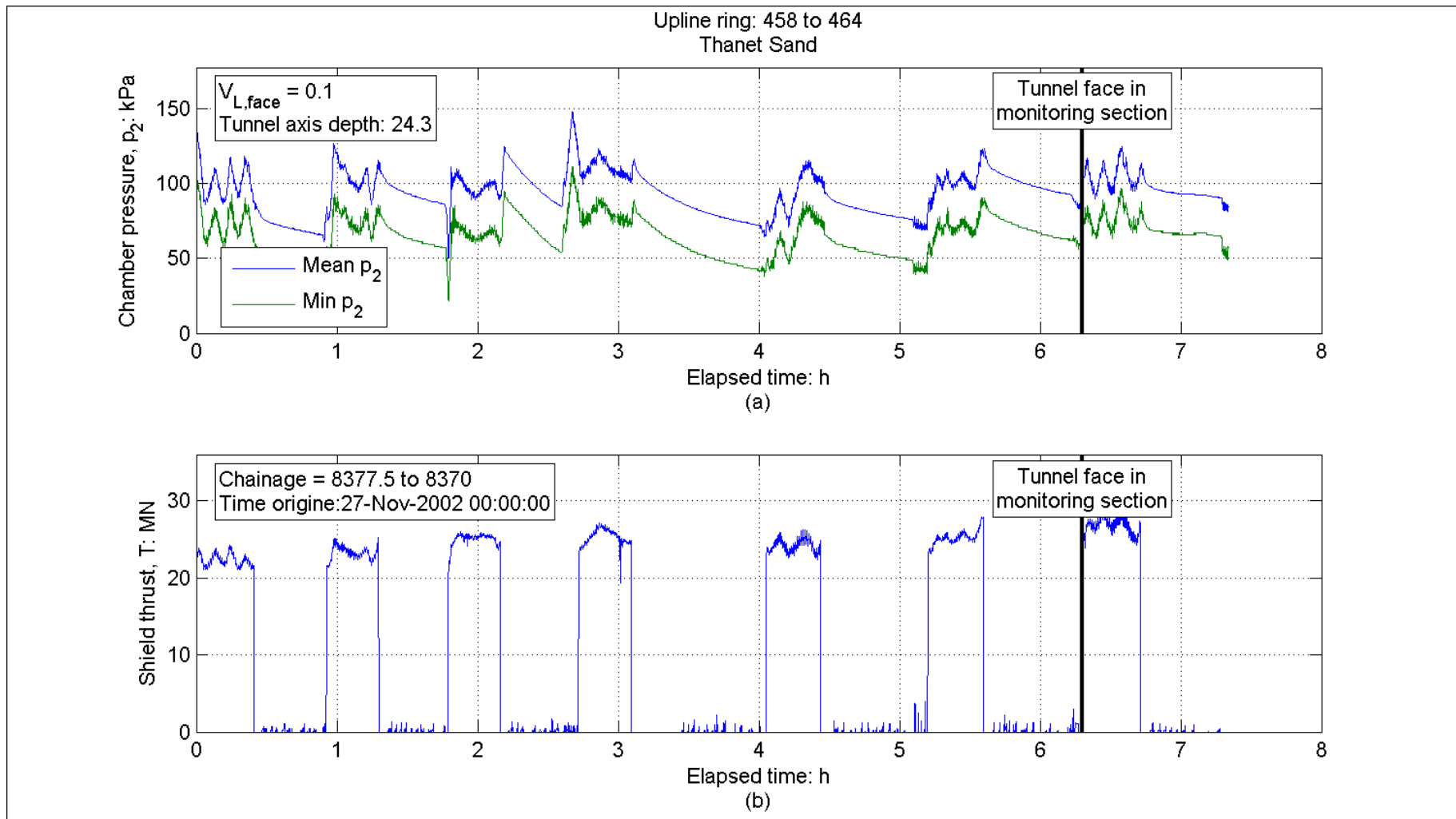


Fig. 7.30. Chamber pressure (a) and total thrust (b) during excavation face progress through the 7.5 m preceding monitoring section

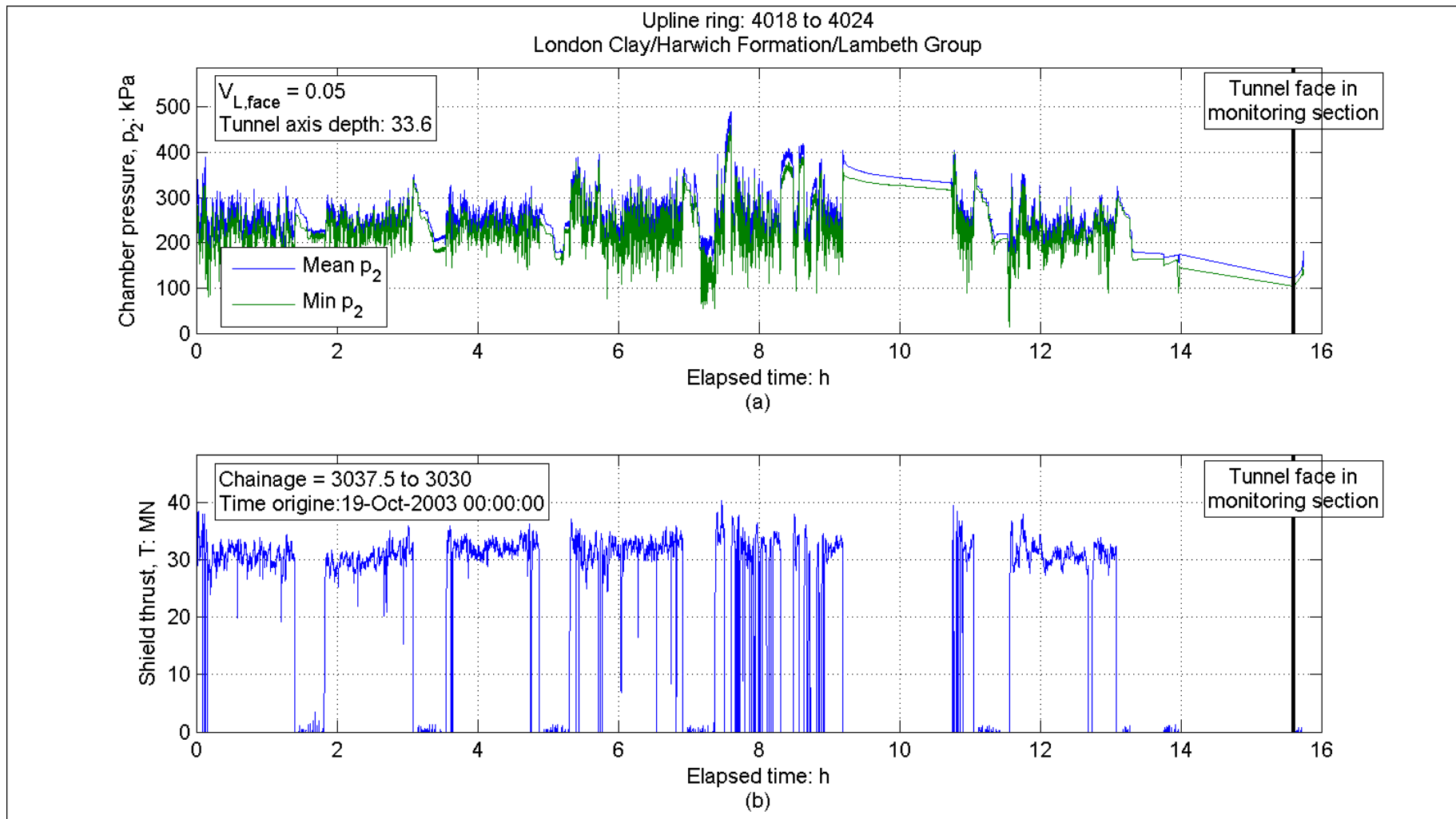


Fig. 7.31. Chamber pressure (a) and total thrust (b) during excavation face progress through the 7.5 m preceding monitoring section

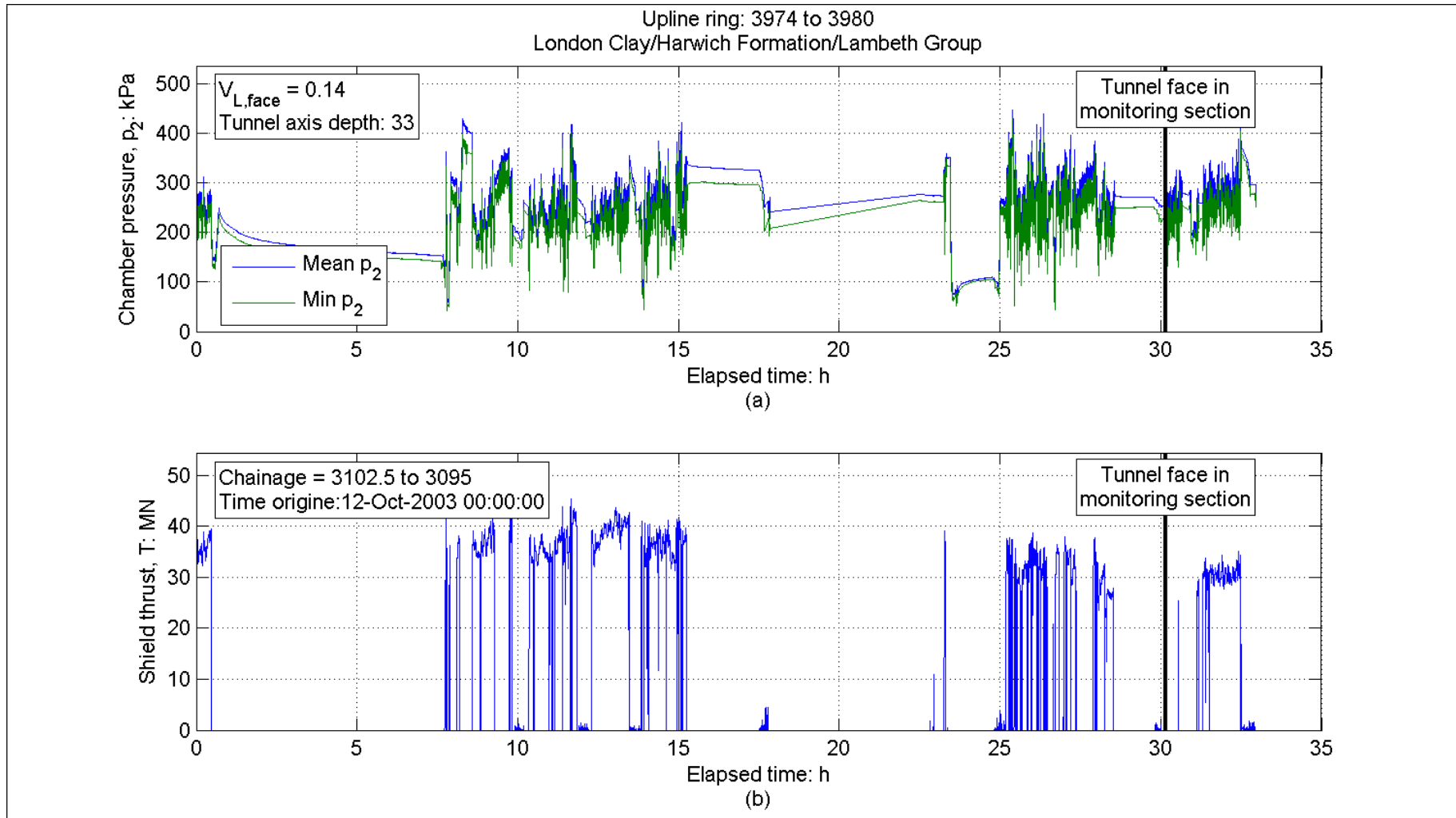


Fig. 7.32. Chamber pressure (a) and total thrust (b) during excavation face progress through the 7.5 m preceding monitoring section

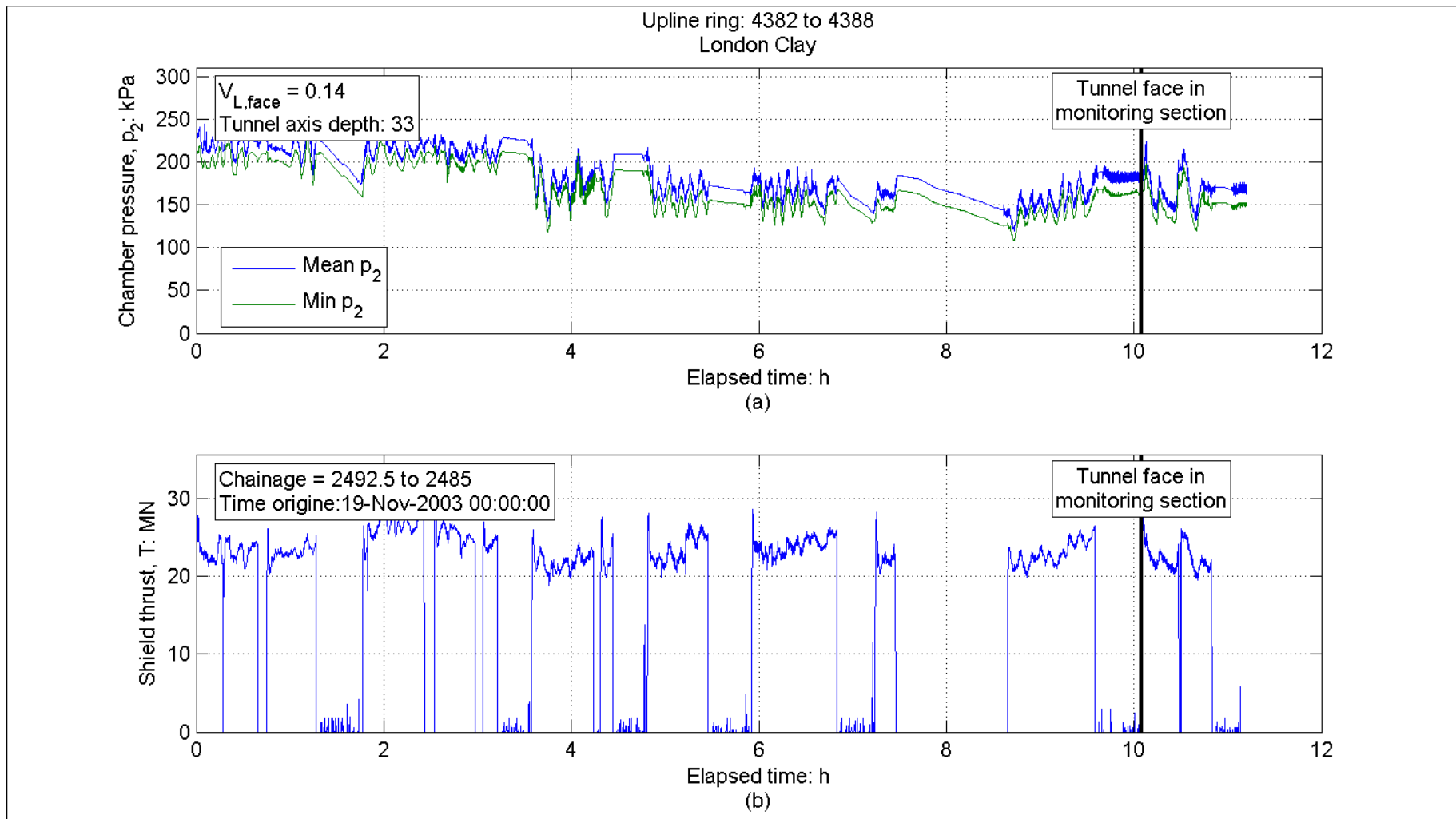


Fig. 7.33. Chamber pressure (a) and total thrust (b) during excavation face progress through the 7.5 m preceding monitoring section

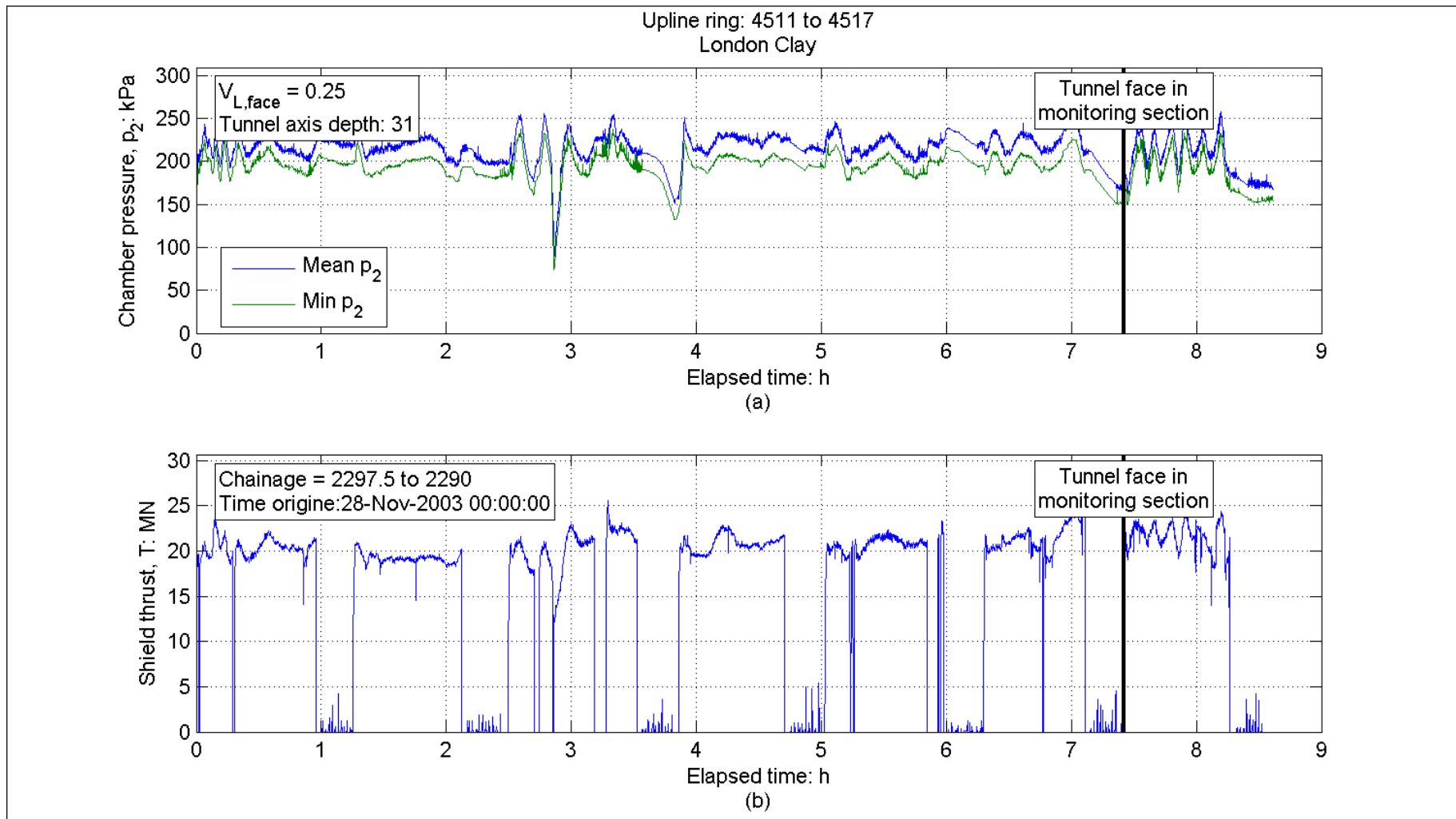


Fig. 7.34. Chamber pressure (a) and total thrust (b) during excavation face progress through the 7.5 m preceding monitoring section

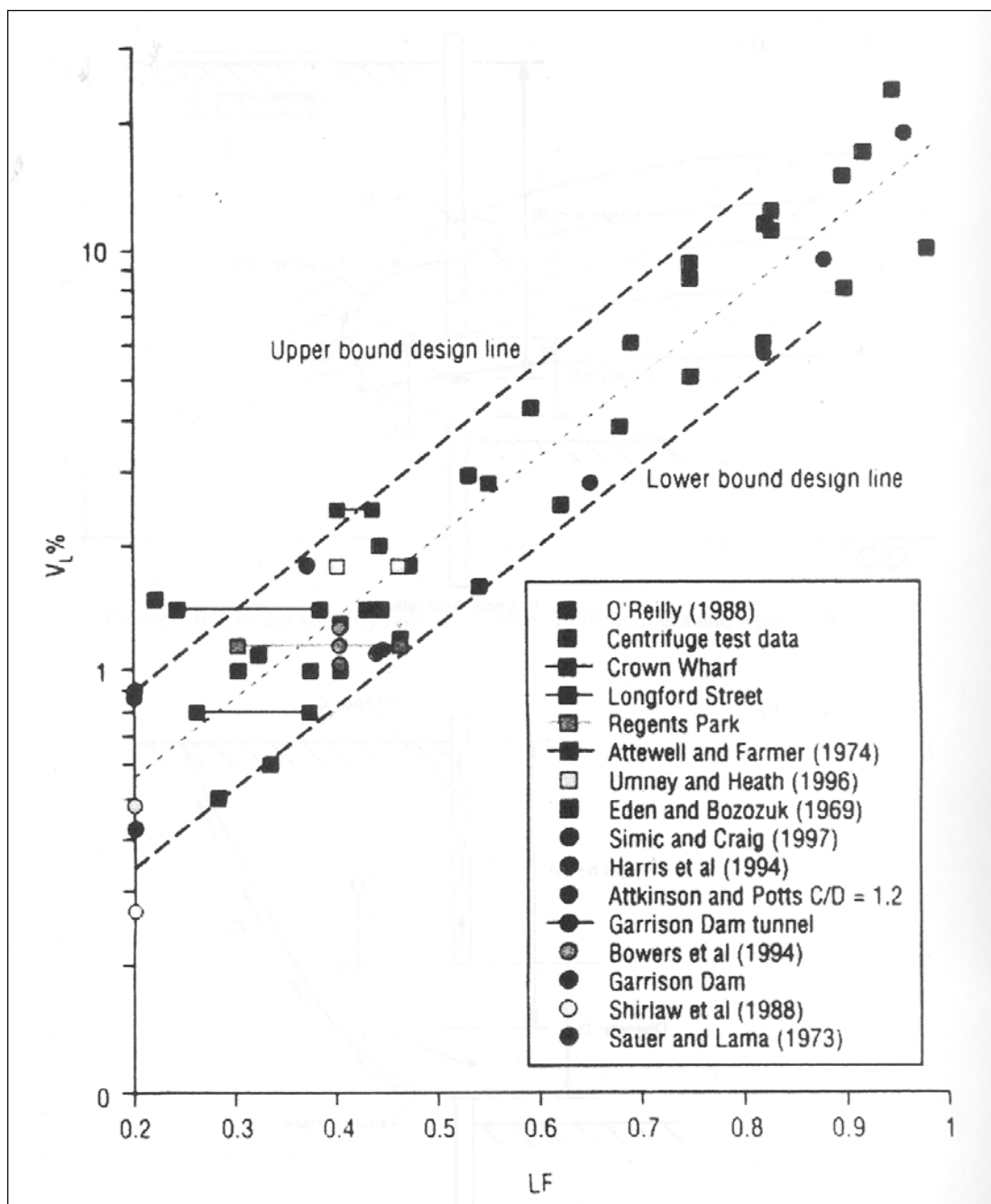


Fig. 7.35. Case history data of volume loss presented against load factor (Macklin, 1999)

## **CHAPTER 8: CONCLUSIONS**

### **8.1 Scope and Outline**

This last chapter summarises the contributions achieved towards the research needs outlined at the outset of this dissertation. Conclusions are drawn from the evidence gained in the experimental and field work and their implications for practical application are suggested. Finally, areas where further work might be appropriate are recommended, either to clarify aspects of the research that remain unexplained or to answer questions that arise from the results presented in this thesis. The structure of this chapter corresponds to the division adopted throughout this work: conclusions relating to lubrication in pipe jacking are presented first (§ 8.2), and are followed by conclusions on the soil conditioning research for *EPB* machines (§ 8.3).

---

## 8.2 Lubrication in Pipe Jacking

### 8.2.1 Conclusions

A review of published experiences of lubrication in pipe jacking was provided in chapter 2. To date, the effects of lubricant products other than bentonite on jacking forces have hardly been investigated and remain poorly understood. Records of jacking loads revealed large differences in unit jacking forces in different projects, and little or no correlation with the main parameters (diameter, undrained shear strength of the clay, overcut size, or lubrication) could be established. Experimental investigations into the interaction between contracting cavities in shale and drilling fluids composed of polymers, potassium brines or silicate were reviewed from the literature of deep well-bore drilling for the oil industry. Contradicting conclusions were sometimes reported, in particular regarding the ability of a given type of chemical to prevent swelling around a borehole. The mechanisms responsible for altering the behaviour of contracting cavities in shales were reviewed. These mechanisms include permeability reduction at or near the cavity wall, alteration of the clay mineral properties by cation exchange, variation of interparticle forces, and osmotic effects causing flow of solute counteracting water ingress into the swelling clay. Depending on the chemical composition of the lubricant or drilling fluid, these mechanisms may combine to produce antagonistic or synergetic effects. The relevance of each mechanism under different sets of circumstances is not yet understood, especially in the context of pipe jacking. As a result, the way in which they are to be taken into account in an analytical or numerical model must be assessed experimentally.

For the research described in this dissertation a novel apparatus was devised and commissioned to identify the key mechanisms governing the interactions between the pipe, the clay and the lubricant and to measure the effects of the chemical composition of lubricants on the pipe loading. The pipe jacking construction process was idealised and its essential features were reproduced under carefully controlled conditions to allow their effect to be measured. A system was devised to excavate a cylindrical cavity, inject lubricant behind an oversized shield and install an instrumented pipe into the clay model. The excavation occurred without prior removal of the surcharge pressure on the clay, and marginal disturbances only were caused to the stresses ahead of the advancing pipe. This allowed the excess pore water pressure due to the unloading of the cavity to be modelled and isolated from uncontrollable and irrelevant effects. The lubrication process was simulated and two types of lubricant were injected during excavation under pressure-controlled

---

conditions. A series of experiments were carried out by varying the type of lubricant but under otherwise identical boundary conditions. Eight pore water pressure transducers (*PPTs*) were installed into the clay, allowing extremely repeatable excess pore water pressure measurements to be obtained in all tests. Meticulous saturation of the *PPTs* under vacuum and accurate insertion of the devices allowed the measurement of large and sudden reduction of pore water pressure just 5 mm away from the excavation boundary, hence obtaining crucial information to understand the clay behaviour close to the cavity wall. In addition, total stresses and fluid pressures on the model pipe were measured throughout its installation and the subsequent consolidation period, thus giving a comprehensive set of data of soil-pipe interaction.

The data gained from this experiment showed that two different tests could be performed under remarkably repeatable boundary conditions, hence allowing the effects of the lubricant type to be isolated. The three main conclusions that can be drawn from the evidence gained in the experimental work may be summarised as follows:

- The permeability of E-Grade kaolin to 0.3% water-based solution of [spell out what *PHPA* is] (*PHPA*) is approximately 400 times smaller than the hydraulic conductivity of E-Grade at identical voids ratio and total isotropic stress.
- The rate of effective stress build-up on the model pipe was significantly reduced by the presence of the *PHPA* in the annulus.
- For the overcut ratio and the boundary conditions used in the model experiment, the use of *PHPA* solution led to a 65% reduction in the long-term effective stresses acting on the pipe.

The effect of the polymer was attributed to the permeability reduction near the cavity boundary. This reduction of permeability greatly reduced the rate of polymer ingress into the clay, which in turn resulted in an increased lubricant pressure as the cavity contracted. Simple analyses using qualitative stress paths for an element of soil at the cavity boundary suggest that a larger zone of softened clay had developed around the pipe in the case where water was used as a lubricant. It was shown that the softening of the ground was associated with larger radial effective stresses on the pipe than in case where less softening had occurred.

The research results demonstrated the beneficial effects of *PHPA* in reducing the radial effective stresses on the pipe. As a result of the widespread belief that polymer lubricants merely reduce jacking forces by reducing the interface shear stress between the pipe and the ground, bentonite is used in most projects to provide radial support to the excavation. While the provision of a filter cake is required to prevent loss of lubricant into the ground where permeable materials are encountered, this research demonstrates that, in clay, polymer alone can effectively reduce the radial stresses between the pipe and the ground. This suggests that, in clay, the use of bentonite may be less beneficial than the use of polymers such as *PHPA*.

### 8.2.2 Recommendations for further work

The experimental procedure allowed the pipe jacking process to be reproduced in a controllable manner and the comprehensive instrumentation of the model provided a detailed picture of the pipe-soil interactions. The tests included most of the features relevant to pipe-soil interaction, and therefore proved adequate in identifying general mechanisms, whilst retaining sufficient simplicity to ensure repeatable test conditions. Because the test combinations were restricted to water and polymer and only two different lubricant pressures, additional tests on a similar apparatus are recommended. In particular, comparing the effects of bentonite to those of polymer and water is required. The current state of knowledge allows neither quantitative nor qualitative predictions of the effects of electrolytes such as potassium cations on the effective stress state of the clay. As discussed above, clay-lubricant interactions involve coupled physicochemical processes, and it is not clear which of these mechanisms governs the interaction for a given clay-lubricant system. Therefore, if such products are to be used in the field, additional experimental evidence should be sought to clarify their effect and, in turn, maximise their potential benefits.

The tests described in chapter 3 should be supplemented by simple laboratory experiments in which the basic interaction between chemicals and clays can be measured under well-defined and controlled boundary conditions. The ability of lubricants to provide an impermeable barrier at the boundary of the excavation was shown to be essential to support the excavation. Therefore, further permeability tests such as those reported in chapter 2 and 5 should be carried out, however with emphasis on clay and lubricant materials that are encountered at shallow depth rather than those typical for deep well-bore drilling. Bentonite is often preferred to polymer because of its ability to form a filtercake in granular materials, and is therefore used even in predominantly clayey ground conditions where limited amount of granular

material is to be encountered. Some polymer treatments of granular materials reported in the context of soil conditioning for *EPB* machines showed that the permeability of sand and sandy gravels may be significantly reduced without the need to inject bentonite. Again, simple laboratory tests are recommended to investigate the potential of polymers to reduce the permeability of granular material, and therefore, to assess the suitability of polymer lubricants in cases where limited intrusions of granular material are likely to appear at the excavation surface of the pipe jack.

The validity of the experimental results should be established by continuing to monitor full scale pipe jacks. Back analysis and comparison of field data of pipe jacking was found to be notoriously difficult. Considerable potential rests with lubricant systems which allow a controlled pressure to be maintained in the overcut during the entire drive. Although such systems sometimes allow the installation of pipe jacks of over 500 m with unusually low unit jacking force, the mechanisms responsible for this outstanding performance have not yet fully been identified. Rigorous monitoring and back analysis of pipe jacking data should be continued to allow these observations to be explained in field situations. It is recommended that the pressure of the lubricant in the annulus be continuously monitored, together with systematic logging of the lubricant composition and the injected volumes.

### **8.3 Soil Conditioning in EPB machines**

#### **8.3.1 Conclusions**

The literature review presented in chapter 6 showed that limited systematic research had been carried out into the effects of soil conditioning in *EPB* machines. This resulted in a lack of recommendations as to the required conditioning in different ground conditions, especially in stiff plastic clays. Few accounts of the behaviour of large diameter tunnels in stiff clay had been reported, and therefore, uncertainties as to the viability of closed-mode operation in the clays of the Lambeth Group and in London Clay remained before construction of the *CTRL* tunnels in London.

An extensive programme of index tests was performed with a view to quantifying the effects of soil conditioning treatments on the shear strength of representative samples taken from the construction of the ventilation shafts on *Contract 220* of the *CTRL* project. This allowed the soil conditioning products to be selected and the range of suitable injection ratios of foam and polymer solution to be estimated. The operation of the *EPB* machines revealed that closed-mode operations were possible in all the ground conditions encountered along the route of *Contract 220*. Foam injection ratios

(*FIR*) of about 50% (at foam expansion ratios (*FERs*) of 10) were usually used in the Thanet Sand and in the Lambeth Group Clays. In addition to foam, polymer solutions were injected at polymer injection ratios (*PIRs*) of 7% and about 10% in the Thanet Sand and the Lambeth Group, respectively. Contrastingly, much lower quantities of foam were used in the London Clay and, as was suggested by the results of the index tests, the benefits of foam in stiff clay are mostly related to its liquid phase. *PIRs* of about 15% with little or no foam were required to remould the clay mixture to an undrained shear strength of  $S_u = 20\text{-}30$  kPa. Evidence is also available to demonstrate that while the absence of conditioning prevented the machine from being operated in closed-mode, the injection of large quantities of foam or polymer sometimes acted counterproductively by exacerbating the drop of pressure in the head chamber during ring build or by preventing the soil from being remoulded into a homogeneous mass.

Remarkably well-controlled chamber pressures were achieved in the London Clay, where high values of over 220 kPa could be maintained within accurate limits and with little or no pressure decay during ring build. These optimal conditions are believed to have been allowed by maintaining steady state operations of the machine, *i.e.* without the need for continuous adjustment of the thrust, the screw speed or the conditioning. Under such conditions, the volume losses induced by stress relief at the tunnel face can be reduced to negligible amounts. In the Lambeth Group, the operation of the machines was more erratic, with more pressure fluctuations in the excavation chamber, and steady state operations could hardly be achieved. High face pressures could nevertheless be maintained, but both the revolution speed of the screw conveyor and the thrust on the machine had to be altered frequently, often resulting in large variations of the chamber pressure.

Volume losses of less than 1% were achieved throughout most of the 15 km drive, with only a few instances of larger volume loss. For the 30 m deep tunnels sections in the London Clay, the volume loss was not significantly affected by the magnitude of the chamber pressure, or indeed by occasional temporary low values of the chamber pressure. This was attributed to the relatively small dependency of the volume loss on face pressure when the load factor is low, in the region of 0.2-0.3%. However, in order to minimise the risk due to unexpected zones of locally high permeability granular material, it is crucial to maintain a full excavation chamber at all times, and therefore, a chamber pressure. It is important not to associate the measurement of large chamber pressures as necessarily meaning a “full” excavation chamber. This is because the pressure may merely result from the compressed air injected with the foam, and excessive amounts of foam in the chamber may not prevent partial collapses of the face.

### 8.3.2 8.3.2 Recommendations for further work

Back analysing the effects of the soil conditioning parameters is rendered difficult by the simultaneous alteration of several machine parameters. Further field monitoring exercises could be of value if soil parameters were varied independently (*i.e.*, while keeping all other parameters constant) throughout the range relevant for their applications. When carrying out such field trials, it is important to maintain the parameters constant for a series of at least two rings in order to allow uniform conditions of the mixture throughout the excavation chamber and the screw conveyor to be established.

Attempts at correlation between the machine parameters affecting the face pressure and the volume loss induced by their operation failed to produce consistent or unambiguous trends. This is partly due to the small range of volume losses observed (5 mm trough depth at the ground surface), the small variation of machine parameters, and the cross-correlation between variables. However, having established that for deep tunnels in stiff clay the volume losses are relatively insensitive to small variations of chamber pressure, research efforts should focus on the back analysis of *EPB* machine parameters where unusually high volume losses, sinkholes or partial face collapse occurred. Identifying the cause of such events could help to improve further the reliability of *EPB* tunnelling machine operations and prevent the recurrence of major sinkholes or tragic collapses.

## References

- Addenbrooke, T.I.** (1996). *Numerical Analysis of tunnelling in stiff clay*. PhD Thesis, University of London, UK.
- Alexanderson, M.** (2001). *Construction of a Cable Tunnel ID 2.6 Vibhavadi*. Proc. 5<sup>th</sup> Int. Symp. on Microtunneling, Bauma, Munich: 139-147.
- Alexanderson, M.** (2005). *Personal communication*.
- Alonso, E., Alejano, L.R., Varas, F., Fdez-Manín, G. & Carranza-Torres, C.** (2003). *Ground response curves for rock mass exhibiting strain softening behaviour*. Int. J. Numer. Anal. Methods Geomech., 27(13): 1153-1185.
- Al Tabaa, A. & Wood, D.M.** (1987). *Horizontal drainage during consolidation. Insights gained from analyses of a simple problem*. Géotechnique, 41(4): 581-585.
- Anagnostou, G.** (1992). *Untersuchungen zur Statik des Tunnelbaus in quellfähigem Gebirge*. PhD Thesis, Swiss Federal Institute of Technology, Zurich, Switzerland. In German.
- Anagnostou, G. & Kovári, K.** (1994). *Die Stabilität der Ortsbrust bei Erddruckschilden*. Publications de la Société Suisse de Mécanique des Sols et des Roches. Frühjahrstagung, 29th April, No. 129. In German
- Anagnostou, G. & Kovári, K.** (1996). *Slurry penetration into coarse grained soils and settlements from a large slurry shield tunnel*. Geotechnical Aspects of Underground Construction in Soft Ground, Mair & Taylor (eds), Balkema, Rotterdam: 453-458.
- Ano, Y.** (2003). *C220 – Stratford to London Portal*. Tunn. Tunn. Int., special supplement CTRL Section 2 Tunnelling, 35(9): 12-15.
- Aristotenas, G.V.** (1992). *Time-dependant behaviour of tunnels excavated in shales*. PhD Thesis, Massachusetts Institute of Technology, Boston, USA.
- Arthur, J.R.F. & Roscoe, K.H.** (1961). *An earth pressure cell for the measurement of normal and shear stresses*. Civil Engineering and Public Work Review, 56: 765-770.
- Atkinson, J.H. & Mair, R.J.** (1981). *Soil mechanics aspects of soft ground tunnelling*. Ground Engineering, 14(5): 20-38.

- Atkinson, J.H. & Mair, R.J.** (1983). *Loads on leaking and watertight tunnel linings, sewers and buried pipes due to groundwater*. *Géotechnique*, 33(3): 341-344.
- Attewell, P.B. & Farmer, I.W.** (1974). *Ground deformations resulting from shield tunnelling in London Clay*. *Can. Geotech. J.*, 11(3): 380-395.
- Atwa, M.** (1996). *Analyses numériques des écoulements d'eau et de la consolidation des sols autour des tunnels creusés dans l'argile*. PhD Thesis, L'École Nationale des Ponts et Chaussée, France. In French.
- Audibert, A., Argillier, J.-F., Ladva, H.K.J., Way, P.W. & Hove, A.O.** (1999). *The role of polymers on Formation damage*. Proc. European Formation Damage Conf., The Hague, The Netherlands: 505-516.
- Auld, F.A.** (1982). *Determination of pipe jacking loads*. Conf. Proc., Pipe Jacking Association, Manchester.
- Babendererde, L.H.** (1998). *Developments in polymer application for soil conditioning in EPB-TBMs*. *Tunnels and Metropolises*, Negro Jr. and Ferreira (eds), Balkema, Rotterdam: 691-695.
- Bailey, L., Denis, J.H. & Maitland, G.C.** (1991). *Drilling fluids and wellbore stability – current performance and future challenges*. In *Chemicals in the Oil Industry: Developments and Applications*, Ogden, P.H. (ed.): 53-70.
- Bailey, L., Reid, P.I. & Sherwood, J.D.** (1994a). *Mechanisms and solutions for chemical inhibition of shale swelling and failure*. In *Recent Advances in Oilfield Chemistry*, Ogden, P.H. (ed.): 13-27.
- Bailey, L., Keall, M., Audibert, A. & Lecourtier, J.** (1994b). *Effect of clay/polymer interactions on shale stabilization during drilling*. *Langmuir*, 10(5): 1544-1549.
- Bailey, L., Sawdon, C., Brady, M. & Cliffe, S.** (1998). *New insight into the mechanisms of shale inhibition using water based silicate drilling fluids*. Proc. of the IADC/SPE Asia Pacific Drilling Technology Conference, Dallas, Texas, USA: 897-902.
- Ballard, T.J., Beare, S.P. & Lawless, T.A.** (1994). *Shale inhibition with water based muds: the influence of polymers on water transport through shales*. In *Recent Advances in Oilfield Chemistry*, Ogden, P.H. (ed.): 38-55.
- Barbour, S.L. & Fredlund, D.G.** (1989). *Mechanisms of osmotic flow and volume change in clay soils*. *Can. Geotech. J.*, 26(4): 551-562.

**Barker, H.R.** (1998). *Physical modelling of construction processes in the Mini-Drum centrifuge*. PhD Thesis, University of Cambridge, UK.

**Barla, G.** (2000). *Tunnelling under squeezing rock conditions*. Eurosummer-School in Tunnel Mechanics, Innsbruck, Austria. At website: [www2.polito.it/ricerca/rockmech/Pubblicazioni/Art\\_convegna/Innsbruck2001.PDF](http://www2.polito.it/ricerca/rockmech/Pubblicazioni/Art_convegna/Innsbruck2001.PDF)

**Barla, M.** (1999). *Tunnels in swelling ground, simulation of 3D stress paths by triaxial laboratory testing*. PhD Thesis, Politecnico di Torino, Italy.

**Barla, M., Borghi, F.X., Mair, R.J. & Soga, K.** (2003). *Numerical modelling of pipe-soil stresses during pipe jacking in clay*. XIII<sup>th</sup> European Conference on Soil Mechanics & Geotechnical Engineering, Prague: 453-458.

**Barratt, D.A. & Tyler, R.G.** (1976). *Measurements of ground movements and lining behaviour on the London Underground at Regents Park*. TRL Laboratory Report LR684.

**Bellwald, P.** (1990). *A contribution to the design of tunnels in argillaceous rocks*. PhD Thesis, Massachusetts Institute of Technology, Boston, USA.

**Benamar, I.** (1996). *Etude des effets différés dans les tunnels profonds*. PhD Thesis, Ecole Nationale des Ponts et Chaussées. Paris, France. In French.

**Bennett, D.** (1998). *Jacking loads and ground deformations associated with microtunnelling*. PhD Thesis, University of Illinois at Urbana-Champaign, USA.

**Bernaud, D., Benamar, I. & Rousset, G.** (1994). *Nouvelle méthode implicite pour le calcul des tunnels dans les milieux elastoplastiques et viscoplastiques*. Revue Française de Géotechnique, 68 : 3-19.

**Bezuijen, A. & Schaminee, P.E.L.** (2000). *Simulation of EPB shield TBM in model test with foam as additive*. Proc. IS-Kyoto Conf. On Modern Tunnelling Science and Technology.

**Bezuijen, A., Talmon, A.M., Joustra, J.F.W. & Grote, B.** (2005). *Pressure gradients and muck properties at the face of an EPB*. Proc. 4<sup>th</sup> Int. Symp. on Geotechnical Aspects of Underground Construction in Soft Ground, Bakker *et al.* (eds), Amsterdam: 195-202.

**Bolton, M.D.** (1979). *A Guide to Soil Mechanics*. Macmillan, London, reprinted by Chung Hwa Books, and published by M.D. and K. Bolton in 1991, and 1998.

- Bolton, M.D. & Whittle, J.P.** (1999). *A non-linear elastic/perfectly plastic analysis for plane strain undrained expansion tests*. Géotechnique, 49(1): 133-141.
- Boone, S.J., Artigiani, E., Shirlaw, J.N., Ginanneschi, R., Leinala, T. & Kochmanova, N.** (2005). *Use of ground conditioning agents for earth pressure balance machine tunnelling*. Proc. AFTES International Congress, Chambéry.
- Bowers, K.H. & Moss, N.A.** (2006). *Settlement due to tunnelling on the CTRL London Tunnels*. Proc. 4<sup>th</sup> Int. Symp. on Geotechnical Aspects of Underground Construction in Soft Ground, Bakker *et al.* (eds), Amsterdam: 203-209.
- Burns, S.E. & Mayne, P.W.** (2002). *Analytical cavity expansion-critical state model for piezocone dissipation in fine-grained soils*. Soils Found., 42(2): 131-137.
- Breen, C.** (1999). *Characterization and use of polycation-exchanged bentonites*. Applied Clay Science, 15(1): 187-219
- Broomfield, J.** (2004). *Long distance pipe jacking in Asia*. Tunn. Tunn. Int., 36(7): 40-42.
- Broms, B.B. & Bennermark, H.** (1967). *Stability of clay at vertical openings*. J. Geotech. Eng., 93(1): 71-94.
- Brown, E.T., Bray, J.W., Ladanyi, B. & Hoek, E.** (1983). *Ground response curves for rock tunnels*. J. Geotech. Eng., 109(1): 15-39.
- Brown, R.** (2003). *C220 – Stratford to London Portal*. Tunn. Tunn. Int., special supplement CTRL Section 2 Tunnelling, 35(9): 5-7.
- Butterfield, R. & Johnson, J.C.** (1973). *The stresses acting on a continuously penetrating pile*. Proc. 8<sup>th</sup> ISSMFE, Moscow, (2): 39-45.
- Cairncross, A.M.** (1973). *Deformations around model tunnels in stiff clay*. PhD Thesis, University of Cambridge, UK.
- Cao, L.F., Teh, C.I. & Chang, M.F.** (2001). *Undrained cavity expansion in modified Cam clay I: Theoretical analysis*. Géotechnique, 51(4): 323-334.
- Caquot, A. & Kerisel, J.** (1966). *Traité de Mécanique des sols*. Gauthier-Villars. In French.
- Carder, D.R. & Krawczyk, J.V.** (1975). *Performance of cells designed to measure soil pressure on earth retaining structures*. Laboratory Report LR689, Transport Research Laboratory, Crowthorne, UK

**Carrier, M.** (2000). *Dielectric measurements over a wide frequency range in e-grade kaolin clay*. PhD Dissertation, University of Cambridge, UK.

**Carter, J.P.** (1988). *A semi-analytical solution for swelling around a borehole*. Int. J. Numer. Anal. Methods Geomech., 12(2): 197-212.

**Cetco Europe Ltd** (2006). *Personal communication*.

**Chapman, D.N. & Ichioka, Y.** (1999). *Prediction of jacking forces for microtunnelling operations*. Trenchless Technology Research, 14(1): 31-41.

**Chen, X., Tan, C.P. & Haberfield, C.M.** (1999). *Effects of induced pore water pressure on stability of wellbores drilled in shales*. Proc. SPE Int. Soc. Mech. Petrol Eng. Conf., 1: 453-460.

**Chen, G., Chenevert, M.E., Sharma, M.M. & Yu, M.** (2003). *A study of wellbore stability in shales including poroelastic, chemical, and thermal effects*. J. Pet. Sci. Eng., 38(3-4): 167-176.

**Chenevert, M.E.** (1970). *Shale control with balanced- activity oil - continuous muds*. J. Petrol. Technol. 22(10): 1309-1316.

**Clarke, B.G.** (1981). *In situ testing of clays using the Cambridge self boring pressuremeter*. PhD Dissertation, University of Cambridge, UK.

**Clough, G.W. & Leca, L.E.** (1989). *EPB shield tunneling in mixed face conditions*. J. Geotech. Eng., 119(10): 1640-1656.

**Collins, I.F. & Yu, H.S.** (1996). *Undrained cavity expansion in critical state soils*. Int. J. Numer. Anal. Methods Geomech., 20(7): 489-516.

**Cook, J.M., Geehan, T.M., Bieber, A.M. & Lecourtier, M.-T.** (1993). *Mud/shale interaction: model wellbore studies using X-ray tomography*. Proc. Drill. Conf., Amsterdam, Netherlands: 491-500

**Craig, R.N.** (1983). *A state-of-the-art review*. CIRIA Technical note 112.

**Darley, P., Carder, D.R., Ryley, M.D. & Hawkins, P.G.** (1996). *Field evaluation of the TRL load cell pressuremeter*. Report TRL209, Transport Research Laboratory Report, Crowthorn, UK.

**Darley, P., Carder, D.R. & Steele, D.P.** (1999). *Field evaluation of the TRL load cell pressuremeter in Gault Clay*. Report TRL427, Transport Research Laboratory, Crowthorn, UK.

**Davis, E.H., Gunn, M.J., Mair, R.J. & Seneviratne, H.N.** (1980). *The stability of shallow tunnels and underground openings in cohesive material*. Géotechnique 30(4): 397-416.

**De Moor, E.K.** (1989). *Modelling of deep tunnel behaviour in clay*. PhD Thesis, City University, London, UK.

**Denis, J.H., Keall, M.J., Hall, P.L. & Meeten, G.H.** (1991). *Influence of potassium concentration on the swelling and compaction of mixed (Na, K) ion-exchanged montmorillonite*. Clay Minerals, 26(2): 255.

**Denys, K.F.J.** (2003). *Flow of polymer solutions through porous media*. PhD Thesis, Delft University, The Netherlands.

**Denys, K.F.J. & Zaitun, A.:** *Bridging adsorption of cationic polyacrylamide in SiC pack*. [www.ucc.ie/research/hmrc/SWERF/proceedings/Schlumberger/karldenys.pdf](http://www.ucc.ie/research/hmrc/SWERF/proceedings/Schlumberger/karldenys.pdf)

**Detournay, E. & Cheng, A.H.-D.** (1988). *Poroelastic response of a borehole in a non-hydrostatic stress field*. Int. J. Rock Mech. Min. Sci., 25: 171-182.

**Di Maio, C.** (1996). *Exposure of bentonite to salt solutions: osmotic and chemical effects*. Géotechnique, 46(4): 695-707.

**Doran, S.R. & Athenoux, J.** (1998). *Storebaelt tunnel-geotechnical aspects of TBM selection and operation*. Tunnels and Metropolises, Negro Jr and Ferreira (eds), Balkema, Rotterdam: 761-766.

**EFNARC** (2001). *Specification and guidelines for the use of specialist products for soft ground tunnelling*. European Federation for Specialist Construction Chemicals and Concrete Systems, Surry, UK. [www.efnarc.org/pdf/TBMGuidelinesApril05.pdf](http://www.efnarc.org/pdf/TBMGuidelinesApril05.pdf)

**Eisenstein, Z. & Samarasekera, L.** (1992a). *Pore water pressure around tunnels in clay*. Can. Geotech. J., 29(4): 819-831.

**Eisenstein, Z. & Samarasekera, L.** (1992b). *Stability of unsupported tunnels in clay*. Can. Geotech. J., 29(4): 609-613.

**Elmes D.R.** (1985). *Creep and viscosity in two kaolin clays*. PhD Thesis, University of Cambridge, UK.

**Evans, D.C.** (1994). *Contaminant migration through intact and damaged clay liners*. PhD Thesis, University of Cambridge, UK.

**Fam, M.A. & Dusseault, M.B.** (1998). *Borehole stability in shales: A physico-chemical perspective*. Proc. SPE/ISRM Rock Mech. Petrol. Eng. Conf., Trondheim, Norway, 461-469.

**Ewy, R.T. & Stankovich, R.J.** (2002). *Shale-fluid interactions measured under simulated downhole conditions*. Proc. SPE/ISRM Rock Mech. Petrol. Eng. Conf., Irving, Texas, USA: 100-109.

**Fam, M.A & Santamarina, J.C.** (1996). *Coupled diffusion-fabric-flow phenomena: an effective stress analysis*. Can. Geotech. J., 33(3): 515-520.

**Feng, Q.L.** (2004). *Soil conditioning for modern EPBM drives*. Tunn. Tunn. Int., 36(12): 18-20.

**Freij-Ayoub, R., Tan, C.P. & Choi, S.K.** (2003). *Simulation of time-dependant wellbore stability in shale using a coupled mechanical-thermal-physico-chemical model*. Proc. SPE/IADC Drill. Conf., Abu Dhabi, United Arab Emirates: 433-439.

**Fritz, P.** (1984). *An analytical solution for axisymmetric tunnel problems in elasto-visco-plastic media*. Int. J. Numer. Anal. Methods Geomech., 8(4): 325-342.

**Gärber, R.** (2002). *Design of deep galleries in low permeable saturates porous medium*. PhD Thesis, Ecole Polytechnique Fédérale de Lausanne, Switzerland.

**Garrubbo, E.** (2003). *Pipe Jacking in argille rigonfianti: prove di laboratorio sul caolino*. MSc. Thesis. Politecnico di Torino, Italy (in Italian).

**Ghaboussi, J. & Gioda, G.** (1977). *On the time-dependant effects in advancing tunnels*. Int. J. Numer. Anal. Methods Geomech., 1(3): 249-269.

**Giraud, A.** (1993). *Couplages thermo-hydro-mécaniques dans les milieux poreux peu permeables: Application aux argiles profondes*. PhD Thesis, Ecole Nationale des Ponts et Chaussées, Paris, France.

**Gourvenec, S.M., Mair, R.J. Bolton, M.D. & Soga, K.** (2005). *Ground conditions around an old tunnel in London Clay*. Geotechnical Engineering 158: 25-33.

**Gray, G.R., Darley, H.C.H. & Rogers, W.F.** (1980). *Composition and properties of oil well drilling fluids*. Fourth edition, Gulf Publishing Company, Houston, Texas.

**Grim, R.E.** (1953). *Clay mineralogy*. McGraw-Hill Series in Geology.

**Hale, A.H., Mody, F.K. & Salisbury, D.P.** (1993). *The influence of chemical potential on wellbore stability*. SPE Drilling and Completion, 8(3): 207-216.

**Herrenknecht, M. & Maidl, U.** (1995). *Applying foam for an EPB shield drive in Valencia*. Tunnel, 5: 10-19.

**Hight, D.W., Ellison, R.A. & Page, D.P.** (2001). *Engineering in the Lambeth Group*. Construction Industry Research and Information Association. Funders Report CP/83.

**Horsrud, P., Bostrom, B., Sonstebo, E.F. & Holt, R.M.** (1998). *Interaction between shale and water based drilling fluids: laboratory exposure tests give new insight into mechanisms and field consequences of KCl contents*. Proc. SPE Annual Technical Conference and Exhibition, New Orleans, Louisiana: 215-225.

**Houlsby, G.T. & Psomas, S.** (2001). *Soil conditioning for pipejacking and tunnelling: properties of sand/foam mixtures*. Proc. Underground Construction 2001, London Docklands, UK: 128-138.

**Hughes, J.M.O.** (1973). *An instrument for the in situ measurement of the properties of soft clays*. PhD Dissertation, University of Cambridge, UK.

**Jáky, J.** (1944). *The coefficient of earth pressure at rest*. In Hungarian (A nyugalmi nyomas tenyezoje). J. Soc. Hung. Eng. Arch.: 355–358.

**Janscecz, S.** (1997). *Modern shield tunnelling in the view of geotechnical engineering: A reappraisal of experiences*. Proc. 14th ICSMFE, Hamburg: 1415-1420.

**Janscecz, S., Krause, R. & Langmaack, L.** (1999). *Advantages of soil conditioning in shield tunnelling: experiences of LRTS Izmir*. Challenges for the 21st Century, Alten *et al.* (eds), Balkema, Rotterdam: 865-875.

**Kasper, T. & Meschke, G.** (2004). *A 3D finite element simulation model for TBM tunnelling in soft ground*. Int. J. Numer. Anal. Methods Geomech., 28(14): 1141-1460.

**Katti, D.R. & Shanmugasundaram, V.** (2001). *The influence of swelling on the microstructure of expansive clay*. Can. Geotech. J.: 38: 175-182.

**Keijzer, T.J.S.** (2000). *Chemical osmosis in natural clayey materials*. “Geologica Ultraiectina, 196, PhD dissertation, University of Utrecht, The Netherlands.

**Kimura, T. & Mair, R.J.** (1981). *Centrifugal testing of model tunnels in soft clay*. Proc. 10<sup>th</sup> Proc. Int. Conf. Soil Mech. Found. Eng., Stockholm, Sweden, 1: 319-322.

**Kippie, D.P., Horton, R.L., Foxenberg, W.E., & Arvie, Jr.M.** (2002). *Chemical Fluid-Loss-Control Systems for Severe Environments: Taking Conventional Systems*

---

*to a Higher Level*. Proc. SPE International Symposium on Formation Damage Control: 657-668.

**König, D., Jessenberger, H.L., Bolton, M.D., Phillips, R., Bagge, G., Renzi, R. & Garnier, J.** (1994). *Pore pressure measurements during centrifuge tests: Experience of five laboratories*, In Leung, Lee and Tan (eds), Centrifuge'94: Rotterdam: Balkema: 101-108.

**Knogle, D.S.** (1979). *The influence of pore-water tension on the undrained shear strength of kaolin*. University of Cambridge, Engineering Tripos Part II Project Report.

**Kusakabe, O., Nomoto, T. & Imamura, S.** (1999). *Geotechnical criteria for selecting mechanised tunnel system and DMM for tunnelling*. Panel discussion, Proc. 14th Int. Conf. Soil Mech. Found. Eng., Hamburg, 4, Balkema, Rotterdam: 2439-2440.

**Krause, T.** (1987). *Schildvortrieb mit flüssigkeits- und erdgestützter Ortsbrust*. PhD thesis, University Carolo-Wilhelmina, Braunschweig, Germany. In German.

**Labieuse V.** (1997). *Numerical and analytical modelling of a new gallery in the Boom Clay formation*. Numerical Models in Geomechanics NUMOG VI, Montreal, Canada, 489-494.

**Labieuse, V.** (1999). *Predictions of hydro-mechanical disturbances around tunnels based on different constitutive models*. Numerical Models in Geomechanics NUMOG VII, Graz, Austria.

**Labieuse, V. & Giraud, A.** (1998). *Analytical solutions for the undrained response of a poro-elastic medium around a cylindrical opening*. Proc. Biot conference on Poromechanics, Thimus *et al.* (eds), Balkema, Rotterdam: 159-164.

**Ladd, C.C.** (1960). *Mechanisms of swelling by compacted clay*. National Research Council -- Highway Research Board -- Bulletin 245: 10-26.

**Lal, M.** (1999). *Shale stability: drilling fluid interaction and shale strength*. Proc. SPE Asia Pacific Oil and Gas Conference and Exhibition, Jakarta, Indonesia, vol./pp.

**Langmaack, L.** (2000). *Advanced technology of soil conditioning in EPB shield tunnelling*. Proc. North American Tunnelling: 525-542.

**Leinala, T., Grabinsky, M., Delmar, R. & Collins, J.R.** (2000). *Effects of foam soil conditioning on EPBM performance*. Proc. North American Tunneling, Ozdemir (ed.), Balkema, Rotterdam: 543-552.

**Lomba, R.F.T., Chenevert, M.E. & Sharma, M.M.** (2000a). *The ion-selective membrane behaviour of native shale*. J. Pet. Sci. Eng., 25(1): 9-23.

**Lomba, R.F.T., Chenevert, M.E. & Sharma, M.M.** (2000b). *The role of osmotic effects in fluid flow through shales*. J. Pet. Sci. Eng., 25(1): 25-35.

**Lyon, J.** (1999). *Drilling fluids*. Proc. No-Dig Int., 10(2): 20-25.

**Macklin, S.R.** (1999). *The prediction of volume loss due to tunnelling in overconsolidated clay based on geometry and stability number*. Ground Engineering, 32(4): 30-33.

**Madsen, F. & Müller-Vonmoos, M.** (1989). *The swelling behaviour of Clays*. Applied Clay Science, 4: 143-156.

**Maidl, U.** (1995). *Erweiterung der Einsatzbereiche der Erddruckschilde durch Bodenconditionierung mit Schaum*. PhD Thesis, Ruhr Universität, Bochum, Germany. In German.

**Mair, R.J.** (1979). *Centrifugal modelling of tunnel construction in soft clay*. PhD Thesis, University of Cambridge, UK.

**Mair, R.J. & Taylor, R.N.** (1993). *Prediction of clay behaviour around tunnel using plasticity solutions*. Predictive soil mechanics, Thomas Telford, London: 449-463.

**Mair, R.J., Taylor, R.N. & Clarke, B.G.** (1992). *Repository tunnel construction in deep clay formations*. Commission of the European Communities Report EUR 13964 EN, Luxembourg: Office for Official Publications of the European Communities.

**Mascagni, M.B.** (2005). *Pipe jacking in argille rignonfianti: prove di permeabilità e rigonfiamento*. Tesi di Laurea, Politecnico di Torino. In English.

**Mascagni, M.B.** (2006). *Personal communication*.

**Marshall, M.A. & Milligan, G.W.E.** (1996). *Pipe jacking through soft alluvial clay near London: A case history*. Geotechnical Aspects of Underground Construction in Soft Ground, Kusakabe, Fujita & Miyazaki (eds), Balkema, Rotterdam: 263-268.

**Marshall, M.A., Milligan, G.W.E. & Mair, R.J.** (1996). *Movements and stress changes in London Clay due to the construction of a pipe jack*. Geotechnical Aspects of Underground Construction in Soft Ground, Mair & Taylor (eds), Balkema, Rotterdam: 751-756.

- Marshall, M.** (1998). *Pipe-jacked tunnelling: jacking loads and ground movements*. PhD Thesis, University of Oxford.
- Marshall, M.A. & Milligan, G.W.E.** (1998). *Geotechnical aspects of pipe-jacked tunnelling*. Proc. Int. Conf. on Urban Ground Engineering, Hong Kong, ICE, London, UK.
- Maynar, M.M., Saavedra, F.M. & Trabada Guijarro, J.M.** (2000). *Tuneladoras de presión de tierra para el plan 1999-2003 de ampliación del Metro de Madrid*. Revista de Obras Públicas, Extraordinario-Diciembre 2000, No 3.405: 131-150. In Spanish.
- Mayne, P.W. & Kulhawy, F.H.** (1982).  *$K_o$ -OCR relationship in soil*. J. Geotech. Eng. Div., Am. Soc. Civ. Eng., 108(6): 851-872.
- McRory, J.A. & Ashmawy, A.K.** (2005). *Polymer treatment of bentonite clay for contaminant resistant barriers*. American Society of Civil Engineers, ASCE. Geotechnical Special Publication, 130-142: 3399-3409.
- Merritt, A.S. & Mair, R.J.** (2001). *Investigation of lubrication and soil conditioning for tunnelling and pipe jacking in clay soils*. Proc. Underground Construction Symposium, London Docklands: 117-127.
- Merritt, A.S., Borghi, F.X. & Mair, R.J.** (2003). *Conditioning of clay soils for earth pressure balance tunnelling machines*. Proc. Underground Construction, London Dockland, UK: 455-466.
- Merritt A.S.** (2004). *Soil conditioning for earth pressure balance machines*. PhD Dissertation, University of Cambridge, UK.
- Michalowski, R.L.** (2005). *Coefficient of earth pressure at rest*. J. Geotech. Geoenviron. Eng., 131(11): 1429-1433.
- Milligan, G.W.E. & Marshall, M.A.** (1998). *The functions and effects of lubrication in pipe jacking*. *Tunnels and Metropolise*. Negro Jr and Ferreira (eds), Balkema, Rotterdam: 739-744.
- Milligan, G.W.E. & Norris, P.** (1999). *Pipe-soil interaction during pipe jacking*. Geotechnical Engineering, Proc. Institution of Civil Engineering, 137(1): 27-44.
- Milligan, G.W.E.** (2000). *Lubrication and soil conditioning in tunnelling, pipe jacking and microtunnelling: A state-of-the-art review*. Geotechnical Consulting Group, London, UK. [www-civil.eng.ox.ac.uk/research/pipejack/soilcond.html](http://www-civil.eng.ox.ac.uk/research/pipejack/soilcond.html)

**Milligan, G.W.E.** (2001). *Soil conditioning and lubricating agents in tunnelling and pipe jacking*. Proc. Underground Construction Symposium 2001, London Docklands, UK: 105-116.

**Mitchell, J.K., Greenberg, J.A. & Witherspoon, P.A.** (1973). *Chemico-osmotic effects in fine-grained soils*. ASCE J. Soil Mech. Found. Div., 99(4): 307-322.

**Mitchell, J.K.** (2003). *Up and down soils - A reexamination of swelling phenomena in earth materials*. American Society of Civil Engineers, ASCE. Geotechnical Special Publication 19: 1-24.

**Mitchell, J.K. & Soga, K.** (2005). *Fundamentals of Soil Behavior*. Third Edition, John Wiley & Sons.

**Mody, F.K. & Hale, A.H.** (1993). *Borehole stability model to couple the mechanics and chemistry of drilling fluid shale interaction*. Proc. Drill. Conf., Amsterdam, Netherlands: 473-490.

**Moroy, F.** (1998). *New developments in earth pressure equipment for boring underground guided transit lines in France (VAL)*. Tunnels and Metropolises, Negro Jr. and Ferreira (eds), Balkema, Rotterdam: 697-701.

**Muir Wood, D.** (1990). *Soil behaviour and critical state soil mechanics*. Cambridge University Press, Cambridge, UK.

**Muir Wood, D.** (2004). *Geotechnical modelling*. Spon Press.

**Muskat, M.** (1949). *Physical principles of oil production*. McGraw-Hill Book Company, Inc. New York.

**Musso, G.** (2000). *Electrokinetic phenomena in soils*. PhD Dissertation, Politecnico di Torino.

**Nadarajah, V.** (1973). *The stress-strain properties of lightly overconsolidated clay*. PhD Thesis, University of Cambridge, UK.

**Nakamura, S. & Uno, T.** (1997). *Effect of lubricants and manicure method on reduction of propulsion force*. Proc. 15<sup>th</sup> Int. No-Dig, Taipei, Taiwan: 2.1.1-2.1.15.

**Nakamura, S. & Uno, T.** (1997). *Survey and study of the propulsion force in 628 pipe jacking execution cases*.

**Norris, P.** (1992). *The behaviour of jacked concrete pipes during site installation*. PhD Thesis, University of Oxford, UK.

- Ogawa, T. & Lo, K.T** (1987). *The effects of dilatancy and yield criteria on displacements around tunnels*. Can. Geotech. J., 24(1): 100-113.
- Olsen, H.W.** (2003). *Coupled chemical and liquid fluxes in earthen materials*. American Society of Civil Engineers, ASCE. Geotechnical Special Publication 19: 57-85.
- Osho, P.A.** (1970). *The influence of electrolytes on the stress-strain behaviour of soils*. MSc. Thesis, University of Cambridge, UK.
- Page, D. & Skipper, J.** (2000). *Lithological Characteristics of the Lambeth Group*. Ground Engineering, 33(2): 38-43.
- Panet, M. & Guenot, A.** (1982). *Analysis of convergence behind the face of a tunnel*. Int. Symp.: Tunnelling 82, Brighton, UK: 197:204.
- Peck, R.B.** (1969). *Deep excavations and tunnelling in soft ground: state-of-the-art*. Proc. 7<sup>th</sup> Int. Conf. Soil Mech. Found. Eng., Mexico City, State of the Art Volume: 225-290.
- Pellet, A.-L.** (1997). *Analyse des interactions sol-canalisation et sol machine pour la pose de conduites par microtunnelage*. PhD Thesis, INSA, Lyon, France. In French.
- Perron, J.Y. & Marcheselli, P.** (1994). *Construction of the Passante Ferroviario link in Milan, Italy, lots 3P, 5P and 6P, excavation by large earth pressure balanced shield with chemical foam injection*. Tunnelling 94, Institution of Mining and Metallurgy and British Tunnelling Society, Chapman & Hall, London, UK: 679-707.
- Phelipot, A.** (2000). *Interaction sol-canalisation lors de l'opération de microtunnelage*. PhD Thesis, Institut national des sciences appliquées de Lyon. In French.
- Phelipot, A., Dias, D. & Kastner, R.** (2003). *Influence of overcut and lubrication during microtunneling*. Proc. Int. No-Dig, Los Angeles, California, USA. Pp.
- Plank, J.R.** (1991). *Water based muds for drilling high pressure, high temperature wells*. In Chemicals in the Oil Industry: Developments and Applications, Ogden, P.H. (ed.): 99-110.
- Potter, L.J.** (1996). *Contaminant migration through consolidating soils*. PhD Dissertation, University of Cambridge, UK.
- Purwodihardjo, A. & Cambou, B.** (2005). *Time-dependent modelling for soils and its application in tunnelling*. Int. J. Numer. Anal. Meth. Geomech., 29(1), 49-71.

- Quebaud, S.** (1996). *Contribution à l'étude du percement de galeries par boucliers à pression de terre: amélioration du creusement par l'utilisation des produits moussants*. PhD Thesis, University of Lille, France.
- Randolph, M.F. & Wroth, P.** (1979). *Analytical solution for the consolidation around a driven pile in clay*. Int. J. Numer. Anal. Methods Geomech., 3(3): 217-229
- Randolph, M.F., Carter, J.P. & Wroth, P.** (1979). *Driven piles in clay*. Géotechnique, 29(4): 361-393.
- Ridley, A.M. & Burland, J.B.** (1999). *Use of tensile strength of water for the direct measurement of high soil suction: Discussion*. Can. Geotech. J., 36: 178-180.
- Robinet, J.-C. & Tacherifet, S.** (1996). *Simulation numérique du creusement d'une galerie dans un milieu argileux gonflant*. Revue française de Géotechnique, 75: 57-68. In French.
- Rosa, R.C.R.S., Rosa, A.L.A., Farias, S.B., Gracia, M.H. & Coelho, A.S.** (2005). *A new inhibitive water-based fluid: a completely cationic system*. Proc. Latin American and Caribbean Petroleum Engineering Conference, Rio de Janeiro, Brazil, vol./pp.
- Roscoe, K.H., Schofield, A.N. and Wroth, C.P.** (1958). *On the yielding of soils*. Géotechnique, 8: 22-53.
- Roscoe, K.H. & Burland, J.B.** (1968). *On the generalised behaviour of 'wet' clay*. In Engineering plasticity (Heyman, J. & Leckie, F.A., eds), Cambridge University Press: 535-609.
- Rose, A.B.** (1978). *The influence of pore-water tension on the strength of kaolin*. University of Cambridge, Engineering Tripos Part II Project Report.
- Sagasetta, C.** (1987). *Analysis of undrained soil deformation due to ground loss*. Géotechnique, 37(3): 301-320.
- Samarasekera, L. & Eisenstein, Z.** (1992). *Stability of unsupported tunnels in clay*. Can. Geotech. J., 29(4): 609-613.
- Santamarina, J.C. & Fam, M.A.** (1995). *Changes in dielectric permittivity and shear wave velocity during concentration diffusion*. Can. Geotech. J., 32(4): 647-659.
- Santos, H., Diek, A., Da Fontoura, S. & Roegiers, J.-C.** (1997). *Shale reactivity test: a novel approach to evaluate shale-fluid interaction*. Int. J. Rock Mech. Min. Sci.s, 34(3-4): 457.

**Savitzky A. & Golay, M.J.E.** (1964). *Smoothing and Differentiation of Data by Simplified Least Squares Procedures*. Analytical Chemistry, 36: 1627-1639.

**Schlemmer, R., Friedheim, J.E., Growcock, F.B., Bloys, J.B., Headley, J.A. & Polnaszek, S.C.** (2003). *Chemical Osmosis, shale, and drilling fluids*. SPE Drilling and Completion Journal, 18(4): 318-331.

**Schofield, A.N. & Wroth, C.P.** (1968). *Critical state soil mechanics*. McGraw-Hill, New-York.

**Seneviratne, H.N.** (1979). *Deformations and pore water pressure dissipation around tunnels in soft clay*. PhD Thesis, University of Cambridge, UK.

**Sherwood, J.D.** (1993). *Biot poroelasticity of a chemically active shale*. Proc. Royal Society London, A. 440: 365-377.

**Sherwood, J.D. & Bailey, L.** (1994). *Swelling of shale around a cylindrical wellbore*. Proc. Royal Society London, A 444: 161-184.

**Shin, J.H., Addenbrooke, T.I. & Potts, D.M.** (2002). *Numerical study of the effect of groundwater movement on long-term tunnel behaviour*. Géotechnique, 52(6): 391-403.

**Shirlaw, J.N., Ong, J.C.W., Osborne, N.H. & Tan, C.G.** (2002). *The Relationship between Face Pressure and Immediate Settlement due to tunnelling for the North East Line, Singapore*. Proc. 3rd Int. Symp. on Underground Construction in Soft Ground, Toulouse, France: 25-30.

**Shirlaw, J.N., Ong, J.C.W., Rosser, H.B., Tan, C.G., Osborne, N.H. & Heslop, P.E.** (2003). *Local Settlements and Sinkholes due to EPB Tunnelling*. Proc. Institution of Civil Engineering, Geotechnical Engineering, 156(4): 193-211.

**Silva, M.F.** (2005). *Numerical and physical models of rate effects in soil penetration*. PhD Thesis, Universtiy of Cambridge, UK.

**Sloan, S.W. & Assadi, A.** (1993). *Stability of shallow tunnel in soft ground*. Predictive soil mechanics, Thomas Telford, London: 644-663.

**Soderberg, L.O.** (1962). *Consolidation theory applied to time effects*. Géotechnique, 15(3): 217-225.

**Stein, D., Mollers, K. & Bielecki, R.** (1989). *Microtunnelling*. Ernst-Sohn, Berlin, Germany.

**Steiner, W.** (1996a). *Criteria for selecting mechanised tunnelling systems in soft ground*. North American Tunneling'96, Ozdemir (ed.), Balkema, Rotterdam: 483-491.

**Steiner, W.** (1996b). *Slurry penetration into coarse grained soils and settlements from a large slurry shield tunnel*. Geotechnical Aspects of Underground Construction in Soft Ground, Mair & Taylor (eds), Balkema, Rotterdam: 329-333.

**Take, W.A** (2003). *The influence of seasonal moisture cycles on clay slopes*. PhD Dissertation, University of Cambridge, UK.

**Take, W.A. & Bolton, M.D.** (2003). *Tensiometer saturation and the reliable measurement of matric suction*. Géotechnique 53(2):159-172.

**Talmon, A.M. & Bezuijen, A.** (2002). *Muck discharge by the screw conveyor of an EPB Tunnel Boring Machine*. Fourth Int. Symp. Geotechnical Aspects of Underground Construction in Soft Ground - IS Toulouse, Lyon: 23-25.

**Terzaghi, K.** (1943). *Fundamental of soil mechanics*. Wiley, New York, USA.

**Theng, B.K.G.** (1979). *Formation and Properties of Clay-polymer Complexes*. Elsevier, Amsterdam, The Netherlands.

**Thomson, J.** (1993). *Pipejacking and microtunnelling*. Thomson J.C. (ed.), Blackie Academic & Professional (1<sup>st</sup> ed.), London, UK.

**Thushyanthan, T.** (2005). *Behaviour of landfill systems under monotonic and earthquake loading*. PhD Dissertation, University of Cambridge, UK.

**Union Railways Limited** (1997). *London tunnels west geotechnical design basis report, technical report: 220-RUP-LCEEH-00025-AA*. Not published.

**Vaughan, P.R.** (1989). *Non-linearity in seepage problems: theory and field observation*. De Mello Volume, Sao Paulo: Editora Edgard Blucher Ltda: 501-516,

**Vervoort, A. & Van de Steen, B.** (2001). *Support interaction in an underground storage facility of radioactive waste in a clay layer*. FLAC and numerical Modelling in Geomechanics, Billiaux *et al.* (eds), Lyon, France.

**Wallis, S.** (1995). *Foaming success at Valencia*. World Tunnelling, October: 311-316.

- Wang, Y. & Dusseault, M.B.** (1994). *Stresses around a circular opening in an elastoplastic porous medium subjected to repeated hydraulic loading*. Int. J. Numer. Anal. Methods Geomech., 31(6): 597-616.
- Webb, R. & Breeds, C.D.** (1997). *Soft ground EPBM tunnelling-West Seattle, Alki tunnel*. Proc. Tunnelling 97, London, UK: 501-514.
- White, D.J.** (2002). *An investigation into the behaviour of pressed-in piles*. PhD Dissertation, University of Cambridge, UK
- Williamson, G.E., Traylor, M.T. & Higuchi, M.** (1999). *Soil conditioning for EPB shield tunnelling on the South Bay Ocean Outfall*. Proc. Rapid Excavation & Tunneling Conference: 987-925.
- Wongsaroj, J., Borghi, F.X., Soga, K. and Mair, R.J., Sugiyama, T., Hagiwara, T. Minami, T. & Bowers, K.H.** (2005). *Effect of TBM driving parameters on ground surface movements: Channel Tunnel Rail Link Contract 220*. Proc. 4<sup>th</sup> Int. Symp. on Geotechnical Aspects of Underground Construction in Soft Ground, Bakker *et al.* (eds), Amsterdam: 335-341.
- Woods, E.** (2003). *C220 – Stratford to London Portal*. Tunn. Tunn. Int., special supplement CTRL Section 2 Tunnelling, 35(9): 8-10.
- Yeung, A.T. & Mitchell, J.K.** (1993). *Coupled fluid, electrical and chemical flows in soil*. Géotechnique 43(1): 121-134.
- Yoshikawa, T.** (1996a). *Soil pressure drop of screw conveyor for shield machines*. Trans. Japan. Soc. of Mechanical Engineering, Part C, 62(595): 1197-1203.
- Yoshikawa, T.** (1996b). *Soil pressure drop of various screw conveyor structures for shield machines*. Trans. Japan. Soc. of Mechanical Engineering, Part C, 62(599): 2927-2930.
- Yoshikawa, T.** (1996c). *Conditions on soil pressure drop of screw conveyor for shield machines*. Trans. Japan. Soc. of Mechanical Engineering, Part C, 62(599): 2931-2935.
- Yu, H.S. & Rowe, R.K.** (1999). *Plasticity solutions for soil behaviour around contracting cavities and tunnels*. Int. J. Numer. Anal. Methods Geomech., 23(12): 1245-1279.
- Yu, H.S.** (2000). *Cavity Expansion Methods in Geomechanics*. Kluwer Academic Publishers, Dordrecht, The Netherlands.

**Yu, M. Chenevert, M.E. & Sharma, M.M.** (2003). *Chemical-mechanical wellbore instability model for shales: accounting for solute diffusion*. J. Pet. Sci. Eng., 38(3-4): 131-143.

**Zitha, P.L.J., van Os, K.G.S., & Denys, K.F.J.** (1998). *Adsorption of linear flexible polymers during laminar flow through porous media: Effect of the concentration*. Proceedings - SPE Symposium on Improved Oil Recovery, Tulsa, Oklahoma, USA, 2: 225-237.

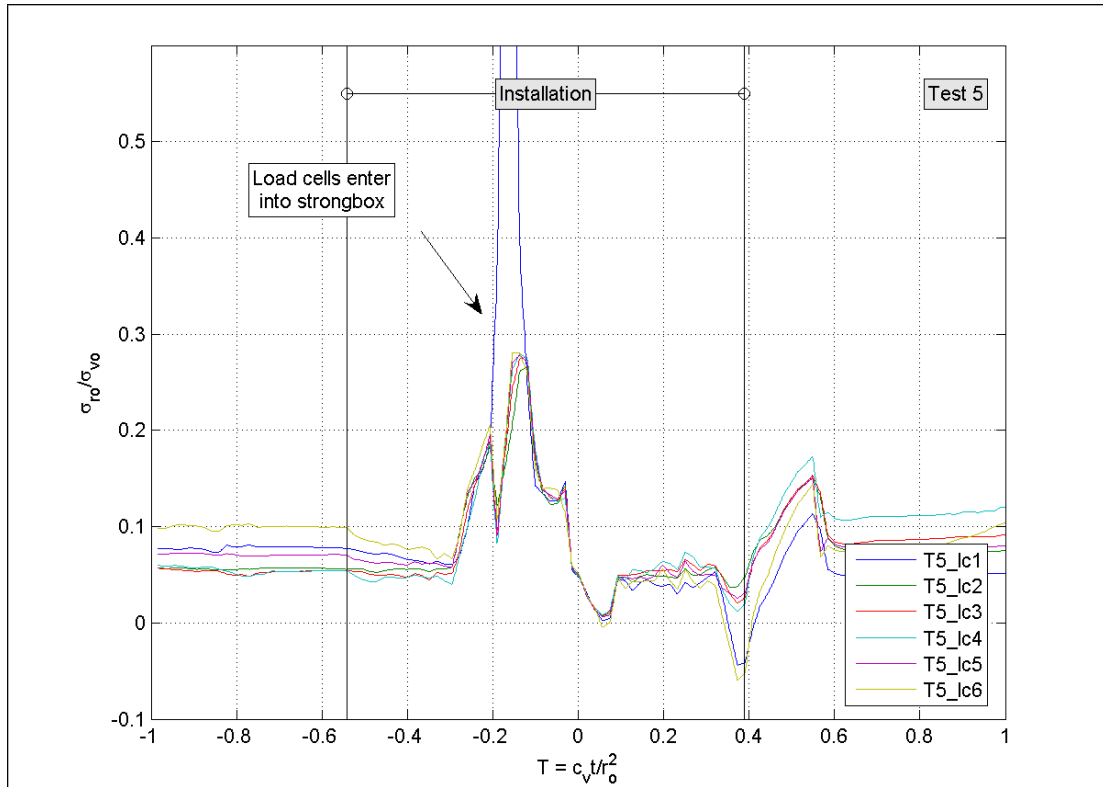


Figure A.1 Total stress on pipe during installation T5

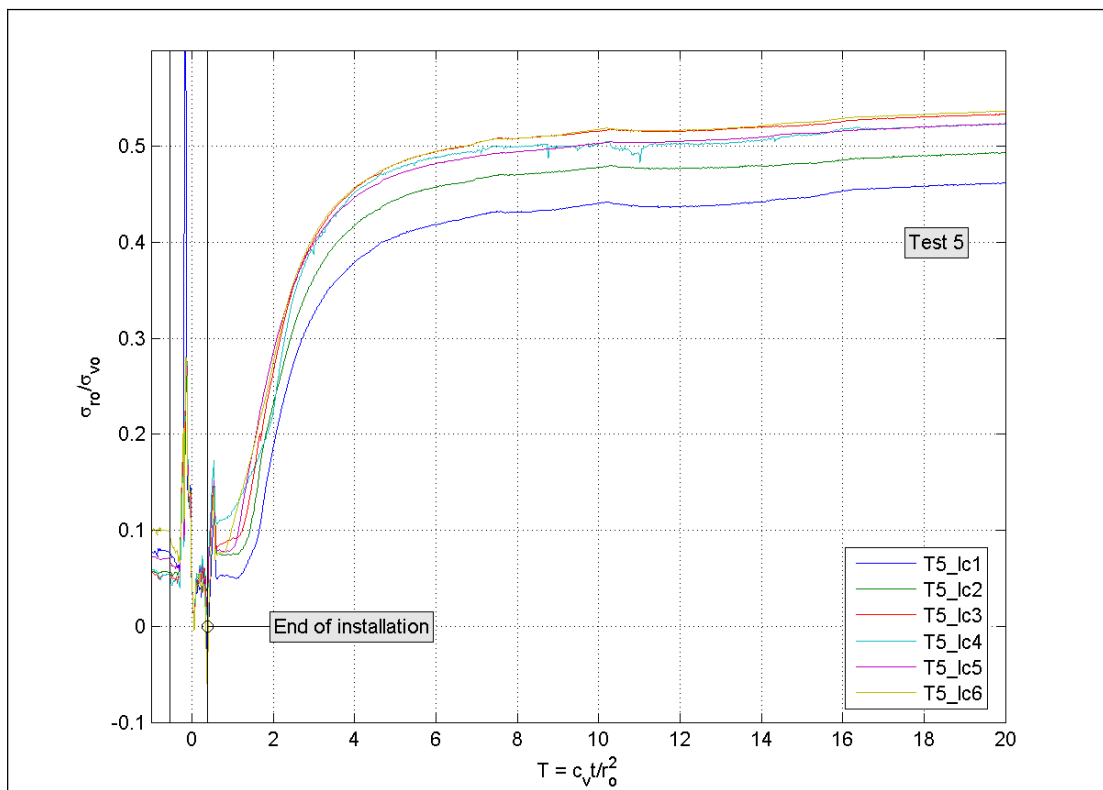


Figure A.2 Total stress on pipe during consolidation T5

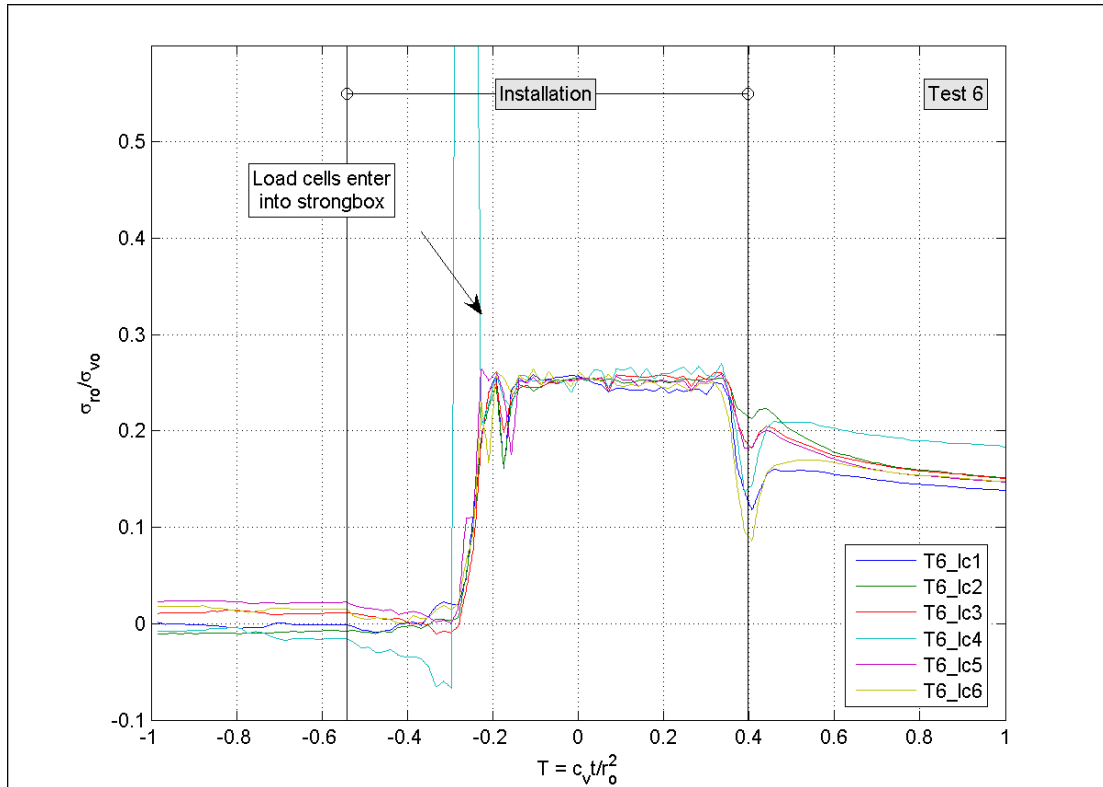


Figure A.3 Total stress on pipe during installation T6

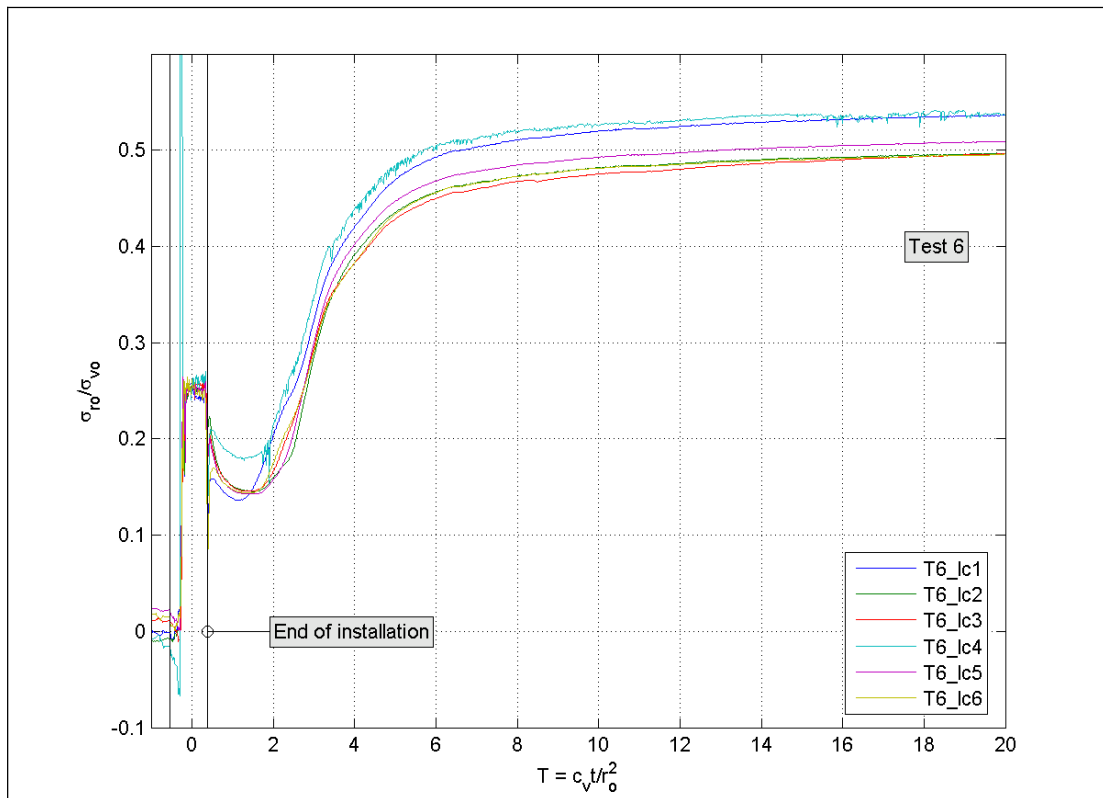


Figure A.4 Total stress on pipe during consolidation T6

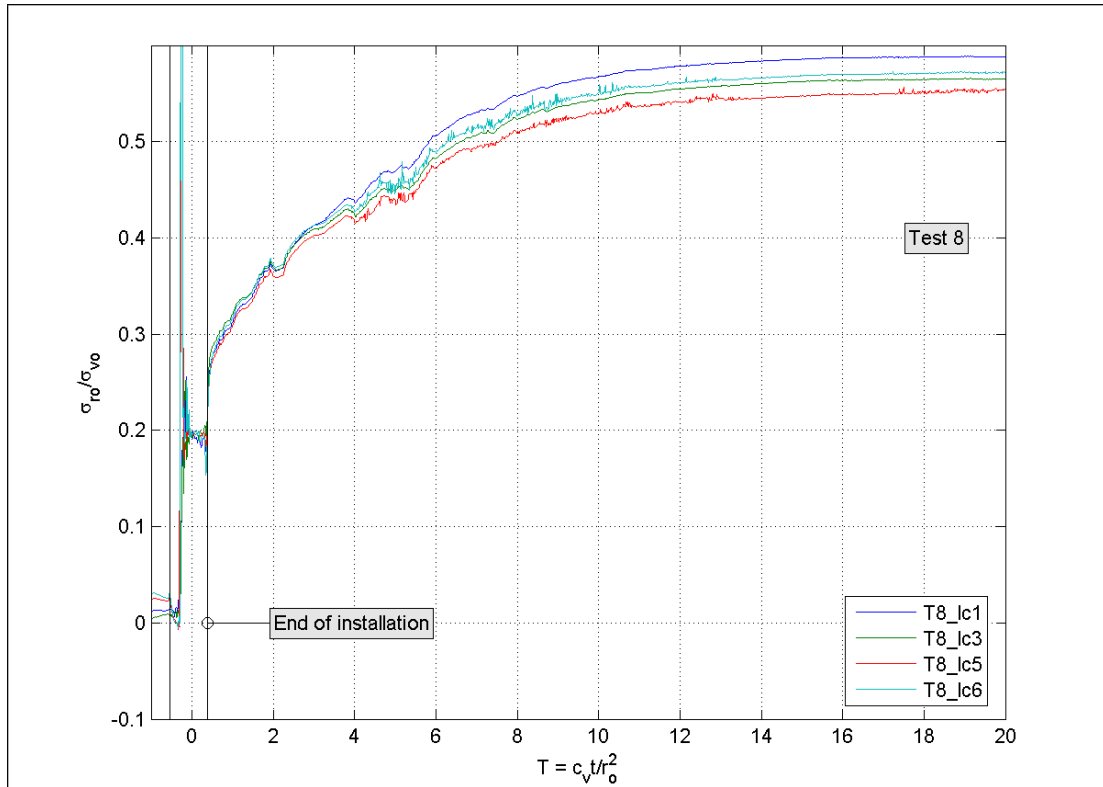


Figure A.5 Total stress on pipe during consolidation T8

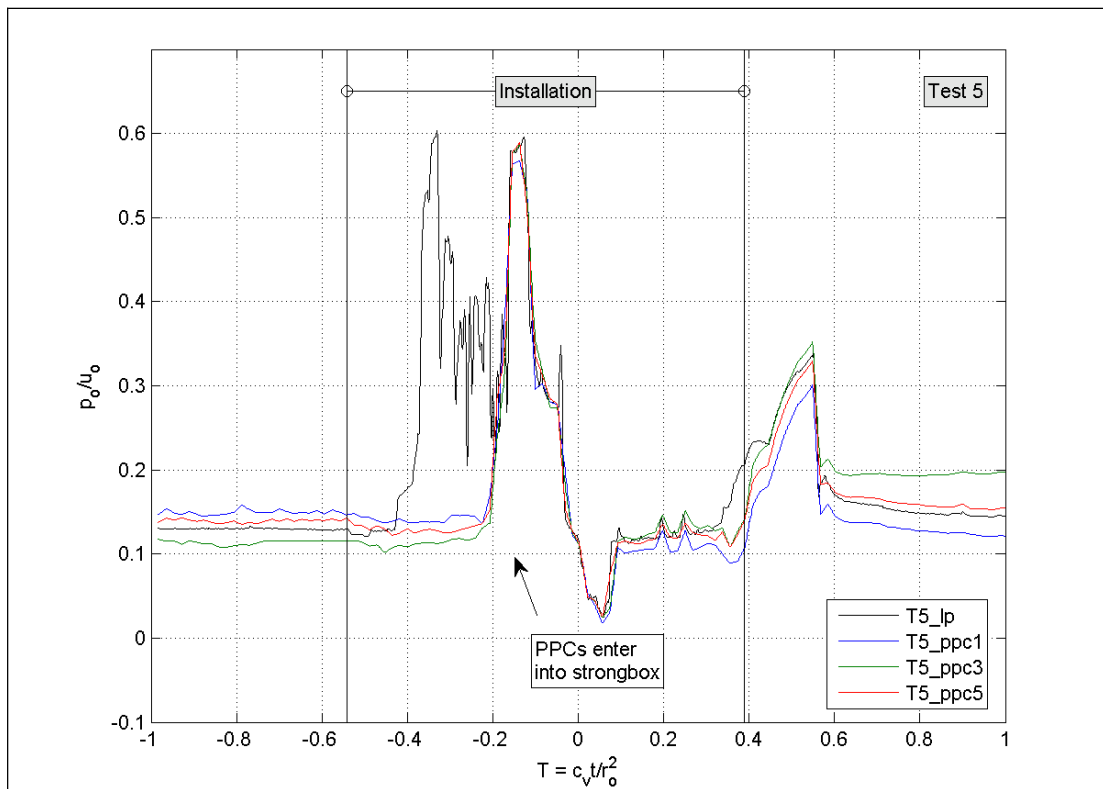


Figure A.6 Fluid pressure on pipe during installation T5

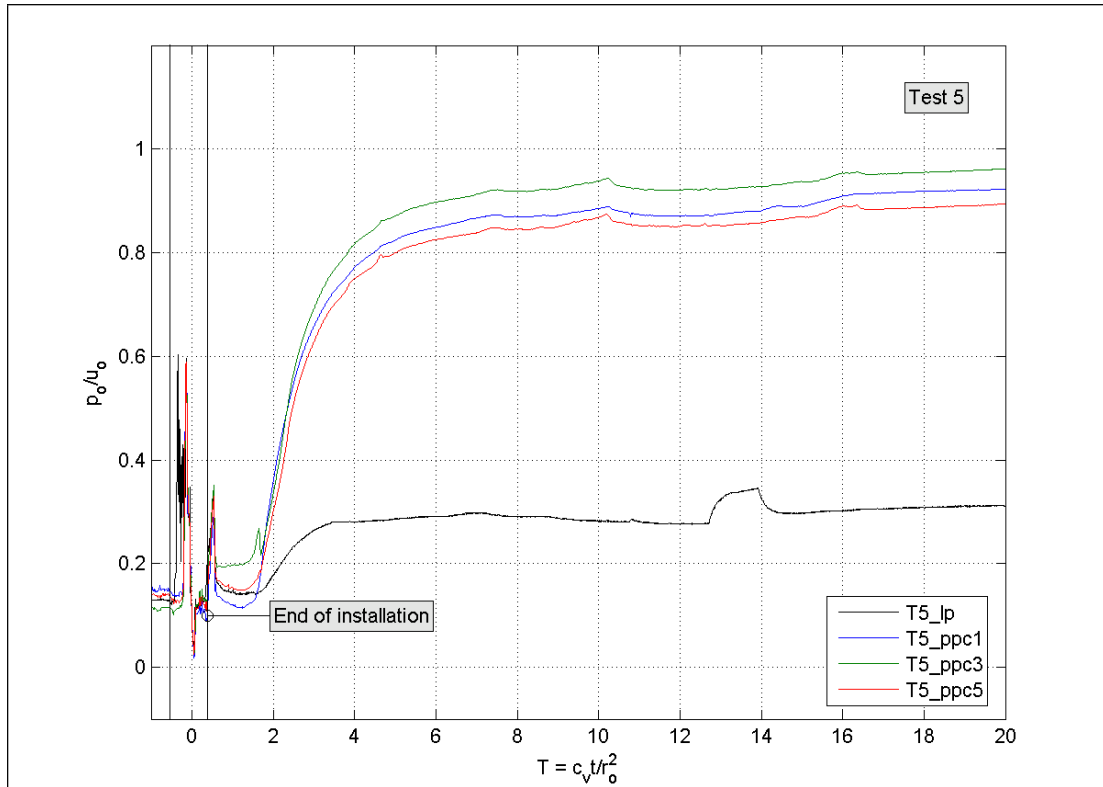


Figure A.7 Fluid pressure on pipe during consolidation T5

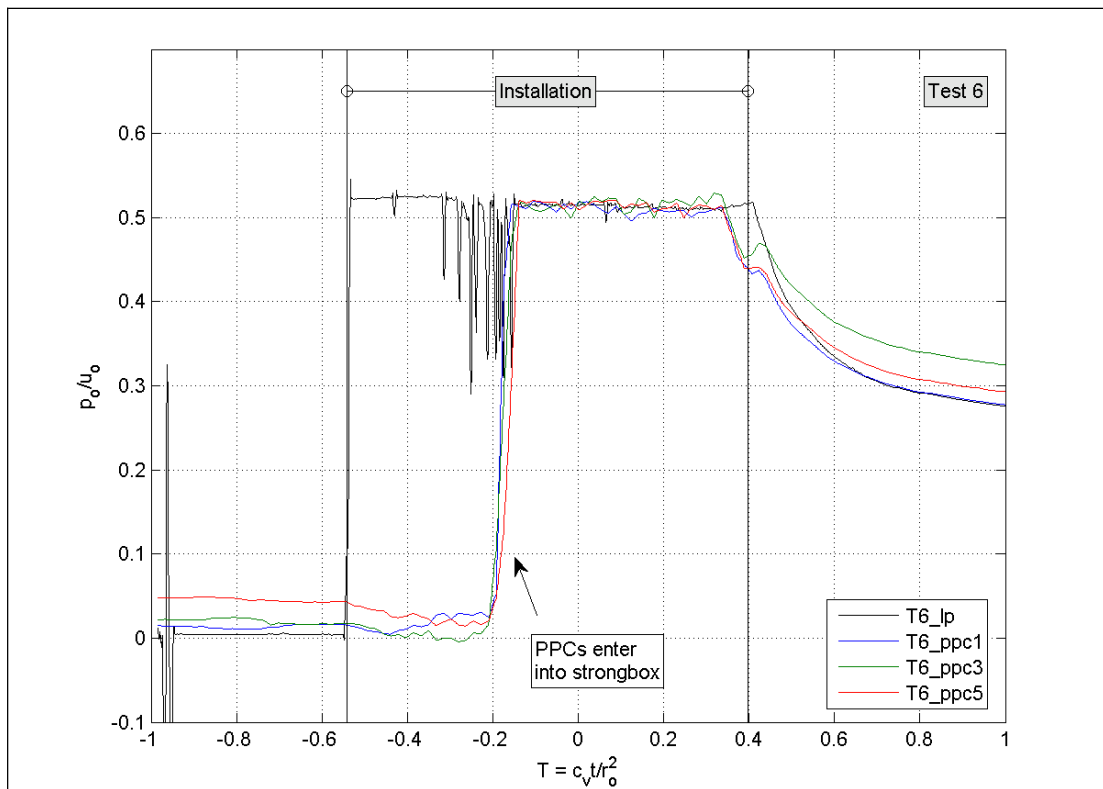


Figure A.8 Fluid pressure on pipe during installation T6

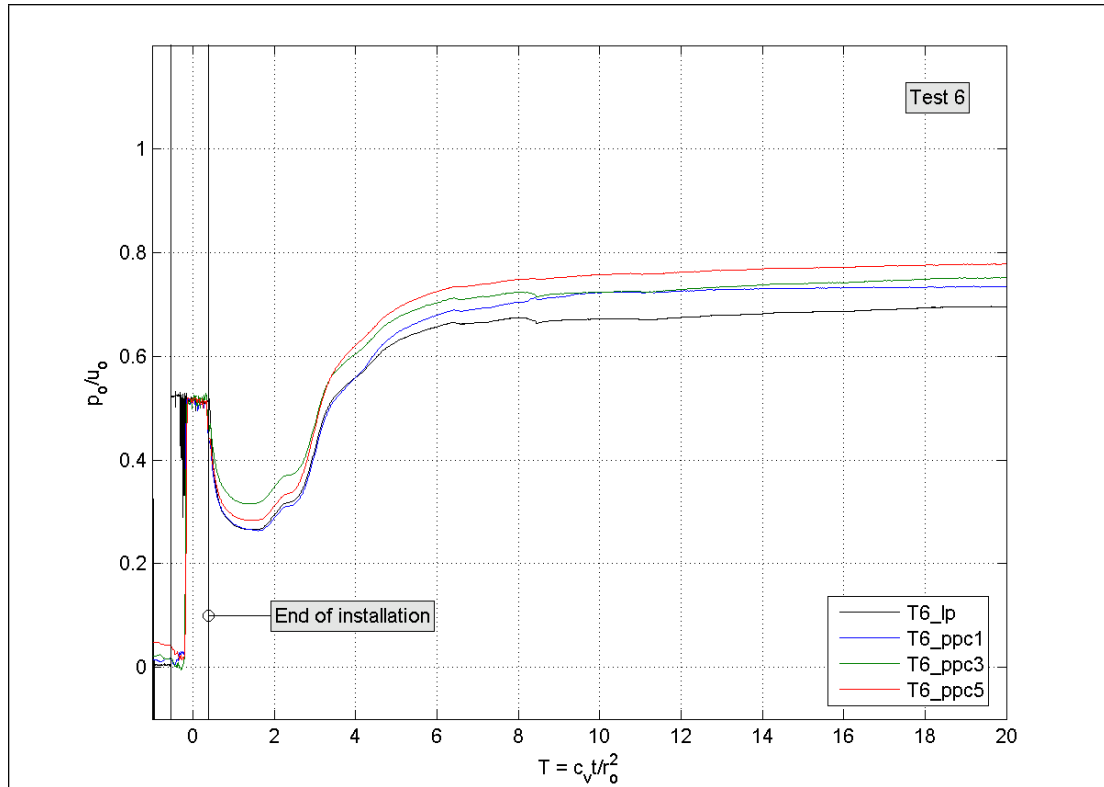


Figure A.9 Fluid pressure on pipe during consolidation T6

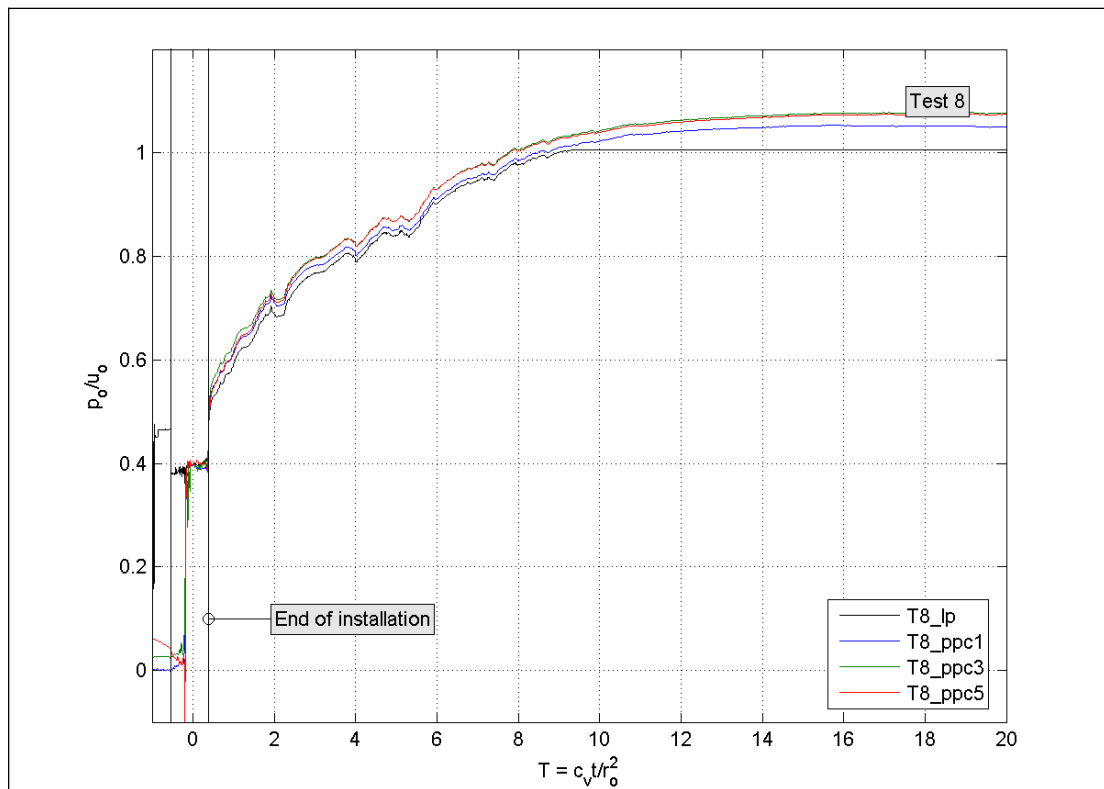


Figure A.10 Fluid pressure on pipe during consolidation T8

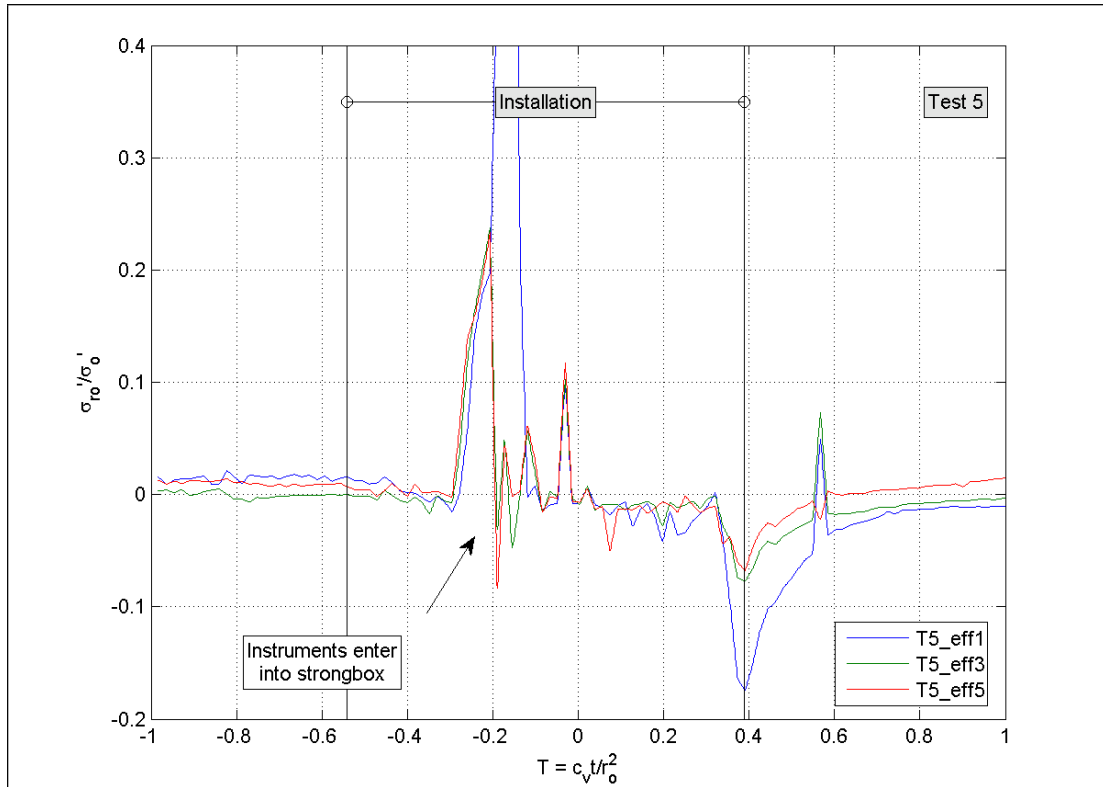


Figure A.11 Effective stresses on pipe during installation T5

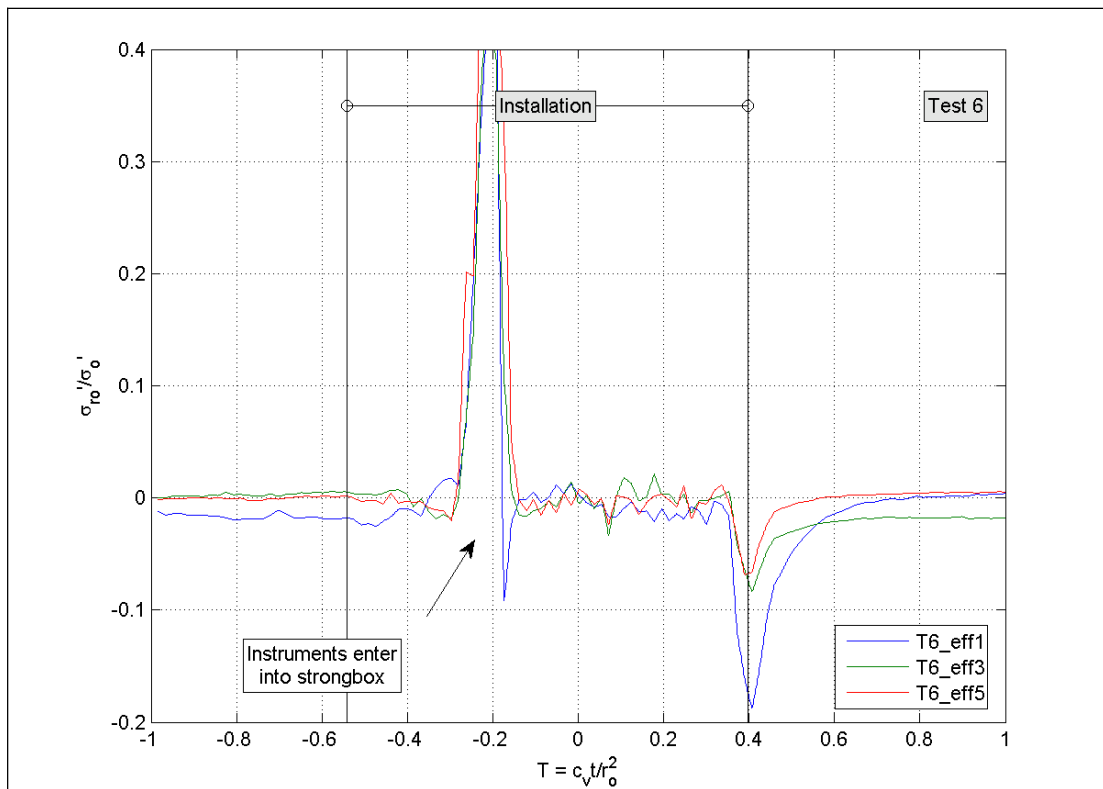


Figure A.12 Effective stresses on pipe during consolidation T5

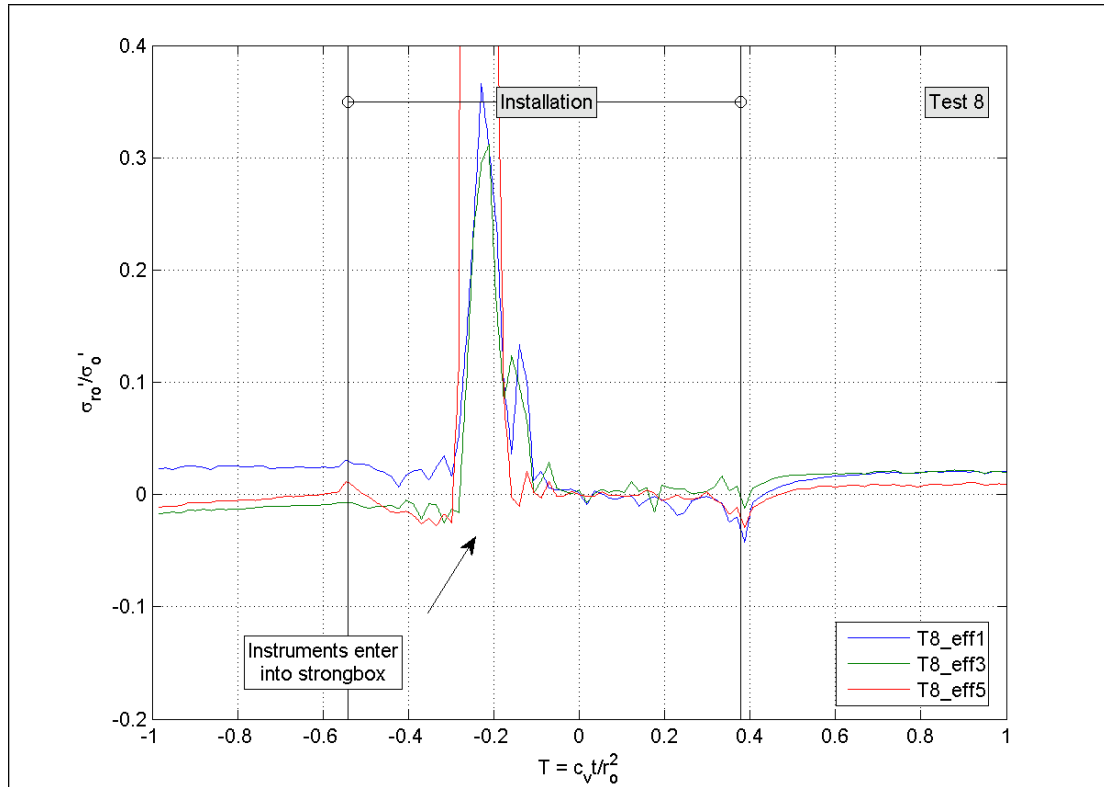


Figure A.13 Effective stresses on pipe during installation T6

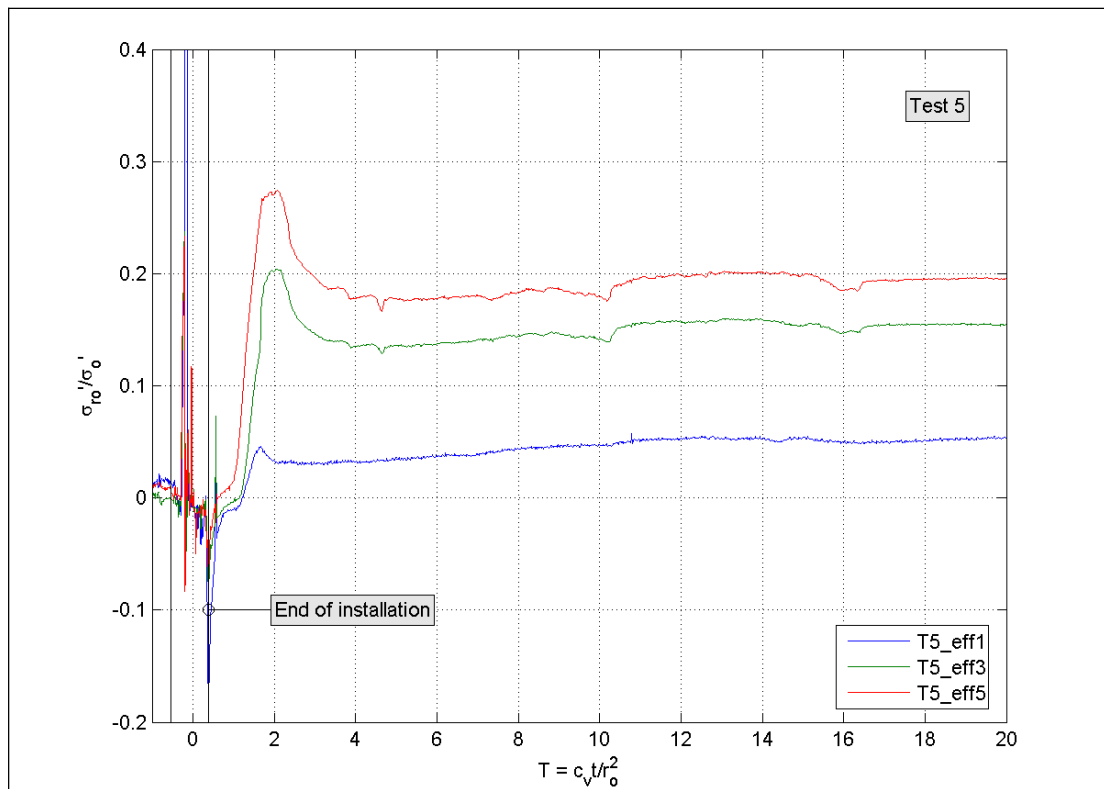


Figure A.14 Effective stresses on pipe during consolidation T6

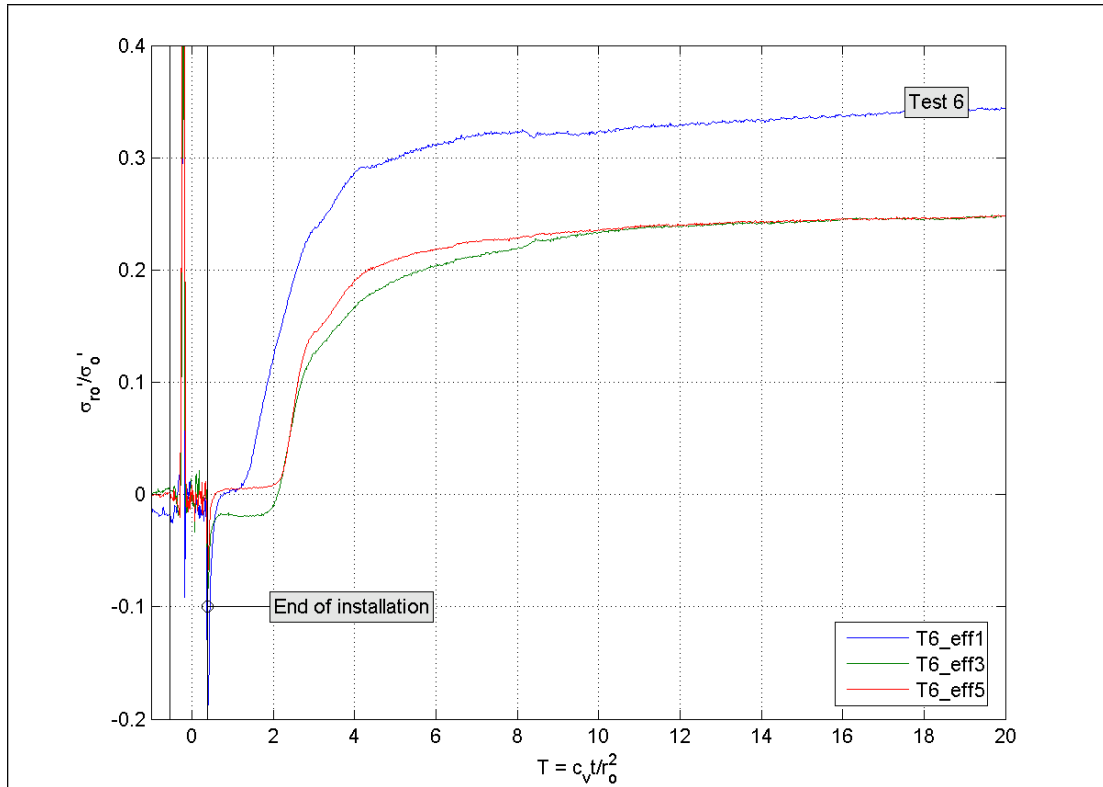


Figure A.15 Effective stresses on pipe during installation T8

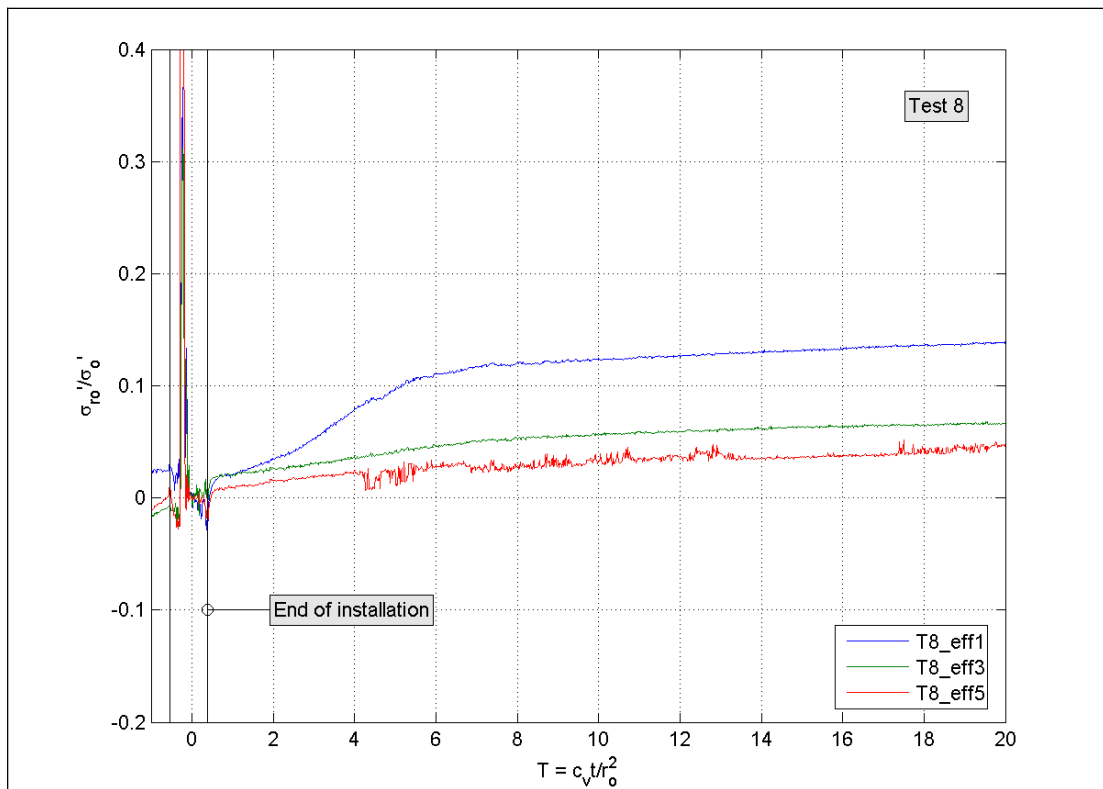


Figure A.16 Effective stresses on pipe during consolidation T8